Geochemical and Environmental Analysis

Geochemical weathering in the sub- and proglacial zone of two glaciated crystalline catchments in the Swiss Alps (Oberaar- and Rhoneglacier)

Ph.D. thesis presented by Kaspar Arn

Université de Neuchâtel
Faculté des Sciences
Institut de Géologie

November 2002

Thesis Jury:

Prof. Karl B. Föllmi (Neuchâtel)	*Director*
Prof. Martin Burkhard (Neuchâtel)	*Examinator*
Dr. Thierry Adatte (Neuchâtel)	*Examinator*
Dr. Virginie Matera (Neuchâtel)	*Examinator*
Prof. Christian Schlüchter (Bern)	*Examinator*
Prof. James I. Drever (Wyoming)	*Examinator*

Oberaar glacier snout on the 29th of June 2000
with tent (Hilleberg Namatji 2GT)

“The feldspar of the granite rock exposed to the atmosphere is corroded very slowly indeed, by the effects of air and moisture...

... this operation of the atmosphere upon the surface of the granite is so extremely slow as to be altogether unmeasurable by man”

James Hutton, Theory of the Earth (1795)

Acknowledgements

First of all, I would like to thank my supervisor Karl Föllmi, who set up this project and allowed me to spend two extra summers in the field and to go on many sampling missions during the winter season. His office door was always open for discussion of the latest results and possible implications, or further questions. He supported all upcoming ideas throughout this time and always motivated me to move a step further. He also initiated the participation of Neuchatel in the Venezuela Field Mission with Sylvain Huon and made it possible for me to travel down there. I especially appreciated his open mind and his tolerance towards me and my guignolism.

I started this work with Rachel Hosein. For four years we shared an office, good and bad weather in the field (during winter and summer), a lab, a field apartment, many liters of coffee, many colored, South American experiences (graçe aux outils suisses), and many hours of talking and discussing. I very much appreciated her as my friend and fellow-sufferer throughout this project! And I also thank her husband David Nisbet for all the hours he spent supporting this whole project.

This study was supported by Swiss National Science Foundation Grants 21-53997.98 and 20-61485.00, who are gratefully acknowledged!

For support in the lab, reviewing paper drafts, and help with many questions around this project I thank Philipp Steinmann, Thierry Adatte, Virginie Matera, André Villars, Sébastien Ryser, Khaoula Hamila, Pierre Schnegg, Roberto Costa, Didier Marquer, Othmar Müntener, Sabine Erb, Gianfranca Cerrito, Elisabeth Kuster, Pierre Tissot, and Urs Eichenberger. Martin Burkhard as “the glaciologist of the institute” was always happy to discuss whether it is the glacier ice or the subglacial meltwater that erodes the glacier bed. He helped enthusiastically on a winter sampling mission and many of the ideas in this work benefited from discussions with him!

My fieldwork was very well supported by the Kraftwerke Oberhasli (KWO). I thank Peter Marti, Walter Nägeli and Aristo von Weissenfluh (for the rides up to the lake during winter and the hospitality in their heated winter room), Theodor Maurer (who interpreted the avalanche risk), Wilhelm Regez and Gianni Biasutti (for the general support of this project). I thank Greti Willener from the Berghaus Oberaar for always having a hot soup for me, especially during the summer snowstorms.

This project benefited from several collaborations. In the early summer of ’99 during my stay at Haut Glacier d’Arolla, British friends of the Arolla project introduced me to the mysteries of glacial geochemistry. I will always remember the Gin-Tonics with glacier ice! I thank Sylvain Huon (Paris) for the trip to Venezuela (Fall ‘99), in which I participated as a technician. I included some pictures of this trip in Appendix E. Jan Kramers (Berne) and Dominique Aubert (Strasbourg) supported the Sr-business. Martin Lee (Glasgow) was always answering biotite-questions incredibly quick. Jérôme Gaillardet helped me to extrapolate the weathering data and questions to a global scale!

I would like to thank all the other PhDs at the institute with whom I spent many happy hours between work during lunches, dinners, and fieldtrips: Pierre, Julia, Baba, Nathalie, Laurent, Federica, Bas, Ronny, Julien, Bastos, J.D., Bernd, Urs, Charles, Guillaume, Olivier, and Claire. Thank you for adapting to my sense of humor!

I thank the students, who gave me a chance during travaux pratiques, breaks, and fieldtrips, despite my foreign language from across the Röschtigraben: Philippe M. (he helped to find the river under 4 m of snow…), Ivann, Laure, Michiel, the staff of the ANEG (geology students association), and all the others.

Besides university life, I was supported by some old friends who always had time to listen to my frustrations and experiences and who helped me to get over many crises. Thanks to Iwan (who sometimes sent me an e-mail and also helped during a sunny winter sampling mission), to Franz and Brigitta (for many time-outs in Italy, before and during the thesis), to Moose and Michelle (for many corrections and dinners in Bern), to Mirjam (for discussions about weathering, research, and life in general), to Sascha (for many deep snow rides and quaternary dream constructions on the balcony), to the entire Schaller clan (for their hospitality in the back country resort of Les Paccots/FR), to Bärni (for motivating me to become an applied geologist in the future), to Christian Schlüchter (the initiator of my interest in glaciers and quaternary geology), and to Peter Schertenleib (for supporting me with much-needed health advisories).

Last but definitively not least, I thank my family who brought me to where I am now. My parents and my brother were constantly interested in my project field areas during my studies in Geology. Thanks to my mum (e.g. for being patient during water filtering and for carrying around iron bars in the field), to my brother (for water sampling while I was in Venezuela and for all the motivating drinks and dinners), and to my dad and Marietta (for field visits and general supervision). My biggest thanks goes to Lena (my Lama), who didn't leave me alone during all this long years, who helped in the field, who re-motivated me during weekends, and who always stood at my side. Thank you for your support and your patience.

Geochemical weathering in the sub- and proglacial zone of two glaciated crystalline catchments in the Swiss Alps (Oberaar- and Rhoneglacier).

Abstract

Within this thesis project subglacial and proglacial chemical weathering processes and the composition of runoff and particulate material from the two glaciated catchments of Oberaar and Rhone glacier (Swiss Alps) were studied. Both areas are contained within the crystalline rocks of the Aar Massif, and the lithologies are quite homogeneous and comparable, except for the presence of a zone of strongly foliated and highly deformed Variscan basement gneisses and schists in the Oberaar cachment, which may contain up to 5 % calcite and are more erodable than the purely granitic bedrock of the Rhone catchment. There are two domaines of weathering in glacial environments, the subglacial and proglacial zones: The subglacial domain is dominated by "short-term" weathering processes driven by the dissolution of freshly ground fine particles in dilute glacial meltwaters. The most reactive mineral in this context is calcite. "Long-term" weathering processes take place in the proglacial area where conditions associated with pedogenesis, such as increased acidity, increase the overall chemical weathering rates.

A first part of this thesis is concerned with the weathering mass balance of the two catchments. Annual weathering fluxes are calculated as the weighted mean of monthly accumulation period and twice daily ablation period meltwater samples collected from July, 1999 to May, 2001, and corrected for precipitation inputs. They are dominated by calcium, which represents 81 % and 55 % of the total cation flux in the Oberaar and Rhone catchments, respectively. A three times higher calcite content of Oberaar suspended sediments compared to the Rhone suspended sediments (2.1 vs. 0.6 %), coupled with the increased erodability and higher sulphide content of the Oberaar bedrock, leads to a five times higher Ca^{2+} flux. This demonstrates the extreme sensitivity of glacial systems to minor changes in the calcite and sulphide content of crystalline bedrock and suggests that short-term CO_2 sequestration associated with the hydrolysis of carbonate may be locally variable. Calcite weathering is more important in these glacial catchments than in non-glaciated catchments underlain by granitoid rocks. The silicate weathering rates we observe in our presently glaciated alpine catchments (and those which are published for other glaciated alpine and Antarctic catchments) fall within the range of temperate, non-glaciated granitoid catchments with the same runoff, implying that silicate weathering is not accelerated in the subglacial environment. The strongly foliated gneissic zone running down the central third of the Oberaar catchment has a major impact also on physical erosion rates compared to those of the the Rhone catchment: Approximately twice as much suspended sediment is exported by the Oberaar meltwaters compared to the Rhone meltwaters during the study period.

In a second part the Sr isotope composition of meltwaters and precipitation as well as bulk suspended sediment and local bedrock was analysed. The Rhone suspended sediment composition is interpreted as a mixture of Grimsel Granodiorite and Central Aar Granite. The lower meltwater Sr ratio is explained by the preferential weathering of disseminated calcite which has a relatively low calcite $^{87}Sr/^{86}Sr$ ratio. Furthermore, early and nonstoichiometric Sr release from silicates may be visible as well in this purely granitic catchment. Oberaar meltwaters show a higher isotopic ratio compared to Oberaar suspended sediment which reflects the preferential weathering of the calcite contained within the Variscan Gneisses. The Sr concentration of rain corresponds to 8 – 9 % of that in the meltwaters. Together with its low Sr isotopic ratio this suggests that the atmospheric contribution is not visible in the meltwaters. Disseminated calcite exerts a major impact not only on the meltwater major ion composition but also on its Sr systematics.

In a third part of this thesis the clay mineralogy of glacial sediments from the two proglacial areas were analysed using XRD techniques, in order to identify processes and rates of alteration of moraine material in the glacier forefield. The well-dated sediments provide a chronosequence consisting of (A) recent suspended sediment in meltwater; (B) terminal moraines dating from the Little Ice Age (LIA 1300-1850); and (C) tills dating from the retreat of Younger Dryas (YD 11'600 y BP). The suspended sediment is derived from mechanically abraded freshly eroded bedrock without being stored and altered subglacially and secondary weathering products have not been observed. Chemical weathering becomes increasingly important once glacial sediment is deposited in the

proglacial area. With increasing age a vegetation cover develops on the morainic deposits and the initial umbrepts undergo podzolisation. XRD data in this chronosequence show an increase in pedogenically formed vermiculite and a continuous decrease in biotite with increasing sediment age. Biotite contents in the top 30 cm of the soils decrease by 25 – 50 % within 140 – 270 years. Feldspar weathering becomes apparent in proglacial sediments older than 270 years.

Biotite weathering rates were calculated using the difference in biotite content between the C-horizon and the top 30 cm of a soil profile. Reactive mineral surface areas were estimated geometrically, for their total as well as for their edge surface. The weathering rates obtained are several orders of magnitude faster than known field weathering rates. Two potential explanations are offered: (1) The predominance of fine-grained particles (<63 μm) in glacial sediment which are mechanically disaggregated and preferentially leached; (2) The studied glacial sediments are well drained and highly permeable and no heterogeneities in flow paths through soils were observed. It is confirmed that glacially derived material is subjected to enhanced chemical weathering, starting immediately after deposition in the pro-glacial zone and subsequently continuing for thousands of years after glacier retreat.

In a fourth part apatite dissolution textures and long-term detrital phosphorus (P) weathering rates were determined from the chronosequences. Apatite grains were graded relative to weathering-induced changes in their surface morphologies. Present-day apatite grains are heavily indented and dissolution rounded. Little Ice Age grains from two 0-10 cm depth samples already showed extensive dissolution etching, similar to surface grains from the Younger Dryas profile. The weathering front deepened progressively due to bio-corrosion in the evolving acidic pedosphere, with mechanical indentations on grains acting as sites for preferential dissolution. Ironbound, organic, and detrital P concentrations were measured in the chronosequences: Organic and ironbound P replaces detrital P in the Younger Dryas profiles. During the first 300 yrs of glacial sediment exposure P dissolution rates were ca. 70 times higher than the mean global riverine dissolved P flux from ice-free continents. Calculated for the Younger Dryas profiles, the flux is 2.5 times the global mean. These data strengthen the argument for changes in the biolimiting P flux on glacial-interglacial timescales.

A fifth part of this thesis compares the different forms of phosphorus with different bioavailabilities in the tropical Apure (Venezuela) and glacial Rhone, Oberaar, and Rhone tributary catchments. The tropical waters generally contain more conditionally bioavailable forms of P (DOP, ironbound and organic P), while runoff from the presently glaciated catchments is dominated by scarcely bioavailable detrital P (97 %). However, glacial processes play an important regenerative role in bringing large volumes of freshly ground detrital phosphorus to the biosphere. The increased flux of weathering-derived soluble reactive phosphorus from the recently deglaciated Rhone tributary catchment indicates that the dissolution of detrital P is accelerated in proglacial sediments compared to the global mean. In contrast the main source of soluble reactive phosphate in the Apure catchment is probably atmospheric. Glaciers and periods of glaciation may therefore lead to complex changes in the P dynamics and productivity of terrestrial and aquatic ecosystems.

Summarizing, the global impact of subglacial versus proglacial weathering is not fully clear yet, there is still a need for more data to address the different problems outlined in this thesis. Our data seems to indicate that there is no direct impact of subglacial chemical weathering on global silicate weathering rates. But the present data situation implies, that there is certainly a significant potential for the indirect impact on global chemical weathering via the readily weatherable glacially derived material deposited in the proglacial area. This work confirms the positive coupling of physical and chemical weathering: The coupling is intensified in environments whose weathering regimes are dominated by weathering-limited glacial processes. Global denudation is assumed to be weathering-limited during glaciations.

Résumé

Dans ce projet de thèse ont été étudiés à la fois les processus d'altération chimique proglaciaire et subglaciaire ainsi que la composition des ruissellements et de la fraction particulaire des deux bassins versants glaciaires de l'Oberaar et du Rhône (Alpes suisses). Ces deux sites d'étude se trouvent sur les roches cristallines du Massif de l'Aar. Les lithologies sont homogènes et comparables, exception faite de la présence d'une zone fortement foliée et déformée du socle varisque, composée de gneiss et de schistes, dans le bassin versant de l'Oberaar. Ce dernier peut localement contenir plus de 5% de calcite et est plus érodable que le bassin versant rhodanien, purement granitique. Il existe deux domaines d'altération dans les environnements glaciaires : ce sont les zones subglaciaire et proglaciaire. Le domaine subglaciaire est dominé par les processus d'altération à court-terme matérialisés par les phénomènes de dissolution des particules fines non-altérées présentes dans les eaux de fonte glaciaire diluées. Le minéral le plus réactif dans ce contexte est la calcite. Les processus d'altération à long-terme prennent place dans les zones proglaciaires, où les conditions associées avec la pédogenèse, telle que l'acidité, augmentent le taux général d'altération chimique.

La première partie de cette thèse concerne le bilan de masse de ces deux bassins versants. Les flux d'altération annuels sont calculés en utilisant une moyenne pondérée sur une période d'accumulation mensuelle, ainsi que par un échantillonnage bi-journalier des eaux de fonte de juillet 1999 à mai 2001. Ces derniers sont corrigés par rapport aux précipitations. Ils sont dominés par le calcium qui représente respectivement 81% et 55% du flux total de cations dans les bassins versants de l'Oberaar et du Rhône. La teneur en calcite est trois fois plus élevée pour les sédiments en suspension de l'Oberaar par rapport à ceux du Rhône (2.1% contre 0.8%). Couplé avec une plus grande érodabilité et une plus forte teneur en sulfures des roches présentes dans le bassin versant de l'Oberaar, ceci mène à un flux de Ca^{2+} cinq fois plus élevé. Ceci démontre l'extrême sensibilité des systèmes glaciaires à des changements mineurs de la teneur en calcite et en sulfures des roches cristallines et suggère que la séquestration à court-terme du CO_2, associée à l'hydrolyse des carbonates, peut être localement variable. L'altération de la calcite est plus importante dans les bassins versants glaciaires que dans les non-glaciaires, ceci pour de régions granitiques. Les taux d'altération des silicates que nous avons mesurés dans ces bassins versants alpins actuellement englacés (ainsi que ceux publiés pour d'autres bassins versants glaciaires des Alpes et de l'Antarctique) sont du même ordre de grandeur que ceux de bassins versants granitiques tempérés non-glaciaires à débits similaires. Ceci implique que l'altération des silicates n'est pas accélérée dans les environnements subglaciaires. La zone de gneiss fortement foliés que l'on trouve dans le tiers central du bassin versant de l'Oberaar a également un impact majeur sur le taux d'érosin physique. En comparaison avec le bassin versant du Rhône, durant la période de la présente étude, l'exportation de matières en suspension dans les eaux de fonte de l'Oberaar était environ deux fois plus importante que dans celles du Rhône.

Dans la deuxième partie de cette thèse, la composition isotopique du strontium des eaux de fonte, des précipitations, des sédiments en suspension et du socle a été analysée. La composition des sédiments en suspension du Rhône est interprètée comme étant un mélange de Granodiorite du Grimsel et de Granite Central de l'Aar. Le faible rapport isotopique du strontium des eaux de fonte est expliqué par l'altération préférentielle de la calcite disséminée, qui a un rapport $^{87}Sr/^{86}Sr$ relativement bas. De plus, dans les bassins versants purement granitiques, une libération précoce et non-stoechiométrique du strontium peut être visible. Les eaux de fonte de l'Oberaar montrent un rapport $^{87}Sr/^{86}Sr$ plus élevé par rapport à celui des sédiments en suspension de même provenance, ce qui reflète l'altération préférentielle de la calcite présente dans les gneiss varisques. La concentraton en strontium des eaux de pluie correspond à 8-9% de celle des eaux de fonte. Leur faible rapport $^{87}Sr/^{86}Sr$ suggère que la contribution atmosphérique n'est pas importante dans les eaux de fonte. La calcite disséminée exerce un impact majeur non seulement sur la composition des ions majeurs des eaux de fonte, mais également sur la systématique des isotopes du strontium.

En troisième partie, la minéralogie des argiles des sédiments glaciaires des deux zones proglaciaires a été examinée par diffraction des rayons X afin de déterminer les processus et les taux d'altération du matériel morainique de la marge proglaciaire. Les sédiments datés fournissent une chronoséquence consistant en : (A) des sédiments en suspension récents provenant de l'eau de fonte, (B) des moraines terminales (frontales) datant du Petit Age Glaciaire (années 1300-1850) et (C) des moraines datant du retrait de Dryas Récent (11'600 ans BP). Les sédiments en suspension, qui sont dérivés de l'abrasion mécanique du socle, ont été récemment érodés et n'ont subi ni stockage et ni altération subglaciaire. De plus, aucun produit secondaire d'altération n'a été observé. L'altération chimique devient de plus en plus importante dès que les sédiments proglaciaires sont déposés dans la zone proglaciaire. Avec l'augmentation de l'âge, une couverture végétale se développe sur les dépôts morainiques et les umbrets initiaux subissent une podzolisation. Les données de diffraction des rayons X dans cette chronoséquence montrent une augmentation de la vermiculite d'origine pédogénique et une diminution continue de la biotite avec l'augmentation de l'âge du sédiment. La teneur en biotite dans les trente premiers centimètres du sol décroît de 25% à 50% en un laps de temps de 140-270 ans. L'altération des feldspaths devient apparente pour des sédiments proglaciaires de plus de 270 ans.

Les taux d'altération de la biotite ont été calculés en utilisant les différences de concentration en biotite entre l'horizon C et les 30cm supérieurs d'un profil de sol. Les surfaces de réaction des minéraux ont été estimées géométriquement, aussi bien pour leur surface totale que pour leur surface de bordure. Les taux d'altération ainsi obtenus sont plus rapides de plusieurs ordre de grandeur que ceux trouvés dans la littérature.

Deux explications sont proposées : (1) La prédominance des particules de faible diamètre (<63 μm) dans les sédiments glaciaires qui, ayant subi une désaggrégation mécanique, sont lessivées de manière préférentielle. (2) Les sédiments glaciaires étudiés sont très bien drainés et hautement perméables et aucune hétérogénéité des directions d'écoulement n'a été observée. Il est confirmé que les matériaux d'origine glaciaire sont sujets à une forte altération chimique commençant immédiatement après leur dépôt dans la zone proglaciaire et se poursuivant durant des milliers d'années après le retrait des glaces.

Dans une quatrième partie, les textures de dissolution de l'apatite ainsi que les taux d'altération à long terme du phospore ont été déterminés à partir des chronoséquences. Les grains d'apatite ont été classés selon les changements de morphologie de leur surface provoqués par l'altération. Les grains d'apatite récents sont fortement indentés et arrondis par dissolution. Les grains du Petit Age Glaciaire provenant d'échantillons récoltés entre 0cm et 10cm de profondeur montrent déjà une dissolution extensive, similaire à celle observée sur des grains provenant de profils du Dryas Récent.

Le front d'altération s'approfondit progressivement à cause de la bio-corrosion dans la pédosphère acide en évolution, avec une indentation des grains agissant comme site*s* de dissolution préférentiels.

Les concentrations de phosphore lié au fer, organique et détritique ont été mesurées dans les chronoséquences : le phosphore lié au fer et le phosphore organique remplacent le phosphore détritique dans les profils du Dryas Récent. Durant les 300 premières années d'exposition des sédiments glaciaires, les taux de dissolution du phosphore étaient environ 70 fois plus élevés que le flux global moyen de phosphore dissous dans les rivières drainant des continents libres de glace. Calculé pour les profils du Dryas Récent, le taux est égal à 2.5 fois la moyenne globale. Ces données renforcent l'argumentation en faveur des changements du flux de phosphore bio-limitant pour des échelles de temps de l'ordre glaciaire-interglaciaire.

Une cinquième partie de cette thèse compare les différentes formes de phosphore. Elle montre les différentes bio-disponibilités, dans l'Apure (climat tropical, Venezuela) et dans les parties englacées des bassins versants du Rhône, et de ses affluents, et de l'Oberaar. Les eaux tropicales contiennent généralement des formes de phosphore plus bio-disponibles (POD, organique et lié au fer), alors que les écoulements en provenance des bassins versants actuellement englacés sont dominés par le phosphore détritique (97%), difficilement bio-disponible. Cependant, les processus glaciaires jouent un important rôle de régénération en apportant de grandes quantités de phosphore détritique fraichement broyé à la biosphère. L'augmentation du flux de phosphore réactif soluble dérivé de l'altération, provenant d'un affluent du Rhône récemment désenglacé, indique que la dissolution du phosphore détritique est

accélérée dans les sédiments proglaciaires par rapport à la moyenne globale. Au contraire, dans le bassin versant de l'Apure, la principale source de phosphore soluble est probablement atmosphérique. Les glaciers ainsi que les périodes glaciaires peuvent donc induire des changements complexes dans la dynamique du phosphore et dans la productivité des écosystèmes terrestres et marins.

Pour résumer, l'impact global de l'altération subglaciaire, comparée à l'altération proglaciaire, n'est pas encore complètement clair, de nombreuses données étant encore nécessaires pour résoudre les différents problèmes évoqués dans cette thèse.

Nos données semblent indiquer qu'il n'y a pas d'impact de l'altération subglaciaire sur le taux d'altération global des silicates. Cependant, l'état actuel de nos données implique qu'il y a certainement un potentiel significatif pour un impact indirect sur l'altération chimique globale par l'intermédiaire de matériaux d'origine glaciaire, facilement altérables, déposés dans les zones proglaciaires. Ce travail confirme le couplage positif de l'altération physique et chimique ; le couplage augmente dans les milieux dont les régimes d'altération sont dominés par des processus glaciaires limités par l'érosion. L'érosion globale est considérée comme étant limitée par l'altération durant les périodes de glaciation.

Zusammenfassung

Im Rahmen dieses Projektes wurden sub- und proglaziale Verwitterungsprozesse und die Zusammensetzung von Abflusswasser und partikulärem Material von den zwei vergletscherten Einzugsgebieten vom Oberaar und Rhonegletscher (Schweizer Alpen) studiert. Beide Gebiete liegen in den kristallinen Gesteinen des zentralen Aarmassif. Die Lithologien sind homogen und vergleichbar, mit Ausnahme einer Zone von stark gefalteten und deformierten Variskiden Basementgneisen und -schiefer im Oberaargebiet (die sog. Gneis-Schiefer-Zwischenzone). Diese können bis 5 % Calcit enthalten und sind einfacher erodierbar als die puren granitischen Grundgesteine des Rhonegebietes. In vergletscherten Gebieten sind generell zwei Verwitterungsbereiche bekannt; der sub- und der proglaziale Bereich. Der subglaziale Bereich ist wird dominiert durch “kurzfristige” Verwitterungsprozesse, welche durch die Auflösung von frisch gemahlenen feinen Gesteinspartikel im schwachkonzentrierten Schmelzwasser angetrieben werde. Das reaktivste Mineral in diesem Zusammenhang ist Calcit. “Langfristige” Verwitterungsprozesse finden im proglazialen Bereich statt, wo die Bedingungen in Verbindung mit der Pedogenese (z.B. Versäuerung) die gesamte chemische Verwitterungsrate erhöhen.

Der erste Teil dieser Arbeit befasst sich mit einer Verwitterungsmassenbilanz der beiden Einzugsgebiete. Jährliche Verwitterungsfluxe werden aus dem gemittelten Schnitt von Wasserproben berechnet (monatliche Beprobung während der Akkumulationsperiode, zweimal täglich während der Ablationsperiode). Die Schmelzwasserflüsse wurden zwischen Juli 1999 und May 2001 beprobt und die Werte wurden niederschlagskorrigiert. Sie sind dominiert von Calcium, welches 81 resp. 55 % vom totalen Kationenflux im Oberaar- resp. Rhonegebiet ausmacht. Der drei mal höhere Calcitgehalt des suspendierten Sedimentes vom Oberaargletscher verglichen mit dem Rhonegletscher (2.1 resp. 0.5 %), verbunden mit der leichteren Erodierbarkeit und dem höheren Sulphidgehalt des Grundgesteines im Oberaargebiet, führt zu einem fünf mal grösseren Ca^{2+} flux. Dies zeigt die extreme Empfindlichkeit von glazialen Systemen gegenüber kleinsten Änderungen im Calcit- und Sulphidgehalt von kristallinem Grundgesteinen und weist darauf hin, dass die kurzfristige CO_2-Bindung in Zusammenhang mit der Hydrolyse von Karbonaten lokal variabel ist. Calcitverwitterung in diesen vergletscherten Gebieten ist wichtiger als in nicht-vergletscherten Gebieten in granitoidem Grundgestein. Die Silikatverwitterungsraten in unseren zur Zeit vergletscherten alpinen Einzugsgebieten entsprechen (zusammen mit publizierten Daten anderer vergletscherter alpiner und antarktischer Gebiete) den Werten von temperierten, nicht-vergletscherten, granitoiden Einzugsgebieten mit ähnlichem Abfluss. Dies bedeutet, dass die Silikatverwitterung im subglazialen Bereich nicht beschleunigt ist. Die Zone stark zerfalteten Gneise im Mittleren Drittel vom Oberaareinzugsgebiet hat ferner einen grossen Einfluss auf die mechanischen Erosionsraten verglichen mit dem Rhonegebiet. Während der Untersuchungsperiode wird ungefähr doppelt soviel suspendiertes Sediment aus dem Oberaargebiet exportiert verglichen mit dem Rhonegebiet.

In einem zweiten Teil geht es um die Sr-Isotopenzusammensetzung von Schmelz- und Niederschlagswasser sowie von suspendiertem Sediment und lokalem Grundgestein. Die Zusammensetzung von suspendiertem Sediment vom Rhonegletscher wird als Gemisch aus Grimsel-Granodiorit und Zentralem Aaregranit interpretiert. Das tiefere Sr-Verhältnis im Schmeltwasser wird mit der bevorzugten Lösung von disseminiertem Calcit erklärt, welcher ein relativ tiefes Sr-Verhältnis aufweist. Zudem kann in diesem vollständig granitoiden Gebiet frühe nicht-stoichiometrische Sr-Lösung von Silikaten sichtbar sein. Oberaarschmelzwässer zeigen höhere Isotopenverhältnisse verglichen mit der entsprechenden Suspension. Dies wiederspiegelt die bevorzugte Auflösung vom in den Variskiden Gneisen enthaltenen Calcit. Die Sr-Konzentration von Regen entspricht ca. 8 – 9 % von derjenigen im Schmelzwasser. Zusammen mit dem tieferen Sr-Isotopenverhältnis deutet dies darauf hin, dass im Schmeltwasser kein atmosphärischer Einfluss sichtbar ist. Disseminierter Calcit übt den Haupteinfluss aus, nicht nur auf die Zusammensetzung der Hauptionen im Schmelzwasser, sondern auch auf deren Sr-Systematik.

In einem dritten Teil dieser Arbeit wurde die tonmineralogische Zusammensetzung von Gletschersedimenten

der zwei proglazialen Gebiete untersucht, mit Hilfe von XRD-Technik, um Einblick in die Prozesse und Raten von der Verwitterung von Moränenmaterial im Gletschervorfeld zu erhalten. Die gut datierten Sedimente stellen eine Chronosequenz dar aus (A) rezentem suspendiertem Sediment in Schmeltwasser; (B) Endmoränen aus der kleinen Eiszeit (LIA, 1300-1850), und (C) Moränen vom Rückzug der Ausdehnung der Jüngeren Dryas (YD, 11'600 y BP). Das suspendierte Sediment stammt von der mechanischen Abrasion von frischem Grundgestein, es wurde weder zwischengelagert noch verwittert im subglazialen Bereich und sekundäre Verwitterungsprodukte konnten nicht beobachtet werden. Chemische Verwitterung wird zunehmend wichtig, sobald das Gletschersediment im proglazialen Bereich deponiert wird. Mit wachsendem Alter entwickelt sich eine Vegetationsdecke auf den Moränenablagerungen und die ursprünglichen "Umbrepts" durchlaufen eine Podzolisation. XRD daten von diesen Chronosequenzen zeigen die Zunahme von pedogenetisch geformtem Vermikulit und eine kontinuierliche Abnahme von Biotit mit wachsendem Alter. Der Biotitgehalt in den obersten 30 cm der Böden nimmt in 140 – 270 Jahren um 25 – 50 % ab. Feldspatverwitterung wird in den proglazialen Sedimenten nach mehr als 270 Jahren sichtbar.

Biotitverwitterungsraten wurden berechnet unter Zuhilfenahme der Differenz im Biotitgehalt zwischen dem C-Horizont und den obersten 30 cm vom Bodenprofil. Die reaktive Mineraloberflächen wurden geometrisch bestimmt, für die totale sowie für die randliche Oberfläche. Die erhaltenen Verwitterungsraten sind mehrere Grössenordnungen schneller als bekannte Feldverwitterungraten. Zwei mögliche Erklärungen werden abgegeben: (1) Die starke Anreicherung von feinen Partikelgrössen (< 63 μm) in glazialen Sedimenten mit mechanischen Defekte werden bevorzugt gelöst; (2) die untersuchten glazialen Sedimente sind gut drainiert und durchlässig und heterogene Fliesspfade durch die Böden konnten nicht beobachtet werden. Damit wurde bestätigt, dass Material glazialen Ursprungs stärkerer chemischer Verwitterung unterliegt, welche direkt nach der Ablagerung im proglazialen Bereich beginnt und während tausender von Jahren nach einem Gletscherrückzug fortschreitet.

In einem vierten Teil wurden anhand von Apatit-Lösungsstrukturen und aus den Chronosequenzen langfristige detritische Phosphorverwitterungsraten ermittelt. Apatitkörner wurden eingeteilt relativ zu verwitterungsbedingten Änderungen in ihrer Oberflächenmorphologie. Heutige Apatitkörner sind stark gemahlen und lösungsgerundet. Körner der kleinen Eiszeit von zwei oberflächennahen Proben (aus 0 – 10 cm Tiefe) zeigen bereits extensive Lösungserscheinungen, ähnlich oberflächennahen Körnern aus Profilen von der Jüngeren Dryas. Die Verwitterungsfront vertieft sich fortlaufend durch Biokorrosion in der sich entwickelnden sauren Pedosphäre, und unter bevorzugter Lösung der Körner entlang mechanischer Defekte ihrer Oberflächen. In den Chronosequenzen wurden eisengebundene, organische und detritische Phosphorkonzentrationen gemessen: organischer und eisengebunderer Phosphor ersetzt detritischer Phosphor in den Profilen der Jüngeren Dryas. Während den ersten 300 Jahren der Freisetzung von glazialem Sediment waren die Phosphorlösungsraten ca. 70 mal höher als der globale Durchschnitt von gelöstem Phorphor im Abfluss von eisfreien Kontinenten. Über die Jüngeren Dryas Profile gerechnet ist der Flux 2.5 mal höher als der globale Durchschnitt. Diese Daten bestätigen die Möglichkeit von Änderungen im biolimitierenden Phosphorflux in glazial-interglazialen Zeiträumen.

In einem fünften Teil dieser Arbeit werden verschiedene Formen von Phosphor mit unterschiedlicher biologischer Verfügbarkeit verglichen zwischen dem tropischen Apure-Einzugsgebiet (Venezuela) sowie dem vergletscherten Rhone- und Oberaargebiet und einem Nebenfluss der Rhone. Die tropischen Wässer enthalten generell mehr teilweise bio-verfügbare Formen von Phosphor (DOP, eisengebunder und organischer P), während der Abfluss von den heute vergletscherten Gebieten von schlecht bio-verfügbarem detritischem Phosphor dominiert ist (97 %). Glaziale prozesse spielen jedoch eine wichtige regenerative Rolle, indem sie grosse Mengen von frisch gemahlenem detritischem Phosphor in die Biosphäre bringen. Der erhöhte Fluss von gelöstem reaktivem Phosphorus aus dem eisfreien Rhone Nebenflussgebiet (welcher aus der Verwitterung stammt) weist auf eine beschleunigte Lösung von detritischem Phosphor in proglazialen Sedimenten hin, verglichen mit dem globalen Durchschnitt. Im Apure-Einzugsgebiet hingegen ist der hauptsächliche Ursprung von gelöstem reaktivem Phosphor wahrscheinlich die Athmosphäre. Gletscher und Vergletscherungsperioden können darum zu komplexen Änderungen in der Phosphordynamik und der Produktivität von terrestrischen und aquatischen Ökosystemen führen.

Zusammenfassend kann gesagt werden, dass der globale Einfluss von subglazialer verglichen zu proglazialer Verwitterung noch nicht vollständig klar ist, nach wie vor besteht ein grosser Bedarf an weiteren Daten, um die verschiedenen Probleme anzugehen, welche in dieser Arbeit vorgestellt wurden. Unsere Daten zeigen, dass die subglaziale chemische Verwitterung kaum einen Einfluss auf die globalen Silikatverwitterungsraten hat. Die heutige Situation der Daten bestätigt jedoch das signifikante Potential der indirekten Einflussnahme durch die leicht verwitterbaren Sedimente glazialen Ursprungs im proglazialen Bereich. Die Arbeit bestätigt die positive Beziehung zwischen physikalischer und chemischer Verwitterung: Diese Verbindung ist verstärkt in Gebieten, welche von verwitterungs-limitierten, glazialen Prozessen dominiert sind. Globale Erosion wird während Vergletscherungen als verwitterungs-limitiert angenommen.

CHAPTER 1

Introduction

General introduction to geochemical weathering

Chemical weathering of continental rocks is extremely important for the generation of soils, for the evolution of landscape, and as a main source of inorganic nutrients for plant growth (White, 1995). In addition it is the mechanism that provides the solutes to streams and rivers (Garrels and Mackenzie, 1967). A major interest in chemical and physical denudation of rocks is due to its potential to affect the global carbon cycle and thereby global climate by the consumption of atmospheric CO_2 (Walker et al., 1981, Raymo and Ruddiman, 1992, Berner, 1995). The efficiency of atmospheric CO_2 drawdown is dependent on the type of rock being weathered: Only CO_2 consumed by the weathering of silicate rocks is fixed on geologic timescales. This weathering process begins when atmospheric CO_2 dissolves in water to form carbonic acid:

$$CO_2 + H_2O = H_2CO_3$$

During chemical weathering of silicate minerals aqueous H_2CO_3 is converted into HCO_3^-, which is transported to the ocean by rivers and removed from seawater in form of carbonate minerals or organic matter in sediments (Berner, 1995). Either way there is a net loss of atmospheric CO_2. Two model example reactions for silicate weathering are:

$$\underset{\text{Sodium feldspar}}{NaAlSi_3O_8} + 2H_2CO_3 + 9H_2O = 2Na^{2+} + 2HCO_3^- + 4H_4SiO_4 + \underset{\text{weathered feldspar surface}}{H_2Al_2Si_2O_8}$$

$$\underset{\text{Wollastonite}}{CaSiO_3} + 2H_2CO_3 + H_2O = Ca^{2+} + 2HCO_3^- + \underset{\text{silicic acid}}{H_4SiO_4}$$

Because one of the two original molecules of CO_2 is fixed upon calcite precipitation in the ocean this overall reaction creates a net loss of CO_2 from the atmosphere:

$$Ca^{2+} + 2HCO_3^- = CaCO_3 + H_2O + CO_2$$

Carbonate and other rock types are less important on the long term because either the weathering reactions do not consume atmospheric CO_2 (e.g. evaporites), or the amount of CO_2 delivered by calcite precipitation in the ocean equals the amount of CO_2 consumed by continental weathering flux from carbonates. Weathering of carbonates has, however, a short term impact on global CO_2, depending on the residence time of HCO_3^- in continental and marine systems, as outlined by the following two reactions of weathering of carbonates:

$$CaCO_3 + H_2O + CO_2 = Ca^{2+} + 2HCO_3^-$$

and calcite reprecipitation:

$$Ca^{2+} + 2HCO_3^- = CaCO_3 + H_2O + CO_2.$$

The HCO_3^- residence time in seawater is $10^2 - 10^5$ years (Berner, 1995).

Besides CO_2 other weathering agents are important: (1) Organic acids in soils that are photosynthetic derivates of CO_2, (2) oxygene (O_2) used in the oxidation of iron in silicates and sulphides, sulfur in sulphides, and organic carbon in sedimentary rocks to form acids that act as further proton sources (e.g. sulfuric acid H_2SO_4), (3) HNO_3 from precipitation, and (4) water in the dissolution of quartz and major evaporites (NaCl, $CaSO_4$, $CaSO_4 \bullet H_2O$; Berner, 1995).

The susceptibility of the bedrock itself affects the weathering rate, and mineral stabilities vary considerably according to their composition and crystal lattice (Stallard, 1992). For igneous and metamorphic minerals, stability at the surface of the Earth is approximately the reverse of the Bowen's reaction series (Goldich, 1938). The most stable minerals are often physically eroded before they have a chance to decompose chemically. On a global scale lithology plays a dominant role. The influence of single lithologies on chemical

weathering rates was studied by Meybeck, 1987) for french monolithical streams which drain major rock types. Based on his studies, he proposed that the relative chemical weathering rates of continents range from 1 for granite and gneiss to 12 for limestones and 80 for evaporite rocks.

Also climate itself exerts an impact on chemical weathering (White and Blum, 1995). Atmospheric variables like temperature and precipitation have a direct influence as well as an indirect one over vegetation, runoff, and glacial/periglacial phenomena. Minerals dissolve faster with higher temperatures (e.g. salt dissolution in water). Higher temperatures lead to increased precipitation and higher runoff which increases the weathering (influence not linear). In general low runoff leads to silicate weathering being more important than carbonate weathering whereas in high runoff regimes carbonate weathering exceeds silicate weathering (Stallard, 1995).

The role of vegetation is given by the following mechanisms for biochemical weathering of silicates: (1) Growing roots and fungal hyphae physically disrupt minerals, exposing new fresh mineral surfaces and increasing mineral surface areas available for reaction, (2) soil stabilisation through plant cover increases water retention, lengthening the time for weathering reactions to occur, (3) production of organic acid accelerates weathering rates, (4) organic ligands directly attack mineral surfaces or form complexes with ions in solution which change the saturation state, (5) complex extracellular polymers moderate the water potential, maintain diffusion channels, act as ligands or chelators, and serve as nucleation sites for authigenic mineral formation, (6) the nutrient absorption of e.g. K, Fe, and P, decreases the solution saturation state and enhances weathering. However, plant cover can also act as an isolating cover, preventing the landscape from physical erosion and therefore decreasing the intensity of chemical weathering of fresh underlying bedrock (Berner, 1995, Stallard, 1995, White, 1995).

Weathering processes in specific regions depend on factors like geographical latitude as well as on altitude. Chemical weathering is enhanced in warm and moist regions as well as in regions with much vegetation. Physical weathering on the other hand is enhanced in cold and dry regions and furthermore in steep terrains, where relief increases overall weathering rates. Global weathering acts as climate feedback mechanism: The high atmospheric CO_2 concentrations under greenhouse conditions (Walker et al., 1981) lead to increased temperatures, which accelerate the hydrological cycle and, in combination with the temperature, increase chemical weathering on continents. By consuming atmospheric CO_2 the increased silicate weathering results in stabilisation and decrease of global temperatures on geological time scales (negative feedback on climate warming, Walker et al., 1981, Föllmi et al., 1994). Such feedback mechanisms are used by many authors which model the evolution of atmospheric CO_2 and therefore climate over geological time scale (e.g. Berner et al., 1983, Berner and Kothavala, 2001).

As a limitation on weathering two end-member states are considered as controls on chemical denudation (e.g. Stallard, 1992, Kump et al., 2000): the transport-limited and weathering-limited erosional regimes. In most areas the erosional regimes correspond to a mixture of the two end-members. Transport-limited watersheds have thick and mature soils, often with well developed vegetation covers, which isolate the underlying bedrock from contact with through-flowing soil waters. Primary minerals have been altered to secondary minerals. Water travels along major hydrological flowpaths through cation depleted soils (Ca^{2+}, Mg^{2+}, Na^{+}, K^{+}) without interacting much with bedrock. The denudation rates of such regimes are independent of the lithology. The limiting factor is the rate of physical erosion of the soil mantle which itself may be limited by slow or negative rates of surface uplift.

In contrast, soils in weathering limited watersheds are thin, and rain and soil water percolate easily to the soil bedrock interface, where they interact with fresh minerals. Because of the rather short water-rock interaction time the minerals that are more susceptible to dissolution dominate water chemistry. The limiting factor of such regimes is physical erosion. Chemical weathering rates therefore depend on factors controlling mineral dissolution rates, which are mineralogy, water supply, soil-water pH, and temperature. Weathering limitation becomes more important in tectonically active areas with high uplift rates and significant relief, as physical erosion processes are dominant. In weathering limited regimes material is only partially weathered, most rocks lose structural integrity before complete chemical decomposition. Vegetation on steep

slopes may increase chemical weathering as it anchers the soil and favors water retention. Gaillardet et al. (1999), comparing data from 60 world rivers, conclude, that their good correlation between chemical and physical denudatoin of silicates can be seen as a sort of mixing line between the two extreme regimes of weathering: The transport-limited and the weathering-limited regimes. After Kump et al. (2000) chemical denudation by the world's rivers is strongly weathering-limited.

Summarizing, rock weathering is a key process in the evolution of the Earth surface and the knowledge of the rates for present day weathering as well as of the controlling parameters are needed to understand the past and to predict the future. Understanding the processes on a small scale is of major importance to be able to extrapolate on a global scale.

Glacial geochemical weathering

Subglacial chemical weathering

There are several motivations to studying chemical weathering in alpine glaciated catchments: (1) Glacial meltwaters show a strong enrichment in dissolved ions over relatively short distances of a few kilometers between their origin as dilute snow and icemelt (conductivities of 2 – 6 μS cm^{-1} at Oberaar glacier) and the glaciers snout (conductivities up to 80 μS cm^{-1} during the accumulation period at Oberaar glacier), (2) anthropogenic influences are often low in glaciated environments, which allows for the investigation of natural controls on streamwater composition, (3) the role of soil and vegetation development on chemical weathering can easily be analysed in the proglacial area where glacial sediment is initially deposited as fresh material (Chapter 3 of this work, Anderson et al., 2000), and, (4) high flushing rates of fresh and finely ground, geochemically reactive sediment contrast with many other Earth surface environments, where biological activity and soil formation may significantly impact weathering rates.

Chemical weathering in glaciated environments might play an important role in regulation atmospheric CO_2 contents by proton consumption during hydrolytic weathering reactions: One source of protons may be the dissociation of carbonic acid derived from the dissolution of atmospheric CO_2 as described earlier. Proton consumption is more rapid with increasing discharge and suspended sediment concentration and cannot be fully counterbalanced by the rate of resupply by CO_2 dissolution. This leads to increased pH and a reduction in CO_2 partial pressure, and consequently the rate of diffusion of atmospheric CO_2 into solution is increased (Tranter et al., 1993). Therefore, where meltwaters are in contact with atmosphere, this could be an important mechanism for the drawdown of atmospheric CO_2 on glacial/interglacial timescales (e.g. Sharp et al., 1995a). Where meltwater is isolated from the atmospheric source of CO_2 as may be the case in subglacial environments, other proton sources become more important, e.g. the oxidation of sulphides (Tranter et al., 2002) and organic carbon (Sharp et al., 1999). Carbonate weathering by protons from sulphide oxidation leads to increased CO_2 partial pressure, and, subsequently, as meltwaters get in contact again with the atmosphere, they may serve as source of CO_2 to the atmosphere. The most important subglacial chemical weathering reactions are (after Tranter et al., 2002):

- Carbonation of feldspar surfaces:
  $CaAl_2Si_2O_8(s) + 2CO_2(aq) + H_2O(l) =$
  anorthite
  $Ca^{2+}(aq) + 2HCO_3^-(aq) + H_2Al_2Si_2O_8(s)$
  weathered feldspar surface

- Carbonation of carbonates (calcite):
  $CaCO_3(s) + CO_2(aq) + H_2O(l) =$
  $Ca^{2+}(aq) + 2HCO_3^-(aq)$

- Sulphide oxidation coupled to carbonate dissolution:
  $4FeS_2(s) + 16CaCO_3(s) + 15O_2(aq) + 14H_2O(l) =$
  pyrite
  $16Ca^{2+} + 16HCO_3^-(aq) + 8SO_4^{2-}(aq) + 4Fe(OH)_3(s)$
  ferric oxyhydroxides

- Carbonate hydrolysis:
  $CaCO_3(s) + H_2O(l) =$
  $Ca^{2+}(aq) + HCO_3^-(aq) + OH^-(aq)$

- Feldspar hydrolysis (and analogue silica and pyroxene hydrolysis):
  $KAlSi_3O_8(s) + H_2O(l) =$
  K-feldspar
  $K^+(aq) + OH^-(aq) + HAlSi_3O_8(s)$
  weathered feldspar surfaces

- Oxidation of organic carbon:
  $C_{org}(s) + O_2(aq) + H_2O(l) =$
  $CO_2(aq) + H_2O(l) = H^+(aq) + HCO_3^-(aq)$

Studies of chemical weathering in glaciated environments started about 30 years ago when Slatt (1972) analysed the meltwater streams from nine Alaskan valley glaciers eroding five different bedrock types. He found that the streams were similar in that Ca^{2+} was the most abundant of the major ions (Na^+, K^+, Ca^{2+}, Mg^{2+}). Recent studies in glacierised catchments suggest that the negative effects of low temperature, sparse vegetation, and poorly developed soils on chemical weathering rates are counterbalanced by factors such as high meltwater fluxes and flushing rates as well as freshly ground very fine grained sediment, which has high relative surface areas and is very reactive (e.g. Tranter et al., 1993, Gurnell et al., 1994, Sharp et al., 1995b, Anderson et al., 1997, Wadham et al., 1998, Fairchild et al., 1999, Chapter 2).

Analysis of variations in meltwater composition (particulate/dissolved) is a useful tool to get insight into the configuration and dynamics of the inaccessible subglacial environment and to investigate the geochemical processes which take place there. The composition of the ionic load reflects the solute provenance: There are different types of chemical weathering reactions and processes during which the initially very dilute glacial ice meltwaters get charged. These reactions are controlled by varying hydrological flowpaths and sediment composition as the subglacial hydrological system evolves through the ablation season. Factors like proton availability, grain-sizes, shape, and surface morphology of subglacial sediments, water:rock ratio and interaction time and mobilisation of suspended sediment exert a major impact on the chemical evolution of meltwaters beneath a glacier.

A simple two component mixing model is used to describe the general pathways of meltwater and the reaction processes they undergo in glaciers prior to their sorting at the snout (Fig. 1.1). This separation of total discharge into two hydrological components was first proposed by Collins (1977, 1979): (1) Quick-flow waters flow rapidly (> 0.5 – 1 m s^{-1}, beneath Haut glacier d'Arolla, Brown, 2002) through a discrete channelized system which is either incised in the basal ice layer or engraved in the underlying bedrock (Röthlisberger and Lang, 1987, Nye, 1973). In such arterial conduits significant quantities of suspended sediment are mobilised, transported and evacuated by the turbulent meltwaters (Willis et al., 1996, Hubbard and Nienow, 1997). Water:rock contact times are short and limit the potential for solute acquisition to rapid surface exchange reactions (Tranter et al., 1993). During the progressing ablation season this channelised system expands headwards of the catchment, following the retreat of the seasonal snowcover (Brown et al., 1994, Nienow et al., 1996). (2) Delayed flow waters pass relatively slowly (< 0.05 m s^{-1}, beneath Haut Glacier d'Arolla, Brown, 2002) through a distributed drainage system at the ice-bedrock interface. Water is transported as film-flow and porous flow through permeable subglacial sediments (Clarke, 1987), linked cavities, and broad, low canals (Walder and Fowler, 1994, Brown, 2002). Water:rock ratios are high and waters interact with particles from physical erosion and crushing: Finely ground glacial flour, debris-rich basal ice and subglacial till material. As the water-rock contact times are long the weathering processes include slower dissolution as well as surface exchange reactions (Tranter et al., 1993).

This two-component mixing model is simplified and imposes many problems, as it assumes conservative mixing of the two flow components, with no post-mixing solute acquisition (Brown et al., 1994). Furthermore it cannot account for temporal variations in chemical composition of the two components, which may result from factors such as variable residence times, lateral and headwards channel migration (Nienow et al., 1998), variable suspended sediment concentrations (Brown et al., 1994), and chemical fractionation of atmosphere-derived protons from the seasonal snowcover (Fountain, 1996, Tranter and Jones, 2001).

Proglacial weathering

Proglacial environments are important for the understanding of global CO_2 cycling on glacial/interglacial timescales as they made up a significant amount of the global land surface during the Quaternary due to the advance and retreat of glaciers and ice sheets (Gibbs and Kump, 1994). The proglacial area is a potential zone of high geochemical reactivity due to the availability of freshly ground reactive material (subglacially derived), high water:rock ratios and contact times, high permeabilities, and constant supply of dilute waters

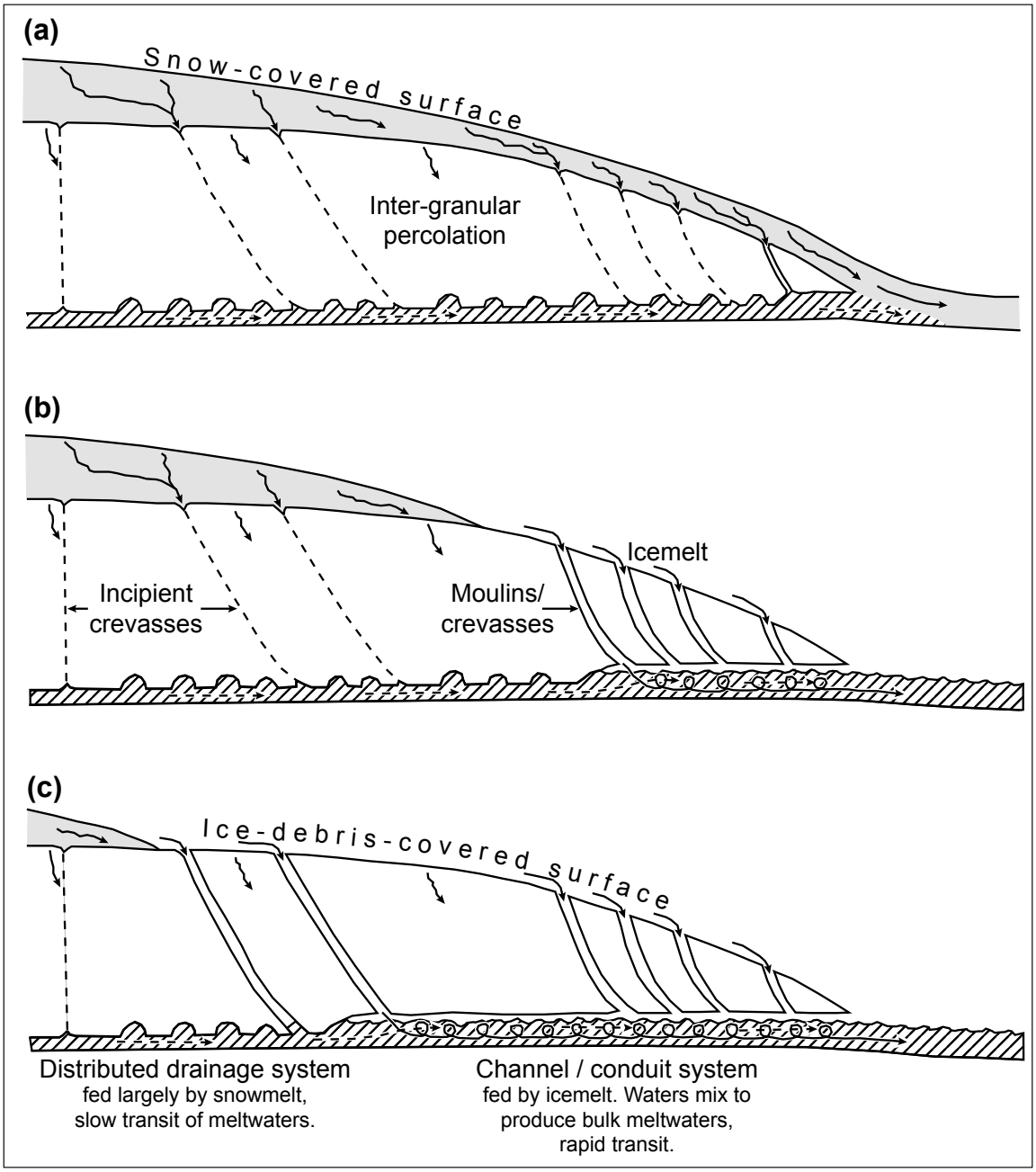

Fig. 1.1: Schematic representation of the seasonal development of the subglacial drainage system beneath an alpine glacier (after Brown, 2002): As the melt season progresses through June (a), July (b), and August (c), the seasonal snow-cover retreats upglacier. The position of the transient snowline is closely associated with the upglacier development of the subglacial channelised drainage system (Nienow et al. 1996).

(meltwaters and rain/snowmelt) to percolate through the deposits. Furthermore, significant soil development is low in terrains which have been deglaciated over timescales of 100s of years. Proglacial weathering intensities depend mainly on the lithology (e.g. highly reactive minerals like carbonates and sulphates vs. crystalline rocks), the rate of supply of fresh rock material to the proglacial zone, the age of exposure, and the character of the proglacial hydrological drainage system. In young areas (< 100 years) proglacial chemical weathering rates are high and result primarily from the dissolution of the most reactive phases (e.g. Wadham et al., 2001), the predominant process is coupled sulphide oxidation and carbonate dissolution. In contrary, in older proglacial areas (up to 10,000 years), the exhaustion of sulphides may increase the degree to which CO_2 is drawn down from the atmosphere during chemical weathering. Here, silicate weathering gets more signifi-

cant with distance from the glacier snout (Anderson et al., 2000).

Physical erosion

Also the important role of glaciers and glaciations as agents in physical erosion has long been recognised. Glacial erosion produces huge quantities of sediments ranging from decameter to silt size. Given the close connection between climate and weathering (Raymo and Ruddiman, 1992), the following question becomes important: Are rates of physical and chemical weathering greater in glaciated than in non-glaciated regions? There exist several difficulties in evaluation the relative rates of glacial and non-glacial weathering processes (Hallet et al., 1996): (1) Besides the climatic circumstances, the lithological control of the physical erosion rate has important implications for the comparison and correlation of different catchments, (2) the importance of sediment storage is often difficult to estimate, and (3) the variability of sediment output from glaciated basins throughout the season and from year to year should be taken into account in basin studies. Furthermore some other important glacial variables also control sediment yields: The speed of basal sliding (cold based versus temperate glaciers), glacier size, ice flux, and meltwater production and routing to the glacier snout. The relationship between present day yields from glaciated basins and present day sediment production by glacial erosion is likely to be complex because of the possible changes in subglacial sediment storage (Harbor and Warburton, 1993). Furthermore, rapid sliding and basal motion which accompany rapid terminus retreat accelerate erosion of bedrock. Present-day erosion rates are thought to be substantially higher than long-term rates because deglaciation is a period of anomalously high ice flux and rapid basal ice motion (Koppes and Hallet, 2002). Compilations of sediment yields from different glacial basins are given in Hallet et al. (1996) and Gurnell et al. (1996). Our values are discussed in Chapter 7.

The ideal parent material

In soil chronosequence studies the question of the ideal and fresh parent material remains generally unsolved. Normally the composition of the C-horizon is used as fresh parent material for weathering rate calculations (also in this work, Chapter 3). However, in glacial chronosequences this may impose a problem: During times of glacier advance the equilibrium line moves downwards, increasing the areas of the accumulation as well as of the ablation zone (Ehlers, 1996, Benn and Evans, 1998). Depending on the extent of the glaciers readvance, the equilibrium line can move beyond the the initial glacier margin and lie within the proglacial area. Thus the accumulation zone overlies former proglacial areas where weathering and soil formation previously occurred. Therefore the material of the C-horizon contains a mixture of reworked, pre-weathered glacial material and fresh glacially eroded bedrock, and the age of these soils might not strictly be 140 or 10,000 years.

Todays suspended sediment of temperate valley glaciers represents freshly eroded bedrock that was mechanically abraded at the glacier base and its mineralogy shows an average bedrock composition of todays glacier catchments. The lack of any secondary mineral phases in the suspended sediment implies that there are no subglacial reworking processes of old, pre-weathered material. Major subglacial sedimentation processes normally take place below the equilibrium line (Benn and Evans, 1998; Drewry, 1986). At present in temperate valley glacier catchments major subglacial erosion processes like grinding and abrasion must therefore take place above the equilibrium line, where the sediment retention time is rather short: The subglacial sediments are evacuated from the system too quickly to be significantly incongruently weathered. This could hold true for stationary downwasting glaciers like the Rhone and Oberaar glaciers. Eventhough suspended sediment could therefore hold for the ideal parent material, it was not used in this work to calculate a weathering rate because of differences in transport processes as well as in grainsize distributions between suspended sediment and morainic deposits.

Introduction to the project

The project of this thesis stands in the framework of a long-term research program which has been developed at the Geological Institute of the University of Neuchatel and is entitled: “Continent-ocean interactions and their geological records”. The general aim of this program is to trace continental weathering by all means and to establish feedback mechanisms between

continental weathering, productivity, and (paleo-)climate. The starting point of this program is a compilation of all meaningful phosphorus (P) burial data published in the proceedings of the Deep Sea Drilling Project (DSDP) and subsequent Ocean Drilling Program (ODP). This compilation is used as a proxy for variations in global P flux rates over the last 160 million years (Föllmi, 1995). P flux rates are linearly dependent on continental weathering rates, since a major P phase in the atmosphere is lacking and hydrothermal P output rates are negligible. For this reason, the P burial rate compilation can be used as a quantitative approximation of changes in global weathering rates. A comparison of the burial curve to the long-term sea-level record as compiled by Haq et al. (1987) suggests a positive coupling between climate warming, long-term sea-level change, and continental weathering for the period between the Callovian and the Oligocene (160 – 32 ma). For the time period between the Oligocene and the present this coupling is inverse (32 – 0 ma). Therefore, in an ice-free greenhouse world, intensified weathering would exert a negative feedback on climate warming due to the acceleration of the global carbon and phosphorus cycle and the accelerated sequestering of atmospheric CO_2 (e.g. Berner, 1992, Föllmi et al., 1994). During ice-house conditions, the feedback would be positive: intensified glacial weathering would increase CO_2 drawdown and global cooling and provoke further cooling.

The goal of this thesis project (entitled: "Present-day biogeochemical weathering in glaciated areas") is to identify the impact of glaciation on global biogeochemical cycles and climate, both directly, through the consumption of CO_2 during chemical weathering of glacially derived material, as well as indirectly, through the regulation of important nutrient fluxes such as phosphorus, silicium, and iron, which stimulate continental and marine productivity. To do so two temperate valley glaciers have been chosen (Fig. 1.2): the Oberaar and the Rhone glacier in the central Swiss Alps. There are several reasons why this research is performed in these two catchments: (1) The catchments are small and well defined, (2) both glaciers have focussed and single meltwater outlets and are more or less accessable

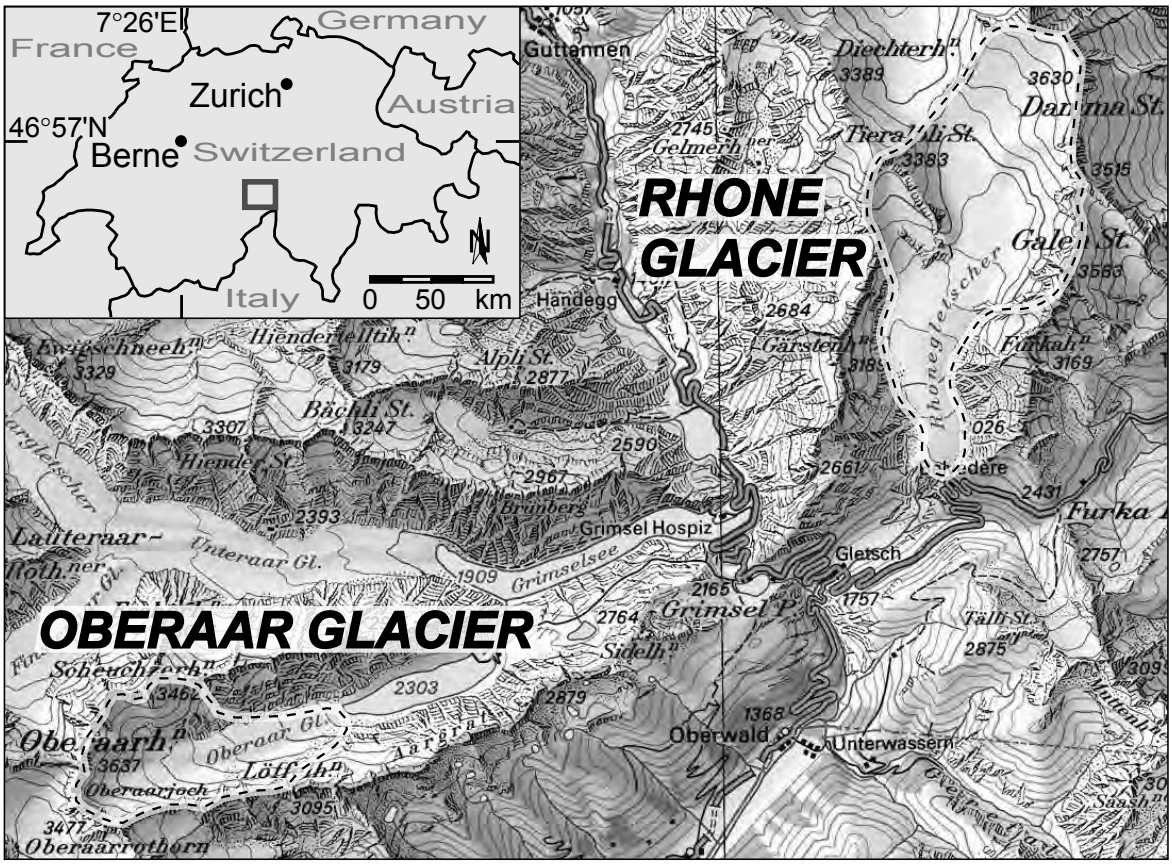

Fig. 1.2: Overview map with Oberaar and Rhone glacier. Reproduziert mit Bewilligung des Bundesamtes für Landestopographie (BA024559).

throughout the whole year, meaning also during the accumulation season, (3) beside these logistic advantages the two catchments are showing quite a homogeneous lithology: Both are embedded in crystalline rocks of the Aar massif. Small differences in the lithology between the two areas should simplify a comparison of the weathering processes within the two areas. A considerable amount of published research exists on glacial geochemistry in catchments lying on metasedimentary and mixed lithologies, whereas purely granitic settings like the Rhone catchment are poorly documented.

The research is done according to a chemical mass balance approach:

Input	=	Output
bedrock weathering		solutes
+	=	+
atmospheric input		particulate

Main meltwater chemistry (dissolved ions) as well as suspended sediment (mechanical erosion) and morainic deposits in the proglacial area were analysed. The regional geology and tectonics of the area are well known (e.g. Stalder, 1964). As atmospheric input, precipitation and eolian dust were collected and analysed chemically and mineralogically. Atmospheric variables like precipitation, dust, and temperatures exert a strong impact on the atmospheric input as well as on glacier dynamics (glacial mass balance) and transport processes. These, in turn, influence especially particulate output due to, e.g., mechanical abrasion and storage effects. The chemical composition of meltwaters as well as the mineralogical composition of suspended sediment give insight into recent subglacial weathering processes in the two catchments (see Chapters 2 and 4). Chemical and mineralogical analysis of the proglacially deposited moraines and tills of different ages show the importance of subsequent weathering processes after glacier retreat (see Chapters 3 and 5).

Besides the chemical mass balance approach (direct impact), we also tried to attack the indirect impact of glaciers/glaciations on the global biogeochemical cycling through the regulation of the oceanic nutrient budget, biological productivity, and carbon drawdown. Different forms of phosphate were measured directly in the meltwaters as well as in the proglacial sediments. Special attention was given to apatite, the main particulate phosphorus phase in granitic rocks, which shows a particularly fast weathering rate (see Chapters 5 and 6). This work as a whole should help to improve the general understanding of the coupling processes between climate, active tectonics, continental weathering, and productivity on a global scale.

Introduction to field areas

Geography:

Oberaar glacier is a west-east sloping valley glacier which lies about 12 km southwest of the Grimsel pass in central Switzerland (see Fig. 1.2 and Fig. 1.3a,b (Ap-

	Oberaar			**Rhone**		
Geographical position	46° 32' N 8° 14' E			46° 35' N 8° 23' E		
Surface of catchment	11.2 km2			23 km2		
Altitude	2310 - 3631 m above sea level (a.s.l.)			1750 - 3630 m a.s.l.		
Glacier cover today (%)	57%			73%		
Annual mean temperature *	- 1° C§			+ 1.2° C§		
Annual mean precipitation *	2100 mm			2200 mm		
Geology of catchments:	Today	LIA	YD	Today	LIA	YD
Central Aar Granite	38%	38%	25%	90%	82-86%	40%
Grimsel Granodiorite	7%	7%	12%	10%	8-9%	20%
Variscan gneisses	42%	42%	38%		10-5%	20%
Ultramafic Inclusions	1%	1%	1%			
Southern Aar Granite	12%	12%	24%			
Mesozoic metasediments						20%

* Schwab etal., 2001
§ within proglacial area; 2300 m at Oberaar, 1757 m at Rhone.
LIA Little Ice Age; YD Younger Dryas

Table 1.1: Catchment parameters.

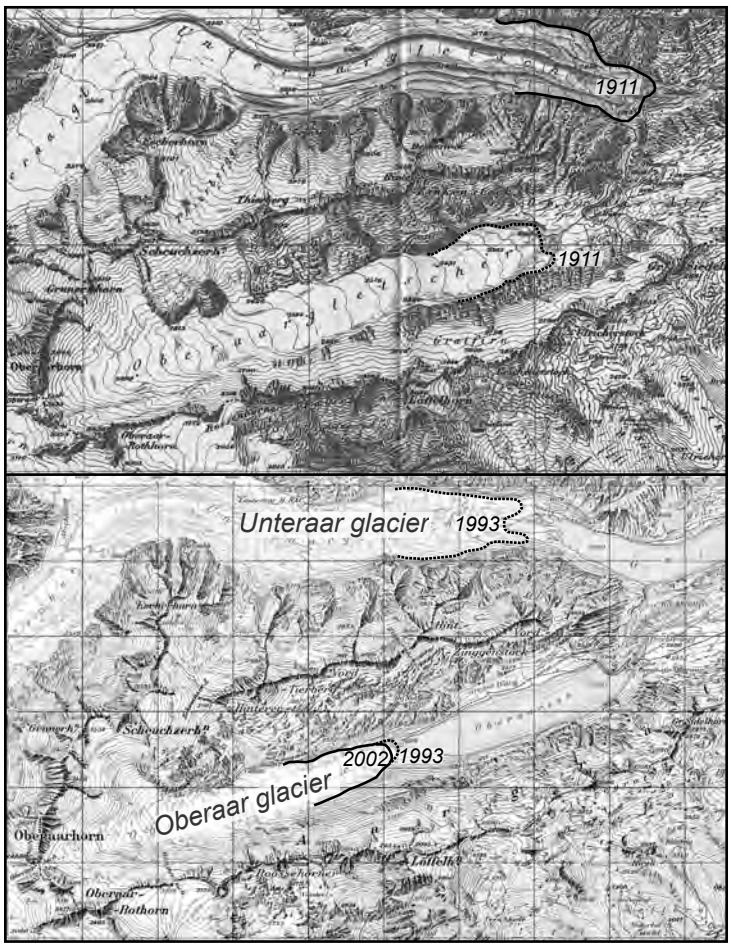

Fig. 1.4 a: Oberaar and Unteraar glaciersnout comparison: 1911 - 1993 - 2002, scale 1:100'000. Reproduced with permission of the Swiss Federal Office of Topography (BA024559).

pendix E) as well as Table 1.1). Its basin is elongated with the Oberaar Joch (3216 m) and the Oberaarhorn (3631 m) on the western end and Oberaarsee (2303 m), a dammed lake for electric power supply, at the snout. The main mountain peaks in the south are the Oberaar Rothorn (3477 m), the Löffelhorn (3095 m) and the Grosses Siedelhorn (2872 m). In the north the main mountain peaks are the Grunerhorn (3432 m), the Scheuchzerhorn (3456 m), Hinterer (3081 m) and Vorderer Tierberg (3111 m), and Hinterer (3040 m) and Vorderer Zinggenstock (2915 m). The Oberaar catchment area is about 11.03 km^2, of which 57 % are glacier covered.

The snout of the Rhone glacier lies about 4 km northeast of the Grimsel pass (see Fig. 1.2 and Fig. 1.3b (Appendix E) as well as Table 1.1). The main part of this glacier is north-south oriented with the snout west of the Belvédère at about 2300 m. West of the glacier are the Gärstenhörner (3166 – 3189 m) and the Hintere Gelmerhörner (3097 – 3191 m). In the north are the Tieralplistock (3383 m), the Eggstock (3556 m), and the Schneestock (3608 m). The eastern boarder of the catchment is Dammastock (3630 m), the Galenstock (3583 m), and the Furkahorn (3169 m). The Rhone catchment area is about 26.2 km^2, of which 73 % are glacier covered.

Photos of the two catchments are given in the color figure section of this thesis (Appendix E).

Climate:

The two areas receive 2100 – 2200 mm of precipitation per year, and snow makes up for about 60 % of total precipitation. The average temperatures are –1 °C and +1.2 °C in the forefields of Oberaar (2300 m) and Rhone glaciers (1757 m; Schwab et al., 2001, Table 1.1). The vegetation cover in the forefield of the Oberaar glacier consists of pioneer plants typical for proglacial areas that recently became ice free (proxi-

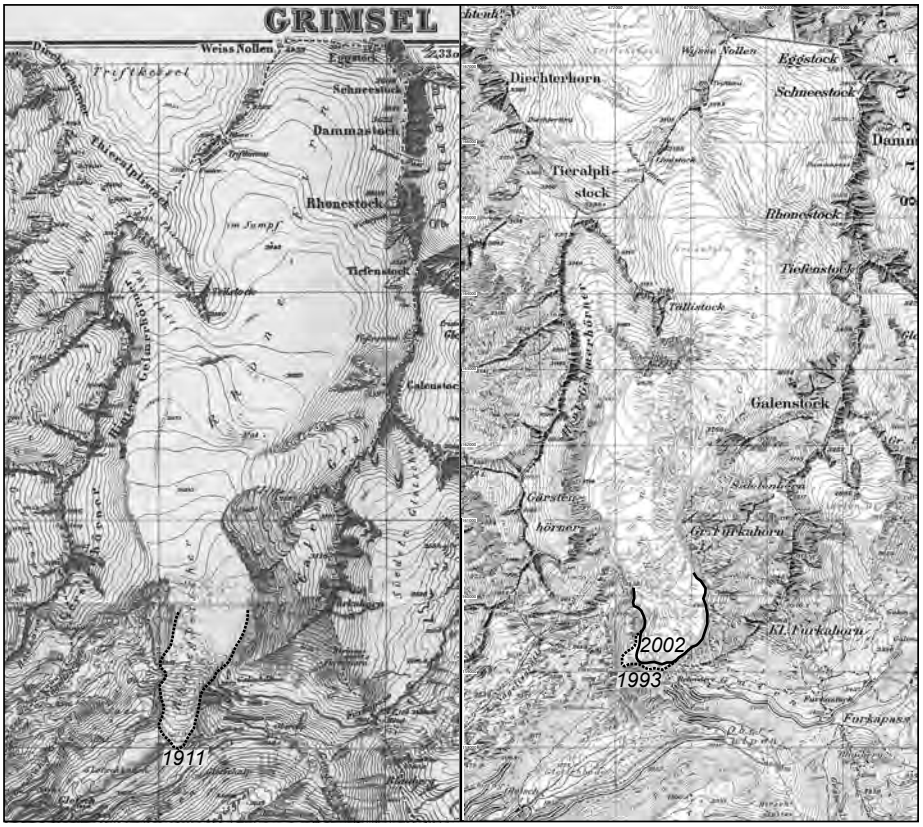

Fig. 1.4 a: Rhone glaciersnout comparison: 1911 - 1993 - 2002, scale 1:100'000. Reproduced with permission of the Swiss Federal Office of Topography (BA024559).

mal), but also some alpine meadows and peatlands in the rather distal parts. This has been documented by Ammann, 1977), who studied the succession of plant communities and also dated the different moraine ridges from the Little Ice Age (1300 – 1850) present in the forefield. The vegetation of Rhone glacier forefield (1757 m) mainly consists of alpine meadows and peatlands with alder bushes. Both glaciers are recently subjected to substantial retreat in ice volume. Maps of the two glaciers show the glaciers 1911 compared to the recent situation (Fig. 1.4a & b), and two pictures (Fig. 1.4c) taken at Oberaar snout in the years 1950 and 2001 document the retreat as well.

Geology:

The lithology of the region (Fig. 1.5) consists of the crystalline rocks of the Central Aar massif (e.g. Stalder, 1964, Oberhänsli et al., 1988). All rocks

Fig. 1.4 c: Oberaar glaciersnout comparison: Photograph left from the fifties (during or shortly after damm construction, picture from Kraftwerke Oberhasli KWO); photograph right from August 2001. Photographs taken from slightly different positions, retreat nevertheless visible if comparing snout relative to peak indicated by arrow (Roossehörner, peak 3111 m).

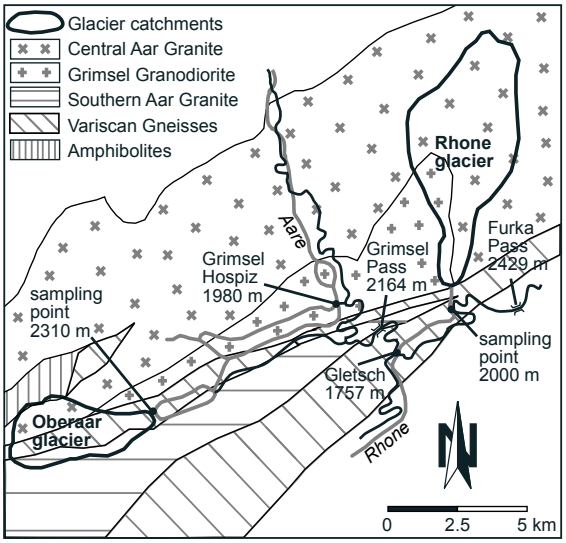

Fig. 1.5: Field geology with glacier catchments indicated (cf. Fig. 1.2).

contain measurable amounts of calcite. Whereas the Rhone catchment is lying entirely in the granitic rocks of the Central Aar granite and Grimsel granodiorite, the lithology of the Oberaar catchment includes in addition Variscan basement gneisses, highly deformed and foliated gneissic rocks of granitic composition which contain up to 5 wt% of calcite and which cover ca. 42 % of the total catchment area. The influence of this so called Gneiss-Schiefer-Zwischenzone is visible in whole rock mineralogy and in the dissolved chemistry in most of the Oberaar samples.

At Oberaar the lithological architecture is visible from the broad geomorphological framework: The main valley incision was performed on the easier erodable zone of Variscan Gneisses which make up approximately 60 % of the total glacier covered area (Table 1.1). The remaining 40 % at the glaciers sides are composed of granitic rocks which are harder and less erodable. The lithologies are elongated parallel to the main valley geometry from the glacier snout to the top of the catchment (the Oberaar Joch).

Recent / Anthropogenic history of area:

Louis Agassiz was the first person who did glacial research in the area of Oberaar glacier: His mission in the Alps in the year 1839 included a visit to Grimsel pass and Unteraar glacier. In the year 1840 they mounted a first hut on the medial moraine of Unteraar glacier, the famous "Hôtel des Neuchâtelois" (Fig. 1.6), constructed underneath a big boulder. During their stay they soon realised, that the boulder was moving slowly. In the same year a first visit to the Oberaar glacier was reported (Gos, 1928). The group of 7 people had several goals: L. Agassiz with help from M. F. Pourtalès collected data on the local climate (temperature, precipitation, weather, and barometry). M. Vogt observed the red snow (caused by algae that grow on the snow almost every season) and drew and studied the different organic appearances associated with this phenomenon. M. Nicolier collected and studied the flora of the glacier and its vicinity. E. Desor studied glacier-specific phenomena, such as its structure, its appearance under different atmospheric conditions, and the nature and origine of the moraines. He was helped by M. H. Coulon. L. Agassiz was "chef de l'expédition", who collected the findings of everyone. In February of 1841, L. Agassiz had the idea to climb up to the glacier in wintertime, and in the beginning of March they succeeded to get there. The group didn't have any helpful utilities like skis or snowshoes why this journey was described as a nightmare. These first missions to the area are well described by Gos (1928). Later missions to the Alps are described by Desor (1845).

The region in front of the Oberaar glacier was used several centuries as mountain pasture by the community of Törbel (VS), it was called the "Törbjer Alpe Oberaar" (pers. comm., U. Magoni & C. Boren, www.maboart.ch). On the 16 of October 1514 the community of Törbel (VS) in the Vispervalley bought the "Oberaaralpe für 850 Pfund Pfennige Münz – mit Steg, mit Weg, mit Weid, mit Grund, mit Grat, mit Mitte, mit Legne, mit Zilen und Marchen, mit Schaden und Nutz" (with trails and tracks, with pasturage and peaks, with defects and profits). It is not well known why Törbel (VS) wanted to buy a pasturage that far away; probably they just needed more space for their animals. They mainly put sheep and cattle up there; in earlier times also mules. Mid June to beginning of July herdsmen and helpers drove the cattle up to the pasturage in a troublesome three-days journey. On a first day the herdsmen and drivers hiked to Lax (VS), on the second day to Obergesteln (VS). In both villages the community of Törbel (VS) possessed an area with folds for the cattle. On the third day they climbed Triebtenseelicke (2639 m) to finally reach the pasturage. In 1948 the pasturage was sold to the Oberhasli power plant company who started 1949/1950 with the construction of the

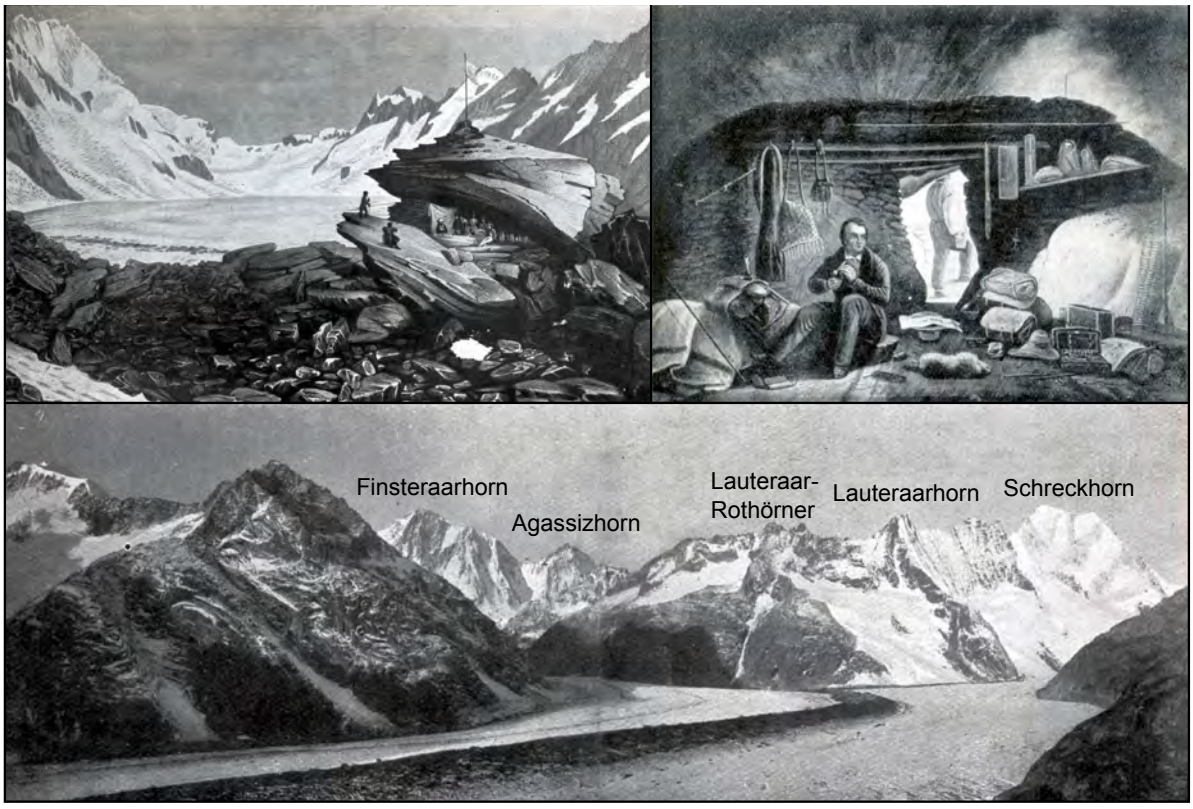

Fig. 1.6: The "Hôtel des Neuchâtelois" (top left); Louis Agassiz within his hut (top right); panorama of Unteraar glacier, with the hut situated somewhere on the median moraine (bottom).

damm. Since 1953 the lake is used for the production of electricity; it is maintained by the Kraftwerke Oberhasli (www.kwo.ch).

Recent research in area:

The glaciology group of the Laboratory of Hydraulics, Hydrology, and Glaciology (VAW) at the ETHZ maintains two projects at Unteraar glacier (pers. comm., U. H. Fischer, www.vaw.ethz.ch/pub_eng/dpt/glaciology/project/uaar.html): (1) Measurements and modeling of ice deformation at Unteraar glacier (PhD of J. Helbling), and (2) Hydro-mechanical conditions beneath Unteraar glacier (PhD of T. Schuler, 2002, e.g. Schuler et al., 2002).

The Institute of Hydromechanics and Water Resources Management (IHW; www.baug.ethz.ch/ihw/) at the ETHZ was involved in research on turbidity, temperature and sediment concentration in waters flowing out of the Oberaar lake (pers. comm., H. Bühler). Their goal was to get insight into the sediment balance of Oberaar lake and how this balance is affected by the water pumping actions (for the production of electricity) between Oberaar and Grimsel lake.

The Limnogeology Laboratory of the ETH Zürich (www.geology.ethz.ch/ESS/LimnoLab/Limno.html), in cooperation with the Kraftwerke Oberhasli KWO, is investigating the modern lacustrine sedimentation in the Grimsel lakes (pers. comm., F. Anselmetti). The goal is to quantify the proglacial sedimentation and to calculate the infilling rates of the lakes. In addition, instrumental meteorological data are compared with the annual sediment record from the last 70 years, allowing for a unique calibration of proglacial lacustrine sedimentation with environmental parameters. For this purpose, a dense grid of high-resolution seismic lines were acquired in Grimsel, Räterichsboden, and Oberaar lakes, imaging the sediment thickness, which amounts to a maximum of 10 meters in the central Grimsel lake. A series of vibrocores, taken in winter from the frozen lake surface, provides the necessary sedimentological record. In addition to the modern history of artifical lakes, these cores also document underneath the proglacial sediments the old organic-rich lacustrine sediments of the old, natural Grimsel lakes, so that the impact from the damming on a high-alpine lakesystem can be investigated.

Methods

Sampling maps

On the maps of the two field areas (Fig. 1.3ab and Fig. 1.3c) the main locations of research and data collection are shown, like sampling points for meltwaters, side rivers, snowprofiles, moraines, rain, as well as the raingauging stations of MeteoSwiss. In the following chapter a short description is given of what was sampled with which aim. Short recipies of the analytical methods, which are not described in the following main chapters, are given in the appendices section (Appendix B).

Samples taken in the field

Glacial meltwaters were sampled on a regular basis, i.e. twice daily during the ablation season as well as monthly during the accumulation season to get insight into the subglacial weathering processes. A major goal was the construction of a chemical mass balance, and for this purpose the major ions (Ca^{2+}, Mg^{2+}, Na^{+}, K^{+}, Cl^{-}, NO_3^{-}, SO_4^{2-}, and HCO_3^{-}) and Fe^{3+} and Al^{3+} were analysed (see Chapter 2). Furthermore a selection of the meltwaters was analysed for establishing the Sr isotope systematics (see Chapter 4).

The proglacial sidestreams were sampled in addition, albeit on an irregular timescale, to characterise the chemistry of waters draining older glacial material (Appendix A).

Suspended sediment was obtained by filtering meltwaters. The flux of suspended sediment gives information on the mechanical erosion rates of the two glaciers (Chapter 7). Furthermore suspended sediment samples give a good average mineralogical composition of what is recently subglacially abraded (Chapter 3). They were also used to analyse the concentration of adsorbed cations within the meltwaters (Chapter 2).

Rain and snow were sampled during the entire project to calculate the quantity as well as to measure the chemistry of precipitation. The chemistry was analysed in analogy to the other water samples. The quantity of precipitation was measured using existing data from gauging stations and totalisators (MeteoSwiss, Grimsel Hospiz, Oberaar Joch, Kl. Siedelhorn, and Albert Heim Hütte) as well as using our own totalisators (analogue to Otz, 1998), which were distributed within the catchments and two rain gauges with data loggers which were put up in front of the two glaciers during the ablation seasons (Appendix A.3). During winter missions snowprofiles were dug and fresh snow was sampled in both areas.

Two dust collectors measured the particulate flux entering the Rhone catchment during the 1999 and the 2000 ablation season. Dust samples were analysed for quantity, mineralogy and Sr isotope systematics (see Chapter 2).

Several soil profiles were dug in chronosequences of glacially derived sediments within the proglacial areas of the two glaciers. Clay mineralogical and chemical analyses of the moraine profiles gave insight into the soil forming processes on glacial sediment after its deposition (Chapters 3 and 5).

The major lithologies of local bedrock were sampled in front of the Oberaar glacier. The mineralogical analyses give a control on the mineralogy of the suspended sediment. They further help to confirm the chemical mass balance of the catchments (e.g. calcite content; Chapter 2 and 3).

In front of Rhone glacier several sondes were installed during the ablation seasons 1999, 2000, and 2001, measuring the water height (pressure sonde), the electrical conductivity, and the turbidity (suspended sediment concentration). Such data allow for the correlation of suspended sediment concentration with total phosphorus as well as with discharge. Conductivity was used as an ion-flux control (Hosein, 2002). In front of the Oberaar glacier several attempts were undertaken with a turbidity sonde (ablation season 2000, Appendix E). However, the fast moving braided meltwater system did not allow for measurements over significant periods of time (< 5 days). The available data are presented in Appendix A.1.

Organisation of this thesis:

This thesis consists of an Introduction, five main chapters, and the Conclusions. Chapter 2 was written together with Rachel Hosein. Chapter 3 and 4 as well as the Introduction and the Conclusions were written by myself whereas chapter 5 and 6 were prepared by Rachel Hosein.

References

Ammann, K., 1977. Der Oberaargletscher im 18., 19., und 20. Jahrhundert. Zeitschrift für Gletscherkunde und Glazialgeologie, XII(2): 253-291.

Anderson, S.P., Drever, J.I., Frost, C.D. and Holden, P., 2000. Chemical weathering in the foreland of a retreating glacier. Geochimica et Cosmochimica Acta, 64(7): 1173-1189.

Anderson, S.P., Drever, J.I. and Humphrey, N.F., 1997. Chemical weathering in glacial environments. Geology, 25(5): 399-402.

Berner, R.A., 1992. Weathering, plants, and the long-term carbon cycle. Geochimica et Cosmochimica Acta, 56: 3225-3231.

Berner, R.A., 1995. Chemical Weathering and its effect on atmospheric CO2 and climate. Reviews of Mineralogy, 31: 565-583.

Berner, R.A. and Kothavala, Z., 2001. GEOCARB III: a revised model of atmospheric CO2 over Phanerozoic time. American Journal of Science, ???: 182-204.

Berner, R.A., Lasaga, A.C. and Garrels, R.M., 1983. The carbonate-silicate geochemical cycle and its effect of atmospheric carbon dioxide over the past 100 million years. American Journal of Science, 283: 641-683.

Brown, G.H., 2002. Glacier meltwater hydrochemistry. Applied Geochemistry, 17: 855-883.

Brown, G.H., Sharp, M.J., Tranter, M., Gurnell, A.M. and Nienow, P.W., 1994. Impact of post-mixing chemical reactions on the major ion chemistry of bulk meltwaters draining the Haut Glacier d'Arolla, Valais, Switzerland. Hydrological Processes, 8: 465-480.

Clarke, G.K.C., 1987. Subglacial till: a physical framework for its properties and processes. Journal of Geophysical Research, 92: 9023-9036.

Collins, D.N., 1977. Hydrology of an alpine glacier as indicated by the chemical composition of meltwater. Zeitschrift für Gletscherkunde und Glazialgeologie, 13(1/2): 219-238.

Collins, D.N., 1979. Hydrochemistry of meltwaters draining from an Alpine glacier. Arctic and Alpine Research, 11(3): 307-324.

Desor, E., 1845. Nouvelles excursions et séjours dans les glaciers et les hautes régions des Alpes, de M. Agassiz et de ses compagnons de voyage. J.-J. Kissling, Neuchâtel, 266 pp.

Fairchild, I.J., Killawee, J. A., Sharp, M. J., Spiro, B., Hubbard, B., Lorrain, R. D., and Tison, J.-L., 1999. Solute generation and transfer from a chemically reactive alpine glacial-proglacial system. Earth Surface Processes and Landforms, 24(13): 1189-1211.

Föllmi, K.B., 1995. 160 m. y. record of marine sedimentary phosphorus burial: Coupling of climate and continental weathering under greenhouse and icehouse conditins. Geology, 23(9): 859-862.

Föllmi, K.B., Weissert, H., Bisping, M. and Funk, H., 1994. Phosphogenesis, carbon-isotope stratigraphy, and carbonate-platform evolution along the Lower Cretaceous northern Tethyan margin. Geol. Soc. Am. Bull., 106: 729-746.

Fountain, A.G., 1996. Effect of snow and firn hydrology on the physical and chemical characteristics of glacial runoff. Hydrological Processes, 10: 509-521.

Gaillardet, J., Dupré, B., Louvat, P. and Allègre, C.J., 1999. Global silicate weathering and CO2 consumption rates deduced from the chemistry of large rivers. Chemical Geology, 159: 3-30.

Garrels, R.M. and Mackenzie, F.T., 1967. Origin of the chemical compositions of some springs and lakes. Equilibrium Concepts in Natural Water Systems. American Chemical Society, Washington D.C., pp. 222-242.

Gibbs, M.T. and Kump, L.R., 1994. Global chemical erosion during the Last Glacial Maximum and the present: sensitivity to changes in lithology and hydrology. Paleoceanography, 9(4): 529-543.

Goldich, S.S., 1938. A study in rock weathering. Journal of Geology, 46: 17-58.

Gos, C., 1928. L'Hôtel des Neuchâtelois. Un épisode de la conquête des Alpes. Librairie Payot & Cie, Lausanne, Genève, Neuchatel, Vevey, Montreux, Berne, 168 pp.

Gurnell, A.M., Brown, G.H. and Tranter, M., 1994. Sampling strategy to describe the temporal hydrochemical characteristics of an alpine proglacial stream. Hydrological Processes, 8: 1-25.

Gurnell, A.M., Hannah, D. and Lawler, D., 1996. Suspended sediment yield from glacier basins. International Association of Hydrological Sciences Publication, 236: 97-104.

Hallet, B., Hunter, L. and Bogen, J., 1996. Rates of erosion and sediment evacuation by glaciers: A review of field data and their iplications. Global and Planetary Change, 12: 213-235.

Haq, B.U., Hardenbol, J. and Vail, P.R., 1987. Chronology of fluctuating sea levels since the Trias. Science, 235: 1156-1167.

Harbor, J. and Warburton, J., 1993. Relative rates of glacial and nonglacial erosion in Alpine environments. Arctic and Alpine Research, 25(1): 1-7.

Hosein, R., 2002. Glacial Weathering. Unpublished PhD Thesis, University of Neuchatel, Neuchatel, CD ROM.

Hubbard, B.P. and Nienow, P., 1997. Alpine subglacial hydrology. Quaternary Science Reviews, 16: 939-955.

Koppes, M.N. and Hallet, B., 2002. Influence of rapid glacial retreat on the rate of erosion by tidewater glaciers. Geology, 30(1): 47-50.

Kump, L.R., Brantley, S.L. and Arthur, M.A., 2000. Chemical weathering, atmospheric CO2, and climate. Annual Reviews in Earth and Planetary Sciences, 28: 611-667.

Meybeck, M., 1987. Global chemical weathering of surficial rocks estimated from river dissolved loads. American Journal of Science, 287: 401-428.

Nienow, P., Sharp, M.J. and Willis, I.C., 1996. Velocity-discharge relationships derived from dye-tracer experiments in glacial meltwaters: implications for subglacial flow conditions. Hydrological Processes, 10: 1411-1426.

Nienow, P., Sharp, M.J. and Willis, I.C., 1998. Seasonal changes in the morphology of the subglacial drainage system, Haut Glacier d'Arolla, Switzerland. Earth Surface Processes and Landforms, 23: 825-843.

Nye, J., 1973. Water at the bed of the glacier. International Association of Hydrological Sciences Publication, 95: 189-194.

Oberhänsli, R., Schenker, F. and Mercolli, I., 1988. Indications of Variscan nappe tectonics in the Aar Massif. Schweizerische Mineralogisch Petrographische Mitteilungen, 68: 509-520.

Otz, M.H., 1998. Die hydrogeologischen Verhältnisse im oberen Valle Santa Maria, Lucomagno, Ticino. Unpublished Masters Thesis, University of Berne, Berne, 150 pp.

Raymo, M.E. and Ruddiman, W.F., 1992. Tectonic forcing of late Cenozoic climate. Nature, 359: 117-122.

Röthlisberger, H. and Lang, H., 1987. Glacial Hydrology. In: A.M. Gurnell and M.J. Clark (Editors), Glacio-fluvial sediment transfer. John Wiley and Sons Ltd., Chichester, pp. 207-284.

Schuler, T., 2002. Investigation of water drainage through an apline glacier by tracer experiments and numerical modelling. Unpublished PhD Thesis, ETH Zurich, Zurich.

Schuler, T., Fischer, U.H., Sterr, R., Hock, R. and Gudmundsson, G.H., 2002. Comparison of modeled water input and measured discharge prior to a release event: Unteraargletscher, Bernese Alps, Switzerland. Nordic Hydrology, 33(1): 27-46.

Schwab, M., Frei, C., Schär, C. and Daly, C., 2001. Mean annual precipitation throughout the European Alps 1971-1990. In: Federal Office for Water and Geology (Editor), The Hydrological Atlas of Switzerland. Federal Office for Topography, Berne.

Sharp, M., Brown, G.H., Tranter, M., Willis, I.C. and Hubbard, B., 1995a. Comments on the use of chemically based mixing models in glacier hydrology. Journal of Glaciology, 41(138): 241-246.

Sharp, M.J., Tranter, M., Brown, G.H. and Skidmore, M., 1995b. Rates of chemical denudation and CO2 drawdown in a glacier-covered alpine catchment. Geology, 23(1): 61-64.

Sharp, M., Parkes, J., Cragg, B., Fairchild, I.J., Lamb, H., and Tranter, M., 1999. Widespread bacterial populations at glacier beds and their relationship to rock weathering and carbon cycling. Geology, 27(2): 107-110.

Slatt, R.M., 1972. Geochemistry of meltwater streams from nine alaskian glaciers. Geological Society of America Bulletin, 83: 1125-1132.

Stalder, H.A., 1964. Petrographische und mineralogische Untersuchungen im Grimselgebiet (Mittleres Aarmassiv). Schweizerische Mineralogische und Petrographische Mitteilungen, 44: 187-389.

Stallard, R.F., 1992. Tectonic processes, continental freeboard, and the rate controlling step for continental denudation. In: S.S. Butcher (Editor), Global biogeochemical cycles. Acacemic, pp. 93-121.

Stallard, R.F., 1995. Relating chemical and physical erosion. Reviews in Mineralogy, 31: 553-564.

Tranter, M., Brown, G., Raiswell, R., Sharp, M. and Gurnel, A., 1993. A conceptual model of solute acquisition by Alpine glacial meltwaters. Journal of Glaciology, 39(133): 573-581.

Tranter, M. and Jones, H.G., 2001. The chemistry of snow: processes and nutrient cycling. In: H.G. Jones, J.W. Pomeroy, D.A. Walker, and R. Hoham (Editors), Snow ecology. Cambridge University Press, Cambridge.

Tranter, M. et al., 2002. Geochemical weathering at the bed of Haut Glacier d'Arolla, Switzerland - A new model. Hydrological Processes, 16: 959-993.

Wadham, J.L., Cooper, R.J., Tranter, M. and Hodgkins, R., 2001. Enhancement of glacial solute fluxes in the proglacial zone of a polythermal glacier. Journal of Glaciology, 47(158): 378-386.

Wadham, J.L., Hodson, A.J., Tranter, M. and Dowdeswell, J.A., 1998. The hydrochemistry of meltwaters draining a polythermal-based, high Arctic glacier, south Svalbard: I. The ablation season. Hydrological Processes, 12: 1825-1849.

Walder, J.S. and Fowler, A.C., 1994. Channelized subglacial drainage over a deformable bed. Journal of Glaciology, 40: 3-15.

Walker, J.C.G., Hays, P.B. and Kasting, J.F., 1981. A negative feedback mechanism for the long term stabilization of the earth's surface temperature. Journal of Geophysical Research, 86: 9776-9782.

White, A.F., 1995. Chemical weathering rates of silicate minerals in soils. Reviews in Mineralogy, 31: 407-461.

White, A.F. and Blum, A., 1995. Effects of climate on chemical weathering in watersheds. Geochimica et Cosmochimica Acta, 59(9): 1729-1747.

Willis, I.C., Richards, K.S. and Sharp, M.J., 1996. Links between proglacial stream suspended sediment dynamics, glacier hydrology and glacier motion at Midtdalsbreen, Norway. Hydrological Processes, 10: 629-648.

CHAPTER 2

Carbonate and silicate weathering in two presently glaciated, crystalline catchments in the Swiss Alps

Abstract

We present a weathering mass balance of the presently glaciated Rhone and Oberaar catchments located within the crystalline Aar massif, central Switzerland. The centre of the Oberaar catchment is underlain by a strongly foliated gneissic zone containing up to 5 % calcite, which is more erodable than the granitic and granodioritic bedrock of the Rhone catchment that contains less than 1 % calcite. Annual weathering fluxes are calculated as the weighted mean of monthly accumulation period and twice daily ablation period meltwater samples collected from July, 1999 to May, 2001, and corrected for precipitation inputs. They are dominated by calcium, which represents 81 % and 55 % of the total cation flux in the Oberaar and Rhone catchments respectively (i.e. 555 and 82-96 keq km^{-2} yr^{-1}). An increase of less than 2 % in the calcite content of Oberaar suspended sediments compared to the Rhone suspended sediments, coupled with the increased erodability and higher sulphide content of the Oberaar bedrock, increases the Ca^{2+} flux by an order of magnitude. This demonstrates the extreme sensitivity of glacial systems to minor changes in the calcite and sulphide content of crystalline bedrock and suggests that short-term CO_2 sequestration associated with the carbonation driven hydrolysis of carbonate may be locally variable. Silica fluxes from the two catchments are comparable with each other and with other catchments with crystalline bedrock and similar runoff, irrespective of whether they are glacier covered.

Introduction

Glaciers and periods of glaciation may have a significant impact on global weathering, changing the interplay between physical and chemical weathering processes by putting large volumes of dilute meltwaters and fine grained sediment in contact with each other. Glaciers are significant agents of physical erosion, for example glaciated valleys in Alaska and Norway have an order of magnitude higher mechanical denudation than equivalent non-glaciated basins (Hallet et al., 1996). Hay (1998) suggests that today's global, glacially derived yield of detrital sediments is about half the fluvial detrital yield, but that the two systems' yields were possibly equal before the advent of man. Furthermore the nature of glacially derived sediments may also pre-dispose them to increased chemical weathering compared to sediments derived by fluvial erosion processes. Abrasion and quarrying at the glacier sole generates large volumes of silt sized grains (Boulton, 1979; Dreimanis & Vagners, 1969, 1971; Drewry, 1986) which are heavily indented and fractured (Mahaney, 1995, and references therein) leading to larger surface areas, complicated microtopographies and increased chemical reactivities (White and Brantley, 1995 and references therein). Reaction of this sediment with dilute, close to neutral meltwaters leads to solute fluxes from glacial catchments that are three times Summerfield's (1991) estimated global average denudation rate of 14.8 t km^{-2} yr^{-1} (Sharp et al., 1995). The characteristic chemical signature of glacial meltwaters is strongly linked to the susceptibility of minerals to comminutation and the temperature dependence of mineral dissolution rates (White et al., 1999a). Catchment studies by numerous authors (e.g. Eyles et al., 1982; Drever and Hurcomb, 1986; Sharp et al., 1995; Anderson et al., 1997, 2000) find glacial meltwaters elevated in dissolved Ca^{2+} and K^{+} relative to non-glacial runoff, but depressed with respect to silica (e.g. Anderson et al., 1997, 2000; West et al., 2002) due to the temperature dependent nature of silicate weathering (White et al., 1999a). It is widely concluded that the

This chapter by Rachel Hosein, Kaspar Arn, Philipp Steinmann, Thierry Adatte, and Karl B. Föllmi has been submitted for publication in *Geochimica et Cosmochimica Acta*.

predominant reactions in glacial meltwaters are calcite dissolution and the nonstoichimetric dissolution of K^+ from micas (e.g. Drever and Hurcomb, 1986).

Calcite is highly reactive in dilute glacial meltwaters because its softness (3 on Moh's scale) causes it to be easily milled into ultra-fine particles, (e.g. Fairchild et al., 1999). Also at near neutral pH the dissolution rate of calcite (10^{-5} mol m^{-2} s^{-1}; Plummer et al., 1978) is approximately 7 orders of magnitude faster than the dissolution rate of plagioclase feldspar (ca 10^{-12} mol m^{-2} s^{-1}; Blum, 1994). Calcite is not confined to catchments with carbonate or metasedimentary geology, but is also present as an accessory phase in crystalline rocks and provides up to 98% of the calcium flux from freshly ground granitoid rocks in laboratory leaching experiments (White et al., 1999b). Glacial weathering may optimise carbonate dissolution in catchments with crystalline bedrock, firstly as calcite and quartz are abraded more effectively when ground together, rather than separately (Fairchild et al., 1999) and secondly because crystalline bedrock generally has a lower permeability than carbonate bedrock. This may have implications for weathering on the icesheet scale, whereby ice underlain by crystalline rock may have higher basal water pressures, facilitating increased basal slip and erosion of during glacial maxima compared to areas of ice underlain by carbonate formations (Sugden, 1978). Crystalline rocks form over 20 % of the continental area (granites = 10.4 %, gneisses = 10.4 %; Meybeck, 1987) and predominate over carbonate rocks at latitudes which were ice covered at the last glacial maximum (Gibbs and Kump, 1994, and references therein). Therefore defining the relative contribution of accessory calcite to weathering fluxes in presently glacier covered, monolithological crystalline catchments is an important goal in assessing the potential feedbacks between glaciation, weathering of continental rocks and atmospheric CO_2 (e.g. Berner, 1991; Ludwig et al., 1998).

In this study we measure the influence of accessory calcite on meltwater chemistries draining two small, presently glaciated, crystalline catchments in central Switzerland, containing the Rhone and Oberaar glaciers. These geographically and glaciologically comparable watersheds are seated in the Aar massif, comprised of Hercynian aged granites and granodiorites, which contain measurable amounts of calcite (< 1% calcite; Keusen et al., 1989). The Rhone catchment sits squarely on these two lithologies. The Oberaar watershed, on the other hand, is centred on a strongly foliated gneissic zone, which represents 42% of the catchment area and contains up to 5% calcite (Stalder, 1964). We assess weathering intensity by measuring the concentrations of dissolved ions and suspended sediment in the meltwaters. The annual variation in meltwater composition for the catchments is presented, including samples taken during two accumulation periods, when discharge is minimal and sediment-water in-

	Oberaar			**Rhone**		
Geographical position	46° 32' N 8° 14' E			46° 35' N 8° 23' E		
Surface of catchment	11.2 km2			23 km2		
Altitude	2310 - 3631 m above sea level (a.s.l.)			1750 - 3630 m a.s.l.		
Glacier cover today (%)	57%			73%		
Annual mean temperature *	- 1° C[§]			+ 1.2° C[§]		
Annual mean precipitation *	2100 mm			2200 mm		
Geology of catchments:	Today	LIA	YD	Today	LIA	YD
Central Aar Granite	38%	38%	25%	90%	82-86%	40%
Grimsel Granodiorite	7%	7%	12%	10%	8-9%	20%
Variscan gneisses	42%	42%	38%		10-5%	20%
Ultramafic Inclusions	1%	1%	1%			
Southern Aar Granite	12%	12%	24%			
Mesozoic metasediments						20%

* Schwab etal., 2001
[§] within proglacial area; 2300 m at Oberaar, 1757 m at Rhone.
LIA Little Ice Age; YD Younger Dryas

Table 2.1: Different parameters of the two catchments. For geology see also Fig. 2.1.

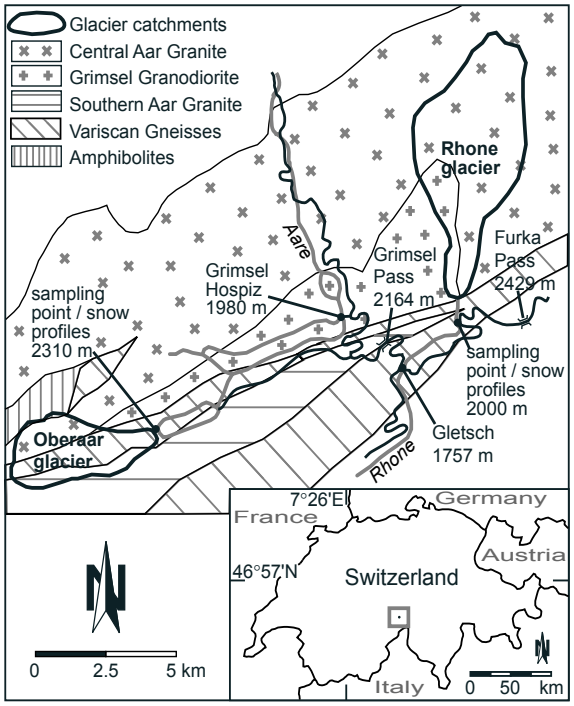

Fig. 2.1: Map of the field areas with geology of the Aar Massif modified after Oberhänsli et al. (1988) and todays glacier catchments.

teraction times should therefore be of longer duration. Silica fluxes from the two catchments are comparable with each other and with other catchments with crystalline bedrock and similar runoff, irrespective of whether they are glacier covered. In contrast the total cation flux from the Rhone glacier (147-175 keq km^{-2} yr^{-1}) is significantly below Livingstone's global average (390 keq km^{-2} yr^{-1}; 1963), whereas the Oberaar's total cation flux (681 keq km^{-2} yr^{-1}) is significantly higher (fluxes are corrected for precipitation inputs). This is due to the dissolved calcium flux from the Oberaar catchment being approximately 4-5 times higher than from the Rhone catchment (555 keq km^{-2} yr^{-1}, and 82-96 keq km^{-2} yr^{-1} respectively; i.e. 81 % 55 % of the total cation flux). We attribute this difference in calcium flux to the higher sediment flux from the Oberaar catchment (773 t km^{-2} yr^{-1} compared to 388-491 t km^{-2} yr^{-1} from the Rhone) and calcite concentrations which are on average 1.8 %, or 4.6 times higher in the Oberaar meltwaters. This result underlines the extremely reactive nature of calcite in presently glaciated environments.

Methods

Field areas and field methods

This study focuses on the catchments of the Rhône and Oberaar glaciers, in central Switzerland (Fig. 2.1). The present-day ice cover of Rhone catchment is 73% and the Oberaar catchment is 57 %. The catchments are of comparable size, altitude, and climate (Table 2.1) and have a simple geometry with one focussed meltwater outlet. The geology of the catchments is similar as they are both situated on the crystalline Aar massif. The bulk mineralogical content of the Central Aar Granite and the Grimsel Granodiorite, on which the Rhone glacier sits, was documented by Keusen et al. (1989; Table 2.2). The Oberaar catchments geology is more complex. The central part of the catchment (42% of the catchment area) is strongly foliated and is referred to by Stalder (1964) as the "Gneiss-Schiefer-Zwischenzone". The sides of the catchment are made up of 38 % Central Aar granite, 12 % Southern Aar granite and 8 % Grimsel granodiorite (Oberhänsli & Schenker, 1988; Stalder, 1964; see Fig. 2.1 for a geological map).

Meltwater samples from the glaciers' outwash streams were collected on a daily basis during the 1999 and 2000 ablation periods. Samples were taken

	n	Quartz	K-Feldspar (Microcline)	Plagioclase (Albite)	Calcite	Phyllosilicates[%]	Unquantifiable[*]	Epidote
Rhone suspended sediment [$]	23	21.8 ± 6.9	17.2 ± 11.1	27.9 ± 16.7	0.5 ± 0.4	14.2 ± 10.8	23.7 ± 27.7	
Oberaar suspended sediment [$]	23	24.3 ± 13.5	6.5 ± 5.7	25.4 ± 11.5	2.3 ± 1.8	13.7 ± 5.5	28.5 ± 17.9	
Central Aar Granite [†]		32.8	34.1	20.9	<1	8.7 [#]		2.3
Grimsel Granodiorite [†]		28.3	24.4	29.1	<1	14.8 [#]		2.0

[$] Amphibole did not enter the calculation

[†] Microscopical quantification after Keusen (1989)

[%] Individual phyllosilicates, e.g. phengite, biotite etc cannot be quantified in the bulk mineralogy (Adatte et al., 1996)

* Minerals cannot be quantified due to differences in chemical composition between the samples and the reference standards used, e.g. different Ca:Na ratios in the plagioclase feldspars. Calcite is not contained within the unquantifiable minerals

[#] Including biotite, chlorite, and white mica

Table 2.2: Mineralogical composition of the glacial suspended sediments and the bedrock (Central Aar Granite and Grimsel Granodiorite).

at 10:00 and 17:00 h, when the daily minimum and maximum discharge occurs (Gurnell et al., 1994). In 1999 sampling commenced on the 6-July-99, due to the late clearance of snow from the mountain passes. But discharge started to rise at the hydrographic station at Gletsch (Fig. 2.1) on the 1-May-99 and we interpret this as the start of the ablation period. We estimate that the ablation period ended on the 1-November-99. The discharge dropped below 1 $m^3 s^{-1}$ at Gletsch on this date and continued to fall, with the first snowfall lying on the 7-November-99. In 2000 the discharge began to rise on the 20-April-00 and the last of the winter's snow fell on the 25-April-00. The discharge dropped below 1 $m^3 s^{-1}$ on the 8-November-00 and the regression continued from this date. We therefore consider the months May to October inclusively as the ablation period. Throughout the winters of 1999-2000 and 2000-2001 samples were taken on a monthly basis from October until April.

On each sampling 500 ml of meltwater was filtered immediately in the field, as recommended by Slatt (1972) using 0.45μm cellulose nitrate filters and a Nalgene filter unit and hand pump. Conductivity and pH were immediately determined on the filtered samples in the field, using a WTW Multiline P4 meter. In the Rhone catchment alkalinity was measured within 15 minutes of sampling during the 1999 ablation season, measurments were made on filtered meltwaters by titration with 0.1 M Titrisol HCl. HCO_3^- concentrations were also calculated as the difference between each sample's summed cation and anion concentrations. This calculation is performed on both uncorrected and precipitation corrected meltwater chemistries. In both field areas sample manipulations were performed in tents to limit contamination by dust or precipitation.

Snow samples were taken from 40-80 cm deep sample pits, dug in fresh snow in the proglacial areas of the two catchments during the accumulation periods. Rainwater samples were taken during the ablation periods: A polypropylene bottle was connected to a plastic funnel via a polypropylene tube and the bottle was left for a maximum of 24 hours before the rainwater was filtered and stored. The funnel was protected from dust between samples by covering it with a plastic bag. All filtered samples were bottled in duplicate, kept in the dark at 2°C and analysed within 2 months. Samples intended for anion analysis were stored in polypropylene bottles, pre-leached with ultra-pure deionised water. Samples intended for cation analysis were stored in polypropylene bottles that had been pre-leached with 10 % supra-pure HNO_3 and then rinsed 3 times with ultra-pure deionised water. The sediment-laden filters were stored in individual perspex boxes.

Dry precipitation (dust) entering the Rhone catchment during the 1999 and 2000 ablation periods was measured using two 0.32 m diameter, 60 L plastic barrels, which had been preleached with 10 % supra-pure HNO_3 and thoroughly rinsed. The barrels were mounted in open, elevated positions, to avoid collecting saltating grains; a large flat topped erratic boulder approximately half way up the glacier (the up glacier barrel) and a flat grassy step to the right of the glacier snout (the down glacier barrel). Dust was prevented from being blown back out of the barrels by placing a 5 cm deep slatted container holding glass marbles at the mouth of the barrel (the marbles were also cleaned in the same way as the barrel; Marith Reheis, U.S. Geological Survey, pers. comm.). The barrels were left for 48 days in 1999 and 107 days in 2000 and then the contents were siphoned off and filtered through 0.45 μm filter papers, the barrels were thoroughly rinsed out with several washings of ultra-pure deionised water, which were also filtered.

Laboratory methods

The major cations and anions (Mg^{2+}, Ca^{2+}, K^+, Na^+, and SO_4^{2-}, NO_3^-, Cl^-) were measured using ion chromatography IC (Dionex DX-500). The error is 5 % for concentrations of < 100 ppb and ca 2 % for concentrations > 100 ppb. Relative Fe^{3+} and Al^{3+} were measured using a graphite furnace AAS. The error for Fe^{3+} was 10 % for concentrations of < 15 ppb and 5 % for concentrations of > 15 ppb. The error for Al^{3+} was 20 % for concentrations of < 15 ppb, 10 % for concentrations of 15–50 ppb, and 3 % for concentrations of > 50 ppb. Adsorbed cation concentrations were measured following Lorrain and Suchez (1972). The filters were washed three times with 10ml 1M ammonium acetate (pH 7), pumping each aliquot through a Nalgene filter unit. The resultant combined leachate was filtered and analysed for Mg^{2+}, Ca^{2+}, Na^+, and K^+ using flame atomic absorption FAA (Perkin Elmer 5100 PC). The blanks were 10 times lower than samples in each series, apart from the Rhone Ca^{2+} values and all the Na^+ values, which were

the same as the blanks. Dissolved silicon was measured colorimetrically (molybdate blue) by FIA (tecator 5017) (modified from Mullin and Riley, 1955) The relative error for these two methods is 5% or better.

Filters were dried at 40° C, weighed and corrected for the original filter weight to calculate the mass of suspended sediment. The mineral content of the suspended sediment was determined by X-ray diffraction (XRD), while the sediment was still on the filter papers (partial orientation), using a Scintag XDS 2000. The dust samples were passed under the X-ray on silver coated stubs. The bulk mineralogy of the suspended sediments was determined by semi-quantitative analysis using external standards (Adatte et al., 1996). The limit of detection for calcite is 0.2 %. Un-orientated powder samples have an error of 5 % and we estimate that our partially orientated powder samples have an error of < 10 %. The granulometry of the suspended sediment and dust samples was determined using a Laser Oriel granulometer. The chemistry of the suspended sediment was determined by XRF, at the University of Fribourg, using a sequential X-ray spectrophotometer (PW-2400), with a relative error of 0.2-1 % for major elements.

Precipitation input corrections

We calculate the input flux for wet precipitation in two ways: Firstly by correcting each meltwater sample for precipitation inputs in proportion to its chloride concentration and secondly based on the estimated volumes of rain and snow falling in the catchments.

In the first approach the concentration of ions in each meltwater sample, X_m, are corrected, to give the weathering derived concentrations in the meltwaters, X_m^*. The relative input of ions by wet precipitation is calculated by multiplying the chloride concentration in the meltwaters Cl_m by a factor, where X_p is the mean concentration of each ion in precipitation and Cl_p is the

Sample:	Date(s)	Na^+	K^+	Mg^{2+}	Ca^{2+}	Fe^{3+}	Al^{3+}	Cl^-	SO_4^{2-}	NO_3^-	NH_4	Si
Rain												
Rhone	28-Aug-99	8.70	7.16	5.76	43.91	n.a.	n.a.	5.64	54.76	15.64	n.a.	n.a.
Rhone	7-Sep-99	10.87	6.14	4.11	33.43	1.51	1.68	3.67	33.31	28.22	n.a.	6.61
Rhone	22-Sep-99	4.78	2.05	1.65	2.50	1.99	2.36	1.41	5.41	5.32	n.a.	n.a.
Rhone	31-May-00	2.15	1.52	0.00	5.17	0.09	1.01	1.69	7.29	9.84	n.a.	0.57
Rhone	7-Jun-00	4.03	6.16	1.31	23.29	0.05	0.61	4.23	28.11	32.42	n.a.	8.29
Rhone	28-Jun-00	5.96	5.19	4.62	21.41	n.a.	n.a.	4.23	24.36	23.39	n.a.	n.a.
Oberaar*	11-Jul-00	16.96	3.58	10.70	134.23	0.12	0.38	3.10	12.91	10.97	n.a.	52.74
Oberaar	13-Jul-00	2.75	1.28	0.00	8.37	0.56	0.79	2.26	50.59	5.00	n.a.	64.06
Rhone	15-Jul-01	n.a.	2.30	2.47	10.98	0.14	0.86	4.22	29.72	17.61	n.a.	n.a.
Rhone	27-Jul-00	3.57	1.84	1.56	5.25	0.62	0.87	3.10	20.40	16.93	n.a.	n.a.
Rhone	1-Aug-00	3.09	2.27	0.59	3.10	0.60	0.61	5.36	16.24	13.22	n.a.	1.81
Rhone	7-Aug-00	2.47	1.51	1.37	16.76	n.a.	n.a.	1.68	19.57	17.10	n.a.	n.a.
Rhone	3-Aug-01	2.61	3.07	1.65	7.49	0.33	n.a.	1.94	12.59	6.44	n.a.	n.a.
Oberaar	3-Aug-01	3.04	4.35	2.47	17.47	0.18	n.a.	3.80	38.18	21.58	n.a.	n.a.
Oberaar	8-Aug-01	2.61	7.67	1.65	11.48	0.05	0.77	3.74	15.84	14.18	n.a.	n.a.
Rhone	17-Aug-01	4.35	9.21	4.11	25.95	0.14	1.11	6.21	19.52	18.01	n.a.	n.a.
Rhone	30-Aug-01	6.09	8.18	6.58	53.39	n.a.	0.88	8.46	17.08	19.97	n.a.	n.a.
Snow (sample depth)												
Rhone (0-85 cm)	18-Jan-01	6.52	2.30	0.82	2.00	0.28	1.05	n.a.	n.a.	n.a.	n.a.	2.87
Oberaar (0-5 cm)	18-Jan-01	5.22	8.16	0.38	4.00	0.30	1.27	9.87	2.58	3.85	n.a.	0.45
Oberaar (0-40 cm)	6-Mar-01	2.75	2.57	0.47	16.96	n.a.	n.a.	5.36	2.07	3.60	n.a.	n.a.
Oberaar(0-5cm)	6-Mar-01	2.45	1.88	0.29	14.31	b.d.	0.80	2.81	2.30	2.94	n.a.	n.a.
Rhone (0-5 cm)	7-Mar-01	0.29	0.99	0.00	1.42	n.a.	n.a.	n.a.	n.a.	n.a.	n.a.	n.a.
Rain average	1999-2001	4.47	4.37	2.49	18.12	0.52	1.05	3.85	24.56	16.55		11.62
Snow average	1999-2001	3.45	3.18	0.39	7.74	0.19	1.04	5.14	2.54	4.87		0.83
Average (ratio 40:60)	**1999-2001**	**3.86**	**3.65**	**1.23**	**11.89**	**0.33**	**1.04**	**4.63**	**11.35**	**9.54**		**5.15**
Other swiss sites												
Alptal (annual average) †		5.65	1.28	1.65	12.48	0.59	0.56	4.51	6.25	4.19	0.01	7.12
Haut Glacier d'Arolla #	1993-1995	0.40	1.10	0.70	3.80			3.80	3.30	5.80		<0.1

n.a.: not analysed
b.d.: below detection
* Rain collected during Saharan red dust event and not included in the mean
† non glaciated; average annual precipitation 2300 mm
# mean snowpack winters 93-95, Tranter et al. (2002)

Table 2.3: Precipitation compositions in µeq l^{-1}.

mean chloride concentration of the precipitation:

$$X_m^* = X_m - Cl_m \cdot X_p/Cl_p$$

14 rain and 5 snow samples, collected between August 1999 and September 2001 are used to determine the mean rain and snow concentrations (Table 2.3). These means are weighted according to the relative proportions of rain and snowfall in (water equivalents) recorded at the Grimsel Hospiz during the study period (60 % snow: 40 % rain; MeteoSwiss, station no. 5010), yielding a mean annual precipitation composition (Table 2.3). The Hospiz is located at 1980 m, on the northerly side of the Grimsel Pass, approximately 4 km from the Rhone and 8 km from the Oberaar glacier snouts (Fig. 2.1.) and provides a daily record of precipitation volumes. Regarding the second, volumetric approach mean annual precipitation data at the Hospiz for 1997, 1999 and 2000 average 2040 mm per year, slightly higher than the average precipitation rate from 1988-2000:1990 mm. Precipitation was assumed to fall as snow from November to April yielding an average snow/total precipitation ratio of 0.68 for September 1999-2000 and 0.53 for September 2000-2001. In the Rhone catchment Bernath (1991) recorded annual inputs ranging between 2108-2845 mm for the period 1979-1983, based on a detailed net of climatological stations. Estimates based on a 20-year local climate record (1971-1990) give an average of 2050 mm of precipitation (Schwab et al., 2001). Because a slightly higher than average precipitation volume is recorded at the Hospiz during our study period we estimate an annual precipitation input of 2200 mm in the Rhone catchment with 60 % of this volume falling as snow. In the Oberaar catchment an annual mean precipitation of 2020 mm has been observed (Schwab et al., 2001). Again, to reflect the elevated precipitation volume recorded at the Hospiz, we use a slightly higher value: 2100 mm, with snowfall representing 60 % of this volume. These rain and snow volumes are multiplied by the mean rain and snow composition to calculate the wet precipitation input to each catchment, which is subtracted from the meltwater fluxes to obtain a denudation rate.

All ion corrections are subject to some error, firstly because we use mean rain and snow composition, whereas ion concentrations vary significantly during individual rain events (Table 2.3) and secondly because ions are eluted at different rates from the snow pack, leading to a non-linear relationship between Cl^- and other ions at the start of the ablation season. Both correction methods fail to remove approximately half the NO_3^- flux (Table 2.4), but correction for NO_3^- may be especially difficult, for example because NO_3^- maybe influenced by subglacial microbial activity (Sharp et al., 1999) and NH_4^+ in rain. The volumetric correction overestimates the total precipitation volume, as negative Cl^- fluxes are calculated (Table 2.4). We therefore use precipitation ratio values in the discussion section of this paper, and point out that this approach is certainly more robust than using sea salt ratios for catchments located in the continental interior (Table 2.5).

	Precipitation		Sea salt
Ion	***μ*eq l^{-1}**	**Ion / Cl$^-$**	**Ion / Cl$^-$**
Cl^-	4.63	1	1
Na^+	3.86	0.83	0.56
Mg^{2+}	1.23	0.27	0.07
Ca^{2+}	11.89	2.57	0.02
K^+	3.65	0.79	0.02
SO_4^{2-}	11.35	2.45	0.14
NO_3^-	9.54	2.06	-
Fe^{3+}	0.33	0.07	-
Al^{3+}	1.04	0.23	-
Si	5.15	1.11	-

Table 2.5: Seawater and precipitation compositions normalised by chloride.

Flux calculations

Rhone daily discharges for the 1999 and 2000 ablation periods were recalculated from Swiss National Hydrological Survey data (Federal Office for Water and Geology) from the Gletsch gauging station (no. 2268). The gauging station is 2.75 km downstream from the glacier snout and receives water from a 38.9 km^2 catchment. Bernath (1991) made a detailed 5-year hydrological study of the Gletsch catchment and calculated that between 14 % and 18% of the discharge measured at Gletsch comes from outside the Rhone glacier catchment. We calculate all our ablation period daily fluxes based on the Gletsch daily discharge measurements corrected by 14% and 18% and mean daily meltwater concentrations in order to show the discharge related error on our values. Accumulation period discharges

Fluxes (keq km^{-2} year^{-1})	Ca^{2+}	K^{+}	Na^{+}	Mg^{2+}	Fe^{3+}	Al^{3+}	Cl^{-}	SO_4^{2-}	NO_3^{-}	HCO_3^{-}	Si	Suspended Sediment
Uncorrected fluxes												
Rhone	96.4-116.2	29-35.4	28.3-34.1	14.9-18.1	5.4-6.5	11.0-13.3	6.6-8.2	49.9-60.0	34.2-42.5	99.9-120.6	152.3-183.2	388274-490771
Oberaar	589.5	59.7	32.4	37.0	4.8	10.4	5.9	226.8	23.8	467.2	182.2	773076
Corrected by precipitation volume												
Rhone	70.2-90.0	21.0-27.4	19.8-25.6	12.2-15.4	4.7-5.8	8.7-11.0	-(2-3.6)	24.9-35.0	13.2-21.5		141.0-171.9	
Oberaar	564.5	52.0	24.3	34.4	4.1	8.2	-3.8	203.0	3.7		171.4	
Corrected by precipitation ratios												
Rhone	81.5-96.4	24.5-29.3	23.1-27.3	13.6-16.4	2.2-2.7	2.1-2.6	0	33.7-39.3	20.5-24.7	93.2-109.7	145.3-173.2	
Oberaar	554.6	53.3	26.1	33.9	4.4	8.9	0	204.5	11.8	467.6	176.4	

Table 2.4: Annual dissolved fluxes from the catchments in keq km^{-2} year^{-1} and suspended sediment fluxes in kg km^{-2} year^{-1}.

	n	Na^{+}	±	K^{+}	±	Mg^{2+}	±	Ca^{2+}	±	Fe^{3+}	±	Al^{3+}	±	Cl^{-}	±	SO_4^{2-}	±	NO_3^{-}	±	†HCO_3^{-}	±	Si	±	Cond.	±	Disch.#	Model§
Rhone																											
January	1-2	47.4	4.4	33.2	0.8	19.9	1.3	142.2	7.8	2.9	–	5.9	–	5.2	1.7	89.8	12.3	21.4	1.2	137.6	3.2	263.3	–	25.5	1.4	200	55
March	1	47.8	–	35.0	–	20.6	–	163.2	–	1.4	–	3.0	–	n.a.	–	n.a.	–	n.a.	–	n.a.	–	n.a.	–	15.0	–	200	55
April	2	40.2	4.0	33.1	1.7	19.3	2.9	206.3	7.5	0.7	0.4	1.6	0.7	2.3	0.02	79.0	64.9	10.3	0.5	135.0	33.8	230.7	18.8	16.3	–	200	164
May	16	15.4	4.0	15.2	3.5	7.4	3.5	53.6	13.1	1.2	0.2	1.7	0.5	3.7	0.8	26.1	13.0	19.9	2.8	53.8	10.5	57.0	19.1	12.5	5.15	300	949
June	11	9.8	2.9	11.4	4.8	4.9	1.9	33.4	8.3	1.1	0.4	1.3	0.4	2.4	0.4	15.8	3.3	14.2	2.6	31.3	11.8	34.8	16.7	8.7	1.87	2269	3797
July	26-29	7.9	2.8	8.3	2.1	4.1	1.7	27.6	8.1	1.0	0.4	1.2	0.5	2.3	0.6	14.1	3.9	12.6	3.2	25.2	10.0	33.5	8.7	8.1	2.3	5525	6115
August	20	5.1	0.8	5.8	1.2	3.1	3.4	17.5	2.9	0.6	0.4	0.6	0.5	1.7	0.6	8.9	1.9	8.0	1.9	14.8	3.8	22.1	7.4	7.2	4.9	7144	5950
September	20	5.7	3.7	7.1	3.8	3.3	1.1	18.8	5.6	0.9	0.6	1.2	0.7	1.6	0.5	8.7	2.5	6.4	1.3	25.8	13.9	25.5	13.7	5.3	1.6	7787	3450
October	7	12.1	3.7	12.2	3.7	5.5	2.6	45.7	15.0	1.5	0.3	2.4	0.4	2.0	0.9	19.2	8.7	11.3	4.9	43.6	25.1	103.8	65.8	9.9	1.4	4137	1040
November	1	26.2	–	20.8	–	12.7	–	96.0	–	1.2	–	2.4	–	3.4	–	45.4	–	17.6	–	98.0	–	147.9	–	18.0	–	1967	201
December	1	35.2	–	26.6	–	16.5	–	120.8	–	0.6	–	1.3	–	5.0	–	59.6	–	20.0	–	123.7	–	250.7	–	47.0	–	400	91
Oberaar																											
January	1-2	42.5	3.2	64.1	1.6	36.6	2.9	616.9	13.9	0.7	0.0	3.9	0.9	2.7	1.0	395.1	26.9	10.6	5.6	356.6	42.7	180.8	–	86.3	1.2	100	47
March	2	47.1	1.1	61.6	6.5	39.9	6.4	645.2	38.8	0.5	0.1	3.0	0.2	3.0	0.2	300.8	33.0	11.7	3.1	481.9	88.6	n.a.	–	90.0	2.8	100	50
April	2	39.0	7.6	48.1	5.5	30.9	5.1	484.5	50.1	1.3	0.9	3.5	1.0	4.4	1.7	140.3	149.2	21.2	4.7	441.4	76.3	193.7	18.2	67.5	7.7	250	92
May	2	16.0	0.2	26.2	4.9	16.1	3.6	218.0	55.8	2.4	2.2	4.3	3.1	3.4	1.2	54.5	38.3	17.5	6.7	282.6	66.7	113.6	16.5	29.0	5.7	625	832
June	11-12	9.1	1.6	16.7	1.9	10.9	2.2	179.9	23.9	2.3	0.6	3.9	0.7	2.2	0.2	63.7	10.3	10.5	2.6	147.1	17.4	55.8	8.77	23.3	2.3	1700	1689
July	19-21	10.9	4.0	21.1	5.3	14.0	3.4	216.1	50.1	1.9	0.9	4.1	1.3	2.2	0.4	87.0	27.6	10.6	3.2	166.6	51.2	62.5	24.7	29.4	6.9	2105	2352
August	10-11	7.3	1.8	16.9	3.5	11.3	2.0	179.0	34.6	2.2	0.9	4.5	1.4	2.0	0.1	66.4	14.6	6.5	1.7	148.5	20.2	62.0	39.3	25.2	4.6	1978	2149
September	9-10	7.8	3.2	19.9	6.3	14.1	4.6	188.6	57.1	2.1	0.8	4.6	1.2	2.5	0.7	83.2	16.8	6.6	2.2	194.0	30.1	56.4	15.6	30.0	5.4	1859	1505
October	3	16.8	0.6	33.4	2.3	19.6	4.6	313.3	39.3	2.2	2.1	5.3	3.2	3.0	0.8	113.0	51.7	12.6	3.2	262.0	33.4	74.9	52.3	39.9	10.2	750	390
November	1	31.2	–	54.6	–	31.2	–	456.4	–	3.1	–	6.6	–	2.3	–	252.6	–	14.0	–	314.8	–	n.a.	–	64.7	–	250	111
December	1	33.9	–	60.8	–	33.7	–	547.9	–	0.9	–	3.1	–	3.2	–	312.8	–	15.0	–	349.4	–	n.a.	–	76.6	–	200	52

n.a. not analysed

† Calculated HCO_3^{-}

Discharge Rhone measured at Gletsch, Oberaar estimated, see text.

* Modelled discharge for areas from Swiss National Hydrological Survey (Federal Office for Water and Geology), see text.

Table 2.6: Daily mean concentrations in µeq l^{-1}; conductivities in µS cm^{-1}; modelled and measured discharges in l s^{-1}.

are based on visual estimates and agree well with those proposed by Bernath (1991).

Oberaar discharges were estimated visually to the nearest 0.5 $m^3 s^{-1}$ each time a meltwater sample was taken, based on estimated water velocity and channel geometry. The meltwater channel was relatively stable and the accuracy of these estimates was compared to the discharge calculated using the salt dilution method (Federal Office for Water and Geology, 1994). Discharge estimates of 1.5 $m^3 s^{-1}$ were calculated as 1.64, 1.58 and 1.41 $m^3 s^{-1}$ on three separate occasions using salt dilution. The calculated mean monthly discharges for the Oberaar stream, based on these regular estimates agrees well with the mean monthly discharge estimates produced using a model designed by the Swiss National Hydrological Survey, Federal Office for Water and Geology. Fluxes are calculated for each sample as the product of the ion or suspended sediment concentration and the discharge volume. The mean of the 10:00 and the 17:00 h fluxes are taken to represent the daily flux, and in both catchments the daily fluxes are used to calculate monthly fluxes which are summed to give yearly fluxes. Fluxes are normalised by catchment area allowing comparison between catchments. Linear regressions between discharges measured at Gletsch at 10:00 and 17:00 and corresponding ion concentrations (Sharp et al., 1995) show no significant correlation, therefore we do not calculate hourly fluxes based on regression models.

To calculate adsorbed cation fluxes the adsorbed cation concentrations from 10:00 and 17:00 h samples for each day were averaged to calculate a daily mean adsorbed concentrations (mg g^{-1}). Weighted monthly concentrations were averaged to calculate a mean annual adsorbed cation concentration (mg g^{-1}) which was multiplied by the annual sediment flux to obtain annual adsorbed cation fluxes.

Results

Dry precipitation

In 1999 the up glacier barrel recorded a daily dust input of 0.0011 g day^{-1}, unfortunately the second barrel was lost. In 2000 the up glacier barrel recorded a daily dust input of 0.0013 g day^{-1} and the down glacier barrel recorded 0.0015 g day^{-1}. This implies that the dust falling over the glacier is evenly spread and the mean dust input is of the order of 5900 kg km^{-2} yr^{-1} or 1 % of the suspended sediment flux (see below). The dust samples contain quartz, mica, chlorite, potassium and plagioclase feldspars, goethite, calcite, smectite and kaolinite. In 1999 5 filters were the same grey colour as the suspended sediment samples, but one filter was covered in red dust. Red coloured dust was also collected during a rain event in 2000. The red colour of some of the dust and the presence of kaolinite suggest that a component of the dust is not local, it maybe of Saharan provenance (Lenaz et al., 1986; Kübler et al., 1990), although dolomite, another mineral typical of peridesertic environments is not observed in our samples.

Suspended sediment

The annual variation in the 10:00 and 17:00 hour suspended sediment concentrations in the meltwaters of the two catchments and the daily mean discharge recorded at Gletsch are plotted (Fig. 2.2a). Suspended sediment concentrations in the Oberaar meltwaters are consistently higher than the Rhone meltwaters. The Rhone mean ablation concentration is 0.11 g l^{-1} (± 0.05; n=196) and the Oberaar mean concentration is 0.33 g l^{-1} (± 0.10; n=107). The average winter suspended sediment concentrations are lower, 0.03 g l^{-1} (± 0.02; n=6) for the Rhone and 0.04 g l^{-1} (± 0.03; n=6) for the Oberaar meltwaters. The figure also shows that high discharges, associated with the rapid melting of snow and heavy rain events provoke the evacuation of large volumes of sediment. In both catchments rain events coinciding with the snow melt period mobilise large volumes of sediment, for example 3% of the annual sediment yield was discharged from each catchment during the rainstorm on the 6th of July 1999. The highest Rhone suspended sediment concentrations were associated with a two day rain event on the 20th and 21st of September 1999. The event was of a magnitude that only occurs once ever 2.3 years according to the MeteoSuisse and the sediment exported on these two days represented 9 % of the annual suspended sediment flux. This event was not recorded in the Oberaar catchment. The main flushing events in both catchments occur at times in the ablation period when a distributed drainage system is thought to be place which creates more contact between subglacial sediment and meltwaters than channelised systems (e.g. Nienow et al., 1996).

The suspended sediments of the two catchments

both contain quartz, plagioclase, alkali feldspar, phyllosilicates and calcite (XRD values). In addition some of the Oberaar samples contain amphibole. The bulk mineralogical analysis shows that quartz, plagioclase feldspar and phyllosilicate content of suspended sediments in the two catchments are similar, but that the Oberaar suspension contains less potassium feldspar than the Rhone suspension. The phyllosilicates have been identified as biotite, phengite and chlorite (Keusen, 1989). The mean calcite concentration is 4.6 times higher in the Oberaar suspension than the Rhone (2.3% and 0.5% respectively, Table 2.2) although the 1 *sigma* standard deviation around the Oberaar mean is ± 1.8. The mean Na_2O and SiO_2 concentrations of the suspended sediments are similar (XRF, Rhone and Oberaar Na_2O 3.8 & 3.0 %, respectively; Rhone and Oberaar SiO_2 68 % & 63 %, respectively). The mean CaO content of the Rhone suspended sediments is approximately half that of the Oberaar suspended sediments (0.9 % & 2.0 %, respectively). The strontium and barium concentrations are observed to be elevated in the Oberaar suspended sediments (Ba=982 ppm, Sr=238 ppm) with respect to the Rhône (Ba=524 ppm Sr=102). The ferrous iron concentrations are also elevated (Oberaar = 3.2 %; Rhone = 1.8 %).

In the two catchments the suspended sediment has a modal grain size in the 4-8 μm range, with 33% of the sediment in this size fraction. The mineralogy and granulometry of the suspended sediment does not change as a function of discharge, time of day or time of year. The suspended sediment flux from the Oberaar catchment is 773 t km^{-2} yr^{-1} and the suspended sediment flux from the Rhône catchment is 388-490 t km^{-2} yr^{-1}.

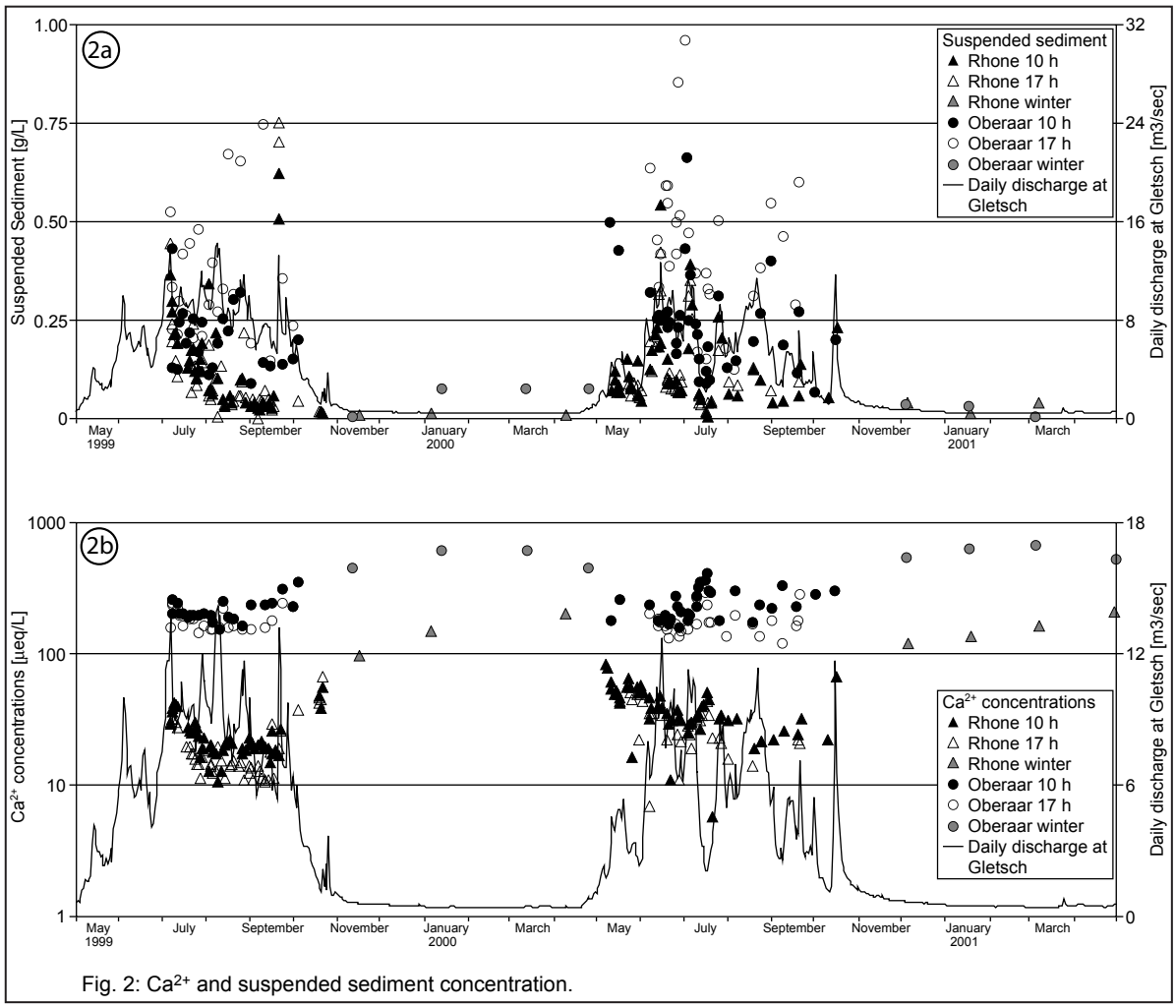

Fig. 2: Ca^{2+} and suspended sediment concentration.

Fig. 2.2: a) Variation in Rhone and Oberaar suspended sediment concentrations over the sampling period July 1999 – May 2001 (g l^{-1}). b) Variation in the Rhone and Oberaar calcium concentrations over the sampling period July 1999 – May 2001 (µeq l^{-1}).

Wet precipitation chemistry

Mean rain and snow chemistries are listed in Table 2.3; we also list average annual precipitation concentrations for the Alptal (P Schleppi, pers. comm.). This non-glaciated valley lies at the northern edge of the Swiss Alps, approximately 80 km from our field areas, between 1100 and 1600 m altitude. Our average annual concentrations agree well with the Alptal dataset, i.e. within 2-3 μeq l^{-1}, the exceptions being the SO_4^{2-} and NO_3^- concentrations, which are approximately twice as high in our glacial catchments. SO_4^{2-} and NO_3^- concentrations in snow agree well with the data for the Haut Glacier d'Arolla (Tranter et al., 2002).

Meltwater chemistry

Concentrations

Calcium dominates the meltwater chemistry of both watersheds (Table 2.6). Fig. 2.2b shows meltwater samples taken at 10:00 h have higher Ca^{2+} concentrations than the corresponding samples taken at 17: 00 h. Mean Ca^{2+} concentrations are higher during the accumulation period (Rhone Ca^{2+} concentrations = 4.5 x higher and Oberaar Ca^{2+} concentrations = 2.6 x higher; see Table 2.6), when discharge is 0.1- 0.3 l s^{-1}, than during the ablation period, when average monthly discharge ranges from 1000- 10'000 l s^{-1}. The trends in Ca^{2+} concentrations are representative for the other dissolved ions. Oberaar meltwater Ca^{2+} concentrations are an order of magnitude higher than Rhone meltwater ones during the 1999 and 2000 ablation periods (Fig. 2.2b) and Oberaar accumulation period samples contain approximately four times as much Ca^{2+} as equivalent Rhône samples. This is reflected in the higher mean annual pH of the Oberaar meltwaters (7.4) compared to the Rhone meltwaters (pH 6.0). The Oberaar meltwaters also have higher K^+, Mg^{2+}, SO_4^{2-}, and calculated HCO_3^- concentrations than the Rhone meltwaters whereas the Na^+, Cl^-, NO_3^-, and Si concentrations are comparable between the two areas (Table 2.6).

Two ternary diagrams show that the Oberaar meltwater compositions plot as a discrete population relative to the Rhone meltwater composition: In the Ca^{2+}-K^+-Na^+ ternary diagram the Oberaar samples are tightly grouped and plot much closer to the Ca^{2+} pole than the Rhone samples (Fig. 2.3a). Similarly in the Si-calculated HCO_3-Ca^{2+} diagram the Oberaar samples plot closer to the Ca-HCO_3 boundary, whereas silica dominantes over HCO_3^- and Ca^{2+} in most of the the Rhone meltwater samples (Fig. 2.3b).

Fluxes

The Ca^{2+}, K^+, Mg^{2+}, calculated HCO_3^- and SO_4^{2-} fluxes calculated for the Oberaar catchment are elevated compared to those calculated for the Rhone (Ca^{2+} by 5-6 times; K^+ by 1.7-2 times; Mg^{2+} by 2-2.5 times; HCO_3^- by 4-4.6 times and SO_4^{2-} by 3.8-4.5 times; Table 2.4). The ranges reflect the possible errors in the Rhone fluxes due to the calculated discharge. The Na^+, Cl^-, and Si fluxes from the two watersheds are comparable. The trend in the mean monthly Ca^{2+} flux is representative for all the dissolved ionic fluxes (Fig. 2.4). Note ablation period Ca^{2+} fluxes are 3-4 times higher than accumulation period Ca^{2+} fluxes. The Rhone calculated and measured HCO_3^- fluxes agree well, (measured = 113'610 keq km^{-2} yr^{-1}, using late October values to

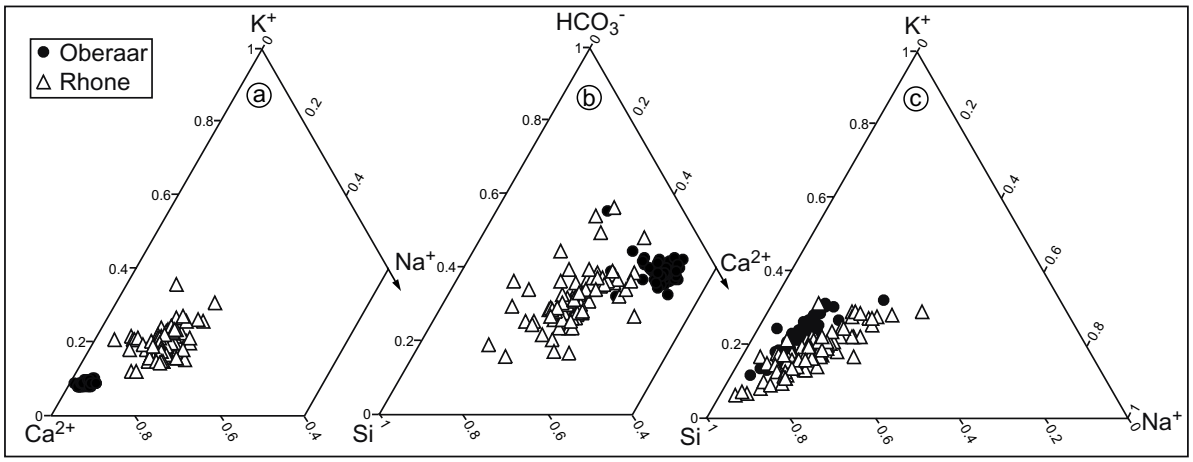

Fig. 2.3: Ternary diagrams comparing the composition of the Rhône and Oberaar meltwaters.

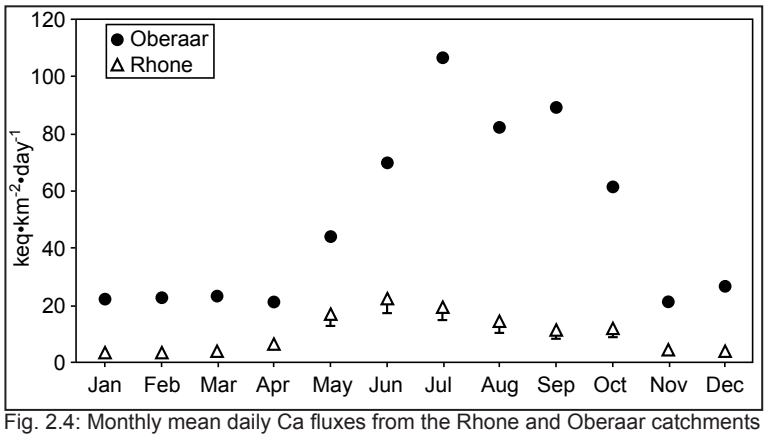

Fig. 2.4: Monthly mean daily Ca fluxes from the Rhone and Oberaar catchments (keq km^{-2} yr^{-1}).

approximate winter values; calculated = 108'638 keq km^{-2} yr^{-1}; both fluxes use Gletsch discharge corrected by 14 %). This would suggest that the error in our lab measurements is small and the calculated HCO_3^- values are robust.

Adsorbed cations

Average summer and winter adsorbed cation concentrations and annual adsorbed fluxes are shown in Table 2.7. Summer concentrations are higher than winter concentrations and the Oberaar annual adsorbed Ca flux is at least 4 times higher than the Rhone. The adsorbed fluxes represent between 2 and 10 % of the dissolved flux. These values are comparable with those of Lorrain and Souchez (1972), who measured adsorbed fluxes from the Moiry glacier catchment, Switzerland, which is also underlain by crystalline bedrock.

Discussion

Carbonate weathering

Calcium denudation appears to be much more important in the Oberaar catchment than the Rhone catchment. Ca^{2+} concentrations in the Oberaar meltwaters are consistently elevated with respect to the Rhone meltwaters and consequently have a higher mean pH and mean calculated HCO_3^- concentration (Figures 2.3a and 2.3b). During the accumulation season the Oberaar Ca^{2+} concentrations are approximately 4 times greater than the Rhone and in July, at the height of the ablation period, the mean Ca^{2+} concentration in the Oberaar meltwaters is 8 times greater than in the Rhone (Fig. 2.2b). This translates to an annual precipitation corrected Ca^{2+} flux from the Oberaar catchment which is approximately 5 times higher than from Rhone catchment (Table 2.4). The Oberaar's elevated Ca^{2+} flux cannot be due to increased plagioclase weathering, given that the suspended sediment from the two catchments contains very similar concentrations of albite (Table 2.2; XRF measurements) and the Na^+ fluxes from the two catchments are comparable (Table 2.4). Therefore other calcium bearing mineral are responsible for the elevated Ca^{2+}:Na^+ molar ratio in the Oberaar (11) relative to the Rhône meltwaters (2). The candidate minerals are amphibole, apatite and calcite, we beleive calcite is the most important as we explain below. Amphibole

	Ca^{2+}	K^+	Mg^{2+}
Oberaar			
mean ablation (µeq g^{-1})	82.34 (±45.91)	2.05 (±1.79)	2.47 (±0.82)
mean accumulation (µeq g^{-1})	27.49	1.46	0.95
keq km^{-2} yr^{-1}	40	1	1
Rhone			
mean ablation (µeq g^{-1})	< 23.95 (±19.96)*	5.88 (± 8.44)*	2.47 (± 0.82)
mean accumulation (µeq g^{-1})	< 16.97	3.36	1.25
keq km^{-2} yr^{-1}	< 8-10	2	1

* Although the blank was as high as the samples we show the calculated values to indicate the maximum possible fluxes.

Table 2.7: Adsorbed composition and fluxes.

was identified in some of the Oberaar suspended sediment samples and Stalder (1964) describes amphibolite lenses in the Oberaar catchment. We beleive that an actinolite composistion is likely (O. Müntener, Neuchatel, pers. comm.) As the peak amplitude (XRD) is less than that of calcite, this suggests that actinolite is present at concentrations of < 1%, although exact quantification is not possible. Amphibole was not detected in the Rhone suspended sediment, and therefore maybe a potential source of additional calcium in the Oberaar catchment. However, we assume that the significance of the amphibole in the Oberaar catchment is negligible because (a) it probably constitutes around 1 % of the sediment load and (b) its weathering rate (ca 10^{-15} mol m^{-2} s^{-1}; Schott et al., 1981) is ten orders of magnitude lower than that of calcite at near neutral pH. Apatite is unlikely to augment the Oberaar Ca^{2+} flux, because orthophosphate concentrations are similar in the meltwaters of the two catchments and apatite weathering is minimal at neutral pH (Stumm and Morgan, 1996). We suggest that the most likely cause of the elevated Oberaar Ca^{2+} flux is the increased mass of finely ground calcite in contact with meltwaters in the Oberaar catchment. As the modal grain size of the suspended sediment in the two catchments is between 4-8 μm and calcite tends to be concentrated in the finer size fractions (Fairchild et al., 1999) it is highly reactive in dilute meltwaters, especially as laboratory experiments show that the dissolution rate of calcite at neutral pH is ca 10^{-5} mol m^{-2} s^{-1} (Plummer et al., 1978). XRD bulk mineralogy shows that approximately 4.6 times as much calcite is present in the suspended sediment exported from the Oberaar as from the Rhone catchment (Table 2). This observation is supported by our XRF observations, which show that there is twice as much CaO in the Oberaar suspended sediments (the discrepancy is probably due to differences between the methods). In addition the average concentration of sediment in the Oberaar meltwaters is 0.31 g l^{-1} (the mean of accumulation and ablation period average concentrations), whereas the average concentration of sediment in the Rhone meltwaters is 0.07 g l^{-1}. So averaged over a year 7.1 mg l^{-1} of calcite may be in contact with meltwaters in the Oberaar catchment, compared to 0.4 mg l^{-1} in the Rhone catchment, asssuming 2.3 % and 0.5 % of the sediment is calcite. Consequently the total mass of calcite transported by the Oberaar meltwaters on an annual basis is much higher (of the order of 17.7 t km^{-2} yr^{-1}) than that transported by the Rhone meltwaters (2.5 t km^{-2} yr^{-1}). Many authors have underlined the dominant influence of calcite weathering on the chemical signature of glacial meltwaters draining crystalline catchments (e.g. Eyles et al., 1982, Drever and Hurcomb, 1986, Anderson et al., 1997, 2000, West et al., 2002). We would like to stress the extreme sensitivity of glacial systems to minor changes in the accessory calcite concentration of crystalline bedrock. The difference of less than 2 % in the calcite content of the suspended sediments of these two catchments, coupled with the increased erodability of the latter sediments, appears to increase Ca^{2+} fluxes by an order of magnitude, from 10's of keq km^{-2} yr^{-1} to 100's of keq km^{-2} yr^{-1}. Fig. 2.5 compares the Ca/Na ratios in runoff from presently glacier covered and non-glacier covered catchments with granitoid bedrock. The Rhône catchment, with it's low calcite content plots within the scatter of non-glaciated catchments, whereas the Oberaar catchment plots with other glacierised catchments whose bedrock geologies contain more carbonate minerals.

CO_2 drawdown

Total CO_2 drawdown in the catchments is calculated based on the chloride normalised fluxes (mol km^{-2} yr^{-1}) as the difference between the total dissolved inorganic carbon flux (calculated HCO_3^-; DIC_{tot}; Rhone = 109'792; Oberaar = 467'997) and the HCO_3^- flux from calcite dissolution ($DIC_{calcite}$), as one mole of HCO_3^- comes from the calcite mineral itself:

$$CaCO_3 + H_2O + CO_2 = Ca^{2+} + 2HCO^{3-}$$

We assume that $DIC_{calcite}$ is equal to the Ca flux (Ca; Rhone = 48'291; Oberaar = 277'774), minus the Ca component from the weathering of plagioclase (Ca_{plag}) and that amphibole weathering is negligable. Our plagioclase feldspar is of albitic composition (Keusen et al., 1989) therefore we assume stoichiometric dissolution and calculate Ca_{plag} as 10 % of the Na flux (Ca_{plag} ; Rhone = 2'727; Oberaar = 2'605).

$$CO_2 \text{ drawdown} = DIC_{tot} - DIC_{calcite}$$

Total CO_2 drawdown is 192'828 mol km^{-2} yr^{-1} in the Oberaar catchment and 64'299 mol km^{-2} yr^{-1} in the

Catchment	(A) Cations from calcite	(B) Cations from silicates	(C) Total cations weathered	% $Ca_{calcite}$	% $Cations_{silicate}$	(D) CO_2 drawdown	(E) Supply from aerosols and sulphides†
Rhone	45564	80945	126509	36	64	64532	102542
Oberaar	275169	127369	402538	68	32	193118	250619

	SCENARIO A				**SCENARIO B**		
Catchment	Aerosols and sulphides to weather calcite	Aerosols and sulphides to weather silicates	CO_2 to weather calcite	CO_2 to weather silicates	CO_2 to weather calcite	CO_2 to weather silicates	Total additional protons
Rhone	36932	65611	8632	15335	23242	41290	61977
Oberaar	171320	79299	103850	48069	132012	61105	209420

All cation fluxes are in eq km^{-2} yr^{-1}, CO_2 is in moles km^{-2} yr^{-1}

† Note uncorrected values are used to include acid aerosols from precipitation inputs

Table 2.8: Long-term CO_2 drawdown in the Rhone and Oberaar catchments.

Rhone catchment. The Oberaar value is comparable with CO_2 drawdown calculated for the Haut Glacier d'Arolla catchment, which has a schistose bedrock geology (1989 = 166'660 mol km^{-2} yr^{-1}; 1990 = 206'410 mol km^{-2} yr^{-1}; Sharp et al., 1995). Determining what portion of this drawdown is long-term (LT), i.e. used in the acid hydrolysis of silicate minerals is more complex. Raiswell (1984) demonstrated that acid hydrolysis reactions are largely driven by protons derived by carbonation and sulphide oxidation in the subglacial environment. Tranter et al. (1993) observed an inverse relationship beween sulphate mass fraction (SO_4^{2-}/(SO_4^{2-} + HCO_3^-); working in eq l^{-1}) and discharge at the Haut Glacier d'Arolla. They interpreted this as evidence that sulphide oxidation is the dominant proton source for subglacial acid hydrolysis reactions within distributed drainage systems and argued that sulphide oxidation and carbonate dissolution reactions are coupled (SO-CD). The observation that silica concentrations are low in such distributed systems is used to bolster their argument (Tranter et al., 2002). But, in this study silica concentrations are observed to increase by an order of magnitude during the accumulation season, implying that silicate weathering is on-going when a distributed drainage system prevails. Furthermore, a significant correlation between the sulphate mass fraction and discharge is lacking in the Oberaar and Rhone catchments (using precipitation corrected meltwater compositions), and the mean sulphate mass fractions (0.3 and 0.26 respectively) imply that weathering reactions are driven by both protons released by carbonation and sulphide oxidation reactions in the meltwaters (Tranter et al., 1993). Hodson et al. (2002) point out that assuming SO-CD leads to maximum estimates of LT CO_2 drawdown (e.g. Sharp et al., 1995). Therefore in order to estimate more realistic LT CO_2 drawdown we presume protons are shared equally between the carbonate and silicate derived cations and present minimum (A) and maximum (B) LT CO_2 drawdown scenatios (Table 2.8):

(A) = preferential weathering by protons derived from sulphide oxidation and acid aerosols, with the remainder of the cations balanced by protons derived from carbonation reactions.

(B) = preferential weathering by protons derived from carbonation and the remainder to the cation balanced by to aerosols and sulphide oxidation.

Using approach (A) 25 % and 24 % of the CO_2 drawdown is LT in the Oberaar and Rhone catchments respectively (48'069 and 15'335 mol km^{-2} yr^{-1}), whereas with approach (B) 32 % and 64 % of the CO_2 drawdown is LT (Oberaar = 61'705 mol km^{-2} yr^{-1}; Rhone = 41'151 mol km^{-2} yr^{-1}). Scenario (A), with the same proportion of LT CO_2 drawdown in both catchments, appears more likely and is in better agreement with the literature.

Silicate weathering

Silicate weathering is temperature dependant (Vebel, 1993; White and Blum, 1995). Replotting the values of White and Blum (1995) to include glacial catchments with granitoid bedrock (Fig. 2.5) shows that the silica fluxes from the Rhone and Oberaar catchments are similar to each other, and to other presently glaciated mountain basins and icesheets underlain by granitoid rocks. The silicate fluxes from the presently glaciated catchments plot amongst the lowest from the non-glaciated granitoid catchments, but they do not form a separate population (Table 2.4; Fig. 2.5). Our two catchments therefore fit into the scheme proposed

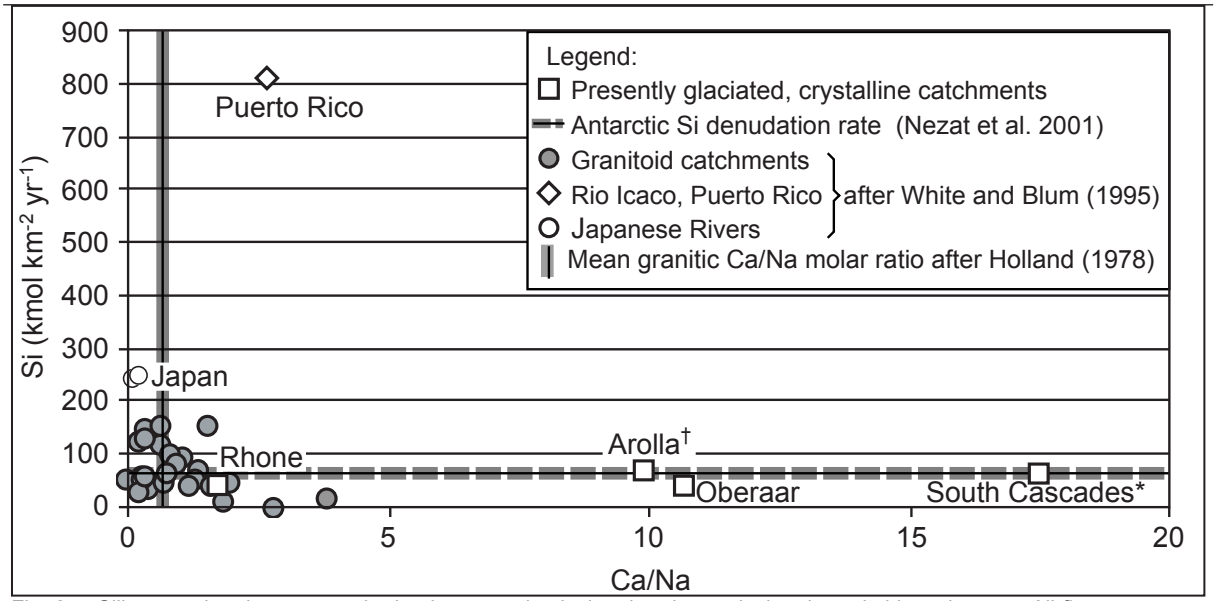

Fig. 2.5: Silicate and carbonate weathering in presently glaciated and non-glaciated granitoid catchments. All fluxes are corrected for precipitation inputs: † Sharp et al. (1995) and * Axtmann and Stallard (1995) => cyclic salt corrections; White and Blum (1995) => volumetric correction.

by Anderson et al. (1997), who used a very similar data set.

Cations derived from silicate weathering (kmol km^{-2} yr^{-1}; $\sum K^+$, Mg^{2+}, Na^+ and Ca_{plag}) are 1/3 greater from the Oberaar catchment than the Rhone (Oberaar = 99; Rhone = 65). The higher sulphide content of the Oberaar catchments bedrock contributes to the increased chemical weathering of both carbonates and silicates in the Oberaar catchment. The Oberaar's higher sulphate flux (approximately 5 times greater than the Rhone's when corrected for wet precipitation inputs) points towards a higher concentration of metal sulphides in the Oberaar catchment, which are probably associated with the strongly foliated gneissic zone. Elevated iron concentrations in the Oberaar suspended sediment (XRF data) also give an indirect indication of a higher sulphide content in the Oberaar suspended sediment compared to the Rhone. The approximately doubled Oberaar sediment flux may also be the cause of increased weathering of cations from silicate minerals

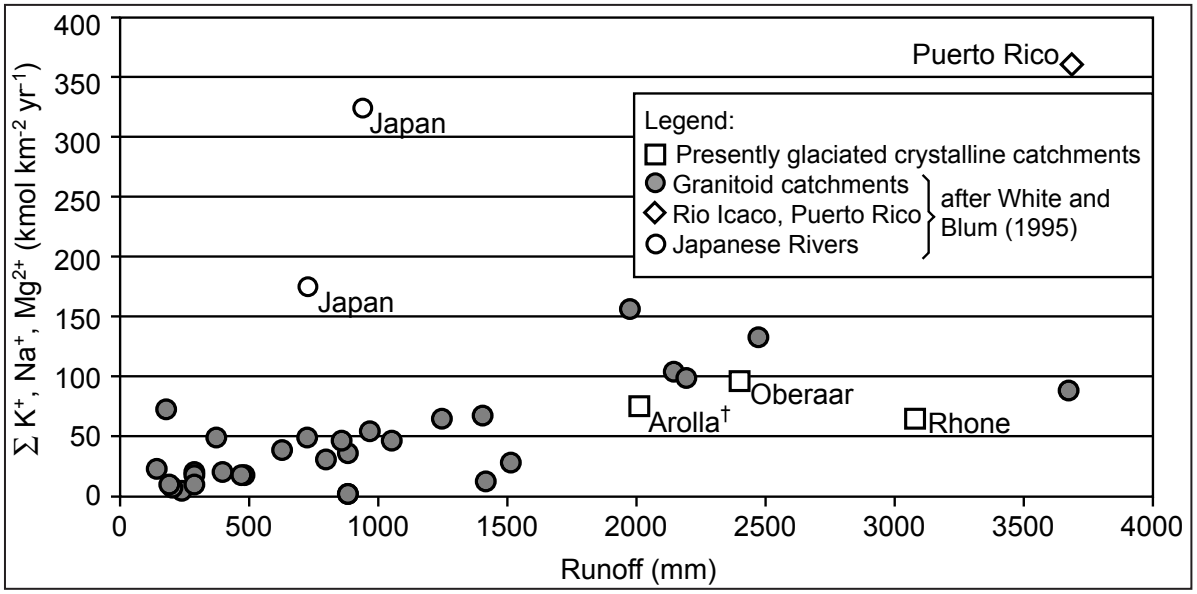

Fig. 2.6: Molar fluxes of cations derived from silicate weathering against runoff in presently glaciated and non-glaciated granitoid catchments. All fluxes are corrected for precipitation inputs: † Sharp et al. (1995) => cyclic salt corrections; White and Blum (1995) => volumetric correction.

and greater CO_2 drawdown within this catchment. We note the Oberaar K^+ flux is double the Rhone K^+ flux (Table 2.4; Fig. 2.3c; the proportion of phyllosilicates in the suspended sediments from both catchments is the same). The vermiculatisation of micas leads to the preferential release of K^+ ions in glacial waters (Drever and Hurcomb, 1986; Anderson et al., 1997). Our data indicates that the K^+ flux maybe directly proportional to the mass of phyllosilicates in suspension. The silicate derived cation fluxes ($\sum K^+, Mg^{2+}, Na^+$) from this study plot in the same range as those from non-glacial catchments with similar runoff, located at similar latitudes (Fig. 2.6; Ca_{plag} is not included, as is not known for the published data compiled in White and Blum, 1995).

Conclusions

The strongly foliated gneissic zone running down the central third of the Oberaar catchment has a major impact on physical and chemical erosion rates measured within this watershed compared to those of the the Rhone catchment, which lies on granitic and granodioritic rocks. Approximately twice as much suspended sediment is exported by the Oberaar meltwaters compared to the Rhone meltwaters during the study period (1999-2001), due to the greater erodability of the Oberaar catchment. This greater erodability, coupled with the larger mean calcite content of the Oberaar suspended sediment (2.3 % compared to 0.5 % for the Rhone suspension), the presence of amphibole and 5 times more sulphide derived sulphate in the Oberaar catchment, leads to 5 times more dissolved calcium being denuded from the Oberaar watershed, most of which comes from carbonate dissolution. Calcite weathering is more important in this glacial catchment than in non-glaciated catchments underlain by granitoid rocks (judging by the Ca/Na molar ratios; Fig. 2.5). Yet the silicate weathering rates we observe in our presently glaciated alpine catchments and those which are published for other glaciated alpine and Antarctic catchments fall within the range of temperate, non-glaciated granitoid catchments with the same runoff implying that silicate weathering is not accelerated in the subglacial environment.

Acknowledgements

We thank Daniel Arn, David Nisbet, Katharine Nisbet, and Marlen Schaller for field support and Giulio Galetti, Khaoula Hamila and Sebastian Ryser for laboratory assistance. This study was supported by Swiss National Science Foundation grants 21-53991.98. and 20-61485.00.

References

Adatte, T., Stinnesbeck, W., and Keller, G., 1996. Lithostratigraphic and mineralogical correlations of near K/T boundary clastic sediments in northeastern Mexico: Implications for origins and nature of deposition. In: G. Ryder, D. Fastovsky and S. Gartner (Editors), The Cretaceous-Tertiary event and other catastrophes in Earth history. Sp. Papers Geol. Soc. Of America, 307, 211-226.

Anderson, S.P., Drever, J.I., and Humphery, N.F. ,1997. Chemical weathering in glacial environments. Geology, 25, 399-402.

Anderson, S.P., Drever, J.I., Frost, C.D. and Holden, P., 2000. Chemical weathering in the foreland of a retreating glacier. Geochimica Cosmochimica Acta, 64, 1173-1189.

Axtmann, E.V. and Stallard, R.F., 1995. Chemical weathering in the South Cascade Glacier basin, comparison of subglacial and extra-glacial weathering. In: K. A. Tonnessen, M. W. Williams and M. Tranter (Editors), Biogeochemistry of seasonally snow-covered catchments. International Association of Hydrological Sciences Publication 228, 431-439.

Bernath, A., 1991. Zum Wasserhaushalt im Einzugsgebiet der Rhone bis Gletsch. Züricher Geographische Schriften, 43, pp. 383.

Blum, A.E., 1994. Feldspars in weathering. In: I. Parson (Editor), Feldspars and their reactions. NATO Advanced Study Inst., Kluwer Academic, Netherlands, pp. 595-629.

Boulton, G.S., 1979. Processes of glacier erosion on different substrata. Journal of Glaciology 23, 15-38.

Dreimanis, A. and Vagners, U. J., 1969. Characteristics of the composition of till derived from the basal and the englacial drift. Geological Society of America

Bulletin, 6, 12.

Dreimanis, A. and Vagners, U.J., 1971. The dependence of the composition of till upon the rule of bimodal distribution. In: Etudes sur le Quaternaire dans le Monde, 2, Bulletin de l'Association Francaise pour l'Etude du Quaternaire 4, pp. 787-789.

Drever, J.I. and Hurcomb, D.R., 1986. Neutralization of atmospheric acidity by chemical weathering in an alpine drainage basin in the North Cascade Mountains. Geology 14, 221-224.

Drewry, D., 1986. Glacial Geological Processes. Edward Arnold Ldt., London, pp 276.

Eyles, N., Sassevilee, D.R., Slat,t R.M. and Rogerson, R.J., 1982. Geochemical denudation rates and solute transport mechanisms in a maritime temperate glacier basin. Canadian Journal of Earth Sciences, 19, 1570-1581.

Fairchild, I.J., Bradby, L., Sharp, M. and Tison, J-L., 1994. Hydrochemistry of carbonate terrains in Alpine glacial settings. Earth Surface Processes and Landforms, 19, 33-54

Fairchild, I.J., Killawee, J.A., Hubbard, B. and Derybrodt, 1999. Interactions of calcareous suspended sediment with glacial meltwater: A field test of dissolution behaviour. Chemical Geology, 155, 243-263.

Federal Office for Water and Geology, 1994. Technischer Bericht: Manual für die Abflussmessung nach dem Salzverdünnungsverfahren. pp. 23.

Gibbs, M.T. and Kump, L.R., 1994. Global chemical erosion during the Last Glacial Maximum and the present: Sensitivity to changes in lithology and hydrology. Paleoceanography, 9, 529-543.

Gurnell, A.M., Brown, G.H. and Tranter, M., 1994. Sampling strategy to describe the temporal hydrochemical characteristics of an alpine proglacial stream. Hydrological Processes, 8, 1-25.

Hallet, B., Hunter, L. and Bogen, J., 1996. Rates of erosion and sediment evacuation by glaciers: A review of field data and their implications. Global and Planetary Change, 12, 213-235.

Hay, W.W., 1998. Detrital sediment fluxes from continents to oceans. Chemical Geology 145, 287-323.

Hoch, A.R., Reddy, M.J. and Drever, J.I., 1999. Importance of mechanical disaggregation in chemical weathering in a cold alpine environment. Geological Society of America Bulletin, 2, 304-314.

Hodson, A., Tranter, M. and Vatne, G., 2002. Contemporary rates of chemical denudation and atmospheric CO_2 sequestration in glacier basins: an Arctic perspective. Earth Surface Processes and Landforms 25, 1447-1471.

Holland, D.H., 1978. The chemistry of the Atmosphere and the Oceans. Wiley-Interscience, New York, pp 351.

Keusen, H.R., Ganguin, J., Schuler, P., Buletti, M., 1989. Felslabor Grimsel, Geologie. NAGRA technischer Bericht, 87-14, pp. 120.

Kübler, B., Jantschik, R. and Houn, S., 1990. Minérologie et granulométrie des poussières éoliennes, dites "Sahariennes", du 24 avril 1989 à Neuchâtel. Leur importance pour l'environnment, les sols et les sédiments. Bulletin de la Société neuchâteloise des Sciences naturelles, 113, 75-98.

Lenaz, R., Landuzzi, V. and Tomadin, L., 1986. Apports et concentration des masses de poussières éoliennes sur le bassin oriental et occidental de al Méditerranée. Mem. Soc. Geol. It. 36, 189-200.

Livingstone, D.A., 1963. Chemical compositions of rivers and lakes. U.S. Geological Survey Professional Paper 440-G, 64 pp.

Lorrain, R.D. and Souchez, R.A., 1972. Sorption as a factor of in the transport of major cations by meltwaters from an Alpine glacier. Quaternary Research 2, 253-256.

Ludwig, W., Amiotte-Suchet, P., Munhoven, G. and Probst, J.-L., 1998 Atmospheric CO_2 consumption by continental erosion: present-day controls and implications for the Last Glacial Maximum. Global and Planetary Change, 16, 107-120.

Mahaney, W.C., 1995. Glacial crushing, weathering and diagenetic histories of quartz grains inferred from scanning electron microscopy. In: John Menzies (Editor): Modern glacial environments. Processes, Dynamics and Sediments in Glacial Environments, Volume 1, xx-xx.

Meybeck, M., 1987. Global chemical weathering of surficial rocks estimated from river dissolved loads. American Journal of Science, 287, 401-428.

Mullin, J. and Riley, J.P., 1955. The colorimetric determination of silicate with special reference to sea and natural waters. Analytica Chimica Acta, 27, 162-176.

Nezat, C.A, Lyons, B.W. and Welch, K.A., 2001.

Chemical weathering in streams of a polar desert (Taylor Valley, Antarctica). Geological Society of America Bulletin, 113, 1401-1408.

Nienow, P., Sharp, M. and Willis, I., 1996. Temporal switching between englacial and subglacial drainage pathways: Dye tracer evidence from the Haut Glacier d'Arolla, Switzerland. Geografiska Annaler 78, 51-59.

Oberhänsli, R. and Schenker, F., 1988. Indications of Variscan nappe teconics in the Aar Massif. Scheizerische Mineralogisch Petrographische Mitteilungen, 68, 509-520.

Plummer, L. N., Wigley, T. M. L., and Parkhurst, D.L., 1978. The kinetics of calcite dissolution in CO_2-water systems at 5-60°C and 0.0-1.0 atm CO_2. American Journal of Science, 278, 179-216.

Raiswell, R., 1984 Chemical models of solute aquisition in glacial meltwaters. Journal of Glaciology, 30, 49-57.

Schott, J., Berner, R.A. and Sjoberg, E.L., 1981. Mechanism of pyroxene and amphibole weathering – I. Experimental studies of iron-free minerals. Geochimica et Cosmochimica Acta, 45, 2123-2135.

Schwab, M., Frei, C., Schär, C. and Daly, C., 2001 Mean annual precipitation throughout the European Alps 1971-1990. In: Federal Office for Water and Geology (Editor), The Hydrological Atlas of Switzerland. Federal Office for Topography, Bern.

Slatt, R.M., 1972. Geochemistry of meltwater streams from nine Alaskan glaciers. Geological Society of America Bulletin, 83, 1125-1132.

Sharp, M., Tranter, M., Brown, G.H. and Skidmore, M., 1995. Rates of chemical denudation and CO_2 draw down in a glacier-covered alpine catchment. Geology, 23, 61-64.

Sharp, M., Parkes, J., Cragg, B., Fairchild, I.J., Lamb, H. and Tranter, M., 1999. Widespread bacterial populations at glacier beds and their relationship to rock weathering and carbon cycling. Geology, 27, 107-110.

Souchez, R.A. and Lemmens, M.M., 1987. Solutes. In: A.M. Gurnell and M.J. Clark (Editors), Glacio-fluvial sediment transfer: An alpine perspective. John Wiley & Sons, New York, pp. 285-303.

Stadler, H. A., 1964. Petrographische und mineralogische Untersuchungen im Grimselgebiet (Mittleres Aarmassiv). Schweizerische Mineralogische und Petrographische Mitteilungen, 44, 187-389.

Stumm, W. and Morgan, J.J., 1996. Aquatic Chemistry. Wiley Interscience, New York, pp. 1022.

Sugden, D.E., 1978. Glacial erosion by the Laurentide ice sheet. Journal of Glaciology, 20, 367-394.

Tranter, M., Brown, G., Raiswell, R., Sharp, M. and Gurnell, A., 1993. A conceptual model of solute acquisition by Alpine glacial meltwaters. Journal of Glaciology, 39, 573-581.

Tranter, M., Sharp, M.J., Lamb, H.R., Brown, G.H., Hubbard, B.P. and Willis, I.C., 2002. Geochemical weathering at the bed of Haut Glacier d'Arolla, Switzerland – A new model. Hydrological Processes 16, 959-993.

Vebel, M.A., 1993. Temperature dependence of silicate weathering in nature: How strong a negative feedback on longterm accumulation of atmospheric CO_2 and global greenhouse warming? Geology 21, 1059-1062.

West, J.A., Bickle, M.J., Collins, R. and Brasington, J., 2002. Small-catchment perspective on Himalayan weathering fluxes. Geology, 30, 355-358.

White, A.F. and Brantley, S.L., 1995. Chemical weathering rates of silicate minerals: An overview. In: A.F. White and S.L. Brantley (Editors), Chemical weathering of Silicate Minerals. Reviews in Mineralogy, 31, p. 1-21.

White, A.F., Blum, A.E., Bullen, T.D., Vivit, D.V., Schulz, M.S. and Fitzpatrick, J., 1999a. The effect of temperature on experimental and natural chemical weathering rates of granitoid rocks. Geochimica et Cosmochimica Acta, 63, 3277-3291.

White, A.F., Bullen, T.D., Vivit, D.V., Schulz, M.S., and Clow, D.W., 1999b. The role of disseminated calcite in the chemical weathering of granitoid rocks. Geochimica et Cosmochimica Acta 63, 1939-1953.

CHAPTER 3

Chemical weathering in a glacial chronosequence in the forefields of Rhone and Oberaar Glaciers (Swiss Alps): Rate and mechanism of biotite weathering

Abstract

We analysed the clay mineralogy of glacial sediments in the two catchment areas of the Rhone and Oberaar glaciers (Swiss Alps) using XRD techniques, in order to identify processes and rates of alteration of moraine material in the glacier forefield. The well-dated sediments provide a chronosequence consisting of (A) recent suspended sediment in meltwater; (B) terminal moraines dating from the Little Ice Age (LIA 1300-1850); and (C) tills dating from the retreat of Younger Dryas (YD 11'600 y BP). The suspended sediment is derived from mechanically abraded freshly eroded bedrock without being stored and altered subglacially and secondary weathering products have not been observed. Chemical weathering becomes increasingly important once glacial sediment is deposited in the proglacial area. With increasing age a vegetation cover develops on the morainic deposits and the initial umbrepts undergo podzolisation. XRD data in this chronosequence show an increase in pedogenically formed vermiculite and a continuous decrease in biotite with increasing sediment age. Biotite contents in the top 30 cm of the soils decrease by 25 – 50 % within 140 – 270 years. Feldspar weathering becomes apparent in proglacial sediments older than 270 years.

Biotite weathering rates were calculated using the difference in biotite content between the C-horizon and the top 30 cm of a soil profile. Reactive mineral surface areas were estimated geometrically, for their total as well as for their edge surface. The weathering rates obtained using the total mineral surface area (WR_T) are in the order of 10^{-10} – 10^{-12} $mol_{biotite}$ m^{-2} sec^{-1}. The weathering rates using the edge surface area (WR_E) are in the order of 10^{-10} – 10^{-11} $mol_{biotite}$ m^{-2} sec^{-1}. The calculated rates are several orders of magnitude faster than known field weathering rates. This is related to: (1) The predominance of fine-grained particles (<63 μm) in glacial sediment which are mechanically disaggregated and preferentially leached; and (2) The studied glacial sediments are well drained and highly permeable and no heterogeneities in flow paths through soils were observed. We suggest that glacially derived material is subjected to enhanced chemical weathering, starting immediately after deposition in the proglacial zone and subsequently continuing for thousands of years after glacier retreat.

Introduction

Glaciers are important agents of physical erosion and glacial abrasion produces a considerable fraction of fine-grained sediment (<63 μm). The high surface: mass ratio and the presence of strained minerals in this fraction condition the material for subsequent chemical weathering. This process begins immediately after erosion and mobilisation in the subglacial domain of temperate glaciers (e.g. Tranter et al., 1993, Gurnell et al., 1994, Sharp et al., 1995, Anderson et al., 1997, Fairchild et al., 1999, and Hosein et al., submitted). It may also continue once the sediment is beyond the glacier margins, within proglacial deposits such as moraines and alluvial plains where chemical weathering may be intensified after glacier retreat (Anderson et al., 2000).

The interest in chemical weathering processes in glacial domains is related to its impact on the global carbon cycle: directly, by the consumption of atmospheric CO_2 during silicate weathering, as well as indirectly, by the mobilisation of nutrients such as phosphorus, iron, potassium, and calcium, which regulate productivity rates and photosynthetic uptake of atmospheric CO_2 (Sharp et al., 1995, Föllmi, 1995, and

This chapter by Kaspar Arn, Rachel Hosein, Thierry Adatte, Philipp Steinmann, and Karl B. Föllmi has been submitted for publication in *Chemical Geology*.

Hallet et al., 1996). A better understanding of changes in the global carbon cycle related to glacial periods depends, therefore, on a better understanding of chemical weathering processes in glaciated areas and glacial sediments of different ages. Extensive literature exists on soil development in glacially derived sediments in chronosequences (e.g., Claridge and Campbell, 1984, Birkeland et al., 1987, Lidmar-Bergström et al., 1999, Righi et al., 1999, and Egli et al., 2001).

In glacial environments the vermiculitisation of biotite leads to the preferential release of K^+ ions in glacial meltwaters (Drever and Douglas, 1986, Anderson et al., 1997). Biotite as the source of K^+ could hold as a proxy of chemical weathering in glacial regimes. Biotite field weathering rates in different climatic regimes are commonly calculated by a mass balance method (e.g., Swoboda-Colberg and Drever, 1993, Nagy, 1995, Murphy et al., 1998). Reported laboratory based biotite weathering rates are calculated for different conditions (Table 3.6b); they are normally two to three orders of magnitude higher than field rates (e.g., Velbel, 1993a, Turpault and Trotignon, 1994, Nagy, 1995, Kalinowski and Schweda, 1996).

In this contribution we studied the forefields of the Rhone and Oberaar glaciers, located in the Swiss Alps (Fig. 3.1). The areas experience similar climatic conditions and underwent comparable deglaciation phases in the Holocene. Both glaciers are presently subjected to considerable retreat and loss in volume. Both areas are contained within the crystalline rocks of the Aar Massif (Stalder, 1964, and Abrecht, 1994; Fig. 3.1). The lithologies are quite homogeneous and comparable (Table 3.1), except for the presence of a zone of highly deformed Variscan basement gneisses and schists in the Oberaar catchment area (Oberhänsli et al., 1988).

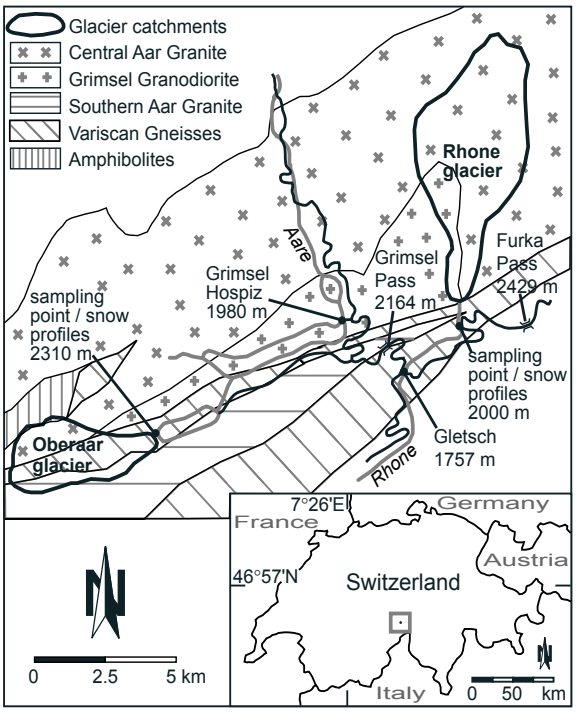

Fig. 3.1: Map of the field areas with geology of the Aar Massif modified after Oberhänsli et al. (1988) and todays glacier catchments.

The goals of this study are threefold: 1) To reconstruct processes and timing of weathering of primary minerals in the proglacial zone; 2) to calculate biotite

	Oberaar			Rhone		
Geographical position	46° 32' N 8° 14' E			46° 35' N 8° 23' E		
Surface of catchment	11.2 km2			23 km2		
Altitude	2310 - 3631 m above sea level (a.s.l.)			1750 - 3630 m a.s.l.		
Glacier cover today (%)	57%			73%		
Annual mean temperature *	- 1° C[§]			+ 1.2° C[§]		
Annual mean precipitation *	2100 mm			2200 mm		
Geology of catchments:	Today	LIA	YD	Today	LIA	YD
Central Aar Granite	38%	38%	25%	90%	82-86%	40%
Grimsel Granodiorite	7%	7%	12%	10%	8-9%	20%
Variscan gneisses	42%	42%	38%		10-5%	20%
Ultramafic Inclusions	1%	1%	1%			
Southern Aar Granite	12%	12%	24%			
Mesozoic metasediments						20%

* Schwab etal., 2001
[§] within proglacial area; 2300 m at Oberaar, 1757 m at Rhone.
LIA Little Ice Age; YD Younger Dryas

Table 3.1: Different parameters of the two catchments. For geology see also Fig. 3.1.

weathering rates based on the decreasing biotite content of soil profiles over 100s to 1000s of years; and 3) to consider the impact which glaciers may exert on global weathering rates.

Sampling sites

Two profiles (O_{140A} and O_{140B}; Fig. 3.2) were dug in a moraine ridge that was deposited during the maximum extent of the Little Ice Age (LIA) within the Oberaar catchment (1860, Ammann, 1977). Another profile (O_{YD}) was dug within a patchy till cover beyond the extent of the LIA-moraines: This till is interpreted to date back to the retreat of the glacier after the Younger Dryas (YD; 11'600 BP; C. Schlüchter, Berne, pers.comm.). Hormes et al. (2001) show evidence for eight Holocene phases of reduced glacier extent in the area of the Unteraargletscher, a glacier catchment adjacent to the Oberaar. Their first post YD phase of glacier contraction, with glaciers smaller than at present, occured 9910-9550 cal yr BP (14-C dated woods). "YD" is used in this work as age for glacial sediments dating back to this first post YD phase. Vegetation cover in the proximal forefield of the Oberaar glacier (ca. 2300 m above sea level, a.s.l.) consists of pioneer plants typical for proglacial areas that recently freed from ice. Some alpine meadows and peat lands appear in the more distal parts (Ammann, 1977).

The maximum extent of the Rhone glacier during the Little Ice Age (LIA) was around 1600 (Zumbühl, 1988). Two profiles (R_{270A}, and R_{270B}; Fig. 3.2) were dug in moraine ridges dating from the beginning of the 18th century, and one profile (R_{145A}) was made in the terminal moraine dating from 1856. A further profile (R_{YD}; Fig. 3.2) was dug in a patchy till cover in a scoured morphology beyond the limits of LIA, which also dates back to the retreat of YD, as described in the Oberaar catchment. The vegetation in the glacier forefield (at 1750 m a.s.l.) mainly consists of alpine meadows and peat lands with alder bushes.

Soil profiles

The LIA profiles are located on the crest of moraine ridges. All moraine profiles show a sandy to silty texture and contain some clay, and the YD profiles are not significantly enriched in clays. The general grainsize distribution implies a good porosity , allowing precipitation to percolate through the tills. Soil description are given in Table 3.2 (the names of soil types and horizons are given according to USDA, 1998, USDA, 1999; soil types are also given according to the recommendations of A.F.E.S., 1998).

The young soils dating back to 1856 – 1860 are best described as orthent (entisols) or "regosols" after USDA and AFES, respectively: In these profiles (O_{140A}, O_{140B}, R_{145A}) an organo-mineral Ah horizon of 5 cm was observed which overlies a transition zone (AC) of 30 – 40 cm and the unweathered C-horizon. A Bw horizon could not be distinguished with certainty. The 270 year old soils (R_{270A}, R_{270B}) were found to be umbrebts (inseptosols) or "brunisol oligosaturé" after USDA and AFES, respectively: An organo-mineral Ah horizon (5 cm) covers a 10 to 15 cm thick Bw horizon. The underlying transition zone reaches down to at least 50 cm. Within the top 30 cm of all the LIA profiles the root density is high and the moraines are of a browny (top) to rusty color. Below 30 – 40 cm the moraines look fresh and grey in color, and roots rarely reach below 30 – 40 cm.

The oldest soils dating back to the retreat of the YD are humods (spodosols) or "podzosols ocriques" after USDA and AFES, respectively. The YD profiles from both areas are strongly weathered throughout. In profile O_{YD} (Oberaar) a discontinuous E horizon of 10 cm thickness is present under a 5 cm thick Oh and a 5 – 10 cm thick Ah horizon. Below that a Bhs (at 20 – 30 cm depth) overlies a Bw horizon (at 30 – 60 cm depth). At 60 cm depth the profile reaches unweathered consolidated bedrock (R). In profile R_{YD} (Rhone) a typical E horizon of 10 cm thickness is present under a 10 cm thick Ah horizon. Below that a Bhs (at 20 – 40 cm depth) overlies a Bw horizon (at 40 – 70 cm depth). Between 30 and 40 cm depth a rusty layer is visible, pointing to the periodic existence of a water layer. At the bottom of the YD profiles is a Bw horizon, and a C horizon could not be distinguished. The top 30 cm of these profiles are organic rich and of a dark brownish color (matrix) including lighter zones. Below that the soil is of a rusty color and some roots reach down to the bottom of the profiles. The clasts are strongly weathered and decay easily.

	Oberaar glacier forefield							**Rhone glacier forefield**									
Soiltype †	**Orthent (Entisols)**				**Humod (Spodosols)**			**Orthent (Entisols)**			**Umbrebt (Inseptisols)**				**Humod (Spodosols)**		
"Référence" §	**Regosol (140 y)**				**Podzosol ocrique (10 ky)**			**Regosol (145 y)**			**Brunisol oligosaturé (270 y)**				**Podzosol ocrique (10 ky)**		
sample depth	soil depth	soil	O_{140A}	O_{140B}	soil depth	soil	O_{YD}	soil depth	soil	R_{145A}	soil depth	soil	R_{270A}	R_{270B}	soil depth	soil	R_{YD}
(cm)	(cm)	horizon†	pH	pH	(cm)	horizon†	pH	(cm)	horizon†	pH	(cm)	horizon†	pH	pH	(cm)	horizon†	pH
		Oh			0-5	Oh			Oh			Oh				Oh	
0-10	0-5	Ah	5.4	7.6	5-10	Ah	6.7	0-5	Ah	5.0	0-5	Ah	4.6	4.6	0-10	Ah	n.a.
10-20	5-30	AC	6.3	6.7	10-20	E	6.5	5-30	AC	5.2	5-20	Bw	4.8	4.7	10-20	E	5.4
20-30			6.7	6.6	20-30	Bhs	6.1			6.0	20-30	BwC	4.9	5.3	20-30	Bhs	5.4
30-40	30-	C	7.1	6.6	30-40	Bw	5.5	30-	C	6.4	30-40	(Bw)C	5.9	6.0	30-40	Bhs *	5.5
40-50			7.2	6.6	40-50	Bw	5.7			6.6	40-	C	6.0	6.1	40-50	Bw	5.5
50-60			7.2	7.1	50-60	Bw	5.8			6.5			6.1	6.5	50-60	Bw	5.9
60-70			7.7	7.5		R				6.4			6.2	n.a.	60-70	Bw	5.8
70-80			7.9	7.2						6.5			6.3	6.5			
80-90			8.2	7.1						6.7			6.5				
90-100			8.1	6.9						6.9			6.2				

† USDA (1998, 1999)

§ A.F.E.S. (1998)

* former water layer visible (rusty rocks)

n.a. not analysed

Table 3.2: Chronosequence parameters.

Laboratory methods

Integrated samples (2 – 3 kg) were taken in soil profiles every 10 cm down to a depth of 60 – 100 cm. The measured parameters of each 10 cm slice were averaged for the top 30 cm and for the bottom 20 – 30 cm, which corresponds to the C-horizon for the LIA profiles. This division was used because of the significant transitions observed at 30 cm depth in all profiles: The rhizosphere is restricted to the top 30 cm layer, and changes in clay mineralogy, pH, and colour of the samples are observed at this limit as well. Suspended sediment was collected from both glaciers during the two ablation seasons (1999 and 2000) by filtering meltwaters through 0.45 μm cellulose-acetate filters in the field. Bedrock was randomly sampled within the areas.

All samples were analysed at the GEA laboratory of the Geological Institute of the University of Neuchatel. Prior to analysis samples were oven-dried at 40 °C and divided into subsamples. Granulometric analyses of the glacial sediments were performed using sieving sizes of 4 cm to 63 μm and the fraction < 63 μm was analysed on a Granulometry Laser Oriel CIS, together with the suspended sediment samples. Bulk rock and clay mineralogy of the samples were analysed following the procedure of Adatte et al. (1996). Approximately 20 g of each bedrock sample was ground with a "jaw" crusher to obtain small chips (1 to 5 mm). Approx. 5 g of dried glacial sediment and bedrock chips were ground to a homogenous powder with particle sizes <40μm.

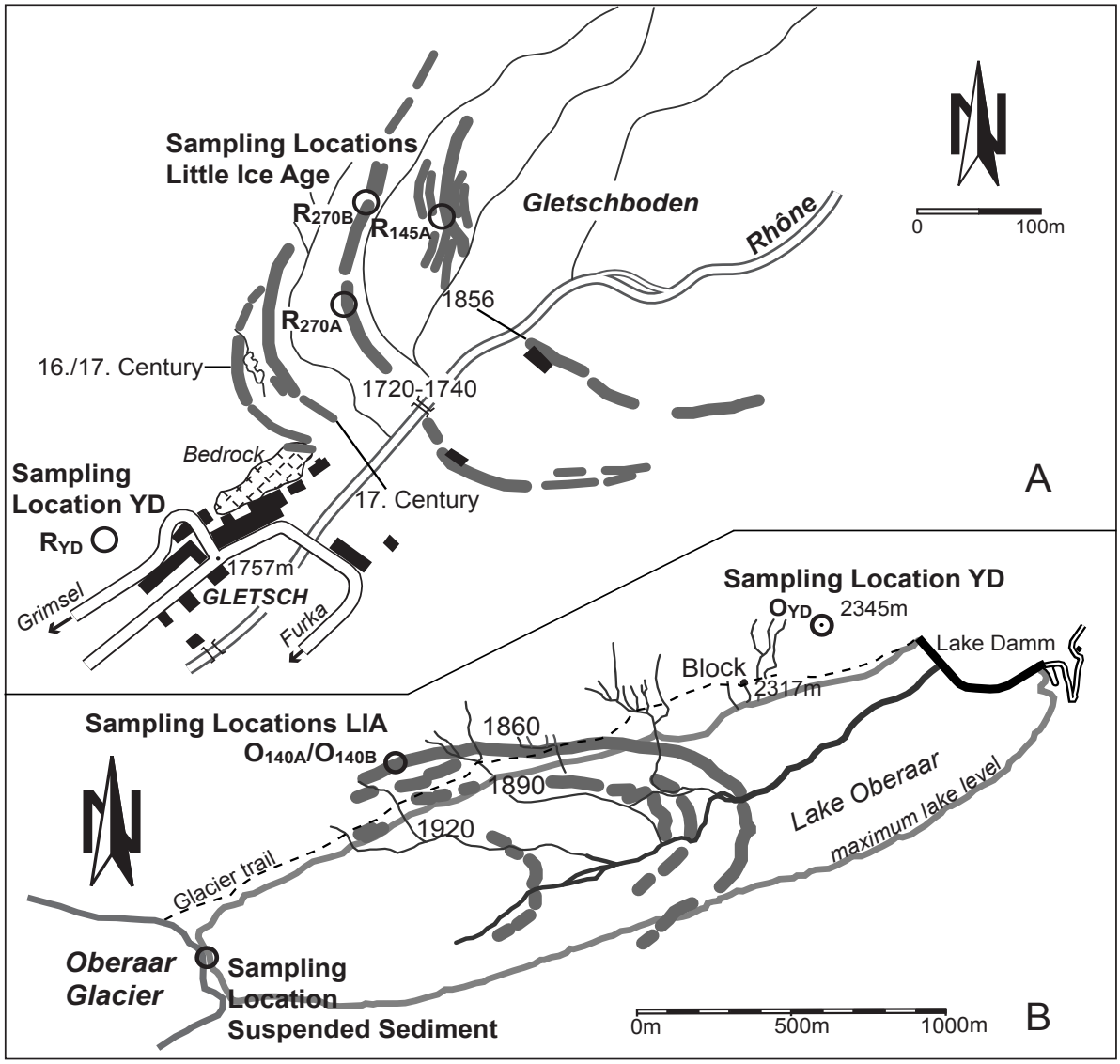

Fig. 3.2: Situation maps of glacier forefields: (A) Rhone after Zumbühl (1988), and (B) Oberaar after Ammann (1977).

800 mg of this powder were pressed (20 bars) in a powder holder covered with blotting paper and analysed by XRD. Bulk rock composition was determined by XRD (SCINTAG XRD 2000 Diffractometer) based on methods described by Klug and Alexander (1974), Kübler (1983), and Adatte et al. (1996). This method for the semi-quantitative analysis of the bulk rock mineralogy uses external standards.

Separation of different grain-size fractions (< 2μm and 2-16 μm) for clay mineralogy analysis of glacial sediments and dust was obtained by centrifugation using the time-settling method based on Stokes law. Each fraction was pipetted onto a glass plate and air-dried at room temperature. The analyses were performed with a SCINTAG XRD 2000 Diffractometer. The intensities of selected XRD peaks characterising each clay mineral present in the size fraction (chlorite, phengite, biotite, biotite-vermiculite mixed-layers, and vermiculite) were measured. Detection limit is ca. 0.3 %. In the 2-16 μm fraction also quartz, K-feldspar, plagioclase, and calcite were measured. Mineral ratios were calculated using raw intensity data (peak heights). Determination of biotite-vermiculite mixed-layers is achieved by the method of Moore and Reynolds (1997). Peaks of biotite (B001), phengite (P001), vermiculite (V001), and biotite-vermiculite mixed layers (B-V001) have been obtained by deconvolution of the 5-10 ° 2θ – interval, by using a Pearson seven function. The samples were pretreated with ethylene-glycol solvation and heated to 450° C. Positions of peaks of vermiculite and biotite-vermiculite mixed layers did not move in the glycol sample and collapsed to 10 Å in the heated one (Fig. 3.3).

Soil pH was measured with a glass electrode on 1:1

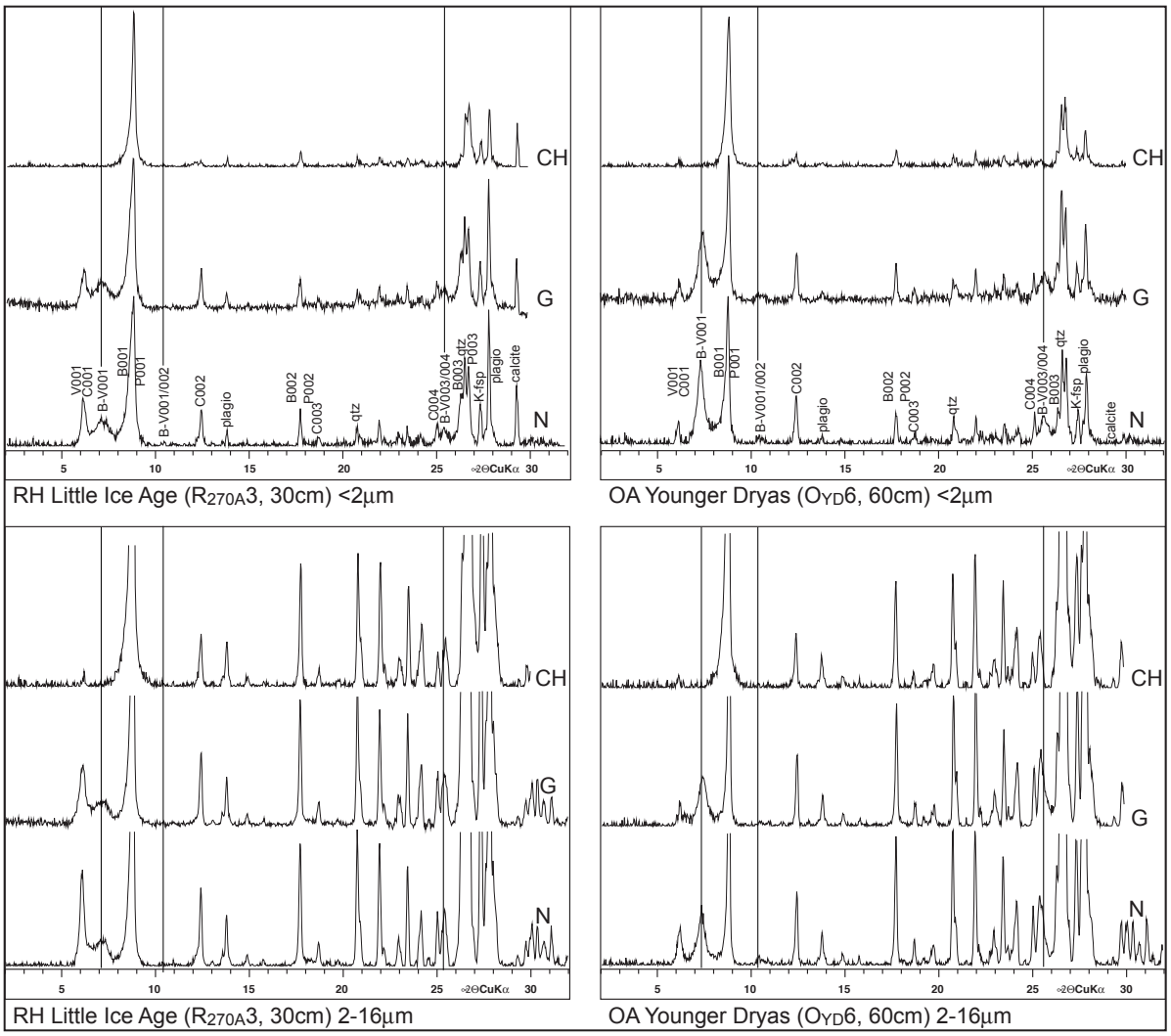

Fig. 3.3: XRD-plots after different pretreatments (<2 µm and 2-16 µm fraction of samples $R_{270A}3$ and $O_{YD}6$): (N) normal, air dried; (G) ethylen-glycol solvation; (CH) heated for two hours at 450 °C; see text for discussion.

Age	Sample	Depth	fraction < 2µm		fraction 2-16µm				
			v + bv / biotite	biotite/ phengite	v + bv / biotite	biotite/ phengite	qtz/K-fsp	qtz/plagio	cc/qtz*
Oberaar moraine samples									
LIA	$O_{140A}1$	0-10	0.592	0.755	0.487	0.309	0.160	0.027	n.d.
140y	$O_{140A}2$	10-20	0.396	0.745	0.540	0.449	0.444	0.071	n.d.
	$O_{140A}3$	20-30	0.577	0.733	0.311	0.435	0.264	0.042	0.149
	$O_{140A}4$	30-40	0.521	0.794	0.373	0.474	1.243	0.128	0.202
	$O_{140A}5$	40-50	0.372	0.652	0.267	0.522	0.316	0.037	0.068
	$O_{140A}6$	50-60	0.527	0.670	0.370	0.353	0.074	0.014	0.076
	$O_{140A}7$	60-70	0.307	0.924	0.187	0.689	0.479	0.078	0.254
	$O_{140A}8$	70-80	0.472	0.929	0.182	0.622	0.210	0.035	0.168
	$O_{140A}9$	80-90	0.321	0.953	0.189	0.538	0.362	0.045	0.095
	$O_{140A}10$	90-100	0.556	0.907	0.264	0.544	0.159	0.040	0.264
Av.	Top <30	0-30	0.522	0.744	0.446	0.398	0.290	0.047	0.149
	stdev		*0.109*	*0.011*	*0.120*	*0.077*	*0.144*	*0.022*	
Av.	Bottom C	>70	0.449	0.929	0.211	0.568	0.244	0.040	0.175
	stdev		*0.119*	*0.023*	*0.045*	*0.047*	*0.106*	*0.005*	*0.085*
LIA	$O_{140B}1$	0-10	1.483	0.311	0.339	0.608	0.519	0.091	0.042
140y	$O_{140B}2$	10-20	0.612	0.412	0.663	0.359	0.445	0.047	0.034
	$O_{140B}3$	20-30	1.051	0.540	0.726	0.321	0.837	0.107	0.047
	$O_{140B}4$	30-40	0.186	1.179	0.410	0.303	0.249	0.043	0.052
	$O_{140B}5$	40-50	0.184	1.945	0.236	0.509	0.215	0.031	0.148
	$O_{140B}6$	50-60	0.164	1.697	0.275	0.497	0.272	0.033	0.065
	$O_{140B}7$	60-70	0.147	1.930	0.118	0.548	0.147	0.022	0.033
	$O_{140B}8$	70-80	0.083	0.856	0.288	0.544	0.516	0.090	0.056
	$O_{140B}9$	80-90	0.339	0.555	0.193	0.653	0.235	0.038	0.087
	$O_{140B}10$	90-100	0.220	1.422	0.232	0.556	0.317	0.059	0.057
Av.	Top <30	0-30	1.049	0.421	0.576	0.430	0.600	0.082	0.041
	stdev		*0.435*	*0.115*	*0.208*	*0.156*	*0.208*	*0.031*	
Av.	Bottom C	>70	0.214	0.944	0.238	0.584	0.356	0.062	0.067
	stdev		*0.128*	*0.440*	*0.047*	*0.060*	*0.145*	*0.026*	*0.018*
YD	$O_{YD}1$	0-10	1.343	0.332	0.593	0.399	1.176	0.948	n.d.
10ky	$O_{YD}2$	10-20	1.274	0.142	0.316	0.311	0.086	0.046	n.d.
	$O_{YD}3$	20-30	3.592	0.247	0.498	0.359	3.302	0.461	0.027
	$O_{YD}4$	30-40	2.737	0.371	2.191	0.193	1.031	0.317	0.070
	$O_{YD}5$	40-50	1.816	0.291	0.974	0.303	0.459	0.152	0.116
	$O_{YD}6$	50-60	1.631	0.492	0.895	0.445	0.961	0.264	0.098
Av.	Top <30	0-30	2.069	0.240	0.469	0.356	1.521	0.485	
	stdev		*1.319*	*0.095*	*0.140*	*0.044*	*1.636*	*0.452*	
Av.	Bottom C	>40	1.724	0.391	0.935	0.374	0.710	0.208	0.107
	stdev		*0.131*	*0.142*	*0.055*	*0.101*	*0.355*	*0.079*	*0.013*
Oberaar suspended sediment samples									
recent	O36 F290		0	1.618	0	1.513	0.472	0.124	
	K46 F223		0	1.431	0	1.024	0.287	0.045	
	K39 F217		0	1.631	0	1.140	0.308	0.051	
	K8 F41		0	2.001	0	1.282	0.828	0.128	
	Av. (n=24)			1.670		1.240	0.474	0.087	0.35 **
	stdev			*0.239*		*0.210*	*0.250*	*0.045*	*0.280*

v = vermiculite, bv = biotite-vermiculite mixed-layers
*) cc/qtz ratios from whole rock analysis
**) average cc/qtz ratios from suspended sediment
n.d. not detected

Table 3.3: Clay mineralogy of the fraction <2 µm and 2 – 16 µm of glacial sediments from Oberaar catchment.

Age	Sample	Depth	fraction < 2µm		fraction 2-16µm				
			v + bv / biotite	biotite/ phengite	v + bv / biotite	biotite/ phengite	qtz/K-fsp	qtz/plagio	cc/qtz*
Rhone moraine samples									
LIA	$R_{145A}1$	0-10	0.292	0.732	0.045	0.947	0.131	0.048	0.0607
145y	$R_{145A}2$	10-20	0.259	0.664	0.077	0.526	0.374	0.137	0.0949
	$R_{145A}3$	20-30	0.266	0.556	0.442	0.423	0.198	0.065	0.101
	$R_{145A}4$	30-40	0.414	0.696	0.050	0.862	0.201	0.070	0.0552
	$R_{145A}5$	40-50	0.379	0.497	0.093	0.383	0.149	0.062	0.148
	$R_{145A}6$	50-60	0.141	0.902	0.065	1.319	0.099	0.043	n.d.
	$R_{145A}7$	60-70	0.363	0.791	0.120	0.908	0.147	0.056	0.0897
	$R_{145A}8$	70-80	0.168	0.723	0.074	0.921	0.160	0.068	0.139
	$R_{145A}9$	80-90	0.215	0.664	0.052	1.021	0.191	0.075	0.0349
	$R_{145A}10$	90-100	0.182	0.712	0.049	1.207	0.215	0.090	0.2155
Av.	Top <30	0-30	0.272	0.651	0.188	0.632	0.235	0.083	0.086
	stdev		*0.017*	*0.089*	*0.221*	*0.278*	*0.125*	*0.047*	*0.022*
Av.	Bottom C	>70	0.189	0.700	0.058	1.050	0.189	0.078	0.130
	stdev		*0.024*	*0.032*	*0.014*	*0.145*	*0.027*	*0.011*	*0.091*
LIA	$R_{270A}1$	0-10	1.105	0.290	0.478	0.189	0.181	0.051	0.148
270y	$R_{270A}2$	10-20	1.421	0.316	0.403	0.457	0.232	0.076	0.114
	$R_{270A}3$	20-30	0.711	0.875	0.295	0.902	0.487	0.192	0.057
	$R_{270A}4$	30-40	0.236	0.868	0.146	0.712	0.091	0.037	0.023
	$R_{270A}5$	40-50	0.861	0.483	0.142	0.812	0.325	0.098	0.051
	$R_{270A}6$	50-60	0.035	0.734	0.323	0.800	0.066	0.027	0.102
	$R_{270A}7$	60-70	0.105	0.716	0.225	0.917	0.458	0.148	0.221
	$R_{270A}8$	70-80	0.222	1.049	0.115	0.825	0.089	0.031	0.064
	$R_{270A}9$	80-90	0.278	1.105	0.090	0.746	0.078	0.033	0.037
	$R_{270A}10$	90-100	0.087	1.006	0.220	0.776	0.000	0.000	0.141
Av.	Top <30	0-30	1.079	0.494	0.392	0.516	0.300	0.106	0.107
	stdev		*0.356*	*0.331*	*0.092*	*0.360*	*0.164*	*0.075*	*0.046*
Av.	Bottom C	>70	0.196	1.053	0.142	0.782	0.056	0.021	0.081
	stdev		*0.098*	*0.049*	*0.069*	*0.040*	*0.048*	*0.019*	
LIA	$R_{270B}1$	0-10	0.823	0.349	0.262	0.236	0.186	0.056	0.180
270y	$R_{270B}2$	10-20	0.949	0.676	0.420	0.431	0.183	0.051	0.122
	$R_{270B}3$	20-30	0.669	0.891	0.339	0.606	0.232	0.070	0.080
	$R_{270B}4$	30-40	0.586	0.667	0.723	0.636	0.155	0.065	n.d.
	$R_{270B}5$	40-50	0.806	0.443	0.266	0.910	0.062	0.030	n.d.
	$R_{270B}6$	50-60	0.356	0.927	0.138	0.685	0.126	0.059	0.044
	$R_{270B}8$	70-80	0.143	0.764	0.167	0.829	0.075	0.038	0.089
Av.	Top <30	0-30	0.814	0.638	0.341	0.425	0.200	0.059	0.127
	stdev		*0.140*	*0.273*	*0.079*	*0.185*	*0.027*	*0.010*	*0.050*
YD	$R_{YD}1$	0-10	1.203	0.366	0.128	0.565	1.328	0.189	n.d.
10 ky	$R_{YD}2$	10-20	1.032	0.247	0.277	0.365	1.237	0.178	0.089
	$R_{YD}3$	20-30	1.589	0.437	0.342	0.463	0.606	0.147	0.044
	$R_{YD}4$	30-40	n.a.	n.a.	0.925	0.375	0.424	0.087	n.d.
	$R_{YD}5$	40-50	4.301	0.413	1.083	0.492	0.987	0.204	n.d.
	$R_{YD}6$	50-60	4.605	0.226	0.859	0.485	0.547	0.134	0.024
	$R_{YD}7$	60-70	2.335	0.399	0.623	0.322	1.352	0.166	n.d.
Av.	Top <30	0-30	1.274	0.342	0.515	0.401	0.756	0.137	0.067
	stdev		*0.286*	*0.134*	*0.357*	*0.054*	*0.427*	*0.046*	
Av.	Bottom C	>50	3.470	0.312	0.741	0.403	0.949	0.150	0.024
	stdev		*1.605*	*0.122*	*0.167*	*0.115*	*0.569*	*0.023*	
Rhone suspended sediment samples									
recent	F272		0	1.633	0	1.528	0.264	0.104	
	F91		0	3.705	0	0.488	0.314	0.122	
	F235		0	0.225	0	0	0.306	0.127	
	F74		0	0.172	0	0.444	0.222	0.092	
	Av. (n=23)			1.434		0.615	0.277	0.111	0.09 **
	stdev			*1.659*		*0.647*	*0.043*	*0.016*	*0.072*

Table 3.4: Clay mineralogy of the fraction <2 µm and 2 – 16 µm of glacial sediments from Rhone catchment (abbreviations and footnotes see Table 3.3).

deionized water: soil suspension.

Results

The whole rock mineralogical analyses show that all moraine and suspended sediment samples reflect the bedrock mineralogy of the two areas; which consists of quartz, potassic feldspar (microcline), plagioclase (albite), phyllosilicates, calcite, and chlorite, with some additional amphibole (actinolite) in the Oberaar catchment.

The XRD analysis of clay minerals shows the presence of chlorite, phengite, biotite, biotite-vermiculite mixed layers (= hydrobiotite, Moore and Reynolds, 1997), and vermiculite (Tables 3.3 & 3.4). The existence of some traces of smectite, mica-smectite mixed-layers or gibbsite can not be excluded; their maximum concentration, however, is less than 0.5 % in samples from the most developped horizons of the profiles, thus they are not considered to be significant in our work. In the <2 μm and 2-16 μm fractions of the moraine samples several trends in mineral distribution are visible in the evolution from the LIA to the YD profiles. The mineral ratios are plotted in a chronological order in Figures 3.4, 3.5, and 3.6.

The relative content of secondary minerals in the LIA profiles is generally higher in the top 30 cm of the profiles. In the YD profiles this trend is reversed, with a higher relative content of secondary minerals in the bottom parts of the profiles (except for the <2 μm fraction of Oberaar). The relative vermiculite content (2-16 μm fraction) of the top 30 cm of the YD profiles is even lower than in the LIA profiles. The YD profiles are more deeply weathered than the LIA profiles. Fig. 3.7 shows how the vermiculite content increases with depth within the Rhone R_{YD} profile.

In the 140 year old moraines at Oberaar the ratios of (vermiculite + biotite-vermiculite mixed layers)/biotite are twice as high in the top 30 cm of the profiles as in the bottom parts (Fig. 3.4). The ratio in the Oberaar YD profile is again two times higher with higher values for the bottom parts of the profiles (except OA < 2 μm fraction). The biotite content decreases correspondingly: The biotite/phengite ratios are half as high in the

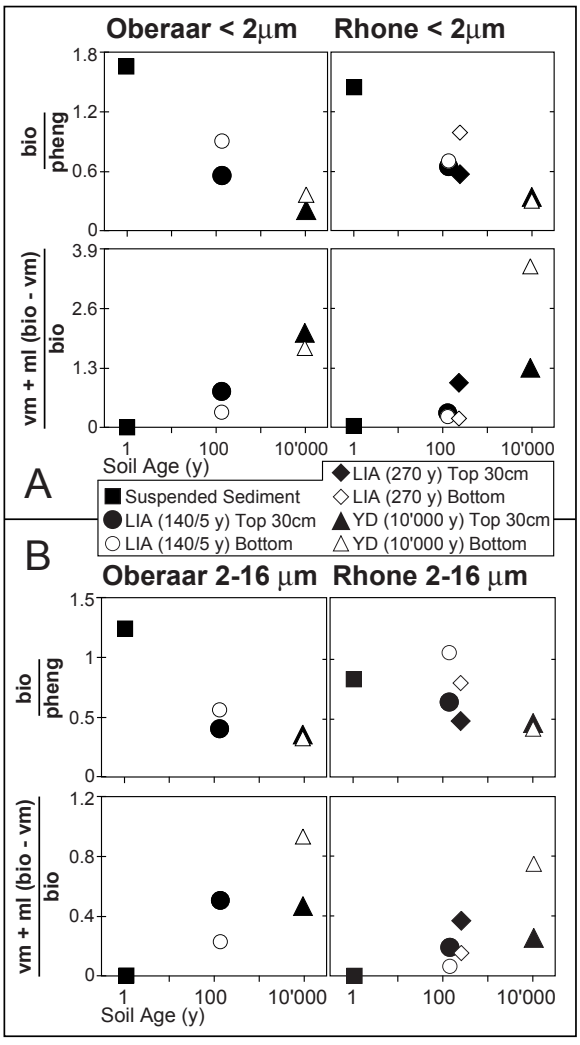

Fig. 3.4: Raw intensity ratios (biotite/phengite & (vermiculite + biotite-vermiculite mixed-layers)/biotite) of Oberaar and Rhone sediments of different ages (moraines and suspended sediment; vm = vermiculite, ml(bio-vm) = biotite-vermiculite mixed-layers).

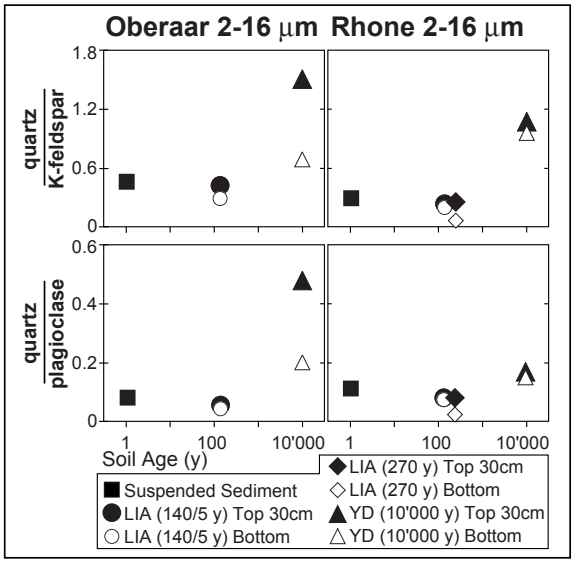

Fig. 3.5: Raw intensity ratios (quartz/K-feldspar & quartz/plagioclase) of Oberaar and Rhone sediments of different ages (moraines and suspended sediment, 2-16 μm fraction).

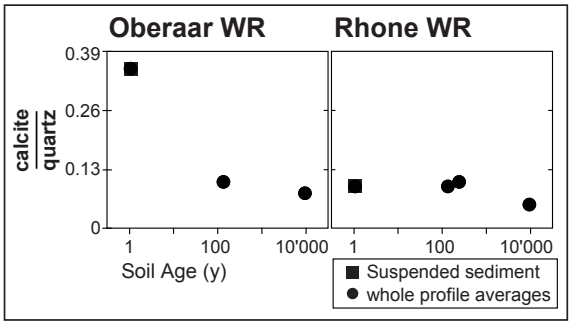

Fig. 3.6: Raw intensity calcite/quartz ratios of suspended sediment and entire profiles calculated from whole rock analysis (XRD). Suspended sediment (OA n = 19; RH n = 15).

LIA profiles compared to the suspended sediments, and again half as high in the YD profile compared to the LIA profiles, always having higher values for the bottom parts of the profiles. The moraine profiles of Rhone glacier catchment show the same trends. The biotite content of Rhone suspended sediment is comparable to the LIA profiles (R_{270A} & R_{270B}).

Oberaar quartz/K-feldspar ratios are almost twice as high as the Rhone ones (Fig. 3.5). Compared to the suspended sediment the values from the LIA profiles are 6 to 36 % and 15 to 75 % lower for top 30 cm and bottom parts and for Oberaar and Rhone profiles, respectively. In the YD profiles the ratios are approximately doubled, with significantly higher values for the top 30 cm of the profiles. The quartz/plagioclase ratios in the LIA profiles are comparable between the two areas. They are 26 to 41 % and 25 to 75 % lower than in the suspended sediments for top 30 cm and bottom parts and for Oberaar and Rhone profiles, respectively.

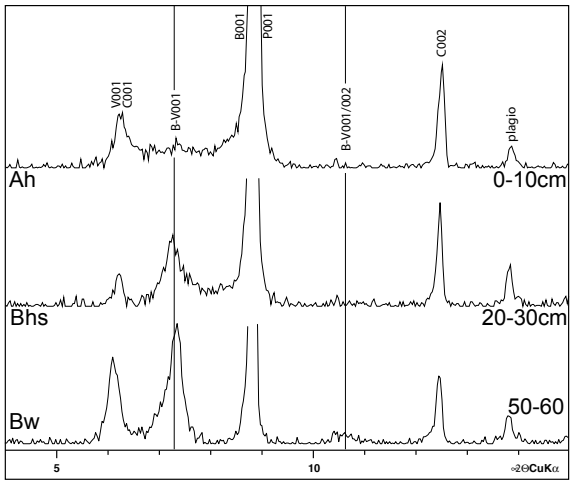

Fig. 3.7: Accumulation of vermiculite as a function of depth in the 2-16 µm fraction of the R_{YD} profile.

In the YD profiles the ratios are approximately doubled, with significantly higher values for the top 30 cm of the profiles especially at Oberaar.

The calcite/quartz ratio of the suspended sediment (calculated on bulk profiles from whole rock mineralogy; Fig. 3.6 and Table 3.3 & 3.4) is higher for Oberaar than for Rhone (0.35 vs. 0.09). In the Oberaar LIA profiles this ratio is diminished by 69 % (to 0.11) relative to the suspended sediment (0.35). The ratio is again decreased in the YD profile (0.08). The Rhone calcite/quartz ratio in the LIA profiles is comparable to the suspended sediment (0.09 to 0.10), only the YD profile shows significantly lower values (0.05).

Biotite field weathering rate

We calculated the decrease in biotite by comparing the biotite/phengite ratio between the C-horizon (bottom 30 cm) and the top 30 cm of the profiles in % for the 0 – 2 and 2 – 16 μm fractions that were analysed for clay minerals (Tables 3.3 & 3.4). Consequently we calculated the amount of biotite (kg) contained within the C-horizon using the corresponding biotite content (%) of the two analysed grain-size fractions (0 – 2 and 2 – 16 μm) combined with the average moraine density of 1500 kg m^{-3} (Egli et al., 2001). We also took into consideration the overestimation in clay minerals of these grain-size fractions which is due to preparation as well as orientation effects: By comparing the phyllosilicate/quartz ratio obtained by whole rock XRD analysis (bulk samples) to the corresponding grain-size fraction data (clay mineral analysis), the overestimation in clay minerals was calculated to be ≥ 20 times for the 0 – 2 μm and 2 – 8 times for the 2 – 16 μm fraction, which corresponds to 95 – 100 % and 50 – 85 % of clay minerals in these grain-size fractions, respectively. This gives us an upper and lower boundary limit for the weathering rates. With a biotite formula by Marquer (1987 & pers. comm.), who worked in the same area and performed several chemical analyses of the micas contained within Grimsel Granodiorite (biotite = $(K_{0.952}, Na_{0.012})$ $(Mg_{1.164}, Fe_{1.276}, Al^{VI}_{0.294}, Ti_{0.099}, Mn_{0.023}, Cr_{0.003})$ $(Si_{2.826}, Al^{IV}_{1.175})$ $O_{10}(OH)_2$) we calculated the amount of biotite which is lost per year relative to the amount of biotite in the C-horizon (t = 0). However, the detailed composition of biotite does not significantly influence the final weathering rates.

Using the grain-size distribution for particles < 16

Grainsize fraction	OA_{140A}	RH_{145A}	RH_{270A}
16µm	34.62	35.18	42.39
8µm	37.44	37.83	37.36
4µm	20.95	19.78	15.62
2µm	5.33	5.47	3.65
1µm	1.142	1.180	0.719
0.5µm	0.391	0.411	0.209
0.2µm	0.095	0.102	0.041
0.1µm	0.032	0.036	0.012

Table 5: Grainsize distribution in different soil profiles, fractions < 1 µm from interpolation of fractions < 16 µm.

μm we interpolated the distributions of the particles < 1 μm using an exponential function (Table 3.5). We obtained $R^2 \geq 0.95$. In order to calculate the relative surface area of biotite using a geometric approach we assume that biotite breaks down into regular shaped flakes or platelets with a constant diameter/thickness ratio. We use radius/height (r/h) ratios of 5, 10, and 15 (cf. Swoboda-Colberg and Drever, 1993) which gives us average surface areas for each grain-size division (surface of cylinder: $S_c = 2\pi r^2 + 2\pi rh$). With a biotite density of 3.09 g cm^{-3} we calculated the total relative surfaces S_T (m^2 g^{-1}; S_c/V; $S_c = 2\pi r^2 + 2\pi rh$ and $V = \pi r^2 h$) as well as the relative edge surfaces S_E (m^2 g^{-1}; S_e/V; $S_e = 2\pi rh$ and $V = \pi r^2 h$), where dissolution processes most likely happen (Nagy, 1995).

The results for the biotite weathering rate are summarised in Table 6a and are further explained in the discussion section. Table 6a shows biotite loss in % of the two grain-size fractions and in mol yr^{-1}. Total surface areas S_T (m^2 g^{-1}) are given for the different radius/height ratios (5, 10, and 15) together with the corresponding edge surface areas S_E (m^2 g^{-1}). The latter remain constant for different radius/height ratios. Finally the calculated weathering rates are shown for total surface area (WR_T, pmol m^{-2} sec^{-1}) as well as for edge surface area (WR_E, pmol m^{-2} sec^{-1}, Table 3.6a). Table 3.6b consists of a compilation of different weathering rates calculated by different approaches, and are discussed below.

Discussion

Validity of data: a) Reworked material

We suggest that the amount of pre-weathered material in our soil profiles is rather small and well homogenised with the freshly eroded sediments for several reasons: 1) Our profiles show characteristic soil zonation processes which already occur in the young LIA moraine profiles (Table 3.2) and a gradient is visible in the distribution of secondary minerals: the contents of secondary minerals of the top 20 – 30 cm of the LIA profiles are significantly higher than the ones of the C horizons (below 30 – 40 cm depth) in these profiles (Fig. 3.4). This suggests that a significant amount of secondary minerals is newly formed. 2) The YD profiles lie in the same altitude as the LIA ones and correspond to the altitudes of the YD accumulation zone. The YD material is therefore deposited during the YD retreat of the glaciers. The glaciers "cleaned out" their systems during the maxima, meaning that the material of our soil profiles was deposited as fresh material during the retreat, when the equilibrium line was already back up in the catchment. 3) Furthermore, apatite mineral grains from suspended sediment and bottom LIA profiles (C horizons) do not show significant differences with regard to their surface morphologies, suggesting that the material of the C horizons is not chemically weathered to a larger extent (Hosein et al., submitted).

b) Geology of catchments during different times

During LIA and YD the surface areas of our two glaciers were larger and consequently included different lithologies than they do recently. Approximate bedrock distributions for different times are given in Table 3.1. Lithological distribution of the Oberaar LIA catchment corresponds to the present-day distribution (Fig. 3.1 & 3.2). During YD the Oberaar glacier filled its catchment more completely, and larger portions of the Grimsel Granodiorite and the Southern Aar Granite were ice covered than today. However, we expect only small differences in the composition of the initial parent materials between LIA and YD soil profiles.

During the maximum extent of YD, two glaciers existed in the Rhone catchment, which joined each other in the plane of Gletsch: The Rhone glacier from the north and the Mutt glacier from the south-east (Furkapass, see Fig. 3.1). The confluence of these two glaciers led to an overdeepening of the valley and finally, with their retreat, to a glacial sediment infill consisting of a mixture of the lithologies which were contained in the glacier catchment at that time (Fig. 3.1 & 3.8A). A first order estimation of the lithologies of

the YD glacier catchment gives a distribution of 40 % Central Aar Granite, 20 % Grimsel Granodiorite, 20 % Variscan Gneisses, and 20 % Mesozoic metasediments. The initial parent material of our YD soil profile contained therefore also Variscan Gneisses and Mesozoic metasediments, and is for this reason not directly comparable to the parent material of LIA soil profiles. During LIA, the Mutt glacier did not join the Rhone glacier (Zumbühl, 1988). The Rhone glacier spread out widely over the plane of Gletsch, not eroding the YD valley infill but depositing the LIA terminal moraines on top of it (Fig. 3.2 & 3.8A). The 5 – 10 % of Variscan Gneisses were isolated and protected from reworking processes. Therefore the lithological distribution is comparable between Rhone LIA and todays catchment.

Biotite weathering: a) General

The clay mineralogy of the suspended sediment of both glaciers is comparable as is also the mica compositions of various sediment samples from both glacier catchments (Fig. 3.9). We may therefore compare their decay processes between our two catchment areas.

The zone of increased weathering of biotite coincides with the zone of high root density, which suggests that weathering is biochemically accelerated by the network of roots and associated microorganisms. Mechanically disaggregated biotite (by abrasion) is preferentially leached to release different cations (specially K, Mg, Fe, and Si; Barker et al., 1997 and Barker et al., 1998). The marginal zones of the frayed-out biotite are gradually opened up and transformed into biotite-vermiculite mixed-layers and subsequently into vermiculite. Therefore glacially derived sediments should show increased biotite weathering rates (see below). Fresh inner parts of the biotites (that were not glacially disaggregated to the same extent) are leached

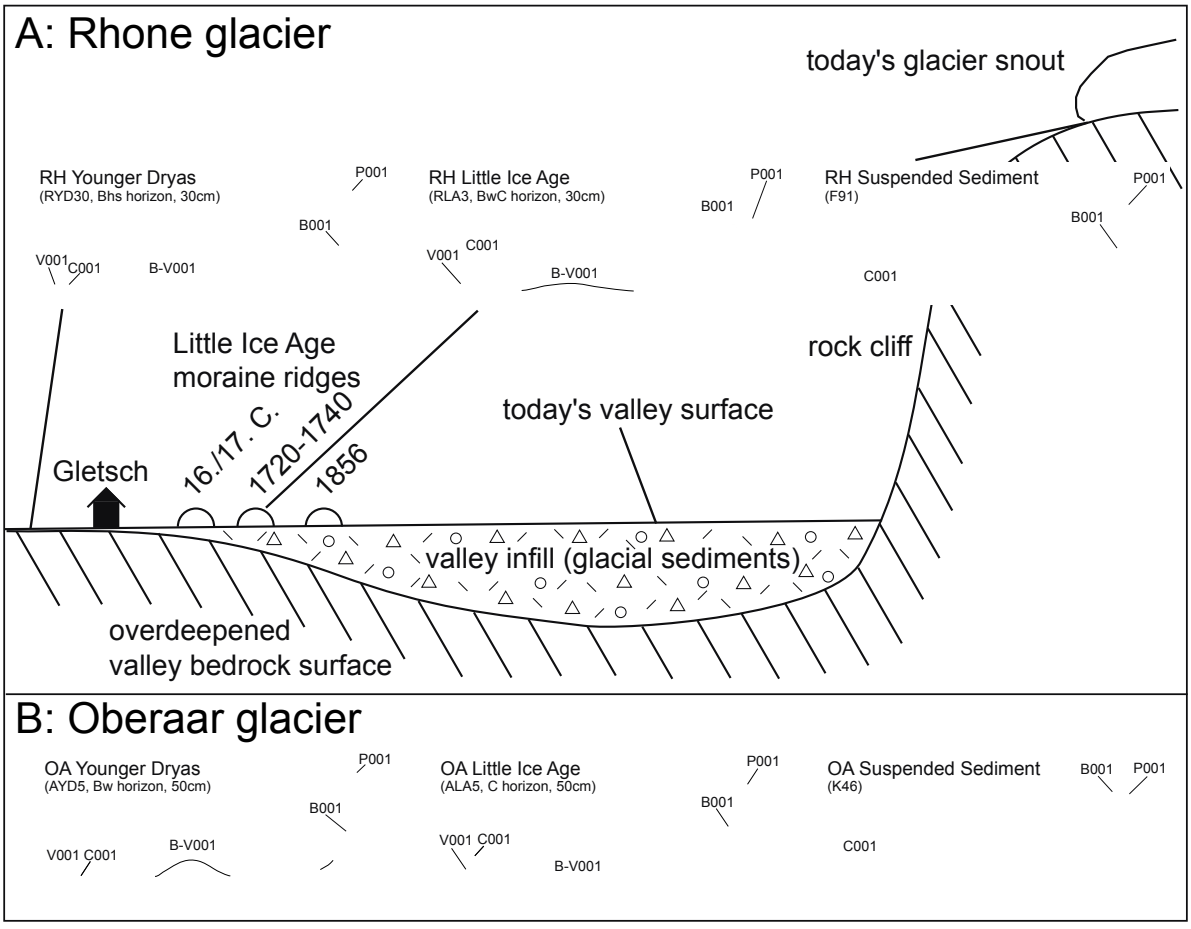

Fig. 3.8: (A) Schematic profile along valley floor of the Rhone proglacial area. Bedrock surface is overdeepened during LGM and YD because two glaciers joined here; overdeepening exaggerated. Valley infill isolated and prevented bedrock surface from active erosion processes during LIA glacier advance. Time mineralogical evolution of different sediments (2-16 µm fraction): suspended sediment => LIA moraines => YD moraines. (B) The mineralogic evolution of different sediments from Oberaar glacier (2-16 µm fraction): suspended sediment => LIA moraines => YD moraines.

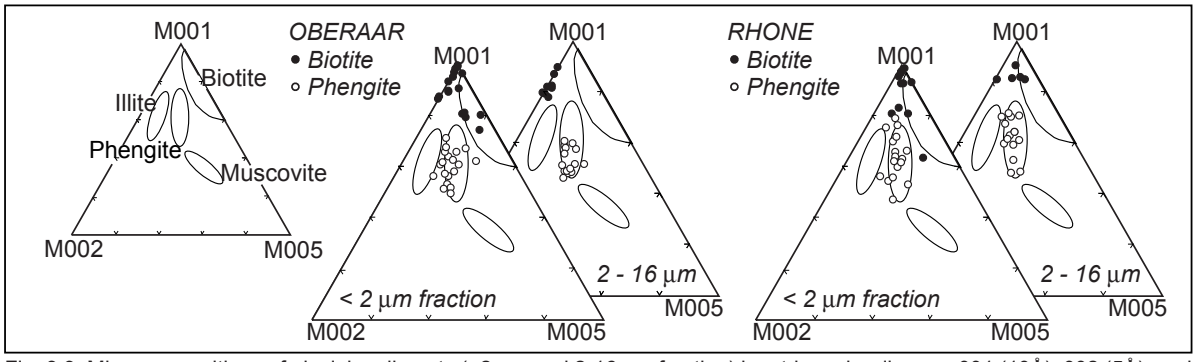

Fig. 3.9: Mica compositions of glacial sediments (<2 µm and 2-16 µm fraction) in a triangular diagram 001 (10Å), 002 (5Å), and 005 (2Å) after Rey and Kübler, 1983.

much more slowly.

The chronosequential evolution of the glacial sediments we analysed is clearly visible in Fig. 3.8: Secondary minerals are missing in the suspended sediment, but they build up within LIA moraines and are widespread in YD moraines. In more developed and consequently more mature soils (at lower altitude and on forested site) compared to this work, Righi et al. (1999) found partially weathered dioctahedral phengite within the eluvial horizon, which was transformed into a mica-smectite mixed-layer mineral. In our area we do not see a decrease in the phengite content within this layer over time and we do not find significant traces of any gibbsite, smectite, or mica-smectite mixed-layers within any of our soil samples.

b) Biotite weathering rate

One important aspect of calculating biotite weathering rates and comparing them to literature values is that due to its perfect basal cleavage, the basal surfaces of biotite flakes are not very reactive during weathering, and most of the dissolution occurs at the edges of the grains (Turpault and Trotignon, 1994). Smaller grains will have much more edge relative to basal surface than larger grains. Therefore the total weathering rates (WR_T) which are calculated using total surface area S_T (including the basal surfaces) may be lower than the edge weathering rates (WR_E) using edge surface areas S_E.

Our edge weathering rates WR_E are one order of magnitude higher than our total weathering rates WR_T (Table 3.6a) which is due to the different relative surface areas used. The edge weathering rates WR_E are the same for the different r/h ratios as the radius stays constant per size fraction and changes in r/h therefore correspond to changes in h which do not affect the relative surface areas S_E ($m^2\ g^{-1}$) as they are normalised to volume. Our field-based, total weathering rates WR_T calculated using total surface area S_T are in the same order of magnitude as fast laboratory rates (10^{-10} - 10^{-12} $mol_{biotite}\ m^{-2}\ s^{-1}$; Acker and Bricker, 1992, Nagy, 1995, Murphy et al., 1998, Table 3.6b). If we compare the weathering rates calculated using edge surface area S_E (WR_E, 10^{-10} – 10^{-11} $mol_{biotite}\ m^{-2}\ s^{-1}$), they are two orders of magnitude slower than the analogue laboratory rates by Turpault and Trotignon (1994). This discrepancy between field and laboratory rates is well known (e.g. Swoboda-Colberg and Drever, 1993, Velbel, 1993a).

The weathering rates calculated for LIA soil profiles are comparable between Rhone and Oberaar, their variance is due to the differences in biotite loss (%) within the profiles and initial biotite contents at time t = 0. Due to their age the weathering rates calculated for YD soil profiles are 1 – 2 orders of magnitude slower. YD total weathering rates (WR_T) correspond to laboratory rates obtained by Swoboda-Colberg and Drever (1993). LIA soil profile C-horizon values are used to calculate YD weathering rates. For Oberaar this assumption might be valid, as the eroded lithologies did not change much between YD and LIA (Table 3.1). For Rhone, however, this assumption is less solid, as outlined above. Therefore, this approach to calculate longer-term weathering rates might not be very sensitive.

c) Possible explanations for the higher weathering rates

We base our calculation on material which is enriched in small particle fractions through glacial mechanical abrasion processes. Mechanically disaggregated and frayed-out biotites are preferentially leached. Due to the alpine environment total precipitation and

Catchment	Timespan	Loss % 0-2µm	Loss % 2-16µm	Loss (mol yr^{-1})	Loss (mol yr^{-1})	r/h	S_T m^2 g^{-1}	S_E m^2 g^{-1}	WR_T pmol m^{-2} sec^{-1}		WR_E pmol m^{-2} sec^{-1}	
	yrs			low	high				high	low	high	low
Oberaar	140	19.93	30.00	24.88	40.60	5	1.357	0.226	104.24	106.15	625.46	636.87
						10	2.487		56.86	57.90		
						15	3.618		39.09	39.80		
Rhone	145	6.94	39.80	79.32	133.85	5	1.358	0.226	128.73	132.93	772.41	797.59
						10	2.489		70.22	72.51		
						15	3.620		48.28	49.85		
Rhone	270	53.11	34.04	14.53	23.31	5	1.127	0.188	82.14	80.59	492.82	483.52
						10	2.065		44.80	43.96		
						15	3.004		30.80	30.22		
Oberaar*	10,000	74.14	51.26	0.67	1.05	5	1.357	0.226	2.80	2.74	16.81	16.45
						10	2.487		1.53	1.50		
						15	3.618		1.05	1.03		
Rhone a[§]	10,000	66.77	40.61	0.47	0.75	5	1.127	0.188	2.67	2.61	16.00	15.65
						10	2.065		1.45	1.42		
						15	3.004		1.00	0.98		
Rhone b[†]	10,000	49.97	55.73	1.74	2.85	5	1.358	0.226	2.82	2.83	16.94	17.00
						10	2.489		1.54	1.55		
						15	3.620		1.06	1.06		

* Surface areas calculated from C-horizon of profile O_{140A}
§ Surface areas calculated from C-horizon of profile RH_{270A}
† Surface areas calculated from C-horizon of profile RH_{145A}

Table 3.6a: Biotite weathering rates compilation for different soil profiles and assumed parameters. r/h = ratio radius / height of platelet, where radius = average of particle size fraction (see Table 3.5).

therefore throughflow is probably increased compared to other field sites. Therefore our glacially derived material may show faster biotite weathering rates.

Due to effects of sample preparation, we are looking at size fractions < 16 μm. Larger size fractions have less relative reactive surface area (Hodson, 2002), especially with regard to edge surface area S_E. As we use a geometric approach to calculate the relative surface area, the r/h ratio remains a major uncertainty. In other weathering rate studies BET surfaces were used, calculated according to Brunauer et al. (1938). The surface areas calculated nongeometrically are always higher than the geometric areas, due to surface roughness and surface steps (Swoboda-Colberg and Drever, 1993) as well as to interlayer surface area (Kalinowski and Schweda, 1996). Our final weathering rates may be increased by this effect and should be seen as maximum rates.

Our study is performed in highly permeable and well-drained glacial sediments where waters percolate easily through the soil matrix and are furthermore rather dilute (low-ionic strength rain waters). The effect of heterogeneities in flow path through soils is of minor importance compared to most field studies, in which weathering rates for silicate minerals are calculated with mass balance equations using surface and groundwater ion concentrations related to estimated mineral surface area (Swoboda-Colberg and Drever, 1993, Velbel, 1993b, White, 1995, Murphy et al., 1998). This effect is quite dominant in such studies, where dissolution may be minimized because soil porewaters only percolate along macropores. In these studies, such effects explained the large discrepancy between field weathering rates and laboratory rates. In laboratory studies, the solutions flow through the matrix (micropores); this increases the overall solute concentration and may have a negative effect on the weathering rate. However, electrolyte effects on dissolution kinetics of biotite at low temperature are small (Kalinowski and Schweda, 1996).

As biotite dissolves and secondary phases (vermiculite) increase there is a loss of reactive surface area in field conditions. Less and less biotite might be in direct contact to soil porewaters. This effect should be taken

Study	What	Surface approach	Approx. weathering rates
Laboratory			
Acker and Bricker 1992	acidic solutions; H_2SO_4; pH 3 - 5.5; 22 ± 1.5 °C oxidizing / reducing solutions saturated vs. unsaturated flow conditions	BET	10^{-11} - $10^{-12.5}$
Swoboda-Colberg and Drever 1993	75 - 150 µm size fraction of soil from field site room temperature pH 4 - 4.5 (analogue pH of bulk soil solution field site) deionised water, HCl to adjust pH	geometric r/h = 10	$10^{-11.4}$
Turpault and Trotignon 1994	0.1N HNO_3; pH 1.08 ± 0.02; 24 °C Single cut crystals of biotite with decr. thickness => $S_T \approx$ const.; S_E decr. const. thickness cut along external (001) interface => ST incr.; SE ≈ const. const. thickness cut perpendicular to external (001) interface => ST ≈ const.; SE incr.	"geometric" S_E vs. S_T norm. to S_E	$\approx 10^{-8}$
Kalinowski and Schweda 1996	aqueous solutions; pH 1 - 4; room temperature	BET	$10^{-11.9}$ †
Field			
Swoboda-Colberg and Drever 1993	plot irrigation with HCl; pH 2 - 3 soil solution combined with grain-size distribution and mineralogy of soil	geometric r/h = 10	10^{-14}
Murphy et al. 1998	mass-balance equation inclusive density and volume of phyllosilicate grains, porewater chemistry and flux & soil porosity	BET	10^{-15}

† as cited in Murphy et al. 1998

Table 3.6b: Compilation of weathering rates of biotite measured in laboratory and field experiments.

into consideration for the longer time step of 10,000 years that we are looking at.

Other observed weathering reactions

Calcite is highly reactive in dilute waters (glacial meltwaters or dilute soil waters) because of its dissolution rate at near neutral pH (10^{-5} mol m^{-2} s^{-1}; Plummer et al., 1978), which is approximately seven orders of magnitude higher than the dissolution rate of plagioclase feldspar ($\approx 10^{-12}$ mol m^{-2} s^{-1}; Blum and Stillings, 1995). Oberaar suspended sediment contains three times as much calcite as Rhone (Hosein et al., submitted), which is due to the presence of calcite bearing Variscan Gneisses (with up to 5 wt% calcite, Stalder, 1964). Calcite in the Oberaar LIA moraine profiles is decreased to one third compared to the suspended sediment (Fig. 3.6). In Rhone LIA profiles this dissolution effect is less visible. In both areas the calcite content is again decreased in the time step to the YD profiles. The short-term weathering of calcite starts as soon as the bedrock-flour becomes in contact with dilute meltwater in the subglacial environment. At Oberaar it is well advanced after 140 years. However, in both areas it continues after 140 – 270 years and its effects are still visible in the longer term (time-step to YD).

The quartz/K-feldspar and quartz/plagioclase ratios show the differences in bedrock between the two catchments (Tables 3.3 & 3.4). Suspended sediment is taken here as the average composition of the bedrock that is recently eroded. Oberaar suspended sediment is richer in plagioclase (lower quartz/plagioclase ratios) in comparison to the Rhone catchment. Rhone glacier suspended sediment, on the other hand, contains more K-feldspar (Fig. 3.5). This difference may be explained by the smaller content of K-feldspar within the Variscan Gneisses of the Oberaar catchment compared to the other lithologies (Stalder, 1964). The feldspar content of the different LIA profiles corresponds more or less to the suspended sediment values (Fig. 3.5). The differences are due to different transport mechanisms (e.g. ice, water). The increased quartz/K-feldspar and quartz/plagioclase ratios in the top parts of the profiles show the more intense weathering of K-feldspar and plagioclase in the top soil layers compared to the bottom parts. The ratios increase with time: In the YD profiles they are more than doubled (Fig 3.5). Therefore the weathering of K-feldspar and plagioclase is rather slow and only becomes significant on time scales longer than 270 years.

Conclusions

There are two domaines of weathering in glacial environments, the subglacial and proglacial zones: "Long-term" weathering processes take place in the proglacial area where conditions associated with pedogenesis, such as increased acidity, increase the overall chemical weathering rates. The calcite concentration of proglacial sediments decreases drastically in the first hundred years after deposition and the chemical weathering of biotite and feldspar grains is also increased after their deposition in the proglacial area. Biotite weathers to form biotite-vermiculite mixed-layer clays and subsequently vermiculite after 140 years (LIA moraine profiles, especially within the top 30 cm of the soils), and continues more slowly in YD profiles.

We present a new approach to calculate weathering rates using the decrease of biotite between the C-horizon and the top 30 cm of the soils and a geometrical calculation of the mineral surface area. We calculate weathering rates using total mineral surface area in the order of 10^{-10} – 10^{-11} $mol_{biotite}$ m^{-2} sec^{-1} for a time-scale of hundreds of years. Weathering rates using the edge surface area are in the order of 10^{-10} $mol_{biotite}$ m^{-2} sec^{-1}. These elevated weathering rates are due to a combination of the enrichment in small particles which are glacially abraded and the high throughflow due to the high precipitation volumes at these alpine fieldsites. However, the particle sizes as well as the geometrical approach considered here could have a further effect on our calculation. Therefore our weathering rates should be seen as maximum rates. A slow-down of the weathering processes is visible comparing weathering rates calculated over hundreds and thousands of years.

The subglacial domain is dominated by "short-term" weathering reactions driven by the dissolution of freshly ground fine particles in dilute glacial meltwaters. The most reactive mineral in this context is calcite.

Acknowledgements

We thank David Nisbet and Marlen Schaller for field support. The manuscript benefited from the dis-

cussions with M. Lee, J.-M. Gobat (soil science), S. Bleuler and C. Schlüchter. This study was supported by Swiss National Science Foundation Grants 21-53997.98 and 20-61485.00.

References

A.F.E.S., 1998. A sound reference base for soils. The "référentiel pédologique". INRA, Paris, 322 pp.

Abrecht, J., 1994. Geologic units of the Aar massif and their pre-Alpine rock associations: a critical review. Schweizerische Mineralogisch-Petrographische Mitteilungen, 74: 5-27.

Acker, J.G. and Bricker, O.P., 1992. The influence of pH on biotite dissolution and alteration kinetics at low temperature. Geochimica et Cosmochimica Acta, 56: 3073-3092.

Adatte, T., Stinnesbeck, W. and Keller, G., 1996. Lithostratigraphic and mineralogic correlations of near K/T boundary clastic sediments in NE Mexico: Implications for origin and nature of deposition. In: G. Ryder, D. Fastovsky and S. Gartner (Editors), The Cretaceous-Tertiary events and other catastrophes in Earth history. Sp. Papers Geol. Soc. of America, pp. 211-226.

Ammann, K., 1977. Der Oberaargletscher im 18., 19., und 20. Jahrhundert. Zeitschrift für Gletscherkunde und Glazialgeologie, XII(2): 253-291.

Anderson, S.P., Drever, J.I., Frost, C.D. and Holden, P., 2000. Chemical weathering in the foreland of a retreating glacier. Geochimica et Cosmochimica Acta, 64(7): 1173-1189.

Anderson, S.P., Drever, J.I. and Humphrey, N.F., 1997. Chemical weathering in glacial environments. Geology, 25(5): 399-402.

Barker, W.W., Welch, S.A. and Banfield, J.F., 1997. Biogeochemical weathering of silicate minerals. Reviews in Mineralogy; Mineralogical Society of America, 35: 391-428.

Barker, W.W., Welch, S.A., Chu, S. and Banfield, J.F., 1998. Experimental observations of the effects of bacteria on aluminosilicate weathering. American Mineralogist, 83: 1551-1563.

Birkeland, P.W., Burke, R.M. and Shroba, R.R., 1987. Holocene alpine soils in gneissic cirque deposits, Colorado Front Range. U.S. Geological Survey Bulletin, 1590: 21pp.

Blum, A.E. and Stillings, L.L., 1995. Feldspar dissolution kinetics. Reviews In Mineralogy, 31: 291-351.

Brunauer, S., Emmett, P.H., Teller, E., 1938. Adsorption of gases in multimolecular layers. Journal of the American Chemical Society, 60: 309-319.

Claridge, G.G.C. and Campbell, I.B., 1984. Mineral transformation during the weathering of dolerite under cold arid conditions in Antarctica. New Zealand Journal of Geology and Geophysics, 27: 537-545.

Drever, J.I. and Hurcomb, D.R., (1986). Neutralization of atmospheric acidity by chemical weathering in an alpine drainage basin in the North Cascade Mountains. Geology, 14, 221-224.

Egli, M., Mirabella, A. and Fitze, P., 2001. Clay mineral formation in soils of two different chronosequences in the Swiss Alps. Geoderma, 104(1-2): 145-175.

Fairchild, I.J., Killawee, J.A., Hubbard, B. and Derybrodt, 1999. Solute generation and transfer from a chemically reactive alpine glacial-proglacial system. Earth Surface Processes and Landforms, 24(13): 1189-1211.

Föllmi, K.B., 1995. 160 m. y. record of marine sedimentary phosphorus burial: Coupling of climate and continental weathering under greenhouse and icehouse conditins. Geology, 23(9): 859-862.

Gurnell, A.M., Brown, G.H. and Tranter, M., 1994. Sampling strategy to describe the temporal hydrochemical characteristics of an alpine proglacial stream. Hydrological Processes, 8: 1-25.

Hallet, B., Hunter, L. and Bogen, J., 1996. Rates of erosion and sediment evacuation by glaciers: A review of field data and their iplications. Global and Planetary Change, 12: 213-235.

Hodson, M. E., 2002. Variation in element release rate from different mineral size fractions from the B horizon of a granitic podzol. Chemical Geology, in press.

Hormes, A., Müller, B. U., Schlüchter, C., 2001. The Alps with little ice: evidence for eight Holocene phases of reduced glacier extent in the Central Swiss Alps. The Holocene, 11(3): 255-256.

Hosein, R., Arn, K., Steinmann, P., Adatte, T. and Föllmi, K. Calcite, the principal control on cation fluxes from the Rhone and Oberaar glaciers, Switzerland. *Submitted to* Geochimica et Cosmochimica Acta.

Hosein, R., Arn, K., Lee, M., Steinmann, P., Föllmi, K. Apatite weathering in glacial chronosequences (Rhone and Oberaar Glaciers, Switzerland). *Submitted to* Geology.

Kalinowski, B.E. and Schweda, P., 1996. Kinetics of muscovite, phlogopite, and biotite dissolution and alteration at pH 1-4, room temperature. Geochimica et Cosmochimica Acta, 60(3): 367-385.

Klug, H.P. and Alexander, L., 1974. X-ray diffraction procedures for polycrystalline and amorphous materials. John Wiley and Sons Inc., New York.

Kübler, B., 1983. Dosage quantitatif des minéraux majeurs des roches sédimentaires par diffraction X. Cahiers de l'Institut de Géologie de Neuchâtel, Série ADX(1): 1-12.

Lidmar-Bergström, K., Olsson, S. and Roaldset, E., 1999. Relief features and paleoweathering remnants in formerly glaciated Scandinavian basement areas. Special Publications of the international Association of Sedimentology, 27: 275-301.

Marquer, D., 1987. Transfert de matière et déformation progressive des granitoïdes. Exemple des massifs de l'Aar et du Gothard (Alpes centrales suisses). Unpublished PhD thesis, Rennes, 250 pp.

Moore, D. and Reynolds, R., 1997. X-ray diffraction and the identification and analysis of clay-minerals. Oxford University Press, Oxford, 332 pp.

Murphy, S.F., Brantley, S.L., Blum, A.E., White, A.F. and Dong, H., 1998. Chemical weathering in a tropical watershed, Luquillo Mountains, Puerto Rico: II. Rate and mechanism of biotite weathering. Geochimica et Cosmochimica Acta, 62(2): 227-243.

Nagy, K.L., 1995. Dissolution and precipitation kinetics of sheet silicates. Reviews In Mineralogy, 31: 173-233.

Oberhänsli, R., Schenker, F. and Mercolli, I., 1988. Indications of Variscan nappe tectonics in the Aar Massif. Schweizerische Mineralogisch Petrographische Mitteilungen, 68: 509-520.

Plummer, L.N., Wigley, T.M.L. and Parkhurst, D.L., 1978. The kinetics of calcite dissolution in CO2-water systems at 5 - 60 °C and 0 - 1.0 atm CO2. American Journal of Science, 278: 179-216.

Rey, M. and Kübler, B., 1983. Identification des micas des séries sédimentaires par diffraction X, à partir de la série harmonique (001) des préparations orentées. schweizerische Mineralogisch Petrographische Mitteilungen, 63: 13-36.

Righi, D., Huber, K. and Keller, C., 1999. Clay formation and podzol development from postglacial moraines in Switzerland. Clay Minerals, 34: 319-332.

Schwab, M., Frei, C., Schär, C. and Daly, C., 2001. Mean annual precipitation throughout the European Alps 1971-1990. In: Federal Office for Water and Geology (Editor), The Hydrological Atlas of Switzerland. Bundesamt für Landestopographie, Bern.

Sharp, M.J., Tranter, M., Brown, G.H. and Skidmore, M., 1995. Rates of chemical denudation and CO2 drawdown in a glacier-covered alpine catchment. Geology, 23(1): 61-64.

Stalder, H.A., 1964. Petrographische und mineralogische Untersuchungen im Grimselgebiet (Mittleres Aarmassiv). Schweizerische Mineralogische und Petrographische Mitteilungen, 44: 187-389.

Swoboda-Colberg, N.G. and Drever, J.I., 1993. Mineral dissolution rates in plot-scale field and laboratory experiments. Chemical Geology, 105: 51-69.

Tranter, M., Brown, G., Raiswell, R., Sharp, M. and Gurnel, A., 1993. A conceptual model of solute acquisition by Alpine glacial meltwaters. Journal of Glaciology, 39(133): 573-581.

Turpault, M.-P. and Trotignon, L., 1994. The dissolution of biotite single crystals in dilute HNO3 at 24°C: Evidence of an anisotropic corrosion process of micas in acidic solutions. Geochimica et Cosmochimica Acta, 58(13): 2761-2775.

USDA, 1998. Keys to soil taxonomy. United States Department of Agriculture, 328 pp.

USDA, 1999. Soil taxonomy: A basic system of soil classification for making and interpreting soil surveys. United States Department of Agriculture, 870 pp.

Velbel, M.A., 1993a. Constancy of silicate-mineral weathering-rate ratios between natural and experimental weathering: Implicatioins for hydrologic control of differences in absolute rates. Chemical Geology, 105: 89-99.

Velbel, M.A., 1993b. Temperature dependence of silicate weathering in nature: How strong a negative feedback on longterm accumulation of atmospheric CO2 and global greenhouse warming? Geology, 21: 1059-1062.

White, A.F., 1995. Chemical weathering rates of silicate minerals in soils. Reviews in Mineralogy, 31:

407-461.

Zumbühl, H.J., 1988. Der Rhonegletscher in den historischen Quellen. In: H.J. Zumbühl and H. Holzhauser (Editors), Alpengletscher in der Kleinen Eiszeit. Die Alpen, Schweizer Alpen-Club SAC, Bern, 64(3), pp. 166-233.

CHAPTER 4

Sr isotope systematics in two glaciated crystalline catchments: Rhone and Oberaar Glaciers (Swiss Alps)

Abstract

We studied subglacial chemical weathering processes and the Sr isotope composition of runoff and particulate material in the two glaciated catchments of Oberaar (OA) and Rhone (RH) glacier (Swiss Alps). Both areas are contained within the crystalline rocks of the Aar Massif, and the lithologies are quite homogeneous and comparable, except for the presence of a zone of highly deformed Variscan basement gneisses and schists in the Oberaar cachment, that may contain up to 9 % calcite.

We analysed meltwaters and precipitation as well as bulk suspended sediment and local bedrock. Furthermore we analysed the easy leachable fraction from the rocks and suspended sediment, using a 4.2 M acetic acid attack.

Ca/Na ratios are 5.0 – 13.3 and 1.8 – 2.4 in OA and RH meltwaters, respectively, which indicates that meltwaters in both catchments are enriched in Ca compared to suspended sediments. This suggests that the main source of Sr in meltwaters is derived by preferential weathering of calcite. Sr ratios of RH meltwaters ($^{87}Sr/^{86}Sr$ = 0.7251 – 0.7258) are lower than those of RH bulk suspended sediment (0.7279 – 0.7334). The Rhone suspended sediment composition is interpreted as a mixture of Grimsel Granodiorite (0.7101) and Central Aar Granite (0.7449). We explain the lower meltwater Sr ratio by the preferential weathering of disseminated calcite which has a relatively low calcite $^{87}Sr/^{86}Sr$ ratio (estimated 0.720 – 0.730). Furthermore early and nonstoichiometric cation release exert another impact on the meltwater signal. OA meltwaters (0.7137 – 0.7174) show a higher isotopic ratio compared to OA suspended sediment (0.7130 – 0.7148) which reflects the preferential weathering of the calcite contained within the Variscan gneisses (estimated 0.7160 ± 0.001).

The $^{87}Sr/^{86}Sr$ ratio measured in rain is 0.7104 (n = 5). An influence of rain on Rhone meltwater $^{87}Sr/^{86}Sr$ ratio is not neglectable. The high Sr isotopic singature of Oberaar meltwaters compared to that of the corresponding suspended sediment and also to the low Sr isotopic ratio of rainwater (0.7104) suggests that the atmospheric contribution is not visible in the Oberaar meltwaters.

Disseminated calcite exerts a major impact not only on the meltwater major ion composition but also on its Sr systematics.

Introduction

Flux rates and isotopic ratios of Sr have been analysed in stream water settings in order to trace mineral weathering reactions and weathering rates of individual silicate phases and compare them with the isotopic characteristics of the catchments source rocks (e.g., Blum et al., 1993, Blum and Erel, 1995, Taylor and Blum, 1995, Clow et al., 1997). The chemical weathering of Sr from minerals is not necessarily stoichiometric and is dominated by the rapid dissolution of Sr-rich and highly reactive minerals or mineral inclusions; e.g., disseminated calcite (Clow et al., 1997, Blum et al., 1998, Jacobson and Blum, 2000, Jacobson et al., 2002) or apatite (Aubert et al., 2001). Biotite releases considerable amounts of highly radiogenic Sr during the initial stages of weathering, where the initial weathering rates may exceed those for feldspar (Blum and Erel, 1995, Blum and Erel, 1997, Arn et al., submitted). In laboratory dissolution experiments Brantley et al. (1998) show that early Sr release from feldspars is nonstoichiometric and not isotopically identical to the starting material. The nonstoichiometric release is attributed to secondary phases present in minute propor-

This chapter by Kaspar Arn, Rachel Hosein, Karl B. Föllmi, Philipp Steinmann, Dominique Aubert (Strasbourg), and Jan Kramers (Berne) has been prepared for submission to Schweizerische Mineralogisch-Petrographische Mitteilungen.

tions, and/or to leaching of cations from damaged sites. They further propose that abraded feldspar particles formed during glaciation will show this initial transient nonstoichiometric release.

Recently detailed studies of the meltwater chemistry (major ions as well as Sr systematics) were performed in glaciated catchments draining different types of rock substrata (e.g., Anderson et al., 2000, Sharp et al., 2002, Tranter et al., 2002). In these studies it was shown that carbonate weathering has a dominant influence on bulk meltwater chemistry, even in catchments of predominantly silicate lithologies with only trace amounts of carbonates (Clow et al., 1997, Blum et al., 1998, Anderson et al., 2000, Jacobson and Blum, 2000, Jacobson et al., 2002, Tranter et al., 2002).

Sr flux rates and isotopic ratios in stream waters also reflect the intensity of weathering. Sr isotopic budgets for Himalayan rivers are used to infer increased erosion rates in this mountain range (Galy et al., 1999, Galy and France-Lanord, 2001). They are relevant as indicators of silicate weathering rates and of the relative importance of carbonate and silicate weathering sources within different Himalayan settings (Harris, 1995, English et al., 2000).

The Sr isotopic ratios in continental riverine runoff are used as a proxy for the rate of chemical weathering on continents. They control the Sr isotopic signature of deposited marine carbonates together with other Sr sources, such as submarine hydrothermal sources and deep-sea sediment pore waters (Blum and Erel, 1995, Palmer and Edmond, 1989, Hodell et al., 1990, Hodell and Woodruff, 1994). Steep gradients in the Sr isotopic ratio towards more radiogenic values in marine carbonates in the late Eocene – Holocene are explained by the intensified weathering of continental source rocks associated with the uplift of the Tibetian plateau and Himalayan mountain range (e.g. Raymo et al., 1988, Raymo and Ruddiman, 1992, Edmond, 1992).

Subglacial and proglacial weathering processes increase the chemical weathering of primary minerals (Sharp et al., 1995, Hallet et al., 1996, Anderson et al., 1997; Tranter et al., 2002, Hosein et al., submitted) and enhance the release of Sr by several mechanisms: (1) glacial grinding and abrasion of rock generating ultrafine particles (< 63 μm) with increased total reactive surface area, (2) selective weathering of bedrock components with relatively high Sr isotopic ratios, (3) the continuous supply of these minerals and the larger discharge and increased flushing of glacial sediments and soils, (4) the presence of mechanically damaged surfaces, enhancing the nonstoichiometric dissolution due to their transiently reactive surface area.

	Oberaar		**Rhone**	
Geogr. Position	46° 32' N 8° 14' E		46° 35' N 8° 23' E	
Surface of catchment	11.2 km^2		23 km^2	
Altitude	2310 - 3631 m a.s.l.		1750 - 3630 m a.s.l.	
Glacier cover today (%)	57%		73%	
Annual mean temperature †	- 1° C §		+ 1.2° C §	
Annual mean precipitation †	2100 mm		2200 mm	
Geology of catchments:	total*	ice covered#	total*	ice covered¥
Central Aar Granite	38%	26%	90%	76±1%
Grimsel Granodiorite	7%	3%	10%	24±1%
Variscan gneisses	42%	60%		
Ultramafic Inclusions	1%			
Southern Aar Granite	12%	11%		

† Schwab (2001)
§ within proglacial area; 2300 m at Oberaar, 1757 m at Rhone
* from geological maps of areas, see text for references.
# Ultramafic inclusions neglected, see text for explanations.
¥ calculated in this work, see text for explanations.

Table 4.1: Different parameters of the two catchments. For geology see also Fig. 4.1.

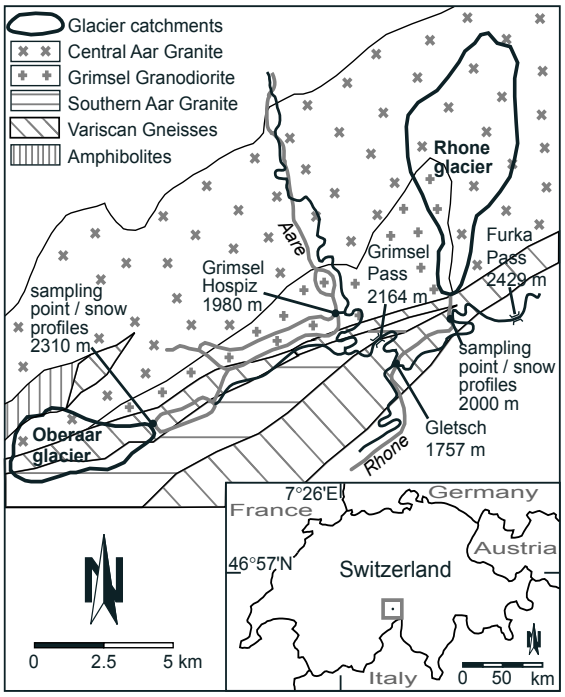

Fig. 4.1: Map of the field areas with geology of the Aar Massif modified after Oberhänsli et al. (1988) and todays glacier catchments.

We studied subglacial chemical weathering processes and the Sr isotope composition of bedrock, runoff and particulate material in the two glaciated catchments of Oberaar (OA) and Rhone (RH) Glaciers (Swiss Alps), which are both situated in the crystalline rocks of the Aar massif. Our goal was to estimate the influence of preferential dissolution of major and trace minerals on the bulk meltwater signal. We suggest that the lithological differences between the two areas in this framework of granitic rocks exert major influences on the bulk meltwater isotope chemistry and the mineralogy of the particulate flux (suspended sediment). We show that dissolution of disseminated calcite and non-stoichiometric Sr release from silicates are important sources of Sr and determine Sr isotopic ratios in runoff. A novel element in this work is that glaciated purely crystalline terrains have not been studied in the same detail as mixed crystalline sedimentary or sedimentary terrains.

Field areas

The Rhone and Oberaar Glaciers are located to the east and west of the Grimselpass (2100m above sea level) in the central Swiss Alps, respectively (Fig. 4.1 and Table 4.1). The glaciers experience similar climatic conditions (Schwab et al., 2001) and are presently subjected to considerable retreat and loss in volume. Both areas are contained within the crystalline rocks of the Aar Massif (Stalder, 1964, and Abrecht, 1994; Fig 4.1), and the lithologies are quite homogeneous and comparable, except for the presence of a zone of highly deformed Variscan basement gneisses and schists in the Oberaar area (Oberhänsli et al., 1988).

The Central Aar Granite and the Southern Aar Granite contain quartz, potassic feldspar (microcline), plagioclase (albite), and micas (mainly biotite). The Grimsel Granodiorite is richer in mica (biotite) and contains several meter to decameter sized basic lenses higher up in the Oberaar catchment.

The Variscan Gneisses show recrystallized quartz, plagioclase (20 – 50 vol%; albite), and 8 – 20 % biotite and may contain some potassic feldspar (microcline). These gneisses are heterogeneous on a small scale and contain up to 9 wt% calcite (compare also Stalder (1964), who found up to 5 vol% calcite). Sulfide mineralization is evident in these rocks, as visible in many rusty stains on weathered surfaces and the higher SO_4 flux in the meltwater (Hosein et al., submitted).

Sampling and analytical methods

Weekly (summer) to monthly (winter) bulk meltwater samples (1000 ml) were taken at both glaciers throughout the years 1999 to 2001 and a representative collection was used for Sr-analyses. The samples were immediately filtered in the field using 0.45 μm cellulose nitrate filters, acidified using suprapure HNO_3, and stored in prewashed (10% HNO_3) polypropylene bottles at 4° C. Suspended sediment was collected from both glaciers during the ablation seasons (1999 to 2001) by filtering meltwaters in the field. The sediment samples were oven-dried at 40° C. Rain samples were taken during the 2000 and 2001 ablation seasons: A polypropylene bottle was connected to a plastic funnel via a polypropylene tube (all equipment was prewashed with 10% HNO_3). The bottle was left for a maximum of 24 hours before the rainwater was filtered and stored like the meltwaters. 17 samples of bedrock were randomly taken within the proglacial areas and on the valley walls beside the glaciers. The bedrock samples include the major lithologies of the two catchment areas. Subglacially precipitated carbonate depos-

its were sampled in both catchments, they appear quite widespread in front of the retreating glaciers. Whole-rock samples plus carbonate deposits were crushed and milled to a fine powder in an agate mill.

A first series of samples was analysed at the Geological Institut of the University of Berne according to the following procedure:

Approximately 100 ml of water was evaporated and the residue dissolved in 1 ml of 3M HNO_3. From a first serie of suspended sediment and rock powders, 1 – 2 g were leached with 4.2M acetic acid for 30 min (weak acid samples, WA). The supernatant was centrifuged twice, evaporated, dissolved with 14M HNO_3 and again evaporated, before being dissolved in 1 ml of 3M HNO_3. The leaching residue was dried, approximately 0.15 mg was digested for 72 hours at 120°C in closed Savilex vessels containing a mixture of 35M HF and 14M HNO_3 (residue total digestion samples, RT). The evaporated samples were taken into solution with 6M HCl and H_2O (pure), evaporated again and subsequently dissolved in 1 ml of 3M HNO_3. In a second serie approximately 0.06 mg of suspended sediment (4 samples) and of carbonate deposit (1 sample) was digested for 72 hours at 120°C in closed Savilex vessels with 14M HNO_3 (strong acid samples, SA). The supernatant was centrifuged, evaporated and subsequently dissolved in 1 ml of 3M HNO_3.

All samples were spiked with approximately 0.05 – 0.06 mg of an ^{84}Sr spike, all acids used were purified by double distillation. All samples were centrifuged prior to the separation of Sr from other ions using columns with Sr spec-pure resin. Strontium samples were stored in 0.01M HNO_3 and some of them were diluted with 0.35M HNO_3 prior to analyses. The samples were analysed on a Nu Instruments® Multiple Collector Inductively Coupled Plasma-Mass Spectrometer (MC-ICP-MS) in static mode. During the analyses 19 standards (NBS 987) were measured with an average $^{87}Sr/^{86}Sr$ of 0.710286 (2 s.d. = 0.000019).

A second serie of samples was analysed in the Centre de Géochimie de la Surface in Strasbourg. Bedrock samples representative for the catchment lithologies and two suspended sediment and meltwater samples were analysed for their Sr isotopic composition and their chemistry. The chemistry, including Sr, was measured on an ICP-MS. For the analyses of the Sr isotopic composition powders of the samples were digested for 7 days in closed Savilex vessels containing a HF, HNO_3, and $HClO_4$ mixture (bulk samples, TD). Strontium was separated from other ions using a cation exchange resin with 1.5 and 4M HCl as eluents. The total procedural blank was < 0.5 ng. $^{87}Sr/^{86}Sr$ ratios were determined on a VG Sector® multicollector thermal ionisation mass spectrometer (TIMS). Strontium was deposited on a W filament with Ta_2O_5 as activator. Mass fractionation corrections were applied by normalising the average $^{87}Sr/^{86}Sr$ ratios to the $^{86}Sr/^{88}Sr$ ratio of 0.1194. The accuracy of the $^{87}Sr/^{86}Sr$ analyses was evaluated by determining the NBS 987 standard. A mean value of $^{87}Sr/^{86}Sr = 0.710258$ (2 s.d. = 0.000026, n = 9) was obtained during analyses.

A third serie of samples was analysed at the Geochemical and Environmental Analyses (GEA) Laboratory of the University of Neuchatel. 1 – 2 g from the bedrock and subglacial carbonate powders were leached with 4.2 M acetic acid for 30 min (WA samples). The supernatant was pipetted of and filtered using 0.45 μm cellulose nitrate filters and a syringe. The leachates were measured on a quadrupole ICP-MS together with 10 further meltwater samples. Detection limit of this quantitative method is < 100 ppt for Ca and < 1 ppt for Sr.

Total inorganic carbon was determined on about 100 mg of ground rock powder, using Rock Eval 6 standard bulk rock pyrolysis (Espitalié et al., 1986 and Lafargue et al., 1996). The inorganic or mineral carbon contents (MINC) were calibrated with marble standards and expressed as wt% calcite. For low concentrations the error is 20 % (RSD); for higher concentrations (≥ 0.5 wt%) the error is 5 % (RSD) or less.

Major cations of the meltwater samples were measured by ion chromatography (Dionex DX 500, Hosein et al., submitted). The error is ± 5 % for concentrations of < 100 ppb and ± 2 % for concentrations of 100 ppb – 1 ppm.

Results

The results of the chemical and Sr isotopic analyses are given in Table 4.2 & 4.3 and Fig. 4.2 & 4.3. Our obtained $^{87}Sr/^{86}Sr$ ratios for bedrock correspond well with previously published data of the same rocks. The $^{87}Sr/^{86}Sr$ ratio for Central Aar Granite (0.7449) concurs with the data from Challandes (2001). Also the Grim-

Sample			Sr	$^{87}Sr/^{86}Sr$		2σ	Calcite *	Ca	Ca/(1000*Sr)	Na	Ca/Na
			µmol g^{-1}			error	wt%	µmol g^{-1}		µmol g^{-1}	
Bedrock											
Central Aar Granite											
R17	TD	SB	0.422	0.744946	±	0.000026	0.11	52	0.122	526	0.098
R17	RT	BE	0.413	0.745898	±	0.000012					
R17	WA	BE	0.019	0.736238	±	0.000072					
R17	WA	NE	0.007					9.4	1.328		
CAGr		¥	1.050	0.747077	±	0.000109		159	0.151	660	0.240
Aar10		#	0.902	0.731928	±	0.000028					
	Bio		1.142	0.741252	±	0.000167					
	K-Feldspar		0.711	0.733796	±	0.000058					
Aar12		#	0.799	0.737147	±	0.000032					
	Bio		6.518	0.739120	±	0.000043					
	Plagio		0.833	0.744114	±	0.000269					
Aar17		#	0.811	0.744057	±	0.000056					
	Bio		0.148	0.748567	±	0.000098					
	Plagio		0.822	0.743363	±	0.000079					
Grimsel Granodiorite											
R6	TD	SB	1.941	0.711526	±	0.000024	0.27	185	0.096	874	0.212
R6	RT	BE	1.488	0.711554	±	0.000025					
R6	WA	BE	0.004	0.717531	±	0.000020					
R6	WA	NE	0.003					4.2	1.565		
R1		SB	3.139	0.716050	±	0.000024		285	0.091	597	0.478
R9		SB	3.630	0.710569	±	0.000026		503	0.138	911	0.552
Aar31		#	4.212	0.708837	±	0.001640					
	Bio		0.594	0.716423	±	0.000046					
	Kfs		3.311	0.710056	±	0.000085					
AD20		#	2.686	0.710093	±	0.000029					
	Bio		1.435	0.713651	±	0.000394					
	Plagio		1.498	0.710527	±	0.000075					
ACIIh		#	2.573	0.711382	±	0.000053					
	Bio		0.726	0.715351	±	0.000074					
	Plagio		3.409	0.711191	±	0.051440					
Southern Aar Granite											
SAGr		¥	0.869	0.735627	±	0.005317					
Variscan gneisses											
R8	TD	SB	1.792	0.712059	±	0.000024	0.15	1818	1.014	450	4.040
R8	RT	BE	2.282	0.711808	±	0.000014					
R8	WA	BE	0.003	0.716165	±	0.000020					
R8	WA	NE	0.011					1.2	0.104		
R15	TD	SB	4.121	0.707763	±	0.000022	9.01	1230	0.298	321	3.832
R15	RT	BE	2.990	0.707828	±	0.000014					
R15	WA	BE	0.865	0.707644	±	0.000050					
R15	WA	NE	0.494					403	0.816		
Suspended sediment											
Oberaarglacier											
OAP6	TD	SB	1.838	0.714783	±	0.000013		241	0.131	569	0.423
OA3	RT	BE	2.193	0.713794	±	0.000032					
OA3	WA	BE	0.134	0.713426	±	0.000024					
OA1	SA	BE	2.717	0.712984	±	0.000014		355	0.131	453	0.783
OA2	SA	BE	2.705	0.713787	±	0.000008		351	0.130	500	0.702
Rhoneglacier											
RH3.8.	TD	SB	1.164	0.730245	±	0.000015		141	0.121	639	0.220
RH3	RT	BE	1.117	0.730570	±	0.000013					
RH3	WA	BE	0.055	0.733371	±	0.000016					
RH1	SA	BE	1.142	0.730583	±	0.000021		162	0.142	621	0.261
RH2	SA	BE	1.176	0.727853	±	0.000029		168	0.143	597	0.281
Carbonate deposit											
OK1		BE	1.725	0.7164363	±	0.000013					
OK1	WA	NE	0.100					385	3.858		
RH1		BE	0.160	0.719159	±	0.000024					

SB measured at Centre de Géochimie de la Surface in Strasbourg
BE measured at Geologisches Institut, University of Berne
NE measured at GEA Lab, University of Neuchatel
¥ Schaltegger et al. 1990
Challandes et al. 2002
* From RockEval analyses, GEA Lab, University of Neuchatel

TD bulk samples
RT residue total digestion samples
WA weak acid leachates
SA strong acid leachates

Table 4.2: Results of the different bedrock and suspended sediment analyses.

Sample		Sr* µmol l^{-1}	$^{87}Sr/^{86}Sr$		2σ error	Ca µmol l^{-1}	Ca/(1000•Sr)	Na$^{\#}$ µmol l^{-1}	Ca/Na
Meltwater									
Oberaarglacier									
O51	BE	0.403	0.715619	±	0.000024	203.74	0.51	23.04	8.84
O65	BE	0.197	0.713730	±	0.000023	86.78	0.44	6.52	13.31
O75	BE	0.146	0.715419	±	0.000020	90.27	0.62	9.57	9.44
O80	BE	0.109	0.717371	±	0.000046	67.48	0.56	16.96	3.97
P6	SB	0.125	0.715950	±	0.000013	69.98	0.56	14.00	5.00
P4	NE	0.218				136.90	0.63		
P7	NE	0.079				83.40	1.05		
K8	NE	0.301				136.77	0.45	14.35	9.53
P8	NE	0.240				108.87	0.45		
P9	NE	0.479				231.07	0.48		
K25	NE	0.238				99.52	0.42	6.52	15.26
Rhoneglacier									
A111	BE	0.013	0.725554	±	0.000159	9.48	0.75	3.91	2.42
A142	BE	0.018	0.725840	±	0.000192	12.22	0.67	6.09	2.01
RH3.8.	SB	0.011	0.725067	±	0.000014	9.00	0.84	5.00	1.80
P046	NE	0.008				23.65	2.82	10.00	2.37
A067	NE	0.007				20.18	2.77	7.83	2.58
P093	NE	0.006				9.10	1.51	4.35	2.09
P071	NE	0.009				19.31	2.09	8.26	2.34
P142	NE	0.010				27.77	2.87	6.09	4.56
A169	NE	0.027				45.06	1.69	15.65	2.88
Rain									
O45R	BE	n.a.	0.712375	±	0.000010	67.08	-	16.96	3.96
RR1	BE	n.a.	0.709957	±	0.000108	2.49	-	2.17	1.15
RR2	BE	n.a.	0.709745	±	0.000024	11.72	-	3.91	3.00
RR3	BE	n.a.	0.709788	±	0.000013	n.a.	-	n.a.	-
RR4	BE	n.a.	0.709972	±	0.000033	n.a.	-	n.a.	-

* measured using quadrupole ICP-MS at GEA Lab, University of Neuchatel
$^{\#}$ measured using ion chromatography at GEA Lab, University of Neuchatel
BE measured at Geologisches Institut, University of Berne
SB measured at Centre de Géochimie de la Surface in Strasbourg
NE measured at GEA Lab, University of Neuchatel

Table 4.3: Results of the different meltwater and rain water analyses.

sel Granodiorite $^{87}Sr/^{86}Sr$ ratios (0.7106 & 0.7115) correspond to published data (0.7088 – 0.7114, Challandes, 2001) with exception of sample R1 (0.7161). For Southern Aar Granite a $^{87}Sr/^{86}Sr$ ratio of 0.7356 from Schaltegger and Krähenbühl, 1990) was adopted. For the Variscan Gneisses two $^{87}Sr/^{86}Sr$ ratios (0.7121 and 0.7078) were measured. Published values for this lithology lack. For Rhone suspended sediments we obtained $^{87}Sr/^{86}Sr$ ratios between 0.7279 and 0.7306, for Oberaar suspended sediments the values lie between 0.7130 and 0.7148.

The meltwaters of both glaciers have comparable Sr concentrations: 0.006 – 0.027 and 0.079 – 0.479 μmol l^{-1} for Rhone and Oberaar meltwater samples, respectively. The $^{87}Sr/^{86}Sr$ ratios of the meltwaters sampled throughout the ablation season show little variation (0.7251 – 0.7258 for Rhone and 0.7137 and 0.7174 for Oberaar samples).

The $^{87}Sr/^{86}Sr$ ratios of the rain samples measured are quite similar (0.7097 – 0.7100), except for one sample (0.7124) that was taken during a one day rain event associated with the precipitation of brownish to redish colored dust suggesting its provenance is from outwith the catchment and may have a Saharan source (Lenaz et al., 1986, Kübler et al., 1990). The chemistry of this water shows a high Ca concentration, and the $^{87}Sr/^{86}Sr$ ratio is slightly higher than the average of the other analysed rain samples (Fig. 4.3).

The weak acid attack (WA) of Central Aar Granite gave a $^{87}Sr/^{86}Sr$ ratio of 0.7362 which is lower than that of the corresponding total digested sample (R17, TD = 0.7449). The WA $^{87}Sr/^{86}Sr$ ratio of Grimsel Grano-

diorite is higher than the corresponding TD (R6, WA = 0.7175 and TD = 0.7115). One WA $^{87}Sr/^{86}Sr$ ratio of the two samples of Variscan Gneisses is higher than the corresponding TD (R8, WA = 0.7162 and TD = 0.7121) whereas the other WA $^{87}Sr/^{86}Sr$ ratio is approximately the same (R15, WA = 0.7076 and TD = 0.7078).

All bedrock lithologies of the two catchments contain measurable amounts of calcite (Table 4.2). The calcite content in Grimsel Granodiorite (0.11 wt%) is lower than in Central Aar Granite (0.27 wt%). The Variscan Gneisses contain 9 and 0.15 wt% of calcite, respectively. The large differences in calcite contents in the Variscan Gneisses point towards the heterogeneity of these rocks (Arn et al., submitted).

The strong acid attack of Oberaar suspended sediment (SA samples: 0.7130 & 0.7138; 14M HNO_3) gave ratios close to the residue sample (RT, 0.7138) but smaller than the bulk sample (TD, 0.7148). The WA $^{87}Sr/^{86}Sr$ ratio of the suspended sediment (0.7134) is similar, and lies between the two WA $^{87}Sr/^{86}Sr$ ratios of the Variscan Gneisses (0.7076 & 0.7162). The heterogeneity of the Variscan Gneisses is also reflected in the scattering of the suspended sediment samples. The Rhone suspended sediment WA $^{87}Sr/^{86}Sr$ ratio (0.7334) is higher than the residue (RT, 0.7306) and the bulk sample (TD, 0.7302), and may be comparable to the WA $^{87}Sr/^{86}Sr$ ratio of Central Aar Granite (0.7362). The strong acid attack (SA: 0.7279 & 0.7306; 14M HNO_3) gives values comparable to the residue and the bulk sample, which is probably related to the leaching of a significant part of silicate minerals. Due to the more homogeneous bedrock of the Rhone catchment its suspended sediment shows less scatter. In the suspended sediment leaving a glacier a significant amount of minerals may already be leached subglacially and the further leaching of suspended sediment might not correspond to the initial leach. Therefore we do not use the suspended sediment WA $^{87}Sr/^{86}Sr$ ratios for the following discussion of Sr sources in the meltwaters.

Discussions

General

The Sr isotopic signal of the meltwaters is usually dominated by contributions from disseminated calcite due to its high dissolution rate and its preferential weathering in subglacial environments (as is reported from other glaciated areas, e.g., Tranter et al., 1993, Tranter et al., 2002, Anderson et al., 1997, White et al., 1999, Hosein et al., submitted). Compared to the suspended sediment, the meltwaters from both glaciers show a Ca enrichment relative to Na (increased Ca/Na ratio) which points towards the preferential weathering of a mineral with a high Ca concentration (calcite, apatite; Fig. 4.3). For Oberaar glacier the Ca enrichment is higher. As the concentrations of PO_4 measured in meltwaters from both glaciers are comparable (Hosein et al., submitted), the main source of Sr in the meltwaters can not be apatite but rather disseminated calcite contained within the different bedrock lithologies. Furthermore, easily hydrated ions derived from freshly cleaved silicate surfaces may exert another impact on the meltwater signal. Their early release is nonstoichiometric and may not correspond to the bulk mineral signature (Brantley et al., 1998).

All granitic rocks in our areas contain measurable amounts of disseminated calcite, with up to 9 wt% calcite in the Variscan Gneisses (Table 4.2). For all the rock and suspended sediment samples, the $^{87}Sr/^{86}Sr$ ratios of WA samples (which are dominated by disseminated calcite) are quite similar to the ratios measured in the bulk samples (TD samples). Disseminated calcite seems to have more or less equilibrated with the surrounding rock during Alpine metamorphism of the Aar Massif (O. Müntener, pers. comm.). However, the small differences in the $^{87}Sr/^{86}Sr$ ratios of the WA samples compared to the bulk rock values allow us to discuss the different sources of Sr present in the meltwaters.

Suspended sediment represents bedrock that was recently mechanically abraded at the glacier base (Benn and Evans, 1998, Drewry, 1986) and its mineralogy shows an average of the different bedrock compositions of todays glacier catchments (Arn et al., submitted). The composition of suspended sediment is affected by the composition of glacier covered bedrock type, by mechanical effects of abrasion and transport, as well as by the overall resistance (or hardness) of a lithology and its minerals against mechanical erosion.

Rhone systematics: a) Suspended sediment vs. catchment lithologies.

Using a mass balance approach we calculate the portions of the two bedrock lithologies within the

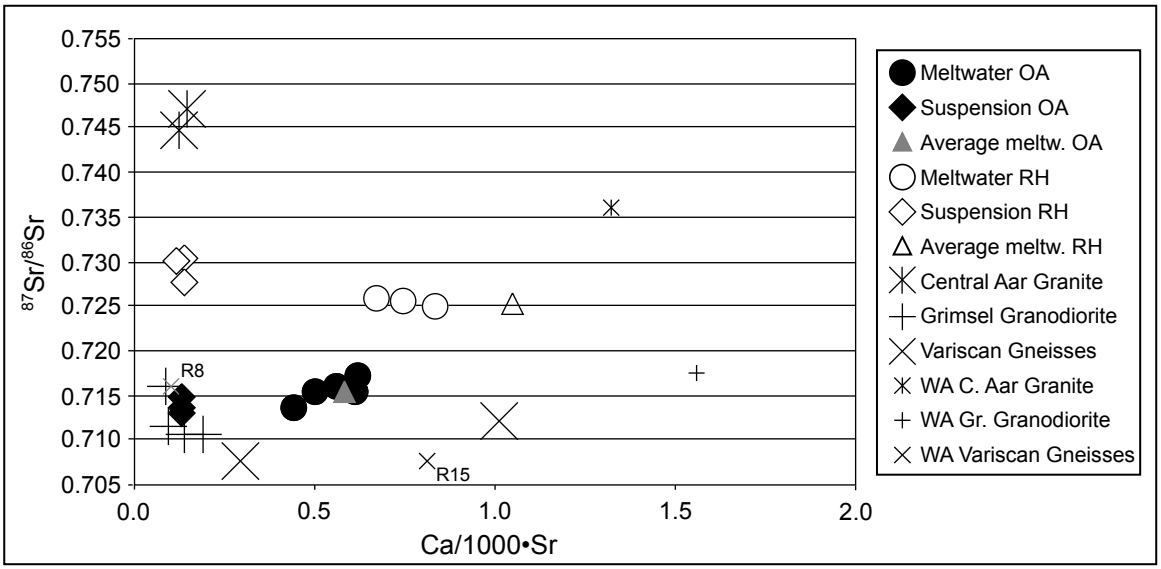

Fig. 4.2: $^{87}Sr/^{86}Sr$ vs. Ca/(1000•Sr) for water, bedrock and suspended sediment samples from both catchments.

catchment. Knowing the $^{87}Sr/^{86}Sr$ ratios and Sr concentrations of the two main lithologies in the Rhone catchment (Table 4.2) and considering suspended sediment to be a mixture of the two recently mechanically eroded bedrock lithologies (see above; bulk suspended sediment (TD) $^{87}Sr/^{86}Sr$ ratio and Sr concentration) we calculated the portions of these lithologies within the suspended sediment. This calculation gives approximately 76 ± 1 % of Central Aar Granite and 24 ± 1 % of Grimsel Granodiorite (Table 4.1). Assuming equal erodability (no difference in the overall hardness) indicates that also the areal distribution of the two lithologies is approximately 76 and 24 %. The values are quite different from an estimated distribution using different maps, which give approximately 90 and 10 % for Central Aar Granite and Grimsel Granodiorite, respectively (Table 4.1). However, the available maps are not precise for the glacier covered parts of the catchment, hence our calculated distribution of the two lithologies is probably more reliable.

b) Rhone meltwater signal

At Rhone glacier the $^{87}Sr/^{86}Sr$ ratio of the meltwater is smaller than of the suspended sediment. Meltwater $^{87}Sr/^{86}Sr$ ratios lie between the two bedrock WA samples (Central Aar Granite 0.7362; Grimsel Granodiorite 0.7175, Fig. 4.2 & 4.3, Table 4.2 & 4.3) but according to the lithological distribution they are not corresponding to the WA values. We propose four reasons for this fact: (1) During the weak acid attack more than calcite was dissolved, the WA signal is influenced by other minerals. As the Central Aar Granite WA value (0.7362) lies below the TD value (0.7449) and other single mineral values are higher (0.7371 – 0.7486, except 0.7338 for one K-feldspar sample; see Table 4.2) the pure granite calcite $^{87}Sr/^{86}Sr$ ratio has to be lower than the WA value. Accordingly, as the WA $^{87}Sr/^{86}Sr$ ratio of Grimsel Granodiorite is the highest of all Granodiorite values (Table 4.2), the pure granodiorite calcite $^{87}Sr/^{86}Sr$ ratio has to be equal or more likely higher admitting that also for Grimsel Granodiorite more than calcite was leached by the weak acid attack (WA). As a broad estimation we propose the disseminated calcite of Rhone catchment lithologies to be between 0.7200 (granodiorite) and 0.7300 (granite) with a higher Ca/1000•Sr ratio than the average meltwater. Because the Ca enrichment relative to Na in Rhone meltwaters compared to Rhone suspended sediment is significant, we assume that calcite dissolution exerts the dominant impact on the meltwater chemistry. (2) The nonstoichiometric Sr release during initial subglacial weathering could have a lowering effect on the $^{87}Sr/^{86}Sr$ ratios which is visible in our meltwaters. The feldspars from Grimsel Granodiorite have a higher Sr concentration (1.498 – 3.409 μmol g^{-1}) compared to Central Aar Granite feldspars (0.711 – 0.822 μmol g^{-1}). They could therefore dominate the nonstoichiometric Sr release, and, according to their lower $^{87}Sr/^{86}Sr$ ratios (0.7101 – 0.7112 compared to 0.7338 – 0.7441 for Central Aar Granite feldspars), they could have a decreasing effect

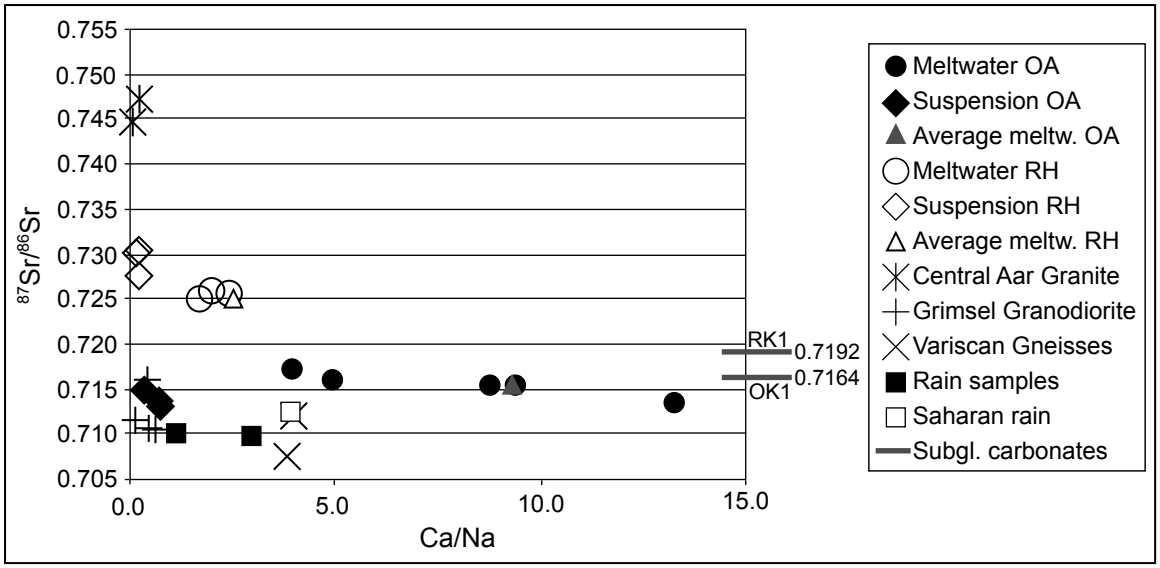

Fig. 4.3: $^{87}Sr/^{86}Sr$ vs. Ca/Na for water, bedrock and suspended sediment samples from both catchments.

on the meltwater $^{87}Sr/^{86}Sr$ ratios. (3) The dissolution of subglacially precipitated carbonate could exert another lowering influence on the meltwater values (0.7192, Fig. 4.3). The significant occurrence of such carbonates in front of Rhone glacier assumes them to exist also beneath the actual glacier, where they can get involved in the subglacial weathering processes. (4) At Rhone the lower $^{87}Sr/^{86}Sr$ ratios in meltwaters compared to bulk suspended sediment may imply that atmospheric input (with its low $^{87}Sr/^{86}Sr$ ratio and high Ca/Na values) also exerts a visible impact on the meltwater signal (Fig. 4.3).

a) Oberaar systematics: Comparing Oberaar lithologies and suspension

At Oberaar the lithological architecture is visible from the broad geomorphological framework: The main valley incision was performed on the easier erodable zone of Variscan Gneisses which make up approximately 60 % of the total glacier covered area (Table 4.1). The remaining 40 % at the glaciers sides are composed of granitic rocks which are harder and less erodable. The lithologies are elongated parallel to the main valley geometry from the glacier snout to the top of the catchment (the Oberaar Joch). Taking into account the ratio of glacier cover, the average suspended sediment flux (kg km^{-2} yr^{-1}) of Oberaar glacier is 2 times higher than Rhone glacier (Hosein et al., submitted). Knowing the areal distribution of 60 % : 40 % and taking the erodability of granitic rocks to equal 1 we calculate the erodability of the Variscan Gneisses to be 2.7 to get an overall flux that is 2 times higher. This corresponds to an influence of the gneiss on the bulk suspended sediment of 73 %. Beside the areal distribution this higher influence is due to effects of anisotropy and glacier dynamics (e.g., higher ice overweight along central parts of glacier).

b) Oberaar meltwater signal

In accordance to the values of the two samples of Variscan Gneisses the $^{87}Sr/^{86}Sr$ ratios of Oberaar suspended sediment (TD) and the meltwater are lower than the ones of Rhone (Fig. 4.2 & 4.3, Table 4.2 & 4.3). The Oberaar meltwaters show a stronger Ca-enrichment relative to Na compared to the suspended sediment than Rhone meltwaters (Fig. 4.3). This is due to the clear dominance of the Variscan Gneisses (with their higher erodability and their higher calcite content compared to the granitic lithologies) in this catchment. Watching the WA $^{87}Sr/^{86}Sr$ ratios of the two samples of Variscan Gneisses, the meltwater $^{87}Sr/^{86}Sr$ ratios would be expected to plot lower, which implies that our two samples do not seem to be representative for the Variscan Gneisses (=> outliers!). This shows clearly the high heterogeneity of these gneisses, they are not adequately represented by the two samples we measured (cf. also the different calcite content of the two samples, R8 = 0.15 wt%, R15 = 9 wt%). According to the Sr ratio of the meltwaters, we would expect an average gneiss calcite $^{87}Sr/^{86}Sr$ ratio to be 0.7160 ±

0.001. Furthermore, the $^{87}Sr/^{86}Sr$ ratio of a sample of subglacially precipitated carbonate deposits is about the same (0.7164, Fig. 4.3), whereas its Ca/Na ratio is higher than all the meltwater samples measured. As the carbonate deposits are quite widespread in this catchment (own observations at the glacier snout), their subglacial dissolution could also exert a major impact on our meltwater signals.

Because Oberaar meltwater $^{87}Sr/^{86}Sr$ ratios are higher than the suspended sediment (and than all the rain values), the atmospheric impact is minor relative to the other discussed Sr sources (Fig. 4.3).

Comparison to other works

Sharp et al. (2002) discuss the relationship between subglacial weathering processes and the Sr isotope systematics of meltwater runoff from Robertson Glacier, (Alberta, Canada) a glacier that rests on predominantly carbonate bedrock. During times of quick flow conditions with high discharge, when meltwaters are dilute and their residence times within the glacier are short, the contribution of carbonates to the Sr flux in runoff dominates. Opposite, during distributed flow conditions, when meltwater-rock contact times are long, significant amounts of K-silicate minerals present in the catchment exert a visible impact on the meltwaters.

On the other hand, Anderson et al. (2000) show in their research for streams draining the catchment of the retreating Bench Glacier (south-central Alaska, glacier within metagraywacke-metapelite bedrock), that the dominant contribution to solute flux in the glacier outlet stream is by generally biotite alteration. The carbonate source only became dominant in proglacial streams draining sediments of increasing age of exposure.

The measured $^{87}Sr/^{86}Sr$ ratios of our meltwaters lie too close to each other (& their Sr concentrations are scattering too much) to significantly attach their values to such trends (and they are too few).

Conclusions

This is the first work which analyses Sr isotopes in purely crystalline glaciated terrains. Generally, meltwaters draining crystalline glaciated catchments reflect the high $^{87}Sr/^{86}Sr$ ratios of the underlying bedrocks. Meltwater composition is defined by different short-term subglacial processes: At Oberaar we showed that the dissolution of disseminated calcite exerts a major impact not only on meltwater major ion composition but also on its Sr systematics. Also Rhone glacier meltwaters draining a solely granitic catchment show a clear impact of disseminated calcite dissolution. Here the influence of nonstoichiometric Sr release from silicates and from precipitation seems to be visible as well.

The dominance of calcite dissolution was confirmed in the Oberaar catchment (where the Variscan Gneisses contain more calcite and are easier erodable than the other granitic rocks) by comparing the $^{87}Sr/^{86}Sr$ ratio of the meltwaters to the $^{87}Sr/^{86}Sr$ ratios of disseminated (& subglacially precipitated) calcite.

Outlook

In this work we analysed the Sr systematics of crystalline glaciated terrains. We showed clearly that disseminated calcite exerts a dominant impact on meltwater Sr characteristics, even in a pure crystalline catchment, e.g., the Rhone catchment. Hosein et al. (submitted) show that as soon as there is a higher amount of calcite (2.3 % in Oberaar compared to 0.5 % in Rhone catchment) it dominates the meltwater dissolved load. Sr isotope systematics help to clarify our knowledge about subglacial weathering processes. On the other hand our work also shows the limits of the Sr systematics, where heterogeneities in Sr content of lithologies complicate the interpretations (Oberaar catchment with Variscan Gneisses).

To resolve the remaining uncertainties with our findings we would therefore propose several points to consider during a continued survey of the two catchment areas:

(1) In order to get insight in the exact Sr systematics of disseminated calcite we propose step wise leaching experiments starting with ultrapure water and weaker acids (pH 4), in analogue to the work of Sharp et al. (2002). Leaching with 4.2M acetic acid was shown to be too strong.

(2) During a further field mission we would try to get more samples of the Variscan Gneisses ($n > 10$) as well as of the granitic rocks, in order to compare the scatter between them and to be able to conclude what could be an average value for the gneisses of the area.

(3) Same time we would get more meltwater and

suspended sediment samples (n = 15 – 20), in order to get insight in their variance and trends (quick-flow / dilute-flow) during the ablation season. Accumulation season samples could give information about weathering processes during longer sediment-water contact times.

(4) The calcite content should be measured on all bedrock samples and on suspended sediments.

(5) During a further field mission several rainwater samples could be collected to countercheck the data obtained within this work.

Acknowledgements

This work benefited from the collaboration with Dominique Aubert (Strasbourg) and Jan Kramers (Berne) who are gratefully acknowledged. We thank Virginie Matera (Neuchatel) and Ingeborg Hebeisen (Berne) for laboratory assistance. This study was supported by Swiss National Science Foundation Grants 21-53997.98 and 20-61485.00.

References

Abrecht, J., 1994. Geologic units of the Aar massif and their pre-Alpine rock associations: A critical review. Schweizerische Mineralogisch-Petrographische Mitteilungen, 74: 5-27.

Anderson, S.P., Drever, J.I., Frost, C.D. and Holden, P., 2000. Chemical weathering in the foreland of a retreating glacier. Geochimica et Cosmochimica Acta, 64(7): 1173-1189.

Anderson, S.P., Drever, J.I. and Humphrey, N.F., 1997. Chemical weathering in glacial environments. Geology, 25(5): 399-402.

Arn, K., Hosein, R., Adatte, T., Steinmann, P. and Föllmi, K.B., submitted. Chemical weathering in a glacial chronosequence in the forefields of Rhone and Oberaar Glaciers (Swiss Alps): Rate and mechanism of biotite weathering. Chemical Geology.

Aubert, D., Stille, P. and Probst, A., 2001. REE fractionation during granite weathering and removal by waters and suspended loads: Sr and Nd isotopic evidence. Geochimica et Cosmochimica Acta, 65(3): 387-406.

Benn, D.I. and Evans, D.J.A., 1998. Glaciers and glaciation. Arnold Publishers, London, 734 pp.

Blum, J.D. and Erel, Y., 1995. A silicate weathering mechanism linking increases in marine 87Sr/86Sr with global glaciation. Nature, 373: 415-418.

Blum, J.D. and Erel, Y., 1997. Rb-Sr isotope systematics of a granitic soil chronosequence: The importance of biotite weathering. Geochimica et Cosmochimica Acta, 61(15): 3193-3204.

Blum, J.D., Erel, Y. and Brown, K., 1993. 87Sr/86Sr ratios of Sierra Nevada stream waters: implications for relative mineral weathering rates. Geochimica et Cosmochimica Acta, 58: 5019-5025.

Blum, J.D., Gazis, C.A., Jacobson, A.D. and Chamberlain, C.P., 1998. Carbonate versus silicate weathering in the Raikhot Watershed within the High Himalayan Crystalline Series. Geology, 26(5): 411-414.

Brantley, S.L., Chesley, J.T. and Stillings, L.L., 1998. Isotopic ratios and release rates of strontium measured from weathering feldspars. Geochimica et Cosmochimica Acta, 62(9): 1493-1500.

Challandes, N., 2001. Comportement des systèmes isotopiques 39Ar-40Ar et Rb-Sr dans les zones de cisaillement: Exemples du massif de l'Aar (Massifs cristallins externes) et de la nappe de Suretta (Alpes centrales suisses). PhD Thesis, Université de Neuchâtel, Neuchâtel, CD-ROM.

Clow, D.W., Mast, M.A., Bullen, T.D. and Turk, J.T., 1997. Strontium 87/strontium 86 as a tracer of mineral weathering reactions and calcium sources in an alpine/subalpine watershed, Loch Vale, Colorado. Water Resources Research, 33(6): 1335-1351.

Drewry, D., 1986. Gacial Geologic Processes. Edward Arnold Ldt., London, 276 pp.

Edmond, J.M., 1992. Himalayan tectonics, weathering processes, and the strontium isotope record in marine limestones. Science, 258: 1594-1597.

English, N.B., Quade, J., DeCelles, P.G. and Garizone, C.N., 2000. Geologic control of Sr and major element chemistry in Himalayan Rivers, Nepal. Geochimica et Cosmochimica Acta, 64(15): 2549-2566.

Espitalié, J., Deroo, G. and Marquis, F., 1986. La pyrolyse Rock-Eval et ses applications - III partie. Rev. Inst. Fr. Pet., 41(1): 73-89.

Galy, A. and France-Lanord, C., 2001. Higher erosion rates in the Himalaya: Geochemical constraints on riverine fluxes. Geology, 29(1): 23-26.

Galy, A., France-Lanord, C. and Derry, L.A., 1999. The strontium isotopic budget of Himalayan Rivers in Nepal and Bangladesh. Geochimica et Cosmochimica Acta, 63(13/14): 1905-1925.

Hallet, B., Hunter, L. and Bogen, J., 1996. Rates of erosion and sediment evacuation by glaciers: A review of field data and their iplications. Global and Planetary Change, 12: 213-235.

Harris, N., 1995. Significance of weathering Himalayan metasedimentary rocks and leucogranites for the Sr isotope evolution of seawater during the early Miocene. Geology, 23(9): 795-798.

Hodell, D.A., Mead, G.A. and Mueller, P.A., 1990. Variation in the strontium isotopic composition of seawater (8 Ma to present): Implications for chemical weathering rates and dissolved fluxes to the oceans. Chemical Geology, 80: 291-307.

Hodell, D.A. and Woodruff, F., 1994. Variations in the strontium isotopic ratio of seawater during the Miocene; stratigraphic and geochemical implications. Paleoceanography, 9(3): 405-426.

Hosein, R., Arn, K., Steinmann, P., Adatte, T., Huon, S., and Föllmi, K.B., submitted. Phosphorus weathering: 4 case studies from the Swiss Alps and Venezuela. Biogeochemistry.

Hosein, R., Arn, K., Steinmann, P., Adatte, T., and Föllmi, K.B., submitted. Carbonate and silicate weathering in two presently glaciated, crystalline catchments in the Swiss Alps. Geochimica et Cosmochimica acta.

Jacobson, A.D. and Blum, J.D., 2000. Ca/Sr and $^{87}Sr/^{86}Sr$ geochemistry of disseminated calcite in Himalayan silicate rocks from Nanga Parbat: Influence on river-water chemistry. Geology, 28(5): 463-466.

Jacobson, A.D., Blum, J.D., Chamberlain, C.P., Poage, M. and Sloan, V.F., 2002. Ca/Sr and Sr isotope systematics of a Himalayan glacial chronosequence: Carbonate versus silicate weathering rates as a function of landscape surface age. Geochimica et Cosmochimica Acta, 66(1): 13-27.

Kübler, B., Jantschik, R. and Huon, S., 1990. Minéralogie et granulométrie des poussières éoliennes, dites "Sahariennes", du 24 avril 1989 à Neuchâtel. Leur importance pour l'environnment, les sols et les sédiments. Bulletin de la Société Neuchâteloise des Sciences naturelles, 113: 75-98.

Lafargue, E., Espitalié, J., Marquis, F. and Pillot, D., 1996. Rock Eval 6 applications in hydrocarbon exploration, production and in soil contamination studies, Latin American Congress on Organic Geochemistry, Cancun.

Lenaz, R., Landuzzi, V. and Tomadin, L., 1986. Apports et concentration des masses de poussières éoliennes sur le bassin oriental et occidental de la Méditerrannée. Memoires de la Société Geologique Italienne, 36: 189-200.

Oberhänsli, R., Schenker, F. and Mercolli, I., 1988. Indications of Variscan nappe tectonics in the Aar Massif. Schweizerische Mineralogisch Petrographische Mitteilungen, 68: 509-520.

Palmer, M.R. and Edmond, J.M., 1989. The strontium isotope budget of the modern ocean. Earth and Planetary Science Letters, 92: 11-26.

Raymo, M.E. and Ruddiman, W.F., 1992. Tectonic forcing of late Cenozoic climate. Nature, 359: 117-122.

Raymo, M.E., Ruddiman, W.F. and Froelich, P.N., 1988. Influence of late Cenozoic mountain building on ocean geochemical cycles. Geology, 16: 649-653.

Schaltegger, U. and Krähenbühl, U., 1990. Heavy rare-earth element enrichment in granites of the Aar Massif (Central Alps, Switzerland). Chemical Geology, 89: 49-63.

Schwab, M., Frei, C., Schär, C. and Daly, C., 2001. Mean annual precipitation throughout the European Alps 1971-1990. In: Federal Office for Water and Geology (Editor), The Hydrological Atlas of Switzerland. Federal Office for Topography, Berne, Switzerland.

Sharp, M.J., Creaser, R.A. and Skidmore, M., 2002. Strontium isotope composition of runoff from a glaciated carbonate terrain. Geochimica et Cosmochimica Acta, 66(4): 595-614.

Sharp, M.J., Tranter, M., Brown, G.H. and Skidmore, M., 1995. Rates of chemical denudation and CO2 drawdown in a glacier-covered alpine catchment. Geology, 23(1): 61-64.

Stalder, H.A., 1964. Petrographische und mineralogische Untersuchungen im Grimselgebiet (Mittleres Aarmassiv). Schweizerische Mineralogische und Petrographische Mitteilungen, 44: 187-389.

Taylor, A. and Blum, J., 1995. Relation between soil

age and silicate weathering rates determined from the chemical evolutin of a glacial chronosequence. Geology, 23: 979-982.

Tranter, M., Brown, G., Raiswell, R., Sharp, M. and Gurnel, A., 1993. A conceptual model of solute acquisition by Alpine glacial meltwaters. Journal of Glaciology, 39(133): 573-581.

Tranter, M. et al., 2002. Geochemical weathering at the bed of Haut Glacier d'Arolla, Switzerland - A new model. Hydrological Processes, 16: 959-993.

White, A.F., Bullen, T.D., Vivit, D.V., Schulz, M.S. and Clow, D.W., 1999. The role of disseminated calcite in the chemical weathering of granitoid rocks. Geochimica et Cosmochimica Acta, 63(13/14): 1939-1953.

CHAPTER 5

Elevated apatite weathering rates in alpine glacier forefields (Rhone and Oberaar glaciers, central Switzerland)

Abstract

Apatite dissolution textures and long-term detrital phosphorus (P) weathering rates were determined from chronosequences in the Oberaar and Rhone glacier forefields, central Switzerland. Apatite grains from present-day outwash sediments, Little Ice Age moraines and Younger Dryas tills were graded (1-4) relative to weathering-induced changes in their surface morphologies. Present-day apatite grains are heavily indented and dissolution rounded (grade 1). Little Ice Age grains from two 0-10 cm depth samples already showed extensive dissolution etching, similar to surface grains from the Younger Dryas profile (mean grades 2.7, 3.5 and 3.5 respectively). The weathering front deepened progressively due to bio-corrosion in the evolving acidic pedosphere, with mechanical indentations on grains acting as sites for preferential dissolution. Ironbound, organic, and detrital P concentrations were measured in the chronosequences: Organic and ironbound P in the Younger Dryas profiles replaces detrital P. Detrital P weathering rates are calculated as 0.31 and 0.28 g m^{-2} yr^{-1} for Little Ice Age moraines and 0.01g m^{-2} yr^{-1} for Younger Dryas tills. During the first 300 yrs of glacial sediment exposure P dissolution rates were ca. 70 times higher than the mean global riverine dissolved P flux from ice-free continents. Over 11.6 kyr the flux is 2.5 times the global mean. These data strengthen the argument for changes in the biolimiting P flux on glacial-interglacial timescales.

Introduction

Phosphorus (P) is an essential nutrient and its supply to the biosphere fosters and may even limit primary productivity (Broecker and Peng, 1982; Haselwandter et al., 1983; Tyrell, 1999). Physical weathering is the first order control on the supply of the principal P-bearing mineral apatite to the biosphere (Syers and Walker, 1976; Filippelli and Delaney, 1994). Rates of subsequent biogeochemical weathering of apatite are controlled by its quantity and reactive surface area, the ambient temperature and the supply of weathering solution (Guidry and Mackenzie, 2000). Physical abrasion in the subglacial environment produces large volumes of silt sized sediment grains with complicated microtopographies and consequently enhanced reactive mineral surface areas (e.g. Mahaney, 1995). Apatite is particularly susceptible to comminutation, owing to its (weak) cleavage and relatively low hardness. Moreover, although the near-neutral pH of glacial meltwaters probably renders apatite chemically unreactive in the subglacial environment (Stumm and Morgan, 1996), deposition of mechanically preconditioned apatite grains in proglacial sediments and their exposure to pedogenic processes may accererate biogeochemical P weathering rates. Our study of glacial chronosequences in the Rhone and Oberaar forefields, Switzerland, demonstrates elevated apatite weathering rates in their proglacial zones compared to the average global riverine P flux (Meybeck, 1993). Weathering intensities were assessed by observing changes in grain morphologies, quantifying different forms of P (organic, detrital and ironbound; see below) and calculating weathering rates of detrital P over the last 11.6 kyr. We suggest that apatite dissolution rates are enhanced in proglacial settings due to a combination of physical and chemical factors: i.e. the mechanical abrasion of sediment and the percolation of porewaters that are acidified by atmospheric aerosols and pedogenic processes.

This chapter by Rachel Hosein, Kaspar Arn, Martin R. Lee†, Philipp Steinmann, and Karl B. Föllmi has been submitted for publication in *Geology*.

† Division of Earth Science, Gregory Building, Lilybank Gardens, University of Glasgow, Glasgow G128QQ, UK.

Field areas, sampling, soil identifications, and methods

We sampled a chronosequence (present-day, Little Ice Age = LIA and Younger Dryas = YD sediments) in each glacial forefield. The forefields are approximately 10 km apart and are comparable in their present vegetation (alpine flowers, grasses, and shrubs), altitude (Rhone, 1750 m; Oberaar, 2310 m), climate (mean annual temperature and precipitation for Rhone: +1.2°C, 2200 mm; Oberaar: -1°C, 2100 mm; EDI, 1992) and geology (the crystalline rocks of the Aar massif). The Rhone bedrock consists of Hercynian aged granites (ca. 90%) and granodiorites (ca. 10%), whereas the Oberaar bedrock is a mixture of strongly foliated gneisses (ca. 40%), granites (ca. 50%) and granodiorites (ca. 10%). These distributions hold for the LIA ice extent of both glaciers, and the YD ice extent in the Oberaar catchment. But the Rhone YD ice would have also covered the foliated gneissic zone (ca. 20%) and been joined with the adjacent Mutt glacier, which is underlain by metamorphosed Mesozoic sedimentary rocks (ca. 20 %) in addition to the granite and granodiorite (ca. 40 %).

Fresh outwash sediment from the Rhone glacier snout and suspended sediment in the two glaciers' meltwaters were considered as present-day material (Rhone: $R_{0yr\ outwash}$, $R_{0yr\ susp.}$; Oberaar: $O_{0yr\ susp.}$). LIA moraine ridges dated as 140 and 145 yr and 260-280 yr old were sampled (Oberaar: O_{140yr}; Rhone: R_{145yr} and R_{270yr}; Ammann, 1977; Zumbühl, 1988). We also sampled tills that are interpreted to have been deposited during the rapid, globally synchronous breakdown of the YD glaciers 11.6 kyr ago, and to have remained ice-free after this event (Rhone: $R_{11.6kyr}$ and Oberaar: $O_{11.6\ kyr}$; Zumbühl, 1988; Alley et al., 1993; Hormes et al., 2001). 1 m profiles were dug in the LIA moraine walls and integrated samples were taken at 10 cm intervals. The YD section $O_{11.6\ kyr}$ terminated in bedrock at 60 cm and the YD section $R_{11.6\ kyr}$ was dug to a Bw horizon at 70 cm depth (soil classification according to USDA, 1998, 1999). Table 5.1 contains general soil descriptions, soil pH's, the ratio of the < 2 mm fraction, detrital P and TiO_2 concentrations, and the bulk densities.

Apatite grains were isolated in samples from sites $R_{0yr\ outwash}$, O_{140yr}, R_{270yr}, and $R_{11.6kyr}$: Approximately 500 g of sediment sample was wet sieved in order to ascertain the granulometry. Apatite grains from the 125-250 μm fraction (approx. 30-120 g) were concentrated by heavy liquids and magnetic separation; confirmation of their chemical composition was obtained using an energy dispersive X-ray spectroscopy (EDS). The surface morphologies of all the apatite grains found whilst combing each sample for a minimum of 4 hours were assessed with an environmental scanning electronic microscope (ESEM; Philips XL30 FEG EDS). Observations were made with regard to the scale, intensity, and location of biogeochemical weathering features on the individual apatite grains.

We also performed two sets of analyses on the < 2 mm fraction of samples from sites O_{140yr} and $O_{11.6\ kyr}$, and R_{145yr}, R_{270yr}, and $R_{11.6kyr}$, which were ground up in an agate mill for 3 minutes. Firstly, we determined TiO_2 concentrations using an X-ray spectrometer (XRF PW 24000), in order to correct for volume change in the profiles. Secondly, we measured ironbound, detrital, and organic P concentrations by sequential extraction (SEDEX; Ruttenberg, 1992; Tamburini, 2001). The SEDEX method was originally designed for use on marine sediments and has applied to lake and river sediments (e.g. Filippelli and Souch, 1999). We interpret the "authigenic" P phase extracted by the sodium acetate step as detrital P, based on a test series of SEDEX analyses on pure apatite grains (Hosein, unpublished data) and on the observation that prolonged grinding enhances dissolution of the detrital analog phase in the sodium acetate extraction step (Ruttenberg, 1992). Furthermore authigenic P does not normally form in acidic soils (Sharpley, 2000) and was not observed on any detrital grains in the ESEM study. A spectrophotometer (Perkin Elmer UV/VIS Lambda 10) was used to determine the detrital and organic P, and an ICP-AES (Perkin Elmer Optima 3000) to quantify the ironbound P.

Calculating detrital P weathering rates

We calculated detrital P weathering rates for the more complete and chemically homogenous Rhone chronosequence using a method analogous to Taylor and Blum (1995): The present-day phosphorus inventory (L) is for a surface of 1 m^2 and a depth of 1 m (minimal apatite grain dissolution is observed in

	140/145 yr							270 yr							11.6 kyr						
sample depth (cm)	Soil type & horizon	Det_P (mg g^{-1})	TOC %	pH	TiO_2 (mg g^{-1})	bulk density [§]	< 2mm	soil type & horizon	Det_P (mg g^{-1})	TOC %	pH	TiO_2 (mg g^{-1})	bulk density [§]	< 2mm	soil type & horizon	Det_P (mg g^{-1})	TOC %	pH	TiO_2 (mg g^{-1})	bulk density [§]	< 2mm
Rhone	Orthent (Entisol)							Umbrept (Inceptisol)							Humod (Spodosol)						
0-10	Oh-Ah-Ac	0.16	0.24	5.0	0.22	1.02	0.55	Oh-Ah-Bw	0.10	0.67	4.6	0.21	0.91	0.59	Oh-Ah	0.05	5.05	-	0.34	0.60	0.66
10-20	Ac	0.19	0.15	5.2	0.20	1.30	0.56	Bw	0.15	0.37	4.8	0.22	1.22	0.50	E	0.02	1.45	5.4	0.33	1.32	0.39
20-30	Ac	0.24	<0.1	6.0	0.18	1.20	0.67	BwC	0.15	0.19	4.9	0.21	1.24	0.45	Bhs	0.04	1.93	5.4	0.40	1.28	0.46
30-40	C	0.20	<0.1	6.4	0.20	1.30	0.52	(Bw)C	0.15	<0.1	5.9	0.19	1.37	0.47	Bhs[†]	0.10	1.12	5.5	0.43	1.24	0.42
40-50		-	<0.1	6.6	0.19	1.30	0.71	C	0.16	<0.1	6.0	0.20	1.53	0.39	Bw	0.23	1.01	5.5	0.35	1.55	0.63
50-60		0.28	<0.1	6.5	0.22	1.30	0.47		0.11	<0.1	6.1	0.17	1.53	0.39	Bw	0.25	0.68	5.9	0.35	1.56	0.88
60-70		0.25	<0.1	6.4	0.22	1.30	0.62		0.16	<0.1	6.2	0.17	1.53	0.45	Bw	0.27	0.37	5.8	0.32	1.56	0.80
70-80		0.28	<0.1	6.5	0.2	1.30	0.65		0.16	<0.1	6.3	0.2	1.53	0.55							
80-90		0.16	<0.1	6.7	0.21	1.30	0.68		0.19	<0.1	6.5	0.21	1.53	0.55							
90-100		0.24	<0.1	6.9	0.19	1.30	0.78		0.20	<0.1	6.2	0.21	1.53	0.44	BC[§]						
Oberaar	Orthent (Entisol)														Humod (Spodosol)						
0-10	Oh-Ah	0.63	0.11	5.4	0.46										Oh-Ah	0.17	24.09	6.7	0.28		
10-20	AC	0.83	<0.1	6.3	0.41										E	0.14	9.00	6.5	0.33		
20-30	C	0.80	<0.1	6.7	0.40										Bhs	0.13	3.49	6.1	0.42		
30-40		0.75	<0.1	7.1	0.35										Bw	0.40	1.54	5.5	0.43		
40-50		0.47	<0.1	7.2	0.33										Bw	0.39	1.03	5.7	0.39		
50-60		0.71	<0.1	7.2	0.34										Bw		<0.1	5.8	0.39		
60-70		0.51	<0.1	7.7	0.36										R						
70-80		0.79	<0.1	7.9	0.37																
80-90		0.69	<0.1	8.2	0.38																
90-100		0.47	<0.1	8.1	0.38																

[†]A rust layer was observed within this level, we interpret it as the presence of a former water table.
[§](Egli et al. 2001)

Table 5.1: Chronosequence parameters.

the LIA samples at this depth and Egli et al. (2001) define 1 m as the BC horizon of the YD profile). L is calculated as the sum of 10 cm thick soil slices (L_j): $L_j = P_j \bullet \rho_j \bullet F_j \bullet V_j$, where P_j is the present-day detrital P concentration. The soil density, ρ_j, is taken from Egli et al. (2001) and F_j is the weight fraction of < 2 mm material of the total mass of the till (Table 5.1; a positive bias may be introduced as large clasts > 4 cm are not included). V_j is the volume of soil slice j.

The mass of P initially present in each soil slice, prior to any weathering, is $S_j = P_j/X_j$, where X_j is the depletion factor. Based on the assumption that titanium is immobile in these granitic soils, the depletion factor can be calculated as $X_j = (P_j/P_0)/(Ti_j/Ti_0)$, where Ti_j is the measured concentration of Ti in the soil slice j and Ti_0 is the Ti concentration of the parent material. The concentration of detrital P (mg g^{-1}) in the parent material is P_0.

Finally, subtracting the summed inventories of present day P from the summed inventory of initial P, gives the amount of P weathered: $W_P = \Sigma S_j - \Sigma L_j$. The long term P weathering rate at each site (R_{LT}), is W_P divided by the soil age.

Results

Biogeochemical weathering and apatite grain surface morphology

From observations of the morphology of apatite grain surfaces we identify four different grades of chemical weathering (Fig. 5.1):

1. Mechanically and slightly biogeochemically weathered: Whole grains show "fresh", unaltered surfaces, with the exception of the presence of localised mechanical indentations; zooming in the mechanically indentations show dissolution rounding (Fig. 5.1: 1 and 1a)
2. Mechanically and biogeochemically weathered: Whole grains show rather "fresh" and only slightly altered surfaces, with localised mechanical indentations; zooming in the indentations are locally chemically etched to form a sugary texture and localised denticular margins (Fig. 5.1: 2 and 2a)
3. Predominantly biogeochemically weathered: Whole grains show a "sugary" surface texture; zooming in, the surface is covered by pervasive initial lenticular etch pits and denticular margins (Fig. 5.1: 3 and 3a)
4. Pervasively biogeochemically weathered: Whole grains are heavily etched. Individual pits have coalesced to form pervasive acicular or tower block-like structures (Fig. 5.1: 4 and 4a) and / or extensive enlargement of pits has generated a secondary porosity in the grain.

Sample	Grains analysed	Grade 1	Grade 2	Grade 3	Grade 4	Mean grade
R_{0yr}						
Meltout sediment	5	5				1.0
O_{140yr}						
(0-10 cm)	11	2	3	2	4	2.7
(40-50 cm)	7	4	3			1.4
(90-100 cm)	9	6	3			1.3
R_{270yr}						
(0-10 cm)	11			6	5	3.5
(40-50 cm)	10	5	2	1	1	1.8
(90-100 cm)	10	7	2	1		1.4
$R_{11.6kyr}$						
(0-10 cm)	6			3	3	3.5
(30-40 cm)	4	1	1	2	1	2.6
(60-70 cm)	4		1	3		2.8

Each sample represents the apatite grains concentrated from ≈ 500 g of sample and was combed for at least 4 hours in order to detect a maximum number of apatite grains.

Table 5.2: Weathering grades of the apatite grains.

Each isolated grain was graded according to this scale and a mean grade was established for each sample (Table 5.2). Generally, in grains of grades 1 and 2, mechanically damaged surface areas (e.g., along chatter marks and fractures) are sites of preferential biogeochemical weathering (Fig. 5.1: 3a). We also observed that the mean weathering grades of surface samples from sites O_{140yr} and R_{270yr} (2.7 and 3.5, resp.) are higher than samples from the middle of the profiles (1.4 and 1.8 respectively). The mean grades of weathering in the middle and bottom slices of site $R_{11.6kyr}$ are 2.6 and 2.8 respectively and 68 % fewer apatite grains were observed in these samples compared to those of LIA age, albeit similar amounts of sediment being treated (ca 30-40 g). In general, the intensity of biogeochemical weathering depends on sample age and depth, with highest weathering grade (4) even observed in grains from the top sample of the 140 yr old moraine. At site O_{140yr} (0-10cm), we identified two apatite grains where denticular weathering structures were covered in fungal hyphae (Fig. 5.2).

SEDEX forms of P

Extraction of different P forms by the SEDEX method shows that the mean detrital P concentrations

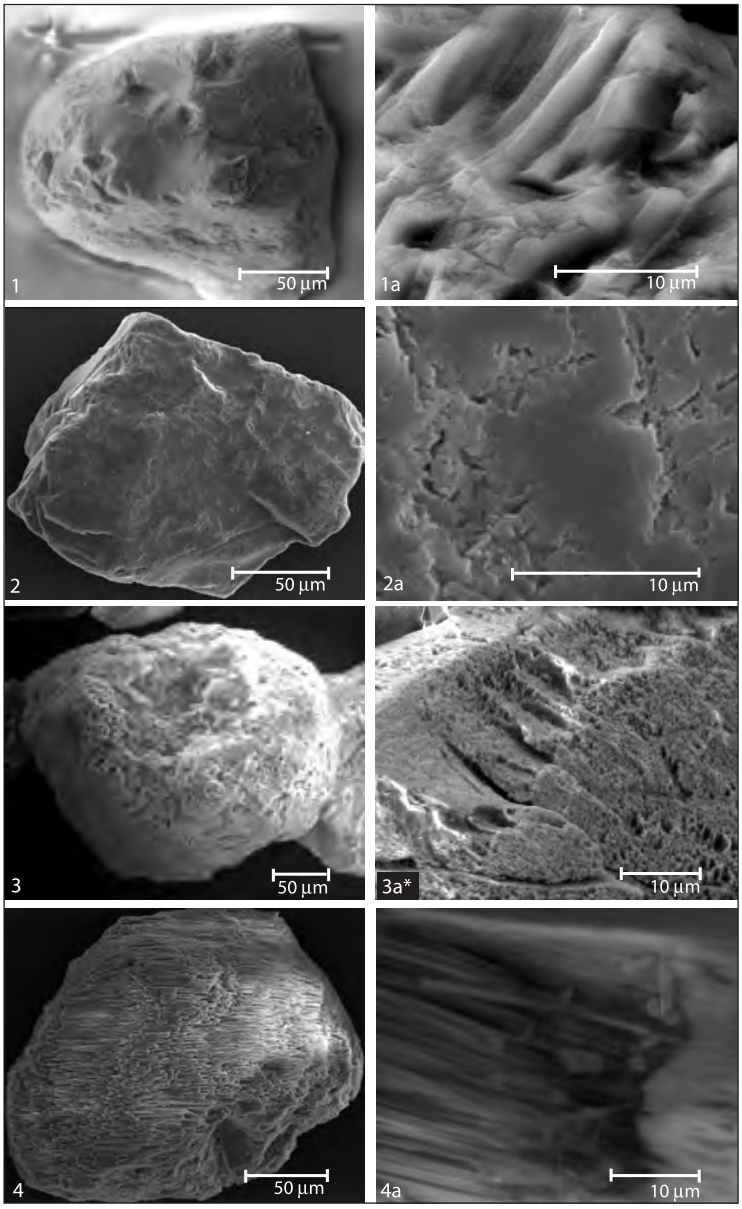

Fig. 5.1: Typical grain morphologies of the four apatite weathering grades. 3a*, the physical erosion feature allows more pervasive chemical etching.

in R_{0yr} susp and O_{0yr} susp are 0.32 mg g^{-1} and 0.58 mg g^{-1} (± 0.05 mg g^{-1}), organic P measures 0.09 mg g^{-1} and 0.14 mg g^{-1} (± 0.005 mg g^{-1}) and ironbound P is below detection (< 0.03 mg g^{-1}). Detrital P remains the predominant P phase at the LIA sites and ironbound P is still below detection; mean C-horizon detrital P values are almost three times higher in the O_{140yr} profile (0.63 mg g^{-1}) than the R_{145yr} profile (0.23 mg g^{-1}; Fig. 5.3). Detrital P is reduced at the YD sites, where Fe-bound P is dominant (especially in the surface samples). The presence of organic P is almost entirely limited to surface samples (max. depth is 30 cm) and its importance increases as a function of age, with nearly 4 times as much organic P in $O_{11.6kyr}$ as $R_{11.6kyr}$. Whereas total P concentrations remain stable throughout the LIA profiles, with a slight tendency to decrease towards the tops, total P increases considerably towards the upper part of the YD sections. Total P values in YD surface samples are 5 to 10 times higher than in LIA samples.

Detrital P weathering rates

We calculate detrital P weathering rates at LIA sites of 0.31 and 0.28 g m^{-2} yr^{-1} (R_{145yr}; R_{270yr}). At YD site $R_{11.6kyr}$ the rate decreases to 0.01 g m^{-2} yr^{-1}. LIA rates are calculated by approximating P_0 as the mean detrital P concentration of present-day suspended sediment and

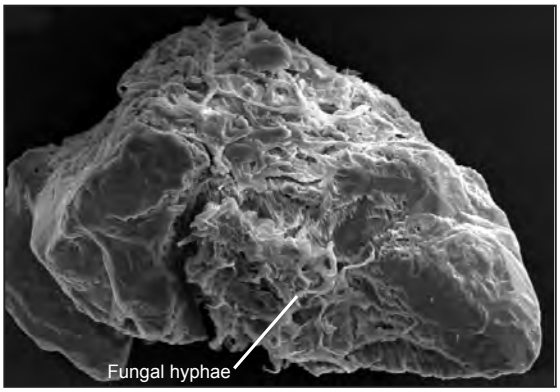

Fig. 5.2: Apatite grain showing denticular weahtering structures and covered in fungal hyphae (O_{140yr}, 0-10 cm).

the R_{145yr} C-horizon (0.29 mg g^{-1}) and Ti_0 as the mean Ti concentration in the R_{145yr} C-horizon (0.21 mg g^{-1}). The change in source rock composition of the YD profile may change its P_0 and Ti_0. Because the YD profile C-horizon was not sampled we estimate P_0 by extrapolating the linear increase in detrital P between 40-70 cm down to 100 cm (the BC horizon after Egli, 2001; 0.34 mg g^{-1} detrital P) and we assume that the Ti_0 measured at 60 and 70 cm remains constant to 100 cm depth (0.32 mg g^{-1}). The use of a P_0 derived from the LIA parent material would double the YD weathering rate.

Discussion and Conclusions

Our observations of the progressive change in surface morphology of whole apatite grains, the systematic shift in the composition of P from detrital to ironbound and organic P forms, and our estimations of the weathering rate of detrital P indicate that apatite is actively biogeochemically weathered in proglacial areas. Fluxes of ions derived from other soft and chemically reactive minerals, i.e. carbonates and metal sulphides are also higher from arctic and alpine Little Ice Aged proglacial sediments with respect to equivalent fluxes from presently ice-covered areas (30-50 %; Anderson et al., 2000; Wadham et al., 2001). Apatite grains are preconditioned for biogeochemical weathering by mechanical abrasion during subglacial transit, facilitated by their (weak) tendency to cleave and fairly low Vickers hardness. Apatite weathering is most intense and detrital P least concentrated at the tops of profiles where pedo-

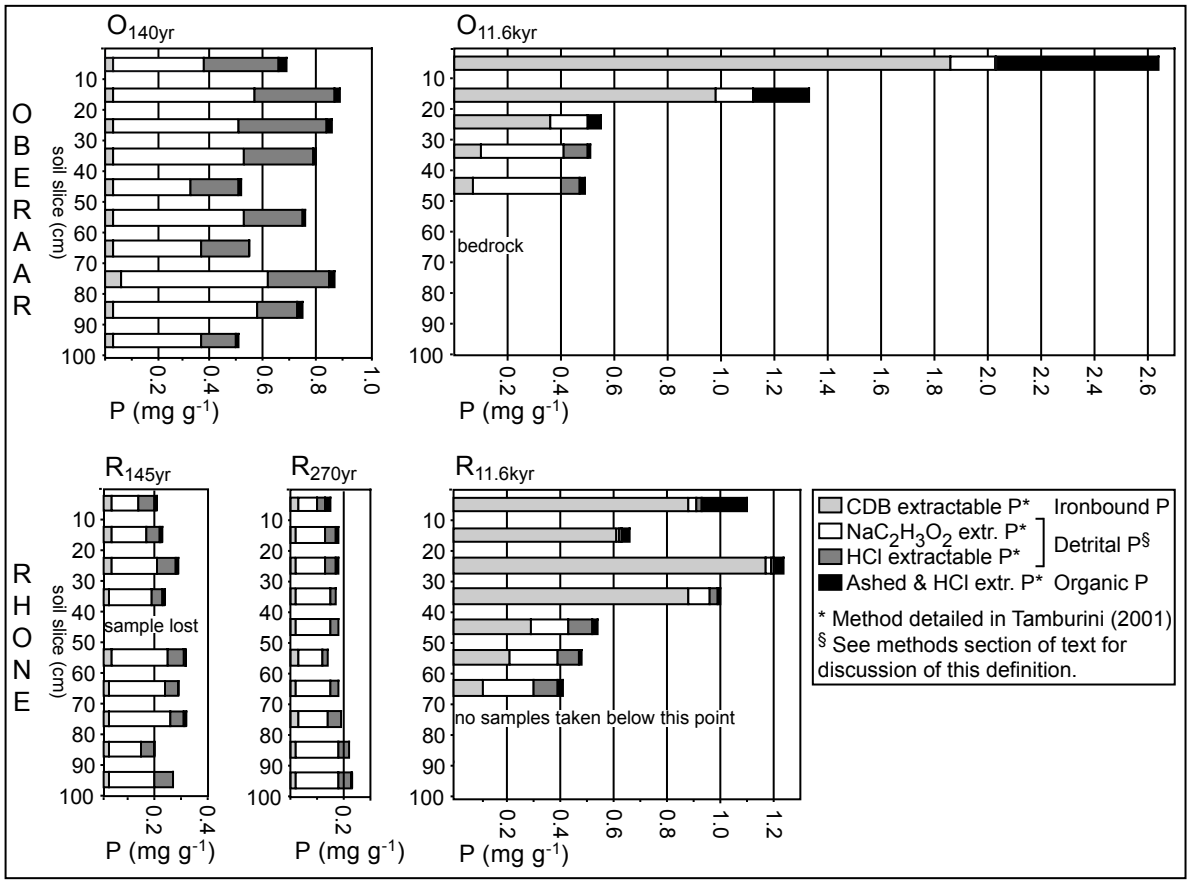

Fig. 5.3: The distribution of phosphorus phases in the chronosequence.

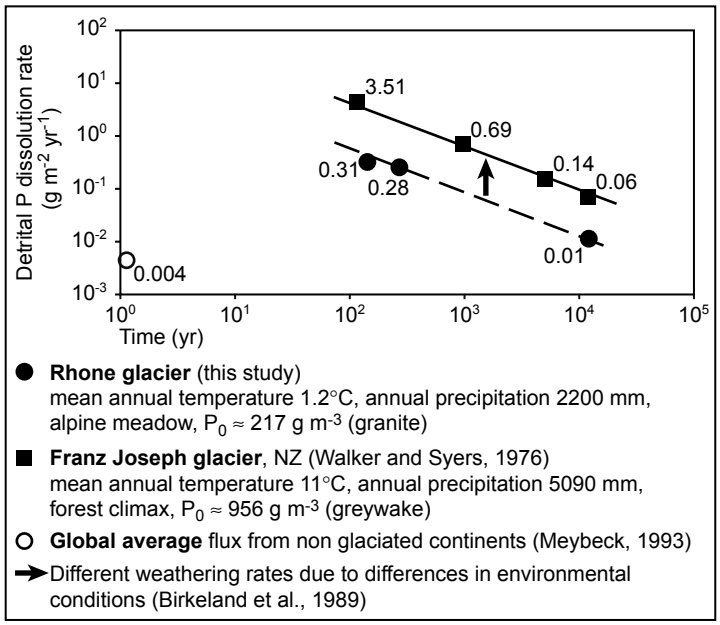

Fig. 5.4: Phosphorus weathering rates in two proglacial chronosequences.

genic and biological processes are localised and the pH may be as low as 4.6 (Table 5.1). Two major modes of acid hydrolysis can be distinguished on the apatite grains. Firstly, diffuse etching is attributed to the acidic soil solution, whose pH is lowered by the rapid oxidation of sulphides in the proglacial environment (e.g. Anderson et al., 2000), acid aerosols and acidifying pedogenic processes. Secondly, intense localised dissolution is interpreted as active biogeochemical weathering (Fig. 5.2; Frossard et al., 1995). After only 140–270 years of exposure a combination of chemical and active biogeochemical processes probably give rise to surficial apatite grains with the same weathering grade as 11.6 kyr grains from 50-70 cm depth.

The detrital P weathering rates reported here are one order of magnitude lower than those calculated by Walker and Syers (1976), although the decrease in weathering intensity with age is comparable (Fig. 5.3). We attribute the difference in weathering intensity to the warmer, wetter climate of Walker and Syers' chronosequence, which is located in the Franz Joseph glacier forefield, New Zealand (Fig. 5.3; see also Birkland et al., 1989). The P dissolution rates we calculate for the Rhone proglacial area are approximately 70 times higher than the world average dissolved P flux from non-glaciated continents (0.004 g P m^{-2} yr^{-1}; Meybeck, 1993). Filippelli and Souch (1999) postulate that the low P binding capacity of proglacial protosoils may allow an important flux of bioavailable P to leak into aquatic ecosystems and enhance productivity. A concomitant increase in terrestrial productivity may only be achieved in a more evolved, conservative pedosphere with more efficient internal recycling of P (Crews et al., 1995). During soil development a combination of biological and abiological mechanisms may also sequester P from precipitation inputs, leading to the enrichment of organic and ironbound P forms and elevated total P concentrations (Haselwandter et al., 1983; Birkland et al., 1989; this study, YD tills). 28 % of the land surface of the Northern Hemisphere may have fallen within the proglacial zone during deglaciation following the last glacial maximum, and fluvial and glacial detrital yields were possibly equal before man (Gibbs and Kump, 1994; Hay, 1998). Consequently elevated dissolution of detrital P potentially has a geographically wide-ranging impact on bioproductivity (Föllmi, 1995). Glacially derived P may influence bioproductivity beyond glacier margins: P becomes bound in occluded and recalcitrant-organic forms in tropical soils after millions of years and the aeolian inputs of detrital P, which limit productivity, are partially derived from glacial sources (Crews et al., 1995, Chadwick et al., 1999, and references therein).

In conclusion, during deglaciation the widespread exposure of reactive proglacial sediment and the rapid dissolution of associated detrital P may increase bioavailable P supply to both terrestrial and aquatic ecosystems on centennial to millennial timescales.

Acknowledgements

Massoud Dadras and Mireille Leboeuf (both Neuchatel) assisted with the ESEM, Giulio Galetti (Fribourg) provided the XRF data, and J. Ondrus and S. Pierrehumbert (SCPE-laboratory, Neuchatel) performed the ICP-AES analysis, and Jean-Michel Gobat (Neuchatel) helped with soil identification. Swiss National Science Foundation grants 21-53997.98 and 20-61485.00 are gratefully acknowledged.

References

Alley, R. B., Meese, D., Shuman, C.A., Gow, A.J., Taylor, K.C., Grootes, P.M., White, J.W.C., Ram, M., Waddingtion, E.D., Mayewski P.A., Zielinski, G.A., 1993. Abrupt increase in Greenland snow accumulation at the end of the Younger Dryas event. Nature, 362, 527-529.

Ammann, K., 1977. Der Oberaargletscher im 18., 19. und 20. Jahrhundert. Zeitschrift für Gletscherkunde und Glazialgeologie. XII (2), 253-291.

Anderson, S.P., Drever, J.I., Frost, C.D., and Holden, P., 2000. Chemical weathering in the foreland of a retreating glacier. Geochimica et Cosmochimica Acta, 64, 1173-1189.

Birkland, P.W., Burke, R.M., and Benedict, J.B., 1989. Pedogenic gradients for iron and aluminium accumulation and phosphorus depletion in Arctic and Alpine soils as a function of time and climate. Quaternary Research. 32, 193-204.

Broecker, W. and T.-H. Peng, 1982. Tracers in the sea. Lamont-Doherty Geological Observatory, Palisades, N.Y, pp. 690.

Chadwick, O.A., Derry, L.A., Vitousek, P.M., Huebert, B.J., and Hedin, L.O., 1999. Changing sources of nutrients during four million years of ecosystem development. Nature, 397, 491-497.

Crews, T.E., Kitayama, K., Fownes, J.H., Riley, R.H., Herbert, D.A., and Mueller-Dombois, D., 1995. Changes in soil phosphorus fractions and ecosystem dynamics across a long chronosequence in Hawaii. Ecology, 76, 1407-1424.

EDI, (Eidgenössisches Department des Innern), 1992, Hydrologischer Atlas der Schweiz. Federal Office for Water and Geology (Editor), Berne, Switzerland, pp. 206.

Egli, M., Fitze, P., and Mirabella A., 2001. Weathering and evolution of soils formed on granitic, glacial deposits: results from chronosequences of Swiss alpine environments. Catena, 45, 19-47.

Filippelli, G.M. and Delaney, M.L., 1994. The oceanic phosphorus cycle and continental weathering during the Neogene. Paleoceanography, 60, 643-652.

Filippelli, G.M. and Souch, C., 1999. Effects of climate and landscape development on the terrestrial phosphorus cycle. Geology, 27, 171-174.

Föllmi, K.B., 1995. 160 m.y. record of marine sedimentary phosphorus burial: Coupling of climate and continental weathering under greenhouse and icehouse conditions. Geology, 23, 859-862.

Frossard, E., Brossard, M., Hedley, M.J., and Metherell A., 1995. Reactions controlling the cycling of P in Soils. In H. Tiessen (Editor), Phosphorus in the global environment: Transfers, cycles and management, SCOPE, 54, Wiley, p. 107-137.

Gibbs, M.T. and Kump L.M., 1994. Global chemical erosion during the last glacial maximum and the present: Sensitivity to changes in lithology and hydrology. Paleoceanography, 9, 529-543.

Guidry, M.W. and Mackenzie, F.T., 2000. Apatite weathering and the Phanerozoic phosphorus cycle. Geology, 28, 631-634.

Hay, W.W., 1998. Detrital sediment fluxes from continents to oceans. Chemical Geology, 145, 287-
323.

Haselwandter, K., Hofmann, A., Holzmann, H. -P., and Read, D.J., (199X). Availability of nitrogen and phosphorus in the nival zone of the Alps. Oecologia, 57, 266-269.

Hormes, A., Mueller, B.U. and Schluechter, C., 2001. The Alps with little ice: evidence for eight Holocene phases of reduced glacier extent in the Central Swiss Alps. The Holocene, 11, 255-265.

Körner, C., 1999. Alpine plant life: Functional plant ecology of high mountain ecosystems. Springer, Germany, pp. 338.

Mahaney, W.C., 1995. Glacial crushing, weathering and diagenetic histories of quartz grains inferred from scanning electron microscopy. In J. Menzies (Editor), Modern glacial environments. Processes, dynamics and sediments, Volume 1, pp. 621.

Meybeck, M., 1993. Natural sources of C, N, P, and S. In R. Wollast, F.T. Mackenzie, and L. Chou (Edi-

tors), Interactions of C, N, P, and S. Biogeochemical Cycles and Global Change: NATO ASI Series, I(4), Springer-Verlarg, Berlin.

Pennington, W., 1981. Records of a lake's life in time: The sediments. Hydrobiologia, 79, 197-219.

Ruttenberg, K.C., 1992. Development of a sequential extraction method for different forms of phosphorus in marine sediments. Limnology and Oceanography, 37, 1460-1482.

Sharpley, A., 2000. Phosphorus Availability. In M.E. Sumner (Editor), Handbook of soil science. CRC Press, D18-36.

Stumm, W. and Morgan, J.J., 1996. Aquatic Chemistry. Wiley, New York, pp. 1022.

Tamburini, F., 2001. Phosphorus in marine sediments during the last 150,000 years: Exploring relationships between continental weathering, productivity, and climate. Unpublished PhD thesis, University of Neuchatel, Switzerland, CD ROM.

Taylor, A. and Blum, J.D., 1995. Relation between soil age and silicate weathering rates from the chemical evolution of a glacial chronosequence. Geology, 23, 979-982.

Tyrell, T., 1999. The relative influences of nitrogen and phosphorus on oceanic primary production. Nature, 400, 525-531.

Wadham, J.L., Cooper, R.J., Tranter, M., and Hodgkins, R., 2001. Enhancement of solute fluxes in the proglacial zone of a polythermal glacier. Journal of Glaciology, 47, 378-386.

Walker, T.W. and Syers, J.K., 1976. The fate of phosphorus during pedogenesis. Geoderma, 15, 1-19.

Zumbühl H. J., 1988. Der Rhonegletscher in den historischen Quellen. In: H.J. Zumbühl and H. Holzhauser (Editors), Alpengletscher in der Kleinen Eiszeit. Die Alpen, Zeitschrift der Schweizen Alpen-Clubs, 64(3), 129-322.

CHAPTER 6

Posphorus weathering: Four case studies from the Swiss Alps and Venezuela

Abstract

The runoff from the Apure watershed contains more conditionally bioavailable P (dissolved inorganic, and organic P and particulate ironbound and organic P; 1.97 kmol km^{-2} yr^{-1}) than glacial meltwaters from the Rhone and Oberaar glaciers (0.29 - 0-39 kmol km^{-2} yr^{-1}). But, the eolian input of bioavailable P to the Apure watershed by Saharan dust is greater than the output flux of conditonally bioavailable P. This implies that soils in the largely transport limited tropical catchment act as a reservoir for P.

In contrast, while runoff from the presently glaciated catchments is dominated by scarcely bioavailable detrital P (97 %), the role subglacial weathering processes play in bringing large volumes of freshly comminuted, detrital P to the biosphere (7 & 11 kmol km^{-2} yr^{-1} in the presently glaciated catchments) may be important in controlling inputs of bioavailable P to the oceans on glacial-interglacial timescales: The weathering-derived SRP flux from the recently deglaciated Rhone tributary catchment (0.17 kmol km^{-2} yr^{-1}) is elevated compared to the weathering-derived SRP flux from the Rhone and Oberaar subglacial environments (0.04 - 0.05 kmol km^{-2} yr^{-1}) and global mean riverine SRP flux (0.13 kmol km^{-2} yr^{-1}). This indicates that the dissolution of detrital P is accelerated in proglacial sediments and that the low P binding capacity of immature, weathering limited, glacial soils allows the leakage of bioavailable P into aquatic ecosystems. We estimate that the annual bioavailable P-flux from half the area exposed by ice melt after the Last Glacial Maximum would have been 1.564 * 109 kmol SRP yr^{-1}. This is more than doubled the maximum, present-day global riverine flux of conditionally bioavailable P to the oceans (dissolved inorganic + dissolved organic + particulate organic + iron bound particulate P; 1.485 * 108 kmol yr^{-1}).

Introduction

Dissolved phosphorus (P) in the form of orthophosphate, is a potentially biolimiting nutrient in terrestrial, freshwater and marine ecosystems (e.g. Schindler, 1977; Cotner, 1997; Chadwick et al., 1999) and may be the ultimate limiting nutrient for oceanic primary productivity on geological timescales (e.g. Broecker, 1982; Tyrell, 1999). The fundamental control on the P flux to the biosphere is the weathering rate of P bearing minerals (Filippelli and Delaney, 1994; Delaney, 1998). Paradoxically, detrital P is scarcely bioavailable in freshwater and marine environments, and in fact 90-99 % of total P is transported fluvially in solid forms that are either only conditionally or scarcely bioavailable (Figs. 6.1 and 6.2; Martin and Meybeck, 1979; Froelich et al., 1982; Boström et al., 1988; Reynolds and Davis, 2001). Biologically reactive P is a limited resource under natural conditions (e.g. Hudson et al., 2000) that is often recycled intrabiotically, with algal biomass forming the main source of P in the oceans and organic matter being a principal source of bioavailable P in 10'000 year old soils (Crews et al., 1995; Chadwick et al., 1999). Although increased physical erosion rates associated with tectonic uplift and possibly glaciation (Southam and Hay, 1981; Guidry, 2000) augment the flux of apatite (the main P bearing mineral) supplied to the biosphere and physically precondition it for chemical weathering, the timescales and mechanisms by which it becomes bioavailable are unclear. Apatite dissolution is limited in rivers, lakes and sea water due to their close to neutral pH's (6 - 8.4; Skirrow, 1975; Meybeck, 1993) and therefore freshly weathered apatite conveyed directly to ocean reservoirs will not be bioreactive.

Consequently it is vital that detrital P should be

This preliminary draft of Chapter 6 by Rachel Hosein, Kaspar Arn, Philipp Steinmann, Thierry Adatte, Sylvain Huon†, and Karl B. Föllmi is in preparation for submission to *Biogeochemistry*.

† Université Pierre et Marie Curie, Laboratoire de Biogéochimie Isotopique (LBI), UMR 7618, Paris 6, Cedex.

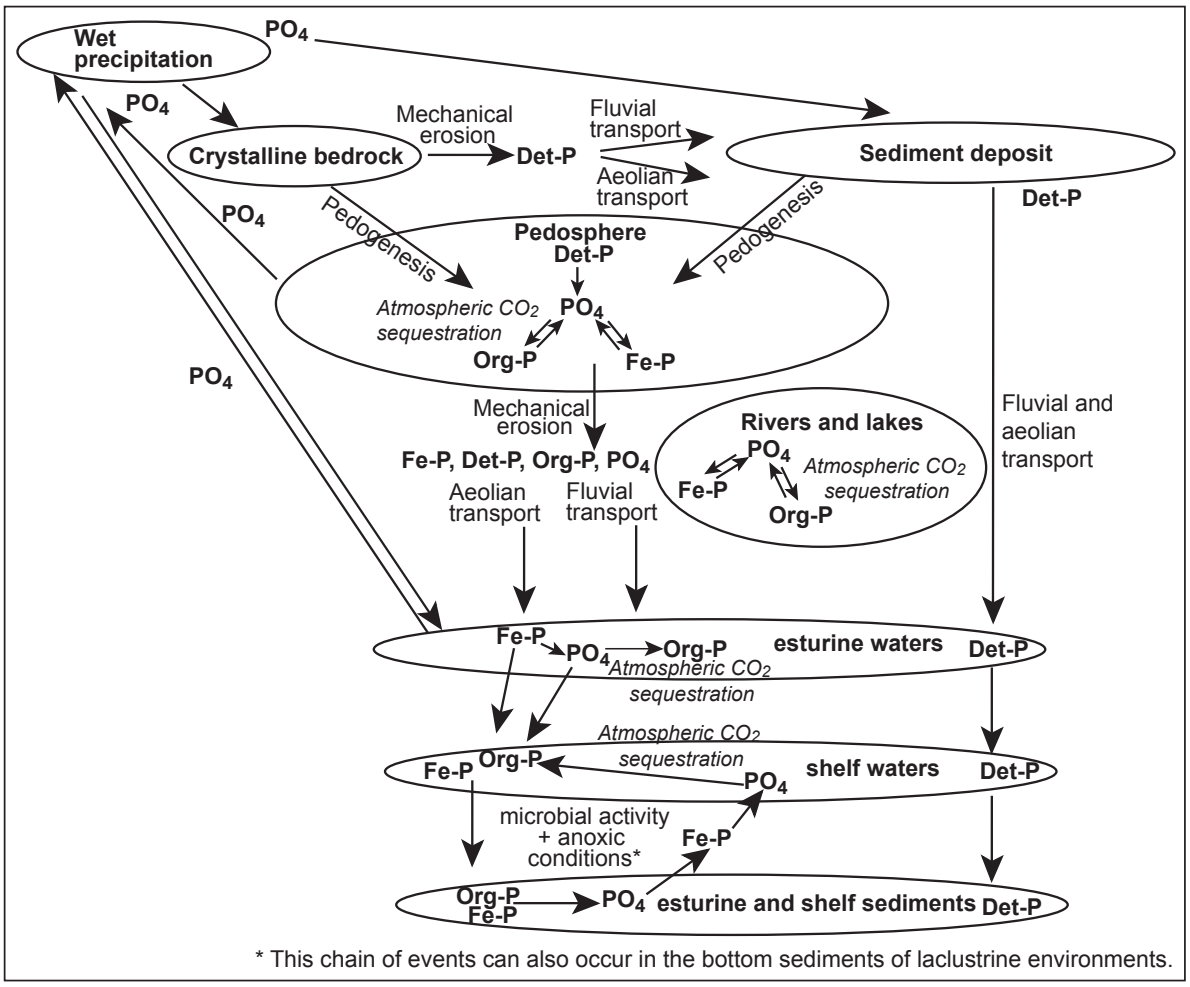

Fig. 6.1: The transfer of different P forms from the continents to oceanic sediments.

retained in terrestrial environments where apatite solubility is enhanced by acidic porewaters (Stumm and Morgan, 1996). Acidic soils increase the dissolution of detrital P through a range of chemical and biogeochemical processes, like acid aerosols, the H^+ pump at root tips and organic acid exudates, such as oxalic acid from rootlets and associated mycorhizal fungi (e.g. Kpomblekou and Tabatabai, 1994). Detrital P is rapidly dissolved in soils, for instance it is no longer detected in 20'000-year-old glacial (Birkland et al., 1989) and Hawaiian soils (Crews et al., 1995). Furthermore, protosoils established on recently deposited sediment have a low P binding capacity due to their low organic matter and iron oxide concentrations and therefore they are often leaky with regard to biologically reactive, dissolved phosphorus, (van der Molen et al., 1997; Filippelli and Souch, 1999) causing an important flux of bioavailable P to drain into aquatic ecosystems.

While soils become impoverished in detrital P, they become enriched in ironbound and organic P phases (e.g. Walker and Syers, 1976; Birkland et al., 1989; Crews, 1995). The organically bound and ironbound P are conditionally bioavailable, i.e., they can become bioavailable under specific environmental conditions: Organic P can take many forms in soils and surface waters, with a whole range of bio-reactivities, giving rise to the recycling of P within ecosystems (Newbold et al., 1984; Lucas et al., 1993; Frossard et al., 1995; Crews et al., 1995; Sharpley, 2000). Some phytoplankton can secrete alkaline phosphatases that separate orthophosphate groups from dissolved organic compounds rendering them bioavailable (Cembella et al., 1984) and microbial activity in coastal marine and lake sediments also releases orthophosphates from organically bound P (Ruttenberg, 1992). Ironbound P is generally only available to specific microbes in the pedosphere that produce siderophores (Frossard et al., 1995; Sharpley, 2000). But if soils are eroded and transported by rivers ironbound P may become available to phytoplankton through desorbtion processes: Flocs of iron oxide are

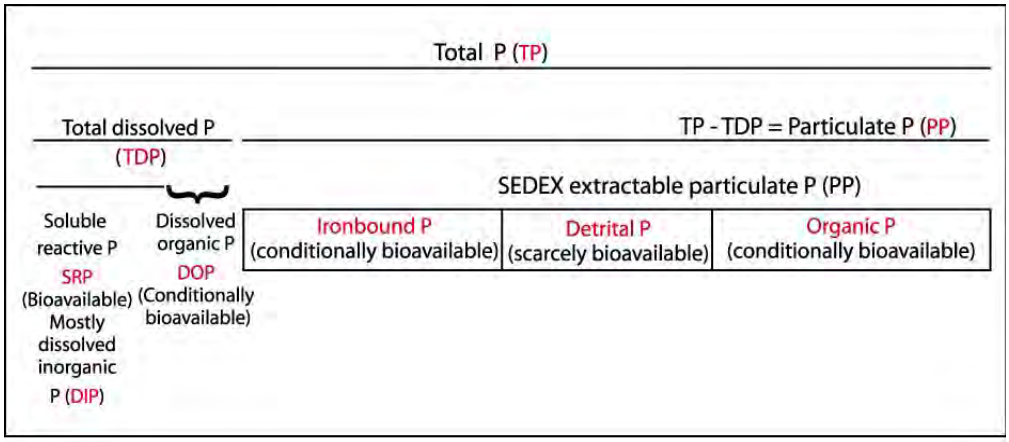

Fig. 6.2: A schematic diagram showing the P forms measured in this chapter and their bioavailabilities (after Boström et al., 1988, and Reynolds and Davis, 2001.

a significant source of orthophosphate in some river estuaries, where P desorbtion is driven by changes in salinity and pH (Fox, 1986) and below the redoxcline of anoxic water bodies, where iron is reduced to its ferric form (e.g., Golterman, 1984). Berner and Rao (1994) studied the various P forms in Amazon River, estuary and shelf sediments using Ruttenberg's (1992) sequential extraction technique and observed a marked drop in organic and ironbound P concentrations in the shelf sediments compared to the river sediments. They attributed this decrease to the solubilisation of P in the sediments, which they estimate represents a source of bioavailable P that is almost three times larger than the dissolved P flux from the Amazon River (18 x 10^{10} gm P yr^{-1}).

In this paper we present four case studies, we compare P forms in the meltwaters from three presently or recently glaciated alpine catchments in central Switzerland, with P forms in the runoff from the tropical Apure catchment which encompasses an area of the Venezuelan Andes and Llanos. In the presently glaciated Rhone and Oberaar catchments the runoff from the tropical Apure catchment which encompasses an area of the Venezuelan Andes and Llanos. In the presently glaciated Rhone and Oberaar catchments derived from the weathering of detrital minerals is negligible, (0.05 kmol km^{-2} yr^{-1}). However, in the recently glaciated Rhone Tributary catchment dissolved P is dominant and the weathering-derived-SRP-flux is 0.17 kmol km^{-2} yr^{-1}. In contrast rivers in the tropical Apure watershed contain conditionally bioavailable dissolved organic P (0.1 - 0.6 μmol l^{-1}), which is not found in the runoff from the glacial catchments. Also sediments in the Apure waters contain an order of magnitude more organic P than sediments in the glacial meltwaters and scarcely bioavailable detrital P is replaced downstream by conditionally bioavailable ironbound P. Therefore, not only is terrestrial productivity higher in the tropical catchment compared to glacial catchments (as evinced by the higher concentrations of organic P), but the tropical sediments might also stimulate more productivity in aquatic ecosystems, because of the higher concentrations of conditionally bioavailable P. Paradoxically the elevated SRP flux from the Apure catchments (0.52 kmol km^{-2} yr; Saunders and Lewis, 1988) could be largely due to atmospheric inputs of P. 1.36 kmol km^{-2} of SRP are delivered to to the Llanos per year (Montes and José, 1989), and a considerable portion of the regional bioavailable P flux is established to come from Saharan eolian input (Reichholf, 1986; Swap et al., 1992). In contrast the Rhone Tributary's rain corrected SRP flux is comparable with the mean global SRP flux from unpolluted non-glaciated catchments (0.13 kmol km^{-2} yr^{-1}; Meybeck, 1993; this flux is not corrected for atmospheric inputs). Therefore we suggest that periods of glacial retreat may have a positive impact on the SRP flux to the biosphere and that glacial preconditioning of grains, coupled with acidifying pedogenic processes may accelerate the dissolution of detrital P minerals.

The glacial and tropical catchments

The presently glaciated Rhone (Rh) and Oberaar (Ob) catchments and the proglacial Rhone tributary catchment are located on crystalline bedrock of the Aar

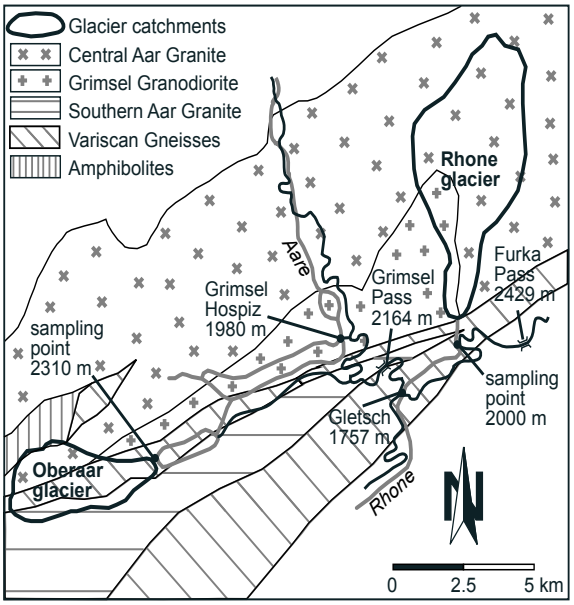

Fig. 6.3: The glacial catchments in the Swiss Alps and their crystalline bedrock geology.

massif in central Switzerland (Table 6.1; Fig. 6.3). The glacial catchments are both pristine and anthropogenic pollution can only influence precipitation inputs to the catchments. The presently glaciated catchments both have well-defined meltwater streams that were sampled up to 100's of meters from the glacier snouts. The catchments have been part of a detailed three-year study and their major anion and cation chemistries and the fluxes of major ions and suspended sediments from the catchments are presented elsewhere (Chapter 2). The Rhone tributary catchments is located on a steep sided (> 25°) adjacent to the Rhone glacier (Fig. 6.3). Approximately 80 % of the catchment contains glacial drift of Younger Dryas age that is undergoing podzolification and has a vegetation cover of alpine flowers, grasses and shrubs. (Zumbühl, 1988; Egli et al., 2001).

The Apure watershed, a fan shaped array of tributaries draining an area of 167'000 km^2, is located in the north-west of Venezuela, with its headwaters beginning at approximately 2000 m in the Venezuelan Andes (Fig. 6.4). We have sampled headwater streams that feed the Bocono River and taken upstream samples of some other important tributaries, Guanare and the Portuguesa. The Bocono joins the Guanare approximately 200 km along its course and the Guanare subsequently joins the Portuguesa after a further 400 km. The Guanare and the Portuguesa are major left bank affluents of the Apure River, which the Portuguesa joins 70 km downstream from its confluence with the Guanare. The Apure joins the Orinoco River 1500 km from its source, having descended approximately 2000 m (Fig. 6.4). The Apure watershed drains the eastern slopes of the Cordillera de Merida and the Cordillera de la Costa, composed of ancient basement rocks and associated metamorphosed sediments and volcanic rocks of Mesozoic age which have been thrust southwards onto Paleogene flysch deposits (Edmond et al., 1996). Having left the Andes the Apure and its tributaries subsequently meander over the alluvial plain of the Llanos: The refluxing of water through these porous sediments has weathered them intensely, transforming them from felsic arenites to quartz sands (Johnsson et al., 1988). The summits of the Cordillera are covered by paramo type vegetation, with the lower slopes being used for arable production, for example coffee, peppers and corn. The Llanos plain is used as pasture for cattle, but there are important riparian zones that are flooded each rainy season. The precipitation maximum occurs

	Oberaar	Rhone	Rhone tributary	Apure
Geographical position	46° 32'N 8° 14'E	46° 35'N 8° 23E	46° 35'N 8° 23E	
Geology	granite & strongly foliated gneiss	granite and granodiorite	granodiorite, with granite and granodiorite drift	crystalline and sediments
Catchment area (km^2)	11.03	26.2	1.5	167000
Glacial cover (%)	57	73	0	0
Temperature (°C)	-1	1.2	1.2	27†
Annual precipitation (mm)	2100	2200	2200	1600
Elevation (m)	2310 - 3631	2050 - 3630	1770 - 2600	≈ 2000 - 50*
Sampling elevation (m a.s.l)	2316m (snout)	1840m	1770 m	-

† Maximum mean annual temperature (Vegas-Vilarrubia et al., 1993)

* Only 15 % of the catchment is > 500 m (Saunders and Lewis, 1988)

Table 6.1: The physical parameters of the Oberaar, Rhone, and Rhone tributary catchments, Switzerland, and the Apure catchment, Venezuela.

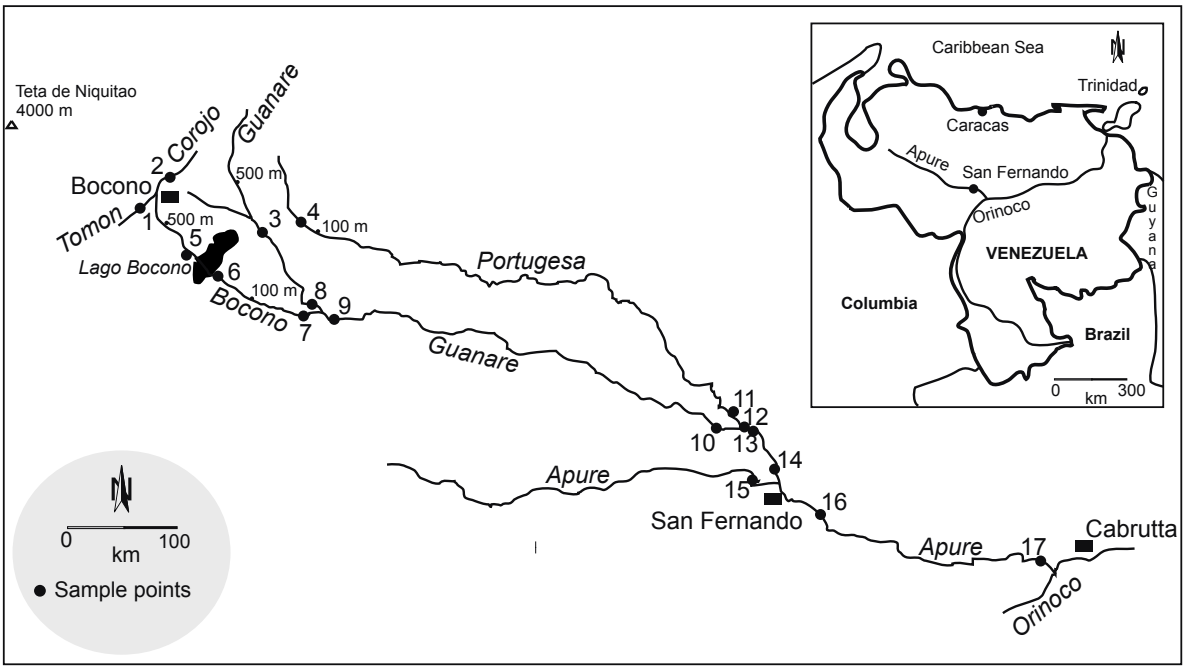

Fig. 6.3: The principal rivers sampled in the Apure watershed, Venezuela.

in June or July and annual rainfall averages 1'600 mm (Lewis and Saunders, 1989)

Methods

Sampling techniques and laboratory analysis.

Weekly meltwater samples were collected from the Rhone and Oberaar catchments during the summers of 1999, 2000 and 2001. In order to calculate daily mean concentrations samples were taken in pairs at the times of minimum and maximum daily discharge (10:00 and 17:00 h; Gurnell et al., 1994). Throughout the winter samples were taken on a monthly basis. In total 70 Rhone meltwater and 50 Oberaar meltwater samples were taken. The Rhone tributary was sampled six times on a monthly basis between May and September 2000. The Apure river system was sampled in February 1999, September 1999 and November 2000. The 1999 campaign coincided with a year when the El Nino –El Nina effect was particularly pronounced, leading to very dry river beds in February and particularly swollen rivers in September.

Samples for total phosphorus (TP) analysis were bottled without filtration, samples for soluble reactive phosphorus (SRP) and total dissolved phosphorus (TDP) analysis were filtered immediately in the field, as recommended by Slatt (1972) using pre-weighed 0.45 μm cellulose acetate filters, a Nalgene filter unit and hand pump. The difference between TSP and SRP is ascribed to dissolved organic phosphorus; DOP. The water samples (approximately 125 ml) were stored in the dark at 2°C. In 1999 all samples were stored in polyethylene bottles, pre-leached with deionised water after Edmund et al. (1996). The 1999 Venezuelan samples were poisoned with several drops of Na_2N_3 since they were only analysed after 2-3 weeks (GEA laboratory, Neuchatel). The 1999 glacial samples were poisoned using $HgCl_2$ to prevent SRP uptake by bacteria (Mackereth et al., 1978). We found the $HgCl_2$ made TDP analysis inaccurate. So in 2000 and 2001 all samples were stored in autoclaved, iodine coated polypropylene bottles that were rinsed three times with river water before filling them to leave no airspace (Mackereth et al., 1978).

5 snow samples were taken from profiles dug during the 2000-2001 accumulation season in front of the Rhone and Oberaar glaciers. 17 rain samples were also collected during the 2000 and 2001 ablation periods by connecting a pre-leached 1 liter polypropylene bottle to a funnel via a polypropylene tube. A fine copper mesh was used to limit particles falling into equipment and the bottle was left for a maximum of 24 hours before the rainwater was filtered and bottled.

Sample	SRP ($\mu eq\ l^{-1}$)	TDP ($\mu eq\ l^{-1}$)	TP ($\mu eq\ l^{-1}$)	Cl ($\mu eq\ l^{-1}$)
Rain				
28-Aug-99				5.64
7-Sep-99				3.67
22-Sep-99				1.41
31-May-00	0.52	0.88		1.69
7-Jun-00				4.23
28-Jun-00	0.93	1.46		4.20
13-Jul-00	0.15			2.26
15-Jul-00				4.22
27-Jul-00	0.30	1.15		3.10
1-Aug-00	0.86	1.23		5.36
7-Aug-00	0.41	0.49		1.68
15-Jul-01			2.08	4.22
23-Jul-01			8.13	
3-Aug-01				3.80
3-Aug-01		1.00	4.71	1.94
8-Aug-01		1.16	3.36	3.74
17-Aug-01			5.18	6.21
30-Aug-01			3.35	8.46
Snow				
18-Jan-01 (Rhone)	0.14	0.24	0.23	2.52
18-Jan-01 (Oberaar)	0.57	0.78	1.09	9.87
6-Mar-01 (0-5 cm; Oberaar)	0.08	0.39		2.80
6-Mar-01 (0-40 cm; Oberaar)	0.04	0.39		5.32
6-Mar-01 (0-5 cm; Rhone)	0.06	0.15	0.30	
mean rain	0.53	1.05	4.47	3.87
mean snow	0.18	0.39	0.54	5.13
weighted average	**0.32**	**0.66**	**2.11**	**4.63**
Alptal, Switzerland (non glaciated; average annual precipitation)[†]				4.51
Haut Glacier d'Arolla, Switzerland[#]				3.80
PO_4^{3-}/Cl	**0.07**	**0.14**	**0.46**	

[†] Mean annual precip. for a non-glaciated valley on the northern border of the Alps; Average annual precipitation 2300 mm; P. Schleppi (pers. comm., Swiss Federal Insititute for Forest, Snow, and Landscape).

[#] Mean winter snowpack 93-95, Tranter et al. (2002)

Values are given in $\mu eq\ l^{-1}$ and P conc. are listed as PO_4^{3-} to show the PO_4^{3-}/Cl^- ratios used to correct the raw data.

Table 6.2: Mean precipitation PO_4^{3-}/Cl^-.

Sediment-laden filters were retained from each sampling event, generally representing the sediment in 500 ml of water; the filters were dried at 40°C, weighed and used to calculate suspended sediment concentrations in the meltwaters. Venezuela bedload samples were also taken using a grab sampler; they were dried at 40° C in the GEA laboratory, Neuchatel, within 3 weeks.

The TDP and TP samples were dissolved with ammonium peroxide at 120 °C and subsequently measured together with the SRP samples using a Perkin Elmer spectrophotometer (molybdenum blue method; Murphy and Riley, 1962). The 5 cm cuvette affords a

limit of detection of 0.03 μmol l^{-1} (± 0.04 μmol l^{-1}).

The ironbound, detrital and organic P concentrations of the suspended and bedload sediments were analysed using a sequential extraction method (SEDEX; Ruttenberg, 1992; Tamburini 2001), which has also been used on river and on lake sediments (Berner and Rao, 1994; Fillipelli and Souch, 1999). The method removes increasingly recalcitrant phosphorus forms in progressive steps. Samples were prepared as follows: Suspended sediment was removed from each filter paper ultrasonically, the sample was immediately centrifuged and the supernatant (deionised water) decanted off. The blank filters were dried and reweighed to calculate the exact mass of sediment transferred (between 0.04 and 0.2 g). Bedload samples were ground for 3 minutes in an agate mill and 0.1 g was used for the extraction. Step 1 of the SEDEX method removes ironbound P using a pH 7.6 citrate-dithionate-bicarbonate solution (CDB). Step 2, an acetic acid-sodium acetate solution buffered at pH 4, was designed to identify marine authigenic phosphorus (Ruttenberg, 1992). We interpret the P extracted by this step as fine detrital P, which can be solublised if sediment grains are not close to 250 μm in diameter (Ruttenberg, 1992). As the modal grain size of our glacial suspended sediment is approximately 4 - 8 μm and the bedload samples are equally fine it is highly likely that detrital P dissolution occurs (Hosein et al., submitted; Hosein, unpublished data). Step 3 extracts detrital P with a 1N HCl digestion and step 4 involves ashing the samples with peroxide at 550 °C and redigesting them with 1N HCl to measure organic P. The solutions obtained from steps 2 - 4 were analysed within 1 week, using the molybdenum blue method in the GEA laboratory. The accuracy of the detrital P measurements is ± 0.64 μmol g^{-1} and the accuracy of the organic P measurements is ± 0.32 μmol g^{-1}. The samples obtained from step 1 were analysed for iron and P at the SCPE-laboratory of Neuchatel by ICP-AES.

The mineralogy of the powdered Venezuelan bedload sediment samples and the glacial and Venezuelan suspended sediments retained on the 0.45 μm cellulose acetate filters were measured by X-ray diffraction (XRD), using a Scintag XDS 2000.

P fluxes were calculated as the product of the P concentrations and discharge volumes (see Chapter 2 for details of how fluxes are calculated in the presently glaciated catchments). In the Rhone tributary catchment discharges are estimated from Bernath (1991) who recorded the tributary's discharges over a three-year period (1981-1984; mean discharges are 250, 277, 150 and 66 l s^{-1} for the months of June, July, August and September respectively; ± 48 l s^{-1}). A winter flux is estimated by taking the lowest discharge recorded by Bernath (1991, 7 l s^{-1}) and the P concentration measured on the 19th of September as a representative winter value. The annual P fluxes are calculated as the mean of the ablation and accumulation period P fluxes, multiplied by 365. In all three catchments "weathering derived P fluxes" are also calculated, using P concentrations that have been corrected for atmospheric P inputs using the cyclical salts method described in Chapter 2; PO_4^{3-}: Cl$^-$ ratios are shown in Table 6.2.

Results

P Concentrations

P concentrations in the glacial catchments: Particulate P (PP), the difference between total dissolved and total P, is the most concentrated P form in the glacial meltwaters (Table 6.3) and at least 96-97% of this P is detrital (RH: 10.00 μmol g^{-1}, ± 1.61; 0.03 %; OA: 18.72 μmol g^{-1}, ± 2.58). The concentration does not vary as a function of discharge or seasonal evolution of the subglacial hydrological system and the mean detrital P concentration of the Rhone suspension is similar to the detrital P concentration of the catchment's bedrock; the Central Aar granite (0.04 - 0.07 % Keusen et al., 1989). The mean concentrations of ironbound and organic P in the glacial suspended sediments are < 1.61 μmol g^{-1} and 0.32 μmol g^{-1} (± 0.32 μmol g^{-1}) respectively.

The partitioning of P is very different in the runoff from the Rhone tributary catchment: P is mostly transported in dissolved forms, and the mean SRP and TDP concentrations of the Rhone tributary waters are approximately double those in the glacial meltwaters (Table 6.3). Suspended particulate matter in the Rhone tributary waters is negligible, therefore we have not analysed its solid P composition. One similarity between the three glacial catchments is that the SRP and TDP concentrations are within experimental error of each other (± 0.04 μmol l^{-1}) in the great majority of the Rhone, Oberaar and Rhone tributary water samples and therefore dissolved inorganic P (DIP) is the predominant dissolved form in the runoff from all three

	n†	Oberaar µmol l^{-1}	Rhone µmol l^{-1}	Tributary µmol l^{-1}	Precipitation µmol l^{-1}
		Ablation Period Runoff			**Rain**
SRP	48; 64; 6	0.08 (± 0.02)	0.05 (± 0.02)	0.14 (± 0.04)	0.18 (± 0.1)
TDP	41; 54; 5	0.10 (± 0.04)	0.07 (± 0.03)	0.17 (± 0.04)	0.35 (± 0.1)
DOP	-	b/d	b/d	b/d	0.17
TP	24; 30; 2	5.58 (± 3.21)	2.17 (±2.39)	0.29 (± 0.01)	1.52 (± 0.7)
Cl^-	111;198; 5	2.23 (± 0.49)	2.23 (±0.88)	2.70 (±0.92)	3.97 (± 1.85)
		Accumulation Period Runoff			**Snow**
SRP	7; 6; 1*	0.11 (± 0.02)	0.09 (± 0.04)	0.09	0.06 (± 0.07)
TDP	4; 4; 1*	0.13 (± 0.03)	0.14 (± 0.06)	0.16	0.13 (± 0.08)
DOP	-	b/d	b/d	0.07	-
TP	3; 3; -	0.26 (± 0.03)	0.23 (± 0.03)	-	0.18 (± 0.16)
Cl^-	7; 6; 1*	3.19 (± 1.10)	4.25 (± 0.05)	3.52	5.13 (± 3.40)

† Oberaar; Rhone; Tributary

* Winter estimate is based on a sample taken on the 19-Sept-00

b/d below detection limit

Table 6.3: P concentrations in glacial runoff and precipitation inputs.

catchments and dissolved organic P (DOP) is below detection.

P concentrations in the rain and snow falling in the glacial catchments: The most important difference between the mean P composition of the glacial runoff and the mean P composition of the precipitation entering the catchments is that the precipitation samples contain DOP. The mean DOP concentration in rain is 0.17 μmol l^{-1}, DOP was also detected in some snow samples (Table 6.3).

Comparing P concentrations in the runoff from the glacial and tropical catchments: The SRP concentration of the Apure tributaries ranges from 0.1 - 1.6 μmol l^{-1}, i.e. 1 - 2 orders of magnitude higher than the mean SRP concentrations of the glacial meltwaters (Table 6.3 & 6.4). Also, in contrast with the glacial meltwaters, DOP is detected in the tropical runoff (0.1 - 0.6 μmol l^{-1}; Table 6.4). In the sediments of the Apure tributaries ironbound, detrital and organic P forms are all detected: ironbound P concentrations are generally higher in the suspension samples (mean suspension = 10.17 μmol g^{-1}; mean bedload = 3.28 μmol g^{-1}) as are organic P concentrations (mean suspension = 4.99 μmol g^{-1}; mean bedload = 2.82 μmol g^{-1}). Detrital P concentrations are generally higher in the bedload samples (mean suspension = 6.80 μmol g^{-1}; mean bedload = 13.34 μmol g^{-1}). We observe a pattern of decreasing detrital P and increasing ironbound P concentrations with distance downriver, whereas organic P concentrations do not appear to change as a function of distance (Fig. 6.5; Table 6.5). The mean particulate P concentrations of suspended sediments from these climatically distinct catchments are similar (RH: 11.93 μmol g^{-1}; OA: 20.65 μmol g^{-1}; Apure = 21.95 μmol g^{-1}), but whereas detrital P represents 96 – 97 % of the particulate P in the glacial suspensions, it only represents 30 % of the average solid P content in the Apure suspended sediments. This is because ironbound and organic P concentrations are on average > 6 and 15 times higher (respectively) in the suspended sediments of the Apure catchment than in the suspended sediments of the glacial catchments.

Comparing the mineralogy of the glacial and tropical sediments: The sediment suspended in the glacial meltwaters contains quartz (21.8 & 24.3 %); potassic feldspar (17.2 & 6.5 %); plagioclase (27.9 & 25.4 %), phyllosilicates (14.2 & 13.7 %), and calcite (0.5 & 2.3 %), with some additional amphibole in the Oberaar catchment (mean values are given for the Rhone and Oberaar glaciers respectively). The Venezuelan suspended and bedload sediments generally contain kaolinite in addition to the minerals found in the glacial catchments.

Glacial P Fluxes

The dominance of solid P forms in the glacial meltwaters leads to a strong correlation between the TP and

Samples *	Distance from the Source	Discharge $m^3 s^{-1}$ †			P-SRP µmol l^{-1}			P-TDP µmol l^{-1}		P-DOP µmol l^{-1}	
		Feb-99	Sep-99	Nov-00	Feb-99	Sep-99	Nov-00	Sep-99	Nov-00	Sep-99	Nov-00
Head waters											
1. Tomon					0.1	0.3		0.5		0.1	
2. Corojo					0.1	0.6		0.7		0.1	
3. Gunare (source)						0.5	0.3	0.5	1.0		0.6
4. Portugesa source						0.3		0.4		0.1	
Intermediate rivers											
5. Mouth Bocono					0.1	0.5		0.7		0.2	
6. Outflow of Bocono dammed lake						0.1		0.3	0.2	0.1	0.0
7. Bocono before Guanare			51			0.2		0.4		0.1	
8. Guanare before Bocono (0-2m)			160			1.1		1.1		0.1	
9. Bocono & Guanare			210			0.9		1.2		0.2	
Llanos river samples											
10. Guanare before Portugesa			175			1.6		1.9		0.3	
11. Portugesa before Guanare			900			0.3		0.6		0.3	
12. Guanare & Portugesa 200 m after the confluence						0.0	0.7	0.0	1.0		0.3
13. Guanare & Portugesa 3km after the confluence						0.3	0.6	0.5	1.1	0.2	0.5
14. Portugesa before Apure		175	1075	625	0.1	0.6	0.4	0.7	0.8	0.1	0.4
15. Apure before Portugesa		375	3225	1875	1.8	0.6	0.6	0.7	0.8	0.1	0.2
16. Apure Boquerones						0.3	0.5	0.6	0.7	0.3	0.3
17. Mouth Apure		650	5000		0.4	0.7		0.4			

* The numbering corresponds to the sample points on Fig. 6.3

† Discharge estimates ± 10%

Table 6.4: Dissolved P in the Apure watershed.

Sample	Sample Date	Distance from source (km)	Det-P	Fe-P	Org-P	Particulate P
Apure sediments [#]						
BEDLOAD						
Head water rivers						
1. Tomon	Mar-99	-	11.31	0.89	0.79	12.98
Vitisy	Sep-99	-	33.05	21.02	25.19	79.26
Tirindi	Sep-99	-	0	0.97	1.82	2.79
2. Corojo	Mar-99	-	36.23	0.97	2.91	40.11
2. Corojo	Sep-99	-	48.76	0.97	2.91	52.63
Average (without Vitisy)		*20*	*17.93*	*0.94*	*1.84*	*20.71*
Intermediate and Llanos Rivers						
5. Bocono entry to lake	Sep-99	100	26.82	1.01	1.14	28.97
3. Guanare, Biscucui	Sep-99	137	12.64	1.97	1.64	16.25
4. Portuguesa, Llanos Road	Sep-99	200	6.61	4.81	4.58	16.01
8. Guanare before Bocono (0 - 2 m)	Sep-99	213	20.77	4.57	3.31	28.66
9. Bocono & Guanare	Sep-99	216	17.81	2.07	2.01	21.89
15. Apure before Purtuguesa, San Fernando	Sep-99	950	0.14	1.2	5.11	6.45
17. Mouth Apure	Mar-99	1247	4.02	9.69	2.91	16.61
Average			*13.34*	*3.28*	*2.82*	*19.44*
SUSPENSION						
Intermediate and Llanos Rivers						
5. Bocono entry to lake	Sep-99	100	13.77	5.63	5.57	24.97
3. Guanare, Biscucui	Sep-99	137	8.44	5.5	3.3	17.24
4. Portuguesa, Llanos Road	Sep-99	200	5.93	3.57	4.79	14.29
8. Guanare before Bocono (0 - 2 m)	Sep-99	213	8.73	8.43	6.36	23.52
9. Bocono & Guanare	Sep-99	216	8.97	7.9	5.77	22.64
10. Guanare before Portuguesa (g)	Nov-00	400	7.56	9.69	5.16	22.41
10. Guanare before Portuguesa (s)	Nov-00	400	7.3	10.33	5.22	22.85
12. Portuguesa + Guanare 800 m (g)	Nov-00	400	5.8	11.62	6.12	23.55
12. Portuguesa + Guanare 800 m (s)	Nov-00	400	4.86	15.18	5.29	25.33
13. Portuguesa + Guanare 15 km (s)	Nov-00	415	5.94	11.95	5.7	23.58
14. Portuguesa before Apure, San Fernando (g)	Nov-00	450	6.72	12.92	5.49	25.13
15. Apure before Portuguesa, San Fernando (g)	Sep-99	950	4.2	17.04	3.23	24.47
15. Apure before Portuguesa, San Fernando (g)	Nov-00	950	6.46	8.72	5.17	20.34
15. Apure before Portuguesa, San Fernando (s)	Nov-00	950	6.12	8.72	5.36	20.2
16. Apure Boquerones	Sep-99	1037	4.51	10.91	3.58	19.01
17. Mouth Apure	Sep-99	1247	3.44	14.55	3.73	21.72
Average			*6.8*	*10.17*	*4.99*	*21.95*
AMAZON RIVER SUSPENSION [†]			6.78	7.43	7.43	21.63
GLACIAL SEDIMENTS						
Rhone (n = 21)	1999-2000	0	10	1.61*	0.32	11.93
Oberaar (n = 15)	1999-2000	0	18.72	1.61*	0.32	20.65

[#] The numbering corresponds to the sample points on Fig. 6.3

[†] Berner and Rao (1994)

* cf. estimates in Table 6.6.

Table 6.5: The detrital (Det-P), ironbound (Fe-P) and organic P (Org-P) compositions of the Apure and Amazon (tropical) and the Rhone and Oberaar (glacial) particulate P fluxes (PP).

suspended sediment concentrations (R^2; OA: 0.92; RH: 0.80). This enables us to use least squares regressions to calculate the TP concentrations in 174 Rhone and 117 Oberaar meltwater samples, based on their suspended sediment concentration. We can thereby calculate a more representative TP flux that includes several flushing events, such as a two day rain event on the 20th and 21st of September 1999 where 9 % of the annual

	Oberaar	Rhone	Tributary
Runoff			
SRP	0.19	0.19	0.29
TP	13.82	8.46	< 2.33
PP	11.18	8.27	-
Rain corrected			
SRP	0.04	0.05	0.17
TP	10.58	7.38	≈ 0.60
PP	10.53	7.33	-

Table 6.6: Fluxes from the glaciated catchments in kmol km^{-2} yr^{-1}.

suspended sediment flux was exported from the Rhone glacier (Chapter 2; The particulate P concentration and the suspended sediment bulk mineralogy were not observed to change as a function of discharge). We obtain average TP fluxes of 8 and 11 kmol km^{-2} yr^{-1} respectively from the Rhone and Oberaar catchments using this method (precipitation inputs of TP are relatively minor; Table 6.6). The larger Oberaar TP flux reflects both the elevated detrital P concentration of the Oberaar suspension and the higher suspended sediment concentration of the Oberaar meltwaters (Hosein et al., submitted). We attribute these differences to the presence of the easily eroded gneissic zone that forms the central part (42 %) of the Oberaar catchment (Fig. 6.3).

The particulate P flux, calculated as the product of the mean particulate P concentration of the suspended sediments (ironbound & detrital & organic P) and the annual suspended sediment fluxes from each glacier, is comparable with the particulate P fluxes calculated as the difference between the TP and SRP fluxes (see Table 6.7).

The SRP fluxes from the presently glaciated Rhone and Oberaar catchments are significantly lower than the SRP fluxes from Rhone tributary catchment. Moreover, when these fluxes are corrected for precipitation inputs, the glacial catchments' SRP fluxes are approximately 4 times less than the SRP flux from the Rhone Tributary catchment (Table 6.3). TP fluxes are not calculated for the Rhone tributary catchment as TP concentrations were only measured on 2 samples, but since the TP concentrations are approximately double the SRP concentrations it would follow that the TP flux should also be approximately double the SRP flux, i.e. ca. 0.6 kmol km^{-2} yr^{-1}.

Discussion

The annual, precipitation corrected, total phosphorus fluxes in the two presently glaciated catchments are 7 and 11 kmol km^{-2} yr^{-1} and more than 99 % of this flux is in particulate form. Our glacial catchments' particulate P fluxes are the same order of magnitude as catchments in tectonically active areas, such as the Ganges, Amazon and Mekong, which also have high suspended sediment fluxes (see Table 6.7). Rivers draining watersheds located in areas that are less tectonically active, such as the Gambia and Congo have particulate P fluxes that are 2 orders of magnitude lower, as do non-glaciated crystalline catchments that are a similar size to the glacierised ones (Table 6.7). Although glacial erosion may potentially produce similar sediment volumes as fluvial erosion (Hay, 1998) the P forms in the runoff from presently glaciated and tropical catchments are different. The Amazon and the Apure, two of the world's major tropical rivers, have now been shown to carry an important load of particulate P in ironbound and organic P forms (Berner and Rao, 1994; this study). Upstream in the Apure catchment detrital P concentrations are higher than ironbound P concentrations in the suspended sediments, but downstream (over 400 km from the headwaters) ironbound P becomes the dominant P forms in the suspended sediments (Fig. 5). This may suggest that detrital P is dissolved during cycles of deposition, colonisation by vegetation, and remobilisation during its transport downriver and is superceded by ironbound P forms. (There may also be an element of transport bias towards potentially lighter flocs of ironbound P and fine organic matter.) Consequently, because of the retention of detrital P in the pedosphere in the tropics and its conversion into biogenic forms (Syers and Walter, 1976; Crews et al., 1995), the P discharged into the marine realm by tropical rivers may contains up to 26 times more conditionally bioavailable P (DIP, DOP, ironbound and organic P) than the P discharged into the marine realm by subglacial meltwaters, where the majority of the particulate P is scarcely bioavailable detrital P (Table 6.7).

Glaciers and periods of glaciation may therefore have great potential to change the P dynamics and productivity of terrestrial and aquatic ecosystems in several ways (Föllmi, 1995; Chadwick et al., 1999). Firstly the great physical erosive force of advancing glaciers (Hallet et al., 1996; Hay, 1998) might have lead firstly to deeply weathered soils being bulldozed off land surfaces, ironbound and organic P in such

River system	Study	Geology	Catchment	Sediment flux[£]	Altitude	PP	TP
			(km^2)	($t\ km^{-2}\ yr^{-1}$)	(m)	($kmol\ km^{-2}\ yr^{-1}$)	($kmol\ km^{-2}\ yr^{-1}$)
Ganges	Martin & Meybeck (1979)		3820000	437	>3000	7.90	
Amazon	Martin & Meybeck (1979)		6150000	195	>3000	10.40	
Orinoco	Lewis & Saunders (1989)		990000	212	>3000	2.32	3.10
Mekong	Martin & Meybeck (1979)		790000	203	>3000	13.08	
Apure	Saunders & Lewis (1988)		167000		1000-3000	1.49	2.20
Vaal 1978-81	Grobler & Silberbauer (1985)	sedimentary	16153		1000-3000		0.03
Limpopo-sub 1980-82	Grobler & Silberbauer (1985)	igneous	1171		1000-3000		0.08
Limpopo-sub 1979-81	Grobler & Silberbauer (1985)	igneous	129		1000-3000		0.03
Rhône	This study	granite-granodiorite	27	491[#]	1000-3000	6*-8°	8.01
Oberaar	This study	granite, foliated gneisse	11	773[#]	1000-3000	11°-16*	11.66
Gambia	Lesack et al. (1984)		42000		500-1000	0.09	0.25
Richmond river	McKee & Eyre (2000)	volcanic	6861		500-1000		0.42[§], 1.64[†]
Congo	Martin & Meybeck (1979)		3820000	11	100-500	0.55	
Thi National Park	Stoorvogel et al. (1997)		1.17		100-500	4.00	4.62
Mean export from 25 forested catchments	Dillon & Kirchner (1975)	plutonic	10-100				0.15
Mean export from 8 for. sedimentary catch.	Dillon & Kirchner (1975)	sedimentary	10-100				0.38
mean export from 7 volcanic catchments	Dillon & Kirchner (1975)	volcanic	10-100				2.32

[£] Milliman and Meade,1985
[#] Hosein et al., (submitted)
[*] Calculated from SEDEX extraction
[°] Calculated as the difference between SRP and TP
[§] Flux calculated from weathering of bedrock
[†] Total Phosphorus

Table 6.7: A comparison of particulate P (PP), total P (TP), and conditionally bioavailable P fluxes ($kmol\ km^{-2}\ yr^{-1}$).

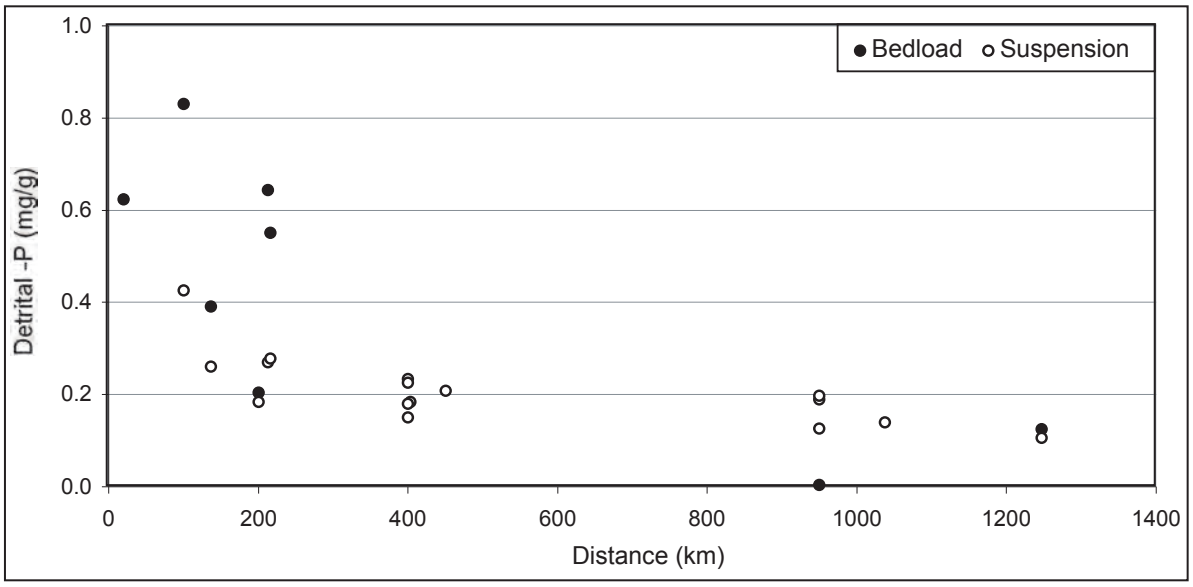

Fig. 6.5: Detrital P concentrations in the bedload and suspended sediments of the Apure watershed.

soils would become conditionally bioavailable in the marine environment (a transfer of 600 Pg of C, after Sigman and Boyal, 2000). Secondly, as large areas of the continents became covered in ice physical weathering rates and export of sediment from subglacial environments may have decreased as the ice masses became predominantly cold based and frozen to their beds (Kump et al., 2000, and references therein). Also the chemical weathering derived SRP flux from any wet based marginal areas of ice sheet would have likely been negligible, judging from the SRP fluxes from the presently glaciated Rhone and Oberaar catchments are (0.05 kmol km^{-2} yr^{-1}), this is probably due to the neutral pH of the subglacial environments (Stumm and Morgan, 1996). Thirdly, periods of deglaciation may have lead to the renewed erosion and export of freshly comminuted detrital P grains in glacial sediments and their deposition over considerable continental areas (28 % of the Northern Hemisphere's land surface may have fallen within the proglacial zone during deglaciation following the last glacial maximum, Gibbs and Kump, 1994). This detrital P may have been rapidly hydrolised to SRP in the proglacial environment. Furthermore, due to the low P binding capacity of protosoils with their thin organic horizons and low oxide contents (Egli et al., 2001; Filippelli and Souch; 1999) proglacial areas may have leaked a considerable flux of SRP into aquatic ecosystems (Pennington, 1981; Filippelli and Souch, 1999).

The integrated detrital P weathering rate we calculate for the 11.6 kyr sediments in the Rhone forefield is 0.32 kmol km^{-2} yr^{-1} (according to Chapter 5). As the chemical erosion rates from the Rhone tributary is 0.17 kmol km^{-2} yr^{-1} this suggests that approximately 47 % of the weathering derived SRP is retained within the soil profile in the Rhone catchment over 11.6 kyr. If we estimate that 20 % of weathering derived SRP was retained in the pedosphere after sediments had been exposed for 1000 yr, but the weathering rate at this time was still 0.32 kmol km^{-2} yr^{-1} (probably a conservative weathering scenario judging from Fig. 5.4, Chapter 5), then the weathering derived SRP flux from a proglacial system that had been ice free for 1000 yr would be 5 times greater than the present day maximum natural SRP flux recorded by Meybeck (1993; i.e. 1.6 kmol km^{-2} yr^{-1}). In fact the flux calculated for in the Rhone tributary catchment might be a rather conservative estimate of an average P flux from proglacial areas, given that SRP fluxes from catchments with plutonic bedrock are lower than SRP fluxes from catchments with sedimentary or volcanic geology (Dillon and Kirchner, 1975). Bearing this in mind if we scale these fluxes up to estimate a leaky P flux during deglaciation after the last glacial maximum, basing our calculation of the proglacial P flux on a time when the LGM ice mass was halved, exposing 9'200'000 km^2 of continental land mass (Gibbs and Kump, 1994), and assuming a conservative chemical SRP erosion flux of 0.17 kmol km^{-2} yr^{-1} we arrive at a flux of $1.564 \cdot 10^9$ kmol SRP yr^{-1} from this recently deglaciated area. This is more than double the

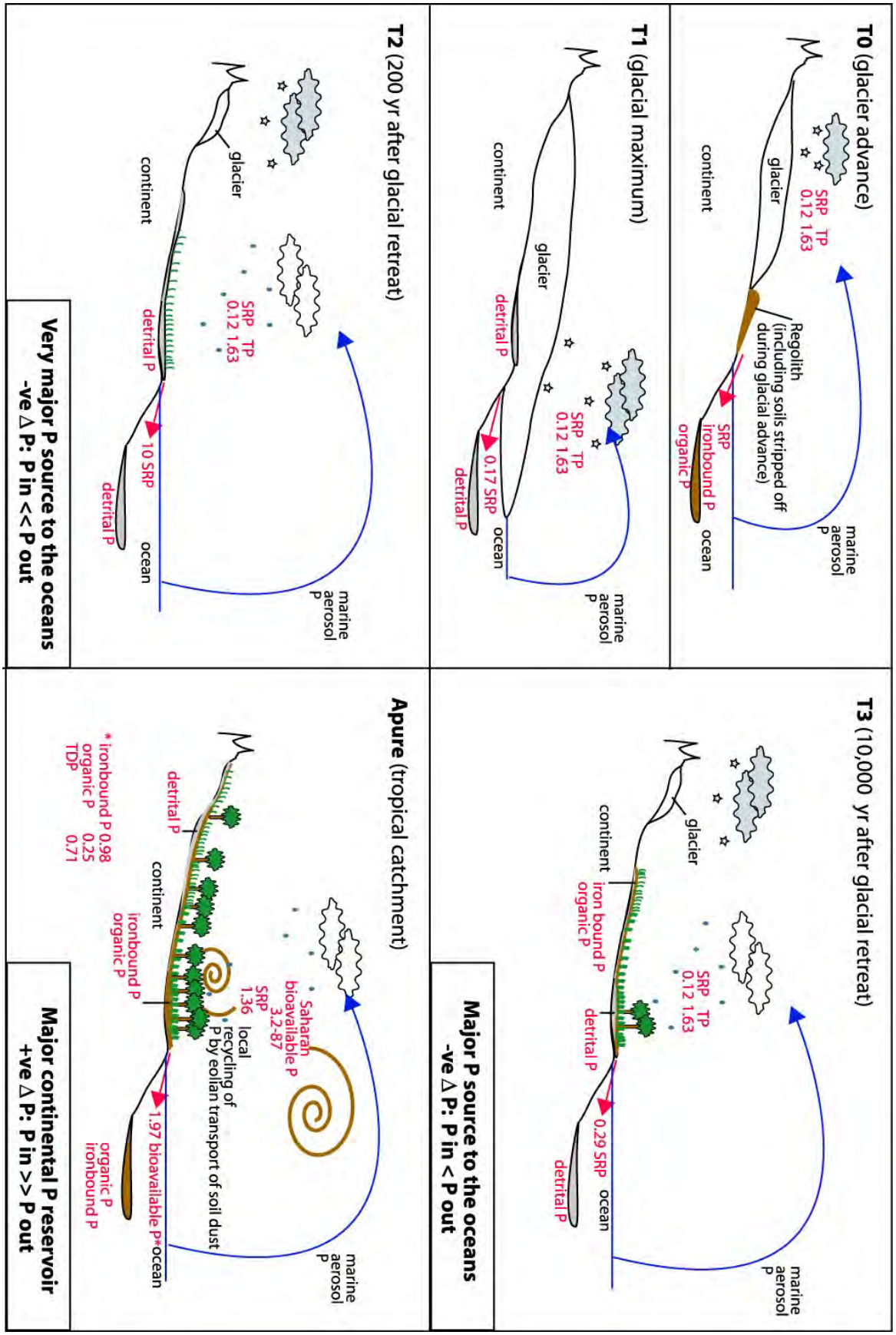

Fig. 6.6: P cycling in glaciated and tropical continental areas, values are taken from Chapters 5 and 6, Reichhof (1986), Montes and San-Jose (1989), and Swamp et al. (1992).

maximum present-day global riverine reactive P flux to the oceans (dissolved inorganic + dissolved organic + particulate organic + iron bound particulate P; 1.485 • 10^8 kmol yr^{-1}; Compton et al., 2000, and references therein).

To compare the SRP fluxes generated by the dissolution of detrital P in glacial environments with SRP fluxes from the tropics, non-weathering inputs of SRP need to be accounted for, namely precipitation and anthropogenic inputs: On average 20 - 30 kg ha^{-1} of mineral P fertiliser were added to Venezuelan soils between 1985 and 1989 (Beaton et al., 1995). The regional input of soluble P by rain and occult deposition is also considerable (SRP = 1.36 kmol km^{-2} yr^{-1}; Montes and Jose, 1989). The literature hints that both locally recycled and distal inputs of SRP may be important sources: P may be recycled internally within the Apure basin by burning vegetation and through the local eolian transport of soil dust (Montes and Jose, 1989, and references therein). But, marine aerosols (Montes and Jose, 1989) and Saharan dust may also account for a portion of the locally bioavailable P (3.2 - 87 kmol P km^{-2} yr^{-1}; Reichholf, 1986; Swap et al., 1992). Since the Llanos soils are oligotrophic and depleted in P (San Jose and Garcia Miragaya, 1982) such external P inputs may be important in maintaining productivity.

Moreover since SRP inputs to the Apure catchment are more than twice as large as SRP outputs (0.52 kmol km^{-2} yr^{-1}, Saunders and Lewis, 1988) even with the potential addition of mineral P fertiliser; and since the lowest estimate of distal eolian bioavailable P input (3.2 kmol P km^{-2} yr^{-1}) is higher than the annual output of biologically available P from the catchment (1.97 kmol P km^{-2} yr^{-1}) it is likely that the Apure catchment acts as a reservoir, trapping SRP as ironbound and increasingly recalcitrant organic P forms (see also Chadwick et al., 1999).

Therefore periods of glaciation (and uplift) may provide important counter mechanisms for reactivating such transport limited regimes by replacing old, deeply weathered soils with immature pedospheres that leak a globally significant fluxes of soluble reactive P into marine environments (Fig. 6.6).

Acknowledgements

J. Ondrus (SCPE-laboratory, Neuchatel) performed the ICP-AES analysis. A. Moreau, M. Cornièles-Vallès and Colonel R. Mena Nava (MARNR-Venezuela) provided invaluable logistical support for the Apure sampling campaign and Swiss National Science Foundation grants 21-53997.98 and 20-61485.00 are also gratefully acknowledged.

References

Beaton, J.D., Roberts, T.L., Halsted, E.H., and Cowell, L.E., 1995. Global transfers of P in fertiliser materials and agricultural commodities. In H.Tiessen (Editor) Phosphorus in the global environment: Transfers, cycles and management: SCOPE 54, Wiley: 107 - 137.

Bernath, A., 1991 Zum Wasserhaushalt im Einzugsgebiet der Rhone bis Gletsch. Züricher Geographische Schriften, 43, pp. 383.

Berner, R.A., and Rao, J.L., 1994. Phosphorus in sediments of the Amazon River and estuary: Implications for the global flux of phosphorus to the sea. Geochimica Cosmochimca Acta, 58, 2333-2339.

Birkland, P.W., Burke, R.M., and Benedict, J.B., 1989. Pedogenic gradients for iron and aluminium accumulation and phosphorus depletion in Arctic and Alpine soils as a function of time and climate. Quaternary Research, 32, 193-204.

Boström, B., Persson, G., and Broberg, B., 1988. Bioavailability of different phosphorus forms in freshwater systems. Hydrobiologia, 170, 133-155.

Broecker, W.S. 1982. Ocean chemistry during glacial times. Geochimica Cosmochimica Acta, 46, 1689-1705.

Cembella, A.D., Antia, N.J., and Harrison, P.J., 1984. The utilisation of inorganic phosphorus compounds as nutrients by eukaryotic mircoalgae: A multidisciplinary perspective. Critical Reviews in Microbiology, 10, 317-391.

Chadwick, O.A., Derry, L.A., Vitousek, P.M., Huebert, B.J., and Hedin, L.O., 1999. Changing sources of nutrients during four million years of ecosystem development. Nature, 397, 491-497.

COHMAP, 1988. Climatic changes of the last 18,000 years: Observations and model simulations. Science, 241, 1043-1052.

Cotner, J.B., Ammerman, J.W., Peele, E.R., and Bentzen, E., 1997. Nutrient-limited bacterioplankton

growth in the Sargasso Sea. Aquatic Microbial Ecology, 13, 141-149.

Crews, T.E., Kitayama, K., Fownes, J.H., Riley, R.H., Herbert, D.A., and Mueller-Dombois, D., 1995. Changes in soil phosphorus fractions and ecosystem dynamics across a long chronosequence in Hawaii. Ecology, 76, 1407-1424.

Delaney, M.L., 1998. Phosphorus accumulation in marine sediments and the oceanic phosphorus cycle. Biogeochemical Cycles, 12, 563-572.

Dillon, P.J. and Kirchner, W.B., 1974. The effects of geology and land use on the export of phosphorus from watersheds. Water Resources, 9, 135-145.

Edmond, J.M., Palmer, M.R., Measures, C.I., Grant, B., and Stallard, R.F., 1995. The fluvial geochemistry and denudation rate of the Guayana Shield in Venezuela, Columbia and Brazil. Geochimica et Cosmochimica Acta, 59, 3301-3325.

Filippelli, G.M. and Delaney, M.L., 1994. The oceanic phosphorus cycle and continental weathering during the Neogene. Paleoceanography, 60, 643-652.

Filippelli, G.M. and Souch, C., 1999. Effects of climate and landscape development on the terrestrial phosphorus cycle. Geology, 27, 171-174.

Föllmi, K.B., 1995. 160 m.y. Record of marine sedimentary phosphorus burial: Coupling of climate and continental weathering under greenhouse and icehouse conditions. Geology, 23, 859-862.

Fox, L.E., Sager, S.L., and Wofsy, S.C., 1986. The chemical control of soluble phosphorus in the Amazon estuary. Geochimica et Cosmochimica Acta, 50, 783-794.

Froelich, P.N., Bender, M.L., Luedtke, N.A., Heath, G.R., and DeVries, T., 1982. The marine phosphorus cycle. American Journal of Science, 282, 474-511.

Frossard, E., Brossard, M., Hedley, M.J., and Metherell, A., 1995. Reactions controlling the cycling of P in Soils. In H.Tiessen (Editor) Phosphorus in the global environment: Transfers, cycles and management: SCOPE, 54, Wiley: 107 - 137.

Gibbs, M.T., and Kump, L.R., 1994. Global chemical erosion during the Last Glacial Maximum and the present: Sensitivity to changes in lithology and hydrology. Palaeoceanography, 9, 529-543.

Golterman, H.L., 1984. Sediments, modifying and equilibriating factors in the chemistry of freshwater. Verh. Internat. Verein. Liminol., 22, 23-59.

Graham, W.F. and Duce, R.F., 1979. Atmospheric pathways of the phosphorus cycle. Geochimica et Cosmochimica Acta, 43, 1195-1208.

Grobler, D.C. and Silberbauer, M.J., 1985. The combined effect of geology, phosphate sources and runoff on phosphate export from drainage basins. Water Research, 19, 975-981.

Guidry, M.W., Mackenzie, F.T., and Arvidson, R.S., 2000. Role of tectonics in phosphorus distribution and cycling. In C.R. Glenn, et al. (Editors) Marine Authegenisis: From global to microbial. SEPM (Society for Sedimentary Geology) Special Publication, 66.

Gurnell, A.M., Brown, G.H., and Tranter, M., 1994. Sampling strategy to describe the temporal hydrochemical characteristics of an alpine proglacial stream. Hydrological Processes, 8, 1-25.

Hay, W.W., 1998. Detrital sediment fluxes from continents to oceans. Chemical Geology, 145, 287-323.

Hudson, J.J., Taylor, W.D., Schindler, D.W., 2000. Phosphate concentration in lakes. Nature, 406, 84 -86.

Johnsson, M.J., Stallard, R.F., and Meade, R.H., 1988. First-cycle quartz sand in the Orinoco River basin, Venezuela and Columbia. Journal of Geology, 96, 263-277

Kpomblekou-a, K. and Tabatabai, M.A., 1994. Effect of organic acids on release of phosphorus from phosphare rocks. Soil Science, 158, 442-453.

Kump, L.R. and Alley, R.B., 1994. Global chemical weathering on glacial time scales. In: T.M. Usselman and W.W. Hay (Editors) Material Fluxes on the Surface of the Earth. Geophysics Study Committee, National Research Council, National Academy Press, Washington D.C., 40-60.

Kump, L.R., Brantley, S.L., and Arthur, M.A., 2000. Chemical weathering, atmospheric CO2, and climate. Annual Reviews in Earth and Planetary Sciences, 28, 611-667.

Lesack, L.F.W., Hecky, R.E., and Melack, J.M., 1984. Transport of carbon, nitrogen phosphous and major solutes in the Gambia River, West Africa. Limnology and Oceanography, 29, 816-830.

Lewis, W.M. and Saunders, J.F., 1989. Concentration and transport of dissolved and suspended substances in the Orinoco river. Biogeochemistry, 7,

203-240.

Ludwig, W., Amiotte-Suchet, P., and Probst, J.-L., 1999. Enhanced chemical weathering of rocks during the Last Glacial Maximum: A sink for atmospheric CO_2? Chemical Geology, 159, 147-161.

Mackereth, F.J.H., Heron, J., and Talling, J.F., 1978. Water Analysis: Some revised methods for limnologists. Freshwater Biological Publication, 36.

Martin, J.M. and Meybeck, M., 1979. Elemental mass balance of material carried by major world rivers. Marine Chemistry, 7, 173-206.

McKee, L.J. and Eyre, B.D., 2000. Nitrogen and phosphorus budgets for the sub-tropical Richmond River Catchment, Austraila. Biogeochemistry, 50, 207-239.

Meybeck, M.,1982. Carbon, nitrogen and phosphorus transport by world rivers. American Journal of Science, 282, 401-450.

Meybeck, M., 1993. Natural sources of C, N, P and S, In R. Wollast, F.T. Mackenzie, and L. Chou, (Editors) Interactions of C, N, P and S Biogeochemical Cycles and Global Change: NATO ASI Series, I 4, Springer-Verlarg, Berlin Heidelberg.

Migon, C. and Sandroni, C., 1999. Phosphorus in rainwater: Partioning inputs and impact on the surface coastal ocean. Limnology and Oceanography, 44, 1160-1165.

Milliman, J.D. and Meade, R.H., 1983. Worldwide delivery of river sediments to ocean. Journal of Geology, 91, 1-19.

Molen, D.T., van der Breeuwsma, A., Boers, P.C.M., and Roest, C.W.J., 1997. Dutch policy towards phosphorus losses in agriculture. In H. Tunney, O.T. Carton, P.C. Brookes, and A.E. Johnston (Editors) Phosphorus losses from soil to water. CAB International, Wallingford, 137-149.

Montes, R. and San-Jose, J.J., 1989. Chemical composition and nutrient loading by precipitation in the Trachypogon savannas of the Orinoco Llanos, Venezuela. Biogeochemistry, 7, 241-256.

Murphy, J. and Riley, J.P., 1962. A modified single solution method for the determination of phosphate in natural waters. Analytica Chimica Acta, 27, 31-36.

Newbold, J.D., Elwood, J.W., O'Neill, R.V., and van Winkle, W., 1981. Measuring nutrient spiralling in streams. Canadian Journal of Aquatic Science, 38, 860-863.

Pennington, W., 1981. Records of a lake's life in time: the sediments. Hydrobiologia, 79, 197-219.

Pye, K., 1984, Loess. Progress in Physical Geography, 8, 176-217.

Reichhof, J.H., 1986. Is Saharan dust a major source of nutrients to the Amazonian rain forest? Neotrop. Faunu Environ., 21, 251-255.

Reynolds, C.S. and Davis, P.S., 2001. Sources and bioavailability of phosphorus fractions in freshwater: A British perspective. Biological Reviews, 76, 27-64.

Roure, F., Carnevali, J.O., Gou, Y., and Subieta, T., 1994. Geometry and kinematics of the North Monagas thrust belt (Venezuela). Marine Petroleum Geology, 11, 347-362.

Ruttenberg, K.C., 1992. Development of a sequential extraction method for different forms of phosphorus in marine sediments. Limnology and Oceanography, 37, 1460-1482.

Ruttenberg, K.C., 1993. Reassesment of the oceanic residence time of phosphorus. Chemical Geology, 107, 405-409.

San-Jose, J.J. and Garcia-Miragaya, J., 1982. Factores operacionales en la produccion de meteria nica de las sabanas de Trachypogon. Boletin de la Sociedad Venezolana de Ciencias Naturales, 139, 347 – 374.

Saunders, J.F. and Lewis, W.M., 1988. Transport of phosphorus, nitrogen, and carbon by the Apure River, Venezuela. Biogeochemistry, 5, 323-342.

Schindler, D.W., 1977. Evolution of phosphorus limitation in lakes. Science, 195, 260-262.

Sharpley, A., 2000. Phosphorus Availability. In M.E. Sumner (Editor) Handbook of soil science, D18-D36, CRC Press.

Sigman, D. and Boyle, E., 2000. Glacial/Interglacial variations in atmospheric carbon dioxide. Nature, 407, 859-869.

Skirrow, G., 1975. The dissolved gases-carbon dioxide. In J.P. Riley and G. Skirrow (Editors) Chemical Oceanography 2, 2nd Edition, Academic Press, London, 245-300.

Slatt, R.M., 1972. Geochemistry of meltwater streams from nine Alaskan galciers. Geological Society of America Bulletin, 83, 1125-1132.

Southam, J.R., and Hay, W.W., 1981. Global sedimentary mass balance and sea level changes. The Sea, 7, 1617-1684.

Stoorvogel, J.J., Janssen, B.H., and van Breemen, N., 1997. The nutrient budgets of a watershed and its forest ecosystem in the Tai National Park in Côte d'Ivoire. Biogeochemistry, 37, 159-172.

Stumm, W. and Morgan, J.J., 1996. Aquatic Chemistry. Wiley, New York, pp. 1022.

Swamp, R., Garstang, M., Greco, S., Talbot, R., and Kallberg, P., 1992. Saharan dust in the Amazon basin. Tellus, 44, 133-149.

Swiss National Hydrological and Geological Service (BWG), 1994. Technischer Bericht: Manual für die Abflussmessung nach dem Salzverdünnungs-verfahren.

Tamburini, F., 2001. Phosphorus in marine sediments during the last 150,000 years: Exploring relationships between continental weathering, productivity, and climate. Ph.D. thesis (CDRom), University of Neuchatel, Switzerland, pp. 219.

Tyrell, T., 1999. The relative influence of nitrogen and phosphorus on oceanic primary production. Nature, 400, 525-531.

Vegas-Vilarrubia, T., Maass, M., Rull, V., Elias, V., Ramon, A., Ovalle, C., Lopez, D., Schneider, G., Depetris, P.J., and Douglas, I., 1993. Small Catchment Studies in the Tropical Zone. In B. Moldan and J. Cerny (Editors) Biogeochemistry of Small Catchments, SCOPE, 51. Wiley.

Walker, T.W. and Syers, J.K., 1976. The fate of soil phosphorus during pedogenesis. Geoderma, 15, 1-19.

CHAPTER 7

Synthesis

Summary of subglacial weathering

Dissolved load

Dissolved load from crystalline glaciated catchments is normally enriched in Ca^{2+}, which is visible in increased Ca/Na ratios (Fig. 7.1, taken from Chapter 2). Our dataset corresponds to this trend. This enrichment is proportional to the content of accessory calcite present in the catchment lithologies. In Fig. 7.1 data from a selection of presently non-glaciated catchments underlain by crystalline geology (from White and Blum, 1995) are plotted as well as the average Ca/Na ratio of granite (whole line, after Holland, 1978). Rhone dissolved load lies within the scatter of the presently non-glaciated, granitoid catchments. Some of these might show increased Ca/Na ratios because they were formerly glaciated and could still be affected by the weathering of glacially derived material. Furthermore, the scatter could just be due to bedrock impurities which are minor in the Rhone catchment. Data from Puerto Rico shows an increased Ca/Na ratio as well as an elevated silica flux which is due to the hotter and wetter (tropical) climate of this site. The Variscan Gneisses play a dominant role in the composition of dissolved load from Oberaar glacier. This zone is mechanically more readily erodable, which is visible in a higher suspended sediment yield as well as in higher dissolved fluxes from Oberaar glacier. The slightly higher content of accessory calcite within these rocks dominates the meltwater chemistry. Due to the significant content of sulphide also the sulphate flux from Oberaar is elevated. The K^+ flux is directly proportional to the biotite flux. Both glaciers suspended sediment contain equal amounts of biotite. At Oberaar, the higher suspended sediment yield therefore leads to an increased K^+ flux. Our silicate weathering derived cation fluxes ($\sum$ K^+, Mg^{2+}, Na^+) lie in the same range as those from non-glaciated granitoid catchments with similar runoff and located at similar latitudes. Looking at our data we conclude that increased physical erosion (cf. Oberaar) seems to have a direct influence on chemical weathering rates.

All silica fluxes (area normalised) from glaciated granitoid catchments are in the same order of magnitude, they plot together with silica fluxes from the Antarctica (dotted line in Fig. 7.1, Nezat et al., 2001). Compared to the non-glaciated granitoid streams their silica fluxes are rather low; however, they do not form a separate population. Therefore we conclude that the

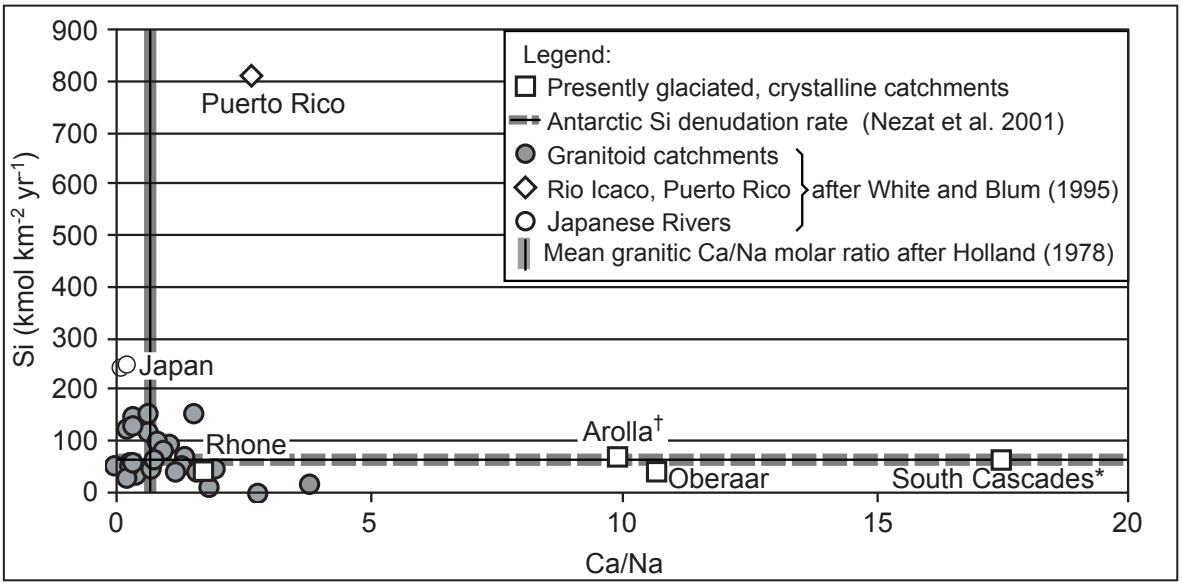

Fig. 7.1: Silicate and carbonate weathering in presently glaciated and non-glaciated granitoid catchments. All fluxes are corrected for precipitation inputs: † Sharp et al. (1995) and * Axtmann and Stallard (1995) => cyclic salt corrections; White and Blum (1995) => volumetric correction.

subglacial environment does not show increased silicate weathering rates. Our data compares well with the compilation of Anderson et al. (1997).

Suspended sediment

There are several factors controlling suspended sediment yield and erosion rate which might vary between glacial catchments (over small distances) and within them as a function of time (between different ablation seasons). This might be a reason for a probably rather high error on our calculations. Following is a recapitulation of the major factors, which could have affected our calculations:

- The underlying bedrock type (Fig. 1.5): Oberaar catchment has higher suspended sediment yields due to the higher erodability of the gneissic rocks (Variscan Gneisses). But also within the Rhone crystalline rocks there might be different/varying erodabilities, especially in border zones between granite and granodiorite, where bedrock might be foliated. Furthermore zones rich in joints and fractures play an important role.
- Quantities and time-scales of subglacial storage and remobilisation of deposits: The remobilisation of sediment deposits beside the glaciers (by precipitation/runoff) will increase the yields calculated for glacier covered areas. This could be inverse proportional to glacier cover, however, it might mainly depend on the catchment geometry and morphology. Rhone glacier snout lies in a small basin (Fig. 7.2) with a rock bar in front (Aellen, 1979). Major sediment pulses were observed during rain events: e.g., on the 20th/21st of September 1999 approximately 9 % of the yearly sediment flux was evacuated and we assume that this basin was flushed.

  Much research on temperate glacier regimes is done in regions which have been glaciated to a higher extent. Therefore todays mechanical erosion rates may still be affected by former higher mechanical erosion rates, during which sediment was stored and is now evacuated. This feature is of minor importance in our areas, because suspended sediment does not contain any secondary minerals which would be an indication for reworking/remobilisation of stored pre-weathered material. Suspended sediment from Oberaar and Rhone glacier is fresh.
- The dynamics of a glacier, such as its sliding speed, but also glacier size and ice flux affect this interplay of active abrasion vs. remobilisation of stored sediment. Koppes and Hallet (2002) worked on mechanical erosion rates in fjordes and discusses the possible importance of a strong correlation of sediment flux and ice flux. They suggest that, for landbased temperate glaciers as well as tidewater glaciers, erosion rates increase with ice flux and much of the erosion is likely to occur during periods of rapid basal motion (important in studying surgeing glaciers). Therefore recent yields may not be representative of long-term rates of erosion averaged over the glacial cycle, but may rather reflect a short-term (10 – 100 yr) acceleration in glacier sliding which often goes together with the glacier retreat.

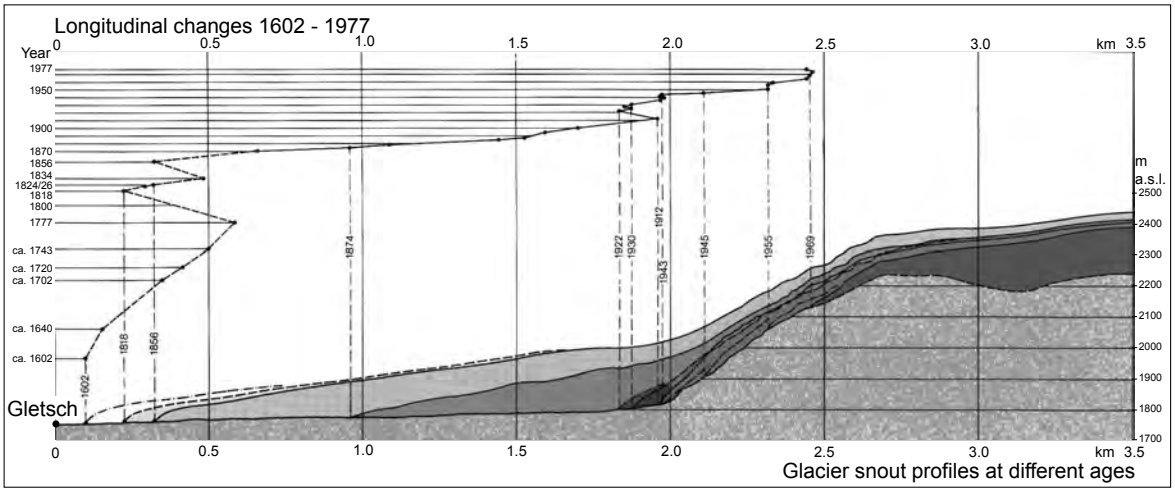

Fig. 7.2: Rhone glacier snout profiles at different ages and longitudinal changes 1602 - 1977 (modified after Aellen, 1979).

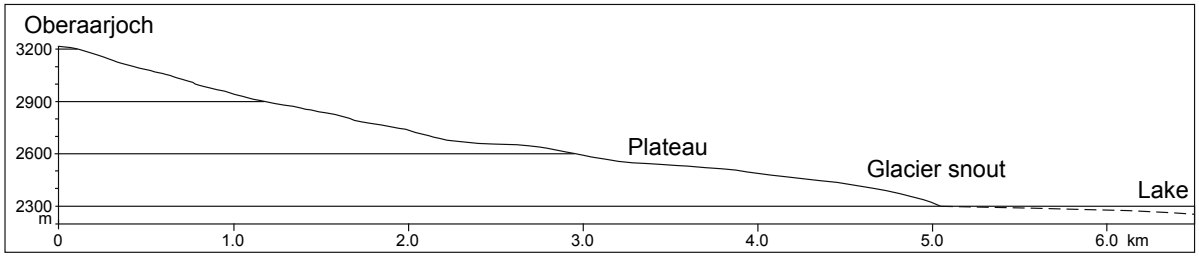

Fig. 7.3: Topographic profile through Oberaarglacier.

- The general hydrology of the basins (cf. Table 7.1A): The complexity of the catchment geometry and subglacial morphology plays a major role in defining zones of ice melting and meltwater routing to the bed. Both glaciers show a plateau-like, plane surface in their lower parts below the equilibrium line (Fig. 7.2 and 7.3, which shows Oberaar surface topography, the subglacial morphology is assumed to be simple). Above is a zone of crevasses which facilitate meltwater inflow during ablation season. Mean annual precipitation of the two glaciers is comparabele (2200 for Rhone and 2100 mm for Oberaar catchment). Due to the larger catchment size of Rhone the total precipitation volume is higher ($5.76 \cdot 10^7$ m^3) than Oberaar ($2.32 \cdot 10^7$ m^3). Rhone has a higher total discharge than Oberaar catchment, which results also in a higher runoff of 3080 compared to 2393 mm yr^{-1} (for Rhone and Oberaar, resp.). The higher Rhone runoff is due to higher glacier cover which leads to more ice melt: The ratio Oberaar/Rhone of glacier cover equals that of runoff. As a consequence the ratio of precipitation/discharge is lower for Rhone.

Keeping these factors in mind, our annual suspended sediment yields and erosion rates (Table 7.1B) compare well with published data compilations from e.g. Gurnell et al. (1996) as well as Hallet et al. (1996) as is visible from Table 7.2. The rather low annual yield for Rhone is probably due to the purely crystalline bedrock the Rhone glacier is lying on. However, also the Oberaar glacier which covers more readily erodable Variscan Gneisses does not show a significantly increased erosion rate compared to other Alpine glaciers (Table 7.2). Furthermore, in our calculation the bedload is neglected. But overall, bedrock type seems to be the factor controlling suspension load (or: mechanical

Parameters		**Oberaar**	**Rhone**	**OA/RH**
A: Hydrology				
Catchment area	km^{-2}	11.03	26.2	
Glacial cover	%	57	73	0.78
Discharge total	m^3 yr^{-1}	$2.64 \cdot 10^7$	$8.07 \cdot 10^7$	
Discharge yield	m^3 km^{-2} yr^{-1}	$2.39 \cdot 10^6$	$3.08 \cdot 10^6$	
Runoff	mm yr^{-1}	2393	3080	0.78
Mean annual precipitation	mm	2100	2200	
Precipitation volume	m^3 yr^{-1}	$2.32 \cdot 10^7$	$5.76 \cdot 10^7$	
Precipitation/discharge		0.88	0.71	
B: Mechanical erosion				
Suspended sediment total	t yr^{-1}	8527	12858	
Suspended sediment yield total	t km^{-2} yr^{-1}	773	491	
Suspended sediment yield glacierized	t km^{-2} yr^{-1}	1356	672	
Mechanical erosion rate total	mm yr^{-1}	0.29	0.18	
Mechanical erosion rate glacierized	mm yr^{-1}	0.50	0.25	
Dust input	kg km^{-2} yr^{-1}	5900	5900	

Table 7.1: Comparison of (A) hydrology and (B) mechanical erosion of the two catchments.

Glacier type	Mechanical erosion rate (mm yr^{-1})
Polar glaciers and thin plateau glaciers on crystalline bedrock	0.01
Temperate valley glaciers on crystalline bedrock in Norway	0.1
Scandinavian glaciers in general (from Bogen 1989)	0.1 - 0.5
Small temperate glaciers on different bedrock in the Swiss Alps (Bezinge 1987)	0.41 - 1.7
Large & fast moving temperate valley glaciers in tect. active range of SE Alaska	10 - 100

Table 7.2: Comparison of mechanical erosion rates from Hallet et al. (1996).

erosion) when catchments in similar physical erosion regime (glaciated) and climate (runoff) are compared.

Summary of proglacial weathering

In our work we confirm that in the proglacial area chemical weathering rates are increased. The increased chemical reactivities in the proglacial zone is due to the freshly ground subglacial material which is deposited in a chemically reactive environment. Rock-water contact times are high and there is abundant water supply from the glacierized environment. Sediments deposited in the proglacial area are furthermore highly permeable and show good drainage capacities. We observe, for instance, significantly higher weathering rates for biotite compared to existing biotite field weathering rates from the literature. The zone of increased biotite weathering coincides with the zone of high root density, which suggests that the weathering is biochemically accelerated by the network of roots and associated mocroorganisms of the initial vegetation cover. Soil development seems to play an important role, initially increasing the weathering rate. Over hundreds and thousands of years, however, a slow-down of the weathering processes is visible.

Recently in several publications the initial weathering of freshly ground material in the proglacial area was described: Anderson et al. (2000) observe a dominance of coupled sulphide oxidation/carbonate dissolution in solute acquisition in young proglacial sediments, and the significance of silicate dissolution increases as reactive minerals such as sulphides and carbonates become exhausted with increasing age of the proglacial deposits. Wadham et al. (2001) show that the annual proglacial chemical weathering rate in the catchment of a polythermal high-Arctic glacier exceeds the rate for the glaciated part of the catchment and confirms the proglacial zone as highly geochemically reactive. Brantley et al. (1998) observe increased nonstoichiometric element release during feldspar weathering and propose that this may be imporant for the huge amounts of glacial sediments deposited in front of glaciers.

Significance of our findings

The problematics of extrapolation

The logical continuation of projects like this one is to finally extrapolate on a bigger scale, from temperate valley glaciers to ice shields and Ice Ages, and to model the impact of glaciations on global element cycles (e.g. C-cycle, P-cycle…). Our data from temperate valley glaciers are comparable to many similar contributions, compiled in, e.g., Anderson et al. (1997) or Hodson et al. (2000). Extrapolating on a global or ice sheet scale (cf. high-latitude cold- or polythermal-based glaciers), however, rises several problems due to several differences between the different regimes:

- Due to their different thermal regime (cold/polythermal based) the subglacial drainage system of ice sheets is significantly different to temperate valley glaciers: In warm-based temperate valley glaciers significant amounts of meltwater flows to the bed, whereas even in polythermal parts of ice sheets meltwaters are often prevented in routing to the bed due to layers of cold englacial ice. Depending on the drainage system, meltwaters are routed either to the glacier margins, where rock-water interactions are weak due to the lower suspended sediment concentrations (compared to the subglacial environment), or, if they are routed to the glacier bed, they could be prevented from leaving the subglacial environment by cold ice near the glacier margins, and therefore could experience prolongated rock-water contact times.
- The influence of runoff on dissolved fluxes should not be neglected in an extrapolation from valley glaciers to an ice sheet scale. Temperate valley glaciers are discharge dominated: Precipitation dominates total runoff, but also ice melt makes up a significant part of it. In contrary, the total runoff of ice sheets is significantly lower, and with the runoff also the rates of solute transport is decreased.

- The common theory assumes that mechanical erosion processes like abrasion take place only underneath temperate-based glaciers and that landscapes are protected beneath cold-based glaciers, which are frozen to their bed (Benn and Evans, 1998). However, Atkins et al. (2002) describe and interpret the geological evidence of erosion and deposition exposed by the retreat of a cold-based glacier in the Allan Hills, Antarctica. The capability of cold-based glaciers to mechanically abrade their underlying surface and their potential influence as a sediment source should be taken into account in future extrapolation works.
- Lithology plays an important if not the dominant role. However, difficulties arise in relating the silicate weathering derived cations to specific runoff or to catchment area due to the difficulty in estimating the surface area underlain by silicate rocks, especially in big scale watersheds. The small sizes of catchments which are normally investigated in glacial chemical weathering studies are a clear advantage to address this problem. Furthermore, it is even easier if areas are chosen (like this work), which are quasi monolithical and whose bedrock composition is clearly known (mostly the case in the Swiss Alps, compared to, e.g., the Himalayan). However, the problem is important if extrapolation is performed from small valley glaciers on ice shield scale due to the higher number of different and varying lithologies. They might be less well known and therefore an average composition has to be estimated with a larger error.

Physical erosion vs. tectonics

Glacially induced processes are weathering-limited: Physical erosion processes play the major role in total denudation (glacial erosion processes like abrasion, producing very fine-grained material which is highly reactive). A control of chemical weathering by physical processes of erosion points to the high potential for a strong tectonical control on chemical weathering rates (e.g., Stallard and Edmond, 1983, Gaillardet et al., 1999, Riebe et al., 2001).

Comparing temperate and polythermal glacier regimes the factor tectonics (and with that relief) becomes extremely important: The existing data for temperate glacier catchments are mostly from areas which are tectonically active (e.g. Alps, Himalaya, Rocky Mountains). This enhances the total weathering rate: Increased physical erosion rates (glacially and tectonically increased, cf. high relief and uplift rates) increase the chemical weathering rates. Data from polythermal glacier regimes, however, are mainly collected in the Arctic on continental shield rocks (Svalbard, Greenland). These shield regions are tectonically inactive zones of the Earth surface. Furthermore, they show a much lower relief. A third set of data exists for icelandic glaciers whose bed geometries approaches the ones of shields. Iceland is not only tectonically active (e.g. subglacial melting due to geothermism, provoking Jökulhlaups; glacier outburst floods) but also consists of highly erodable lithologies (volcanic rocks, basalts), and is, furthermore, significantly influenced by high volumes of precipitation (extreme runoffs).

Conclusions

This thesis emphasizes the continental perspective of the long-term research program "continent-ocean interactions and their geological records" which was described initially (cf. Chapter 1). For a marine perspective the reader is referred to Tamburini (2001).

With our work we confirm the positive coupling of physical and chemical weathering: the coupling is intensified in environments whose weathering regimes are dominated by weathering-limited glacial processes. Global denudation is assumed to be weathering-limited during glaciations. Especially the combination of active tectonic processes with glacial processes has a high potential to increase physical erosion and subsequently chemical weathering. Zones (and periods) of mountain uplift may therefore play an important role on a global scale.

There are two domaines of weathering in glacial environments, the subglacial and proglacial zones:

- The subglacial domain is dominated by "short-term" weathering reactions driven by the dissolution of freshly ground fine particles in dilute glacial meltwaters. The most reactive mineral in this context is calcite.
- The strongly foliated gneissic zone running down the central third of the Oberaar catchment has a major impact on physical and chemical erosion rates measured compared to those of the the Rhone

catchment, which lies on granitic and granodioritic rocks: Approximately twice as much suspended sediment is exported by the Oberaar meltwaters compared to the Rhone meltwaters during the study period (1999-2001). This leads to 5 times more dissolved calcium being denuded from the Oberaar catchment, most of which comes from carbonate dissolution. Calcite weathering is more important in this glacial catchment than in non-glaciated catchments underlain by granitoid rocks.

- Disseminated calcite exert a major impact not only on the meltwater major ion composition but also on its Sr systematics. In purely granitic catchments the influence of nonstoichiometric Sr release from silicates may be visible as well.
- The silicate weathering rates we observe in our presently glaciated alpine catchments (and those which are published for other glaciated alpine and Antarctic catchments) fall within the range of temperate, non-glaciated granitoid catchments with the same runoff, implying that silicate weathering is not accelerated in the subglacial environment.
- "Long-term" weathering processes take place in the proglacial area where conditions associated with pedogenesis, such as increased acidity, increase the overall chemical weathering rates of, e.g., biotite and feldspar grains. Biotite weathers to form biotite-vermiculite mixed-layer clays and subsequently vermiculite after 140 years, and continues more slowly in YD profiles.
- Elevated weathering rates are due to a combination of the enrichment in small particles which are glacially abraded and the high water throughflow due to the high precipitation volumes at these alpine fieldsites. A slow-down of the weathering processes is visible comparing weathering rates calculated over hundreds and thousands of years.
- During deglaciation, the widespread exposure of reactive proglacial sediment and the rapid dissolution of associated detrital phosphorus may over 100 – 1000 years increase bioavailable phosphorus supply to both terrestrial and aquatic ecosystems. Dissolution of detrital phosphorus is accelerated in the proglacial area compared to the global mean.
- Phosphorus is transported in different forms with different bioavailabilities in the tropical Apure, the glacial Oberaar and Rhone, and the proglacial Rhone tributary catchments. The tropical waters generally contain more conditionally bioavailable forms of phosphorus (dissolved organic, ironbound, and organic phosphorus), while runoff from glaciated catchments is dominated by scarcely bioavailable detrital phosphorus. However, glacial processes play an important regenerative role in bringing large volumes of freshly ground detrital phosphorus to the biosphere.

Outlook

Summarizing, the global impact of *subglacial* versus *proglacial* weathering is not fully clear yet, there is still a need for more data to address the different problems outlined above. Our data seems to indicate that there is no *direct* impact of *subglacial* chemical weathering on global silicate weathering rates. But the present data situation implies, that there is certainly a significant potential for the *indirect* impact on global chemical weathering via the readily weatherable glacially derived material deposited in the *proglacial* area. The knowledge of processes in proglacial areas is important to understand in more detail what happens between the glacier snout and the ocean, especially with regard to biolimiting nutrient fluxes like those of phophorus. For our work this would mean to investigate (possible) weathering processes taking place along the Rhone river between Gletsch and Marseille and along the Aare river between the Grimsel Hospiz and Rotterdam. Nowadays this would be extremely difficult due to the high pollution of these rivers, as they drain densely populated, industrialised, and cultivated areas (human activities can easily dominate the major element chemistry of such rivers). Less populated areas and catchments could help to go round such uncertainties; for example, Millot et al. (2002) investigated silicate weathering rates and their coupling with physical erosion on the Canadian Shield.

Especially the *proglacial* weathering regime needs further investigation, not only to trace and understand more clearly the weathering processes and their potential impact on the global CO_2 cycle, but to be able to predict a reasonable time scale during which chemical weathering is increased. It is also important to compare glaciated and non-glaciated areas.

There are many questions remaining:

- How long is a catchments weathering flux "affected" by a former glaciation?

On a global scale this would mean:

- How was the distribution of proglacial area during Ice Ages?
- Is their total area significant during a glaciation?
- By how much is this area increased upon glacier retreat?

Proglacial environments have undergone significant variations in their spatial distribution over the Quaternary due to the advance and retreat of glaciers and ice sheets (Gibbs and Kump, 1994).

- What could be the impact of the drastically increased runoff due to the melting of ice masses?
- Do formerly cold-based regimes change to temperate conditions as the ice masses decay?
- How important is ice sublimation during the retreat of ice shields?
- Could recent calculations of global weathering fluxes to the ocean still be positively influenced by the glacial material from former glaciations, which is still being weathered at an increased rate?

References

Aellen, M., 1979. Neuzeitliche Gletscherschwankungen. In: Schweizerische Verkehrszentrale Zürich (Editor), Die Schweiz und ihre Gletscher. Von der Eiszeit bis zur Gegenwart. Kümmerly + Frey, Bern, Switzerland, pp. 70-89.

Anderson, S.P., Drever, J.I., Frost, C.D. and Holden, P., 2000. Chemical weathering in the foreland of a retreating glacier. Geochimica et Cosmochimica Acta, 64(7): 1173-1189.

Anderson, S.P., Drever, J.I. and Humphrey, N.F., 1997. Chemical weathering in glacial environments. Geology, 25(5): 399-402.

Atkins, C.B., Barrett, P.J. and Hicock, S.R., 2002. Cold glaciers erode and deposit: Evidence from Allan Hills, Antarctica. Geology, 30(7): 659-662.

Benn, D.I. and Evans, D.J.A., 1998. Glaciers and glaciation. Arnold Publishers, London, 734 pp.

Brantley, S.L., Chesley, J.T. and Stillings, L.L., 1998. Isotopic ratios and release rates of strontium measured from weathering feldspars. Geochimica et Cosmochimica Acta, 62(9): 1493-1500.

Gaillardet, J., Dupré, B., Louvat, P. and Allègre, C.J., 1999. Global silicate weathering and CO2 consumption rates deduced from the chemistry of large rivers. Chemical Geology, 159: 3-30.

Gibbs, M.T. and Kump, L.R., 1994. Global chemical erosion during the Last Glacial Maximum and the present: sensitivity to changes in lithology and hydrology. Paleoceanography, 9(4): 529-543.

Gurnell, A.M., Hannah, D. and Lawler, D., 1996. Suspended sediment yield from glacier basins. International Association of Hydrological Sciences Publication, 236: 97-104.

Hallet, B., Hunter, L. and Bogen, J., 1996. Rates of erosion and sediment evacuation by glaciers: A review of field data and their iplications. Global and Planetary Change, 12: 213-235.

Hodson, A.J., Tranter, M. and Vatne, G., 2000. Contemporary rates of chemical denudation and atmospheric CO2 sequestration in glacier basins: an arctic perspective. Earth Surface Processes and Landforms, 25: 1447-1471.

Holland, D.H., 1978. The Chemistry of the Atmosphere and the Oceans. Wiley-Interscience, New York, 351 pp.

Koppes, M.N. and Hallet, B., 2002. Influence of rapid glacial retreat on the rate of erosion by tidewater glaciers. Geology, 30(1): 47-50.

Millot, R., Gaillardet, J., Dupré, B. and Allègre, C.J., 2002. The global control of silicate weathering rates and the coupling with physical erosion: New insights from rivers of the Canadian Shield. Earth and Planetary Science Letters, 196: 83-98.

Nezat, C.A., Lyons, W.B. and Welch, K.A., 2001. Chemical weathering in streams of a polar desert (Taylor Valley, Antarctica). Geological Society of America Bulletin, 113(11): 1401-1408.

Riebe, C.S., Kirchner, J.W., Granger, D.E. and Finkel, R.C., 2001. Strong tectonic and weak climatic control of long-term chemical weathering rates. Geology, 29(6): 511-514.

Stallard, R.F. and Edmond, J.M., 1983. Geochemistry of the Amazon 2. The influence of geology and weathering environment on the dissolved load. Journal of Geophysical Research, 88: 9671-9688.

Tamburini, F., 2001. Phosphorus in marine sediments during the last 150,000 years: exploring relationships between continental weathering, productivity, and climate. PhD thesis, University of Neuchatel,

Switzerland, CD ROM.

Wadham, J.L., Cooper, R.J., Tranter, M., and Hodgkins, R., 2001. Enhancement of glacial solute fluxes in the proglacial zone of a polythermal glacier. Journal of Glaciology, 47(158): 378-386.

White, A.F. and Blum, A., 1995. Effects of climate on chemical weathering in watersheds. Geochimica et Cosmochimica Acta, 59(9): 1729-1747.

APPENDIX A.1
OBERAAR

APPENDIX A.1: Oberaar data

Ca concentrations from Oberaar glacier ablation season 1999-2000 (mg l^{-1}).

Month		**July**			**August**		**September**			**October**		**May**		**June**			**July**			**August**		**September**			**October**	
Day nr.	10	17	**daily**	10	17	**daily**	10	17	**daily**	10	**daily**		10	17	**daily**	10	17	**daily**	10	17	**daily**	10	17	**daily**	10	**daily**
1							4.72	3.05	3.89													4.39	3.55	3.97		
2																									5.65	5.65
3				3.94	3.10	3.52										3.78	3.93	3.86								
4										7.16	7.16					3.56										
5				3.44	3.10	3.27										4.06	3.05	3.55								
6		3.21	3.21													3.95				3.88	4.93					
7	4.12	4.72	4.42																5.97							
8	5.27	4.82	5.05										4.77	4.12	4.45											
9				3.05	3.17	3.11																6.68	2.38	4.53		
10							4.73	3.18	3.96			3.58				4.58	3.41	4.00								
11	4.93	4.39	4.66													5.57	5.36	5.47								
12	4.03	3.95	3.99	5.02	4.39	4.71										6.48										
13													3.62	3.31	3.47	6.95										
14													3.58	3.69	3.63											
15	4.10	3.29	3.70				4.92	3.63	4.28				3.62	3.44	3.53											
16				3.79	3.18	3.49						5.16													6.03	6.03
17																7.37	5.90	6.63								
18	3.85	3.87	3.86													8.17	4.78	6.48					3.31			
19				3.70	3.32	3.51							3.95	3.32	3.63	6.12	3.45	4.78	3.48	3.39	3.44	0.46				
20	3.92	3.65	3.79										3.59	3.09	3.34	5.92	3.47	4.69					3.62			
21													3.43	2.66	3.05								5.74			
22	3.93	3.67	3.80										3.72	3.55	3.64											
23							6.21	4.90	5.56																	
24																			4.73	0.70	2.72					
25				3.27	3.12	3.20																				
26	3.89	2.94	3.42										5.50	3.39	4.45	3.54										
27													4.60		4.60											
28													3.15	2.71	2.93											
29	4.03	3.26	3.65										4.13	2.98	3.56											
30							4.55	4.65	4.60																	

Ca concentrations from Oberaar glacier accumulation seasons 1999-2001 (mg l^{-1}).

Date	mg l^{-1}
11-Nov-99	9.15
13-Jan-00	12.17
12-Mar-00	12.38
25-Apr-00	9.00
5-Dec-00	10.98
18-Jan-01	12.56
6-Mar-01	13.48
1-May-01	10.42

Mean daily Ca concentrations

Month	n	mg l^{-1}	StDev.
January	2	12.4	
Febuary	0		
March	2	12.9	
April	1	9.00	
May	3	6.39	3.58
June	12	3.69	0.54
July	19	4.37	0.97
August	10	3.59	0.69
September	7	4.40	0.59
October	3	6.28	0.79
November	1	9.15	
December	1	10.98	

Seasonal averages

Season	Ablation 10:00 h	Ablation 17:00 h	Accumulation
Average	4.56	3.79	11.39
St.dev.	1.31	1.23	1.74
n	58	58	7

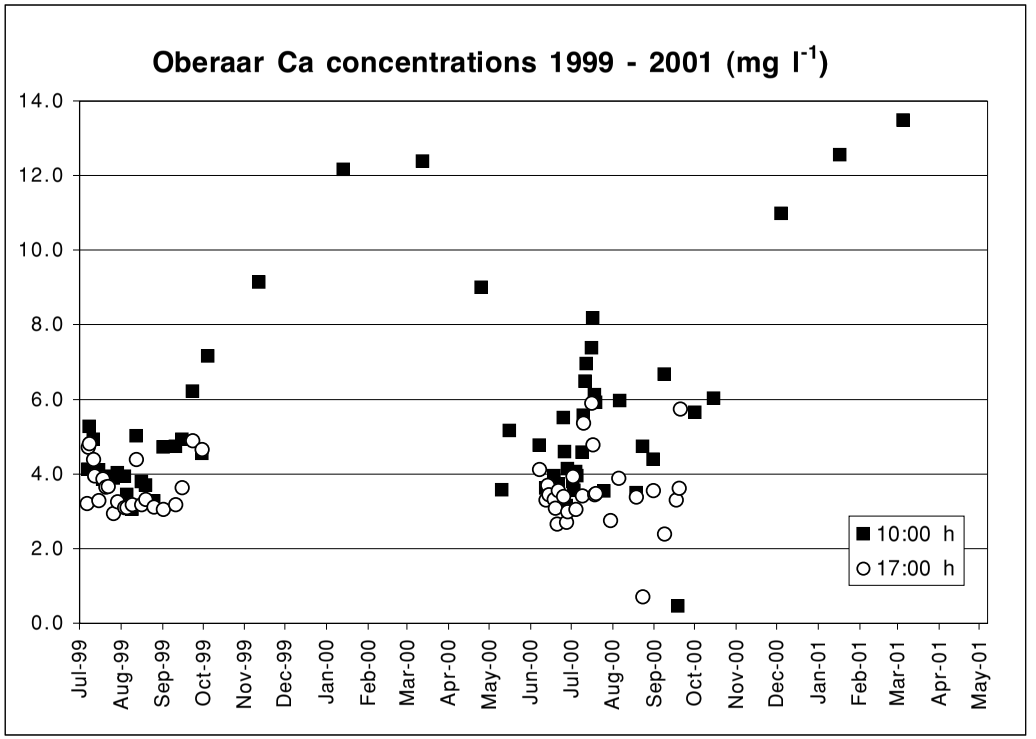

Mg concentrations from Oberaar glacier ablation season 1999-2000 (mg l^{-1}).

Month		**July**			**August**		**September**			**October**		**May**		**June**			**July**			**August**		**September**			**October**	
Day nr.	10	17	**daily**	10	17	**daily**	10	17	**daily**	10	**daily**		10	17	**daily**	10	17	**daily**	10	17	**daily**	10	17	**daily**	10	**daily**
1							0.17	0.11	0.14													0.27	0.11	0.19		
2																									0.19	0.19
3				0.14	0.11	0.13										0.14	0.16	0.15								
4										0.30	0.30					0.14										
5				0.12	0.10	0.11										0.16	0.12	0.14								
6		0.10	0.10													0.15		0.15								
7	0.18	0.18	0.18																0.21							
8	0.22	0.17	0.20										0.16	0.17	0.16											
9				0.11	0.11	0.11																	0.09	0.09		
10							0.18	0.11	0.15			0.16				0.17	0.15	0.16								
11	0.20	0.17	0.19													0.22	0.21	0.21								
12	0.19	0.17	0.18	0.20	0.17	0.19										0.24										
13													0.16	0.14	0.15	0.21										
14													0.15	0.15	0.15											
15	0.15	0.11	0.13				0.19	0.13	0.16				0.10	0.13	0.12											
16				0.15	0.12	0.14						0.23													0.22	0.22
17																0.30	0.24	0.27								
18	0.16	0.16	0.16													0.29	0.17	0.23					0.12			
19				0.15	0.13	0.14							0.14	0.15	0.15	0.25	0.15	0.20	0.14	0.17	0.15	0.27				
20	0.15	0.14	0.15										0.10	0.08	0.09	0.25	0.15	0.20					0.14			
21													0.17	0.10	0.14								0.22			
22	0.15	0.14	0.15										0.11	0.10	0.10											
23							0.23	0.21	0.22																	
24																			0.17	0.10	0.13					
25				0.12	0.11	0.12																				
26	0.16	0.11	0.14										0.19	0.13	0.16	0.16										
27													0.19													
28													0.08	0.11	0.10											
29	0.14	0.12	0.13										0.18	0.11	0.15											
30							0.16	0.18	0.17																	
31																	0.11									
m			**0.15**			**0.13**			**0.17**		**0.30**	**0.20**			**0.13**			**0.19**			**0.14**			**0.14**		**0.21**

Mg concentrations from Oberaar glacier accumulation seasons 1999-2001 (mg l^{-1}).

Date	mg l^{-1}
11-Nov-99	0.38
13-Jan-00	0.42
12-Mar-00	0.43
25-Apr-00	0.33
5-Dec-00	0.41
18-Jan-01	0.47
6-Mar-01	0.54
1-May-01	0.42

Mean daily Mg concentrations

Month	n	mg l^{-1}	StDev.
January	2	0.45	
Febuary	0		
March	2	0.49	
April	1	0.33	
May	3	0.27	0.13
June	11	0.13	0.03
July	20	0.17	0.04
August	9	0.13	0.02
September	7	0.16	0.04
October	3	0.24	0.06
November	1	0.38	
December	1	0.41	

Seasonal averages

Season	Ablation 10:00 h	Ablation 17:00 h	Accumulation
Average	0.18	0.20	0.43
St.dev.	0.05	0.39	0.07
n	57	55	7

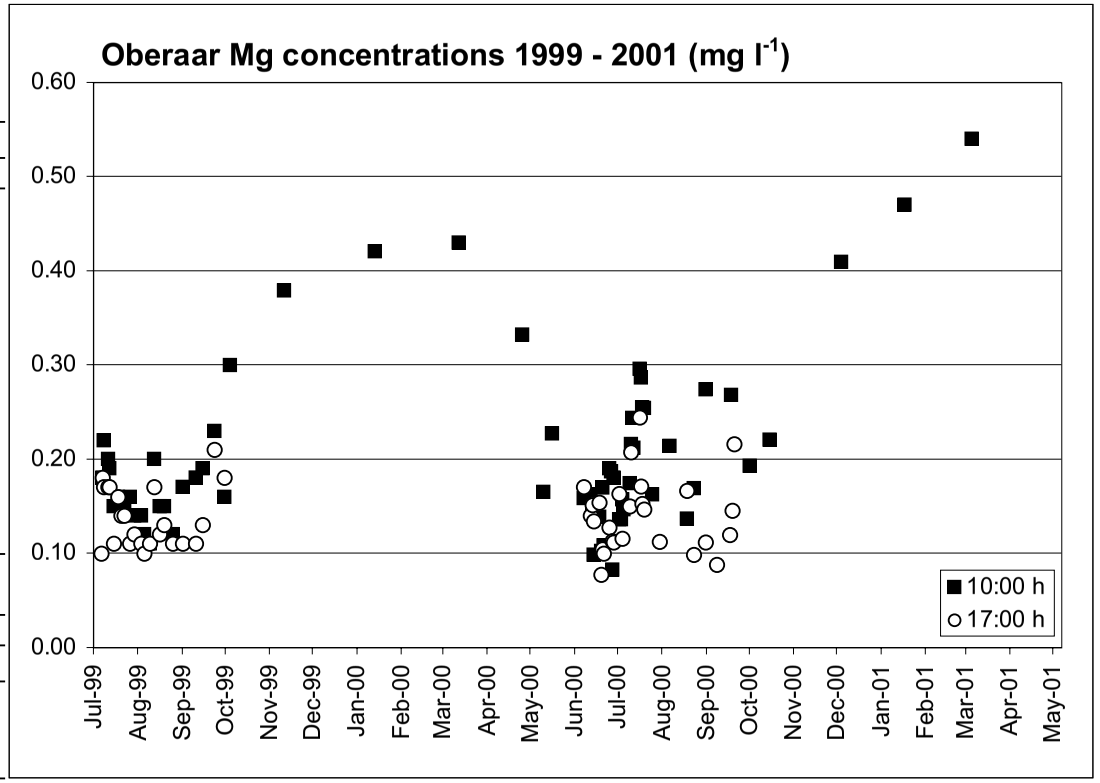

Na concentrations from Oberaar glacier ablation season 1999-2000 (mg l^{-1}).

Month		**July**			**August**		**September**			**October**		**May**		**June**			**July**			**August**		**September**			**October**	
Day nr.	10	17	**daily**	10	17	**daily**	10	17	**daily**	10	**daily**		10	17	**daily**	10	17	**daily**	10	17	**daily**	10	17	**daily**	10	**daily**
1							0.22	0.12	0.17													0.24	0.18	0.21		
2																									0.39	0.39
3				0.17	0.15	0.16										0.19	0.21	0.20								
4										0.40	0.40					0.23										
5				0.15	0.14	0.15										0.21	0.14	0.17								
6		0.31	0.31													0.20		0.20		0.23	0.26					
7	0.28	0.20	0.24																0.28							
8	0.29	0.40	0.35										0.24	0.25	0.24											
9				0.15	0.13	0.14																0.02	0.13	0.07		
10							0.24	0.15	0.20			0.37				0.24	0.21	0.23								
11	0.36	0.38	0.37													0.29	0.29	0.29								
12	0.33	0.23	0.28	0.23	0.20	0.22										0.35										
13													0.22	0.27	0.24	0.36										
14													0.22	0.22	0.22											
15	0.06	0.11	0.09				0.22	0.17	0.20				0.19	0.19	0.19											
16				0.20	0.17	0.19						0.37													0.37	0.37
17																0.40	0.34	0.37								
18	0.19	0.19	0.19													0.53	0.39	0.46					0.16			
19				0.18	0.16	0.17							0.24	0.20	0.22	0.34	0.19	0.26	0.15	0.15	0.15	0.04				
20	0.17	0.17	0.17										0.20	0.16	0.18	0.34	0.18	0.26					0.22			
21													0.20	0.17	0.19								0.27			
22	0.18	0.17	0.18										0.18	0.17	0.18											
23							0.36	0.27	0.32																	
24																			0.20	0.06	0.13					
25				0.13	0.12	0.13																				
26	0.32	0.14	0.23										0.40	0.17	0.28	0.18										
27													0.23													
28													0.15	0.17	0.16											
29	0.17	0.16	0.17										0.24	0.14	0.19											
30							0.29	0.24	0.27																	
31																	0.15									
m			**0.23**			**0.16**			**0.23**		**0.40**	**0.37**			**0.21**			**0.27**			**0.18**			**0.14**		**0.38**

Na concentrations from Oberaar glacier accumulation seasons 1999-2001 (mg l^{-1}).

Date	mg l^{-1}
11-Nov-99	0.72
13-Jan-00	0.93
12-Mar-00	1.06
25-Apr-00	0.77
5-Dec-00	0.78
18-Jan-01	1.03
6-Mar-01	1.10
1-May-01	1.02

Mean daily Na concentrations

Month	n	mg l^{-1}	StDev.
January	2	0.98	
Febuary	0		
March	2	1.08	
April	1	0.33	
May	3	0.59	0.38
June	11	0.21	0.04
July	20	0.25	0.09
August	10	0.17	0.04
September	7	0.20	0.08
October	3	0.39	0.01
November	1	0.38	
December	1	0.41	

Seasonal averages

Season	Ablation 10:00 h	Ablation 17:00 h	Accumulation
Average	0.25	0.26	0.91
St.dev.	0.10	0.38	0.16
n	58	56	7

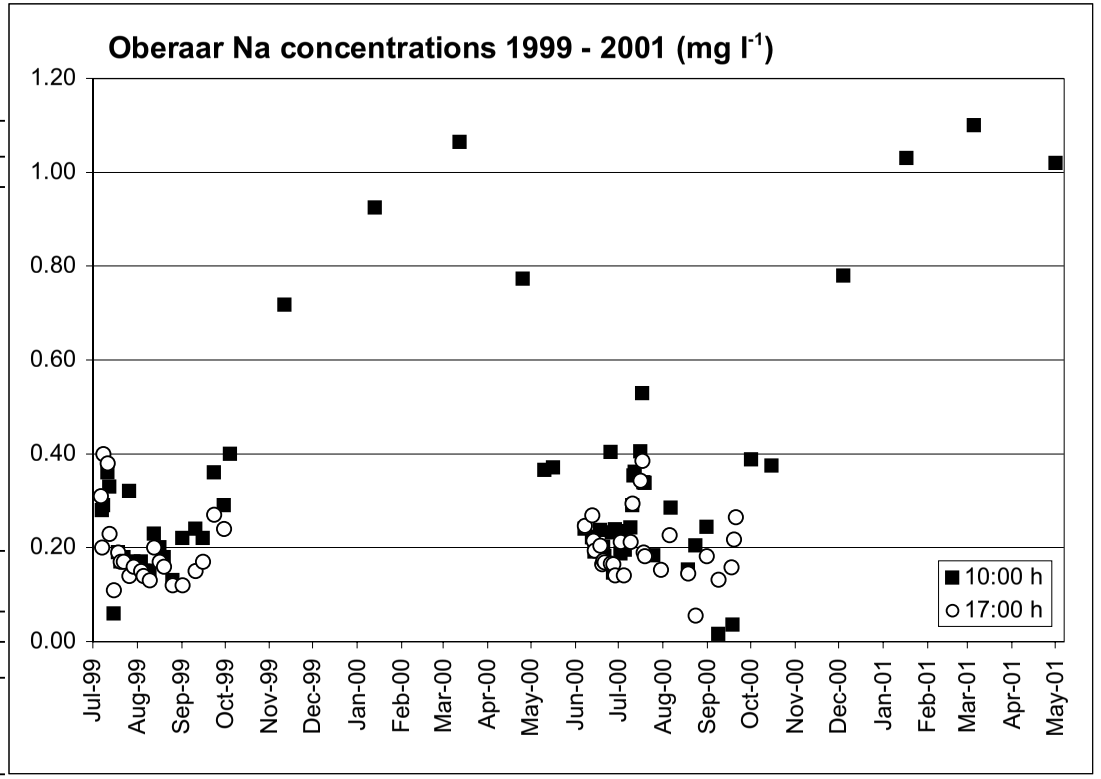

K concentrations from Oberaar glacier ablation season 1999-2000 (mg l^{-1}).

Month		**July**			**August**			**September**			**October**		**May**		**June**			**July**			**August**			**September**			**October**	
Day nr.	10	17	**daily**	10	17	**daily**	10	17	**daily**	10	**daily**		10	17	**daily**	10	17	**daily**	10	17	**daily**	10	17	**daily**	10	**daily**
1							0.90	0.59	0.75													0.88	0.67	0.78		
2																									1.23	1.23
3				0.71	0.57	0.64										0.68	0.68	0.68								
4										1.41	1.41					0.66										
5				0.64	0.59	0.62										0.70	0.53	0.62								
6		0.64	0.64													0.69		0.69		0.78	0.93					
7	0.79	0.85	0.82																1.08							
8	0.94	1.01	0.98										0.81	0.71	0.76											
9				0.56	0.55	0.56																1.49	0.61	1.05		
10							0.91	0.58	0.75			0.89				0.86	0.72	0.79								
11	0.90	0.90	0.90													1.06	1.04	1.05								
12	0.76	0.72	0.74	0.92	0.81	0.87										1.25										
13													0.64	0.63	0.63	1.30										
14													0.66	0.64	0.65											
15	0.75	0.68	0.72				0.91	0.69	0.80				0.63	0.59	0.61											
16				0.74	0.61	0.68						1.16													1.28	1.28
17																1.43	1.26	1.34								
18	0.71	0.68	0.70													1.37	0.92	1.14					0.66			
19				0.72	0.63	0.68							0.78	0.61	0.70	1.25	0.78	1.01	0.60	0.55	0.58	0.15				
20	0.69	0.64	0.67										0.66	0.58	0.62	1.24	0.74	0.99					0.75			
21													0.59	0.52	0.55								1.13			
22	0.69	0.64	0.67										0.64	0.59	0.61											
23							1.36	1.03	1.20																	
24																			0.83	0.22	0.52					
25				0.57	0.52	0.55																				
26	0.84	0.56	0.70										0.90	0.66	0.78	0.62										
27													0.86													
28													0.57	0.56	0.57											
29	0.68	0.58	0.63										0.80	0.60	0.70											
30							0.97	0.96	0.97																	
31																	0.58									
m			**0.74**			**0.65**			**0.89**		**1.41**	**1.02**			**0.65**			**0.92**			**0.68**			**0.91**		**1.26**

K concentrations from Oberaar glacier accumulation seasons 1999-2001 (mg l^{-1}).

Date	mg l^{-1}
11-Nov-99	2.14
13-Jan-00	2.46
12-Mar-00	2.23
25-Apr-00	1.73
5-Dec-00	2.38
18-Jan-01	2.55
6-Mar-01	2.59
1-May-01	2.03

Mean daily K concentrations

Month	n	mg l^{-1}	StDev.
January	2	2.51	
Febuary	0		
March	2	2.41	
April	1	1.73	
May	3	1.36	0.60
June	11	0.65	0.07
July	20	0.82	0.20
August	10	0.66	0.14
September	7	0.90	0.18
October	3	1.31	0.09
November	1	2.14	
December	1	2.38	

Seasonal averages

Season	Ablation 10:00 h	Ablation 17:00 h	Accumulation
Average	0.87	0.76	2.30
St.dev.	0.27	0.39	0.30
n	58	56	7

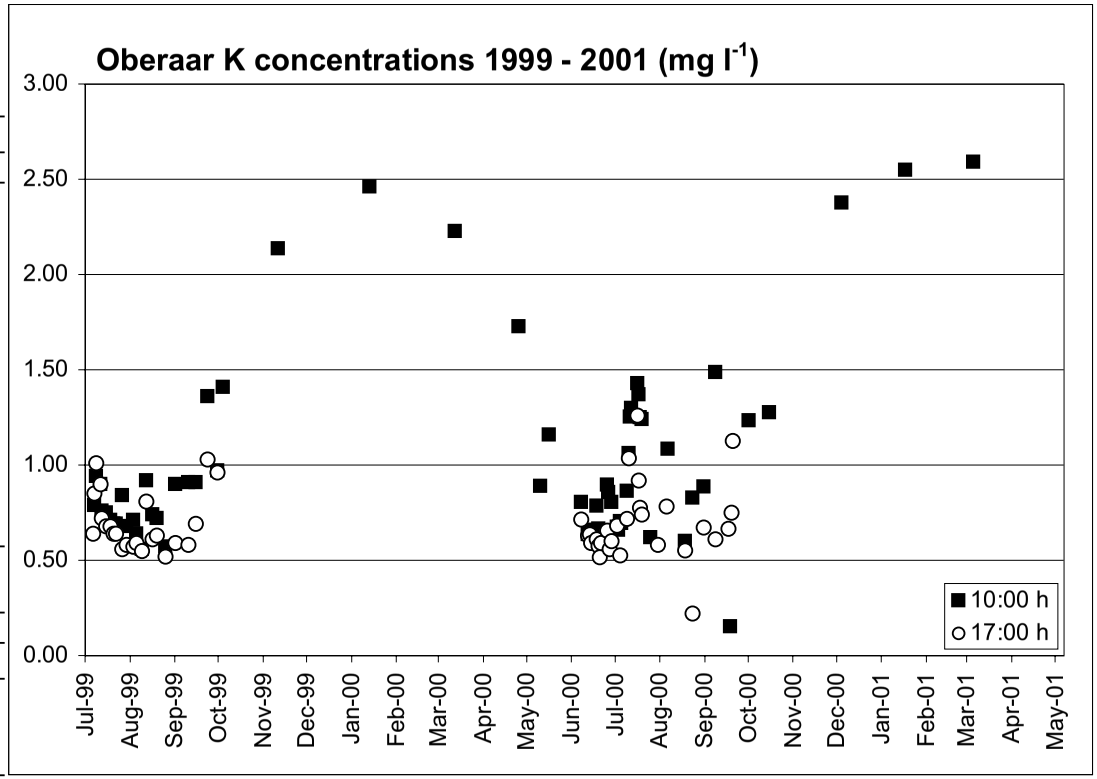

Cl concentrations from Oberaar glacier ablation season 1999-2000 (mg l^{-1}).

Month		**July**			**August**		**September**			**October**		**May**		**June**			**July**			**August**		**September**			**October**	
Day nr.	10	17	**daily**	10	17	**daily**	10	17	**daily**	10	**daily**		10	17	**daily**	10	17	**daily**	10	17	**daily**	10	17	**daily**	10	**daily**
1							0.07	0.08	0.08													0.04	0.02	0.03	0.11	0.11
2																										
3				0.04	0.06	0.05										0.08	0.15	0.12								
4										0.08	0.08					0.22		0.11								
5				0.65	0.04	0.35										0.09	0.07	0.08								
6		0.07	0.07													0.06		0.06		0.08	0.07					
7	0.07	0.07	0.07																0.06							
8	0.09	0.07	0.08										0.08	0.08	0.08											
9				0.04	0.05	0.05																0.05	0.05	0.05		
10							0.07	0.04	0.06			0.15				0.10	0.06	0.08								
11	0.06	0.11	0.09													0.09	0.08	0.09								
12	0.07	0.06	0.07	0.05	0.05	0.05										0.10		0.10								
13													0.07	0.08	0.08	0.08		0.08								
14													0.10	0.10	0.10											
15	0.09	0.07	0.08				0.04	0.04	0.04				0.10	0.08	0.09										0.14	0.14
16				0.03	0.03	0.03																				
17												0.09				0.09	0.07	0.08								
18	0.07	0.10	0.09													0.04	0.05	0.05					0.04	0.10		
19				0.02	0.03	0.03							0.08	0.06	0.07	0.07	0.04	0.06	0.04	0.03	0.04	0.15				
20	0.07	0.13	0.10										0.08	0.05	0.07	0.09	0.04	0.07					0.12	0.12		
21													0.06	0.08	0.07								0.08	0.08		
22	0.05	0.03	0.04										0.06	0.05	0.06											
23							0.07	0.05	0.06																	
24																			0.06	0.07	0.07					
25				0.07	0.04	0.06																				
26	0.31	0.09	0.20										0.08	0.06	0.07	0.07	0.08	0.08								
27													0.06	0.04	0.05											
28													0.05	0.06	0.06											
29	0.07	0.06	0.07										0.07	0.05	0.06											
30							0.05	0.06	0.06																	
31																0.08	0.04	0.06								
m			**0.09**			**0.09**			**0.06**		**0.08**	**0.12**			**0.07**			**0.08**			**0.06**			**0.08**		**0.13**

Cl concentrations from Oberaar glacier accumulation seasons 1999-2001 (mg l^{-1}).

Date	mg l^{-1}
11-Nov-99	0.08
13-Jan-00	0.07
12-Mar-00	0.10
25-Apr-00	0.20
5-Dec-00	0.11
18-Jan-01	0.12
6-Mar-01	0.11
1-May-01	0.11

Mean daily Cl concentrations

Month	n	mg l^{-1}	StDev.
January	2	0.1	
Febuary	0		
March	2	0.1	
April	1	0.20	
May	3	0.12	0.03
June	12	0.07	0.01
July	25	0.08	0.03
August	10	0.08	0.10
September	10	0.07	0.03
October	3	0.11	0.03
November	1	0.08	
December	1	0.11	

Seasonal averages

Season	Ablation 10:00 h	Ablation 17:00 h	Accumulation
Average	0.09	0.11	0.11
St.dev.	0.09	0.38	0.04
n	59	59	7

NO_3 concentrations from Oberaar glacier ablation season 1999-2000 (mg l^{-1}).

Month		**July**			**August**			**September**			**October**		**May**		**June**			**July**			**August**			**September**			**October**	
Day nr.	10	17	**daily**	10	17	**daily**	10	17	**daily**	10	**daily**		10	17	**daily**	10	17	**daily**	10	17	**daily**	10	17	**daily**	10	**daily**
1							0.40	0.21	0.31													0.41	0.26	0.34	0.63	0.63
2																										
3				0.45	0.33	0.39										0.80	0.72	0.76								
4										1.01	1.01					0.89		0.89								
5				0.41	0.28	0.35										0.59	0.59	0.59								
6		0.74	0.74													0.49		0.49		0.36	0.56					
7	0.93	0.98	0.96																0.76							
8	1.10	1.00	1.05										1.09	0.85	0.97											
9				0.31	0.30	0.31																0.54	0.11	0.33		
10							0.30	0.18	0.24			1.38				0.78	0.81	0.80								
11	0.85	0.79	0.82													0.81	0.82	0.82								
12	0.75	0.71	0.73	0.51	0.47	0.49										0.59		0.59								
13													0.88	0.68	0.78	0.85		0.85								
14													0.88	0.84	0.86											
15	0.72	0.58	0.65				0.34	0.25	0.30				0.77	0.75	0.76										0.71	0.71
16				0.38	0.36	0.37																				
17												0.79				0.90	0.73	0.82								
18	0.60	0.58	0.59													0.26	0.50	0.38					0.28	0.41		
19				0.37	0.42	0.40							0.73	0.56	0.65	0.74	0.39	0.57	0.36	0.30	0.33	0.53				
20	0.59	0.53	0.56										0.63	0.39	0.51	0.77	0.37	0.57					0.64	0.64		
21													0.60	0.41	0.51								0.74	0.74		
22	0.53	0.48	0.51										0.61	0.54	0.58											
23							0.47	0.42	0.45																	
24																			0.59	0.64	0.62					
25				0.36	0.30	0.33																				
26	0.52	0.36	0.44										0.73	0.51	0.62	0.69	0.92	0.81								
27													0.67	0.42	0.55											
28													0.50	0.45	0.48											
29	0.61	0.48	0.55										0.64	0.44	0.54											
30							0.38	0.57	0.48																	
31																0.93	0.35	0.64								
m			**0.69**			**0.38**			**0.35**		**1.01**	**1.09**			**0.65**			**0.68**			**0.50**			**0.49**		**0.67**

NO_3 concentrations from Oberaar glacier accumulation seasons 1999-2001 (mg l^{-1}).

Date	mg l^{-1}
11-Nov-99	0.87
13-Jan-00	0.41
12-Mar-00	0.86
25-Apr-00	1.52
5-Dec-00	0.93
18-Jan-01	0.90
6-Mar-01	0.59
1-May-01	1.11

Mean daily NO_3 concentrations

Month	n	mg l^{-1}	StDev.
January	2	0.7	
Febuary	0		
March	2	0.7	
April	1	1.52	
May	3	1.09	0.30
June	12	0.65	0.16
July	25	0.69	0.17
August	10	0.41	0.11
September	10	0.42	0.16
October	3	0.78	0.20
November	1	0.87	
December	1	0.93	

Seasonal averages

Season	Ablation 10:00 h	Ablation 17:00 h	Accumulation
Average	0.65	0.56	0.87
St.dev.	0.23	0.41	0.35
n	59	60	7

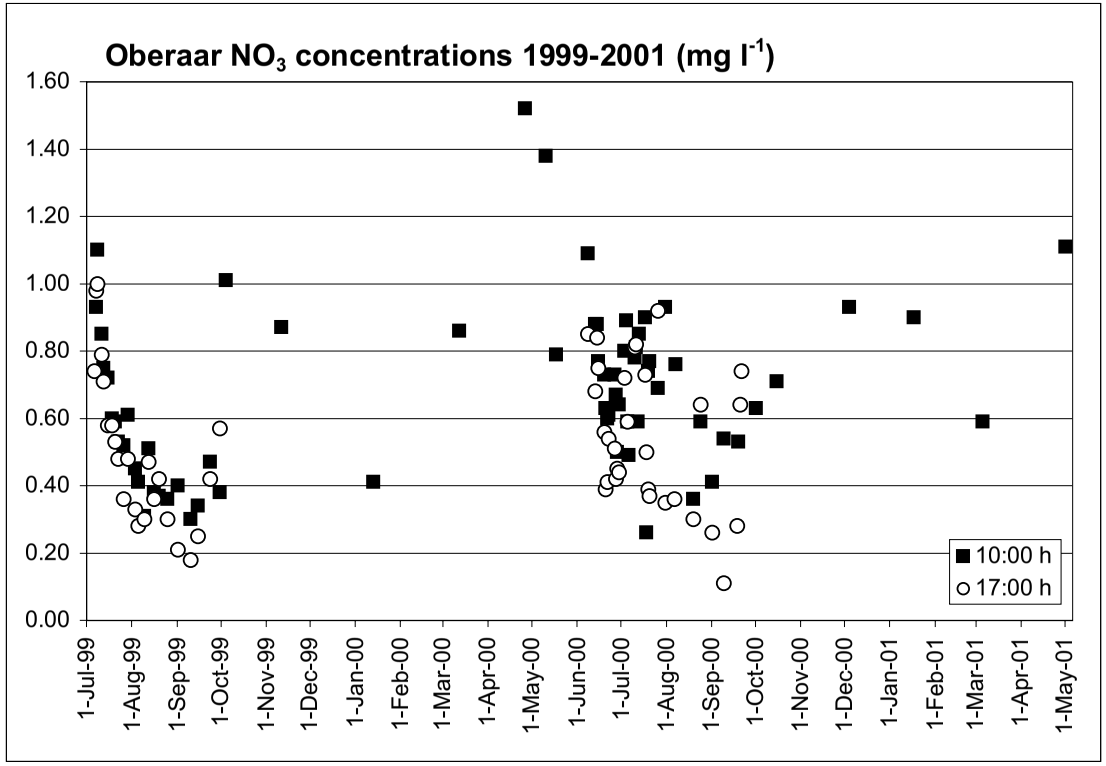

SO_4 concentrations from Oberaar glacier ablation season 1999-2000 (mg l^{-1}).

Month		**July**			**August**			**September**			**October**		**May**		**June**			**July**			**August**			**September**			**October**	
Day nr.	10	17	**daily**	10	17	**daily**	10	17	**daily**	10	**daily**		10	17	**daily**	10	17	**daily**	10	17	**daily**	10	17	**daily**	10	**daily**
1							4.66	2.42	3.54													3.72	2.50	3.11	5.23	5.23
2																										
3				3.87	2.81	3.34										5.87	2.66	4.27								
4										8.00	8.00					2.73		2.73								
5				3.32	2.40	2.86										3.11	3.27	3.19								
6		2.78	2.78													2.12		2.12		2.40	4.13					
7	3.86	4.87	4.37																5.85							
8	5.80	5.32	5.56										4.18	3.20	3.69											
9				2.81	2.66	2.74																7.31	1.18	4.25		
10							4.55	2.10	3.33			1.32				3.47	0.28	1.88								
11	5.90	5.30	5.60													0.79	0.61	0.70								
12	4.40	4.29	4.35	5.02	4.27	4.65										0.53		0.53								
13													3.24	2.44	2.84	7.67		7.67								
14													3.38	3.32	3.35											
15	4.36	3.42	3.89				4.62	3.24	3.93				3.04	3.06	3.05										3.05	3.05
16				3.49	2.43	2.96																				
17												3.92				8.70	6.84	7.77								
18	4.30	4.29	4.30													2.19	4.22	3.21					2.24	3.33		
19				3.31	3.03	3.17							3.92	2.63	3.28	6.82	3.19	5.01	2.70	2.28	2.49	4.41				
20	4.15	3.61	3.88										3.25	1.78	2.52	6.62	3.15	4.89					2.83	2.83		
21													2.90	1.91	2.41								5.63	5.63		
22	4.03	3.68	3.86										3.25	2.78	3.02											
23							6.30	4.86	5.58																	
24																			5.31	0.60	2.96					
25				2.71	2.21	2.46																				
26	3.85	2.59	3.22										4.78	2.87	3.83	0.40	0.79	0.60								
27													4.49	2.47	3.48											
28													2.63	1.89	2.26											
29	3.73	2.95	3.34										3.74	2.30	3.02											
30							3.13	3.67	3.40																	
31																0.77	0.30	0.54								
m			**4.10**			**3.17**			**3.96**		**8.00**	**2.62**			**3.06**			**3.22**			**3.19**			**3.83**		**4.14**

SO_4 concentrations from Oberaar glacier accumulation seasons 1999-2001 (mg l^{-1}).

Date	mg l^{-1}
11-Nov-99	12.13
13-Jan-00	19.89
12-Mar-00	15.57
25-Apr-00	1.67
5-Dec-00	15.02
18-Jan-01	18.06
6-Mar-01	13.33
1-May-01	11.80

Mean daily SO_4 concentrations

Month	n	mg l^{-1}	StDev.
January	2	19.0	
Febuary	0		
March	2	14.5	
April	1	1.67	
May	3	6.39	3.58
June	12	3.69	0.54
July	25	3.61	1.95
August	10	3.17	0.70
September	10	3.89	0.99
October	3	5.43	2.48
November	1	12.13	
December	1	15.02	

Seasonal averages

Season	Ablation 10:00 h	Ablation 17:00 h	Accumulation
Average	4.03	3.03	13.67
St.dev.	1.76	1.68	5.91
n	59	60	7

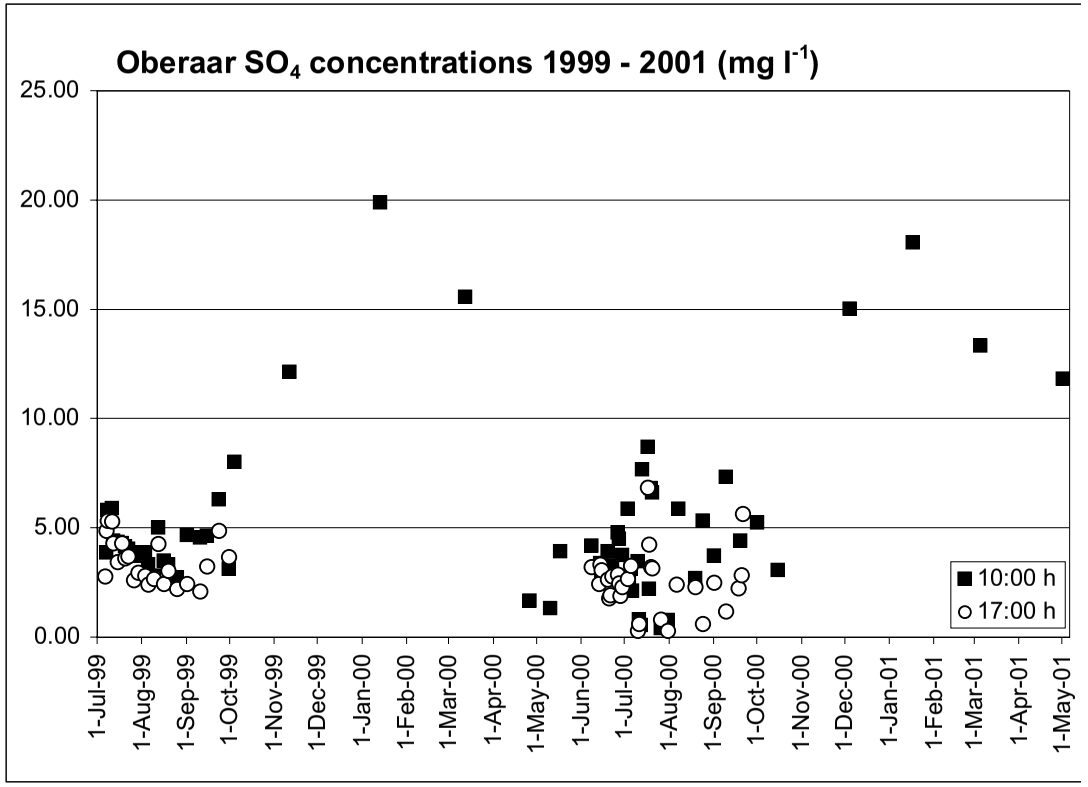

***HCO_3 concentrations from Oberaar glacier ablation season 1999-2000 (mg l^{-1}).**

Month		**July**			**August**		**September**			**October**		**May**		**June**			**July**			**August**			**September**			**October**	
Day nr.	10	17	**daily**	10	17	**daily**	10	17	**daily**	10	**daily**		10	17	**daily**	10	17	**daily**	10	17	**daily**	10	17	**daily**	10	**daily**
1							11.16	8.02	9.59																13.89	13.89
2																										
3				9.02	7.49	8.25																				
4										16.11	16.11					10.55	6.63	8.59								
5				7.91	8.05	7.98																				
6		7.93	7.93																14.07							
7	10.48	10.27	10.38										11.21	10.46	10.84											
8	11.03	10.55	10.79																			13.22	6.30	9.76		
9				7.40	7.86	7.63																				
10							11.69	8.95	10.32			20.13														
11	10.26	9.30	9.78																							
12	9.28	8.72	9.00	11.83	10.47	11.15							8.93	8.82	8.87											
13													8.11	8.79	8.45											
14													8.36	8.14	8.25											
15	8.45	7.16	7.80				11.89	9.04	10.47																17.96	17.96
16				9.60	8.76	9.18										15.53	12.98	14.25								
17												14.37				27.24	12.77	20.00				15.97	9.05	12.51		
18	8.12	8.19	8.15										9.21	8.90	9.06	13.60	8.88	11.24	9.03	9.50	9.26					
19				9.52	8.37	8.94							8.58	8.67	8.62	13.09	8.89	10.99					9.70	12.83		
20	8.52	8.14	8.33										8.80	7.30	8.05								13.45	14.71		
21													8.82	8.85	8.83											
22	8.66	8.29	8.47																							
23							14.92	12.10	13.51										10.08							
24																										
25				8.16	8.43	8.30							13.64	8.43	11.03	12.03										
26	9.79	7.16	8.48																							
27													7.81	7.55	7.68											
28													10.33	7.71	9.02											
29	9.24	7.70	8.47																							
30							13.09	12.57	12.83																	
31																			11.99	9.73	10.86					
m			**8.87**			**8.78**			**11.34**		**16.11**	**17.25**			**8.97**			**13.02**			**10.06**			**12.45**		**15.93**

***HCO_3 concentrations from Oberaar glacier accumulation seasons 1999-2001 (mg l^{-1}).**

Date	mg l^{-1}
11-Nov-99	19.21
13-Jan-00	19.91
12-Mar-00	25.58
25-Apr-00	30.22
5-Dec-00	21.32
18-Jan-01	23.60
6-Mar-01	33.23
1-May-01	23.64

Mean daily *HCO_3 concentrations

Month	n	mg l^{-1}	StDev.
January	2	21.8	
Febuary	0		
March	2	29.4	
April	1	30.22	
May	3	19.32	4.68
June	11	8.97	1.06
July	16	10.17	3.12
August	9	9.06	1.23
September	9	11.84	1.84
October	3	15.99	2.04
November	1	19.21	
December	1	21.32	

Seasonal averages

Season	Ablation 10:00 h	Ablation 17:00 h	Accumulation
Average	11.45	8.99	24.72
St.dev.	3.67	2.95	5.32
n	50	51	7

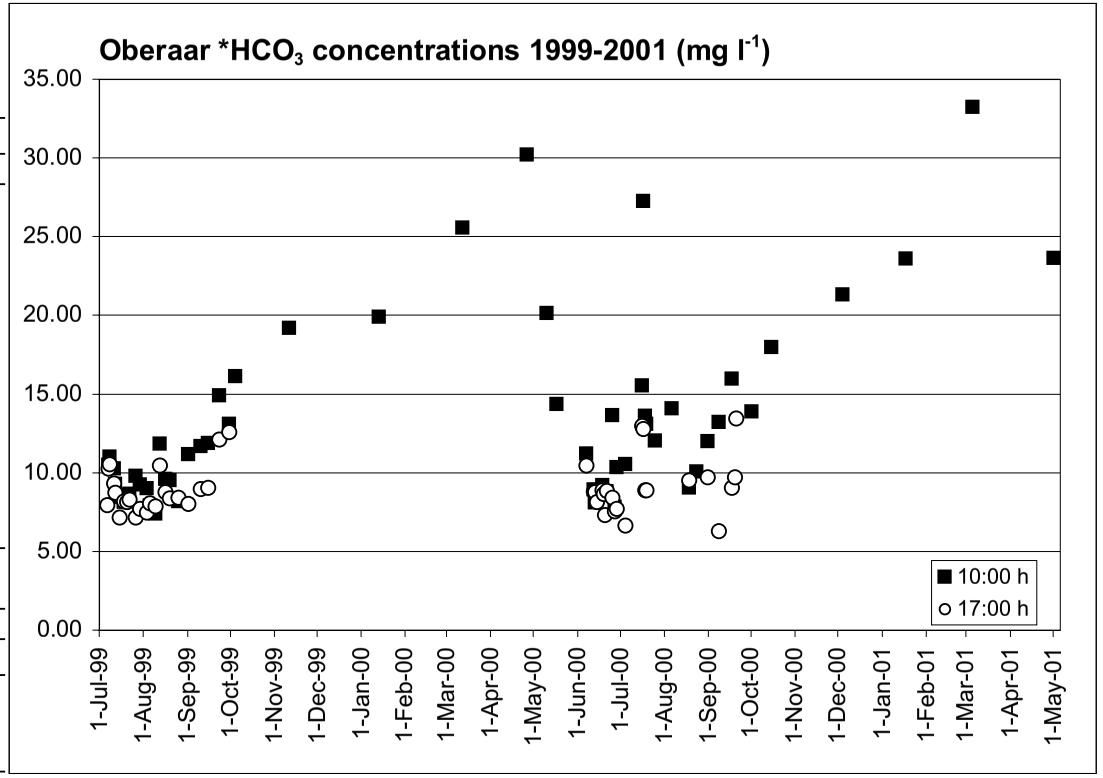

SRP concentrations from Oberaar glacier ablation season 1999-2000 (mg l^{-1}).

Month		**July**			**August**			**September**			**October**		**May**		**June**			**July**			**August**			**September**			**October**	
Day nr.	10	17	**daily**	10	17	**daily**	10	17	**daily**	10	**daily**		10	17	**daily**	10	17	**daily**	10	17	**daily**	10	17	**daily**	10	**daily**
1																			7.00		7.00	8.00	7.00			
2																									6.00	6.00
3																										
4																										
5																										
6																	7.00			5.00						
7																7.00		7.00	11.00		8.00					
8													8.00	6.00	7.00											
9																							5.00	4.00		
10													8.20													
11																8.00	8.00	8.00								
12																9.00		9.00								
13																9.00		9.00								
14																										
15													7.00	7.00	7.00											
16													11.00												12.00	12.00
17																										
18																							5.00			
19								9.10	9.10							10.00	9.00	9.50	7.00	7.00	7.00	9.00				
20																10.00	9.00	7.00					10.00			
21																							9.00			
22	9.10	2.40	5.75										7.00	7.00	7.00								7.00			
23																										
24																			6.00	6.00	6.00					
25																										
26													7.00	6.00	6.50	5.00	6.00	7.00								
27																										
28														8.00	8.00											
29	7.40	11.00	9.20										9.00	6.00	7.50											
30																										
31																	4.00	7.00								
m			**7.48**						**9.10**				**9.60**		**7.17**			**7.94**			**7.00**			**4.00**		**9.00**

SRP concentrations from Oberaar glacier accumulation seasons 1999-2001 (µg l^{-1}).

Date	µg l^{-1}
11-Nov-99	12.62
13-Jan-00	13.00
12-Mar-00	10.40
25-Apr-00	6.60
5-Dec-00	9.80
18-Jan-01	11.50
6-Mar-01	9.40

Mean daily SRP concentrations

Month	n	µg l^{-1}	StDev.
January	2	12.3	
Febuary	0		
March	2	9.9	
April	1	6.60	
May	2	9.60	
June	5	7.00	0.46
July	6	7.81	1.75
August	4	6.75	1.13
September	5	7.87	1.97
October	2	8.60	
November	1	12.62	
December	1	9.80	

Seasonal averages

Season	Ablation 10:00 h	Ablation 17:00 h	Accumulation
Average	8.02	6.67	10.47
St.dev.	1.81	2.00	2.19
n	25	32	7

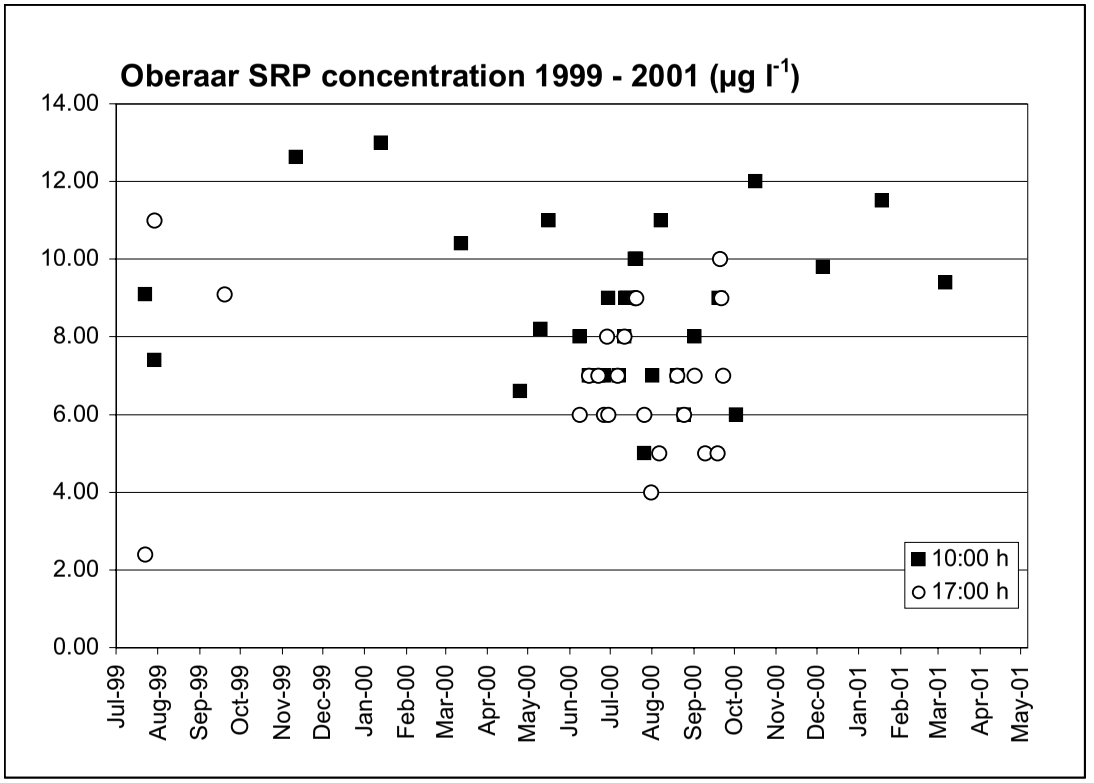

Si concentrations from Oberaar glacier ablation season 1999-2000 (mg l^{-1}).

Month		**July**			**August**			**September**			**October**		**May**		**June**			**July**			**August**			**September**			**October**	
Day nr.	10	17	**daily**	10	17	**daily**	10	17	**daily**	10	**daily**		10	17	**daily**	10	17	**daily**	10	17	**daily**	10	17	**daily**	10	**daily**
1																						0.52	0.30	0.41		
2																									0.62	0.62
3				0.32	0.39	0.35										0.37	0.39	0.38								
4										0.12	0.12					0.37		0.34								
5				0.31	0.34	0.33										0.42	0.32	0.37								
6		0.15	0.15																0.72	0.65	0.69					
7	0.34	0.20	0.27																							
8	0.44	0.47	0.46										0.53	0.30	0.42											
9				0.17	0.27	0.22																0.69	0.24	0.47		
10							0.34	0.16	0.25				0.88			0.51	0.36	0.43								
11	0.31	0.37	0.34													0.68	0.66	0.67								
12	0.35	0.43	0.39	0.41	1.84	1.13										0.81		0.73								
13														0.28	0.43	0.36	0.50		0.63								
14														0.43	0.26	0.34										
15	0.37	0.39	0.38				0.31	0.21	0.26					0.27	0.41	0.34										
16				0.16	0.57	0.36																			0.83	0.83
17													0.72			0.70	0.77	0.73								
18	0.37	0.23	0.30													0.84	0.86	0.85					0.35	0.52		
19				0.31	0.26	0.29								0.48	0.63	0.56	0.55	0.44	0.50	0.46	0.41	0.43				
20	0.25	0.30	0.27											0.43	0.39	0.41	0.75	0.40	0.57				0.53	0.45	0.49	
21														0.38	0.37	0.38								0.51	0.25	
22	0.31	0.44	0.38											0.31	0.34	0.32										
23							0.52	0.43	0.47																	
24																			0.39	0.26	0.32					
25				0.31	0.17	0.24																				
26	0.35	0.26	0.30											0.45	0.33	0.39	0.49	0.28	0.38							
27														0.39	0.48	0.44										
28														0.33	0.39	0.36										
29	0.35	0.29	0.32											0.51	0.29	0.40										
30							0.59	0.28	0.44																	
31																	0.53	0.23	0.38							
m			**0.32**			**0.42**			**0.36**		**0.12**		**0.80**			**0.39**			**0.54**			**0.48**			**0.43**		**0.73**

Si concentrations from Oberaar glacier accumulation seasons 1999-2001 (mg l^{-1}).

Date	mg l^{-1}
11-Nov-99	
13-Jan-00	
12-Mar-00	
25-Apr-00	1.45
5-Dec-00	
18-Jan-01	1.27
6-Mar-01	
1-May-01	1.27

Mean daily Si concentrations

Month	n	mg l^{-1}	StDev.
January	1	1.3	
Febuary	0		
March	0		
April	1	1.45	
May	3	0.96	0.28
June	12	0.39	0.06
July	24	0.44	0.17
August	10	0.44	0.28
September	9	0.40	0.11
October	3	0.52	0.36
November	0		
December	0		

Seasonal averages

Season	Ablation 10:00 h	Ablation 17:00 h	Accumulation
Average	0.47	0.40	1.36
St.dev.	0.21	0.25	
n	58	52	2

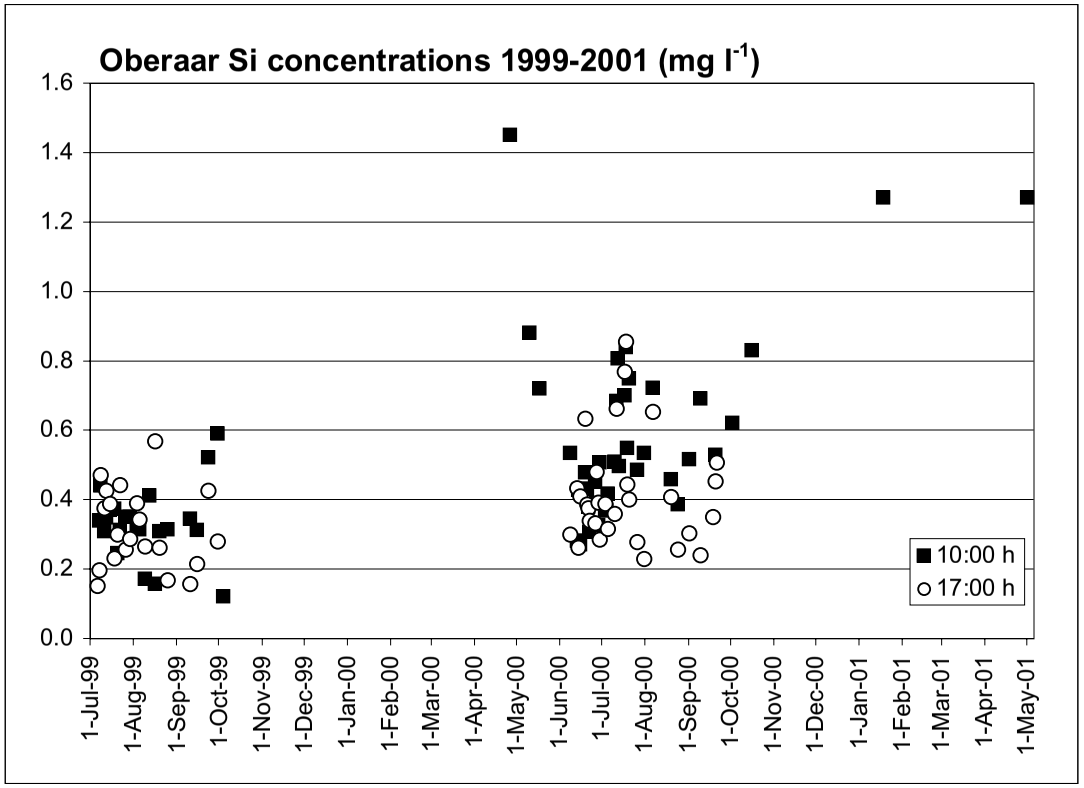

Conductivities from Oberaar glacier ablation season 1999-2001 (µS cm^{-1}).

Month		**July**			**August**			**September**			**October**	**May**		**June**			**July**			**August**			**September**			**October**	**May**	**June**	**July**	**August**	**October**
Day nr.	10	17	**daily**	10	17	**daily**	10	17	**daily**	10		10	17	**daily**	10	17	**daily**	10	17	**daily**	10	17	**daily**	10	10	10	17	10	10
1							33.0	20.0	26.5									35.0		26.5	28.4	21.5	25.0		72.9				53.5
2																								37.5					
3				26.8	20.5	23.7									24.3	23.3	23.8											20.1	
4										47.6					22.6												20		
5				21.4	21.8	21.6									26.7	18.8	22.8												
6		21.9	21.9												25.6				30.0	35.0								
7	28.6	31.5	30.1															40.0										
8	37.8	34.3	36.1										28.0	25.0	26.5														
9				22.5	21.2	21.9															44.7	14.5	29.6						
10							31.9	19.7	25.8			25.0			30.5	23.6	27.1												
11	34.2	31.1	32.7												37.5	36.1	36.8												
12	28.5	27.4	28.0	33.8	29.5	31.7									44.2														
13													23.0	21.0	22.0	46.5													
14													24.0	24.0	24.0												30.9		16.2	
15	28.1	22.4	25.3				33.3	24.7	29.0				24.0	22.0	23.0														
16				33.2	20.5	26.9																		43.8					
17												33.0				49.7	40.6	45.2											
18	26.3	26.4	26.4													45.6	30.2	37.9					32.3	38.7					
19				25.5	22.8	24.2							26.0	20.6	23.3	43.4	22.9	33.2	23.2	20.7	22.0	45.1							
20	27.2	24.2	25.7										24.0	18.9	21.5	43.1	23.3	33.2					23.1	34.1					
21													22.8	16.6	19.7								53.8						
22	26.8	24.2	25.5										24.2	21.8	23.0														
23							42.0	33.2	37.6																				
24																			29.4	17.3	23.4								
25				22.6	21.6	22.1																							
26	25.5	19.4	22.5										32.1	21.9	27.0	23.0	23.0	23.0											
27													30.5	20.6	25.6														
28													24.1	16.5	20.3														
29	27.0	21.9	24.5										29.2	18.5	23.9													20.8	
30							32.0	30.7	31.4																				
31																	18.0												
m			**27.1**			**24.6**			**30.1**	**47.6**		**29.0**			**23.3**			**31.4**			**26.7**			**31.8**	**40.7**	**72.9**				**53.5**

Conductivities from Oberaar glacier accumulation seasons 1999-2001 (µS cm^{-1}).

Date	µS cm^{-1}
11-Nov-99	64.7
13-Jan-00	85.0
12-Mar-00	88.0
25-Apr-00	62.0
5-Dec-00	76.6
18-Jan-01	86.7
6-Mar-01	92.0

Mean daily conductivities

Month	n	µS cm^{-1}	StDev.
January	2	86.3	
Febuary	0		
March	2	90.0	
April	2	67.5	
May	2	29.0	
June	12	23.3	2.3
July	25	29.4	6.9
August	10	25.2	4.6
September	10	30.0	5.4
October	3	39.9	10.2
November	1	64.7	
December	1	76.6	

Seasonal averages

Season	Ablation 10:00 h	Ablation 17:00 h	Accumulation
Average	31.9	24.2	79.3
St.dev.	9.8	6.8	11.9
n	65	54	7

pH from Oberaar glacier ablation season 1999-2000

Month		**July**			**August**			**September**			**October**		**May**		**June**			**July**			**August**			**September**			**October**	
Day nr.	10	17	**daily**	10	17	**daily**	10	17	**daily**	10	**daily**		10	17	**daily**	10	17	**daily**	10	17	**daily**	10	17	**daily**	10	**daily**
1							7.10	7.50	7.26										7.42		7.32	7.08	7.40	7.21		
2																									7.08	7.08
3				7.57	7.56	7.56										7.45	7.51	7.48								
4										7.14	7.14					7.45										
5				7.25	7.95	7.47										7.62	7.51	7.56								
6																7.49				7.03	7.12					
7	7.49	8.20	7.71																7.24							
8	7.70	8.10	7.86										7.00													
9				7.64	8.15	7.82																7.16	7.73	7.36		
10							8.08	8.47	8.23				7.44													
11	7.21	7.48	7.32													7.63	7.63	7.63								
12	7.24	7.61	7.39	7.17	8.10	7.42										7.10										
13													7.59	7.35	7.45	7.48										
14													7.35	7.37	7.36											
15	7.50	7.50	7.50				7.50	7.85	7.64				7.53													
16				7.15	7.25	7.20																				
17													8.50			7.54	7.41	7.47								
18	7.31	7.32	7.31													7.54	7.65	7.59					7.14			
19													7.15	7.56	7.31	7.49	7.48	7.48	7.18	7.32	7.24	7.26		7.26		
20													7.63	7.36	7.47	7.45	7.30	7.37					7.27	7.27		
21													7.23	7.04	7.12								7.67	7.67		
22													7.35	7.26	7.30											
23							7.78	7.82	7.80																	
24																			7.85	7.56	7.68					
25				8.10	8.85	8.33																				
26	6.99												7.69	7.50	7.58	7.18	7.44	7.29								
27													7.57	7.18	7.33											
28													7.31	7.32	7.31											
29													7.45	7.48	7.46											
30							7.11	7.06	7.08																	
31																	7.24									
m			**7.47**			**7.52**			**7.44**		**7.14**		**7.70**			**7.35**			**7.47**			**7.30**			**7.33**		**7.08**

pH from Oberaar glacier accumulation seasons 1999-2001.

Date	pH
11-Nov-99	7.72
13-Jan-00	7.30
12-Mar-00	7.70
25-Apr-00	7.86
5-Dec-00	7.84
18-Jan-01	7.74
6-Mar-01	7.60

Mean daily pH

Month	n	pH
January	2	7.47
Febuary	0	
March	2	7.65
April	1	7.86
May	3	7.60
June	10	7.35
July	14	7.47
August	11	7.42
September	10	7.40
October	3	7.11
November	1	7.72
December	1	7.84

Seasonal averages

Season	Ablation	Accumulation
Average	7.40	7.64
St.dev.	0.30	0.19
n	49	7

Watertemperatures from Oberaar glacier 1999-2001 (°C).

	1999									2000													2001						
Month	July		August		September		October	November		January	March	April	May	June		July		August		September		October	December		January	March	May	June	July	August	Octobe
Day nr.	10	17	10	17	10	17								10	17	10	17	10	17	10	17										
1					0.7	0.2												1.0		1.0	0.9						0.1				0.
2																						2.2									
3			0.8	0.8												1.1	1.1													1.4	
4							0.6									0.9													2		
5			1.0	1.6												1.0	0.9						0.1								
6		0.4														1.0			1.0							0.2					
7	0.6	0.7																1.0													
8	0.7	0.9												1.0																	
9			1.5	1.8																0.7	0.5										
10					0.3	0.2							0.5			1.1	1.7														
11	0.9	1.0						0.3								0.9	1														
12	0.7	0.9	0.8	0.8							0.0					0.9															
13										-0.5				1.0	1.1	1.0															
14														1.0	1.1												0.3		1.3		
15	1.0	2.2			0.3	0.2								0.9																	
16			0.7	0.8																		0.9									
17													0.4			1.1	0.8														
18	1.0	0.9														1.0	0.9				0.7			-0.3							
19			0.7	0.7										1.0	1.5	1.1	1.0	0.8	0.7	2.1	2.3										
20	0.9	1.3												1.1	1.2	0.9	1.1				0.6										
21														1.3	2.9						0.4										
22	0.9	1.0												1.2	1.0																
23					0.4	0.4																									
24																		1.0	1.0												
25			0.6	0.4								0.4																			
26	1.0	1.0												1.0	0.8	1.0	1.0														
27														0.9	0.8																
28														0.8	2.4																
29	1.0	2.1												0.7	0.9															0.3	
30					0.4	0.8																									
31																	1.0														

Discharge from Oberaar glacier ablation season 1999-2001 ($m^3 s^{-1}$)
with daily means used for flux calculations, see chapter 2.

Month		**July**			**August**			**September**			**October**	**May**		**June**			**July**			**August**			**September**			**October**	**May**	**June**	**July**	**August**		**October**
Day nr.	10	17	**daily**	10	17	**daily**	10	17	**daily**	10		10	17	**daily**	10	17	**daily**	10	17	**daily**	10	17	**daily**	10		10						
1							1.00	2.50	1.75									1.50		2.00	1.50	2.50	2.00			0.20					0.50
2																								1.00								
3				1.50	3.00	2.25									1.50	2.50	2.00													2.00		
4										0.50					1.75													3.00			
5				1.50	3.00	2.25									1.50	2.50	2.00															
6		5.00	5.00												1.50				1.50	1.25											
7	2.50	3.00	2.75															1.00														
8	1.50	2.50	2.00										1.50	2.00	1.75																	
9				1.50	3.00	2.25															1.50	2.80	2.15									
10							1.50	2.75	2.13			0.50			1.50	2.50	2.00															
11	1.50	2.50	2.00												1.20	1.50	1.35															
12	1.50	2.50	2.00	1.50	2.50	2.00									1.00																	
13													1.00	2.00	1.50	1.00																
14													1.00	2.00	1.50													0.75		3.00		
15	2.00	3.00	2.50				1.50	2.50	2.00				1.00	1.50	1.25																	
16				1.50	2.50	2.00																		1.00								
17												0.75				0.75	1.00	0.88														
18	2.50	3.00	2.75													1.00	1.50	1.25					2.50	2.00								
19				1.50	2.50	2.00							1.25	2.00	1.63	0.80	2.20	1.50	1.50	2.50	2.00	1.50										
20	2.00	3.00	2.50										1.50	2.00	1.75	1.20	2.20	1.70					3.50	2.50								
21													1.50	2.20	1.85								1.00									
22	2.00	2.50	2.25										1.50	2.20	1.85																	
23							1.00	2.00	1.50																							
24																			1.30	2.20	1.75											
25				1.50	2.50	2.00																										
26	2.00	3.00	2.50										1.25	2.20	1.73	2.50	3.50	3.00														
27													1.25	2.20	1.73																	
28													1.25	3.00	2.13																	
29	2.00	3.00	2.50										1.50	2.00	1.75															1.50		
30							1.00	2.00	1.50																							
31																	2.50															
m			**2.61**			**2.11**			**1.78**	**0.50**		**0.63**			**1.70**			**1.74**			**1.75**			**2.16**	**1.00**		**0.20**					**0.50**

Suspended sediment concentrations from Oberaar glacier ablation season 1999-2001 (g l^{-1}).

Month		**July**			**August**			**September**			**Oct**	**May**		**June**			**July**			**August**			**September**			**Oct**	**May**	**June**	**July**	**August**	**Oct**
Day nr.	10	17	**daily**	10	17	**daily**	10	17	**daily**	10		10	17	**daily**	10	17	**daily**	10	17	**daily**	10	17	**daily**	10	10	10	17	10	10
1							0.090	0.191	0.141									0.130		0.153	0.401	0.545	0.473							0.090
2																														
3				0.110	0.290	0.200									0.431	0.962	0.697													
4										0.199					0.662													0.584	0.620	
5				0.129	0.396	0.263									0.249	0.472	0.360													
6		0.526	0.526												0.364				0.124	0.211										
7	0.128	0.335	0.231															0.149												
8	0.433	0.227	0.330									0.318	0.634	0.476																
9				0.193	0.271	0.232															0.186	0.463	0.324							
10							0.143	0.748	0.445		0.500				0.240	0.369	0.305													
11	0.125	0.213	0.169												0.212	0.171	0.191													
12	0.245	0.298	0.272	0.254	0.329	0.292									0.092															
13												0.251	0.454	0.353	0.151															
14												0.264	0.334	0.299														0.703		0.390	
15	0.266	0.416	0.341				0.132	0.147	0.140			0.249	0.418	0.333																	
16				0.220	0.670	0.445																				0.202					
17											0.425				0.089	0.150	0.119													
18	0.189	0.261	0.225								0.582				0.119	0.368	0.243					0.290	0.203							
19				0.304	0.316	0.310					0.503	0.268	0.591	0.429	0.184	0.328	0.256	0.195	0.310	0.252	0.115									
20	0.219	0.446	0.333									0.269	0.592	0.431	0.098	0.316	0.207					0.601								
21												0.233	0.546	0.389								0.271								
22	0.254	0.203	0.229									0.245	0.385	0.315																
23							0.139	0.356	0.247																					
24																		0.265	0.383	0.324										
25				0.320	0.653	0.486																								
26	0.168	0.480	0.324									0.165	0.418	0.291	0.313	0.501	0.407													
27												0.192	0.500	0.346																
28												0.233	0.856	0.544																
29	0.243	0.208	0.226									0.261	0.516	0.388															0.209	
30							0.151	0.234	0.193																					
31																0.176														
m			**0.291**			**0.318**			**0.233**	**0.199**	**0.503**			**0.383**			**0.309**			**0.235**			**0.333**	**0.202**						

Suspended sediment from Oberaar and Rhone glacier 1999-2001.

Catchment	Oberaar			Rhone		
Season	Ablation 10:00 h	Ablation 17:00 h	Accumulation	Ablation 10:00 h	Ablation 17:00 h	Accumulation
Average	0.259	0.395	0.045	0.125	0.123	0.021
St.dev.	0.146	0.183	0.032	0.114	0.130	0.016
n	64	55	7	96	86	6
	total	glaciericed		total	glaciericed	
yield (kg km^{-2} y^{-1})	7.73E+05	1.36E+06		4.91E+05	6.72E+05	
erosion (m yr^{-1})	2.86E-04	5.02E-04		1.82E-04	2.49E-04	
rate (mm kyr^{-1})	286	502		182	249	

Suspended sediment concentrations from Oberaar glacier accumulation seasons 1999 - 2001 (g l^{-1}).

Date	g l^{-1}
11-Nov-99	0.0051
13-Jan-00	0.0763
12-Mar-00	0.0750
25-Apr-00	0.0750
5-Dec-00	0.0361
18-Jan-01	0.0394
6-Mar-01	0.0054

Mean daily conductivities

Month	n	g l^{-1}	StDev.
January	2	0.0579	
Febuary	0		
March	2	0.0402	
April	1	0.0750	
May	4	0.5025	0.0643
June	12	0.3829	0.0763
July	20	0.2995	0.1308
August	11	0.2880	0.1014
September	8	0.2707	0.1307
October	2	0.2002	
November	1	0.0051	
December	1	0.0361	

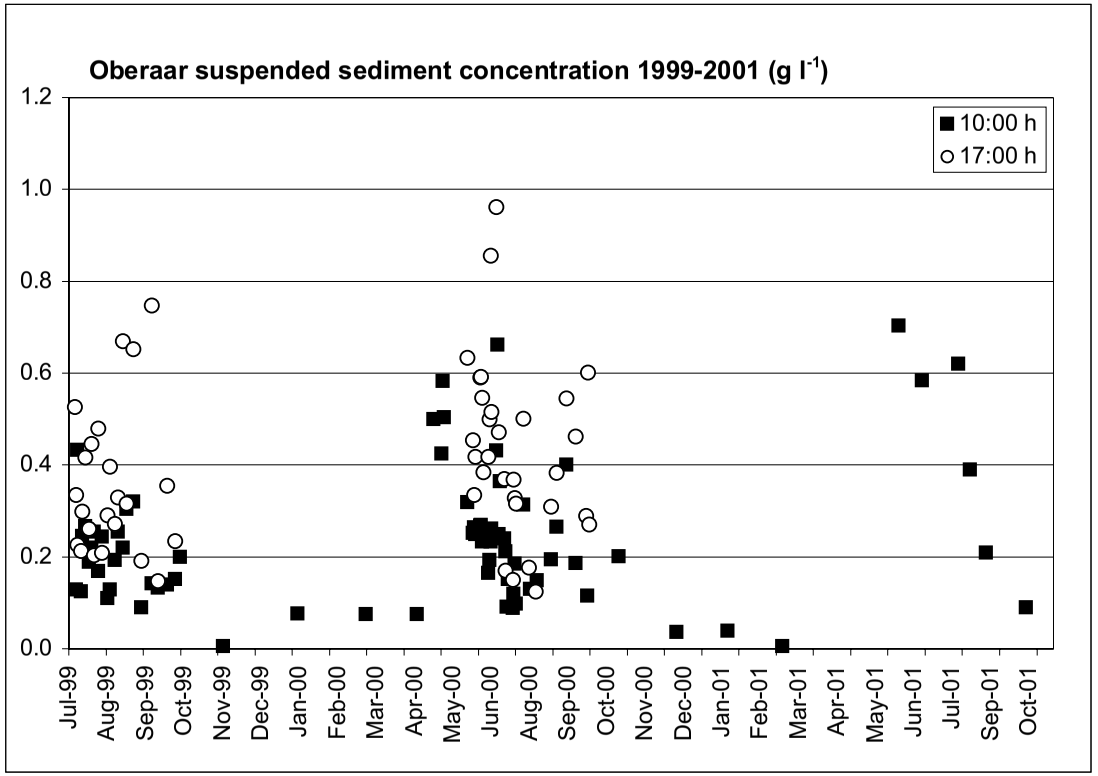

Relationship between total phosphorus (TP) and suspended sediment concentrations in the Oberaar meltwaters (2000-2001)

	TP	Suspended sediment	Suspended sediment outliers†
Dates	mg l^{-1}	g l^{-1}	g l^{-1}
10:00 h			
15-Jun-00	0.55	0.25	
14-Jun-01	0.98	0.70	
4-Jul-01	1.39	1.09	
3-Aug-01	0.82	0.60	
6-Aug-00	0.33	0.15	
24-Aug-00	0.40	0.27	
1-Sep-00	0.56	0.40	
9-Sep-00	0.23	0.19	
19-Sep-00	0.22	0.12	
21-Sep-00	0.40	0.27	
2-Oct-00	0.06	0.07	
16-Oct-00	0.55	0.20	
5-Dec-00	0.03	0.04	
18-Jan-00	0.03	0.03	
7-Mar-01	0.02	0.01	
17:00 h			
15-Jun-00	0.75	0.42	
6-Aug-00	0.31	0.12	
24-Aug-00	0.62	0.38	
1-Sep-00	0.66	0.55	
9-Sep-00	0.65	0.46	
18-Sep-00	0.60	0.29	
20-Sep-00	0.94	0.60	
21-Sep-00	0.08		0.27

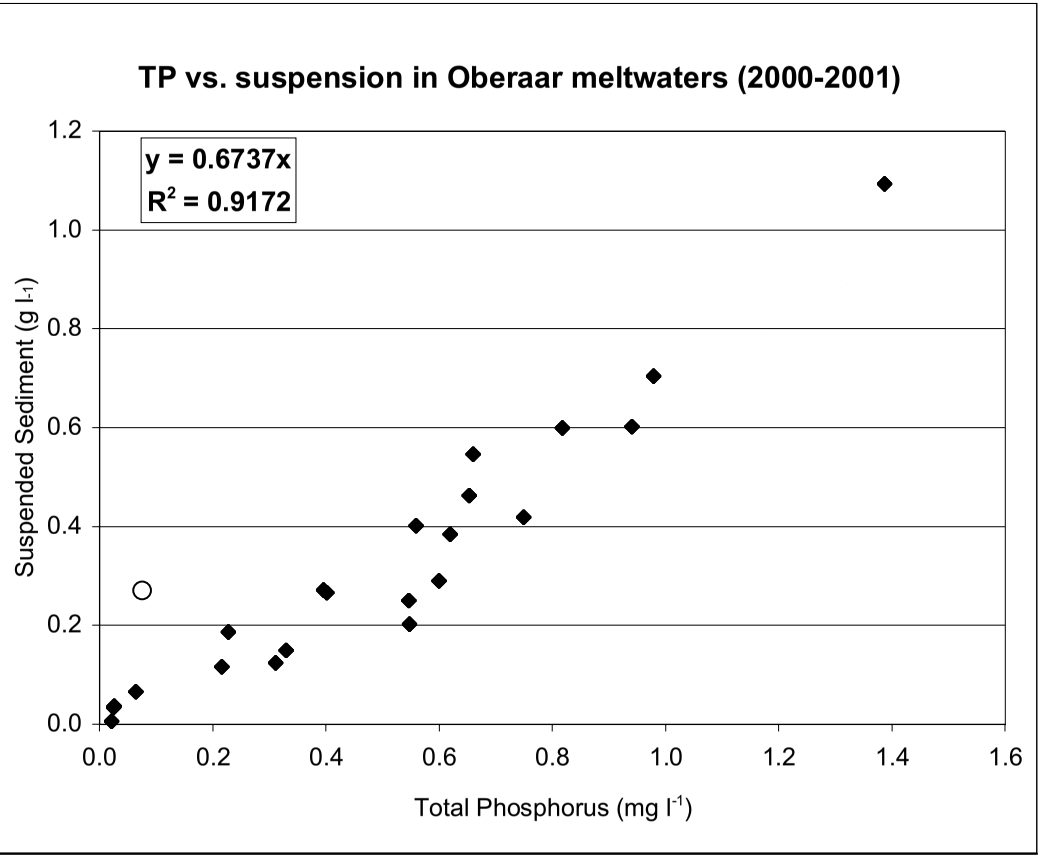

† Outliers were not included in the regression to prevent negative TP concentrations being calculated.
When outliers are included $R^2 = 0.885$

Oberaar 24h sampling campaigns: 28./29. June 2000 and 19./20. July 2000 (Rain as mm during interval to last sample time)

		Fieldparameters						Anions			Cations					
Date	Time	Conductivity	T_{water}	T_{air}	pH	Rain	Discharge	Cl^-	SO_4^{2-}	NO_3^-	Ca^{2+}	Mg^{2+}	Na^+	K^+	Fe^{3+}	Al^{3+}
		µS cm^{-1}	°C	°C		mm	m^3 s^{-1}	mg l^{-1}	mg l^{-1}	mg l^{-1}	mg l^{-1}	mg l^{-1}	mg l^{-1}	mg l^{-1}	mg l^{-1}	mg l^{-1}
28-Jun-00	10:00	24.1	0.8	7	7.31		1.25	0.05	2.63	0.50	3.15	0.08	0.15	0.57	0.0620	0.0443
28-Jun-00	15:00	21.0	1.0	8	7.29	4.55	2.25	0.06	2.66	0.53	n.a.	n.a.	n.a.	n.a.	0.0610	0.0371
28-Jun-00	17:00	16.5	2.4	8	7.32	10.23	3.00	0.06	1.89	0.45	n.a.	n.a.	n.a.	n.a.	0.0495	0.0323
28-Jun-00	18:00	18.0				3.41										
28-Jun-00	19:00	17.9	2.1	6	7.33	0.57	2.75	0.07	2.15	0.49	2.75	0.12	0.19	0.55	0.0462	0.0309
28-Jun-00	20:00	19.8				0										
28-Jun-00	21:00	20.7	1.4	5	7.42	0	2.50	0.06	2.27	0.48	n.a.	n.a.	n.a.	n.a.	0.0304	0.0259
28-Jun-00	23:00	22.1	0.9	5	7.45	1.14	2.50	0.08	2.78	0.57	2.55	n.a.	0.23	0.57	0.0203	0.0200
29-Jun-00	2:00	24.4	0.8	4	7.39	0	2.25	0.07	3.35	0.63	n.a.	n.a.	n.a.	n.a.	0.0368	0.0321
29-Jun-00	5:00	27.4	0.8	3	7.39	0	1.75	0.07	3.71	0.66	n.a.	n.a.	n.a.	n.a.	0.0368	0.0304
29-Jun-00	8:00	29.2	0.8	6	7.42	0	1.50	0.07	3.29	0.60	4.13	n.a.	0.24	0.80	0.0537	0.0436
29-Jun-00	10:00	29.2	0.7	10	7.45	0	1.50	0.07	3.74	0.64	n.a.	n.a.	n.a.	n.a.		
29-Jun-00	12:00	23.2	1.1	10		0	1.50	0.09	2.97	0.53	3.29	n.a.	0.19	0.65	0.0196	0.0187
29-Jun-00	15:00	18.5	0.9	13	7.48	0	2.00	0.05	2.30	0.44	n.a.	n.a.	n.a.	n.a.	0.0277	0.0237
19-Jul-00	10:00	43.4	1.1	9	7.5	0	0.8	0.07	6.82	0.74	n.a.	n.a.	n.a.	n.a.	0.0398	0.0359
19-Jul-00	12:30	33.8	1.1	12	7.6	0	1.3	0.05	4.88	0.53	4.77	n.a.	0.29	1.03	0.0641	0.0474
19-Jul-00	14:00	26.3	0.9			0	1.5									
19-Jul-00	15:00	24.5	1.0	12	7.4	0	1.8	0.04	3.56	0.40	3.44	n.a.	0.01	0.79	0.0706	0.0492
19-Jul-00	16:00	23.5	0.9			0	2.0									
19-Jul-00	17:00	22.9	1.0	12	7.5	0	2.2	0.04	3.19	0.39	n.a.	n.a.	n.a.	n.a.	0.0545	0.0415
19-Jul-00	18:00	22.8	0.7	6		0	2.2									
19-Jul-00	19:00	25.2	0.6			0	2.0									
19-Jul-00	20:00	33.3	0.7	7	7.5	0	2.0	0.05	4.61	0.54	4.27	n.a.	0.25	0.91	0.0473	0.0437
19-Jul-00	21:00	34.5	0.7	6		0	2.0									
19-Jul-00	22:00	34.7	0.7			0										
19-Jul-00	23:00	34.9	0.7	4	7.6	0	1.8	0.06	5.51	0.67	4.78	n.a.	0.25	1.03	0.0450	0.0411
20-Jul-00	2:00	39.4	0.6	1	7.6	0	1.5	0.07	6.26	0.70	n.a.	n.a.	n.a.	n.a.	0.0487	0.0487
20-Jul-00	5:00	40.9	0.5	1	7.6	0	1.3	0.08	6.98	0.77	5.74	n.a.	0.33	1.22	0.0353	0.0395
20-Jul-00	8:00	42.4	0.8	6	7.7	0	1.2	0.10	0.80	0.78	3.67	n.a.	0.22	0.77	0.0413	0.0403
20-Jul-00	9:00	42.8	0.9	6		0	1.2									
20-Jul-00	10:00	43.1	0.9	8	7.5	0	1.2	0.09	6.62	0.77	n.a.	n.a.	n.a.	n.a.	0.0211	0.0334
20-Jul-00	11:00	40.7	0.9	10		0	1.3									
20-Jul-00	15:00	24.8	1.1	13		0	2.0									
20-Jul-00	16:00	23.3	1.1	13	7.3	0	2.2	0.04	3.15	0.37	n.a.	n.a.	n.a.	n.a.	0.0467	0.0394

Airtemperatures from Oberaar glacier 1999-2001 (°C), accumulation period mostly sunny weather => higher airtemperatures!

	1999									2000											2001						
Month	July		August		September		October	November		January	March	April	May	June		July		August		September		October	December	January	March	May	June	July	August	October
Day nr.	10	17	10	17	10	17								10	17	10	17	10	17	10	17									
1																		8.0		7.0	10.0									10.0
2																						1.0								
3			9.0	13.0												11.0	11.0												8.0	
4							5.0									8.0												13.0		
5			11.0	11.0												7.0	16.0						-2.0							
6																10.0			5.6						5.0					
7		5.9																7.3												
8	10.0	13.0												12.0	14.0															
9			11.0	10.0																12.0	19.0									
10					11.5	9.5							7.5			5.0	4.0													
11	9.0	9.0						-1.5								3.0	1.0													
12	7.5	11.0	7.0	5.0							5.0					2.0														
13										-10.0				14.0	15.0	2.0														
14														8.0	14.0												11.0		15.0	
15	15.3	11.5			9.7	11.8								10.0	8.0															
16			9.0	7.0																		2.0								
17													7.5			11.0	7.0													
18	8.7	10.0														7.0	10.0				10.0			-8.0						
19			13.0	8.0										15.0	15.0	9.0	12.0	12.0	13.0	8.0										
20	15.0	15.8												15.0	17.0	8.0	13.0				5.0									
21														13.0	17.0						5.0									
22	10.0	10.0												14.0	13.0															
23					8.9	8.4																								
24																		10.0	14.0											
25			11.0	14.0								7.0																		
26	15.0	15.0												7.0	8.0	19.7	15.2													
27														10.0	14.0															
28														7.0	8.0															
29	11.0	15.5												10.0	13.0														16.0	
30					7.6	4.0																								
31																	17.0													

Oberaar sideriver sampling

		Fieldparameters					Anions			Cations					
Date	Sideriver	Conductivity $\mu S\ cm^{-1}$	T_{water} °C	T_{air} °C	pH	Discharge $l\ s^{-1}$	Cl^- $mg\ l^{-1}$	SO_4^{2-} $mg\ l^{-1}$	NO_3^- $mg\ l^{-1}$	Ca^{2+} $mg\ l^{-1}$	Mg^{2+} $mg\ l^{-1}$	Na^+ $mg\ l^{-1}$	K^+ $mg\ l^{-1}$	Fe^{3+} $mg\ l^{-1}$	Al^{3+} $mg\ l^{-1}$
22-Jun-00	F 3-1	14.10	5.40	15	7.35	5	0.06	0.87	0.26	1.95	0.04	0.42	0.45	0.01	0.01
22-Jun-00	F 4-1	11.00	7.30	15	7.38	20	0.05	0.86	0.28	1.31	0.11	0.54	0.30	0.01	0.01
22-Jun-00	F 8-1	10.50	7.70	15	7.25	20	0.05	0.80	0.14	1.16	0.07	0.55	0.36	0.00	0.02
22-Jun-00	F 11-1	7.30	11.90	15	6.94	5	0.03	0.64	0.01	0.72	0.07	0.38	0.32	0.01	0.03
18-Jul-00	F 3-2	16.20	6.40	15	n.a.	5	0.05	1.16	0.11	1.45	n.a.	0.40	0.40	0.00	0.01
18-Jul-00	F 4-2	10.60	9.80	15	n.a.	20	0.05	0.89	0.16	1.17	n.a.	0.63	0.41	0.01	0.01
18-Jul-00	F 8-2	10.70	9.80	15	n.a.	15	0.04	1.04	0.10	0.87	n.a.	0.63	0.34	0.00	0.02
18-Jul-00	F 11-2	7.70	14.80	15	n.a.	5	0.03	0.91	0.01	n.a.	n.a.	0.01	0.31	0.01	0.02
2-Oct-00	F12.3	19.20	5.60	2	6.95	30	0.14	2.57	0.12	2.45	0.16	0.49	0.69	0.01	0.01
3-Aug-01	F12-4	12.70	9.80	10	n.a.	100	0.07	1.37	0.11	n.a.	n.a.	n.a.	n.a.	n.a.	n.a.
14-Aug-01	F12-5	16.40	13.20	15	n.a.	80	0.04	1.80	0.09	n.a.	n.a.	n.a.	n.a.	0.01	0.02

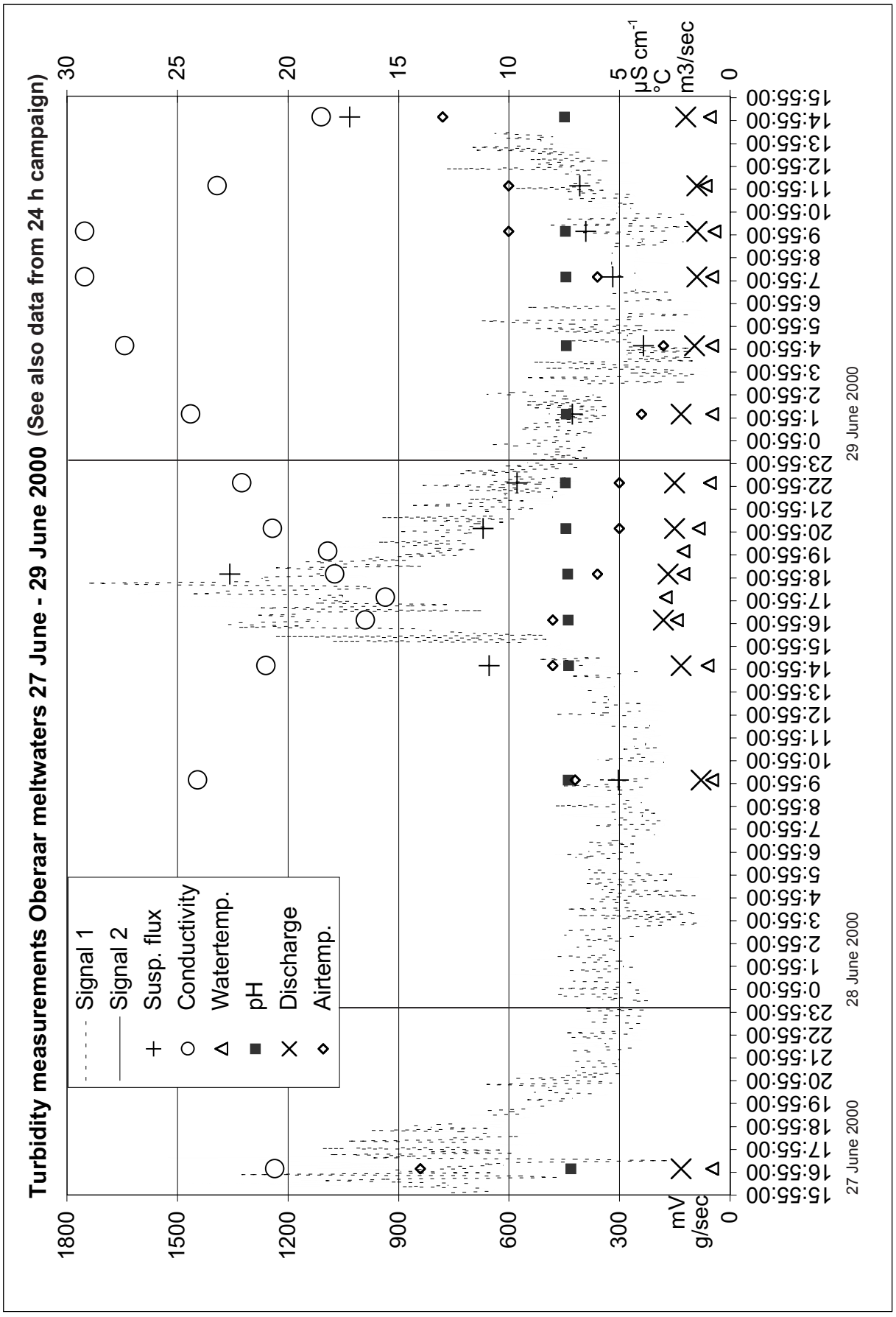
Turbidity measurements Oberaar meltwaters 27 June - 29 June 2000 (See also data from 24 h campaign)
Signal 1
Signal 2
Susp. flux
Conductivity
Watertemp.
pH
Discharge
Airtemp.
mV
g/sec
µS cm-1
°C
m3/sec
27 June 2000
28 June 2000
29 June 2000

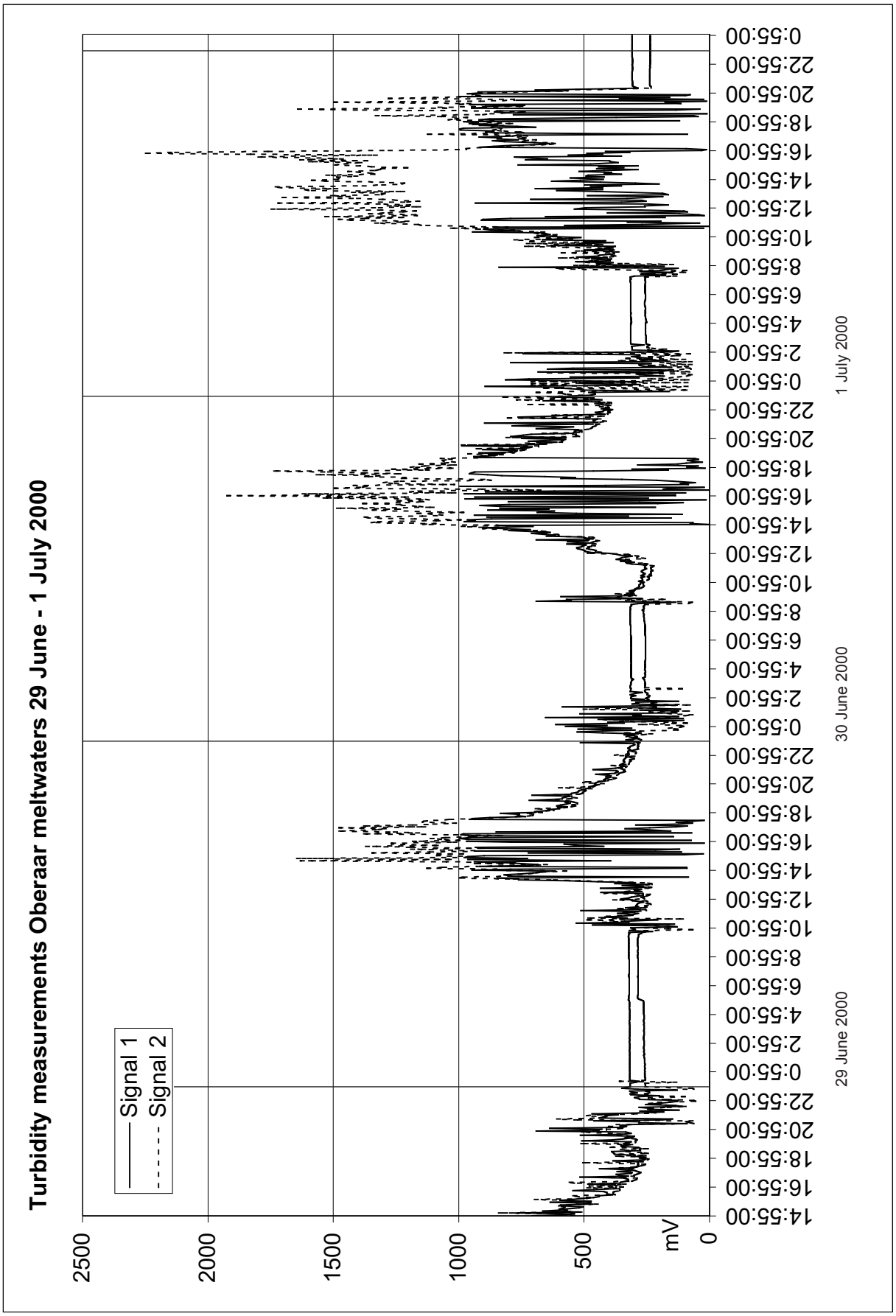
Turbidity measurements Oberaar meltwaters 29 June - 1 July 2000
Signal 1
Signal 2
mV
2500
2000
1500
1000
500
0
29 June 2000
30 June 2000
1 July 2000
14:55:00
16:55:00
18:55:00
20:55:00
22:55:00
0:55:00
2:55:00
4:55:00
6:55:00
8:55:00
10:55:00
12:55:00
14:55:00
16:55:00
18:55:00
20:55:00
22:55:00
0:55:00
2:55:00
4:55:00
6:55:00
8:55:00
10:55:00
12:55:00
14:55:00
16:55:00
18:55:00
20:55:00
22:55:00
0:55:00

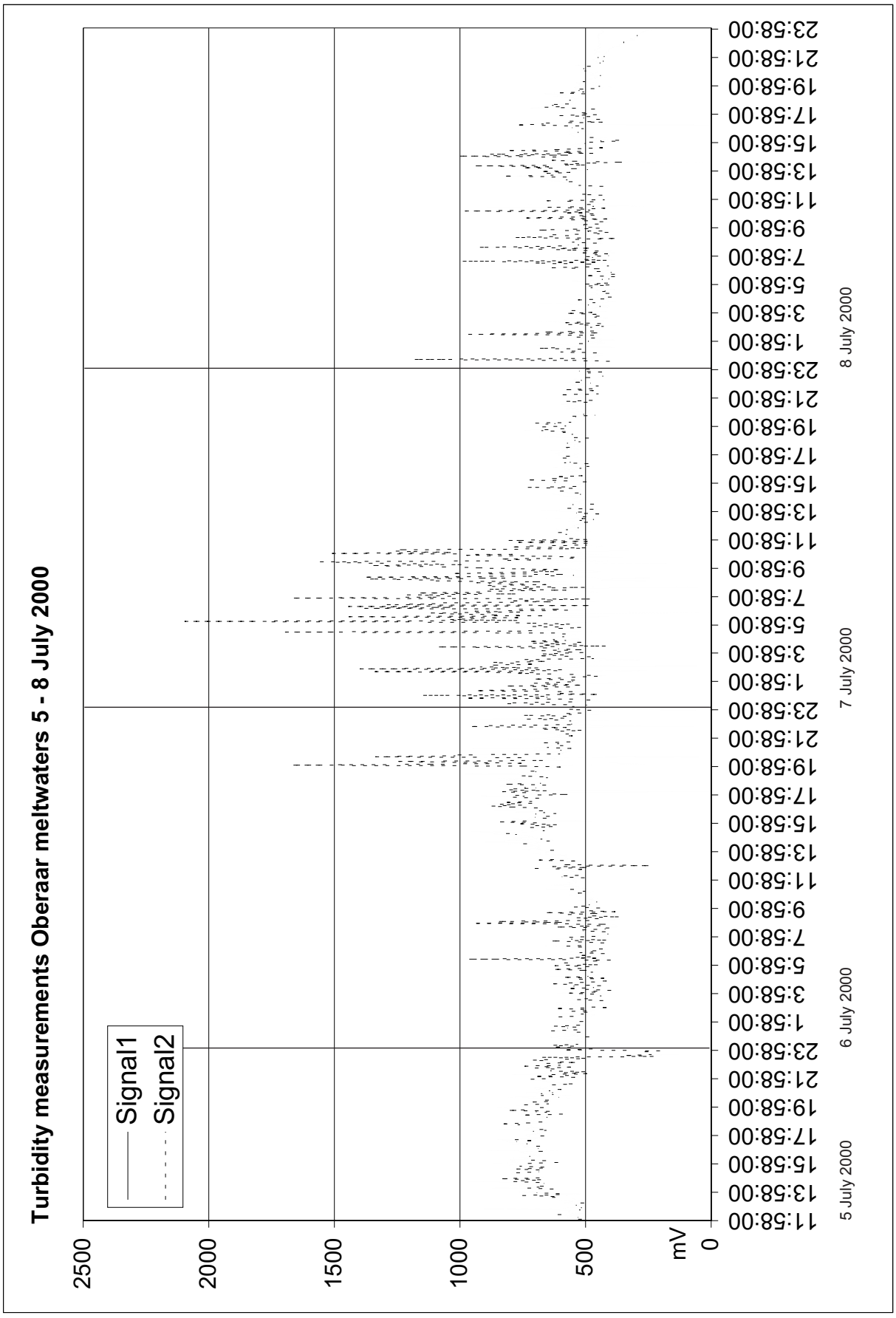
Turbidity measurements Oberaar meltwaters 5 - 8 July 2000
Signal1
Signal2
mV
2500
2000
1500
1000
500
0
11:58:00
13:58:00
15:58:00
17:58:00
19:58:00
21:58:00
23:58:00
1:58:00
3:58:00
5:58:00
7:58:00
9:58:00
11:58:00
13:58:00
15:58:00
17:58:00
19:58:00
21:58:00
23:58:00
1:58:00
3:58:00
5:58:00
7:58:00
9:58:00
11:58:00
13:58:00
15:58:00
17:58:00
19:58:00
21:58:00
23:58:00
1:58:00
3:58:00
5:58:00
7:58:00
9:58:00
11:58:00
13:58:00
15:58:00
17:58:00
19:58:00
21:58:00
23:58:00
5 July 2000
6 July 2000
7 July 2000
8 July 2000

Oberaar adsorbed cation concentrations 1999 - 2001 (mg g^{-1}).

Date	Time	Ca^{2+}	K^{+}	Mg^{2+}
7-Jul-99	15.00	1.314	0.048	0.007
8-Jul-99	10.00	14.413	0.641	0.110
12-Jul-99	10.00	2.215	0.018	0.039
15-Jul-99	10.00	0.655	0.006	0.015
15-Jul-99	17.00	1.780	0.013	0.039
22-Jul-99	10.00	2.033	0.016	0.055
30-Jul-99	10.00	2.176	0.372	0.036
30-Jul-99	17.00	1.723	0.118	0.029
5-Aug-99	10.00	2.606	0.025	0.113
5-Aug-99	17.00	1.888	0.000	0.025
12-Aug-99	10.00	1.216	0.021	0.032
12-Aug-99	17.00	2.343	0.024	0.036
19-Aug-99	17.00	1.161	0.025	0.029
25-Aug-99	10.00	1.312	0.015	0.026
25-Aug-99	17.00	1.616	0.009	0.023
1-Sep-99	10.00	3.074		0.084
1-Sep-99	17.00	2.538		0.051
10-Sep-99	10.00	3.082		0.068
11-Sep-99	17.00	1.037	0.039	0.007
15-Sep-99	10.00	2.146		0.056
15-Sep-99	17.00	2.599		0.057
15-Sep-99	17.00	1.428		0.035
23-Sep-99	17.00	2.412		0.037
30-Sep-99	10.00	1.697		0.036
30-Sep-99	17.00	1.612		0.044
1-Oct-99	12.00	0.830		0.035
4-Oct-99	12.00	2.296		0.022
11-May-00	11.30	0.551	0.057	0.012
14-Jun-00	10.00	1.057	0.069	0.012
14-Jun-00	17.00	1.550	0.054	0.007
29-Jun-00	10.00	1.255	0.069	0.017
29-Jun-00	15.00	0.859	0.050	0.011
29-Jun-00	17.00	0.651	0.032	0.003
29-Jun-00	19.00	0.221	0.028	0.004
29-Jun-00	21.00	1.490	0.084	0.010
29-Jun-00	23.00	1.231	0.087	0.021
30-Jun-00	2.00	1.491	0.121	0.016
30-Jun-00	5.00	1.596	0.098	0.028
30-Jun-00	8.00	1.449	0.073	0.020
30-Jun-00	10.00	0.874	0.069	0.010
30-Jun-00	12.00	1.028	0.073	0.015
30-Jun-00	15.00	0.527	0.040	0.005
18-Jul-00	11.00	1.435	0.400	0.020
18-Jul-00	17.00	0.932	0.243	0.013
20-Jul-00	17.00	0.813	0.046	0.011
20-Aug-00	10.00	1.650	0.077	0.018
20-Aug-00	17.00	1.140	0.042	0.008
10-Sep-00	9.00	1.428	0.077	0.021
10-Sep-00	17.00	0.731	0.027	0.008
21-Sep-00	17.00	0.793	0.073	0.006

APPENDIX 8.2
RHONE

APPENDIX A.2: Rhone data

Ca concentrations from Rhone glacier ablation season 1999-2000 (mg l^{-1}).

Month		**July**			**August**			**September**			**October**				**May**			**June**			**July**			**August**			**September**			**October**	
Day nr.	10	17	**daily**	10	17	**daily**	10	17	**daily**	10	17	**daily**	10	17	**daily**	10	17	**daily**	10	17	**daily**	10	17	**daily**	10	17	**daily**	10	**daily**
1							0.43	0.27	0.35							1.03	0.89	0.96				0.63	0.31	0.47	0.26			0.44	0.44
2				0.26		0.23	0.40	0.22	0.31							1.06													
3				0.40	0.29	0.35	0.38		0.30																				
4				0.39	0.28	0.34					0.75	0.75							0.50	0.58	0.54								
5				0.36	0.25	0.31													0.59	0.49	0.54								
6	0.59	0.60	0.60				0.40	0.28	0.34							0.64	0.71	0.67	0.60	0.38	0.49								
7	0.72	0.65	0.69	0.35	0.26	0.31	0.41	0.26	0.34				1.65		1.65	0.93	0.14	0.53				0.65							
8	0.77	0.65	0.71	0.21	0.39	0.30	0.43	0.23	0.33				1.55		1.55	0.78	0.71	0.74											
9	0.84		0.72																						0.52				
10	0.83	0.60	0.72				0.39	0.21	0.30				1.22		1.22				0.66	0.65	0.66							0.44	0.44
11	0.81	0.56	0.69	0.26	0.31	0.29	0.38	0.22	0.30				1.07		1.07				0.70	0.69	0.70								
12				0.37		0.29										0.81			0.54	0.63	0.58								
13				0.40	0.23	0.32	0.38	0.22	0.30				1.00		1.00				0.79	0.68	0.74								
14				0.43		0.33	0.30	0.36	0.33				1.04		1.04	0.96	0.84	0.90	0.82										
15							0.35		0.19				0.98		0.98	0.78	0.69	0.74											
16							0.52	0.58	0.55				0.93	0.87	0.90													1.33	1.33
17		0.39	0.46	0.44	0.28	0.36		0.23	0.12				0.86		0.86				1.00	0.87	0.94								
18				0.42	0.29	0.36	0.37		0.30		0.86	0.86							0.89	0.69	0.79		0.28	0.33					
19	0.56		0.48		0.31	0.38				0.96	0.94	0.95				0.71	0.44	0.58				0.38			0.49	0.45	0.47		
20	0.52	0.39	0.46				0.34	0.38	0.36	0.78	0.89	0.84				0.58			0.12	0.46	0.29					0.42	0.53		
21	0.51	0.35	0.43				0.54	0.52	0.53	1.13	1.36	1.25				0.22									0.63				
22	0.50	0.35	0.43										1.13		1.13	0.62													
23					0.28								1.31	1.20	1.26														
24	0.61	0.32	0.47		0.30								1.11	1.03	1.07							0.43	0.44	0.43					
25	0.55	0.29	0.42	0.38									0.33	0.90	0.62				0.64	0.46	0.55								
26	0.48	0.29	0.39	0.35												0.74	0.49	0.61											
27	0.33	0.23	0.28		0.22											0.65	0.22	0.44	0.69	0.42	0.55								
28	0.38	0.33	0.36	0.37												0.63	0.43	0.53											
29	0.46	0.37	0.42										1.11	1.00	1.05														
30				0.41	0.25	0.33							1.01	0.44	0.73														
31				0.46	0.28	0.37							1.16	0.99	1.07														
m			**0.51**			**0.32**			**0.33**			**0.93**			**1.07**			**0.67**			**0.61**			**0.41**			**0.50**		**0.74**

Ca concentrations from Rhone glacier accumulation seasons 1999-2001 (mg l^{-1}).

Date	mg l^{-1}
16-Nov-99	1.92
5-Jan-00	2.96
09-Apr-00	4.03
5-Dec-00	2.42
18-Jan-01	2.74
7-Mar-01	3.27
29-Apr-01	4.24

Mean daily Ca concentrations

Month	n	mg l^{-1}	StDev.
January	2	2.9	
Febuary	0		
March	1	3.3	
April	2	4.14	
May	16	1.07	0.26
June	10	0.67	0.17
July	29	0.55	0.16
August	18	0.34	0.06
September	18	0.35	0.11
October	8	0.87	0.33
November	1	1.92	
December	1	2.42	

Seasonal averages

Season	Ablation 10:00 h	Ablation 17:00 h	Accumulation
Average	0.64	0.49	3.08
St.dev.	0.30	0.26	0.84
n	106	82	7

Mg concentrations from Rhone glacier ablation season 1999-2000 (mg l^{-1}).

Month		**July**			**August**			**September**			**October**				**May**			**June**			**July**			**August**			**September**			**October**	
Day nr.	10	17	**daily**	10	17	**daily**	10	17	**daily**	10	17	**daily**	10	17	**daily**	10	17	**daily**	10	17	**daily**	10	17	**daily**	10	17	**daily**	10	**daily**
1							0.05	0.04	0.05							0.06	0.04	0.05				0.06	0.04	0.05	0.05				
2				0.02		0.02	0.04	0.03	0.04							0.07													
3				0.03	0.02	0.03	0.04		0.04																				
4				0.03	0.02	0.03					0.05	0.05							0.06	0.07	0.07								
5				0.02	0.02	0.02													0.06	0.06	0.06								
6	0.05	0.04	0.05				0.05	0.03	0.04							0.04	0.09	0.06	0.06	0.05	0.06								
7	0.06	0.06	0.06	0.02	0.02	0.02	0.04	0.03	0.04				0.16		0.16	0.06		0.06				0.06							
8	0.06	0.06	0.06	0.02	0.37	0.20	0.05	0.03	0.04				0.16		0.16	0.09	0.08	0.09											
9	0.08		0.07																						0.05				
10	0.09	0.05	0.07				0.04	0.03	0.04				0.13		0.13				0.07	0.06	0.06							0.04	0.04
11	0.08	0.05	0.07		0.02	0.02	0.04	0.03	0.04				0.11		0.11				0.07	0.07	0.07								
12				0.02		0.02										0.05			0.07	0.06	0.06								
13				0.02	0.02	0.02	0.04	0.03	0.04				0.11		0.11				0.07	0.06	0.06								
14				0.02		0.02	0.02	0.03	0.03				0.12		0.12	0.08	0.06	0.07	0.07										
15							0.03		0.03				0.10		0.10	0.09	0.06	0.07											
16							0.05	0.07	0.06				0.10	0.09	0.10													0.13	0.13
17		0.03	0.04	0.03	0.02	0.03		0.02	0.01				0.10		0.10				0.09	0.08	0.09								
18				0.02	0.02	0.02	0.03		0.03		0.07	0.07							0.08	0.06	0.07		0.03	0.03					
19	0.11		0.09		0.02	0.02				0.07	0.07	0.07				0.09	0.05	0.07				0.04			0.05	0.04	0.04		
20	0.03	0.02	0.03				0.02	0.04	0.03	0.05	0.06	0.06				0.03			0.01	0.05	0.03					0.05	0.06		
21	0.03	0.02	0.03				0.07	0.06	0.07	0.07	0.09	0.08				0.06									0.07				
22	0.03	0.02	0.03										0.07		0.07	0.08													
23					0.03								0.13	0.08	0.10														
24	0.04	0.03	0.04		0.04								0.08	0.06	0.07							0.05	0.04	0.05					
25	0.04	0.02	0.03	0.04									0.04	0.06	0.05				0.08	0.06	0.07								
26	0.03	0.02	0.03	0.03												0.07	0.06	0.07											
27	0.02	0.02	0.02		0.02											0.08	0.03	0.05	0.08	0.05	0.06								
28	0.03	0.02	0.03	0.03												0.07	0.06	0.06											
29	0.03	0.03	0.03										0.07	0.05	0.06														
30				0.03	0.02	0.03							0.07	0.00	0.03														
31				0.05	0.04	0.05							0.11	0.05	0.08														
m			**0.04**			**0.03**			**0.04**			**0.07**			**0.10**			**0.07**			**0.06**			**0.04**			**0.05**		**0.09**

Mg concentrations from Rhone glacier accumulation seasons 1999-2001 (mg l^{-1}).

Date	mg l^{-1}
16-Nov-99	0.15
5-Jan-00	0.25
09-Apr-00	0.21
5-Dec-00	0.20
18-Jan-01	0.23
7-Mar-01	0.25
29-Apr-01	0.26

Mean daily Mg concentrations

Month	n	mg l^{-1}	StDev.
January	2	0.2	
Febuary	0		
March	1	0.3	
April	2	0.24	
May	16	0.10	0.04
June	10	0.07	0.01
July	29	0.05	0.02
August	18	0.04	0.04
September	18	0.04	0.01
October	7	0.07	0.03
November	1	0.15	
December	1	0.20	

Seasonal averages

Season	Ablation 10:00 h	Ablation 17:00 h	Accumulation
Average	0.06	0.05	0.22
St.dev.	0.03	0.04	0.04
n	104	81	7

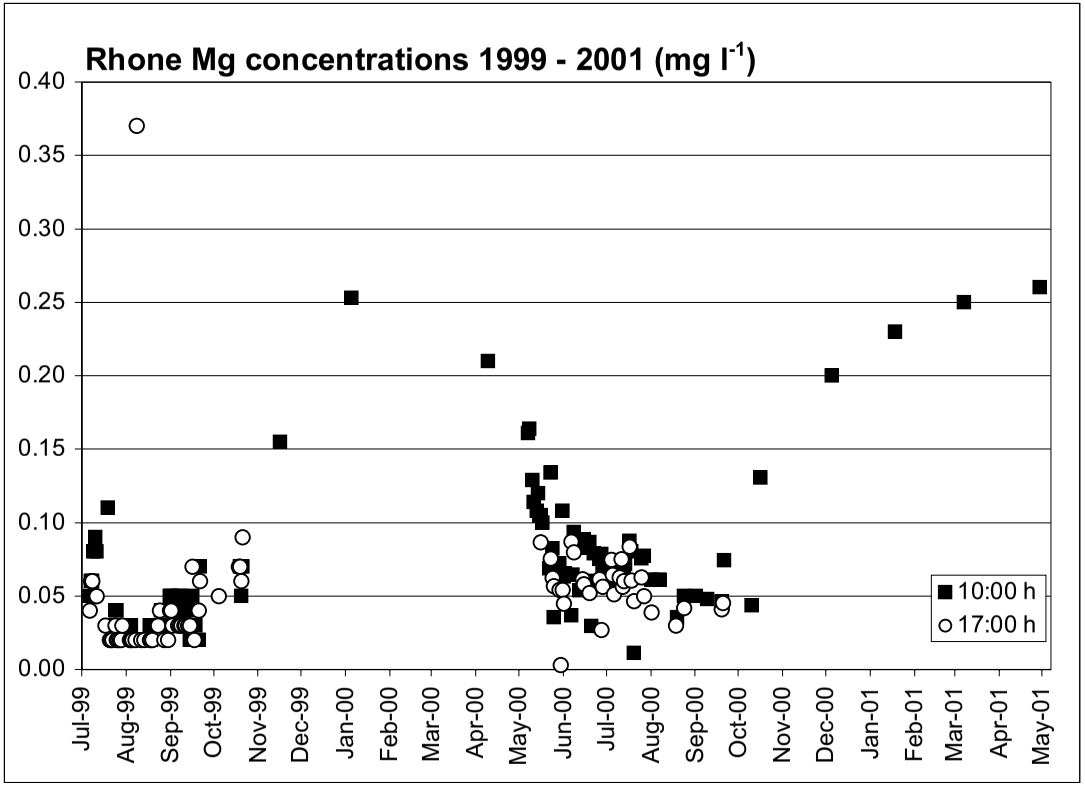

Na concentrations from Rhone glacier ablation season 1999-2000 (mg l^{-1}).

Month		**July**			**August**			**September**			**October**				**May**			**June**			**July**			**August**			**September**			**October**	
Day nr.	10	17	**daily**	10	17	**daily**	10	17	**daily**	10	17	**daily**	10	17	**daily**	10	17	**daily**	10	17	**daily**	10	17	**daily**	10	17	**daily**	10	**daily**
1							0.08	0.09	0.09							0.34	0.29	0.31				0.17	0.10	0.14	0.22				0.00
2				0.11		0.11	0.26	0.03	0.15							0.35													
3				0.10	0.11	0.11	0.03																						
4				0.10	0.09	0.10					0.25	0.25							0.15	0.15	0.15								
5				0.13	0.08	0.11													0.17	0.14	0.15								
6	0.22	0.32	0.27				0.03	0.03	0.03							0.24	0.26	0.25	0.18	0.12	0.15								
7	0.34	0.32	0.33	0.14	0.11	0.12	0.08	0.03	0.06				0.54		0.54	0.39	0.05	0.22				0.18							
8	0.29	0.22	0.26	0.05	0.12	0.09	0.08	0.03	0.06				0.50		0.50	0.27	0.25	0.26											
9	0.35		0.34																						0.15				
10	0.27	0.30	0.29				0.09	0.02	0.06				0.42		0.42				0.17	0.19	0.18							0.11	0.11
11	0.25	0.21	0.23		0.09	0.11	0.07	0.09	0.08				0.36		0.36				0.21	0.20	0.20								
12				0.12		0.12										0.28			0.31	0.17	0.24								
13				0.11	0.11	0.11	0.08	0.05	0.07				0.34		0.34				0.21	0.30	0.25								
14				0.16		0.14	0.08	0.03	0.06				0.35		0.35	0.39	0.31	0.35	0.22										
15							0.17						0.32		0.32	0.29	0.23	0.26											
16							0.32	0.27	0.30				0.28	0.26	0.27													0.36	0.36
17		0.11	0.12	0.17	0.10	0.14		0.14					0.25		0.25				0.26	0.25	0.26								
18				0.14	0.09	0.12	0.13				0.28	0.28							0.24	0.20	0.22		0.10	0.10					
19	0.19		0.15		0.07	0.11				0.33	0.34	0.33				0.21	0.14	0.17				0.09			0.14	0.14	0.14		
20	0.16	0.12	0.14				0.13	0.23	0.18	0.27	0.27	0.27				0.17	0.18	0.17	0.03	0.15	0.09					0.14	0.17		
21	0.14	0.10	0.12				0.32	0.33	0.33	0.35	0.33	0.34				0.10									0.20				
22	0.13	0.11	0.12										0.39		0.39	0.18													
23					0.03								0.43	0.44	0.44														
24	0.18	0.08	0.13		0.03								0.42	0.35	0.39							0.13	0.15	0.14					
25	0.13	0.10	0.12	0.07									0.13	0.30	0.22				0.23	0.16	0.20								
26	0.15	0.10	0.13	0.13												0.20	0.14	0.17											
27	0.15	0.06	0.11		0.07											0.18	0.12	0.15	0.23	0.11	0.17								
28	0.13	0.12	0.13	0.13												0.19	0.14	0.16											
29	0.15	0.10	0.12										0.34	0.31	0.33														
30				0.12	0.13	0.13							0.33	0.14	0.24														
31				0.17	0.13	0.15							0.34	0.31	0.33														
m			**0.18**			**0.12**			**0.12**			**0.30**			**0.35**			**0.23**			**0.19**			**0.13**			**0.16**		**0.16**

Na concentrations from Rhone glacier accumulation seasons 1999-2001 (mg l^{-1}).

Date	mg l^{-1}
16-Nov-99	0.60
5-Jan-00	1.02
09-Apr-00	0.86
5-Dec-00	0.81
18-Jan-01	1.16
7-Mar-01	1.10
29-Apr-01	0.99

Mean daily Na concentrations

Month	n	mg l^{-1}	StDev.
January	2	1.09	
Febuary	0		
March	1	1.10	
April	2	0.93	
May	16	0.35	0.09
June	11	0.23	0.07
July	29	0.18	0.07
August	18	0.12	0.02
September	14	0.12	0.09
October	8	0.24	0.13
November	1	0.60	
December	1	0.81	

Seasonal averages

Season	Ablation 10:00 h	Ablation 17:00 h	Accumulation
Average	0.21	0.16	0.93
St.dev.	0.11	0.10	0.19
n	104	83	7

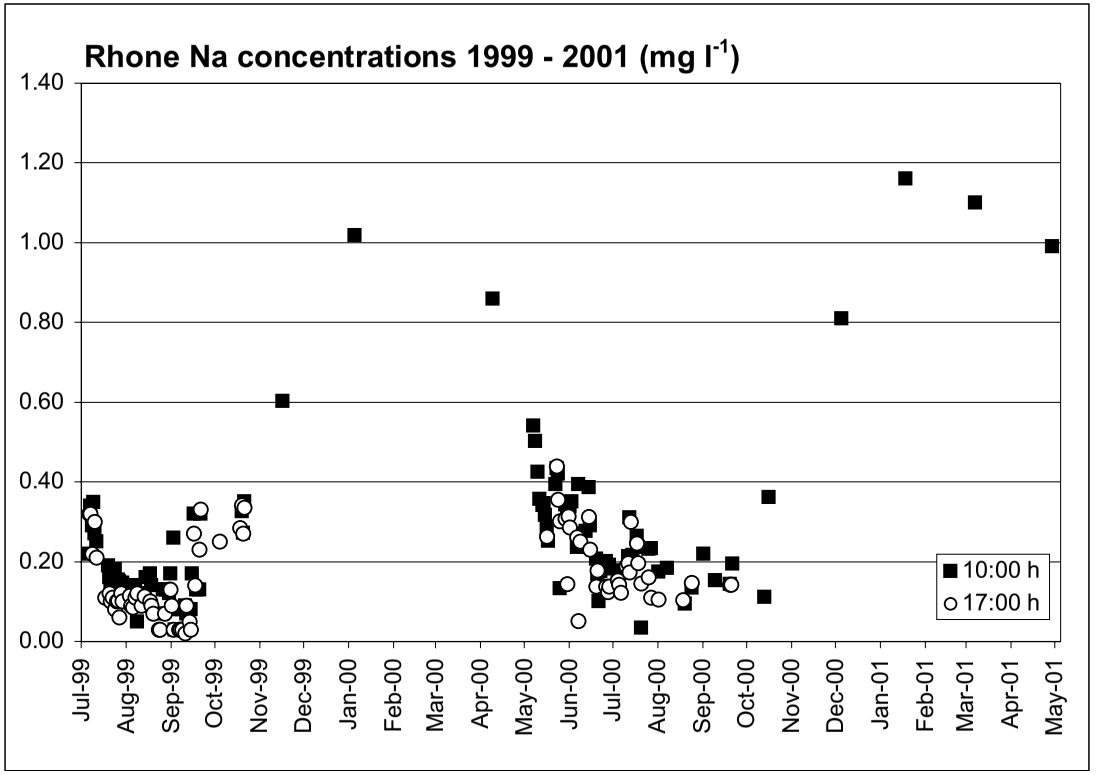

K concentrations from Rhone glacier ablation season 1999-2000 (mg l^{-1}).

Month		**July**			**August**			**September**			**October**				**May**			**June**			**July**			**August**			**September**			**October**	
Day nr.	10	17	**daily**	10	17	**daily**	10	17	**daily**	10	17	**daily**	10	17	**daily**	10	17	**daily**	10	17	**daily**	10	17	**daily**	10	17	**daily**	10	**daily**
1							0.21	0.15	0.18							0.57	0.49	0.53				0.36	0.17	0.26	0.26				
2				0.19		0.19	0.17	0.13	0.15							0.58													
3				0.24	0.17	0.21	0.21																						
4				0.25	0.18	0.22					0.42	0.42							0.28	0.28	0.28								
5				0.21	0.18	0.20													0.41	0.28	0.35								
6	0.40	0.42	0.27				0.21	0.16	0.19							0.50	0.56	0.53	0.35	0.21	0.28								
7	0.48	0.43	0.33	0.24	0.22	0.23	0.22	0.16	0.19				0.79		0.79	0.84	0.12	0.48				0.30							
8	0.51	0.42	0.26	0.16	0.64	0.40	0.23	0.15	0.19				0.79		0.79	0.59	0.50	0.55											
9	0.52		0.34																						0.30				
10	0.52	0.39	0.29				0.22	0.14	0.18				0.67		0.42				0.26	0.36	0.31							0.26	0.26
11	0.41	0.33	0.23		0.19	0.26	0.21	0.14	0.18				0.57		0.57				0.33	0.37	0.35								
12				0.31		0.24										0.59			0.32	0.25	0.28								
13				0.21	0.14	0.18	0.21	0.12	0.17				0.60		0.60				0.31	0.32	0.32								
14				0.19		0.15	0.18	0.14	0.16				0.60		0.60	0.95	0.76	0.86	0.32										
15							0.22						0.55		0.55	0.60	0.51	0.56											
16							0.61	0.46	0.54				0.50	0.46	0.48													0.74	0.74
17		0.28	0.12	0.24	0.16	0.20		0.15					0.45		0.45				0.48	0.34	0.41								
18				0.26	0.20	0.23	0.20				0.45	0.45							0.37	0.29	0.33		0.17	0.20					
19	0.44		0.15		0.17					0.48	0.46	0.47				0.39	0.24	0.32				0.23			0.29	0.40	0.34		
20	0.33	0.29	0.14				0.22	0.48	0.35	0.40	0.47	0.44				0.35	0.25	0.30	0.05	0.22	0.14					0.23	0.29		
21	0.32	0.24	0.12				0.71	0.68	0.70	0.52	0.59	0.56				0.20									0.35				
22	0.42	0.22	0.12										0.68		0.68	0.33													
23					0.14								0.76	0.77	0.76														
24	0.34	0.23	0.13		0.17								0.72	0.63	0.67							0.24	0.22	0.23					
25	0.38	0.19	0.12	0.24									0.10	0.54	0.32				0.51	0.34	0.42								
26	0.30	0.18	0.13	0.28												0.33	0.22	0.28											
27	0.19	0.20	0.11		0.24											0.31	0.13	0.22	0.46	0.30	0.38								
28	0.24	0.23	0.13	0.23												0.34	0.20	0.27											
29	0.28	0.27	0.12										0.60	0.53	0.57														
30				0.21	0.21	0.21							0.56	0.26	0.41														
31				0.25	0.15	0.20							0.57	0.53	0.55														
m			**0.18**			**0.22**			**0.26**			**0.48**			**0.58**			**0.44**			**0.32**			**0.23**			**0.32**		**0.50**

K concentrations from Rhone glacier accumulation seasons 1999-2001 (mg l^{-1}).

Date	mg l^{-1}
16-Nov-99	0.81
5-Jan-00	1.28
09-Apr-00	1.25
5-Dec-00	1.04
18-Jan-01	1.32
7-Mar-01	1.37
29-Apr-01	1.34

Mean daily K concentrations

Month	n	mg l^{-1}	StDev.
January	2	1.3	
Febuary	0		
March	1	1.4	
April	2	1.30	
May	16	0.58	0.14
June	11	0.44	0.19
July	29	0.24	0.10
August	17	0.22	0.05
September	14	0.27	0.16
October	8	0.42	0.21
November	1	0.81	
December	1	1.04	

Seasonal averages

Season	Ablation 10:00 h	Ablation 17:00 h	Accumulation
Average	0.38	0.31	1.20
St.dev.	0.18	0.16	0.20
n	104	83	7

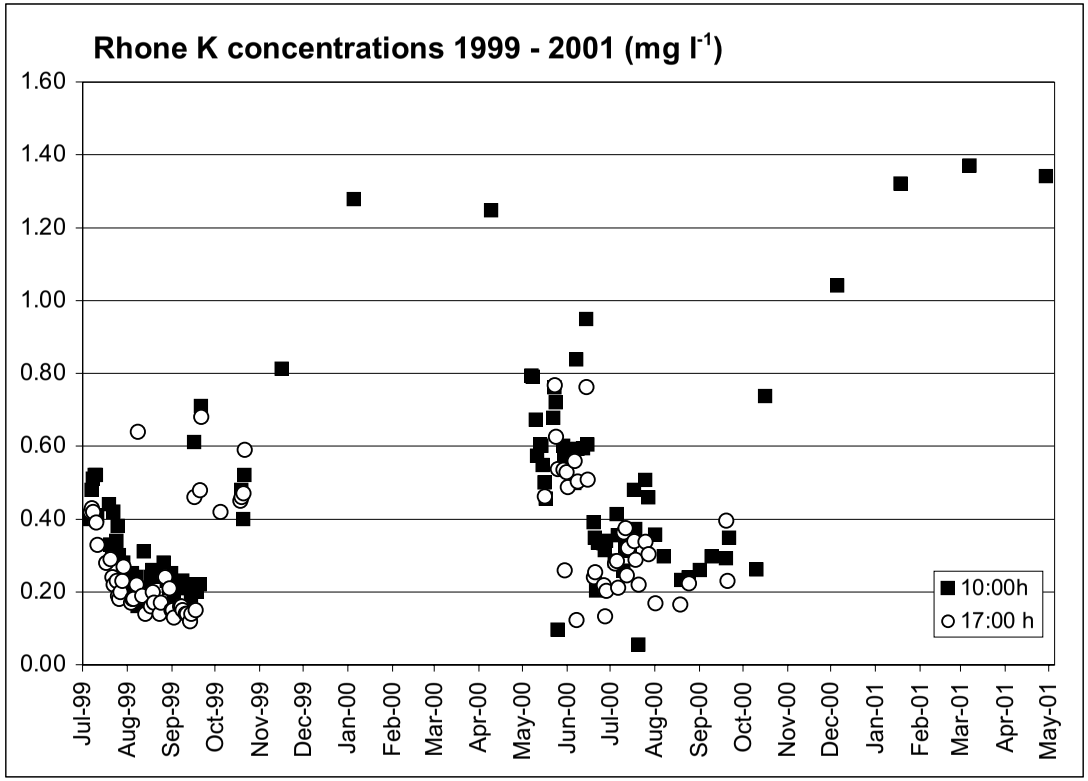

Cl concentrations from Rhone glacier ablation season 1999-2000 (mg l^{-1}).

Month		**July**			**August**			**September**			**October**				**May**			**June**			**July**			**August**			**September**			**October**	
Day nr.	10	17	**daily**	10	17	**daily**	10	17	**daily**	10	17	**daily**	10	17	**daily**	10	17	**daily**	10	17	**daily**	10	17	**daily**	10	17	**daily**	10	**daily**
1							0.06	0.06	0.06							0.11	0.10	0.11				0.09	0.10	0.10	0.09				0.00
2				0.08	0.04	0.06	0.05	0.03	0.04	0.08																			
3				0.06	0.04	0.05	0.10	0.04	0.07																				
4				0.07	0.08	0.08					0.06	0.06							0.08	0.10	0.09								
5				0.03	0.06	0.05													0.08	0.10	0.09								
6	0.07	0.07	0.07				0.05	0.05	0.05							0.09	0.10	0.10	0.11	0.08	0.10								
7	0.08	0.07	0.08	0.05	0.07	0.06		0.04					0.12		0.12	0.12	0.11	0.12				0.07	0.03	0.05					
8	0.09	0.07	0.08	0.04	0.03	0.04	0.06	0.04	0.05				0.17		0.17	0.10	0.09	0.10											
9	0.09																								0.05				
10	0.11	0.08	0.10	0.06	0.05	0.06	0.05	0.04	0.05				0.20		0.20				0.04	0.08	0.06								
11	0.08	0.06	0.07	0.12	0.06	0.09	0.05	0.05	0.05				0.12		0.12	0.09	0.09	0.09	0.09	0.08	0.09								
12				0.14												0.10	0.09	0.10	0.09	0.10	0.10								
13				0.05	0.03	0.04	0.04	0.04	0.04				0.13		0.13	0.09	0.10	0.10	0.05	0.12	0.09								
14				0.05			0.04	0.04	0.04				0.17		0.17	0.09	0.09	0.09											
15							0.08						0.15		0.15	0.08	0.08	0.08											
16							0.05	0.04	0.05				0.13	0.13	0.13													0.08	0.08
17		0.10		0.07	0.04	0.06		0.04					0.10		0.10				0.18	0.11	0.15								
18				0.07	0.03	0.05					0.08	0.08					0.08		0.06	0.08	0.07	0.04	0.03	0.04					
19	0.06				0.03					0.08	0.14	0.11				0.08	0.06	0.07				0.04			0.06				
20	0.10	0.10	0.10				0.07	0.05	0.06	0.07	0.10	0.09				0.08	0.06	0.07	0.11	0.05	0.08					0.10	0.08		
21	0.09	0.08	0.09				0.09	0.07	0.08	0.13		0.07				0.08	0.05	0.07							0.09		0.09		
22	0.10	0.09	0.10		0.07								0.14		0.14	0.09	0.06	0.08											
23					0.04								0.14	0.14	0.14														
24	0.11	0.07	0.09		0.04								0.11	0.12	0.12							0.07							
25	0.08	0.05	0.07	0.06									0.12	0.11	0.12				0.06	0.05	0.06								
26	0.07	0.03	0.05	0.05	0.05	0.05										0.09	0.07	0.08											
27	0.08	0.06	0.07		0.08	0.09										0.10	0.06	0.08	0.08	0.11	0.10								
28	0.05	0.04	0.05	0.09												0.09	0.10	0.10											
29	0.06	0.04	0.05										0.12	0.11	0.12	0.09	0.07	0.08											
30				0.07	0.11	0.09							0.11	0.10	0.11														
31				0.08									0.10	0.09	0.10														
m			**0.07**			**0.06**			**0.05**			**0.10**			**0.13**			**0.09**			**0.09**			**0.06**			**0.09**		**0.04**

Cl concentrations from Rhone glacier accumulation seasons 1999-2001 (mg l^{-1}).

Date	mg l^{-1}
16-Nov-99	0.12
5-Jan-00	0.14
09-Apr-00	0.08
5-Dec-00	0.18
18-Jan-01	0.23
7-Mar-01	
29-Apr-01	0.16

Mean daily Cl concentrations

Month	n	mg l^{-1}	StDev.
January	2	0.2	
Febuary	0		
March	1		
April	2	0.12	
May	16	0.13	0.03
June	17	0.09	0.01
July	26	0.08	0.02
August	17	0.06	0.02
September	14	0.06	0.02
October	7	0.07	0.03
November	1	0.12	
December	1	0.18	

Seasonal averages

Season	Ablation 10:00 h	Ablation 17:00 h	Accumulation
Average	0.09	0.07	0.15
St.dev.	0.03	0.03	0.05
n	106	92	6

NO_3 concentrations from Rhone glacier ablation season 1999-2000 (mg l^{-1}).

Month		**July**			**August**			**September**			**October**				**May**			**June**			**July**			**August**			**September**			**October**	
Day nr.	10	17	**daily**	10	17	**daily**	10	17	**daily**	10	17	**daily**		10	17	**daily**	10	17	**daily**	10	17	**daily**	10	17	**daily**	10	17	**daily**	10	**daily**
1							0.52	0.27	0.40								1.21	1.01	1.11				0.91	0.86	0.89	0.47				
2								0.25		0.81																				
3				0.66	0.45	0.56		0.45																						
4				0.66	0.47	0.57					0.82	0.82								0.80	0.65	0.73								
5				0.42	0.35	0.39														0.80	0.86	0.83								
6	1.07	1.00	1.04				0.46	0.30	0.38								1.04	1.10	1.07	0.89	0.67	0.78								
7	1.16	1.05	1.11	0.56	0.41	0.49		0.25						1.04		1.04	1.24	1.11	1.18				0.62	0.34	0.48					
8	1.28	1.06	1.17	0.52	0.43	0.48	0.47	0.24	0.36					1.59		1.59	1.17	1.04	1.11											
9	1.33																									0.51				
10	1.30	0.91	1.11	0.45	0.38	0.42	0.46	0.21	0.34					1.30		1.30				0.35	0.83	0.59								
11	1.17	0.85	1.01	0.52	0.43	0.48	0.44	0.21	0.33					1.36		1.36	0.89	0.90	0.90	0.27	0.88	0.58								
12				0.60													1.06	0.70	0.88	0.80	0.91	0.86								
13				0.66	0.40	0.53	0.43							1.18		1.18	0.87	0.97	0.92	0.59	0.88	0.74								
14				0.67			0.42	0.24	0.33					1.38		1.38	0.90	1.15	1.03											
15							0.44							1.25		1.25	0.90	0.86	0.88											
16							0.43	0.27	0.35					1.17	1.09	1.13													1.02	1.02
17		0.62		0.58	0.36	0.47		0.40						0.91		0.91				1.06	0.98	1.02								
18				0.54	0.36	0.45					0.71	0.71						0.73		0.72	0.75	0.74	0.49	0.32	0.41					
19	0.93				0.39					0.80	0.78	0.79					0.88	0.65	0.77				0.49			0.51				
20	0.87	0.61	0.74				0.35	0.33	0.34	0.63	0.72	0.68					0.94	0.56	0.75	1.00	0.48	0.74					0.48	0.49		
21	0.84	0.54	0.69				0.49	0.54	0.52	0.98		0.98					0.90	0.54	0.72							0.62		0.55		
22	0.78	0.54	0.66		0.30									1.39		1.39	0.86	0.60	0.73											
23					0.30									1.52	1.33	1.43														
24	0.98	0.54	0.76		0.36									1.09	1.17	1.13							0.64							
25	0.88	0.51	0.70	0.50										1.21	1.10	1.16				0.49	0.43	0.46								
26	0.81	0.44	0.63	0.47	0.41	0.44											0.87	0.62	0.75											
27	0.64	0.39	0.52		0.30	0.45											0.96	0.54	0.75	0.88	1.05	0.97								
28	0.60	0.58	0.59	0.60													0.84	0.67	0.76											
29	0.73	0.49	0.61											1.35	1.11	1.23	0.81	0.56	0.69											
30				0.58	0.32	0.45								1.32	1.13	1.23														
31				0.55										1.06	0.94	1.00														
m			**0.81**			**0.47**			**0.37**			**0.76**				**1.23**			**0.88**			**0.75**			**0.59**			**0.52**		**1.02**

NO_3 concentrations from Rhone glacier accumulation seasons 1999-2001 (mg l^{-1}).

Date	mg l^{-1}
16-Nov-99	1.09
5-Jan-00	1.38
09-Apr-00	0.62
5-Dec-00	1.24
18-Jan-01	1.28
7-Mar-01	
29-Apr-01	1.33

Mean daily NO_3 concentrations

Month	n	mg l^{-1}	StDev.
January	2	1.3	
Febuary	0		
March	0		
April	2	0.98	
May	16	1.23	0.17
June	17	0.88	0.16
July	26	0.78	0.20
August	16	0.49	0.12
September	11	0.40	0.08
October	6	0.83	0.14
November	1	1.09	
December	1	1.24	

Seasonal averages

Season	Ablation 10:00 h	Ablation 17:00 h	Accumulation
Average	0.82	0.63	1.16
St.dev.	0.31	0.29	0.28
n	103	90	6

SO_4 concentrations from Rhone glacier ablation season 1999-2000 (mg l^{-1}).

Month		**July**			**August**			**September**			**October**				**May**			**June**			**July**			**August**			**September**			**October**	
Day nr.	10	17	**daily**	10	17	**daily**	10	17	**daily**	10	17	**daily**	10	17	**daily**	10	17	**daily**	10	17	**daily**	10	17	**daily**	10	17	**daily**	10	**daily**
1							0.50	0.26	0.38							1.08	0.92	1.00				0.67	0.80	0.74	0.46				
2				0.58	0.34	0.46		0.24		0.86																			
3				0.54	0.38	0.46		0.45																					
4				0.54	0.39	0.47					0.98	0.98							0.58	0.62	0.60								
5				0.34	0.29	0.32													0.44	0.88	0.66								
6	0.97	0.84	0.91				0.45	0.30	0.38							0.72	0.77	0.75	0.81	0.65	0.73								
7	0.94	0.86	0.90	0.47	0.36	0.42		0.25					2.86		2.86	0.88	0.84	0.86				0.38	0.33	0.36					
8	1.02	0.85	0.94	0.46	0.37	0.42	0.44	0.21	0.33				1.86		1.86	0.90	0.83	0.87											
9	1.11																								0.54				
10	1.12	0.77	0.95	0.40	0.33	0.37	0.43	0.20	0.32				2.48		2.48				0.50	0.72	0.61								
11	0.92	0.68	0.80	0.45	0.38	0.42	0.39	0.20	0.30				1.47		1.47	0.82	0.81	0.82	0.50	0.84	0.67								
12				0.50												0.94	0.63	0.79	0.69	0.88	0.79								
13				0.53	0.32	0.43	0.41						0.88		0.88	0.82	0.98	0.90	0.50	0.82	0.66								
14				0.58			0.41	0.21	0.31				1.05		1.05	0.90	1.35	1.13											
15							0.43						0.92		0.92	0.90	0.79	0.85											
16							0.44	0.27	0.36				0.85	0.82	0.84													1.43	1.43
17		0.53		0.51	0.31	0.41		0.40					0.62		0.62				1.10	1.02	1.06								
18				0.48	0.33	0.41					0.97	0.97					0.61		0.70	0.71	0.71	0.40	0.27	0.34					
19	0.74				0.35					1.18	1.14	1.16				0.68	0.54	0.61				0.40			0.50				
20	0.69	0.50	0.60				0.50	0.40	0.45	0.90	1.08	0.99				0.73	0.44	0.59	1.03	0.44	0.74					0.61	0.55		
21	0.67	0.45	0.56				0.58	0.58	0.58	1.41		0.71				0.70	0.42	0.56							0.65		0.63		
22	0.62	0.45	0.54		0.28								1.12		1.12	0.67	0.47	0.57											
23					0.27								1.26	1.18	1.22														
24	0.82	0.47	0.65		0.36								0.92	1.02	0.97							0.59							
25	0.70	0.41	0.56	0.48									0.97	0.89	0.93				0.40	0.25	0.33								
26	0.60	0.34	0.47	0.47	0.40	0.44										0.73	0.54	0.64											
27	0.47	0.30	0.39		0.29	0.40										0.82	0.47	0.65	0.79	1.02	0.91								
28	0.44	0.42	0.43	0.50												0.86	0.64	0.75											
29	0.57	0.39	0.48										1.06	0.90	0.98	0.76	0.53	0.65											
30				0.56	0.31	0.44							1.11	0.93	1.02														
31				0.53									0.92	0.83	0.88														
m			**0.65**			**0.42**			**0.38**			**1.04**			**1.26**			**0.76**			**0.70**			**0.48**			**0.59**		**1.43**

SO_4 concentrations from Rhone glacier accumulation seasons 1999-2001 (mg l^{-1}).

Date	mg l^{-1}
16-Nov-99	2.18
5-Jan-00	4.73
09-Apr-00	6.00
5-Dec-00	2.86
18-Jan-01	3.90
7-Mar-01	
29-Apr-01	3.19

Mean daily SO_4 concentrations

Month	n	mg l^{-1}	StDev.
January	2	4.3	
Febuary	0		
March	0		
April	2	4.60	
May	16	1.26	0.62
June	17	0.76	0.16
July	26	0.68	0.19
August	17	0.43	0.09
September	11	0.42	0.12
October	6	1.04	0.24
November	1	2.18	
December	1	2.86	

Seasonal averages

Season	Ablation 10:00 h	Ablation 17:00 h	Accumulation
Average	0.76	0.58	3.81
St.dev.	0.39	0.28	1.39
n	104	91	6

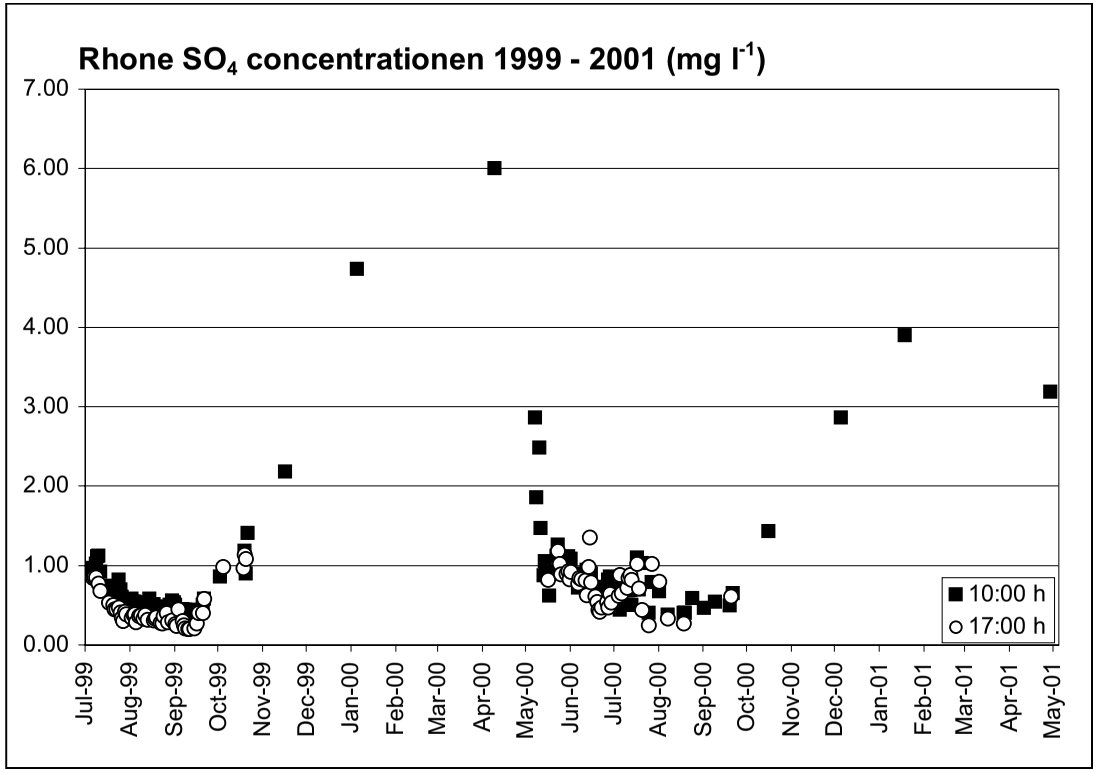

***HCO_3 concentrations from Rhone glacier ablation season 1999-2000 (mg l^{-1}).**

Month		**July**			**August**			**September**			**October**				**May**			**June**			**July**			**August**			**September**			**October**	
Day nr.	10	17	**daily**	10	17	**daily**	10	17	**daily**	10	17	**daily**	10	17	**daily**	10	17	**daily**	10	17	**daily**	10	17	**daily**	10	17	**daily**	10	**daily**
1							1.18	1.24	1.21							2.91	2.48	2.69				1.65			0.96				
2				0.68				1.01																					
3				0.70	0.69	0.70																							
4				0.62	0.43	0.53					2.40	2.40							1.54	1.63	1.59								
5				1.04	0.60	0.82													1.97	0.98	1.47								
6	1.27	1.78	1.53				1.13	0.89	1.01							1.86	2.28	2.07	1.44	0.83	1.13								
7	2.03	2.26	2.15	0.81	0.63	0.72		0.89					4.08		4.08	3.35						2.41							
8	1.76	1.64	1.70	0.18			1.17	0.83	1.00				4.44		4.44	2.33	2.05	2.19											
9	2.10																								1.71				
10	2.57	1.92	2.25				1.10	0.86	0.98				2.03		2.03				2.64	1.91	2.28								
11	1.94	1.73	1.83		0.66		1.14	1.01	1.07				2.60		2.60				2.85	1.83	2.34								
12																2.28			1.69	1.08	1.39								
13							1.23	1.37	1.30				3.21		3.21														
14							0.80	1.27	1.04				2.93		2.93	3.77	2.06	2.91											
15							1.42						3.11		3.11	2.57	2.21	2.39											
16							3.04	4.22	3.63				2.99	2.40	2.70													4.38	4.38
17		1.51		1.59	0.73	1.16		0.79					3.16		3.16				2.51	2.15	2.33								
18				1.16	0.80	0.98					2.99	2.99							2.87	1.83	2.35		1.09	1.08					
19					0.66					2.99	3.19	3.09				2.67	1.28	1.98				1.06			1.50				
20	1.19	0.93	1.06				1.37	2.29	1.83	2.67	2.65	2.66				1.40		0.70		1.46						1.06	1.28		
21	1.14	1.08	1.11				3.09	2.74	2.91	3.05															2.14		1.60		
22	1.32	0.74	1.03										3.35		3.35	1.86		0.93											
23					0.68								4.23	3.71	3.97														
24	1.02	0.90	0.96		0.80								4.33	3.19	3.76							0.97							
25	1.32	0.59	0.95											2.58					2.97	2.14	2.55								
26	1.08	0.86	0.97													2.21	1.49	1.85											
27	0.60	0.47	0.54		0.90	0.93										1.66	1.12	1.39	2.21										
28	0.89	0.75	0.82	0.95												1.22													
29	0.93	1.05	0.99										3.23	2.89	3.06														
30				1.15	1.31	1.23							2.80																
31				1.45									3.98	3.22	3.60														
m			**1.28**			**0.88**			**1.60**			**2.81**			**3.29**			**1.91**			**1.94**			**1.08**			**1.44**		**4.38**

***HCO_3 concentrations from Rhone glacier accumulation seasons 1999-2001 (mg l^{-1}).**

Date	mg l^{-1}
16-Nov-99	5.98
5-Jan-00	8.53
09-Apr-00	9.70
5-Dec-00	7.55
18-Jan-01	8.26
7-Mar-01	
29-Apr-01	13.56

Mean daily *HCO_3 concentrations

Month	n	mg l^{-1}	StDev.
January	2	8.4	
Febuary	0		
March	1		
April	2	11.63	
May	14	3.29	0.64
June	10	1.91	0.72
July	23	1.54	0.61
August	9	0.90	0.23
September	12	1.57	0.85
October	5	3.10	0.76
November	1	5.98	
December	1	7.55	

Seasonal averages

Season	Ablation 10:00 h	Ablation 17:00 h	Accumulation
Average	2.03	1.55	8.93
St.dev.	1.03	0.87	2.58
n	87	70	6

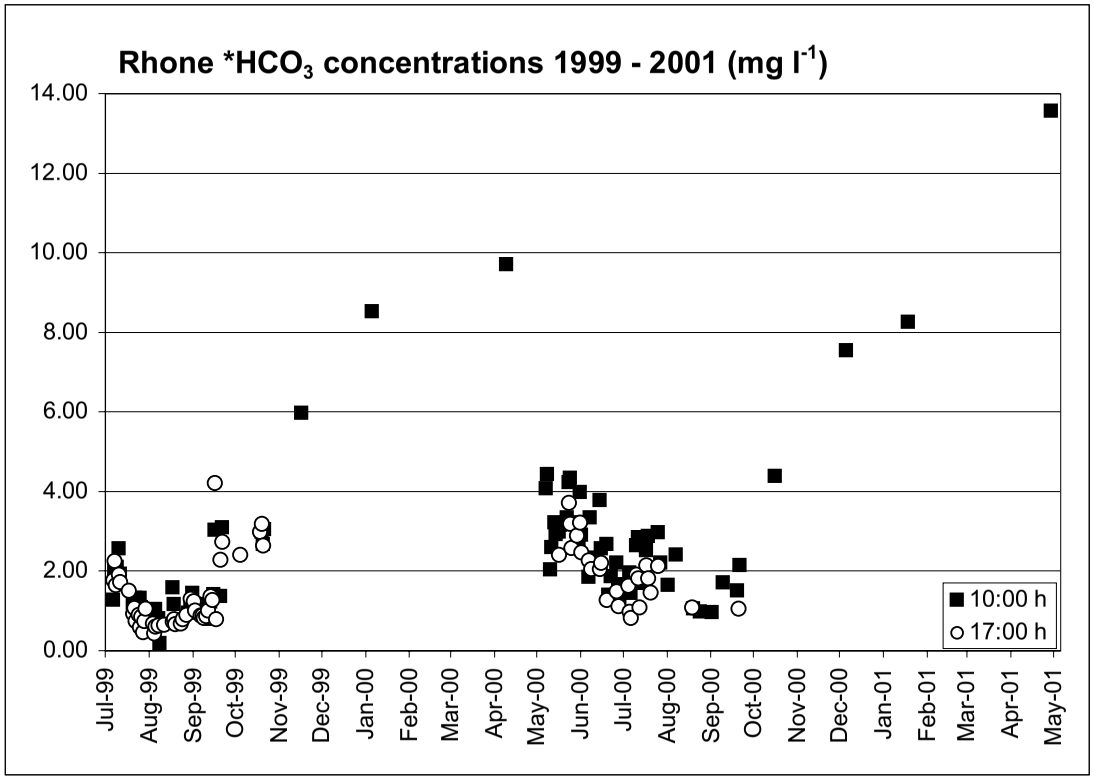

Soluble reactive phosphate (SRP) concentrations from Rhone glacier ablation season 1999-2000 (µg l^{-1}).

Month		**July**			**August**			**September**			**October**			**May**			**June**			**July**			**August**			**September**			**October**	
Day nr.	10	17	**daily**	10	17	**daily**	10	17	**daily**	10	17	**daily**	10	17	**daily**	10	17	**daily**	10	17	**daily**	10	17	**daily**	10	17	**daily**	10	**daily**
1																2.60	2.20	2.40				5.20	6.10		5.90		5.90		
2																												3.80	3.80
3																													
4																			7.20	4.00	5.60								
5				2.90	4.60	3.75													5.80	4.60	5.20								
6																			4.20	4.50	4.35								
7																6.10	16.60	11.35				3.50	3.50	3.50					
8																4.90	4.20	4.55											
9																									1.60		1.60		
10																													
11													7.50		7.50														
12				2.70	4.60	3.65													4.00	3.80	3.90								
13																			3.80	3.60	3.70								
14																5.50	4.80	5.15											
15																5.40	5.40	5.40											
16																												8.60	8.60
17													7.30		7.30														
18																			5.40	5.40	5.40		6.70	6.40					
19					2.90	2.90																6.10			6.00	5.70	5.85		
20																			6.10	6.10	6.10					5.70	5.70		
21																5.40	6.90	6.15							5.90		5.90		
22										1.30		1.30				6.70	6.10	6.40											
23																													
24																						5.70		5.40					
25													3.20	3.00	3.10				4.00	4.00	4.00								
26																													
27																			3.80	4.40	4.10								
28																4.70	4.70	4.70											
29	6.90	5.70	6.30													4.70	3.20	3.95											
30																													
31																							4.20	4.20					
m			**6.30**			**3.43**						**1.30**			**5.97**			**5.56**			**4.71**			**4.88**			**4.99**		**6.20**

SRP concentrations from Rhone glacier accumulation seasons 1999-2001 (µg l^{-1}).

Date	µg l^{-1}
16-Nov-99	2.70
5-Jan-00	11.20
09-Apr-00	10.40
5-Dec-00	13.30
18-Jan-01	7.80
7-Mar-01	3.80
29-Apr-01	

Mean daily SRP concentrations

Month	n	µg l^{-1}	StDev.
January	2	9.5	
Febuary	0		
March	1	3.8	
April	1	10.40	
May	3	5.97	2.48
June	9	5.56	2.48
July	10	4.87	0.97
August	7	4.26	1.22
September	5	4.99	1.90
October	3	4.57	3.71
November	1	2.70	
December	1	13.30	

Seasonal averages

Season	Ablation 10:00 h	Ablation 17:00 h	Accumulation
Average	4.98	5.08	8.20
St.dev.	1.69	2.51	4.23
n	35	29	6

Si concentrations from Rhone glacier ablation season 1999-2000 (mg l^{-1}).

Month		**July**			**August**			**September**			**October**			**May**			**June**			**July**			**August**			**September**			**October**	
Day nr.	10	17	**daily**	10	17	**daily**	10	17	**daily**	10	17	**daily**	10	17	**daily**	10	17	**daily**	10	17	**daily**	10	17	**daily**	10	17	**daily**	10	**daily**
1							0.22															0.30	0.13	0.21	0.07				
2							0.11	0.08	0.09																				
3				0.19	0.10	0.15	0.22																						
4				0.21	0.15	0.18				0.51	0.46	0.49							0.25	0.05	0.15								
5				0.19	0.14	0.17										0.20			0.10	0.32	0.21								
6		0.27	0.27				0.20	0.11	0.16							0.13	0.45	0.29	0.09										
7	0.28	0.26	0.27	0.15	0.12	0.13		0.16					0.34		0.34		0.30					0.33	0.12	0.23					
8	0.31	0.27	0.29	0.15			0.20	0.10	0.15				0.35		0.35	0.09	0.35	0.22											
9	0.32	0.35	0.33																						0.22				
10	0.35	0.26	0.30				0.20	0.08	0.14				0.23		0.23				0.25	0.20	0.22							0.73	0.73
11	0.21	0.28	0.24	0.12	0.12	0.12	0.20	0.11	0.15				0.41		0.41	0.13	0.30	0.21	0.30	0.13	0.22								
12				0.15												0.09	0.20	0.15	0.34	0.16	0.25								
13				0.15			0.19	0.13	0.16				0.29		0.29	0.19	0.28	0.24	0.31	0.31	0.31								
14				0.19			0.16	0.09	0.12				0.18		0.18	0.43	0.66	0.54											
15							0.19						0.50		0.50	0.20	0.30	0.25											
16							0.21						0.19	0.40	0.29													1.76	1.76
17		0.18		0.22	0.14	0.18	0.22	0.13	0.17				0.13		0.13				0.40	0.37	0.38								
18				0.22	0.13	0.17					0.51		0.36		0.36		0.20		0.19	0.31	0.25		0.05	0.08					
19	0.23				0.15					0.56	0.55	0.56	0.56	0.63	0.59	0.19	0.76	0.48				0.12			0.20		0.20		
20	0.21						0.32	0.46	0.39	0.45	0.51	0.48	0.25	0.37	0.31	0.07	0.12	0.10	0.49	0.21	0.35					0.19	0.20		
21	0.22	0.16	0.19				0.40	0.54	0.47	0.60			0.15	1.30	0.72	0.21	0.15	0.18							0.26		0.20		
22	0.20	0.16	0.18										0.18	0.58	0.38	0.25	0.15	0.20											
23					0.09								0.28	0.54	0.41														
24	0.27	0.14	0.21		0.11								0.20	0.57	0.38							0.15							
25	0.27	0.15	0.21	0.14	0.53	0.33							0.64	0.55	0.59				0.36	0.16	0.26								
26	0.23	0.11	0.17	0.14	0.14	0.14										0.20	0.13	0.16											
27	0.19	0.12	0.15	0.05	0.10	0.07											0.12		0.30	0.09	0.19								
28	0.16	0.28	0.22	0.16																									
29	0.18	0.14	0.16																										
30				0.20																									
31					0.09																								
m			**0.23**			**0.16**			**0.20**			**0.51**			**0.38**			**0.25**			**0.25**			**0.17**			**0.20**		**1.24**

Si concentrations from Rhone glacier accumulation seasons 1999-2001 (mg l^{-1}).

Date	mg l^{-1}
16-Nov-99	1.04
5-Jan-00	1.70
09-Apr-00	1.53
5-Dec-00	1.76
18-Jan-01	2.00
29-Apr-01	1.71

Mean daily Si concentrations

Month	n	mg l^{-1}	StDev.
January	2	1.85	
Febuary	0		
March	0		
April	2	1.85	
May	17	0.38	0.15
June	12	0.25	0.13
July	25	0.24	0.06
August	13	0.17	0.07
September	13	0.20	0.11
October	5	0.80	0.54
November	1	1.04	
December	0		

Seasonal averages

Season	Ablation 10:00 h	Ablation 17:00 h	Accumulation
Average	0.26	0.28	1.62
St.dev.	0.20	0.26	0.32
n	101	84	6

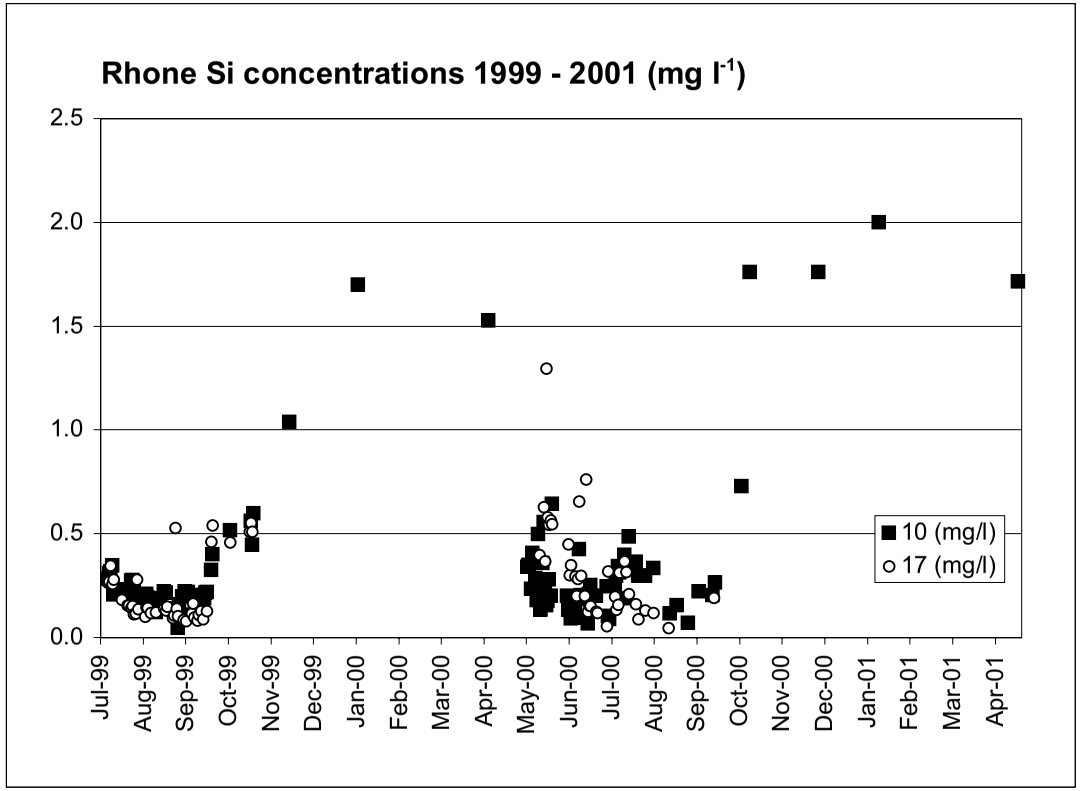

Conductivities from Rhone glacier ablation season 1999-2000 (µS cm-1).

Month		**July**			**August**			**September**			**October**			**May**			**June**			**July**			**August**			**September**			**October**	
Day nr.	10	17	**daily**	10	17	**daily**	10	17	**daily**	10	17	**daily**	10	17	**daily**	10	17	**daily**	10	17	**daily**	10	17	**daily**	10	17	**daily**	10	**daily**
1							7.0	3.0	4.0							10.0	8.0	9.0				6.0	4.0	5.0	4.2				
2							5.0	3.0	4.0																				
3				8.0	25.0	16.5	5.0																						
4				12.0	25.0	18.5				9.0		9.0							6.0	6.0	6.0								
5				24.0	4.0	14.0													7.0	6.0	6.5								
6	8.0	11.0	9.5				5.0	9.0	7.0								9.0		7.0	5.0	6.0								
7	9.0	18.0	13.5	5.0	5.0	5.0		6.0					29.0		29.0	10.0	13.0	11.5				7.0	5.0	6.0					
8	18.0	9.0	13.5				5.0	4.0	4.5				16.0		16.0	9.0	9.0	9.0											
9	12.0																												
10	12.0	11.0	11.5				5.0	3.0	4.0				15.0		15.0				8.0	8.0	8.0							10.1	10.1
11	13.0	7.0	10.0				5.0	3.0	4.0				12.0		12.0	10.0	7.0	8.5	8.0	7.0	7.5								
12				6.0	7.0	6.5										9.0	10.0	9.5	8.0	7.0	7.5								
13							5.0	3.0	4.0				11.0		11.0	10.0	9.0	9.5	9.0	8.0	8.5								
14							6.0	4.0	5.0				12.0		12.0	14.0	11.0	12.5											
15													10.0	9.0	9.5	11.0	11.0	11.0											
16							5.0	4.0	4.5				10.0		10.0														
17		7.0		6.0	5.0	5.5	5.0												10.0	9.0	9.5								
18				8.0	5.0	6.5				9.0		9.0					8.0		10.0	8.0	9.0		3.0	3.5					
19	13.0			4.0						10.0		10.0				8.0	6.0	7.0				4.0			6.0	5.0	5.5		
20	13.0	6.0	9.5				7.0	6.0	6.5	8.0	9.0	8.5				8.0	6.0	7.0	8.0	8.0	8.0					7.0	8.5		
21	9.0	11.0	10.0				8.0	8.0	8.0	12.0	13.0	12.5				8.0	5.0	6.5							10.0				
22	8.0	5.0	6.5				8.0						11.0			7.0	7.0	7.0											
23				4.0									12.0	10.0	11.0														
24	8.0	7.0	7.5	4.0									11.0	10.0	10.5							6.0							
25	7.0	4.0	5.5	5.0									10.0	9.0	9.5				9.0	6.0	7.5								
26	7.0	5.0	6.0	5.0	4.0	4.5										9.0	5.0	7.0											
27	8.0	4.0	6.0	4.0	3.0	3.5										8.0	8.0	8.0	10.0	5.0	7.5								
28	6.0	5.0	5.5													7.0	7.0	7.0											
29													10.0	8.0	9.0														
30	5.2	3.5	4.4		4.0	4.5							10.0	11.0	10.5														
31				5.0	3.0	5.0							11.0	10.0	10.5								3.6	3.9					
m			**8.5**			**8.2**			**5.0**			**9.8**			**12.5**			**8.7**			**7.6**			**4.6**			**7.0**		**10.1**

Conductivities from Rhone glacier accumulation seasons 1999-2001 (µS cm^{-1}).

Date	µS cm^{-1}
16-Nov-99	18.0
7-Dec-99	
05-Jan-00	27.0
9-Apr-00	32.5
5-Dec-00	26.0
18-Jan-01	25.0
7-Mar-01	30.0

Mean daily conductivities

Month	n	µS cm^{-1}	StDev.
January	2	26.0	
Febuary	0		
March	1	30.0	
April	1	32.5	
May	14	12.5	5.1
June	15	8.7	1.9
July	26	8.1	2.3
August	15	7.2	4.9
September	13	5.3	1.6
October	6	9.9	1.4
November	1	18.0	
December	1	26.0	

Seasonal averages

Season	Ablation 10:00 h	Ablation 17:00 h	Accumulation
Average	8.8	7.3	26.4
St.dev.	3.8	4.0	5.0
n	99	82	6

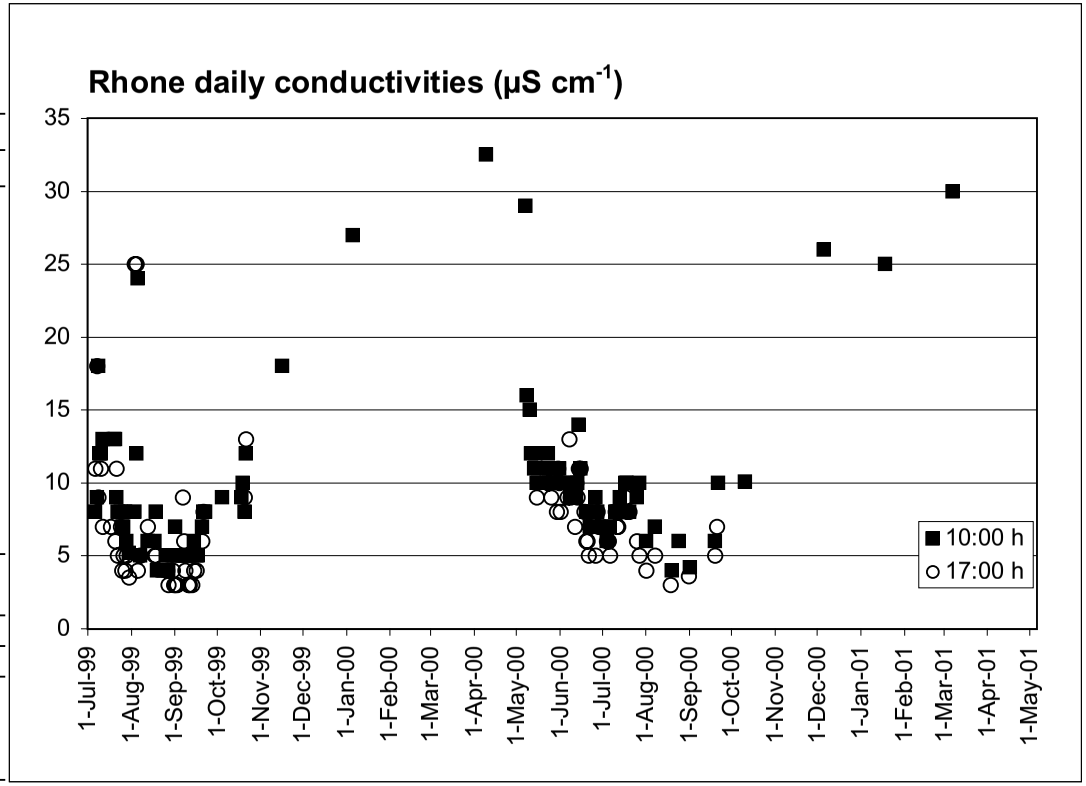

pH from Rhone glacier ablation season 1999-2000

Month		**July**			**August**			**September**			**October**			**May**			**June**			**July**			**August**			**September**			**October**	
Day nr.	10	17	**daily**	10	17	**daily**	10	17	**daily**	10	17	**daily**	10	17	**daily**	10	17	**daily**	10	17	**daily**	10	17	**daily**	10	17	**daily**	10	**daily**
1							5.77	5.45	5.58							6.61	6.97	6.75				6.40	5.67	5.90	6.40	6.06	6.20		
2				6.55	5.98	6.18	5.73	5.60	5.66																				
3				5.42	5.76	5.56	5.60																						
4				5.98	5.85	5.91					6.12								6.46	6.41	6.43								
5				6.88	5.56	5.84													6.43	6.58	6.50								
6	6.35	6.55	6.44				5.72	5.54	5.62								6.65		6.31	5.90	6.06								
7	6.40	6.31	6.35	5.84	5.66	5.74		5.84					7.10	7.10	7.10	6.60	7.76	6.87				6.28	6.30	6.29					
8	6.27	6.21	6.24	5.52	5.63	5.57	5.91	5.65	5.76				7.23	7.23	7.23	6.60	6.45	6.52											
9	6.59																												
10	7.07	6.30	6.53				5.63	5.49	5.55				7.40	7.40	7.40				6.57	6.26	6.39							6.81	6.81
11	6.56	6.19	6.34				5.59	5.43	5.50				6.80	6.80	6.80	5.90	5.53	5.68	6.54	6.41	6.47								
12																6.31	6.29	6.30	6.05	6.52	6.22								
13				5.69	5.69	5.69	5.54	5.51	5.52							6.31	6.24	6.27	6.62	6.37	6.48								
14				5.82			5.72	5.69	5.70				6.85	6.85	6.85	6.74	6.51	6.61											
15							5.38						6.69	6.75	6.72	6.61	6.08	6.27											
16							5.62	5.73	5.67				6.75																
17	7.40			5.84	5.86	5.85		5.40											6.58	6.61	6.59								
18				5.81	5.66	5.73					6.24								6.57	6.59	6.58		6.26						
19	6.42			5.58						6.44	6.18	6.29				6.30	6.10	6.19				6.72		6.43	6.39	6.20	6.28		
20	6.18	5.97	6.06				5.45	5.75	5.57	6.76	6.02	6.25				6.14	6.15	6.14	6.51	6.51	6.51					6.05			
21	6.12	5.97	6.04				5.90	5.69	5.78		6.16					6.50	6.07	6.23							6.23		6.13		
22	6.19	5.59	5.79				5.74						7.10			6.14	6.20	6.17											
23					5.62								7.25	7.10	7.17														
24	6.32	5.45	5.70		5.52								6.70									5.99							
25	6.21	6.00	6.09	5.57									6.83	6.27	6.47				6.58	5.91	6.13								
26	6.19	5.99	6.08	5.62	5.60	5.61										6.27	6.45	6.35											
27	6.24	6.05	6.13													6.45	6.45	6.45	5.89	6.30	6.05								
28	5.87	5.84	5.85	5.97												6.21	5.90	6.03											
29	6.02	5.97	5.99										6.48	6.44	6.46	6.02													
30				5.87	5.56	5.69		7.06					6.12	6.30	6.20														
31				5.59	5.51	5.55							6.04	6.15	6.09														
m			**6.06**			**5.71**			**5.62**			**6.27**			**6.58**			**6.23**			**6.32**			**6.14**			**6.20**		**6.81**

pH from Rhone glacier accumulation seasons 1999-2001.

Date	pH
16-Nov-99	7.50
7-Dec-99	
05-Jan-00	7.40
9-Apr-00	7.30
5-Dec-00	6.91
18-Jan-01	7.25
7-Mar-01	6.99

Mean daily pH

Month	n	pH
January	2	7.32
Febuary	0	
March	1	7.40
April	1	7.86
May	11	6.58
June	15	6.23
July	26	6.16
August	15	5.77
September	14	5.70
October	3	6.39
November	1	7.50
December	1	6.91

Seasonal averages

Season	Ablation	Accumulation
Average	5.97	7.17
St.dev.	0.46	0.23
n	106	6

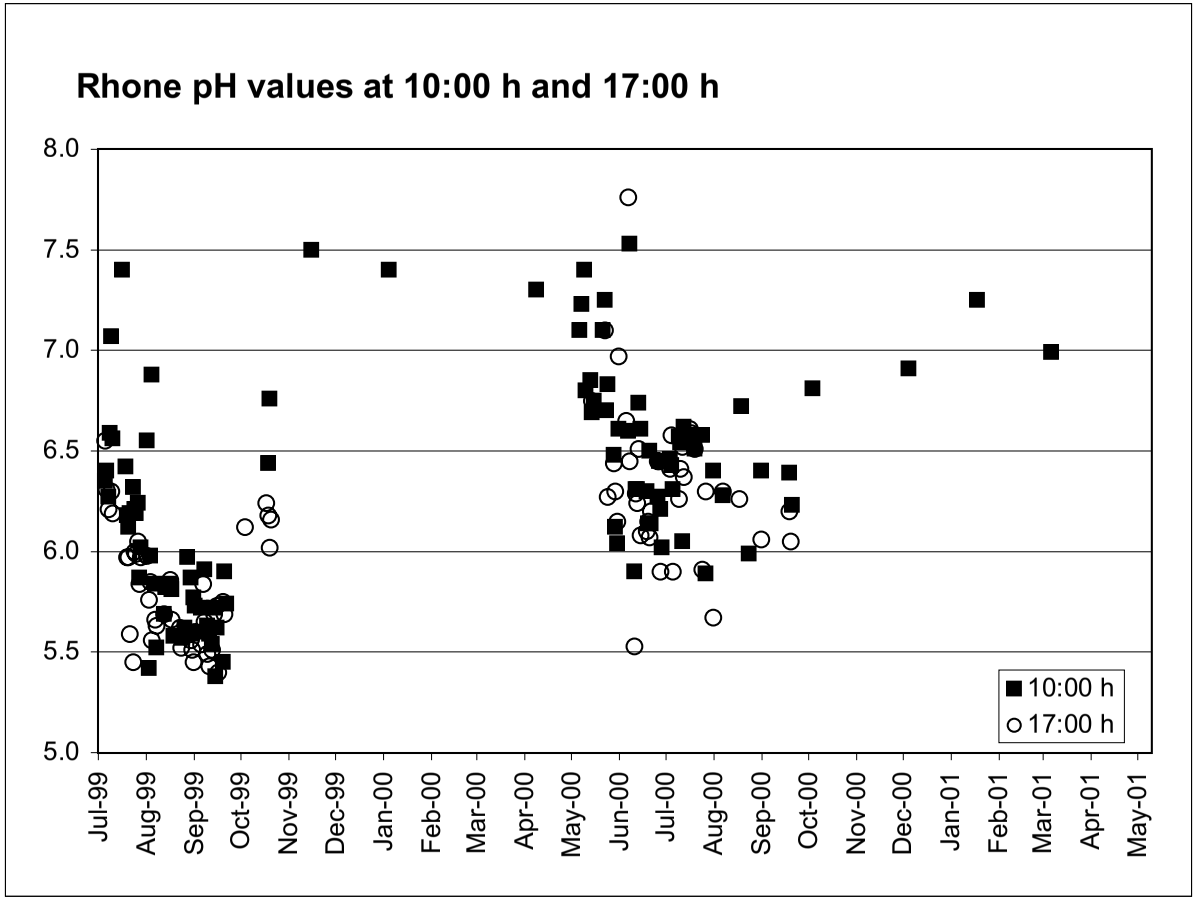

Mean daily discharge from Rhone glacier catchment 1999 - 2001 (l s^{-1})

	1999						2000												2001			
Month Day no.	**Jul**	**Aug**	**Sep**	**Oct**	**Nov**	**Dec**	**Jan**	**Feb**	**Mar**	**Apr**	**May**	**Jun**	**Jul**	**Aug**	**Sep**	**Oct**	**Nov**	**Dec**	**Jan**	**Feb**	**Mar**	**Apr**
1	7285	8160	6834	4641	201	91	55	37	55	164	626	2864	6588	5704	5576	3383	201	91	55	37	55	164
2	7684	8067	6860	4199	201	91	55	37	55	164	706	4030	7344	6086	4590	2015	201	91	55	37	55	164
3	9605	7659	5993	5075	201	91	55	37	55	164	916	5357	8925	5789	3239	1539	201	91	55	37	55	164
4	9945	7472	4701	4318	201	91	55	37	55	164	1075	7560	9435	5202	2805	1488	201	91	55	37	55	164
5	9945	8288	5024	3307	201	91	55	37	55	164	1155	9102	9010	5117	2635	1522	201	91	55	37	55	164
6	11560	10115	5194	2899	201	91	55	37	55	164	1004	6537	8415	6460	2635	1479	201	91	55	37	55	164
7	8670	11815	5653	2746	201	91	55	37	55	164	865	5882	9095	5440	3060	1284	201	91	55	37	55	164
8	7480	12070	5865	2695	201	91	55	37	55	164	937	5984	8840	5330	2499	1114	201	91	55	37	55	164
9	7166	11135	6367	2703	201	91	55	37	55	164	1109	6673	6154	6052	3409	1046	201	91	55	37	55	164
10	**7319**	**11730**	**6307**	**2754**	**201**	**91**	**55**	**37**	**55**	**164**	**1596**	**7072**	**6205**	**6443**	**4327**	**1003**	**201**	**91**	**55**	**37**	**55**	**164**
11	7633	9690	6579	2652	201	91	55	37	55	164	2155	8925	5066	6860	5126	978	201	91	55	37	55	164
12	7829	7752	6579	2414	201	91	55	37	55	164	1961	7897	3587	7455	5211	1148	201	91	55	37	55	164
13	8177	6919	6307	2176	201	91	55	37	55	164	1865	8092	3145	7480	4905	3145	201	91	55	37	55	164
14	9095	6571	6316	2006	201	91	55	37	55	164	2129	9180	3120	7897	5041	6783	201	91	55	37	55	164
15	8118	6860	5661	1811	201	91	55	37	55	164	2276	10370	2474	7769	5058	9945	201	91	55	37	55	164
16	7820	7659	4896	1581	201	91	55	37	55	164	2268	8432	2108	8152	4242	5593	201	91	55	37	55	164
17	7693	7242	5321	1411	201	91	55	37	55	164	2264	7013	2091	7897	3485	4080	201	91	55	37	55	164
18	7956	6078	4845	1250	201	91	55	37	55	164	2113	6936	2474	8058	3902	3128	201	91	55	37	55	164
19	7591	6460	4531	1071	201	91	55	37	55	164	2474	7438	2984	8152	3638	2202	201	91	55	37	55	164
20	**7837**	**7463**	**11220**	**935**	**201**	**91**	**55**	**37**	**55**	**164**	**2474**	**8084**	**3290**	**8670**	**6511**	**1938**	**201**	**91**	**55**	**37**	**55**	**164**
21	8160	7123	9605	1836	201	91	55	37	55	164	1970	8390	3791	9520	4667	1743	201	91	55	37	55	164
22	8245	7285	7463	1165	201	91	55	37	55	164	1558	8050	4429	8755	2950	1607	201	91	55	37	55	164
23	6979	7378	5933	2023	201	91	55	37	55	164	1499	8840	5134	7897	2661	1496	201	91	55	37	55	164
24	6426	8585	5814	1037	201	91	55	37	55	164	1390	7489	7004	7888	2831	1462	201	91	55	37	55	164
25	7055	9605	5806	3120	201	91	55	37	55	164	1445	6248	7200	7650	2924	1386	201	91	55	37	55	164
26	7769	8585	8296	1156	201	91	55	37	55	164	1558	5916	8050	7497	2856	1250	201	91	55	37	55	164
27	8925	9945	7140	816	201	91	55	37	55	164	1583	6044	7302	6834	3128	1233	201	91	55	37	55	164
28	10200	8254	6154	799	201	91	55	37	55	164	1592	6885	7710	6188	2746	1173	201	91	55	37	55	164
29	9095	7795	4913	969	201	91	55	37	55	164	2986	6367	5797	6095	3060	1122	201	91	55		55	164
30	**9180**	**6758**	**5423**	**944**	**201**	**91**	**55**		**55**	**164**	**3402**	**5797**	**4837**	**4956**	**5194**	**1046**	**201**	**91**	**55**		**55**	**164**
31	8441	8466		918			55		55		3146		4828	5202		1165		91	55		55	
m	**8286**	**8354**	**6253**	**2175**	**201**	**91**	**55**	**37**	**55**	**164**	**1745**	**7115**	**5691**	**6919**	**3830**	**2242**	**201**	**91**	**55**	**37**	**55**	**164**

Ablation season values (May to October) calculated as 86% of the daily discharge measured at Gletsch by the Federal Office for Water and Geology (Bernarth, 1981).

Accumulation season values (from November to April) taken from a model by the Federal Office for Water and Geology.

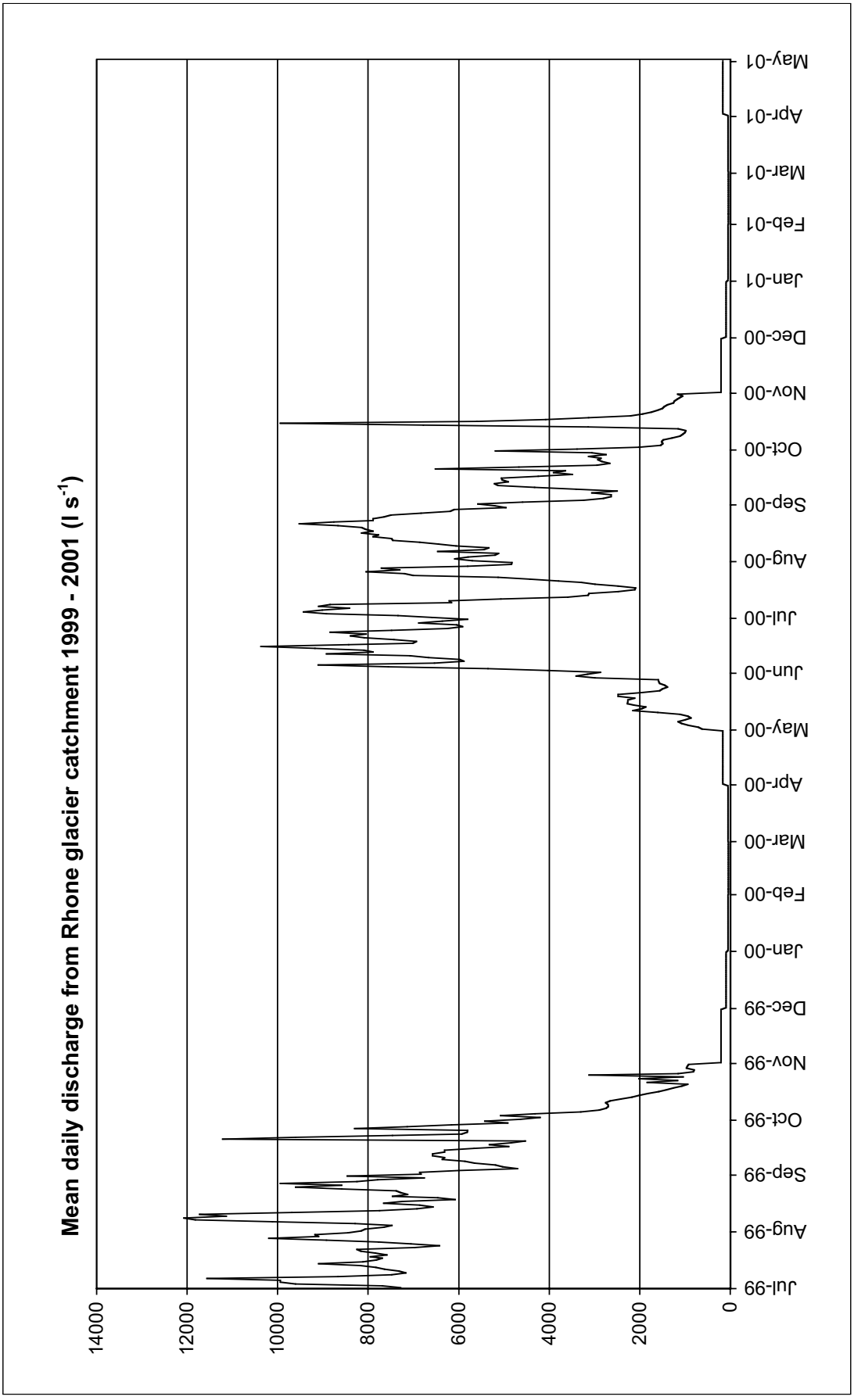
Mean daily discharge from Rhone glacier catchment 1999 - 2001 (l s-1)
14000
12000
10000
8000
6000
4000
2000
0
Jul-99
Aug-99
Sep-99
Oct-99
Nov-99
Dec-99
Jan-00
Feb-00
Mar-00
Apr-00
May-00
Jun-00
Jul-00
Aug-00
Sep-00
Oct-00
Nov-00
Dec-00
Jan-01
Feb-01
Mar-01
Apr-01
May-01

Suspended sediment concentrations from Rhone glacier ablation season 1999-2000 (g l^{-1}).

Month		**July**			**August**			**September**				**October**			**May**			**June**			**July**			**August**			**September**			**October**	
Day nr.	10	17	**daily**	10	17	**daily**	10	17	**daily**	10	17	**daily**	10	17	**daily**	10	17	**daily**	10	17	**daily**	10	17	**daily**	10	17	**daily**	10	**daily**
1							0.032									0.044	0.070	0.057				0.064	0.092	0.078	0.040				
2				0.343	0.186	0.264		0.047																				0.053	0.053
3				0.070	0.059	0.065	0.041																						
4				0.075	0.050	0.063					0.043	0.043							0.178	0.311	0.245								
5				0.062	0.070	0.066													0.392	0.349	0.371								
6	0.365	0.445	0.445				0.027	0.000											0.287	0.252	0.270								
7	0.272	0.194	0.233	0.216	0.100	0.158	0.023	0.047	0.035							0.125	0.196	0.160				0.058	0.086	0.072					
8	0.297	0.241	0.269	0.101	0.003	0.052	0.038	0.045	0.041							0.174	0.120	0.147											
9	0.214																								0.046		0.046		
10	0.219	0.147	0.183				0.039	0.037	0.038																				
11	0.190	0.108	0.149		0.135		0.032	0.069	0.051				0.073		0.073	0.213	0.182	0.197	0.061	0.041	0.051								
12				0.049		0.184										0.229	0.209	0.219	0.064	0.057	0.061								
13				0.032	0.036	0.034	0.036	0.050	0.043				0.121		0.121	0.184	0.314	0.249	0.051	0.036	0.043								
14							0.032	0.042	0.037				0.097		0.097	0.543	0.422	0.483											
15							0.029						0.067		0.067	0.189	0.324	0.257											
16							0.027	0.021	0.024				0.086	0.070	0.078													0.232	0.232
17				0.058			0.057	0.033	0.045				0.065		0.065				0.012	0.016	0.014								
18				0.038	0.036	0.037											0.081	0.040	0.006	0.039	0.023		0.127	0.126					
19	0.128	0.130	0.129		0.046	0.042					0.020	0.020				0.087	0.104	0.096				0.126			0.056		0.076		
20	0.146	0.130	0.138				0.623	0.752	0.687	0.017	0.018	0.018				0.153	0.099	0.126	0.040	0.046	0.043					0.096	0.076		
21	0.172	0.069	0.121				0.506	0.704	0.605	0.015	0.014	0.015				0.097	0.118	0.107							0.136		0.116		
22	0.180	0.238	0.209										0.152			0.089	0.077	0.083											
23					0.056	0.056							0.107	0.091	0.099														
24	0.121	0.131	0.126		0.056	0.056							0.081	0.084	0.082		0.077	0.038				0.096							
25	0.102	0.086	0.094	0.099		0.099							0.073	0.060	0.067				0.257	0.175	0.216								
26	0.125		0.106	0.101	0.093	0.097										0.099	0.072	0.085											
27	0.153	0.122	0.137		0.219	0.219										0.067	0.073	0.070	0.204										
28	0.121	0.150	0.136	0.040	0.055	0.052										0.068	0.111	0.089											
29	0.191	0.141	0.166										0.146	0.086	0.116	0.070	0.095	0.083											
30													0.057	0.061	0.059														
31				0.040	0.035	0.038							0.060	0.055	0.057								0.073						
m			**0.176**			**0.093**			**0.161**			**0.024**			**0.082**			**0.144**			**0.134**			**0.092**			**0.078**		**0.143**

Suspended sediment from Oberaar and Rhone glacier 1999-2001.

Catchment	Oberaar			Rhone		
Season	Ablation 10:00 h	Ablation 17:00 h	Accumulation	Ablation 10:00 h	Ablation 17:00 h	Accumulation
Average	0.259	0.395	0.045	0.125	0.123	0.021
St.dev.	0.146	0.183	0.032	0.114	0.130	0.016
n	64	55	7	96	86	6
	total	glaciericed		total	glaciericed	
yield (kg km^{-2} y^{-1})	7.73E+05	1.36E+06		4.91E+05	6.72E+05	
erosion (m yr^{-1})	2.86E-04	5.02E-04		1.82E-04	2.49E-04	
rate (mm kyr^{-1})	286	502		182	249	

Suspended sediment concentrations from Rhone glacier accumulation seasons 1999 - 2001 (g l^{-1}).

Date	g l^{-1}
16-Nov-99	0.0078
5-Jan-00	0.0115
09-Apr-00	0.0092
5-Dec-00	0.0420
18-Jan-01	0.0144
7-Mar-01	0.0420

Mean daily conductivities

Month	n	g l^{-1}	StDev.
January	2	0.0130	
Febuary	0		
March	1	0.0420	
April	1	0.0092	
May	12	0.0817	0.0216
June	18	0.1437	0.1085
July	25	0.1590	0.1061
August	20	0.0929	0.0652
September	14	0.1371	0.2175
October	6	0.0633	0.0841
November	1	0.0078	
December	1	0.0420	

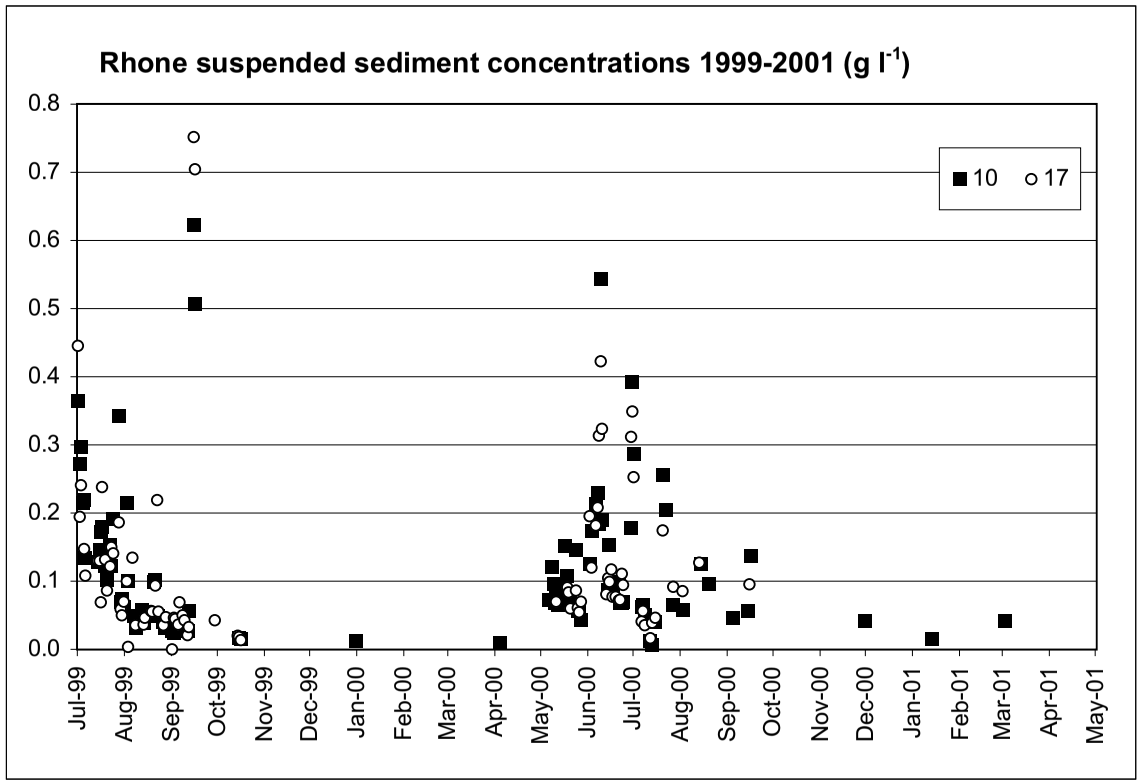

Relationship between total phosphorus (TP) and suspended sediment concentrations in the Rhone meltwaters (2000-2001)

	TP	Suspended sediment	Suspended sediment outliers[†]
Dates	mg l^{-1}	g l^{-1}	g l^{-1}
10:00 h			
14-Jun-00	1.09		0.54
15-Jun-00	0.38		0.19
21-Jun-00	0.22	0.10	
22-Jun-00	0.08	0.09	
1-Jun-01	0.02	0.07	
7-Jul-01	0.51	0.45	
17-Jul-01	0.19	0.23	
7-Aug-00	0.13	0.06	
19-Aug-00	0.18	0.13	
24-Aug-00	0.13	0.10	
3-Aug-01	0.27	0.18	
1-Sep-00	0.05	0.04	
9-Sep-00	0.05	0.05	
19-Sep-00	0.07	0.06	
21-Sep-00	0.14	0.14	
16-Oct-00	0.55		0.23
5-Dec-00	0.02	0.04	
18-Jan-01	0.03	0.01	
7-Mar-01	0.02	0.04	
17:00 h			
8-Jun-00	0.08	0.12	
14-Jun-00	0.59	0.42	
15-Jun-00	0.26	0.32	
21-Jun-00	0.23	0.12	
22-Jun-00	0.21	0.08	
7-Aug-00	0.17	0.09	
18-Aug-00	0.01		0.13
31-Aug-00	0.06	0.07	
19-Sep-00	0.03	0.06	
20-Sep-00	0.09	0.10	
2-Oct-00	0.05	0.05	
29-Aug-01	0.11	0.11	
5-Sep-01	0.06	0.06	
15-Aug-01	0.16	0.16	

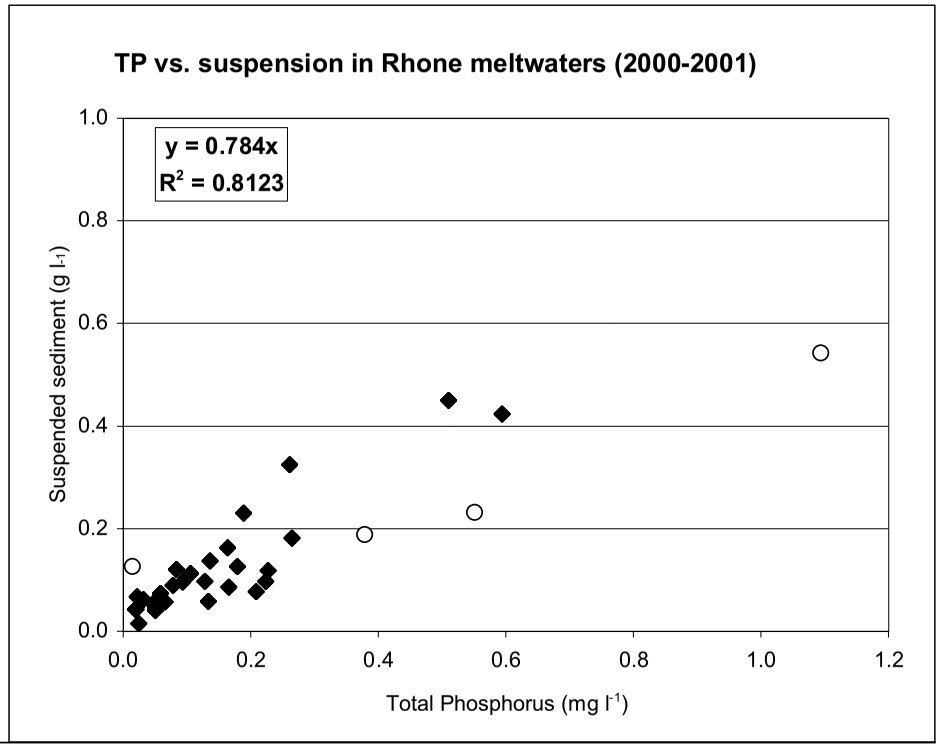

[†] Outliers were not included in the regression to prevent negative TP concentrations being calculated.
When outliers are included $R^2 = 0.730$

Measured HCO_3 concentrations from Rhone glacier ablation season 1999 (mg l^{-1}).

Month	**July**		**August**		**September**		**October**	
Day nr.	10	17	10	17	10	17	10	17
1					0.00	0.76		
2					1.45			
3			5.34					
4			4.58	4.58			2.52	
5					0.76			
6				0.61		0.92		
7			0.23		1.07	0.61		
8								
9						0.84		
10								
11								
12					0.38			
13					0.84	0.99		
14					0.76			
15					1.14	0.53		
16	1.53		0.92	0.92	0.92	1.14		
17			0.23	0.23				
18	2.44		0.23	0.23			2.21	
19		2.44			0.76	0.61	1.98	
20	1.14	0.31			6.48	2.90	1.83	2.29
21	0.69				1.91			2.52
22								
23	4.58							
24	0.84							
25				0.92				
26		1.22						
27	1.91							
28		0.76						
29				0.76				
30				0.46				
31			1.53					

Rhone adsorbed cation concentrations 1999 - 2001 (mg g^{-1}).

Date	Time	Ca^{2+}	K^{+}	Mg^{2+}
7-Jul-99		0.061	0.089	0.034
7-Jul-99		0.179	0.024	0.010
7-Jul-99		0.082	0.074	0.034
7-Jul-99		0.190	0.022	0.014
12-Jul-99		0.166	0.078	0.052
22-Jul-99		0.091	0.079	0.029
22-Jul-99		0.226	0.018	0.011
25-Jul-99		0.186	0.022	0.007
28-Jul-99		0.055	0.059	0.020
28-Jul-99		0.045	0.052	0.020
28-Jul-99		0.230	0.041	0.011
28-Jul-99		0.160	0.032	0.007
29-Jul-99		0.162	0.037	0.008
29-Jul-99		0.067	0.070	0.021
12-Aug-99	1	0.510	0.163	0.073
12-Aug-99		0.236	0.022	0.016
20-Aug-99		0.388	0.041	0.021
25-Aug-99		0.089	0.081	0.053
26-Aug-99		0.351	0.063	0.028
31-Aug-99		0.431	0.120	0.031
9-Sep-99	22	0.667	0.337	0.034
9-Sep-99		0.500	0.118	0.035
16-Sep-99		0.565	0.150	0.026
22-Sep-99		0.083	0.443	0.009
20-Oct-99		0.237	0.715	0.124
21-Oct-99		1.134	0.051	0.043
21-Oct-99		1.143	0.127	0.029
6-Jan-00	12	0.345	0.131	0.015
17-May-00	12	0.176	0.064	0.006
17-May-00	17	0.537	0.226	0.030
25-May-00	10	0.835	0.418	0.046
1-Jun-00	17	0.676	0.278	0.034
2-Jun-00	10	0.905	0.319	0.039
2-Jun-00	17	0.628	0.210	0.015
9-Jun-00	10	0.497	0.189	0.015
9-Jun-00	17	0.560	0.212	0.030
13-Jun-00	10	0.305	0.234	0.016
13-Jun-00	17	0.380	0.124	0.015
22-Jun-00	10	0.543	0.164	0.024
22-Jun-00	17	0.265	0.084	0.011
27-Jun-00	10	0.594	0.182	0.029
27-Jun-00	17	0.809	0.508	0.018
6-Jul-00	10	0.287	0.070	0.007
6-Jul-00	17	0.222	0.063	0.009
13-Jul-00	17	0.532	0.627	0.021
18-Jul-00	10	1.380	0.219	0.036
18-Jul-00	17	1.046	1.057	0.047
19-Aug-00	17	0.300	0.074	0.010
1-Sep-00	17	0.400	0.431	0.017
2-Sep-00	10	0.970	0.297	0.018
12-Jul-99	10	0.582	0.154	0.025
22-Jul-99	17	0.725	0.121	0.032
25-Jul-99	10	0.399	0.107	0.015
17-Sep-99	17	1.391	1.738	0.019
22-Sep-99	10	0.686	0.301	0.046
21-Oct-99	17	1.846	1.914	0.007
22-Oct-99	10	1.968	0.873	0.079
22-Oct-99	17	2.156	2.207	0.013

APPENDIX A.3
MORAINES

APPENDIX A.3: Moraine data

Oberaar glacier forefield

Soiltype †	Orthent (Entisols)						Humod (Spodosols)			
"Référence" §	Regosol (140 y)						Podzosol ocrique (10 ky)			
sample depth	soil depth	soil	O_{140A}		O_{140B}		soil depth	soil	O_{YD}	
(cm)	(cm)	horizon†	pH	TOC	pH	TOC	(cm)	horizon†	pH	TOC
		Oh					0-5	Oh		
0-10	0-5	Ah	5.4	0.11	7.6	0.36	5-10	Ah	6.7	24.09
10-20	5-30	AC	6.3	0	6.7	0.11	10-20	E	6.5	9.00
20-30			6.7	0	6.6	0	20-30	Bhs	6.1	3.49
30-40	30-	C	7.1	0	6.6	0	30-40	Bw	5.5	1.54
40-50			7.2	0	6.6	0	40-50	Bw	5.7	1.03
50-60			7.2	0	7.1	0	50-60	Bw	5.8	<0.1
60-70			7.7	0	7.5	0		R		
70-80			7.9	0	7.2	0				
80-90			8.2	0	7.1	0				
90-100			8.1	0	6.9	0				

Rhone glacier forefield

Soiltype †	Orthent (Entisols)				Umbrebt (Inseptisols)						Humod (Spodosols)			
"Référence" §	Regosol (145 y)				Brunisol oligosaturé (270 y)						Podzosol ocrique (10 ky)			
sample depth	soil depth	soil	R_{145A}		soil depth	soil	R_{270A}		R_{270B}		soil depth	soil	R_{YD}	
(cm)	(cm)	horizon†	pH	TOC	(cm)	horizon†	pH	TOC	pH	TOC	(cm)	horizon†	pH	TOC
		Oh				Oh						Oh		
0-10	0-5	Ah	5.0	0.24	0-5	Ah	4.6	0.67	4.6	1.08	0-10	Ah	n.a.	5.05
10-20	5-30	AC	5.2	0.15	5-20	Bw	4.8	0.37	4.7		10-20	E	5.4	1.45
20-30			6.0	0	20-30	BwC	4.9	0.19	5.3	0.13	20-30	Bhs	5.4	1.93
30-40	30-	C	6.4	0	30-40	(Bw)C	5.9	0	6.0	0	30-40	Bhs *	5.5	0.50
40-50			6.6	0	40-	C	6.0	0	6.1	0	40-50	Bw	5.5	1.12
50-60			6.5	0			6.1	0	6.5	0	50-60	Bw	5.9	1.01
60-70			6.4	0			6.2	0	n.a.		60-70	Bw	5.8	0.68
70-80			6.5	0			6.3	0	6.5	0				
80-90			6.7	0			6.5	0						
90-100			6.9	0			6.2	0						

Weathering specific parameters of minerals of catchments.

Mineral	Formula	molwt	density	log weathering rate	Reference*
		g mol^{-1}	g cm^{-3}	mol cm^{-2} sec^{-1}	
Quartz	SiO_2	60.1	2.62	-16.1	Brady and Walther 1990
Albite10	$Ca_{0.1}Na_{0.9}Al_{1.15}Si_{2.85}O_8$	263.8	2.65	-16.5 to -15.5	Holdren and Berner 1979
Orthoclase 20	$K_{0.8}Na_{0.2}AlSi_3O_8$	275.2	2.56	-16.75	Schweda 1989
Biotite (average)	$K_2Mg_4Fe_2Si_6Al_2O_{20}OH_4$	897.6	3.09	-12.75	Acker and Bricker 1992
Biotite (Granodiorite)	$(K_{0.952}, Na_{0.012})$ $(Mg_{1.164}, Fe_{1.276}, Al^{VI}_{0.294}, Ti_{0.099}, Mn_{0.023}, Cr_{0.003})(Si_{2.826}, Al^{IV}_{1.175})$ O_{10} $(OH)_2$				D. Marquer pers. comm.
Actinolite	$Ca_2Mg_4Fe_1Si_8O_{22}OH_2$	844.0	3.04	-14.8	Schott et al. 1981 Berner and Sjoberg 1981
Calcite	$CaCO_3$	100.1	2.71	-5	Plummer et al. 1978

Geometrical parameters of minerals of catchments.

Mineral	approx. geometry	geom. surface S	geom. volume V	calc. surface (cm^2)	calc. volume (cm^3)	rel. S / part.size	calc. edge; radius (cm)	rel. S / V
				e = 1 cm	e = 1 cm	part.size = const.	V = 1 cm^3	V = const.
Quartz	sphere	$4 \bullet \pi \bullet r^2$	$((4 \bullet \pi)/3) \bullet r^3$	12.57	0.5236	24	0.62	4.84
Albite 10	cube	$6 \bullet e^2$	e^3	6	1	6	1	6
Orthoclase 20	cube	$6 \bullet e^2$	e^3	6	1	6	1	6
Biotite	plate (cylindric, r/h = 5)	$2 \bullet \pi \bullet r^2 + 2 \bullet \pi \bullet r \bullet h$	$\pi \bullet r^2 \bullet h$	1.88	0.0785	24	1.47	16.32
Actinolite	cylindre (r/h = 0.05)	$2 \bullet \pi \bullet r^2 + 2 \bullet \pi \bullet r \bullet h$	$\pi \bullet r^2 \bullet h$	0.33	0.0079	42	0.25	8.35
Calcite	cube	$6 \bullet e^2$	e^3	6	1	6	1	6

S = surface, V = volume, e = edge, r = radius, h = height

*References see Chapter 3.

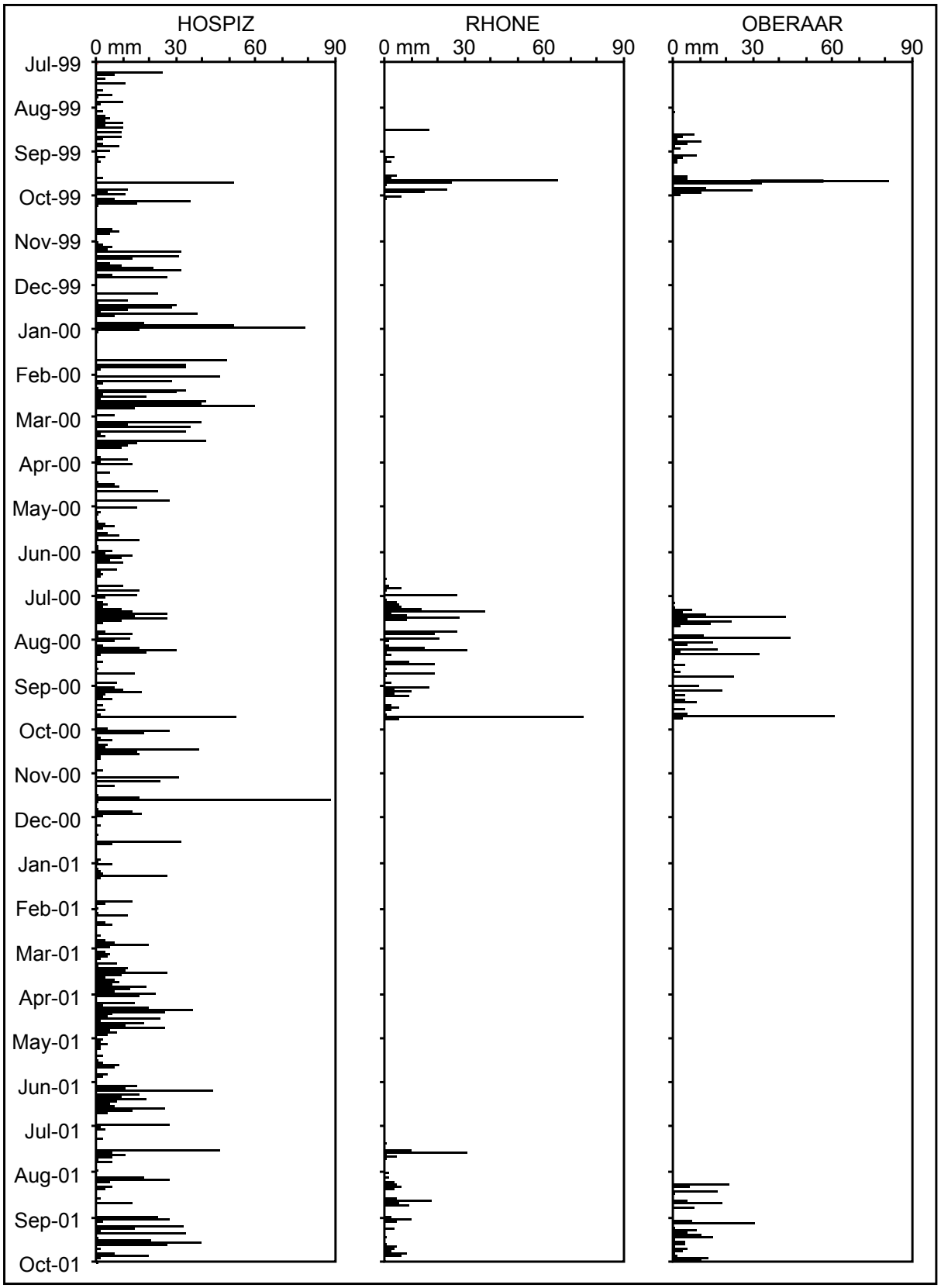

Precipitation pattern from Grimsel Hospiz, Rhone, and Oberaar raingauges (mm day^{-1}).

Precipitation data from fieldarea

Station	Nr	Altitude m a.s.l.	Type	SMA† 99-01 mm	SMA† 91-01 mm	HADES§ mm
Oberaar Joch	5008	3333	Totalisator	1143	2364	25-3000
Kl. Sidelhorn	7015	2428	Totalisator	2033	1789	18-2000
Albert Heim Hütte	4006	2530	Totalisator	2043	1821	16-1800
Grimsel Hospiz	5010	1980	Prec. Station	2089	2047	18-2000

Station	Type	Time		Prec. measured	Grimsel Hospiz	HADES§
		From	Until	mm	mm	mm
Oberaar snout	Gauge	12-Aug-99	30-Sep-99	244	156	18-2000
		27-Jul-00	21-Sep-00	453	456	
		3-Aug-01	1-Oct-01	269	366	
Oberaar snout	Totalisator	3-Aug-99	4-Oct-99	264	242	18-2000
Oberaar wall	Totalisator	3-Aug-99	1-Oct-99	267	186	1600
		1-Oct-99	17-May-00	817	1552	
		17-May-00	20-Jun-00	69	105	
		21-Jun-00	16-Oct-00	641	647	
		16-Oct-00	4-Jul-01	655	1174	
		4-Jul-01	1-Oct-01	340	474	
		1-Oct-99	*1-Oct-01*	*2522*	*3952*	
Rhone (2296 m)	Gauge	12-Aug-99	2-Oct-99	203	162	2000
		18-Jun-00	22-Sep-00	547	483	
		10-Jul-01	26-Sep-01	171	470	
Rhone (1790 m)	Totalisator	4-Aug-99	17-Oct-99	310	243	18-2000
Rhone (2462 m)	Totalisator	4-Aug-99	17-Oct-99	210	243	
Rhone (2600 m)	Totalisator	31-Jul-99	17-Oct-99	250	246	2000
Rhone (2769 m)	Totalisator	31-Jul-99	17-Oct-99	170	246	
Rhone (1790 m)	Totalisator	16-May-99	24-Sep-99	440	470	
Rhone (2462 m)	Totalisator	11-Jun-99	fell down			
Rhone (2600 m)	Totalisator	25-Jun-99	24-Sep-99	350	388	
Rhone (2769 m)	Totalisator	-	-			

† MeteoSuisse

§ Schwab et al. (2001)

Granulometry Oberaar samples I

Sample	weight		>32 mm	>16 mm	>8 mm	>4 mm	>2 mm	>1 mm	>0.5 mm	>250 µm	>125 µm	>63 µm	<63 µm
	wet (g)	dry (g)	(g)	(g)	(g)	(g)	(g)	(g)	(g)	(g)	(g)	(g)	(g)
Oberaar moraines samples LIA 140 y													
$O_{140A}1$		529.40		79.34	24.58	47.49	68.28	72.09	65.51	59.63	43.13	20.09	49.26
$O_{140A}2$		557.71		52.41	45.81	48.08	74.43	77.32	70.61	68.37	61.26	26.71	32.71
$O_{140A}3$		412.32		9.29	18.63	30.03	47.32	55.90	47.28	45.05	45.25	27.50	86.07
$O_{140A}4$		491.80			15.99	34.25	48.07	61.91	68.17	86.58	86.32	56.75	33.76
$O_{140A}5$		478.60		19.21	53.93	24.55	39.03	58.06	62.28	73.98	74.57	42.43	30.56
$O_{140A}6$		500.83		89.92	88.50	56.98	50.13	58.18	45.21	34.10	31.00	20.39	26.42
$O_{140A}7$		515.50		55.66	95.68	58.98	60.35	62.31	50.47	40.45	34.86	20.37	36.37
$O_{140A}8$		510.15		97.39	88.99	68.49	53.62	53.97	43.12	28.36	21.41	15.66	39.14
$O_{140A}9$		536.96		60.64	114.74	65.92	65.93	72.05	50.68	31.49	20.60	15.64	39.27
$O_{140A}10$		512.03		75.06	140.87	89.15	59.05	51.90	19.54	18.94	9.88	6.79	40.85
$O_{140B}1$		547.71		188.74	118.70	49.39	30.86	15.24	18.92	21.08	14.41	11.31	79.06
$O_{140B}2$		541.38		196.13	105.09	49.17	27.53	9.65	15.06	32.97	29.31	14.77	61.70
$O_{140B}3$		423.15		106.33	119.00	55.65	23.44	13.15	9.60	9.27	7.36	3.40	75.95
$O_{140B}4$		466.68		58.65	101.92	57.01	41.06	34.88	31.45	30.59	24.64	16.27	70.21
$O_{140B}5$		500.18		24.54	60.70	50.99	52.03	62.28	64.61	69.78	46.01	23.77	45.47
$O_{140B}6$		495.72		28.28	92.08	60.64	57.36	56.45	54.97	55.82	36.70	21.81	31.61
$O_{140B}7$		496.67		22.93	58.86	57.00	62.93	63.68	60.93	64.09	43.60	19.71	42.94
$O_{140B}8$		532.50		46.52	146.35	94.30	59.98	32.86	30.45	36.14	26.85	18.06	40.99
$O_{140B}9$		535.15		132.20	135.44	76.77	47.49	30.18	28.27	27.43	18.53	11.52	27.32
$O_{140B}10$		528.56		38.44	100.84	76.63	69.95	59.30	52.10	46.45	27.31	17.21	40.33
Oberaar moraines samples YD 10 ky													
$O_{YD}1$		181.16				7.69	10.54	15.75	30.59	38.29	23.39	20.21	34.70
$O_{YD}2$		486.20		7.35		5.67	38.07	43.46	36.32	41.39	60.88	48.06	205.00
$O_{YD}3$		419.79			13.36	17.43	38.64	38.59	32.58	36.31	60.83	71.33	110.72
$O_{YD}4$		493.99		19.79	47.42	28.92	44.03	40.69	36.55	38.33	78.28	58.33	101.65
$O_{YD}5$		638.27		62.43	40.62	32.60	50.15	53.00	50.18	50.23	77.14	77.75	144.17
$O_{YD}6$		660.25		7.48	22.34	47.86	44.54	47.22	46.38	50.53	83.74	80.88	229.28
Oberaar meltout sediment samples													
GSL1		510.88			44.25	84.97	89.12	74.50	50.47	46.16	45.57	33.14	42.70
GSL2		517.88		31.01	107.89	74.56	79.18	61.03	40.14	28.46	16.67	9.60	69.34
GSL2A		618.10		60.19	76.33	53.85	68.80	82.19	71.47	62.27	51.09	39.76	52.15
GSL3		500.81		22.78	62.41	65.49	80.09	64.12	43.53	31.89	25.71	26.50	78.29
GSR1		502.46		19.40	55.20	51.26	50.52	47.79	47.33	48.93	43.73	30.36	107.94
LS1		453.62						0.06	0.53	3.65	7.63	30.67	411.08

Granulometry Oberaar samples II

Sample	<63 µm	>32 µm	>16 µm	>8 µm	>4 µm	>2 µm	>1 µm	>0 µm	>32 µm	>16 µm	>8 µm	>4 µm	>2 µm	>1 µm	>0 µm
	(g)	%	%	%	%	%	%	%	(g)	(g)	(g)	(g)	(g)	(g)	(g)
Oberaar moraines samples LIA 140 y															
$O_{140A}1$	49.26	35.59	30.31	14.74	11.95	5.66	1.37	0.37	17.53	14.93	7.26	5.89	2.79	0.67	0.18
$O_{140A}2$	32.71	30.87	27.10	15.63	16.76	7.53	1.68	0.43	10.10	8.86	5.11	5.48	2.46	0.55	0.14
$O_{140A}3$	86.07	4.67	32.42	25.32	21.80	10.91	3.41	1.47	4.02	27.90	21.79	18.76	9.39	2.93	1.27
$O_{140A}4$	33.76	43.08	26.84	10.79	10.70	5.94	1.99	0.66	14.54	9.06	3.64	3.61	2.01	0.67	0.22
$O_{140A}5$	30.56	17.47	27.34	18.23	20.47	11.16	3.89	1.45	5.34	8.36	5.57	6.26	3.41	1.19	0.44
$O_{140A}6$	26.42	7.31	36.23	21.68	20.45	10.87	2.65	0.81	1.93	9.57	5.73	5.40	2.87	0.70	0.21
$O_{140A}7$	36.37	19.25	29.73	17.91	18.48	10.78	2.93	0.91	7.00	10.81	6.51	6.72	3.92	1.07	0.33
$O_{140A}8$	39.14	15.12	29.97	19.55	19.69	11.49	3.10	1.08	5.92	11.73	7.65	7.71	4.50	1.21	0.42
$O_{140A}9$	39.27	13.75	30.07	18.25	21.81	12.16	3.06	0.91	5.40	11.81	7.17	8.56	4.78	1.20	0.36
$O_{140A}10$	40.85	22.06	33.43	15.92	16.76	9.03	2.18	0.62	9.01	13.66	6.50	6.85	3.69	0.89	0.25
$O_{140B}1$	79.06	19.10	26.43	22.53	21.01	8.59	1.86	0.48	15.10	20.90	17.81	16.61	6.79	1.47	0.38
$O_{140B}2$	61.70	26.72	31.83	11.29	19.05	8.33	2.14	0.63	16.49	19.64	6.97	11.75	5.14	1.32	0.39
$O_{140B}3$	75.95	11.78	36.39	20.07	19.62	9.31	2.19	0.64	8.95	27.64	15.24	14.90	7.07	1.66	0.49
$O_{140B}4$	70.21	44.60	23.31	11.41	12.59	6.24	1.47	0.38	31.31	16.37	8.01	8.84	4.38	1.03	0.27
$O_{140B}5$	45.47	1.81	29.84	22.64	25.33	14.16	4.54	1.68	0.82	13.57	10.29	11.52	6.44	2.06	0.76
$O_{140B}6$	31.61	4.83	32.55	21.70	22.75	12.68	3.98	1.51	1.53	10.29	6.86	7.19	4.01	1.26	0.48
$O_{140B}7$	42.94	7.08	29.89	21.40	21.84	13.70	4.40	1.68	3.04	12.83	9.19	9.38	5.88	1.89	0.72
$O_{140B}8$	40.99	9.18	34.76	19.36	20.47	11.35	3.73	1.15	3.76	14.25	7.94	8.39	4.65	1.53	0.47
$O_{140B}9$	27.32	1.35	23.46	23.39	29.24	16.90	4.44	1.23	0.37	6.41	6.39	7.99	4.62	1.21	0.34
$O_{140B}10$	40.33	31.63	26.57	14.53	16.20	8.46	2.12	0.49	12.76	10.72	5.86	6.53	3.41	0.85	0.20
Oberaar moraines samples YD 10 ky															
$O_{YD}1$	34.70	73.52	18.75	4.36	2.14	0.78	0.30	0.15	25.51	6.51	1.51	0.74	0.27	0.10	0.05
$O_{YD}2$	205.00	62.67	28.72	5.72	2.02	0.71	0.13	0.03	128.47	58.88	11.73	4.14	1.46	0.27	0.06
$O_{YD}3$	110.72	54.76	30.26	9.93	3.67	1.06	0.24	0.07	60.63	33.50	10.99	4.06	1.17	0.27	0.08
$O_{YD}4$	101.65	56.06	27.53	9.33	5.01	1.62	0.35	0.09	56.98	27.98	9.48	5.09	1.65	0.36	0.09
$O_{YD}5$	144.17	53.84	25.89	9.36	7.08	3.02	0.66	0.15	77.62	37.33	13.49	10.21	4.35	0.95	0.22
$O_{YD}6$	229.28	62.63	22.50	5.67	5.54	2.83	0.65	0.18	143.60	51.58	13.00	12.70	6.49	1.50	0.41
Oberaar meltout sediment samples															
GSL1	42.70	40.20	32.13	13.72	9.34	3.68	0.75	0.18	17.17	13.72	5.86	3.99	1.57	0.32	0.08
GSL2	69.34	23.78	28.22	17.22	19.40	9.02	1.93	0.44	16.49	19.57	11.94	13.45	6.25	1.34	0.31
GSL2A	52.15	76.01	15.33	4.17	2.79	1.30	0.32	0.08	39.64	8.00	2.18	1.45	0.68	0.16	0.04
GSL3	78.29	48.91	27.63	11.37	7.65	3.35	0.83	0.26	38.29	21.63	8.90	5.99	2.62	0.65	0.20
GSR1	107.94	22.32	26.23	15.32	19.31	11.38	3.85	1.60	24.09	28.31	16.54	20.84	12.28	4.16	1.73
LS1	411.08	53.02	37.12	7.06	2.00	0.60	0.15	0.04	217.95	152.59	29.02	8.22	2.47	0.62	0.16

Granulometry Rhone samples I

Sample	weight		>32 mm	>16 mm	>8 mm	>4 mm	>2 mm	>1 mm	>0.5 mm	>250 µm	>125 µm	>63 µm	<63 µm
	wet (g)	dry (g)	(g)	(g)	(g)	(g)	(g)	(g)	(g)	(g)	(g)	(g)	(g)
Rhone moraines samples LIA 145 y													
$R_{145A}1$		488.97		71.21	54.97	50.50	45.38	43.77	37.02	32.28	31.64	28.71	93.49
$R_{145A}2$		519.17		103.45	50.90	30.35	42.86	49.68	45.07	39.69	39.81	33.52	83.84
$R_{145A}3$	436.51	422.74		29.07	13.09	46.58	49.24	48.33	39.64	33.72	36.13	26.73	100.21
$R_{145A}4$	466.10	456.42		80.74	49.84	47.51	42.38	47.09	41.88	37.36	31.76	26.93	50.93
$R_{145A}5$	452.62	430.86			31.81	44.23	50.25	60.73	55.56	45.10	47.02	34.08	62.08
$R_{145A}6$	503.12	495.35		94.72	71.49	50.43	43.78	45.13	39.04	36.05	32.90	29.03	52.78
$R_{145A}7$	500.09	475.61		39.70	42.55	49.70	47.36	55.77	49.41	44.27	38.27	38.27	70.31
$R_{145A}8$	483.82	464.97			55.80	56.17	50.14	53.13	47.37	41.86	35.02	38.39	87.09
$R_{145A}9$	477.08	457.69			30.05	59.78	57.99	59.12	50.54	46.74	47.06	39.49	66.92
$R_{145A}10$	484.92	463.79			7.46	41.82	54.41	60.70	54.97	51.87	53.65	42.96	95.95
Rhone moraines samples LIA 270 y													
$R_{270A}1$	394.88	371.62		24.99	40.00	44.58	42.24	37.54	35.31	31.75	31.72	29.33	54.16
$R_{270A}2$	385.84	374.04		25.94	65.61	46.98	49.38	44.30	35.89	28.47	23.82	17.44	36.21
$R_{270A}3$	400.48	394.93		50.26	66.48	45.62	53.61	45.17	34.24	27.84	21.96	17.00	32.75
$R_{270A}4$	452.07	448.81		65.75	56.38	59.01	55.60	48.43	41.77	36.97	33.64	21.41	29.85
$R_{270A}5$	483.87	463.75		113.37	66.17	57.94	47.12	42.21	38.36	32.87	24.99	17.13	23.59
$R_{270A}6$	463.95	483.67		79.41	100.95	58.22	57.32	44.16	38.83	34.54	26.99	17.27	25.98
$R_{270A}7$	414.13	413.96		63.15	44.92	66.50	53.16	44.86	36.59	30.58	24.93	19.01	30.26
$R_{270A}8$	404.40	404.14		32.39	52.31	47.68	49.43	50.60	44.82	38.41	34.71	22.90	30.89
$R_{270A}9$	367.50	367.31		27.92	40.85	46.63	50.05	47.43	39.56	32.15	29.47	22.71	30.54
$R_{270A}10$	484.07	483.84		109.82	58.47	53.95	50.11	44.52	37.28	32.36	32.41	26.18	38.74
$R_{270B}1$	394.43	368.09			23.31	6.42	59.97	51.77	49.52	44.52	30.39	18.87	83.32
$R_{270B}2$	391.54	375.82		80.60	37.42	34.61	34.89	36.84	37.79	35.76	27.11	19.93	30.87
$R_{270B}3$	395.29	386.44		63.02	44.49	54.51	46.07	42.37	42.68	38.63	22.23	12.08	20.36
$R_{270B}4$	444.50	435.42	49.80	71.19	48.16	47.68	40.93	40.23	36.07	31.64	24.16	17.09	28.47
$R_{270B}5$	506.74	495.26		59.83	74.53	60.36	59.84	61.96	51.10	38.44	31.12	21.80	36.28
$R_{270B}6$	472.91	466.90		93.73	77.97	58.79	53.63	48.78	41.25	29.68	20.32	16.02	26.73
$R_{270B}8$	478.39	477.54		88.54	85.37	76.86	51.96	45.34	36.97	27.22	20.87	16.62	27.79
Rhone moraines samples YD 10 ky													
$R_{YD}1$		442.90		7.63	29.89	46.67	66.70	62.15	56.68	49.87	40.74	29.44	53.13
$R_{YD}2$		783.45	66.28	123.67	116.87	86.29	84.50	69.64	60.37	47.41	37.58	32.90	57.94
$R_{YD}3$		875.52		120.92	166.86	89.42	93.72	75.86	69.52	57.76	52.85	42.52	106.09
$R_{YD}4$		622.69		186.02	105.45	35.71	33.12	30.84	33.50	34.35	41.63	41.45	80.62
$R_{YD}5$		482.89		36.18	55.97	37.41	49.20	37.04	36.33	45.35	52.40	45.88	87.13
$R_{YD}6$		459.27			12.11	17.76	27.52	34.33	39.20	54.45	75.61	68.53	129.76
$R_{YD}7$		672.85		40.22	28.75	25.22	39.36	45.84	56.12	71.28	94.72	101.95	169.39
Rhone meltout sediment sample													
RS		475.01							0.13	1.54	128.90	156.88	187.56

Granulometry Rhone samples II

Sample	<63 µm	>32 µm	>16 µm	>8 µm	>4 µm	>2 µm	>1 µm	>0 µm	>32 µm	>16 µm	>8 µm	>4 µm	>2 µm	>1 µm	>0 µm
	(g)	%	%	%	%	%	%	%	(g)	(g)	(g)	(g)	(g)	(g)	(g)
Rhone moraines samples LIA 145 y															
$R_{145A}1$	93.49	31.38	32.35	17.27	12.42	5.05	1.20	0.33	29.34	30.24	16.15	11.61	4.72	1.12	0.31
$R_{145A}2$	83.84	79.03	16.02	2.52	1.52	0.71	0.17	0.04	66.26	13.43	2.11	1.27	0.60	0.14	0.03
$R_{145A}3$	100.21	22.42	26.67	19.65	18.94	9.46	2.29	0.58	22.47	26.73	19.69	18.98	9.48	2.29	0.58
$R_{145A}4$	50.93	39.53	25.95	14.72	12.08	5.89	1.47	0.35	20.13	13.22	7.50	6.15	3.00	0.75	0.18
$R_{145A}5$	62.08	28.83	32.97	16.08	13.38	6.57	1.68	0.48	17.90	20.47	9.98	8.31	4.08	1.04	0.30
$R_{145A}6$	52.78	21.82	33.28	16.48	16.51	9.12	2.22	0.58	11.52	17.57	8.70	8.71	4.81	1.17	0.31
$R_{145A}7$	70.31	70.92	22.08	3.87	2.09	0.82	0.18	0.04	49.86	15.52	2.72	1.47	0.58	0.13	0.03
$R_{145A}8$	87.09	2.15	30.05	22.68	26.34	13.72	3.84	1.23	1.87	26.17	19.75	22.94	11.95	3.34	1.07
$R_{145A}9$	66.92	21.37	31.01	17.55	17.17	9.19	2.77	0.94	14.30	20.75	11.74	11.49	6.15	1.85	0.63
$R_{145A}10$	95.95	24.83	28.76	16.36	17.91	9.20	2.29	0.65	23.82	27.60	15.70	17.18	8.83	2.20	0.62
Rhone moraines samples LIA 270 y															
$R_{270A}1$	54.16	41.47	29.55	13.43	10.30	4.21	0.87	0.17	22.46	16.00	7.27	5.58	2.28	0.47	0.09
$R_{270A}2$	36.21	21.02	33.15	18.77	17.09	7.80	1.67	0.50	7.61	12.00	6.80	6.19	2.82	0.60	0.18
$R_{270A}3$	32.75	16.04	36.32	20.75	17.58	7.27	1.61	0.43	5.25	11.89	6.80	5.76	2.38	0.53	0.14
$R_{270A}4$	29.85	4.96	40.01	19.69	22.10	10.29	2.36	0.59	1.48	11.94	5.88	6.60	3.07	0.70	0.18
$R_{270A}5$	23.59	17.81	34.77	19.01	16.75	8.80	2.28	0.59	4.20	8.20	4.48	3.95	2.08	0.54	0.14
$R_{270A}6$	25.98	3.33	34.93	22.02	23.93	12.21	2.86	0.72	0.87	9.07	5.72	6.22	3.17	0.74	0.19
$R_{270A}7$	30.26	37.53	29.68	14.04	12.01	5.50	1.03	0.22	11.36	8.98	4.25	3.63	1.66	0.31	0.07
$R_{270A}8$	30.89	23.00	33.22	18.53	15.65	7.19	1.89	0.52	7.10	10.26	5.72	4.83	2.22	0.58	0.16
$R_{270A}9$	30.54	22.93	33.59	16.70	17.25	7.30	1.73	0.50	7.00	10.26	5.10	5.27	2.23	0.53	0.15
$R_{270A}10$	38.74	46.98	28.09	11.58	9.14	3.40	0.66	0.15	18.20	10.88	4.49	3.54	1.32	0.26	0.06
$R_{270B}1$	83.32	55.83	24.96	10.51	6.10	2.08	0.42	0.09	46.52	20.80	8.76	5.08	1.73	0.35	0.07
$R_{270B}2$	30.87	49.82	29.96	11.02	6.37	2.30	0.44	0.09	15.38	9.25	3.40	1.97	0.71	0.14	0.03
$R_{270B}3$	20.36	21.84	34.33	17.56	16.96	7.47	1.51	0.33	4.45	6.99	3.58	3.45	1.52	0.31	0.07
$R_{270B}4$	28.47	31.68	37.94	14.58	10.79	4.09	0.76	0.16	9.02	10.80	4.15	3.07	1.16	0.22	0.05
$R_{270B}5$	36.28	16.81	36.34	22.14	16.49	6.57	1.31	0.33	6.10	13.18	8.03	5.98	2.38	0.48	0.12
$R_{270B}6$	26.73	17.57	43.57	18.42	13.43	5.54	1.16	0.31	4.70	11.65	4.92	3.59	1.48	0.31	0.08
$R_{270B}8$	27.79	38.64	34.55	12.99	9.19	3.71	0.73	0.18	10.74	9.60	3.61	2.55	1.03	0.20	0.05
Rhone moraines samples YD 10 ky															
$R_{YD}1$	53.13	59.91	25.75	7.27	4.56	1.92	0.47	0.12	31.83	13.68	3.86	2.42	1.02	0.25	0.06
$R_{YD}2$	57.94	59.74	22.15	7.93	6.44	2.83	0.71	0.20	34.61	12.83	4.59	3.73	1.64	0.41	0.12
$R_{YD}3$	106.09	53.38	25.18	10.44	6.99	3.00	0.77	0.24	56.63	26.71	11.08	7.42	3.18	0.82	0.25
$R_{YD}4$	80.62	57.09	25.99	8.84	5.31	2.07	0.53	0.16	46.03	20.95	7.13	4.28	1.67	0.43	0.13
$R_{YD}5$	87.13	55.50	28.04	8.75	5.42	1.82	0.37	0.11	48.36	24.43	7.62	4.72	1.59	0.32	0.10
$R_{YD}6$	129.76	53.03	29.66	10.47	4.91	1.57	0.30	0.07	68.81	38.49	13.59	6.37	2.04	0.39	0.09
$R_{YD}7$	169.39	63.36	25.91	6.23	3.00	1.19	0.24	0.07	107.33	43.89	10.55	5.08	2.02	0.41	0.12
Rhone meltout sediment sample															
RS	187.56	66.51	28.02	4.06	1.05	0.29	0.06	0.01	124.75	52.55	7.61	1.97	0.54	0.11	0.02

XRD whole rock Oberaar samples

Samples	Phyllosilicates	Quartz	K-Feldspath	Plagioclase	Calcite	Unquantified
Oberaar moraines samples LIA 140 y						
$O_{140A}1$	9.00	16.05	4.66	29.89	0.00	40.40
$O_{140A}2$	5.72	18.55	2.37	18.47	0.00	54.90
$O_{140A}3$	6.21	23.06	1.86	28.57	1.60	38.70
$O_{140A}4$	5.14	13.22	2.22	36.60	2.83	40.01
$O_{140A}5$	3.54	19.54	1.88	40.00	0.41	34.62
$O_{140A}6$	5.84	32.96	7.81	36.24	0.60	16.56
$O_{140A}7$	5.24	22.27	7.51	19.59	0.98	44.41
$O_{140A}8$	7.76	19.10	15.95	38.18	1.54	17.48
$O_{140A}9$	4.89	25.87	7.23	21.98	0.61	39.43
$O_{140A}10$	8.35	32.52	5.37	32.77	1.66	19.33
$O_{140B}1$	6.09	34.90	4.56	30.38	0.00	24.07
$O_{140B}2$	7.56	34.62	7.55	34.22	0.41	15.63
$O_{140B}3$	9.88	18.41	10.06	48.21	0.00	13.45
$O_{140B}4$	9.00	23.22	6.28	45.19	0.00	16.31
$O_{140B}5$	7.86	40.68	6.34	54.79	0.61	0.00
$O_{140B}6$	12.55	28.48	5.06	44.71	0.46	8.74
$O_{140B}7$	11.27	24.07	6.78	54.14	1.15	2.59
$O_{140B}8$	10.46	30.56	8.40	50.96	0.91	0.00
$O_{140B}9$	8.72	41.13	6.47	30.91	0.86	11.91
$O_{140B}10$	9.12	27.07	6.81	38.04	0.62	18.33
Oberaar moraines samples YD 10 ky						
$O_{YD}1$	13.35	11.16	9.00	12.83	0.00	53.66
$O_{YD}2$	4.29	29.90	32.61	28.73	0.00	4.47
$O_{YD}3$	8.12	34.61	50.63	28.44	0.00	0.00
$O_{YD}4$	3.44	33.11	20.49	27.22	0.60	15.13
$O_{YD}5$	5.80	26.36	42.45	27.62	0.67	0.00
$O_{YD}6$	5.50	30.89	21.51	32.93	0.86	8.32
Oberaar meltout sediment samples						
GSL1	9.89	33.03	8.33	64.75	1.51	0.00
GSL2	9.87	44.36	6.38	32.09	0.89	6.41
GSL2A	3.63	16.92	12.94	22.89	0.92	42.70
GSL3	9.48	58.58	8.43	34.32	1.46	0.00
GSR1	5.37	30.20	10.69	35.47	2.35	15.91
LS	4.51	20.08	4.51	10.23	3.65	57.02
Oberaar suspended sediment samples						
k5 8-7-99	17.14	13.09	6.18	20.96	1.10	41.54
k6 11-7-99	27.01	11.82	2.76	12.40	0.51	45.49
k10 15-7-99	9.16	28.91	5.09	40.02	2.85	13.97
k11 15-7-99	6.35	28.78	10.41	22.63	0.00	31.83
k16 22-7-99	23.58	13.39	4.56	17.46	2.98	38.03
k17 22-7-99	11.00	29.06	26.79	32.63	1.98	0.00
k26 5-8-99	14.87	19.01	5.42	29.90	2.55	28.25
k37 12-8-99	13.91	15.13	4.53	13.73	8.03	44.67
k40 19-8-99	6.38	30.37	10.53	30.59	4.90	17.23
k41 19-8-99	13.62	38.87	5.41	16.16	1.94	24.00
k42 25-8-99	10.41	25.45	2.49	31.31	0.00	30.34
k43 25-8-99	17.50	25.51	0.00	0.00	0.00	56.99
k44 1-9-99	13.82	0.00	3.12	16.40	2.40	64.26
k45 1-9-99	14.81	67.23	2.63	27.79	2.91	0.00
k46 10-9-99	11.91	10.69	2.89	26.83	2.45	45.23
k47 10-9-99	10.24	23.23	2.37	27.67	5.02	31.47
k48 15-9-99	23.87	10.70	3.11	16.67	2.16	43.49
k49 15-9-99	8.14	25.32	5.13	24.34	1.39	35.68
k50 23-9-99	12.43	42.56	2.56	22.02	1.93	18.48
k51 23-9-99	17.63	26.21	8.24	27.04	2.28	18.60
k52 30-9-99	10.56	28.97	10.72	27.37	1.84	20.54
k53 30-9-99	12.20	22.45	12.65	48.81	1.76	2.12
k55 4-10-99	7.51	22.35	12.73	51.83	1.46	4.13

XRD whole rock Rhone samples

Samples	Phyllosilicates	Quartz	K-Feldspath	Plagioclase	Calcite	Unquantified
Rhone moraines samples LIA 145 y						
$R_{145A}1$	3.60	20.41	8.64	45.23	0.89	21.22
$R_{145A}2$	1.76	45.08	5.32	41.84	0.45	5.56
$R_{145A}3$	3.20	26.84	24.04	37.86	0.83	7.23
$R_{145A}4$	1.38	17.02	11.66	5.35	0.52	64.07
$R_{145A}5$	3.57	14.97	9.07	7.62	0.00	64.77
$R_{145A}6$	2.08	15.00	7.80	24.18	0.00	50.95
$R_{145A}7$	1.53	20.52	15.05	30.02	0.56	32.32
$R_{145A}9$	2.43	32.73	28.63	36.68	0.55	0.00
$R_{145A}10$	2.88	21.47	6.09	18.42	1.06	50.08
Rhone moraines samples LIA 270 y						
$R_{270A}1$	1.61	25.14	13.60	29.64	0.90	29.11
$R_{270A}2$	2.22	28.78	17.21	34.90	0.00	16.89
$R_{270A}3$	3.08	17.65	8.73	24.73	0.83	44.98
$R_{270A}4$	2.65	12.48	14.94	23.95	0.00	45.98
$R_{270A}5$	1.63	35.07	9.78	16.16	0.54	36.82
$R_{270A}6$	2.46	40.97	22.32	27.08	1.13	6.04
$R_{270A}7$	1.38	26.96	10.80	24.22	0.00	36.64
$R_{270A}8$	3.32	52.90	9.02	28.48	0.00	6.28
$R_{270A}9$	2.54	24.15	19.34	29.58	0.48	23.92
$R_{270A}10$	1.13	26.38	14.73	35.12	1.29	21.34
$R_{270B}1$	4.14	24.88	20.14	33.27	1.60	15.97
$R_{270B}2$	2.30	32.54	19.71	25.84	1.32	18.29
$R_{270B}3$	1.38	29.38	15.71	26.30	0.70	26.54
$R_{270B}4$	2.52	30.03	8.56	24.19	0.97	33.73
$R_{270B}5$	1.68	16.96	13.28	50.09	0.78	17.21
$R_{270B}6$	1.68	16.96	13.28	50.09	0.78	17.21
$R_{270B}8$	3.60	36.77	60.05	28.93	0.65	0.00
Rhone moraines samples YD 10 ky						
$R_{YD}1$	4.23	34.35	9.66	36.86	0.00	14.91
$R_{YD}2$	4.25	26.15	4.30	26.21	0.53	38.56
$R_{YD}3$	4.18	33.69	11.06	25.43	0.00	25.64
$R_{YD}4$	3.10	13.46	8.55	45.88	0.00	29.00
$R_{YD}5$	3.63	47.56	43.40	27.36	0.00	0.00
$R_{YD}6$	11.69	21.10	11.01	32.41	0.36	23.42
$R_{YD}7$	3.65	1.57	18.50	35.27	0.00	41.02
Rhone suspended sediment sample						
RH77 6-7-99	9.47	19.78	19.84	77.29	0.54	0.00
RH79 6-7-99	19.92	21.41	4.74	8.06	1.22	44.66
RH80 6-7-99	8.57	30.46	33.42	39.18	0.82	0.00
RH4 11-7-99	55.03	34.84	1.32	10.37	0.00	0.00
RH115 21-7-99	10.25	35.11	30.55	38.58	0.89	0.00
RH1 22-7-99	9.89	33.82	32.05	42.54	0.22	0.00
RH118 22-7-99	11.45	34.52	41.47	57.33	0.35	0.00
RH132 22-7-99	22.28	21.02	12.90	22.95	0.00	20.86
RH94 25-7-99	13.40	16.83	29.53	26.69	0.00	13.54
RH93 25-7-99	19.24	26.13	17.44	25.55	0.48	11.16
RH151 27-7-99	18.58	24.47	18.98	28.39	0.65	8.94
RH154 27-7-99	18.49	14.53	12.14	23.74	0.77	30.31
RH156 27-7-99	12.14	31.01	26.11	23.27	0.96	6.51
RH157 28-7-99	5.15	34.06	16.71	27.61	0.76	15.71
RH158 28-7-99	9.97	29.30	20.39	38.03	0.45	1.85
RH4 24-8-99	27.57	17.26	18.29	31.66	0.55	4.68
RH2 25-8-99	8.85	12.15	7.94	18.48	0.00	52.58
RH159 28-8-99	12.32	19.66	19.67	33.79	1.05	13.50
RH161 28-8-99	10.29	22.28	14.24	28.53	0.92	23.75
RH244 8-30-99	5.06	9.33	7.13	16.16	0.00	62.33
RH277 9-15-99	5.53	3.64	3.14	5.51	0.35	81.83
RH378 10-18-99	5.42	7.04	4.17	9.25	0.28	73.85
RH384 20-10-99	6.58	2.85	3.15	8.46	0.64	78.32
Recent	0.00	21.67	3.53	8.33	0.00	66.47

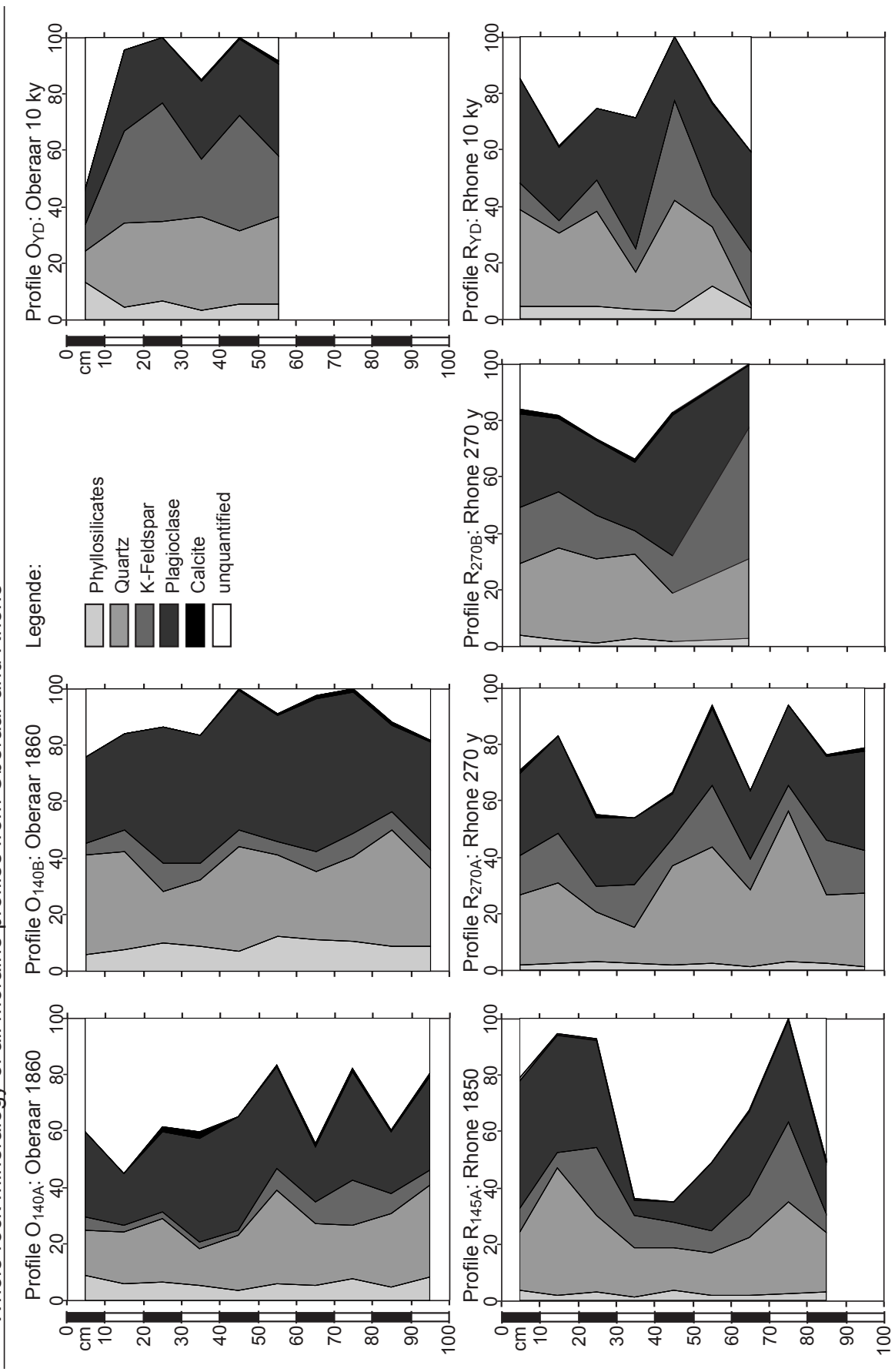
Whole rock mineralogy of all moraine profiles from Oberaar and Rhone
Legende:
Phyllosilicates
Quartz
K-Feldspar
Plagioclase
Calcite
unquantified
Profile O140A: Oberaar 1860
Profile O140B: Oberaar 1860
Profile OYD: Oberaar 10 ky
Profile R145A: Rhone 1850
Profile R270A: Rhone 270 y
Profile R270B: Rhone 270 y
Profile RYD: Rhone 10 ky
cm
0
10
20
30
40
50
60
70
80
90
100

Clay mineralogy Oberaar samples I

Sample	Depth	Fraction <2 µm (%)					Fraction 2-16 µm (%)				
	cm	vermiculite	bio-verm m.-l.	biotite	phengite	chlorite	vermiculite	bio-verm m.-l.	biotite	phengite	chlorite
Oberaar moraines samples LIA 140 y											
$O_{140A}1$	0-10	8.7	4.1	21.5	28.5	37.3	4.8	1.9	13.8	44.7	34.8
$O_{140A}2$	10-20	6.5	1.8	20.9	28.1	42.7	7.3	1.1	15.7	34.9	40.9
$O_{140A}3$	20-30	10.4	1.5	20.6	28.2	39.3	4.2	0.9	16.5	37.8	40.6
$O_{140A}4$	30-40	9.0	1.6	20.4	25.7	43.3	5.5	0.9	17.2	36.2	40.2
$O_{140A}5$	40-50	2.1	5.2	19.6	30.0	43.1	3.5	1.5	18.6	35.7	40.7
$O_{140A}6$	50-60	8.5	2.8	21.4	32.0	35.3	4.0	1.5	14.8	42.0	37.7
$O_{140A}7$	60-70	3.1	4.1	23.4	25.4	44.0	2.1	2.2	22.5	32.6	40.7
$O_{140A}8$	70-80	6.7	4.6	23.9	25.7	39.1	2.6	1.4	22.1	35.4	38.5
$O_{140A}9$	80-90	5.2	3.0	25.4	26.7	39.7	2.3	1.6	20.8	38.6	36.7
$O_{140A}10$	90-100	7.2	8.8	28.7	31.6	23.8	2.9	2.3	19.8	36.3	38.7
$O_{140B}1$	0-10	11.4	4.5	10.7	34.5	38.9	5.4	2.3	22.8	37.5	32.0
$O_{140B}2$	10-20	2.2	6.0	13.4	32.4	46.0	6.6	2.6	13.8	38.5	38.6
$O_{140B}3$	20-30	7.7	11.0	17.7	32.8	30.8	5.9	3.9	13.5	41.9	34.8
$O_{140B}4$	30-40	4.2	1.0	28.2	23.9	42.6	3.9	1.6	13.2	43.8	37.5
$O_{140B}5$	40-50	5.4	0.8	33.5	17.3	43.0	3.5	1.0	19.2	37.7	38.5
$O_{140B}6$	50-60	4.8	0.6	32.9	19.4	42.3	4.3	0.7	18.2	36.7	40.0
$O_{140B}7$	60-70	5.6	0.1	38.4	19.9	36.0	1.5	1.0	20.9	38.2	38.3
$O_{140B}8$	70-80	1.2	1.0	26.6	31.1	40.1	5.0	1.1	21.1	38.7	34.2
$O_{140B}9$	80-90	5.1	1.9	20.6	37.1	35.4	3.4	1.5	25.1	38.4	31.7
$O_{140B}10$	90-100	4.7	2.5	32.8	23.1	36.9	3.9	1.2	21.8	39.3	33.7
Oberaar moraines samples YD 10 ky											
$O_{YD}1$	0-10	15.1	6.1	15.8	47.6	15.4	8.0	1.8	16.5	55.3	18.4
$O_{YD}2$	10-20	6.0	5.9	9.3	65.9	12.8	4.6	1.0	17.8	65.5	11.2
$O_{YD}3$	20-30	19.3	16.5	10.0	40.4	13.8	2.7	4.6	14.7	56.2	21.7
$O_{YD}4$	30-40	13.6	23.9	13.7	36.9	11.9	10.6	10.5	9.6	49.8	19.4
$O_{YD}5$	40-50	8.3	16.1	13.4	46.3	15.9	4.7	10.6	15.7	51.8	17.2
$O_{YD}6$	50-60	9.2	20.3	18.0	36.7	15.8	5.7	12.5	20.4	45.7	15.7

Clay mineralogy Oberaar samples II

Sample	Depth	Fraction <2 µm (%)					Fraction 2-16 µm (%)				
	cm	vermiculite	bio-verm m.-l.	biotite	phengite	chlorite	vermiculite	bio-verm m.-l.	biotite	phengite	chlorite
Oberaar meltout sediment samples											
GSL1		6.2	1.2	21.5	32.8	38.3	6.3	1.3	17.3	42.4	32.7
GSL2		11.6	3.2	20.7	28.8	35.7	4.6	1.2	25.9	38.3	30.0
GSR1		4.5	2.2	30.9	32.1	30.4	6.0	1.2	24.0	32.8	36.1
GSL2A		9.4	2.2	24.0	29.0	35.4	4.1	2.4	18.2	44.0	31.3
GSL3		6.0	2.4	37.3	39.8	14.4	4.0	4.4	28.7	31.0	31.9
Oberaar suspended sediment samples											
O36 F290		0.0	0.0	43.3	26.8	29.9	0.0	0.0	42.7	28.2	29.2
K43 F223		0.0	0.0	37.8	26.4	35.7	0.0	0.0	32.2	31.4	36.4
K39 F217		0.0	0.0	39.2	24.0	36.8	0.0	0.0	33.1	29.0	37.8
K8 F41		0.0	0.0	38.6	19.3	42.1	0.0	0.0	31.9	24.9	43.3
Dust samples											
RHH409		10.2	1.5	24.8	20.5	43.0					
RHH411		5.3	1.0	37.3	35.4	20.9	8.6	4.7	25.2	35.1	26.5

Clay mineralogy Rhone samples I

Sample	Depth	Fraction <2 µm (%)					Fraction 2-16 µm (%)				
	cm	vermiculite	bio-verm m.-l.	biotite	phengite	chlorite	vermiculite	bio-verm m.-l.	biotite	phengite	chlorite
Rhone moraines samples LIA 145 y											
$R_{145A}1$	0-10	2.9	7.0	33.9	46.3	9.9	1.6	0.4	43.6	46.0	8.4
$R_{145A}2$	10-20	4.7	3.6	31.8	48.0	11.9	2.0	0.4	30.3	57.6	9.8
$R_{145A}3$	20-30	2.6	5.3	29.6	53.1	9.4	6.3	4.2	23.7	56.0	9.9
$R_{145A}4$	30-40	4.3	8.0	29.8	42.8	15.1	1.6	0.4	40.6	47.1	10.3
$R_{145A}5$	40-50	3.2	7.1	27.3	54.9	7.4	1.8	0.5	24.6	64.1	9.0
$R_{145A}6$	50-60	1.7	4.1	41.3	45.7	7.2	2.6	0.7	50.2	38.1	8.5
$R_{145A}7$	60-70	5.8	6.4	33.7	42.6	11.6	0.7	4.2	40.5	44.6	10.0
$R_{145A}8$	70-80	1.7	4.0	33.7	46.5	14.2	2.0	1.0	41.0	44.5	11.5
$R_{145A}9$	80-90	2.0	5.3	33.6	50.6	8.6	1.7	0.6	44.2	43.3	10.1
$R_{145A}10$	90-100	3.3	2.9	34.0	47.7	12.1	1.7	0.7	47.0	38.9	11.7
Rhone moraines samples LIA 270 y											
$R_{270A}1$	0-10	9.1	7.7	15.2	52.3	15.8	2.2	4.0	13.1	69.3	11.3
$R_{270A}2$	10-20	12.2	8.8	14.8	46.8	17.4	4.3	5.6	24.6	53.7	11.8
$R_{270A}3$	20-30	14.3	6.6	29.4	33.6	16.2	3.3	6.6	33.6	37.2	19.4
$R_{270A}4$	30-40	4.7	4.5	38.9	44.8	7.1	2.3	2.9	35.1	49.3	10.4
$R_{270A}5$	40-50	0.9	16.6	20.3	42.1	20.1	2.1	3.3	37.9	46.7	10.0
$R_{270A}6$	50-60	0.6	0.6	36.9	50.2	11.6	7.8	3.5	35.0	43.8	9.9
$R_{270A}7$	60-70	2.9	0.9	36.4	50.8	9.0	4.4	4.4	38.9	42.4	10.0
$R_{270A}8$	70-80	4.6	4.4	40.6	38.7	11.6	3.4	1.1	38.6	46.8	10.2
$R_{270A}9$	80-90	4.5	6.7	40.4	36.6	11.7	2.2	1.1	36.9	49.5	10.2
$R_{270A}10$	90-100	3.1	0.7	43.5	43.3	9.4	6.1	1.3	33.7	43.5	15.4
$R_{270B}1$	0-10	7.1	6.3	16.3	46.7	23.6	2.2	2.1	16.3	68.8	10.7
$R_{270B}2$	10-20	7.2	15.6	24.1	35.7	17.3	5.9	4.0	23.6	54.7	11.7
$R_{270B}3$	20-30	11.0	9.0	30.0	33.6	16.4	4.2	6.0	27.5	45.4	8.7
$R_{270B}4$	30-40	5.8	9.9	26.9	40.4	16.9	15.9	3.7	27.0	42.5	11.0
$R_{270B}5$	40-50	12.8	4.0	20.9	47.2	15.1	9.1	1.2	38.6	42.4	8.6
$R_{270B}6$	50-60	10.1	2.0	34.0	36.7	17.1	4.0	0.7	34.4	50.2	10.7
	60-70										
$R_{270B}8$	70-80	3.2	1.6	33.1	43.3	18.9	4.4	2.1	38.6	46.6	8.4

Clay mineralogy Rhone samples II

Sample	Depth	Fraction <2 µm (%)					Fraction 2-16 µm (%)				
	cm	vermiculite	bio-verm m.-l.	biotite	phengite	chlorite	vermiculite	bio-verm m.-l.	biotite	phengite	chlorite
Rhone moraines samples YD 10 ky											
$R_{YD}1$	0-10	11.7	7.8	16.1	44.1	20.3	2.6	1.4	31.2	55.3	9.5
$R_{YD}2$	10-20	7.1	8.5	15.2	61.3	7.8	3.0	3.5	23.6	64.7	5.2
$R_{YD}3$	20-30	13.8	17.1	19.4	44.5	5.2	2.7	5.9	25.2	54.4	11.8
$R_{YD}4$	30-40						9.8	8.9	20.2	53.8	7.3
$R_{YD}5$	40-50	23.5	27.4	11.8	28.7	8.6	8.1	16.6	22.8	46.3	6.2
$R_{YD}6$	50-60	18.2	21.3	8.6	38.0	13.8	8.7	11.1	23.0	47.5	9.7
$R_{YD}7$	60-70	17.3	17.8	15.0	37.6	12.3	16.1	9.6	16.0	49.7	8.7
Rhone meltout sediment samples											
R209		12.6	3.9	21.2	38.2	24.2	8.8	4.4	15.8	47.2	23.9
RS2		1.8	3.5	41.9	43.9	8.9	2.8	0.4	41.5	42.1	13.2
Rhone suspended sediment sample											
F272		0.0	0.0	54.8	33.6	11.7	0.0	0.0	53.6	35.0	11.4
F91		0.0	0.0	68.8	18.6	12.6	0.0	0.0	27.1	55.6	17.3
F235		0.0	0.0	15.1	67.3	17.6	0.0	0.0	0.0	79.0	21.0
F74		0.0	0.0	12.8	74.4	12.9	0.0	0.0	26.5	59.7	13.8

Clay mineralogy of bedrock samples (%)

Sample	Fraction	Rock	bio-verm m.-l.	verm.	biotite	phengite	chlorite	bio/pheng	cc/qtz	qtz/KFsp	qtz/plagio
R1A	< 2µm	GrGr	0	0	37.1	57.3	5.6	0.65			
R6A	< 2µm	GrGr	0	0	42.0	58.0	0.0	0.72			
R8A	< 2µm	VGn	0	0	24.5	36.3	39.2	0.68			
R9A	< 2µm	GrGr	0	0	38.2	47.5	14.3	0.80			
R15A	< 2µm	VGn	0	0	59.9	10.6	29.5	5.62			
R17A	< 2µm	CAGr	0	0	19.9	80.1	0.0	0.25			
R1A	2-16 µm	GrGr	0	0	49.6	44.4	6.0	1.12	0.06	0.23	0.11
R6A	2-16 µm	GrGr	0	0	52.7	47.3	0.0	1.12	0.10	0.09	0.11
R8A	2-16 µm	VGn	0	0	28.3	33.8	37.9	0.84	0.00	0.61	0.09
R9A	2-16 µm	GrGr	0	0	37.0	39.9	23.1	0.93	0.00	0.39	0.08
R15A	2-16 µm	VGn	0	0	42.5	23.0	34.5	1.85	12.73	0.44	0.05
R17A	2-16 µm	CAGr	0	0	35.7	61.0	3.3	0.59	0.11	0.08	0.02

XRF Oberaar samples I

Channel	Unit	Profile O140A, Oberaar LIA, 1860										Profile O140B, Oberaar LIA, 1860						
		$O_{140A}1$	$O_{140A}2$	$O_{140A}3$	$O_{140A}4$	$O_{140A}5$	$O_{140A}6$	$O_{140A}7$	$O_{140A}8$	$O_{140A}9$	$O_{140A}10$	$O_{140B}1$	$O_{140B}2$	$O_{140B}3$	$O_{140B}4$	$O_{140B}5$	$O_{140B}6$	$O_{140B}7$
depth	cm	0-10	-20	-30	-40	-50	-60	-70	-80	-90	-100	0-10	-20	-30	-40	-50	-60	-70
SiO_2	%	71.99	72.46	70.49	73.11	71.86	71.71	71.22	69.89	70.98	70.07	69.55	72.68	71.24	71.89	72.72	72.10	72.11
TiO_2	%	0.36	0.36	0.34	0.31	0.34	0.37	0.37	0.36	0.36	0.47	0.46	0.41	0.40	0.35	0.33	0.34	0.36
Al_2O_3	%	14.30	13.81	14.03	13.45	14.12	14.13	13.79	14.65	14.64	14.61	14.26	13.84	13.92	14.34	14.21	14.36	14.22
Fe_2O_3	%	1.08	0.81	1.03	0.83	0.79	1.05	1.05	1.03	1.03	1.18	1.45	1.23	1.36	1.14	0.98	0.97	0.9
FeO	%	1.17	1.36	1.24	1.03	1.17	1.27	1.77	1.5	1.3	1.39	1.58	1.17	1.29	1.23	1.15	1.19	1.33
MnO	%	0.05	0.05	0.05	0.05	0.05	0.05	0.07	0.06	0.05	0.05	0.07	0.05	0.05	0.05	0.05	0.05	0.05
MgO	%	1.01	1.11	1.09	0.91	0.96	1.01	1.46	1.28	1.02	1.08	1.43	1.10	1.12	1.07	1.00	1.10	1.02
CaO	%	1.38	1.46	1.88	1.80	1.95	1.77	1.9	2.21	1.77	1.96	1.40	1.33	1.57	1.49	1.25	1.49	1.59
Na_2O	%	4.71	4.60	4.70	4.76	4.90	4.72	4.23	4.71	4.74	4.67	4.17	4.47	4.44	4.72	4.84	4.90	4.88
K_2O	%	2.89	2.62	2.79	2.54	2.49	2.80	2.64	2.88	3.12	3.07	2.82	2.70	2.84	2.79	2.69	2.73	2.63
P_2O_5	%	0.13	0.13	0.14	0.14	0.14	0.14	0.1	0.13	0.12	0.12	0.18	0.18	0.16	0.14	0.13	0.13	0.14
LOI	%	1.25	1.24	1.70	1.34	1.38	1.13	1.39	1.55	1.15	1.12	2.02	1.15	1.07	0.98	0.92	1.00	1.02
Fe tot	%	2.38	2.32	2.41	1.98	2.09	2.47	3.01	2.69	2.47	2.72	3.21	2.53	2.79	2.51	2.26	2.29	2.38
Ba	ppm	585	557	591	532	550	566	607	659	652	630	684	612	611	598	609	626	580
Cr	ppm	29	28	32	29	23	29	75	36	31	41	37	40	36	33	30	38	26
Cu	ppm	16	11	17	13	101	22	23	203	19	16	19	28	19	14	16	16	12
Nb	ppm	10	9	8	11	8	11	7	12	12	11	10	9	9	9	8	9	9
Ni	ppm	13	14	18	13	14	13	27	13	12	17	22	20	17	16	13	14	11
Pb	ppm	20	17	24	22	21	20	15	15	15	26	32	21	42	23	22	24	19
Rb	ppm	104	98	97	92	91	98	95	104	111	107	117	100	99	96	93	95	94
Sr	ppm	259	266	290	277	315	268	253	288	262	307	290	273	286	281	276	288	286
V	ppm	42	48	49	42	42	50	53	51	46	51	67	52	53	48	52	49	42
Y	ppm	28	26	25	27	24	25	24	24	29	32	26	29	34	24	22	25	25
Zn	ppm	112	112	116	108	126	111	123	141	112	116	132	118	106	116	112	110	110
Zr	ppm	197	198	190	194	180	205	169	179	172	202	253	247	231	212	178	189	177

XRF Oberaar samples II

Channel	Unit	Profile O140B			Profile OYD, Oberaar YD, 10'000 BP						Meltout/Lake Sediment Oberaar						Suspension	
		$O_{140B}8$	$O_{140B}9$	$O_{140B}10$	$O_{YD}1$	$O_{YD}2$	$O_{YD}3$	$O_{YD}4$	$O_{YD}5$	$O_{YD}6$	GSL1	GSL2	GSL2A	GSL3	GSR1	LS1	OA1	OA2
depth	cm	-80	-90	-100	0-10	-20	-30	-40	-50	-60	Meltout	Meltout	Meltout	Meltout	Meltout	Lakesedi	Susp.	Susp.
SiO_2	%	71.62	71.84	71.45	31.39	67.83	56.70	69.86	70.01	71.64	72.94	69.75	72.82	72.33	71.35	73.73	61.65	63.73
TiO_2	%	0.37	0.38	0.38	0.28	0.33	0.42	0.43	0.39	0.39	0.33	0.38	0.28	0.36	0.36	0.55	0.67	0.65
Al_2O_3	%	13.99	13.79	14.38	5.85	12.85	11.95	13.18	14.10	13.35	13.15	14.34	13.68	13.39	14.50	11.47	16.25	15.68
Fe_2O_3	%	1.00	1.08	1.04	0.05	0.05	0.01	1.12	1.02	1.02	0.83	1.39	0.88	1.15	0.97	1.16	2.31	2.11
FeO	%	1.3	1.36	1.35	2.13	1.82	1.87	1.29	1.04	0.97	1.22	1.58	0.90	1.15	1.15	1.64	3.37	2.93
MnO	%	0.05	0.05	0.05	0.03	0.03	0.02	0.04	0.04	0.04	0.05	0.06	0.04	0.05	0.05	0.07	0.11	0.1
MgO	%	1.11	1.16	1.07	0.36	0.53	0.49	0.77	0.71	0.69	0.98	1.43	0.75	1.00	0.86	1.35	3.1	2.54
CaO	%	1.66	1.57	1.61	0.57	0.97	0.86	1.18	1.07	1.30	1.93	2.01	1.49	1.86	1.92	2.75	1.99	1.97
Na_2O	%	4.59	4.33	4.63	0.98	3.47	2.80	3.73	4.12	3.97	4.4	4.45	4.68	4.43	4.75	3.28	2.81	3.1
K_2O	%	2.67	2.77	2.99	1.17	3.38	2.63	3.25	3.82	3.27	2.61	2.85	3.13	2.66	3.20	2.40	4.31	4.13
P_2O_5	%	0.14	0.14	0.14	0.60	0.10	0.27	0.08	0.10	0.11	0.17	0.17	0.11	0.17	0.13	0.24	0.18	0.18
LOI	%	1.09	1.14	1.00	10.00	8.27	21.69	4.69	3.05	2.71	1.48	1.73	0.90	1.41	1.11	1.66	3.04	2.54
Fe tot	%	2.45	2.59	2.54	1.50	2.07	2.09	2.56	2.17	2.09	2.19	3.15	1.88	2.43	2.25	2.99	6.05	5.37
Ba	ppm	606	638	677	250	647	528	606	738	614	625	678	563	636	625	517	1026	938
Cr	ppm	34	34	31	21	19	30	23	18	17	26	43	21	28	26	38	99	67
Cu	ppm	17	19	13	6	2	2	27	2	3	12	19	14	15	12	23	31	27
Nb	ppm	9	8	10	7	14	13	14	16	16	8	10	9	9	14	16	17	19
Ni	ppm	15	16	14	7	4	5	7	4	6	12	20	12	12	10	20	42	32
Pb	ppm	20	25	20	32	12	16	13	13	17	19	32	19	23	16	17	27	32
Rb	ppm	97	102	110	66	107	89	105	120	110	99	117	104	100	116	101	224	221
Sr	ppm	289	280	271	76	153	136	155	156	167	317	334	235	327	263	306	238	237
V	ppm	47	50	44	32	32	45	42	27	31	38	56	34	43	37	51	100	86
Y	ppm	26	27	24	13	25	22	29	33	39	23	25	26	25	33	40	33	38
Zn	ppm	115	115	118	48	20	17	33	32	29	105	114	26	103	107	120	118	103
Zr	ppm	199	204	219	148	292	275	341	358	345	192	205	226	228	249	404	177	221

XRF Rhone samples I

Channel	Unit	Profile R145A, Rhone LIA, 1856										Profile R270A, Rhone LIA, 1720-1740						
		$R_{145A}1$	$R_{145A}2$	$R_{145A}3$	$R_{145A}4$	$R_{145A}5$	$R_{145A}6$	$R_{145A}7$	$R_{145A}8$	$R_{145A}9$	$R_{145A}10$	$R_{270A}1$	$R_{270A}2$	$R_{270A}3$	$R_{270A}4$	$R_{270A}5$	$R_{270A}6$	$R_{270A}7$
depth	cm	0-10	-20	-30	-40	-50	-60	-70	-80	-90	-100	0-10	-20	-30	-40	-50	-60	-70
SiO_2	%	74.93	74.98	74.87	75.18	75.66	75.67	75.1	75.61	76.36	76.41	74.22	74.50	74.81	74.76	76.17	74.92	75.62
TiO_2	%	0.22	0.20	0.18	0.20	0.19	0.22	0.22	0.2	0.21	0.19	0.21	0.22	0.21	0.19	0.20	0.17	0.17
Al_2O_3	%	13.65	13.73	13.93	13.66	13.36	13.40	13.64	13.39	13.07	13.13	13.17	13.62	13.57	13.75	13.21	13.92	13.36
Fe_2O_3	%	0.41	0.50	0.57	0.53	0.55	0.55	0.59	0.56	0.53	0.53	0.35	0.43	0.58	0.51	0.49	0.53	0.54
FeO	%	0.54	0.52	0.41	0.43	0.45	0.47	0.51	0.47	0.42	0.4	0.75	0.65	0.50	0.59	0.41	0.46	0.42
MnO	%	0.02	0.03	0.02	0.02	0.02	0.03	0.03	0.02	0.02	0.02	0.03	0.03	0.03	0.03	0.03	0.02	0.03
MgO	%	0.32	0.30	0.29	0.29	0.31	0.31	0.35	0.30	0.31	0.30	0.31	0.32	0.32	0.53	0.26	0.31	0.3
CaO	%	0.91	1.03	0.95	0.92	0.90	0.98	1.02	1.03	0.93	0.92	0.91	0.93	0.98	1.08	0.86	0.89	0.87
Na_2O	%	4.54	4.62	4.61	4.68	4.48	4.49	4.41	4.43	4.38	4.46	4.28	4.45	4.44	4.53	4.41	4.54	4.47
K_2O	%	3.87	3.71	3.97	3.84	3.81	3.81	3.88	3.80	3.67	3.61	3.80	3.99	3.98	3.91	3.88	4.14	3.96
P_2O_5	%	0.05	0.06	0.06	0.05	0.05	0.06	0.08	0.07	0.07	0.06	0.05	0.05	0.06	0.05	0.05	0.05	0.05
LOI	%	0.93	0.68	0.48	0.48	0.52	0.36	0.42	0.37	0.38	0.36	1.83	1.15	0.65	0.42	0.37	0.41	0.35
Fe tot	%	1.01	1.07	1.03	1.01	1.06	1.08	1.16	1.09	1	0.98	1.18	1.15	1.13	1.17	0.95	1.04	1.01
Ba	ppm	537	533	552	505	535	526	572	568	511	491	513	558	551	497	514	547	517
Cr	ppm	5	5	5	5	5	7	12	5	7	7	5	5	10	10	5	7	5
Cu	ppm	2	2	2	2	2	2	2	2	2	2	<2	<2	<2	<2	<2	<2	<2
Nb	ppm	18	13	10	16	15	16	13	12	12	12	16	18	16	11	17	10	15
Ni	ppm	3	3	3	3	3	3	3	3	3	3	<3	<3	<3	<3	<3	<3	<3
Pb	ppm	9	12	11	10	9	11	13	11	11	8	10	14	12	10	8	15	14
Rb	ppm	144	143	151	147	155	147	154	139	141	141	152	155	153	152	151	164	158
Sr	ppm	144	156	150	137	141	151	153	157	145	138	140	145	146	138	130	138	133
V	ppm	11	12	16	12	12	16	16	15	13	11	14	13	14	20	10	12	15
Y	ppm	38	32	30	37	32	42	35	33	37	33	36	42	40	31	52	31	36
Zn	ppm	88	93	78	87	82	91	89	95	90	84	87	90	84	85	86	84	79
Zr	ppm	239	227	224	225	211	256	253	272	254	250	266	242	247	185	273	234	217

XRF Rhone samples II

Channel	Unit	Profile R270A			Profile R270B, Rhone LIA, 1720-1740						
		$R_{270A}8$	$R_{270A}9$	$R_{270A}10$	$R_{270B}1$	$R_{270B}2$	$R_{270B}3$	$R_{270B}4$	$R_{270B}5$	$R_{270B}6$	$R_{270B}8$
depth	cm	80	90	100	10	20	30	40	50	60	80
SiO_2	%	75.37	74.51	74.41	71.83	74.35	73.36	74.86	74.74	73.79	74.65
TiO_2	%	0.2	0.21	0.21	0.22	0.22	0.24	0.20	0.21	0.24	0.24
Al_2O_3	%	13.11	13.52	13.52	14.03	13.48	14.14	13.71	13.65	14.16	13.80
Fe_2O_3	%	0.55	0.61	0.64	0.38	0.54	0.63	0.60	0.58	0.67	0.61
FeO	%	0.4	0.45	0.52	0.93	0.62	0.67	0.57	0.57	0.76	0.64
MnO	%	0.03	0.03	0.03	0.03	0.03	0.03	0.03	0.03	0.04	0.03
MgO	%	0.28	0.29	0.34	0.35	0.36	0.47	0.36	0.35	0.41	0.36
CaO	%	0.92	1.03	1.05	1.07	0.85	1.08	0.84	0.92	1.02	1
Na_2O	%	4.37	4.58	4.44	4.56	4.37	4.63	4.33	4.35	4.52	4.51
K_2O	%	3.79	3.81	3.84	3.88	4.04	4.06	4.32	4.16	4.24	3.99
P_2O_5	%	0.06	0.06	0.06	0.06	0.05	0.06	0.06	0.06	0.06	0.06
LOI	%	0.36	0.36	0.43	2.78	1.18	0.63	0.51	0.47	0.47	0.44
Fe tot	%	1	1.11	1.22	1.41	1.23	1.37	1.23	1.22	1.51	1.33
Ba	ppm	506	504	529	511	452	554	476	550	632	525
Cr	ppm	5	5	5	10	5	5	8	5	6	9
Cu	ppm	<2	<2	<2	<2	<2	<2	<2	<2	<2	<2
Nb	ppm	18	19	16	17	20	21	18	22	18	24
Ni	ppm	<3	<3	<3	<3	<3	<3	<3	<3	<3	<3
Pb	ppm	11	13	16	18	12	12	10	14	12	14
Rb	ppm	149	154	149	164	172	167	181	176	173	167
Sr	ppm	139	147	157	155	128	145	121	132	149	143
V	ppm	11	14	20	17	21	18	18	10	17	15
Y	ppm	43	43	37	36	44	44	42	43	43	52
Zn	ppm	87	86	89	96	86	87	90	89	96	98
Zr	ppm	275	272	282	213	259	205	232	201	240	263

XRF Rhone samples III

Channel	Unit	Profile RYD, Rhone YD, 10'000 BP								Suspension	
		$R_{YD}1$	$R_{YD}2$	$R_{YD}3$	$R_{YD}4$	$R_{YD}5$	$R_{YD}6$	$R_{YD}7$	RS	RH1	RH2
depth	cm	10	20	30	40	50	60	70	Meltout	Susp.	Susp.
SiO_2	%	66.91	75.09	72.21	65.62	68.31	69.1	71.97	82.57	67.91	67.63
TiO_2	%	0.34	0.33	0.4	0.43	0.35	0.35	0.32	0.14	0.39	0.4
Al_2O_3	%	11.52	11.84	12.2	14.32	14.53	14.67	13.73	9.44	15.27	15.11
Fe_2O_3	%	0.05	0.42	1	2.17	1.58	1.35	1.19	0.30	1.61	1.8
FeO	%	1.36	0.65	1.02	1.32	0.97	0.89	0.7	0.27	1.77	1.89
MnO	%	0.03	0.07	0.05	0.07	0.04	0.04	0.04	0.02	0.08	0.09
MgO	%	0.49	0.26	0.48	0.67	0.64	0.62	0.53	0.20	1.34	1.51
CaO	%	1.01	0.67	0.9	1.08	1.13	1.23	1.15	0.51	0.91	0.94
Na_2O	%	3.50	3.63	3.57	3.99	4.31	4.41	4.24	3.19	3.85	3.7
K_2O	%	2.55	3.08	2.7	3.17	3.44	3.44	3.35	3.03	4.84	4.82
P_2O_5	%	0.27	0.16	0.29	0.24	0.14	0.14	0.12	0.04	0.09	0.1
LOI	%	11.72	3.45	5.02	6.51	4.03	3.34	2.32	0.25	1.83	1.74
Fe tot	%	1.56	1.14	2.13	3.64	2.66	2.34	1.96	0.60	3.58	3.9
Ba	ppm	621	676	544	578	640	590	561	262	515	533
Cr	ppm	12	11	18	13	12	14	9	5	20	15
Cu	ppm	5	43	3	<2	5	3	29	2	7	9
Nb	ppm	14	11	15	22	14	18	16	18	38	36
Ni	ppm	4	<3	4	3	<3	4	<3	3	7	5
Pb	ppm	34	16	14	13	10	15	12	9	29	27
Rb	ppm	127	110	129	129	134	140	129	132	335	337
Sr	ppm	229	179	178	174	183	183	174	61	100	103
V	ppm	33	29	32	33	26	22	26	7	32	38
Y	ppm	27	20	28	35	33	35	35	47	73	64
Zn	ppm	34	7	16	26	26	23	20	75	66	76
Zr	ppm	262	269	250	271	209	231	307	374	134	151

SEDEX extraction results from moraine samples from the two catchments (mg g^{-1}).

Sample	Depth	Fe-P	Weak acid	Strong acid	Det-P	Org-P	Particulate P
Rhone moraines samples LIA 145 y							
$R_{145A}1$	0-10	0.0300	0.1002	0.0585	0.1587	0.0085	0.1972
$R_{145A}2$	10-20	0.0300	0.1298	0.0558	0.1856	0.0040	0.2196
$R_{145A}3$	20-30	0.0300	0.1726	0.0721	0.2446	0.0074	0.2820
$R_{145A}4$	30-40	0.0300	0.1504	0.0481	0.1985	0.0080	0.2365
$R_{145A}5$	40-50						
$R_{145A}6$	50-60	0.0300	0.2105	0.0654	0.2760	0.0031	0.3091
$R_{145A}7$	60-70	0.0300	0.2094	0.0455	0.2549	0.0031	0.2880
$R_{145A}8$	70-80	0.0300	0.2285	0.0499	0.2785	0.0101	0.3186
$R_{145A}9$	80-90	0.0300	0.1143	0.0497	0.1640	0.0047	0.1987
$R_{145A}10$	90-100	0.0300	0.1688	0.0679	0.2367	0.0031	0.2698
Rhone moraines samples LIA 270 y							
$R_{270}A$	0-10	0.0300	0.0643	0.0371	0.1014	0.0151	0.1465
$R_{270}A$	10-20	0.0300	0.1060	0.0402	0.1463	0.0109	0.1871
$R_{270}A$	20-30	0.0300	0.1101	0.0354	0.1455	0.0076	0.1831
$R_{270}A$	30-40	0.0300	0.1233	0.0263	0.1496	b/d	0.1796
$R_{270}A$	40-50	0.0300	0.1286	0.0314	0.1601	b/d	0.1901
$R_{270}A$	50-60	0.0300	0.0869	0.0202	0.1071	b/d	0.1371
$R_{270}A$	60-70	0.0300	0.1220	0.0363	0.1583	b/d	0.1883
$R_{270}A$	70-80	0.0300	0.1183	0.0402	0.1586	b/d	0.1886
$R_{270}A$	80-90	0.0300	0.1524	0.0413	0.1937	b/d	0.2237
$R_{270}A$	90-100	0.0300	0.1620	0.0396	0.2016	0.0063	0.2379
Rhone moraines samples YD > 10 ky							
$R_{YD}1$	0-10	0.8850	0.0248	0.0264	0.0512	0.1707	1.1068
$R_{YD}2$	10-20	0.6090	0.0177	0.0060	0.0237	0.0260	0.6588
$R_{YD}3$	20-30	1.1760	0.0244	0.0110	0.0354	0.0310	1.2424
$R_{YD}4$	30-40	0.8880	0.0807	0.0188	0.0995	0.0207	1.0082
$R_{YD}5$	40-50	0.2874	0.1495	0.0830	0.2325	0.0197	0.5396
$R_{YD}6$	50-60	0.2139	0.1766	0.0750	0.2517	0.0216	0.4872
$R_{YD}7$	60-70	0.1092	0.1891	0.0858	0.2749	0.0271	0.4113
Oberaar moraines samples LIA 140 y							
$O_{140A}1$	0-10	0.0297	0.3454	0.2812	0.6266	0.0297	0.6860
$O_{140A}2$	10-20	0.0300	0.5342	0.2936	0.8278	0.0285	0.8863
$O_{140A}3$	20-30	0.0300	0.4704	0.3287	0.7992	0.0172	0.8464
$O_{140A}4$	30-40	0.0300	0.4999	0.2499	0.7498	0.0121	0.7919
$O_{140A}5$	40-50	0.0300	0.2901	0.1811	0.4712	0.0124	0.5136
$O_{140A}6$	50-60	0.0300	0.4948	0.2133	0.7081	0.0172	0.7553
$O_{140A}7$	60-70	0.0300	0.3352	0.1728	0.5080	0.0100	0.5480
$O_{140A}8$	70-80	0.0582	0.5586	0.2271	0.7857	0.0176	0.8616
$O_{140A}9$	80-90	0.0300	0.5446	0.1475	0.6920	0.0180	0.7401
$O_{140A}10$	90-100	0.0300	0.3407	0.1263	0.4670	0.0102	0.5073
Oberaar moraines samples YD > 10 ky							
$O_{YD}1$	0-10	1.8660	0.1675	0.0066	0.1741	0.5961	2.6362
$O_{YD}2$	10-20	0.9810	0.1412	0.0000	0.1412	0.2164	1.3386
$O_{YD}3$	20-30	0.3600	0.1359	0.0000	0.1359	0.0587	0.5546
$O_{YD}4$	30-40	0.1002	0.3123	0.0891	0.4014	0.0178	0.5194
$O_{YD}5$	40-50	0.0825	0.3156	0.0698	0.3853	0.0210	0.4889

SEDEX extraction results from suspended sediments from the two glaciers (mg g^{-1}).

Sample	Fe-P	Weak acid	Strong acid	Det-P	Org-P	Particulate P
Rhone Suspension						
7-Jul-99 (10:00)	0.0433	0.1862	0.0984	0.2846	0.0195	0.3474
8-Jul-99 (17:00)	0.0539	0.1690	0.0926	0.2616	0.0049	0.3204
9-Jul-99 (10:00)	0.0610	0.1789	0.0674	0.2463	0.0173	0.3246
21-Jul-99 19:00)	0.0744	0.1910	0.0483	0.2393	0.0106	0.3244
29-Jul-99 (10:00)	0.0330	0.2103	0.1071	0.3174	0.0076	0.3581
2-Aug-99 (10:00)	0.0492	0.1367	0.0917	0.2284	0.0034	0.2810
4-Aug-99 (10:00)	0.2174	0.2196	0.1159	0.3355	0.0101	0.5629
21-Sep-99 (14:00)	0.0098	0.1817	0.1044	0.2861	0.0102	0.3062
21-Sep-99 (10:00)	0.0594	0.2261	0.1203	0.3464	0.0032	0.4090
21-Sep-99 (10:00)	0.0583	0.2196	0.1301	0.3497	0.0000	0.4079
13-May-00 (10:00)	0.0584	0.2622	0.0848	0.3470	0.0089	0.4142
23-May-00 (10:00)	0.0748	0.2244	0.0459	0.2703	0.0107	0.3558
6-Jun-00 (10:00)	0.0267	0.2261	0.1165	0.3426	0.0075	0.3769
15-Jun-00 (10:00)	0.0264	0.1975	0.0971	0.2946	0.0058	0.3268
19-Jun-00 (17:00)	0.0596	0.2124		0.2124	0.0072	0.2792
11-Jun-00 (10:00)	0.0280	0.2037	0.1264	0.3301	0.0104	0.3685
20-Jun-00 (10:00)	0.0589	0.2973	0.0485	0.3458	0.0000	0.4048
4-Jul-00 (10:00)	0.0342	0.1996	0.1228	0.3224	0.0093	0.3660
6-Jul-00 (10:00)	0.0424	0.3041	0.0889	0.3930	0.0059	0.4414
25-Jul-00 (10:00)	0.0316	0.2870	0.1130	0.4000	0.0065	0.4381
25-Jul-00 (17:00)	0.0346	0.2663	0.1180	0.3843	0.0208	0.4397
19-Aug-00 (10:00)	0.0220	0.2158	0.1177	0.3334	0.0088	0.3643
22-Aug-00 (10:00)	0.0391	0.2263	0.1387	0.3650	0.0128	0.4169
average	**0.0520**	**0.2192**	**0.0997**	**0.3146**	**0.0088**	**0.3754**
±	*0.0399*	*0.0414*	*0.0269*	*0.0531*	*0.0053*	*0.0637*
Oberaar Suspension						
7-Jul-99 (10:00)	0.0238	0.3040	0.1431	0.4471	0.0101	0.4811
29-Jul-99 (17:00)	0.0262	0.2972	0.2874	0.5846	0.0128	0.6236
1-Sep-99 (17:00)	0.0302	0.2802	0.2648	0.5450	0.0099	0.5851
5-Aug-99 (10:00)	0.0544	0.3697	0.3582	0.7279	0.0107	0.7930
19-Aug-99 (10:00)	0.0374	0.2688	0.2473	0.5161	0.0097	0.5632
17-May-00 (10:00)	0.0173	0.3097	0.2761	0.5858	0.0153	0.6183
14-Jun-00 (17:00)	0.0216	0.3274	0.2781	0.6054	0.0165	0.6435
26-Jun-00 (17:00)	0.0180	0.3039	0.2676	0.5715	0.0136	0.6031
10-Jul-00 (17:00)	0.0189	0.2858	0.2289	0.5147	0.0267	0.5603
26-Jul-00 (17:00)	0.0235	0.3716	0.2665	0.6381	0.0106	0.6721
26-Jul-00 (17:00)	0.0268	0.3363	0.2836	0.6199	0.0146	0.6612
9-Aug-00 (10:00)	0.0220	0.3089	0.1779	0.4868	0.0247	0.5336
18-Sep-00 (17:00)	0.0205	0.3632	0.2508	0.6140	0.0135	0.6480
sample name lost	0.0455	0.4917	0.2395	0.7312	0.0103	0.7870
20-Sep-00 (17:00)	0.0240	0.3115	0.2624	0.5739	0.0157	0.6137
average	**0.0273**	**0.3287**	**0.2555**	**0.5841**	**0.0143**	**0.6258**
±	*0.0111*	*0.0821*	*0.0862*	*0.1556*	*0.0056*	*0.1602*

SEDEX extraction results from suspended sediments from the two glaciers and the Apure and Amazon (µmol g^{-1}).

Sample	Sample Date	Distance from source (km)	Det-P	Fe-P	Org-P	Particulate P
Apure sediments [#]						
BEDLOAD						
Head water rivers						
1. Tomon	Mar-99	-	11.31	0.89	0.79	12.98
Vitisy	Sep-99	-	33.05	21.02	25.19	79.26
Tirindi	Sep-99	-	0	0.97	1.82	2.79
2. Corojo	Mar-99	-	36.23	0.97	2.91	40.11
2. Corojo	Sep-99	-	48.76	0.97	2.91	52.63
Average (without Vitisy)		*20*	*17.93*	*0.94*	*1.84*	*20.71*
Intermediate and Llanos Rivers						
5. Bocono entry to lake	Sep-99	100	26.82	1.01	1.14	28.97
3. Guanare, Biscucui	Sep-99	137	12.64	1.97	1.64	16.25
4. Portuguesa, Llanos Road	Sep-99	200	6.61	4.81	4.58	16.01
8. Guanare before Bocono (0 - 2 m)	Sep-99	213	20.77	4.57	3.31	28.66
9. Bocono & Guanare	Sep-99	216	17.81	2.07	2.01	21.89
15. Apure before Purtuguesa, San Fernando	Sep-99	950	0.14	1.2	5.11	6.45
17. Mouth Apure	Mar-99	1247	4.02	9.69	2.91	16.61
Average			*13.34*	*3.28*	*2.82*	*19.44*
SUSPENSION						
Intermediate and Llanos Rivers						
5. Bocono entry to lake	Sep-99	100	13.77	5.63	5.57	24.97
3. Guanare, Biscucui	Sep-99	137	8.44	5.5	3.3	17.24
4. Portuguesa, Llanos Road	Sep-99	200	5.93	3.57	4.79	14.29
8. Guanare before Bocono (0 - 2 m)	Sep-99	213	8.73	8.43	6.36	23.52
9. Bocono & Guanare	Sep-99	216	8.97	7.9	5.77	22.64
10. Guanare before Portuguesa (g)	Nov-00	400	7.56	9.69	5.16	22.41
10. Guanare before Portuguesa (s)	Nov-00	400	7.3	10.33	5.22	22.85
12. Portuguesa + Guanare 800 m (g)	Nov-00	400	5.8	11.62	6.12	23.55
12. Portuguesa + Guanare 800 m (s)	Nov-00	400	4.86	15.18	5.29	25.33
13. Portuguesa + Guanare 15 km (s)	Nov-00	415	5.94	11.95	5.7	23.58
14. Portuguesa before Apure, San Fernando (g)	Nov-00	450	6.72	12.92	5.49	25.13
15. Apure before Portuguesa, San Fernando (g)	Sep-99	950	4.2	17.04	3.23	24.47
15. Apure before Portuguesa, San Fernando (g)	Nov-00	950	6.46	8.72	5.17	20.34
15. Apure before Portuguesa, San Fernando (s)	Nov-00	950	6.12	8.72	5.36	20.2
16. Apure Boquerones	Sep-99	1037	4.51	10.91	3.58	19.01
17. Mouth Apure	Sep-99	1247	3.44	14.55	3.73	21.72
Average			*6.8*	*10.17*	*4.99*	*21.95*
AMAZON RIVER SUSPENSION [†]			6.78	7.43	7.43	21.63
GLACIAL SEDIMENTS						
Rhone (n = 21)	1999-2000	0	10	1.61*	0.32	11.93
Oberaar (n = 15)	1999-2000	0	18.72	1.61*	0.32	20.65

[#] The numbering corresponds to the sample points on Fig. 6.3

[†] Berner and Rao (1994)

* cf. estimates in Table 6.6.

Oberaar suspended sediment, fraction 2 - 16 µm, pictures 1 - 3

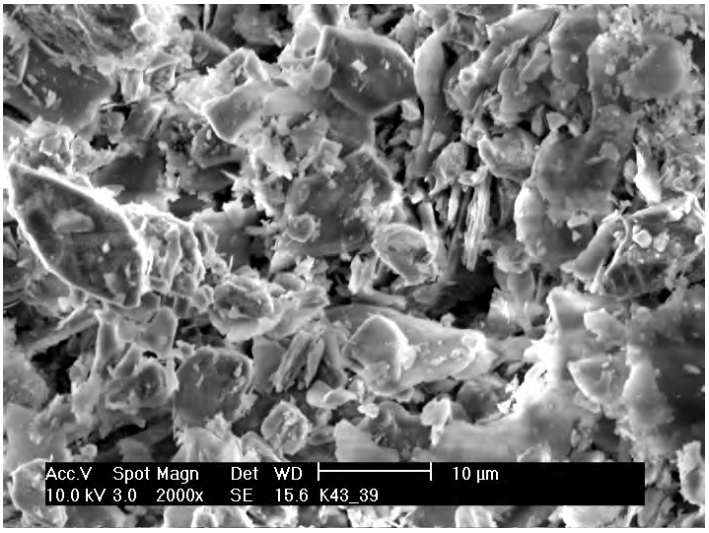

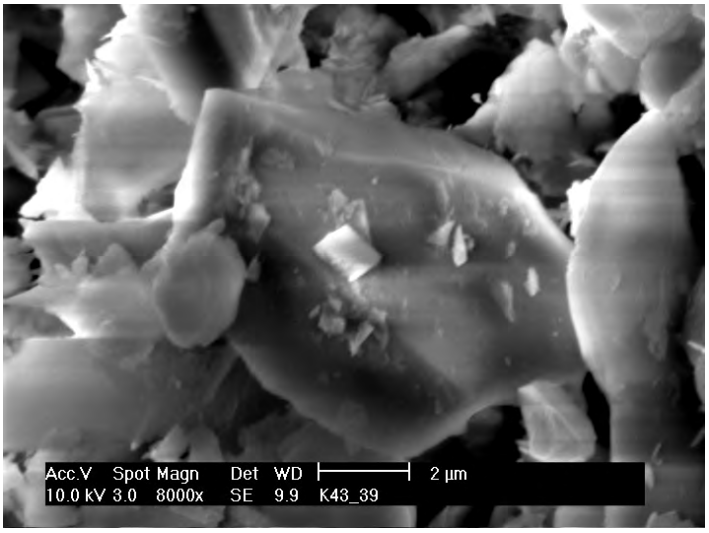

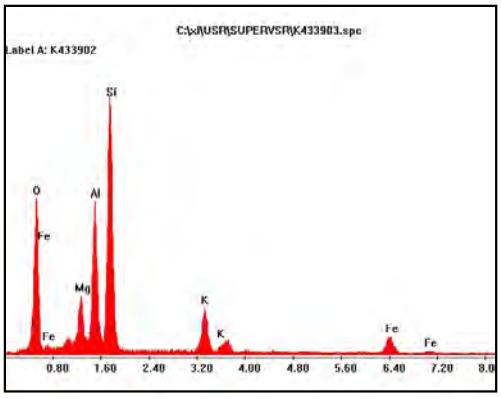

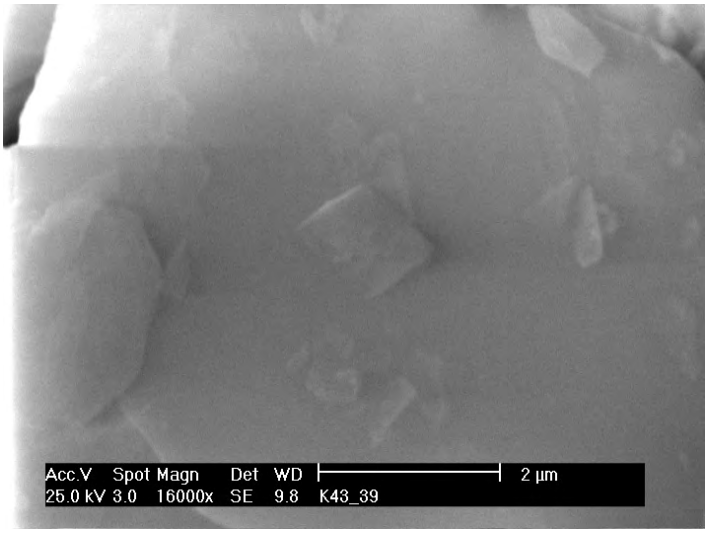

Oberaar suspended sediment, fraction 2 - 16 µm, pictures 4 - 6

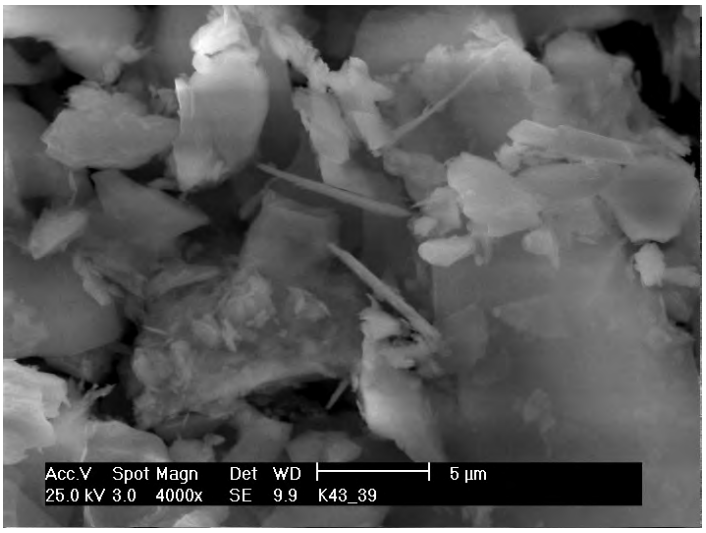

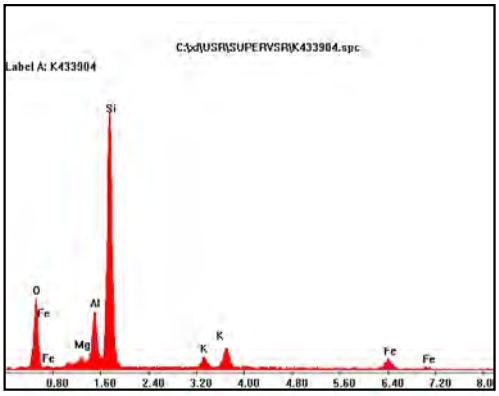

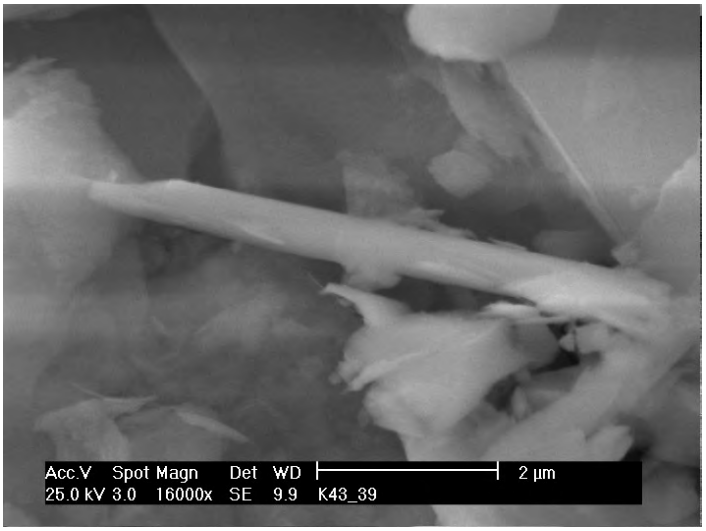

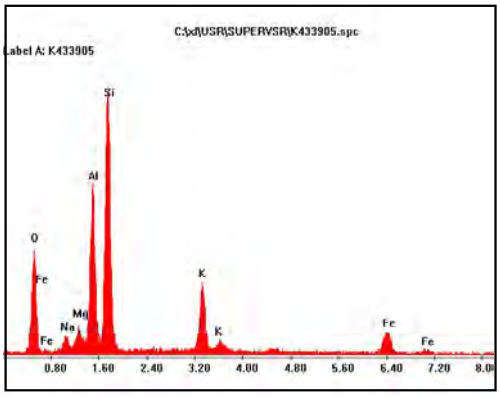

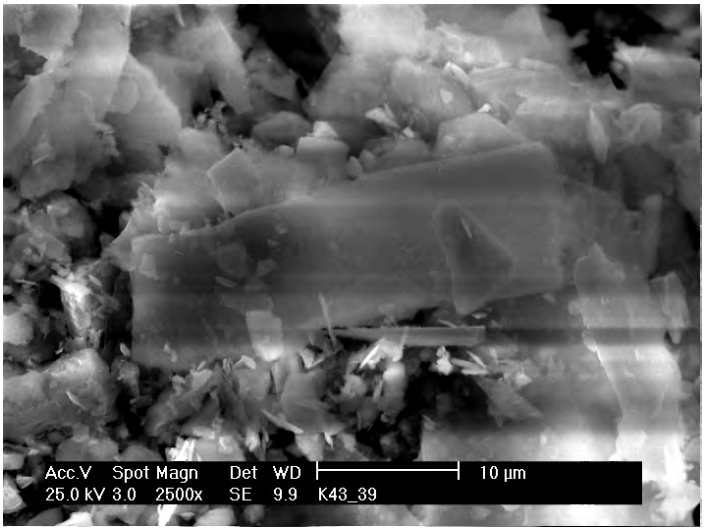

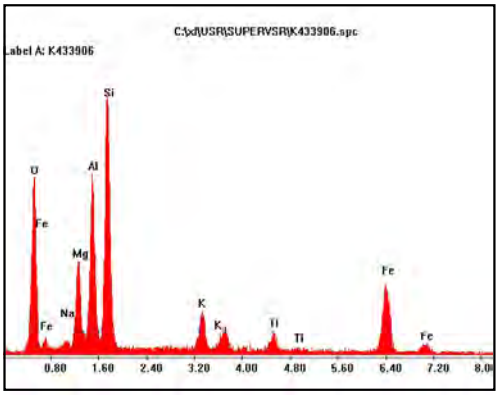

Oberaar suspended sediment, fraction 2 - 16 µm, pictures 7 - 9

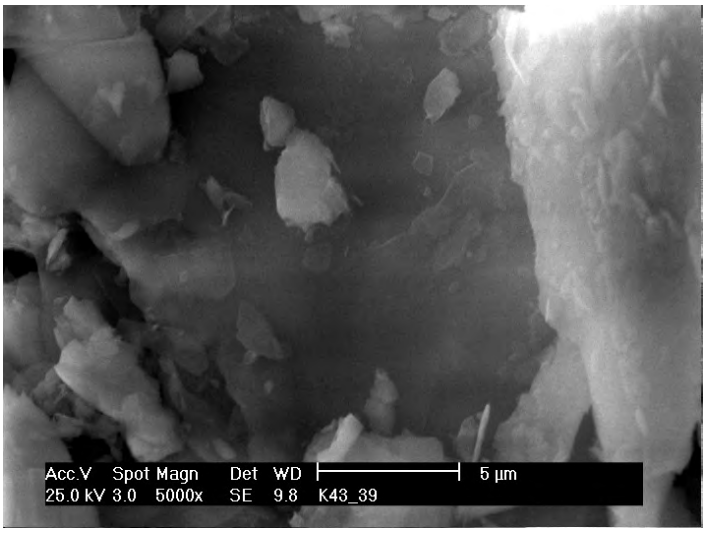

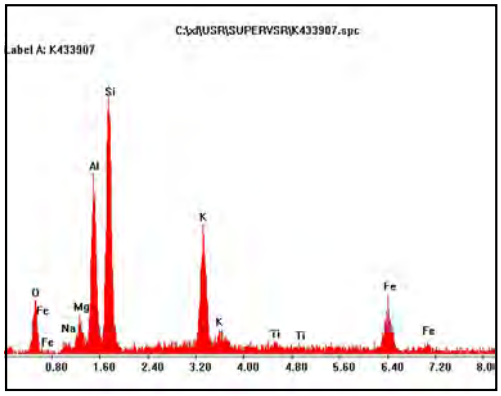

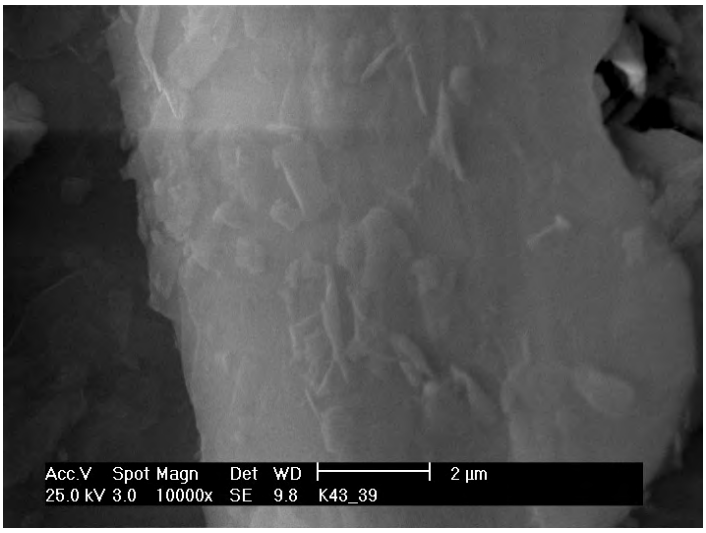

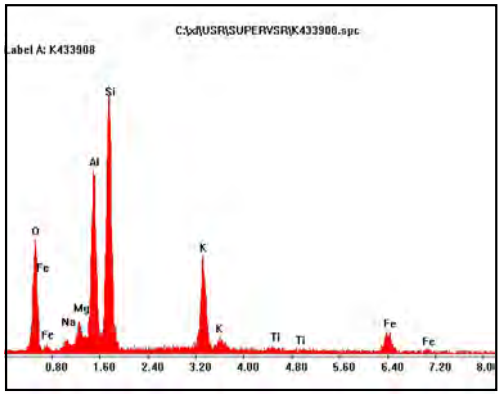

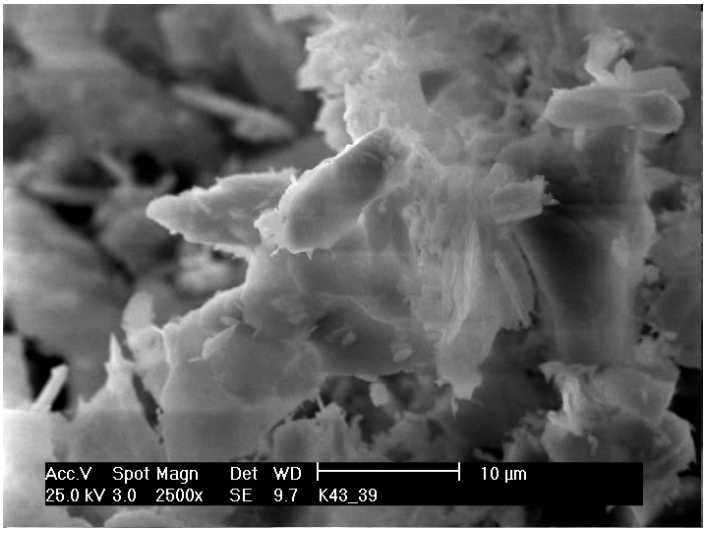

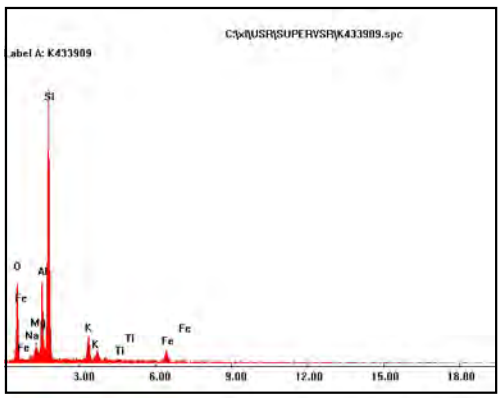

Oberaar suspended sediment, fraction 2 - 16 µm, pictures 10 - 12

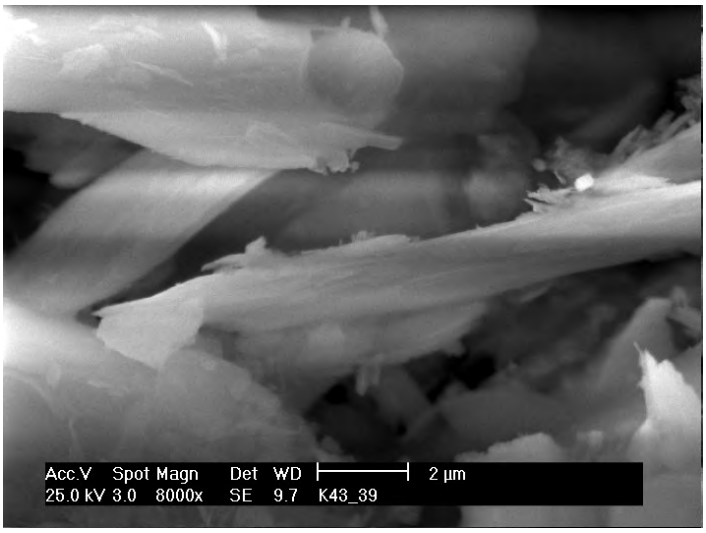

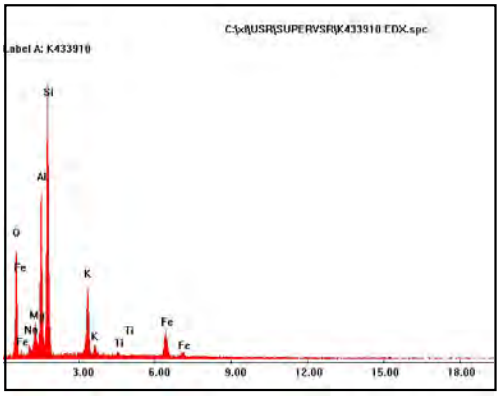

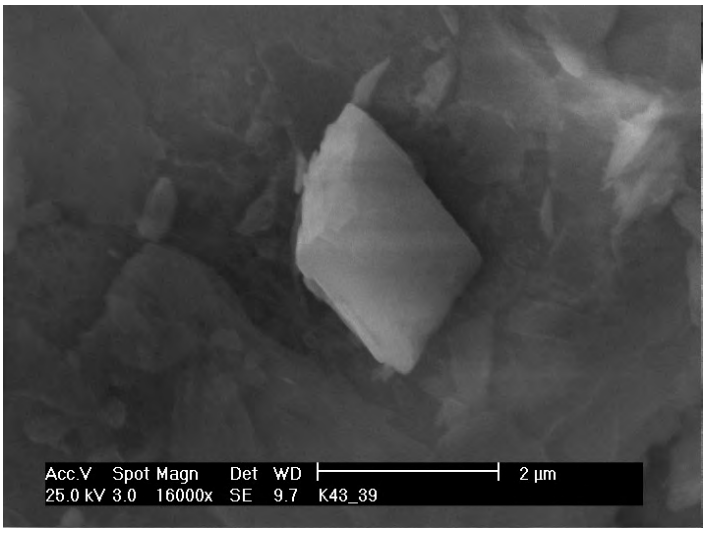

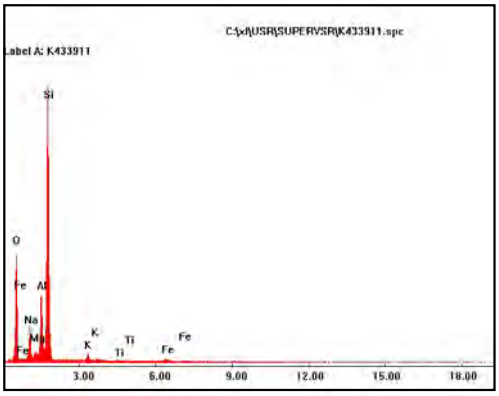

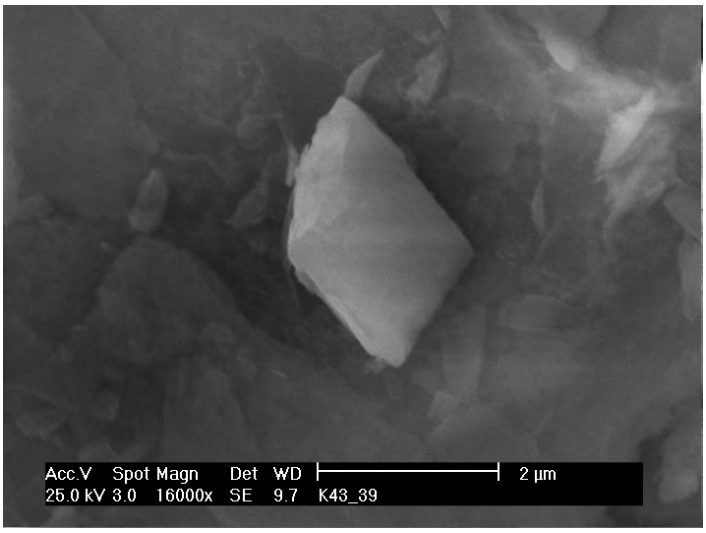

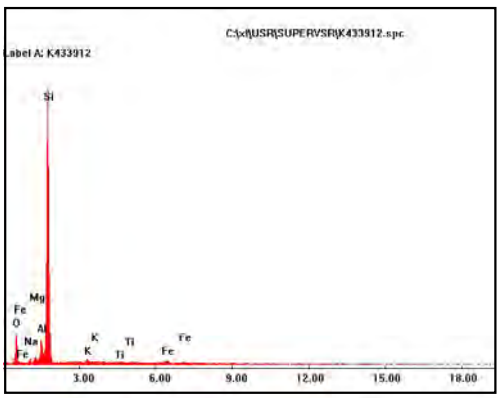

Oberaar suspended sediment, fraction 2 - 16 µm, picture 13

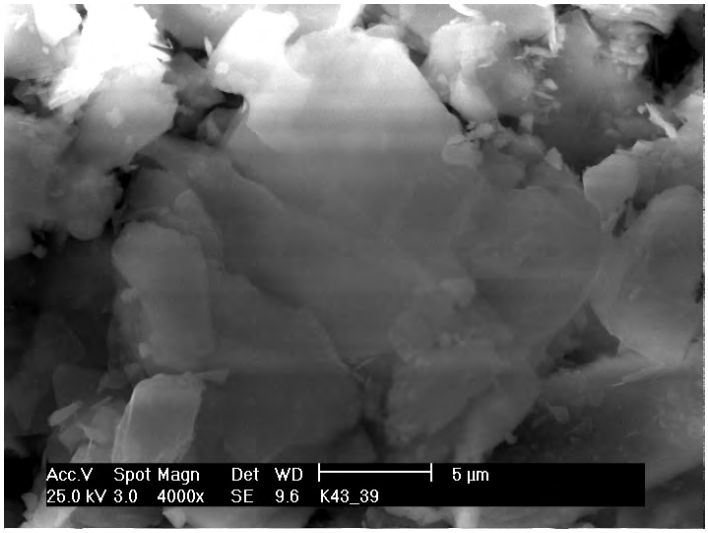

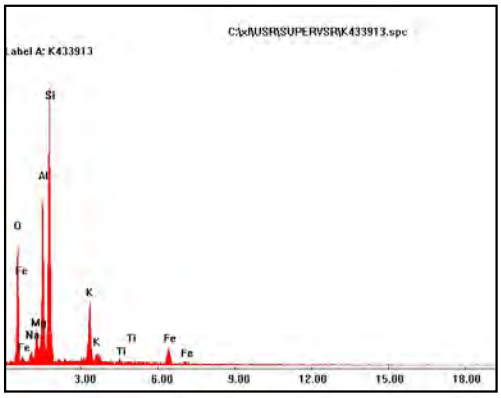

Oberaar YD moraine profile, 50 - 60 cm, fraction 2 - 16 µm, pictures 1 - 3

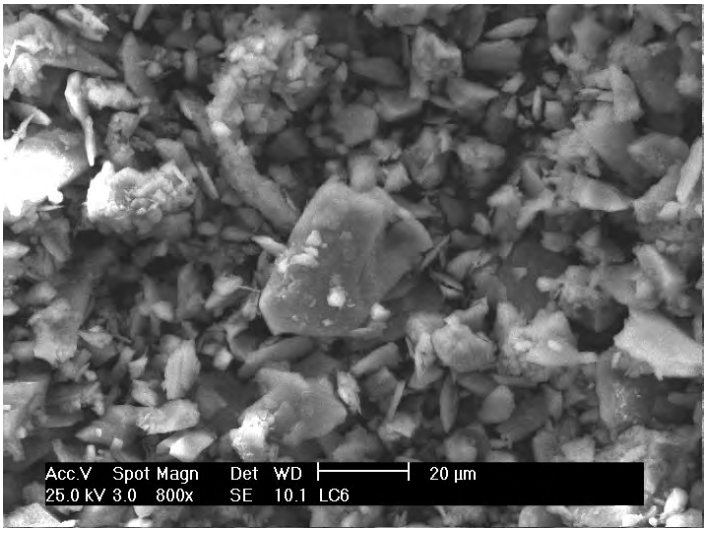

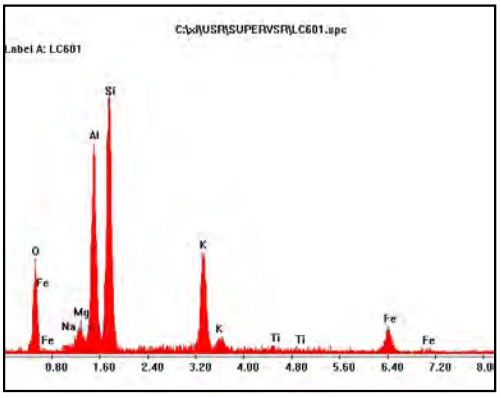

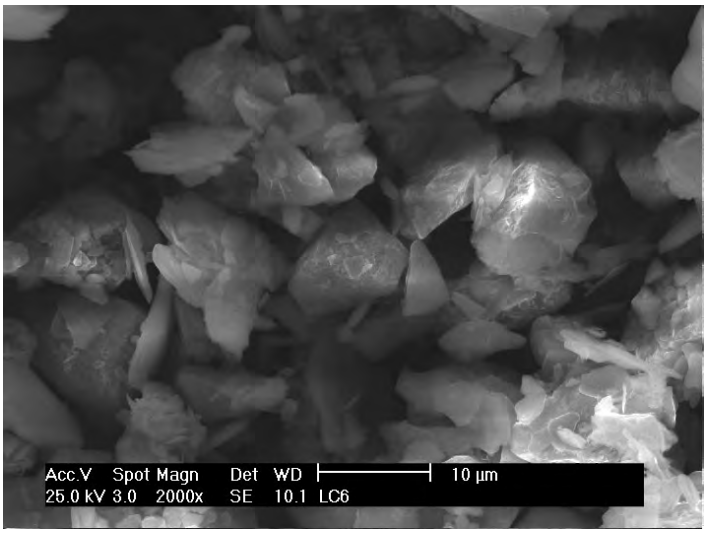

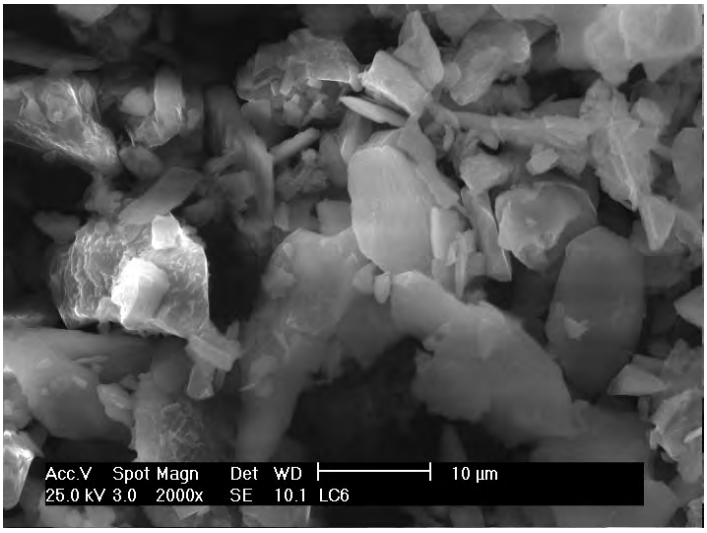

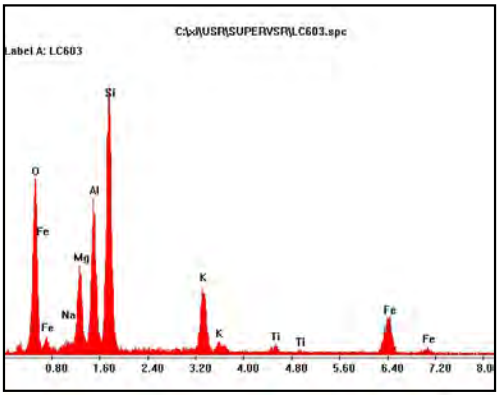

Oberaar YD moraine profile, 50 - 60 cm, fraction 2 - 16 µm, pictures 4 - 6

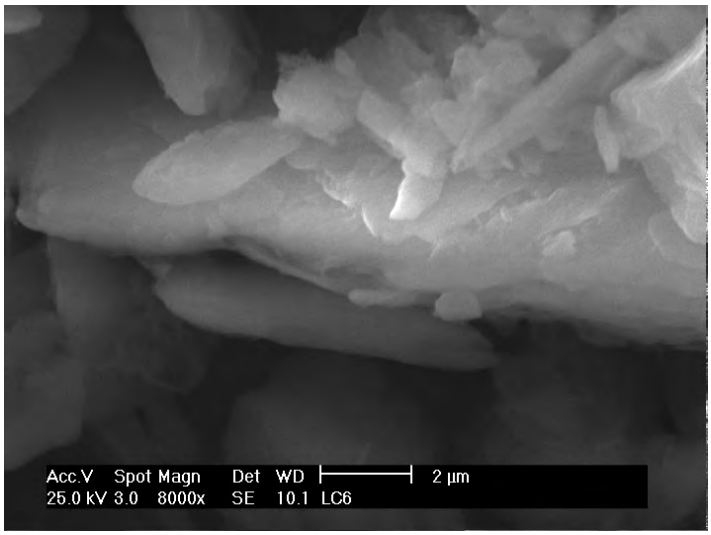

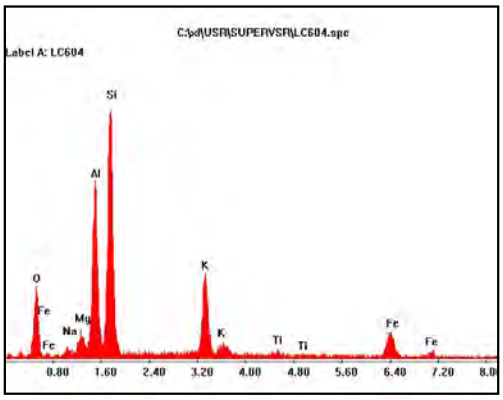

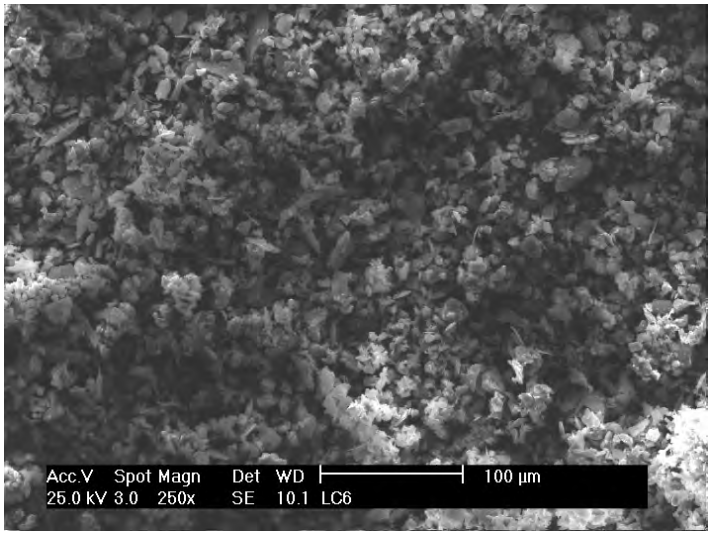

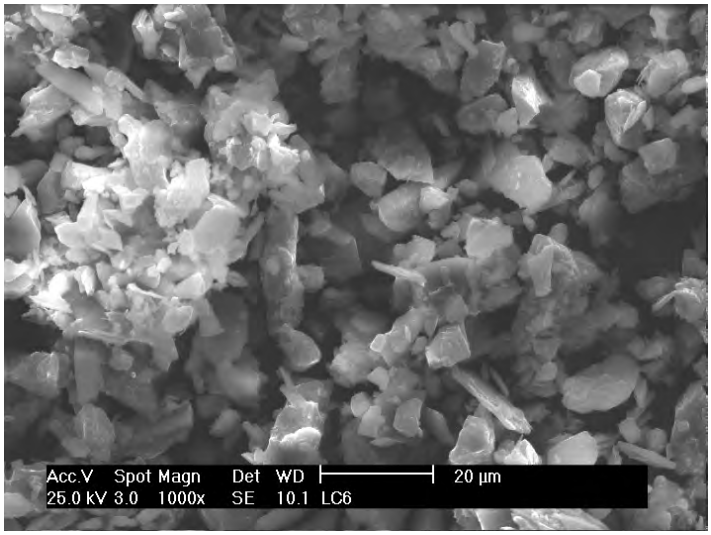

Oberaar YD moraine profile, 50 - 60 cm, fraction 2 - 16 µm, picture 7

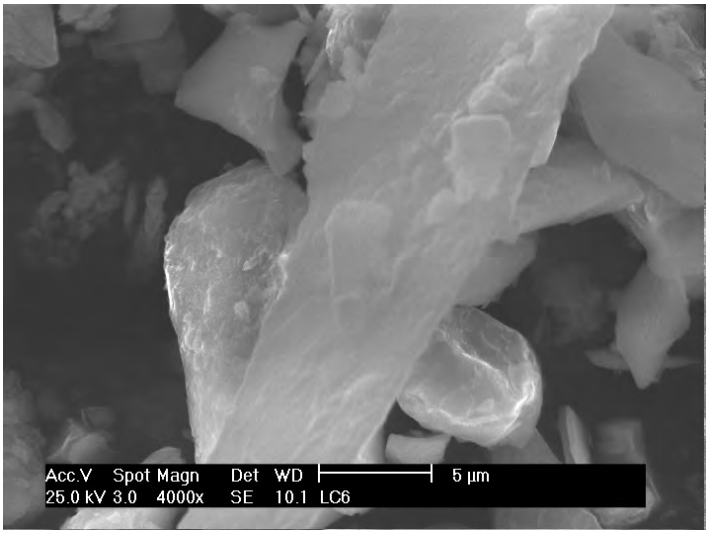

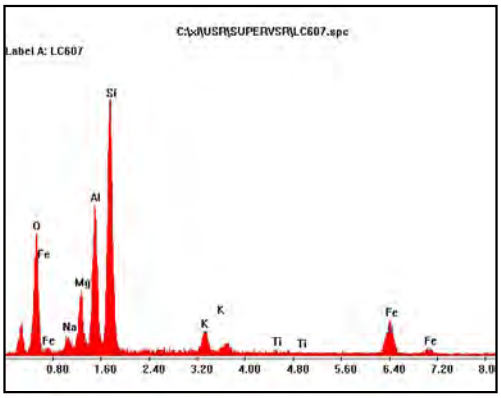

APPENDIX A.4
APATITES

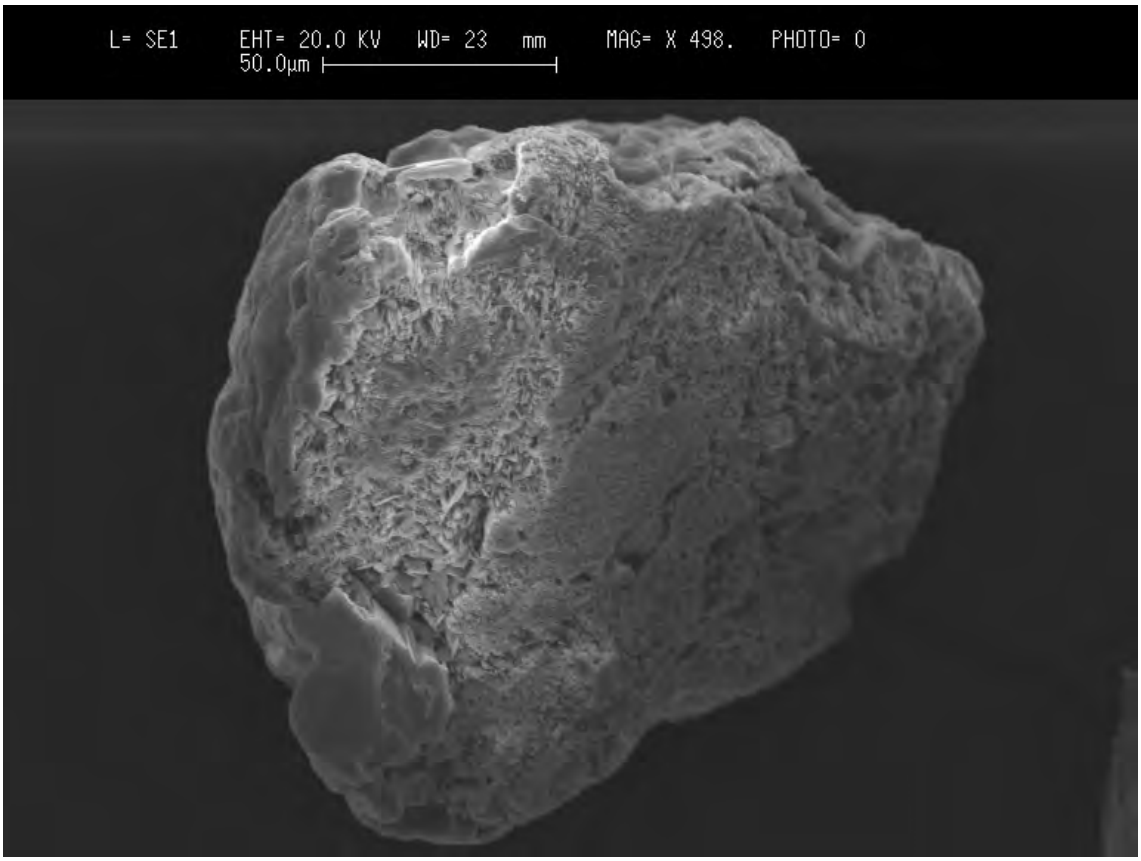

APPENDIX A.3: Apatite data

Apatite characteristics I

Sample	Grade	General grain description				Description of morphological features						Porosity					Biological agents of	
		fresh	flakey	sugary	spongy	sugary indentation	fine cracklike etchings	localised (lenticular) pits	coalseced (lenticular) pits	denticular structures	pervasive towers/ kneedles	surface-porosity	pervasive porosity	secondary preciptate	coatings	rounded grain	bacteria	fungal hyphea
O140 0-10 _1	1	•																
O140 0-10 _2	1	•																
O140 30-40 _1	1	•																
O140 30-40 _2	1	•																
O140 30-40 _3	1	•																
O140 30-40 _6	1	•																
O140 90-100 _3	1	•													•			
O140 90-100 _4	1	•																
O140 90-100 _5	1	•																
O140 90-100 _6	1	•													•			
O140 90-100 _7	1	•																
O140 90-100 _8	1	•																
R11600, 20-30_5	1	•																
R270, 30-40_1	1	•																
R270, 30-40_10	1																	
R270, 30-40_2	1	•																
R270, 30-40_3	1	•																
R270, 30-40_9	1																	
R270, 90-100_10	1	•																
R270, 90-100_4	1	•																
R270, 90-100_5	1	•																
R270, 90-100_6	1	•																
R270, 90-100_7	1	•																
R270, 90-100_8	1	•																
R270, 90-100_9	1	•																
RHOO_1	1	•																
RHOO_2	1	•																
RHOO_3	1	•																
RHOO_4	1	•																
RHOO_5	1	•																
O140 0-10 _3	2					•		•										
O140 0-10 _5	2					•												
O140 0-10 _6	2					•												
O140 30-40 _4	2					•		•										
O140 30-40 _5	2					•		•										
O140 30-40 _7	2					•		•										
O140 90-100 _1	2					•		•							•			
O140 90-100 _2	2		•														•	
O140 90-100 _9	2							•							•			
R11600, 20-30_1	2		•												•			
R11600, 90-100_3	2	•					•											

Apatite characteristics II

Sample	Grade	General grain description				Description of morphological features						Porosity					Biological agents of	
		fresh	flakey	sugary	spongy	sugary indentation	fine cracklike etchings	localised (lenticular) pits	coalseced (lenticular) pits	denticular structures	pervasive towers/ kneedles	surface-porosity	pervasive porosity	secondary preciptate	coatings	rounded grain	bacteria	fungal hyphea
R270, 30-40_4	2							•		•								
R270, 30-40_6	2							•										
R270, 30-40_8	2							•										
R270, 90-100_2	2							•										
R270, 90-100_3	2							•										
O140 0-10 _11	3									•		•						
O140 0-10 -4	3									•		•			•			
R11600, 0-10_1	3								hexagongal								•	
R11600, 0-10_2	3								•	•							•	
R11600, 0-10_4	3									•								
R11600, 20-30_3	3			•														
R11600, 20-30_4	3								•									
R11600, 90-100_1	3		•	•			•											
R11600, 90-100_2	3				•		•											
R11600, 90-100_4	3			•			•											
R270, 0-10_10	3				•							•		•				
R270, 0-10_11	3				•							•						
R270, 0-10_4	3	•									•							
R270, 0-10_5	3									•								
R270, 0-10_7	3								•			•		•				
R270, 0-10_8	3				•								•					
R270, 30-40_5	3								•									
R270, 90-100_1	3								•									
O140 0-10 _10	4										•							•
O140 0-10 _8	4									•								•
O140 0-10 _9	4										•							
O140 0-10 -7	4										•							
R11600, 0-10_3	4				•					•			•		•	•		
R11600, 0-10_5	4										•							
R11600, 0-10_6	4										•		•					
R11600, 20-30_2	4								•		•		•					
R270, 0-10 _1	4								•				•					
R270, 0-10_2	4								•				•					
R270, 0-10_3	4								•				•					
R270, 0-10_6	4								•				•					
R270, 0-10_9	4								•				•					
R270, 30-40_7	4										•			•				

Apatite grading I

Sample, grain	crystal habit	grain grade	blind check	Comments
RH00				
1	2	1		All grains look "greasy" and are heavily pitted or mechanically indented. Crystal form is poorly preserved, 4/5 grains show considerable rounding of the grain edges. All indentations are angular, showing that dissolution rounding of individual indentations is minor. Grain 4 has a 10 um long 1 µm wide striation where is has been abraided by a harder particle.
2	3	1		
3	4	1		
4	1	1		
5	2	1		
O140, 0-10				
1	3	1	1	Indentations are fresh in grain 1
2	3	1	2	Indentations are fresh in grain 2
3	3	2	2	Indentations on grain 3 look sugary and show evidence of localised dissolution etching
4	3	3	4	The dissolution etching is more extensive on the 001 grain surface forming irregular shaped, denticular features perpendicular to the 001 surface. These are sometimes covered by a local surface coating. A microporosity has developed locally between the towers, but does not permeate the whole grain.
5	3	2	2	Grain 5 is covered by small shallow indentations all of which have sugary, diffuse edges.
6	3	2	2	The crystal habit of grain 6 is pristine, there is no dissolution rounding. Its surface is covered by shallow indentations which are sugary
7	3	4	4	Grain 7 shows a "towerblock like structure" which pervades the whole grain, interior following the 001 crystal plane. The sides of the towers are up to several µm wide.
8	3	4	4	Grain 8 is covered in randomly orientated denticular structures, which end in rounded points on some parts of the grain: locally 1-2 µm long, orgainic looking "worms" are localised at the ends of these . Elsewhere on the grain irregular tabular crystals, measuring 1-3 µm in width are observed between the more accicular, denticular structures. Some of the denticular structure are covered by a localised surface coating.
9	3	4	4	Grain 9 shows a "towerblock like structure" which pervades the whole grain, interior following the 001 crystal plane. The ends of the towers are pointed.
10	3?	4	4	The central part of grain 10 is covered with a network of fungal hyphae, several µm wide and up to 40 µm long. The formation of towerblock like structures is localised around the hyphea, the rest of the grain looks fresh.
11	3	3	4	The dissolution etching is more extensive on the 001 grain surface forming irregular shaped, denticular features perpendicular to the 001 surface. A microporosity has developed locally between the towers, but does not permeate the whole grain. The bottom corner of the grain has been protected from etching.
mean grade		**2.7**	**3.0**	
O140, 30-40 cm				
1	4	1	1	Several 30-40 cm grains have very localised pitting, a tendency towards indentations with sugary textures and localised lenticular etch pits. Grain 5 has a characteristic "flakey" texture.
2	2	1	1	
3	3	1	2	
4	3	2	2	
5	3*	2	2	
6	3	1	1	
7	3	2	2	
mean grade		**1.4**	**1.6**	
O140, 90-100cm				
1	4	2	2	Minor pitting and lenticular structures developing on the grain surface. Grain is coated in Al/Si layer in places.
2	4	2	2	Two bacteria possbily observed on zoom 2a, located to a sub hexagonal form. The flakey texture is observed on one side of the of the grain. The texture is similar to RH00 5b, but the indentations are less sharp, implying further etching in the proglacial environment
3	4	1	3	The morphology of grain 3 appears fresh, and similar to RH00 4c in texture. There are some surface coatings on the grain.
4	4	1	1	A fresh grain
5	4	1	1	This grain is very smooth and fresh, from glavio-fluvial dissolution rounding. No secondary etching or pitting is observed.

Apatite grading II

Sample, grain	crystal habit	grain grade	blind check	Comments
O140, 90-100cm continued				
6	4	1	2	The morphology of grain 6 appears fresh, and similar to RH00 4c in texture. There are some surface coatings on the grain.
7	4	1	1	A fresh grain
8	2	1	1	This grain has the same texture as grain RH00 5
9	3	2	1	Minor pitting and lenticular structures developing on the grain surface. Grain is coated in Al/Si layer in places.
mean grade		**1.3**	**1.6**	
R270, 0-10 cm				
1	4	4	3	Grain 1 has a large secondary porosity stemming from the coalescence of pervasive lenticular etch pits. The etchings all have a similar orientation.
2	4	4	3	Grain 2 has a large secondary porosity stemming from the coalescence of pervasive lenticular etch pits to form large cavities in the grain. The etchings all share a common orientation.
3	4	4	3	Grain 3 has a large secondary porosity stemming from the coalescence of pervasive lenticular etch pits to form large cavities in the grain. The etchings all share a common orientation.
4	3	3	4	A third of grain 4 is etched to form the denticular commonly orientated "towerblocks". The remainder of the grain appears fresh, appart from some pitting.
5	4	3	3	The surface of grain 5 is heavily etched forming commonly orientated denticular structures which penetrate the grain most deeply where it is striated.
6	4	4	3	Grain 6 has a large secondary porosity stemming from the coalescence of pervasive lenticular etch pits to form large cavities in the grain. The etchings all share a common orientation.
7	3	3	3	The surface of grain 7 is heavily and deeply pitted, but there has been no coalescence of etch pits. 2 µm raspberry shaped masses, comprised of indivudual " blobs" were observed in a surface depression, this may be a secondary precipiate.
8	4	3	2	The surface of grain 8 is heavily and deeply pitted to give a spongy texture, it is not clear that the porosity is pervasive throughout the grain.
9	4	4	3	Grain 9 has a significant secondary porosity stemming from the coalescence of pervasive lenticular etch pits to form large cavities in the grain. The etchings all share a common orientation.
10	4	3	2	The surface of grain 10 is heavily and deeply pitted to give a spongy texture, it is not clear that the porosity is pervasive throughout the grain. The same precipitate texture as in grain 7 is observed here.
11	4	3	2	The surface of grain 11 is heavily and deeply pitted to give a spongy texture, it is not clear that the porosity is pervasive throughout the grain.
mean grade		**3.5**	**2.8**	
R270 30-40 cm				
1	3	1	2	
2	5	1	1	
3	2	1	2	
4	4	2	2	Etching and the formation of denticular structures is particuarly pronounced around a striation on grain 4
5	4	3	2	Considerable coalescence of lenticular etch pits is observed on grain 5.
6	5	2	2	Etching and the formation of lenticular structures is particuarly pronounced depressions caused by the conchoidal fracture.
7	4	4	4	Grain 7 has the same character as O140, 0-10cm, grain 7. There is a pervasive coalescence of denticular structures to form fine towers and needles. Blocky grains (2-3 µm in length) are observed on the grain (zoom 7a) in a cavity where the needles have broken.
8	4	2	2	There are some deep pits on the surface of grain 8.
9	4	1	2	
10	4	1	1	
mean grade		**1.8**	**2**	

Apatite grading III

Sample, grain	crystal habit	grain grade	blind check	Comments
R270, 90-100 cm				
1	4	3	3	The surface of grain 1 is heavily etched forming deep irreguarlly orientated lenticular structures which penetrate the grain most deeply where it is striated.
2	5	2	4	Lenticular structures are observed on the broken edge of grain 2.
3	5	2	1	Initial lenticular structures are observed on grain 3.
4	4	1	1	
5	4	1	2	
6	5	1	2	
7	4	1	1	
8	4	1	1	
9	4	1	1	
10	4	1	1	
mean grade		**1.4**	**1.7**	
R11.6, 0-10 cm				
1	4	3	3	Grain 1 shows no sign of denticular structures, etchings on the grain are in the form of superimposesed subhexagonal forms. Bacteria are observed on the grain in a crack.
2	4	3	4	Grain 2 is deeply etched to forming series of linear, parallel depressions. Sub mircometer denticular morphologies are observed on the grain (zoom 2d, 2e, 2f) on other parts of the grain the coalesance of 10 µm long lenticular etch pits is observed. Bacteria are observed on this grain surface.
3	4	4	4	Grain 3 is rounded and has a spongy texture due to secondary porosity. There are some secondary coatings in a depression on the grain surface. Zoom 3a shows denticular features.
4	4	3	3	Grain 4 also has denticular features. Chattermarks on the grain surface are also etched, allowing chemical weathering to access more of the grain.
5	4	4	4	Grain 5 is rounded and shows pervasive denticular features which have coalesced throughout the grain.
6	4	4	4	Grain 5 is rounded, with considerable secondary porosity and shows pervasive denticular features which have coalesced throughout the grain. A rootlet is observed on the grain surface.
mean grade		**3.5**	**3.7**	
R11.6, 20-30 cm				
1	4	2	3	Grain 1 has the same flakey texture observed in grain 5, O140, 30-40 and grain 2, O140, 90-100. Surface coatngs are observed.
2	4	4	3	Grain 2 is very deeply etched forming 10 µm wide diamond shaped pits, which generate a high secondary porosity. 50 µm, towerblock shaped margins are also observed.
3	3	3	3	Grain 3 is crumbling in the middle, and has a sugary texture.
4	2	3	3	Grain 4 shows the coalsence of towerblock shaped etchpits (Zoom 4b)
5	4	1	2	Grain 5 looks fresh
mean grade		**2.6**	**2.8**	
R11.6, 90-100 cm				
1	1	3	3	Grain 1 has a flakey/ sugary surface texture and has densly spaced, fine etchings which appear randomly orientated.
2	4	3		etchings.
3	4	2	3	Grain 3 looks fresh and zoom 3a shows that the fine etchings are less densely spaced.
4	4	3	3	Grain 4 has fine, randomly orientated etchings dense etchings and a sugary texture.
mean grade		**2.8**	**3**	

Total number of whole grains: 78

Crystal habit

1. Long prismatic habit
2. Short prismatic
3. Tabular
4. Unknown
5. Fragment with conchoidal fracture
****. Prominent dipyramid***

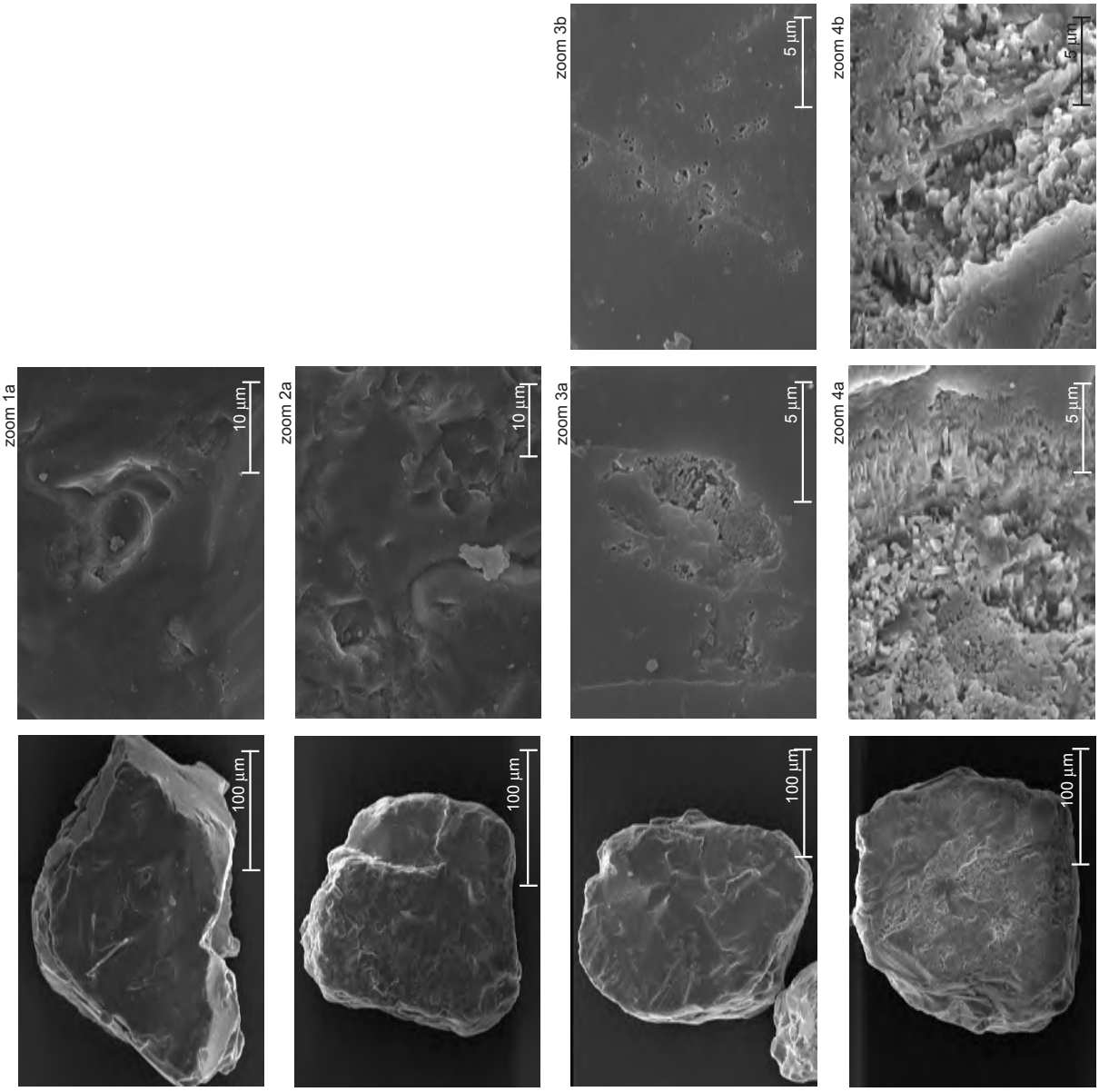

O140 (0-10cm) GRAIN **1** O140 (0-10cm) GRAIN **2** O140 (0-10cm) GRAIN **3** O140 (0-10cm) GRAIN **4**

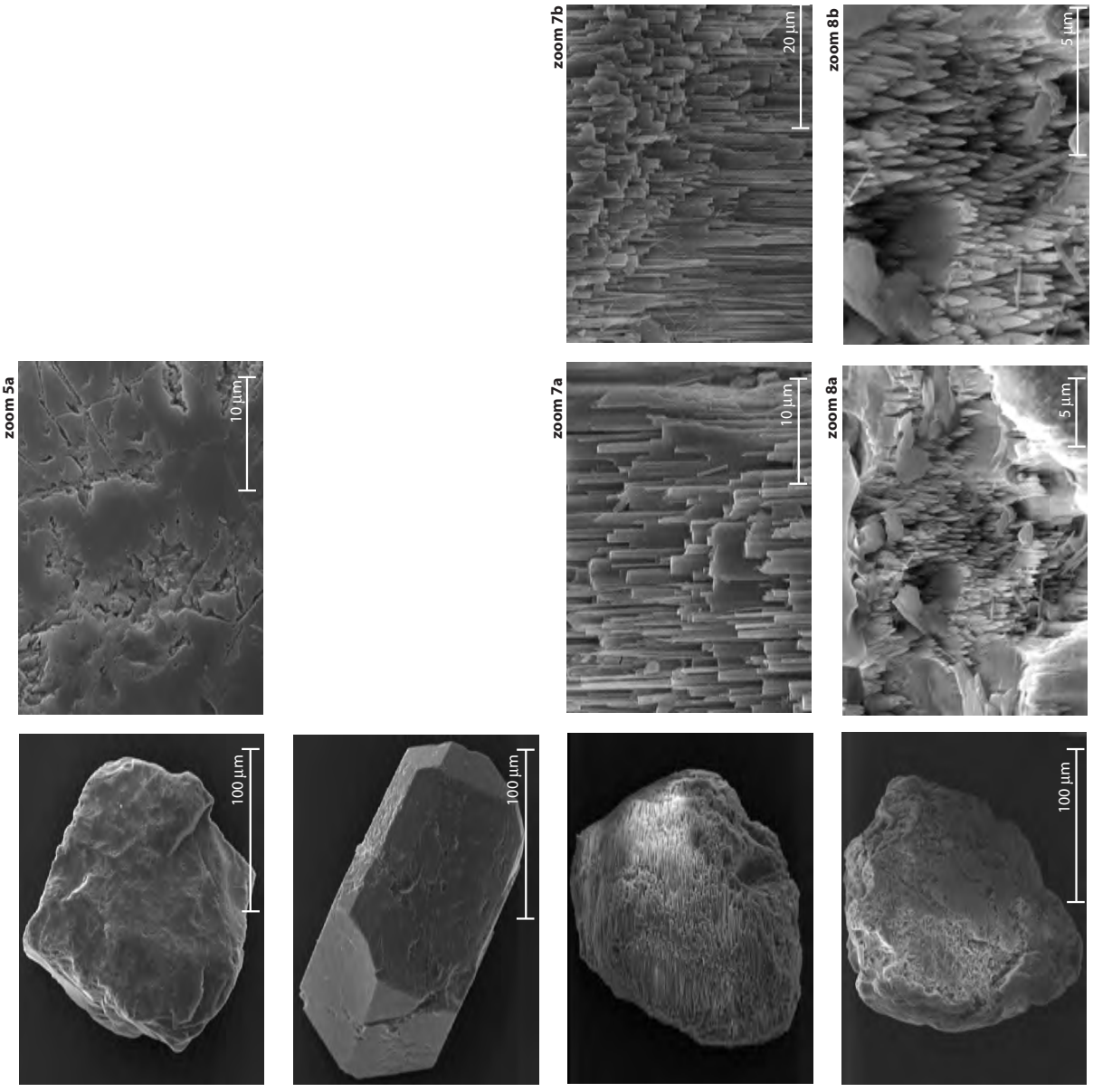

O140 (0-10cm) GRAIN 5. **O140** (0-10cm) GRAIN 6. **O140** (0-10cm) GRAIN 7. **O140** (0-10cm) GRAIN 8.

O140 (0-10cm) grain 8. continued

O140 (0-10cm) GRAIN 9

O140 (0-10cm) GRAIN 10

O140 (0-10cm) GRAIN 11

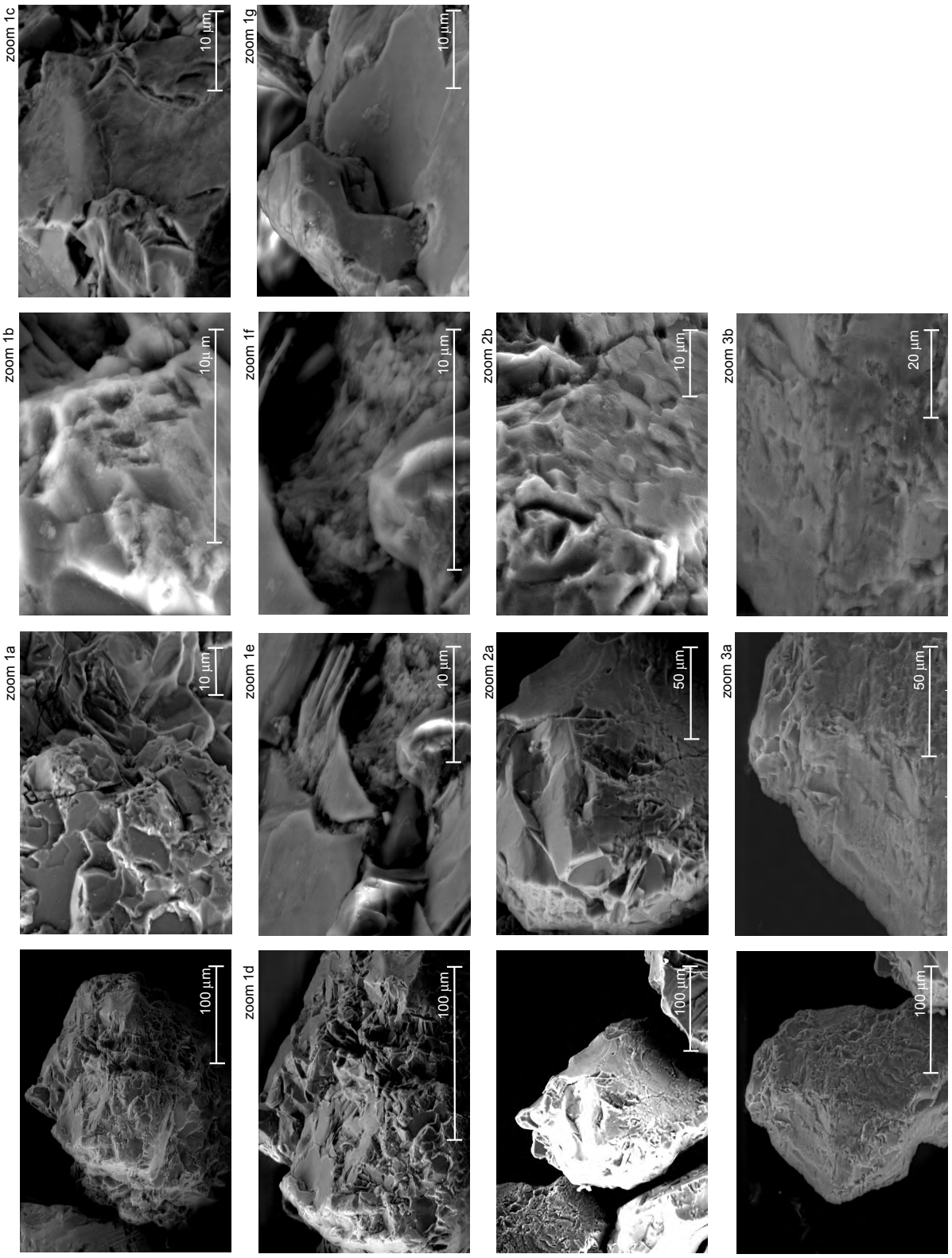

O140 (90-100 cm) GRAIN **1** O140 (90-100 cm) GRAIN **1** O140 (90-100 cm) GRAIN **2** O140 (90-100 cm) GRAIN **3**

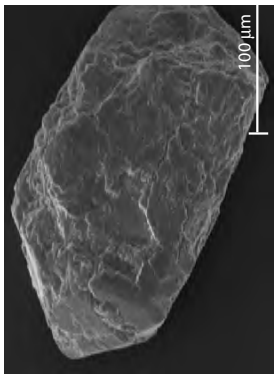

O140 (30-40cm) GRAIN 5.

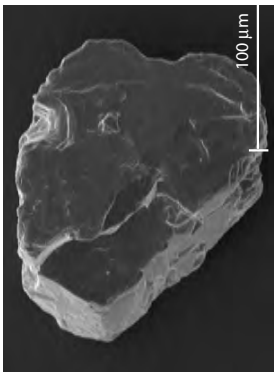

O140 (30-40cm) GRAIN 6.

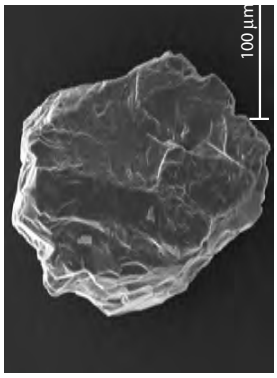

O140 (30-40cm) GRAIN 7.

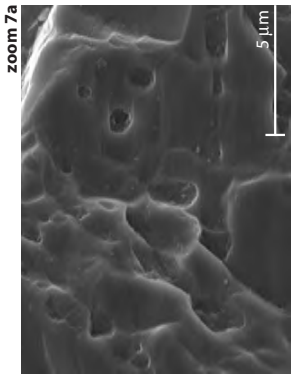

O140 (30-40cm) GRAIN 7

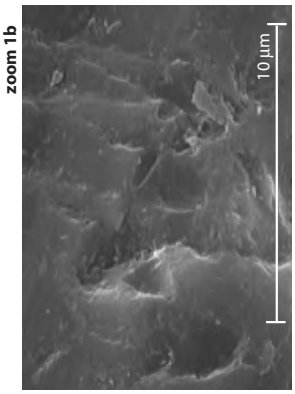

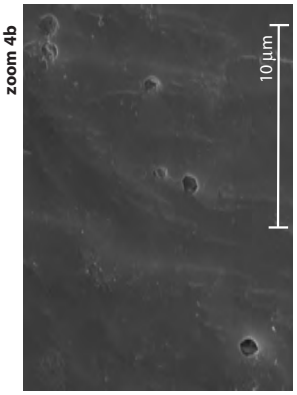

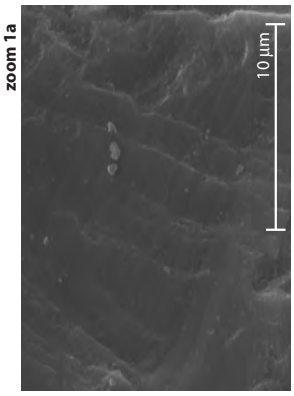

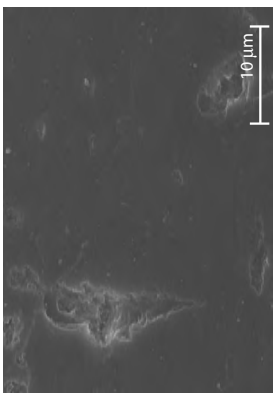

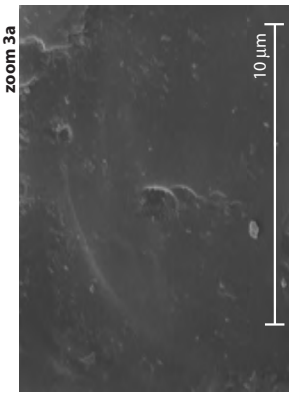

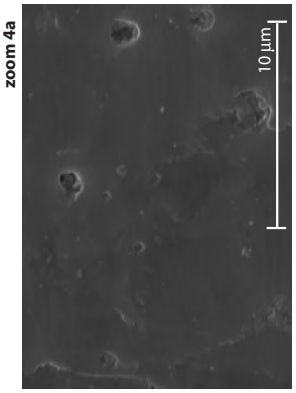

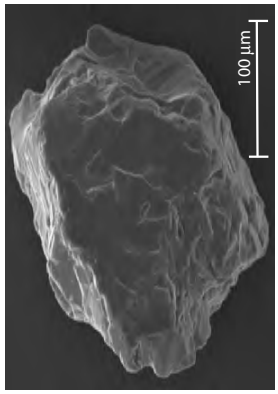

O140 (30-40cm) GRAIN 1.

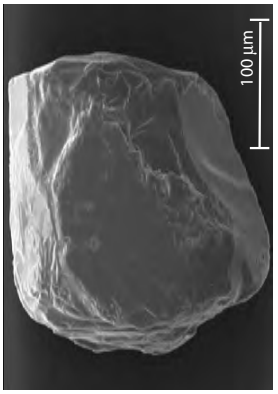

O140 (30-40cm) GRAIN 2.

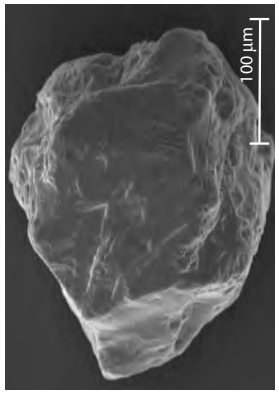

O140 (30-40cm) GRAIN 3.

O140 (30-40cm) GRAIN 4.

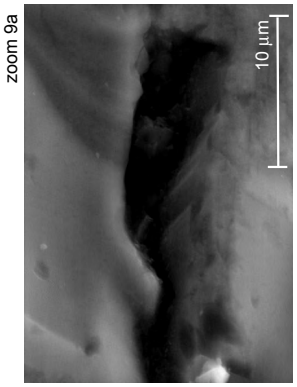

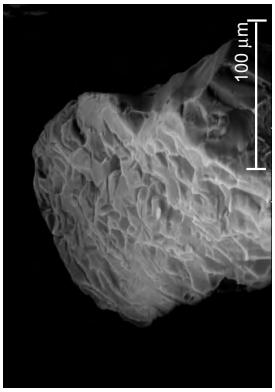

O140 (90-100 cm) GRAIN **8**

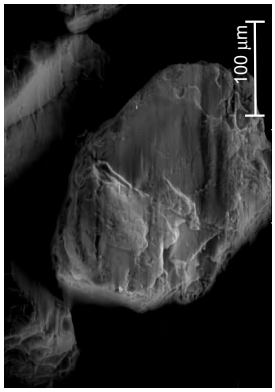

O140 (90-100 cm) GRAIN **9**

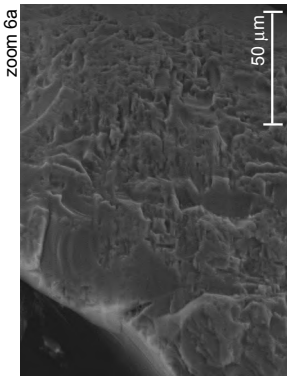

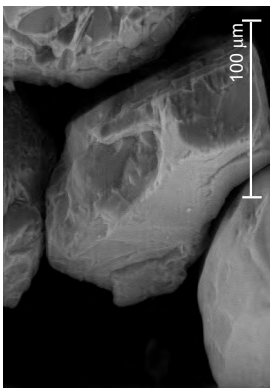

O140 (90-100 cm) GRAIN **4**

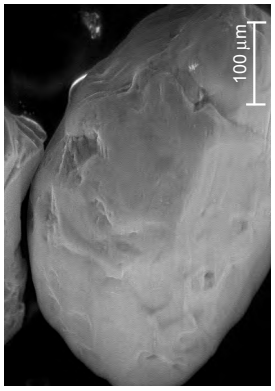

O140 (90-100 cm) GRAIN **5**

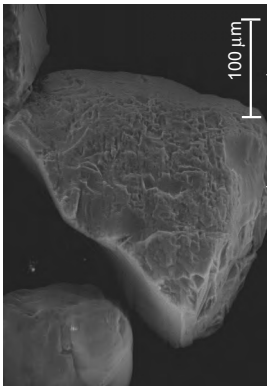

O140 (90-100 cm) GRAIN **6**

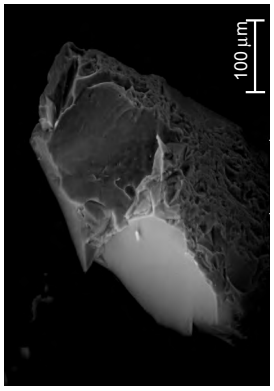

O140 (90-100 cm) GRAIN **7**

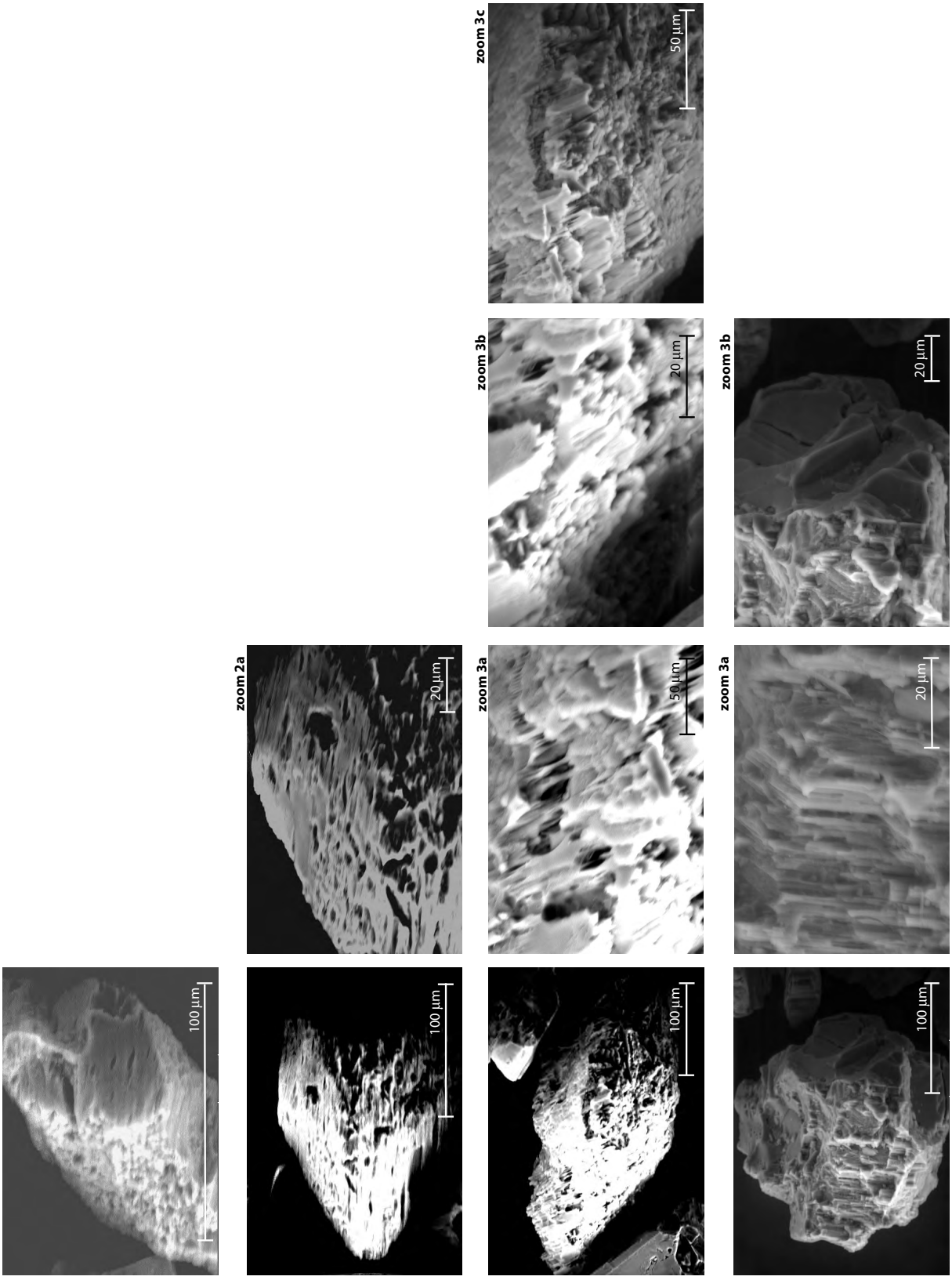

R270 (0-10 cm) GRAIN 1. **R270** (0-10 cm) GRAIN 2. **R270** (0-10 cm) GRAIN 3. **R270** (0-10 cm) GRAIN 4.

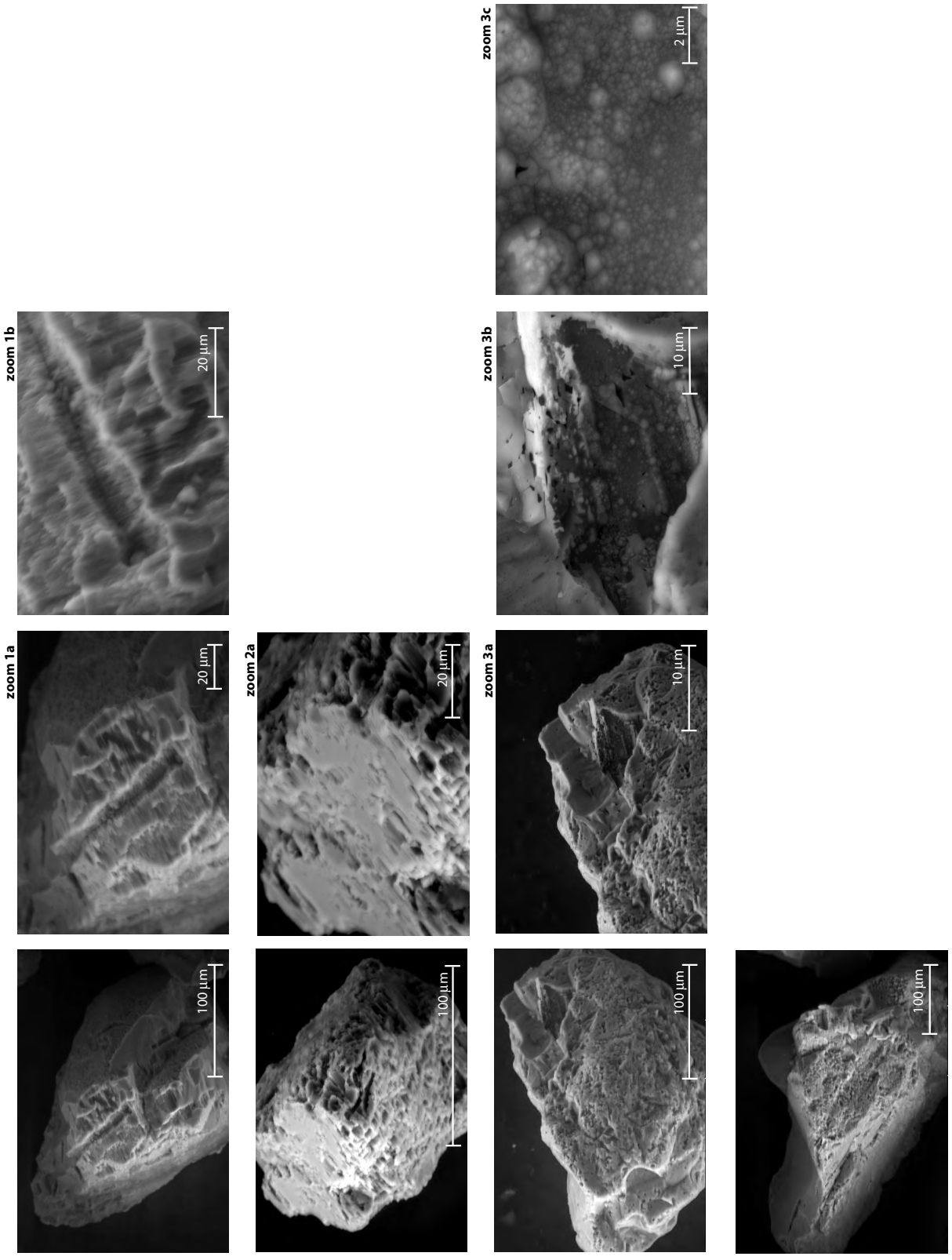

R270 (0-10 cm) GRAIN 5. **R270** (0-10 cm) GRAIN 6. **R270** (0-10 cm) GRAIN 7. **R270** (0-10 cm) GRAIN 8.

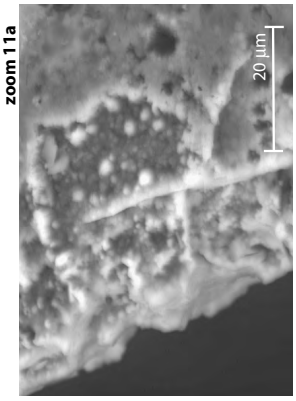

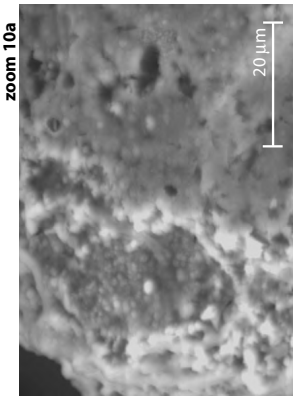

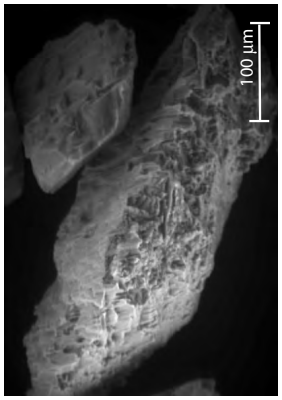

R270 (0-10 cm) GRAIN 9.

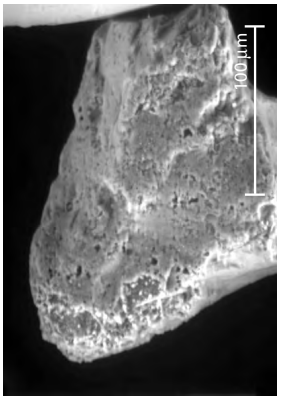

R270 (0-10 cm) GRAIN 10.

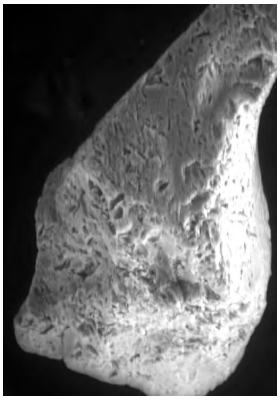

R270 (0-10 cm) GRAIN 11

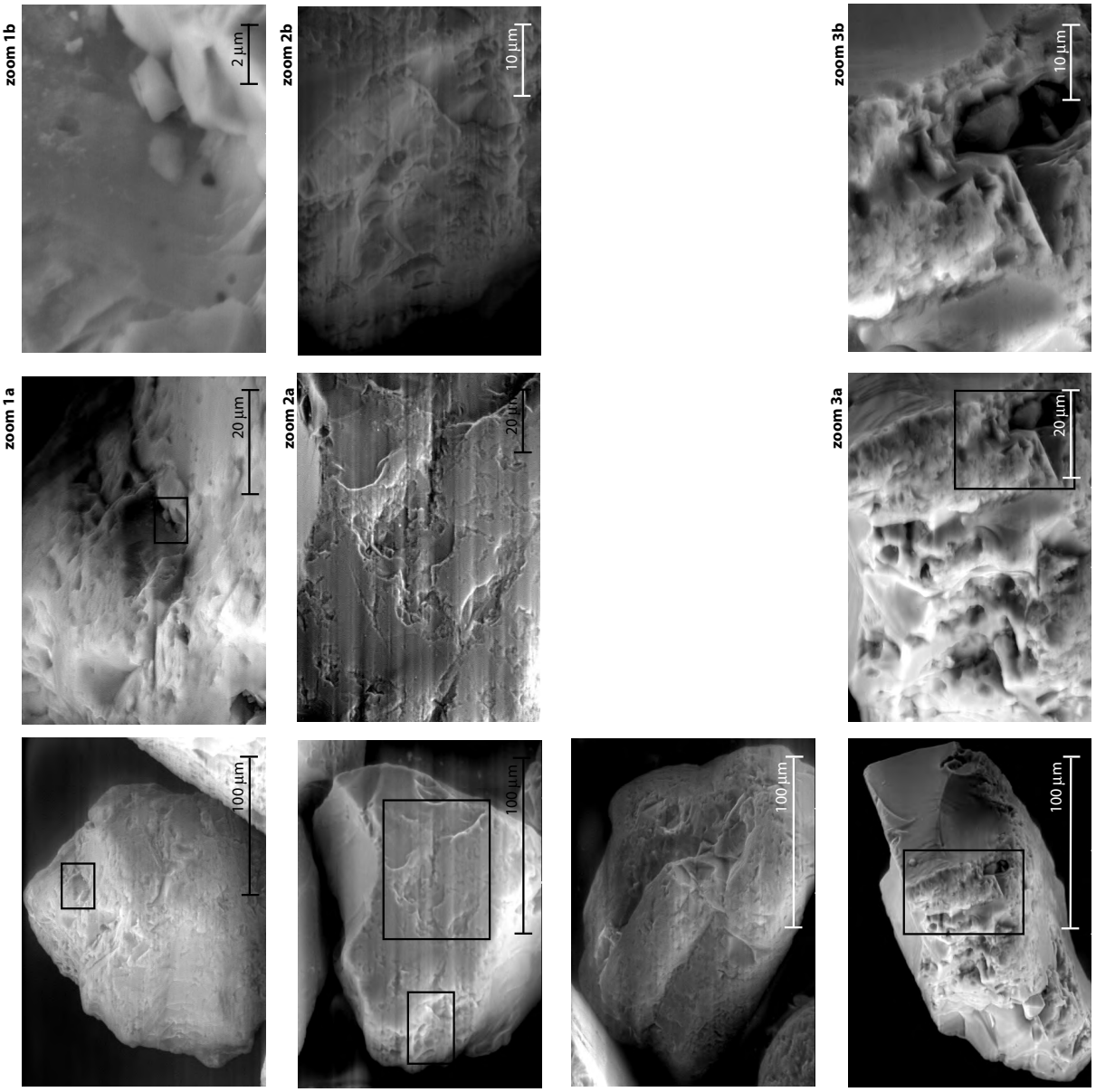

R270 (30-40 cm) GRAIN 1. **R270** (30-40 cm) GRAIN 2. **R270** (30-40 cm) GRAIN 3. **R270** (30-40 cm) GRAIN 4

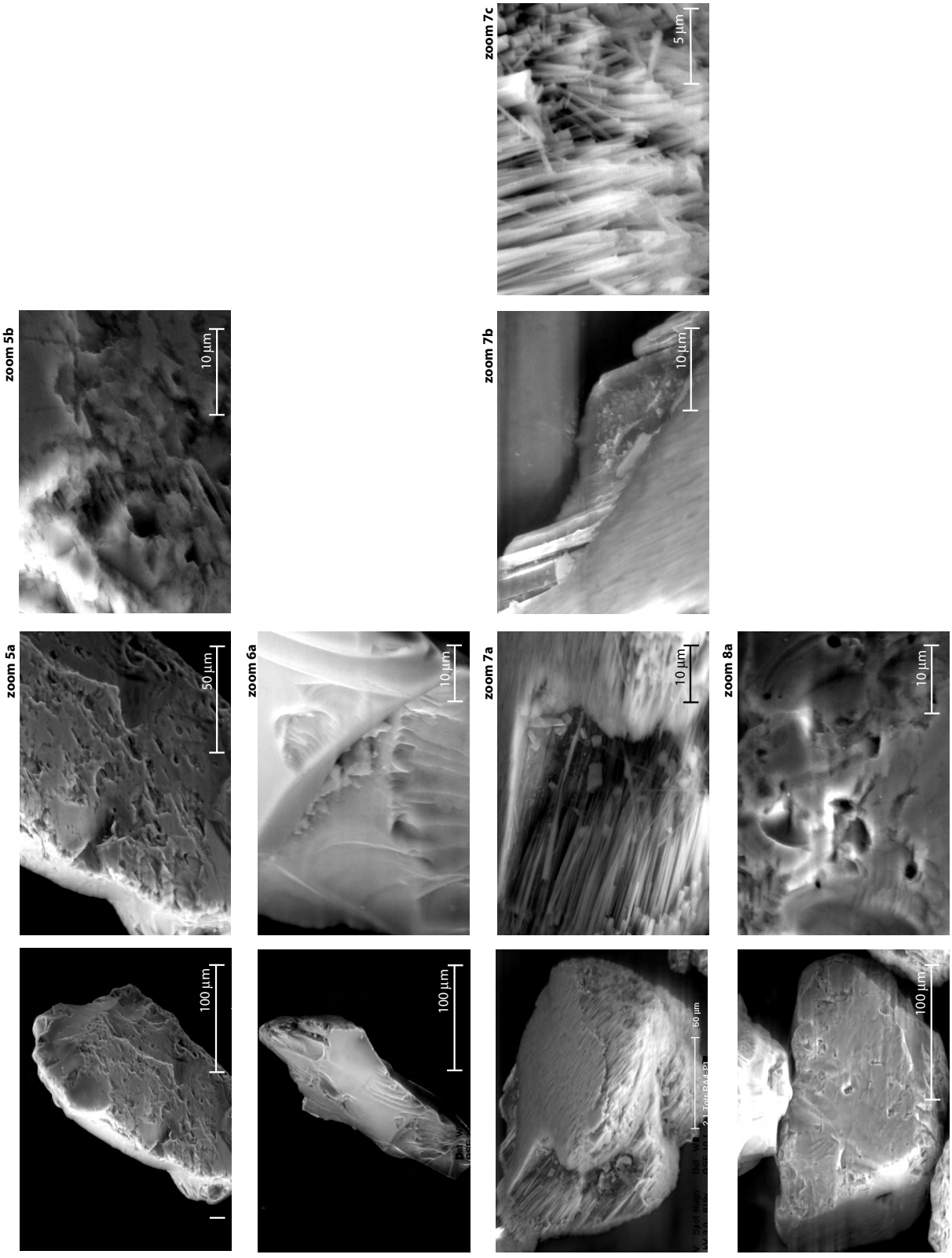

R270 (30-40 cm) GRAIN 5. **R270** (30-40 cm) GRAIN 6. **R270** (30-40 cm) GRAIN 7. **R270** (30-40 cm) GRAIN 8

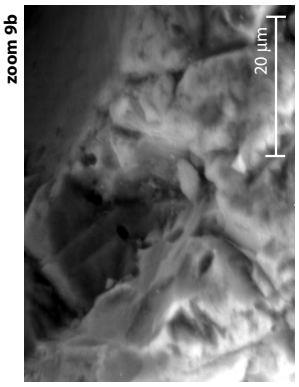

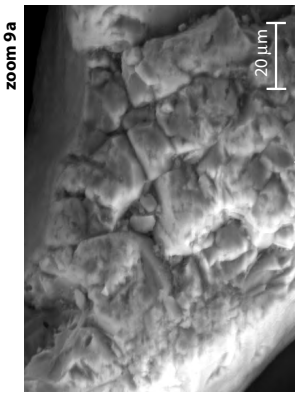

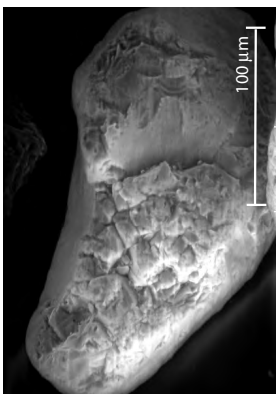

R270 (30-40 cm) GRAIN 9.

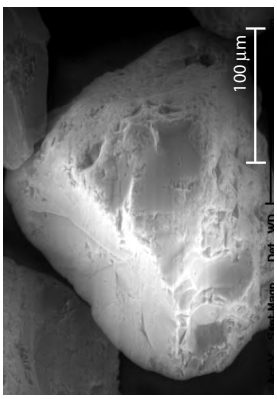

R270 (30-40 cm) GRAIN 10.

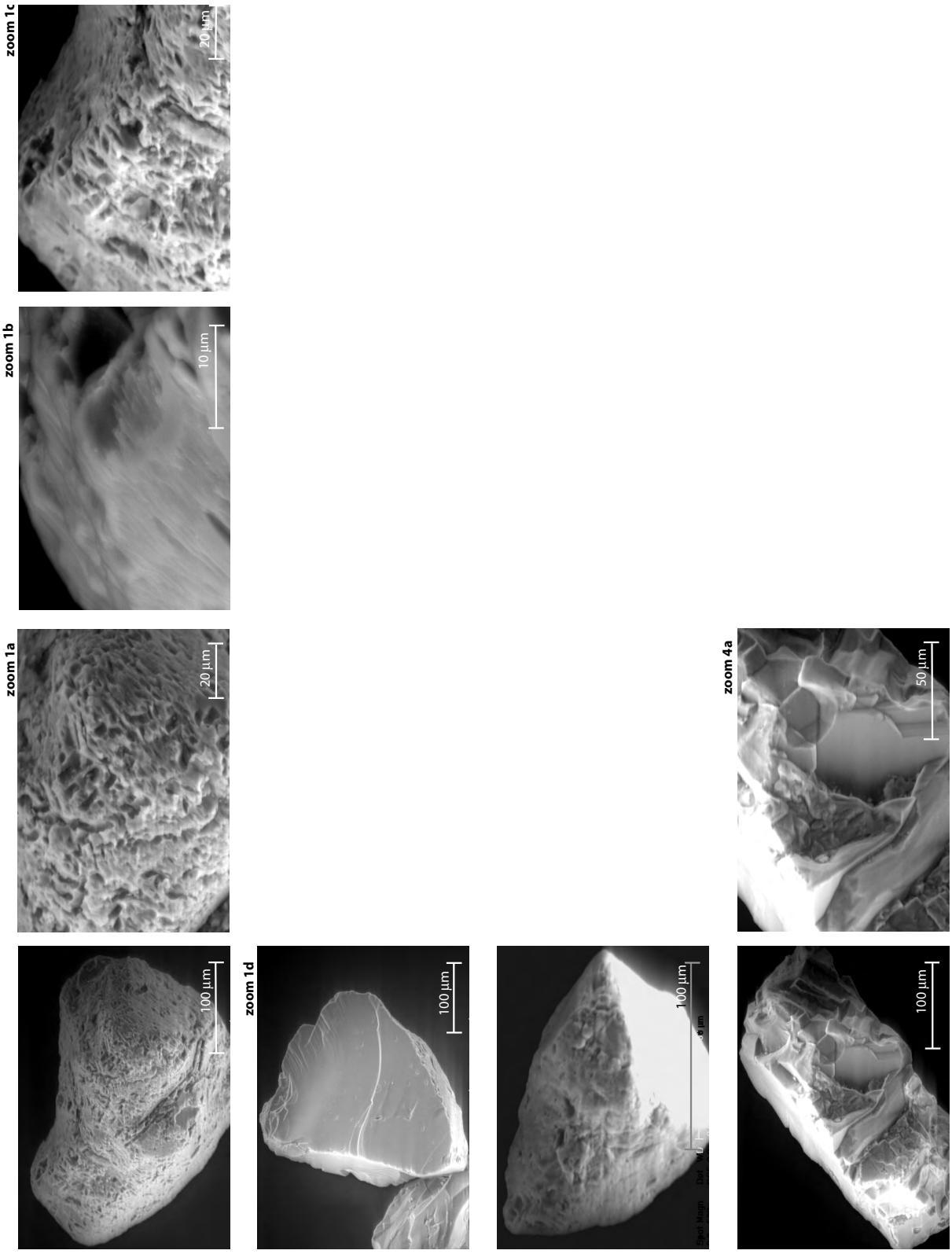

R270 (90-100 cm) GRAIN 1. **R270** (90-100 cm) GRAIN 2. **R270** (90-100 cm) GRAIN 3. **R270** (90-100 cm) GRAIN 4

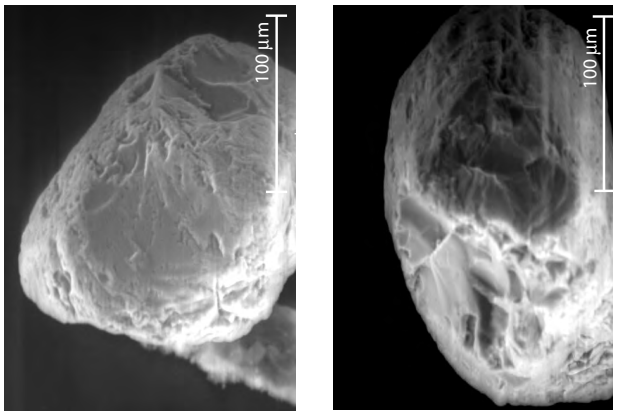

R270 (90-100 cm) GRAIN 9. **R270** (90-100 cm) GRAIN

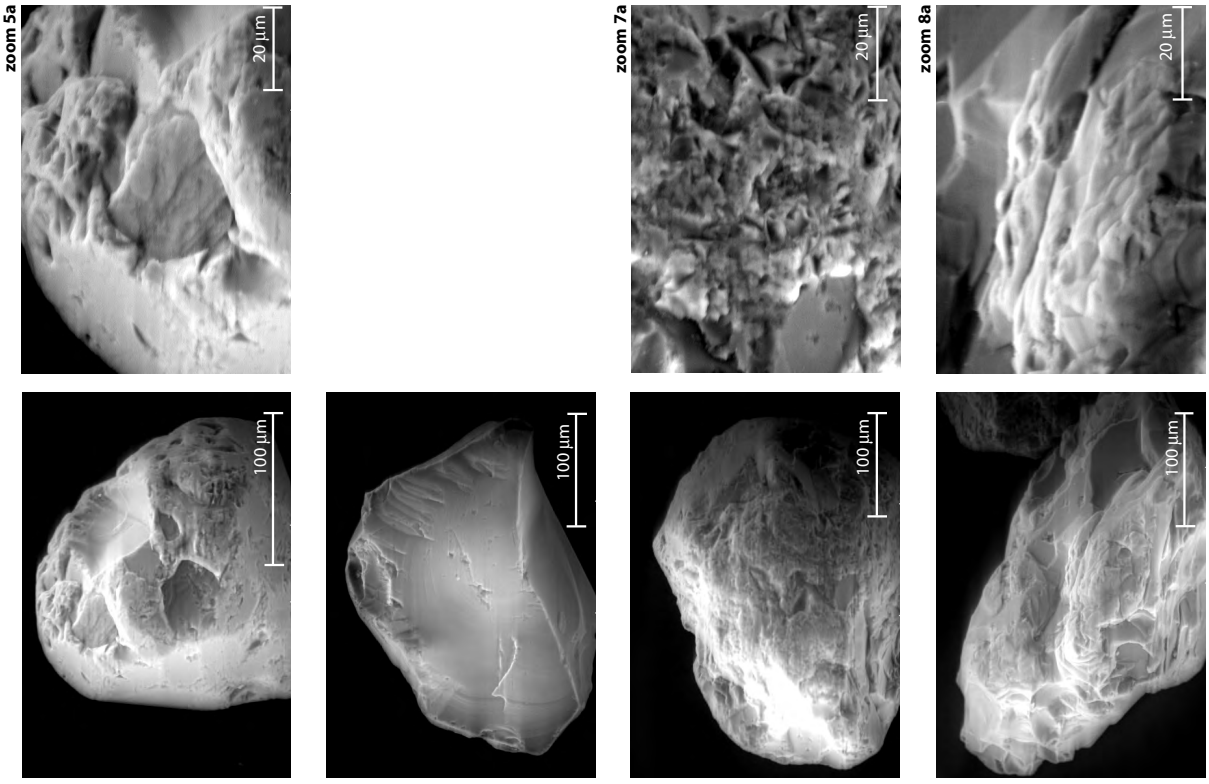

R270 (90-100 cm) GRAIN 5. **R270** (90-100 cm) GRAIN 6. **R270** (90-100 cm) GRAIN 7. **R270** (90-100 cm) GRAIN 8

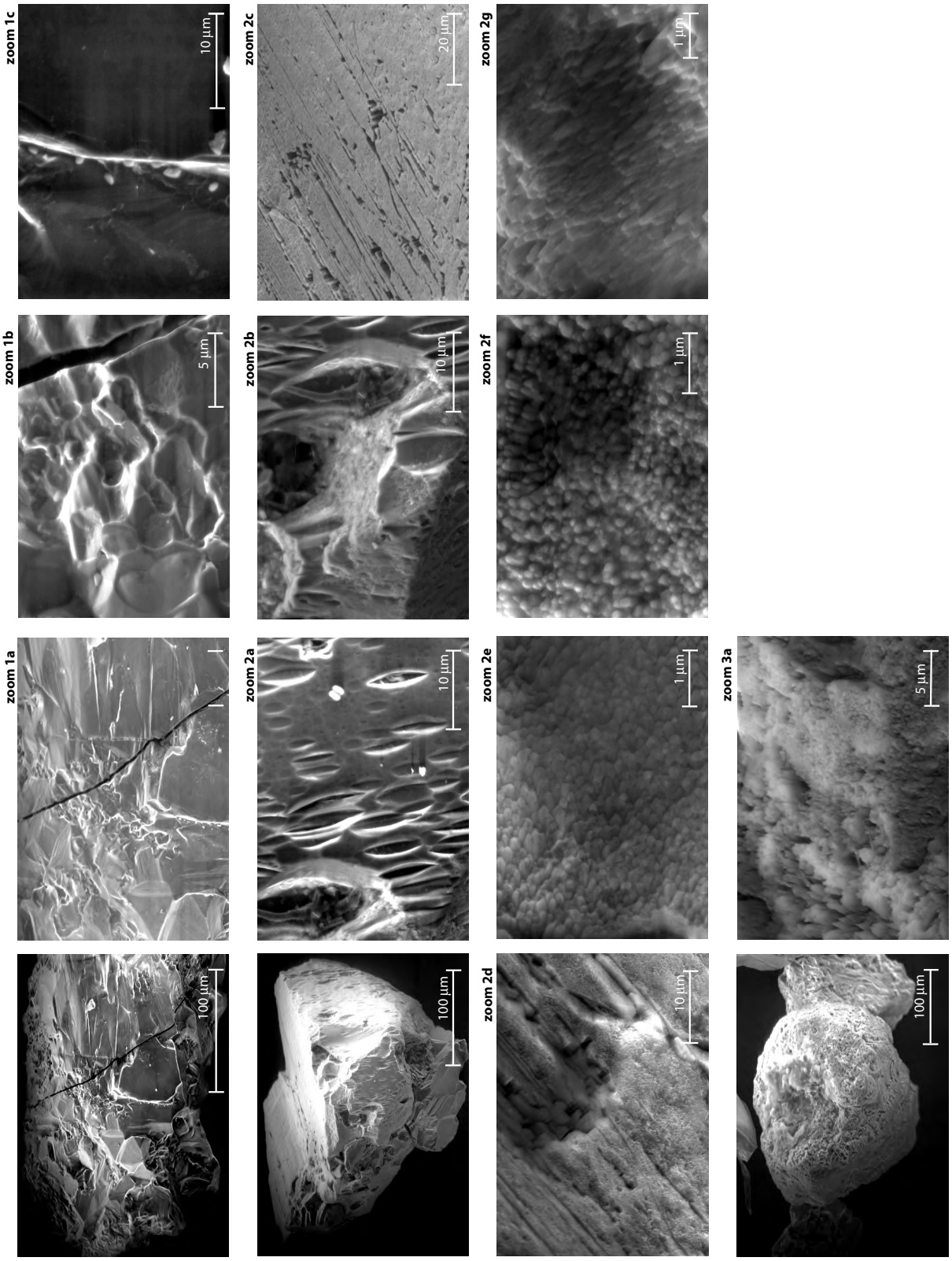

R11.6 kyr (0-10 cm) GRAIN 1. **R11.6 kyr** (0-10 cm) GRAIN 2. **R11.6 kyr** (0-10 cm) GRAIN 2. **R11.6 kyr** (0-10 cm) GRAIN 3

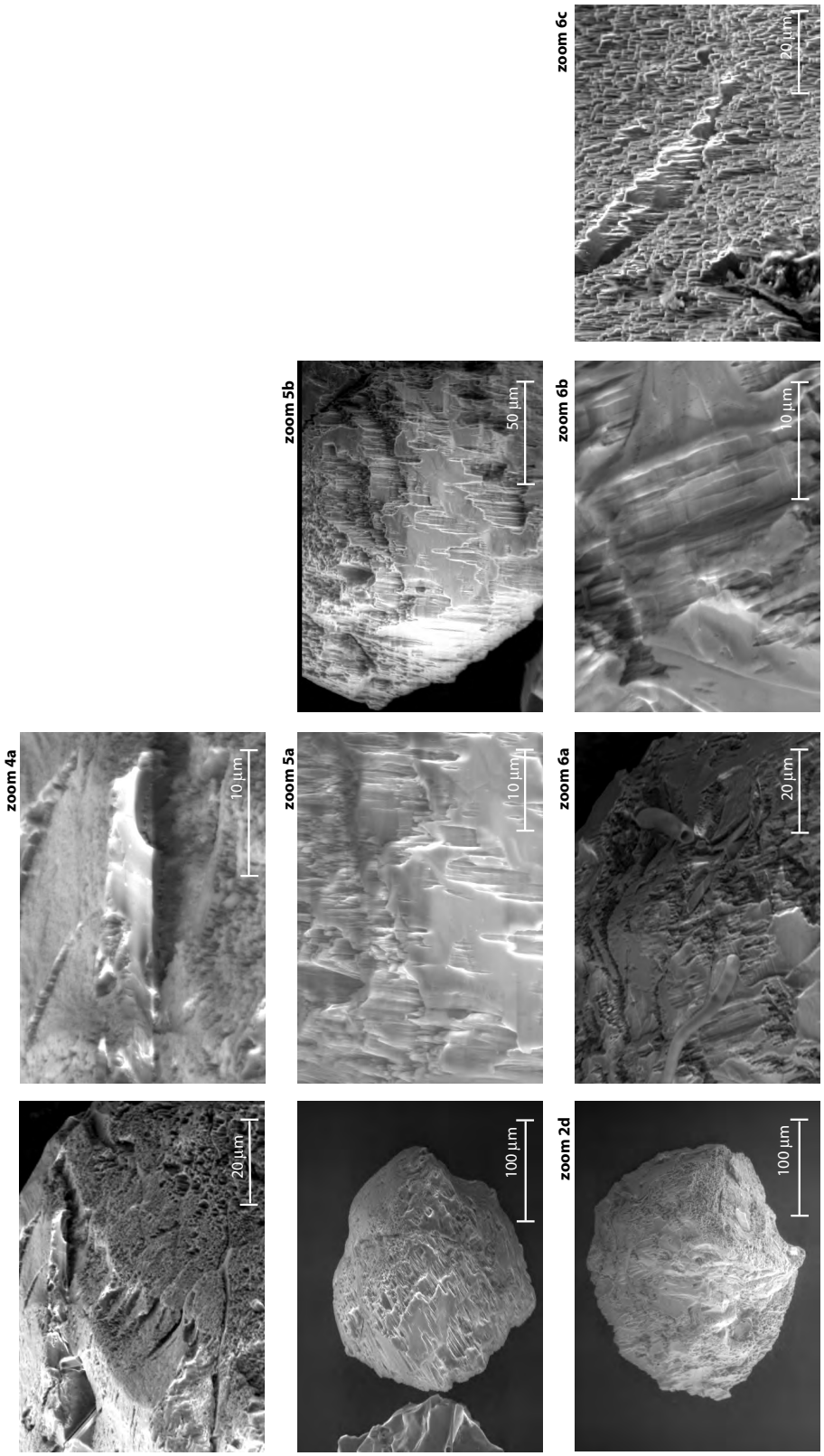

R11.6 kyr (0-10 cm) GRAIN 4. **R11.6 kyr** (0-10 cm) GRAIN 5. **R11.6 kyr** (0-10 cm) GRAIN 6.

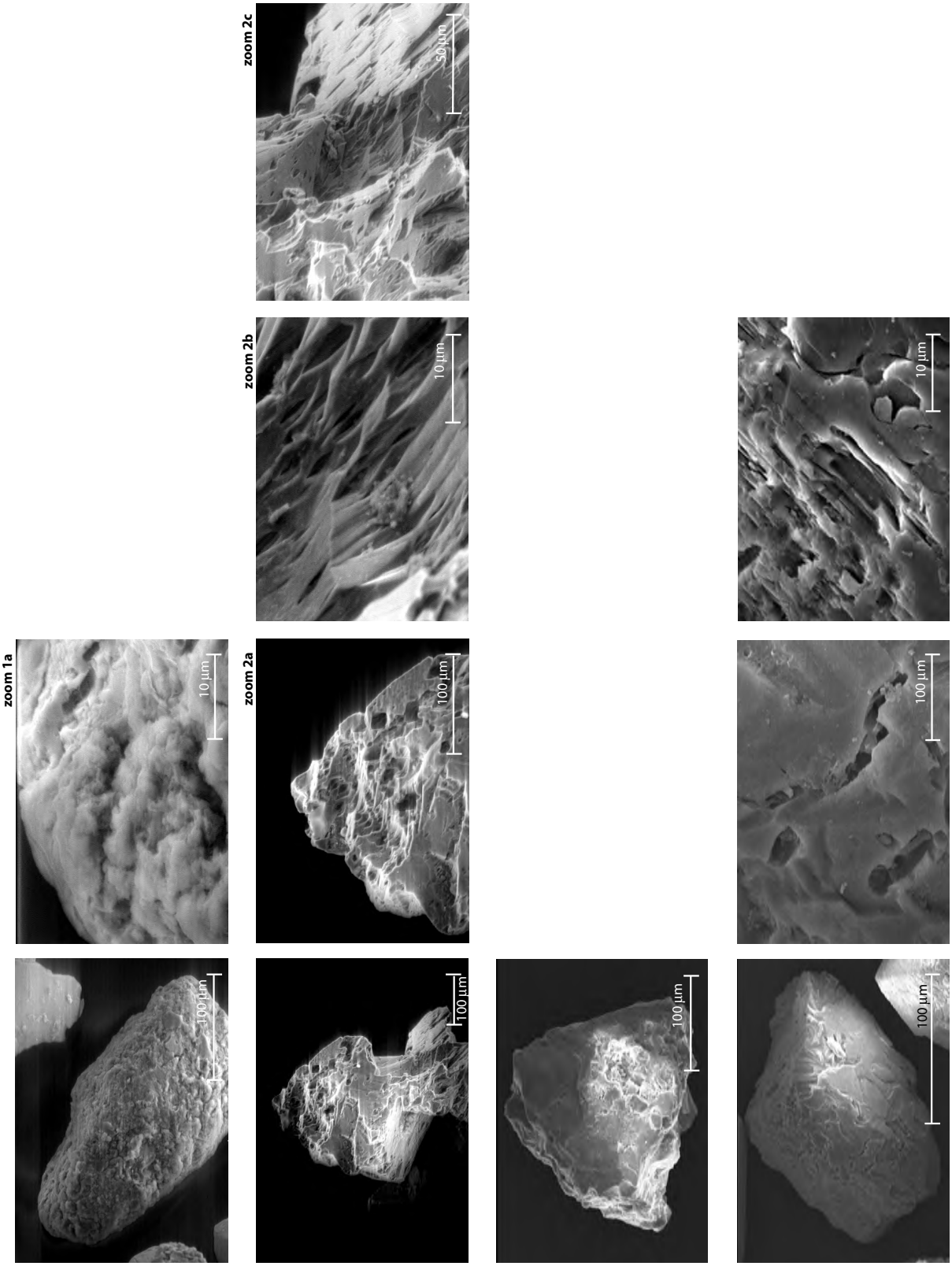

R11.6 kyr (20-30 cm) GRAIN 1. **R11.6 kyr** (20-30 cm) GRAIN 2. **R11.6 kyr** (20-30 cm) GRAIN 3. **R11.6 kyr** (20-30 cm) GRAIN

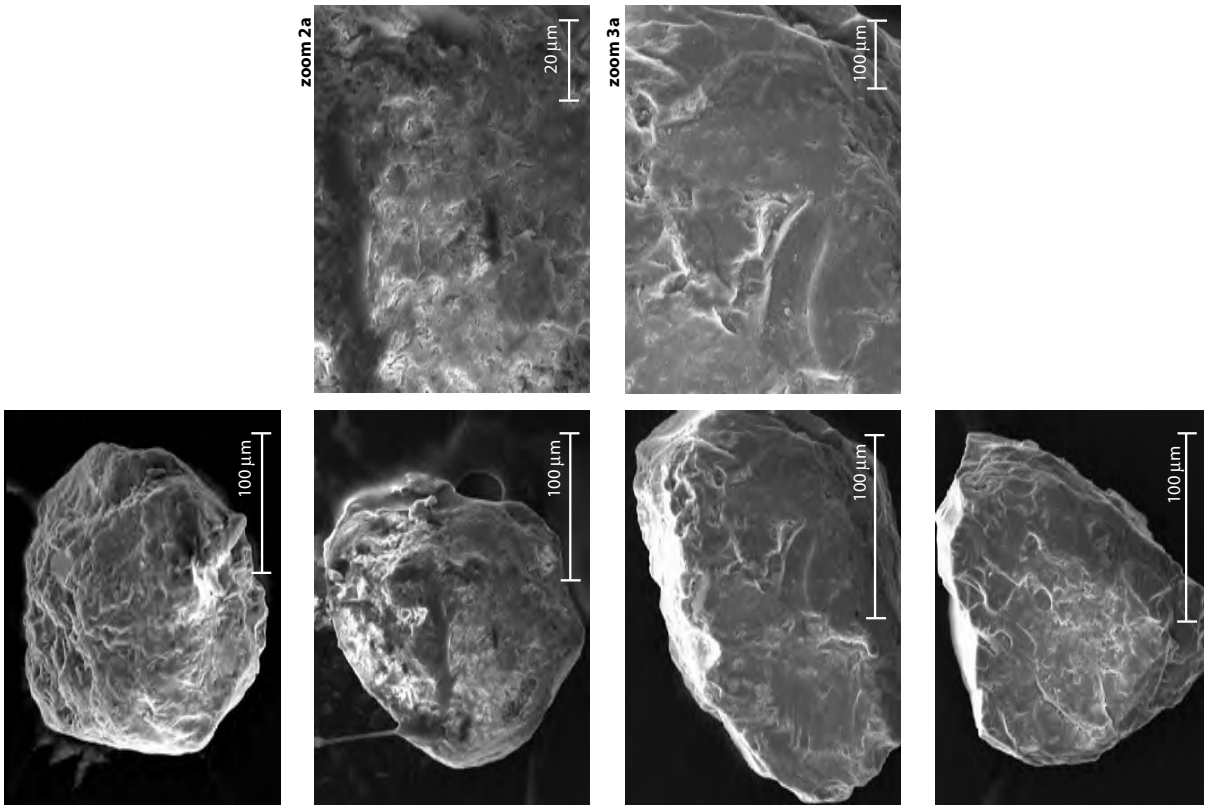

R11.6 kyr (60-70 cm) GRAIN 1. **R11.6 kyr** (60-70 cm) GRAIN 2. **R11.6 kyr** (60-70 cm) GRAIN 3. **R11.6 kyr** (60-70 cm) GRAIN

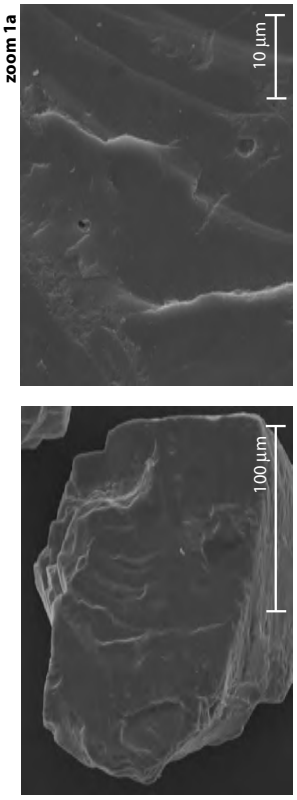

R11.6 kyr (20-30 cm) GRAIN 5

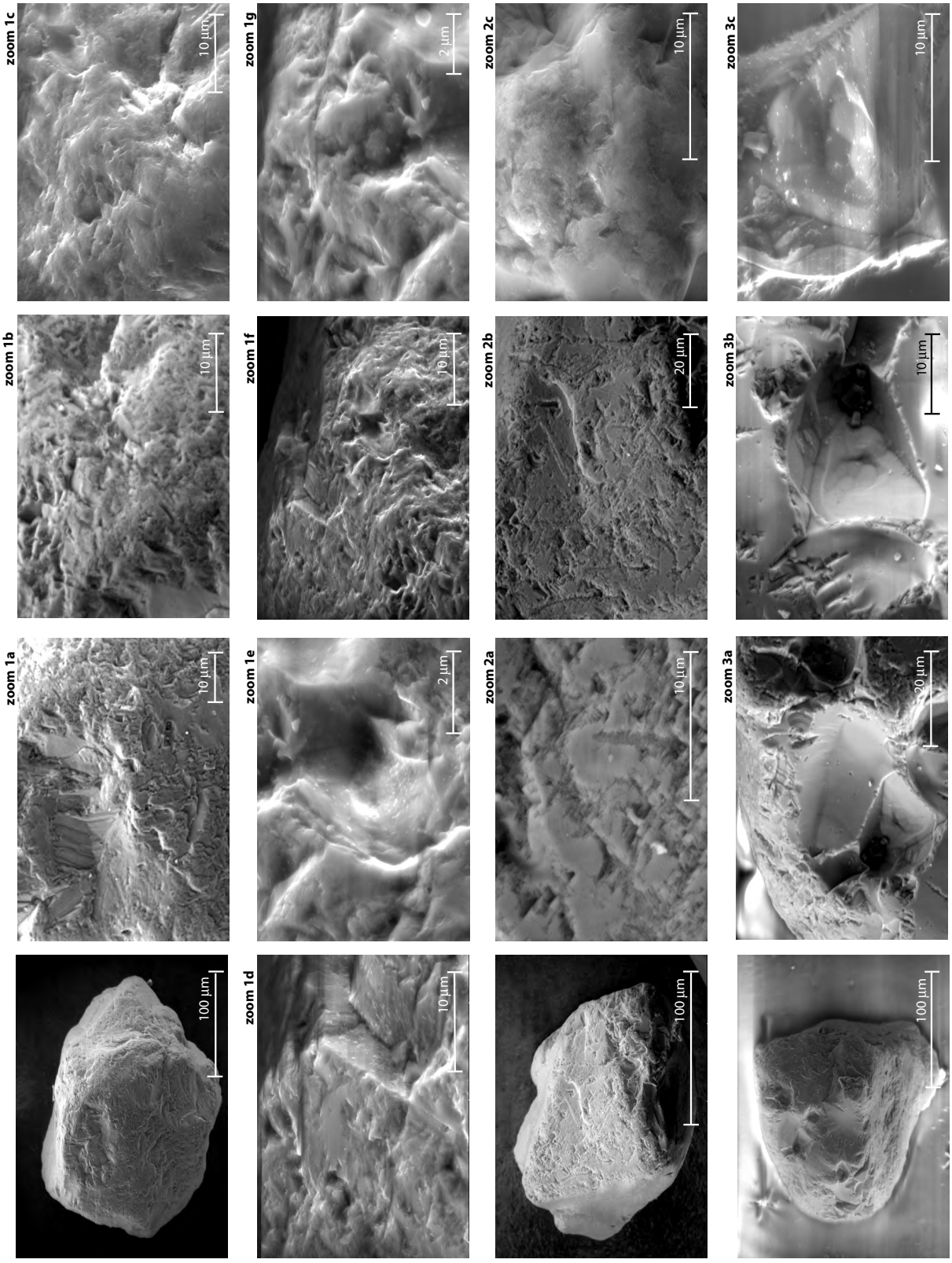

RH00 GRAIN 1. **RH00** GRAIN 1. **RH00** GRAIN 2. **RH00** GRAIN 3.

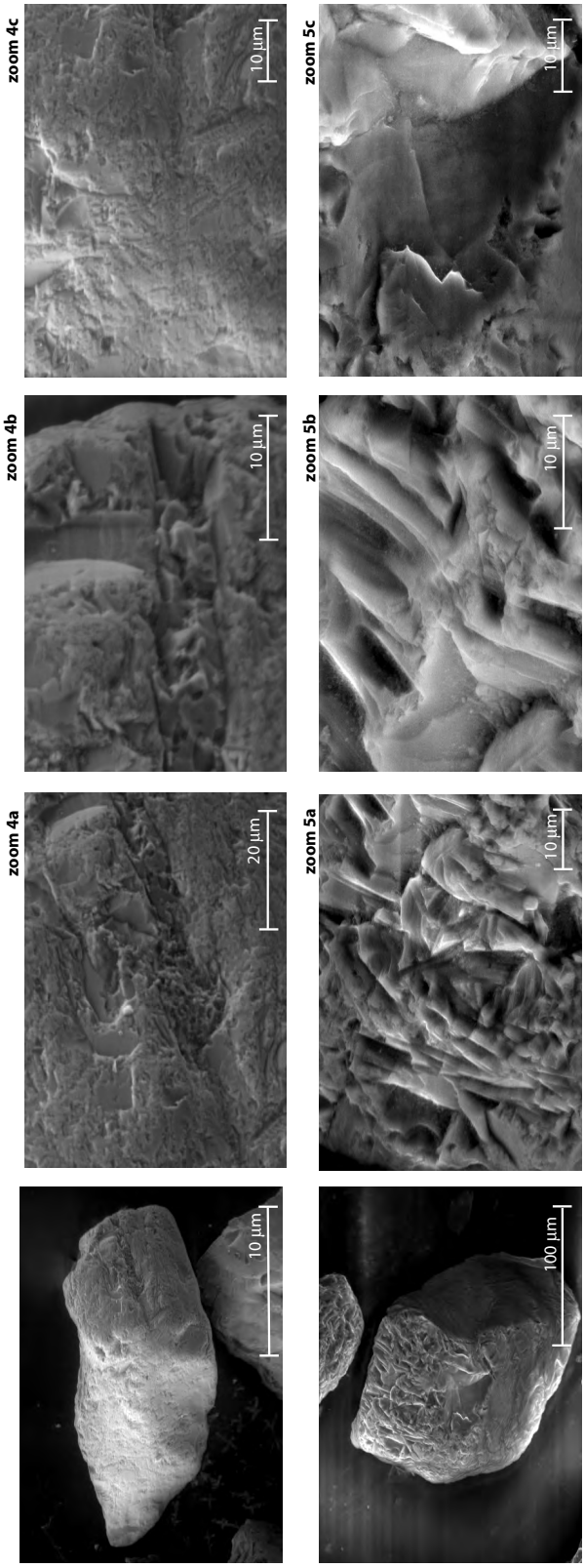

RH00 GRAIN 4. **RH00** GRAIN 5.

APPENDIX B
METHODS

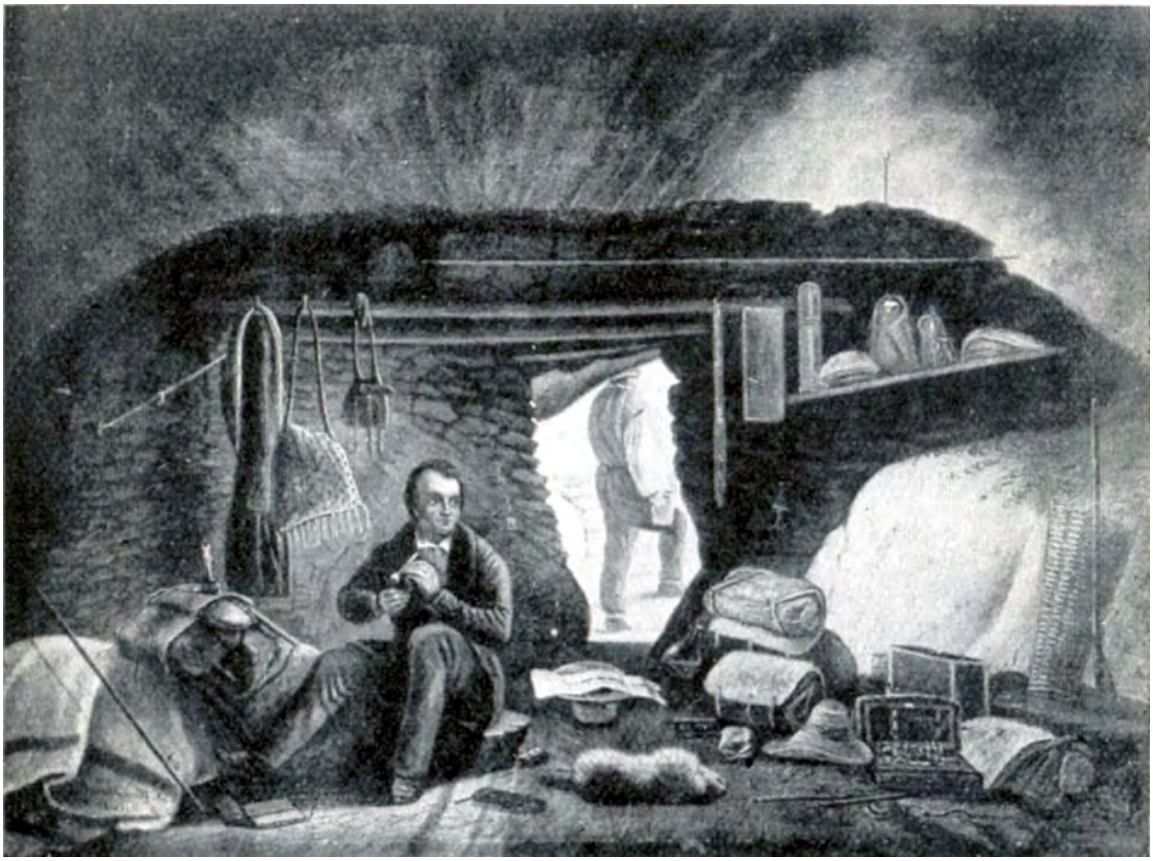

Appendix B: Detailed methods

Field sampling preparation and procedure

A. Preparation of 120 ml polypropylene sample bottles

- Soak cation bottles for 12 hours in 10 % HNO3, then rinse 3 times with deionised water.
- Soak anion bottles for 12 hours in deionised water and then rinse 3 times with deionised water.
- Soak phosphate bottles for 12 hours in deionised water, rinse 3 times with deionised water, add a crystal of iodine and place in oven at 40 °C for 30 minutes. When bottles are coated with a pink film of iodine rinse three times with deionised water and autoclave at 120 °C.

B. Rinse equipment

- Rinse 1 l polypropelyne bottle 3 times in flowing meltwater.
- Take sample ca. 5 – 10 cm below water surface in flowing stream.
- Put a 0.45 µm cellulose acetate filter on the Nalgene filter equipment using plastic tweezers.
- Rinse top chamber with aliquot of sample water, filter to the bottom and rinse bottom chamber subsequently. Pour off filtered water.
- Repeat 3 times.

C. Calibration of WTW pH and conductivity meters

- Calibrate the pH probe once a week, using low-conductivity pH 7 and pH 4 solutions pre-cooled to 4° C.
- Calibrate the conductivity probe once every two months using 0.1 M KCl.

D. Measure Alkalinity, Conductivity & pH

- Add 80 ml of filtered meltwater to an anions bottle.
- Measure pH and conductivity (in that order).
- Add 1 drop of 0.1M HCl acid to sample using a burette.
- Stir well and measure pH.
- Continue, recording the acid volume added at approximately pH 4.7, 4.5, 4.2, and 3.7.

E. Meltwater samples

- Rinse respective sample bottles 3 times with filtered meltwater and fill the bottle. Add 4 drops of 65 % suprapure HNO3 acid to the cation sample using a disposable pipette.
- Take unfiltered sample for total phosphate analysis.

F. Suspended Sediement

Store used filters which contain the susp. sediment

in plastic boxes, subsequently dry them at 40 °C.

Set-up of standards using dilution machine

Prepare standards according to analysis methods using the programmed dilution steps. Rinse machine tubes between different standards.

Ion Chromatography IC

- Major ions: Ca^{2+}, Mg^{2+}, Na^{+}, K^{+}, SO_4^{2-}, NO_3^{-}, Cl^{-}.
- Rinse autosamplerbottle 3 times with sample, put sample charge autosampler
- Machine: Dionex DX-500

A. Cations

- Column: CG 12A / CS 12A
- Eluent: 20 mM MSA (Metasulfonic Acid)
- Eluent flow rate: 1.0 ml/min
- Injection volume: 50 µl
- Detection: Auto suppressed conductivity
- Error: 5 % for concentrations of < 100 ppb; ca. 2 % for concentrations > 100 ppb

B. Anions

- Column: AG11-HC / AS11-HC
- Eluent: 20 mM KOH (Potassiumhydroxid)

- Eluent flow rate: 1.5 ml/min
- Injection volume: 100 µl
- Detection: Auto suppressed conductivity
- Error: 5 % for concentrations of < 100 ppb; ca. 2 % for concentrations > 100 ppb

AAS: furnace/flame

- Fe^{3+}, Al^{3+} measured on Perkin Elmer PC 5100 graphite furnace AAS
- Adsorbed cations: Ca^{2+}, Mg^{2+}, Na^{+}, K^{+}, on Perkin Elmer PC 5100 flame AAS

A. Fe^{3+}, Al^{3+}

- Platform tubes
- Heating steps Fe^{3+}: evaporation at 110 °C, calcination at 1400 °C, atomisation at 2400 °C
- Adsorption Fe^{3+} measured at wavelength of 248 nm
- Error: Fe^{3+} 10 % for concentration of < 15 ppb; 5 % for concentrations of > 15 ppb
- Heating steps Al^{3+}: evaporation at 110 °C, calcination at 1700 °C, atomisation at 2500 °C
- Adsorption Al^{3+} measured at wavelength of 309 nm
- Error: Al^{3+} 20 % for concentration of < 15 ppb; 10 % for concentrations of 15 – 50 ppb; 3 % for concentrations of > 50 ppb.

B. Adsorbed cations

- Flame atomic adsorption
- Adsorption measured at following wavelengths: Ca^{2+} at 422.7 nm, Mg^{2+} at 285.2 nm, Na^{+} at 589.0 nm, K^{+} at 766.5 nm.
- Error: ≤ 5 %, blanks were normaly 10 x lower than samples.

Flow Injected Adsorption (FIA)

- Si-concentrations
- Colorimetrical molybdate blue method (modified from Mullin and Riley, 1955)
- Measured at 695 nm on FIA tecator 5017
- Error: ≤ 5 %

Sr analysis

Described in chapter Sr.

Soluble Reactive Phosphorus (SRP) analyses

(modified after Murphy and Riley, 1962)

A. Reagents (of analytical quality), glassware, standards

A) 70 ml of concentrated sulphuric acid (H_2SO_4), made up to 500 ml in a volumetric flask.

B) 1.3715g of potassium antimony tartrate ($K(SbO)C_4H_4O_6 \bullet 1/2H_2O$) made up to 500 ml in a volumetric flask.

C) 20 g of ammonium molybdate ($(NH_4)_6Mo_7O_{24} \bullet 4H_2O$) made up to 500 ml in a volumetric flask.

D) 1.76 g ascorbic acid ($C_6H_8O_6$) made up to 100 ml in a volumetric flask.

- Reagents A, B, and C can be stored in cool room at 2 °C for several months and reagent D can be stored for up to 1 week.
- Glassware: soak in 10% Deconnex/ultrapur water for < 24h, rinse 3 times with ultra pur deionised water, dry at 80 °C.
- Standards: Merck KH_2PO_4 standard solution, 1000 mg l^{-1}, diluted first to 1mg l^{-1}: 3 µg l^{-1}, 10 µg l^{-1}, 30 µg l^{-1}, 100 µg l^{-1}
- Blank: 20 ml ultra pure deionised water

B. Procedure

1. Prepare 20 ml of filtered samples (0.45 μm cellulose acetate filter papers) and of standards in 30 ml graduated plastic goblets
2. Colour developing solution: Mix 50 ml of A, 5 ml of B, 15 ml of C, and 30 ml of D in a 100 ml volumetric flask (stable for up to 4 hours)
3. Add 3.2 ml of reactive solution to samples/ standards
4. Leave to react for 10-20 min
5. First analyse standards, then blank and samples within an hour.

Perkin Elmer Spectrophotometer

Wavelength: 880 nm

Cuvette: 5 cm glass, pre-rinsed with deionised water

and one washing with the sample
Three readings of each standard and sample

Total Phosphorus (TP) / Total Dissolved Phosphorus (TDP) analysis

Total phosphorus (TP) on unfiltered samples and total dissolved phosphorus (TDP) on filtered samples (0.45 μm cellulose acetate filters)

A. Reagents (of analytical quality), glassware, standards

A) Add 192 ml of concentrated sulphuric acid (H_2SO_4) to approx. 500 ml of deionised water in a 1000 ml flask

B) Dissolve 0.4571 g of potassium antimonyl tartrate ($K(SbO)C_4H_4O_6 \cdot 1/2\ H_2O$) in approx. 100 ml of deionised water.

C) Dissolve 16 g of ammonium molybdate ($(NH_4)_6Mo_7O_{24} \cdot 4H_2O$) in approx. 200ml deionised water.

A') Add B and C to the 1000 ml flask containing reagent A and make up to 1000 ml with deionised water. A' can be kept in cool room at 2 °C for several months.

D) 3.3g of ascorbic acid ($C_6H_8O_6$) made up to 50 ml with deionised water in a volumetric flask.

E) 4 g of ammonium peroxodisulphate ($MnSO_4 \cdot H_2O$) in 100ml of deionised water.

Glassware: soak in 10% Deconnex/ultrapur water for < 24h, rinse 3 times with ultrapur deionised water, dry at 80° C.

Standards: Merck KH_2PO_4 standard solution, 1000 mg l^{-1}, diluted first to 1mg l^{-1}: 3 µg l^{-1}, 30 µg l^{-1}, 100 µg l^{-1}, 500 µg l^{-1}, 1000 µg l^{-1}

Blank: 20 ml ultrapure deionised water

B. Procedure

1. Prepare 20 ml of samples and of standards in 30 ml graduated plastic goblets.
2. Transfer to glass tubes.
3. Add 1.2 ml of reagent E to each tube.
4. Close caps on tubes tightly and microwave for 1/2 h at 120 °C.
5. Return samples to their plastic goblets and when cooled add 1.2 ml of reagent A' and 0.6 ml of reagent D.
6. Leave to react for 10-20 minutes.
7. First analyse standards, then blank and samples within an hour.

Perkin Elmer UV/VIS Lambda 10 Spectrophotometer
Wavelength: 650 nm
Cuvette: 5 cm glass, pre-rinsed with deionised water and one washing with the sample
Three readings of each standard and sample

Sequential extraction of phosphorus phases SEDEX

Part A. Phosphorus extraction method (Ruttenberg, 1992)

1. Chemicals formulae

Sodium citrate $C_6H_5Na_3O_7 \cdot 2H_2O$
Sodium bicarbonate $NaHCO_3$
Sodium dithionite $Na_2O_4S_2$
Magnesium chloride $MgCl_2$
Na-acetate $CH_3COONa \cdot 3H_2O$
Magnesium nitrate $Mg(NO_3)_2 \cdot 6H_2O$
Acetic acid $C_6H_8O_6$
Chloridric acid HCl (5N)
Ultrapure deionised water

2. Extraction outline

- ***Step I: Reductible Mn & Fe-***bound P phase

Reduction of Fe by dithionite and subsequent complexation by citrate

Step II: Weak acid extractable P, including reactive detrital P

Acid dissolution at moderately low pH and chelation of Ca by acetate.

Step III: Detrital apatite

Acid dissolution at pH 1.

Step IV: Organic-bound P

Dry oxidation of organics and acid dissolution of ashed residue.

3. General points

- After each extraction and wash substep centrifuge samples for 12 minutes at 3000 rpm and pour off the supernatant into the same 30 ml/ 50 ml polypropylene collecting bottle, to obtain one sample per

extraction, leaving the sediment in the Falcon tube for the next step.

Include a reagent blank for each step.

Measure P concentrations in step I using ICP-AES and in steps II, III, and VI using spectrophotometer.

4. Solutions

A. CBD solution (0.5 l)

Mix sodium citrate (32.35 g) and sodium bicarbonate (4.62 g) and add deionised water.

Add the sodium dithionite 11.31 g just before use, (oxidises rapidly).

B. MgCl2 solution (0.5 l)

Add MgCl2 (101.65 g) to 0.5 l deionised water and shake well.

C. Na-acetate solution (0.5 l)

Add Na-acetate (68.04 g) to 0.3 l deionised water, mix well to dissolve.

Add 80 ml acetic acid and adjust with the remaining water for 0.5 l of pH 4 final solution.

D. 1 N HCl (1 l)

Add 200 ml HCl (5N) to 600 ml of deionized water and make up to 1 l.

E. 50% weight/volume $MgNO_3$ solution

(100 g of solute in 100 ml of deionized water).

5. Procedure

Step I:

1) Add 10 ml CBD solution to each 0.1 g sample in a Falcon tube, seal tubes, agitate by hand releasing gas if necessary and shake for 6 h.
2) Wash the sediment with 10 ml $MgCl_2$ per tube, agitating the samples by hand before shaking for 2 h.
3) Add 10 ml of deionized water into each tube, agitating the samples by hand before shaking for 2 hours.

Step II:

1) Add 10 ml of Na-acetate solution to each 0.1 g sample, shake for 5 hours.
2) Wash with 10 ml of the $MgCl_2$ solution in, agitating the samples by hand before shaking for 2 hours.
3) Repeat $MgCl_2$ wash.
4) Add 10 ml of deionized water into each tube, agitating the samples by hand before shaking for 2 hours.

Step III:

1) Add 10 ml of HCl solution to each sample agitating the samples by hand before shaking for 16 hours (overnight).

Step IV:

1) Transfer the solid samples from the Falcon tubes to porcelain cups, using deionized water.
2) Evaporate the water overnight in oven at 80°C.
3) Add 1 ml of the $MgNO_3$ solution to each sample and ash at 550°C for 2 hours.
4) Transfer ashed samples back into their respective Falcon tubes same tubes using a plastic spatula and 1N HCl and make up to 10 ml HCl per tube, agitating the samples by hand before shaking for 24 hours.

Part B. Spectrophotometeric analysis of steps II, III & VI (Eaton et al., 1995)

Hardware

- Perkin-Elmer UV/VIS spectrophotometer Lambda 10 with computer interface (UV WinLab software package for Windows).
- 5-cm quartz cuvette.

Chemicals Formulae

Ammonium molybdate $(NH_4)_6Mo_7O_{24}\cdot 4H_{2O}$

Antimony K tartrate $K(SbO)C_4H_4O_6\cdot 1/2H_2O$

Ascorbic acid $C_6H_8O_6$

Sulphuric acid H_2SO_4 (5N)

Ultrapure deionised water

Mixing reagent solution (0.75 l)

A) Add 6 g ammonium molybdate to 250 ml deionized water.

B) Make up 5N H_2SO_4 (74 ml H_2SO_4 in 426 ml deionised water).

Add 0.1454 g antimony K tartrate to H_2SO_4

Mix A and B (stable for about 2 months).

Color developing reagent

C) Add the ascorbic acid to the mixing reagent (0.053 g each 10 ml of solution;

stable for about 1 hour)

Procedure

1) Dilute samples and standards by a factor of 10 (1 ml of solution: 9 ml of deionised water).

2) Add 1 ml of the color developing reagent and place samples in the dark.
3) Analyse with the spectrophotometer after 15 minutes.

Detection Limit of Phosphorus (Tamburini, 2001)

Step I	0.03 mg g^{-1}
Step II	0.025 mg g^{-1}
Step III	0.003 mg g^{-1}
Step IV	0.004 mg g^{-1}

The 1 sigma error on the sum of steps II and III, weak and strong acid extractable P is < 0.03 mg g^{-1}, according to glacial samples remeasured on different extraction runs (n = 5).

The 1 sigma error on step VI is < 0.01 mg g^{-1} (n = 4).

Sediment granulometry analysis

Sieving of > 63 µm

- Weigh ca 500 g of sediment
- Reweigh when dried at 40 °C
- Put sediment in Retsch VS 1000 sieving column, sieving sizes 16, 8, 4, 2, 1 mm; 500, 250, 125, 63 µm. Sieve with water (shaking) for ca 30 min.
- Gain the off-flowing < 63 µm fraction
- Put sediment from individual sieves into plastic bowls, dry at 40 °C, and reweight.

Analysis of < 63 µm

- Analysis of the fraction < 63 µm on a Galai CIS 1 laser oriel.
- Put 1 – 2 drops of suspension in deionised water in disposable 1 cm cuvette. Measure as the machine counts 3500 – 4200 particles per run.
- The relative error is 10 %.

XRD / XRF

- Sample preparation fo whole rock and clay mineralogy analysis is described in chapter moraines.
- Analysis of the total inorganic chemistry were performed on powdered samples at the Geological Institut at the University of Fribourg, using a Sequential X-ray Spectrometer PW2400.

Total organic carbon TOC

Total organic carbon (TOC) was determined on about 100 mg of dried and ground sediment, using Rock Eval 6 standard bulk rock pyrolysis (Espitalié et al., 1986 and Lafargue et al., 1996).

Raingauge

- Put up gauge (Précis Mécanique Pluviometre 3029) away from big obstacles (boulders) at least 1.20 m high. Fix plateau with wires. Adjust balance precisely horizontal.
- Connect datalogger (Mitec Instruments SatelLite-U) to gauge, and put funnel back on.
- Pour one liter of water and count number of turns of balance.
- Not exact time of installation.
- Download on PC and convert signals into mm rain.

References

Eaton A. D., Clesceri L. S., and Greenberg A. E. (1995) Standard methods for the examination of water and wastewater.

Espitalié J., Deroo G., and Marquis F. (1986) La pyrolyse Rock-Eval et ses applications - III partie. Rev. Inst. Fr. Pet. 41(1), 73-89.

Lafargue E., Espitalié J., Marquis F., and Pillot D. (1996) Rock Eval 6 applications in hydrocarbon exploration, production and in soil contamination studies. Latin American Congress on Organic Geochemistry, Cancun.

Mullin J. and Riley J. P. (1955) The colorimetric determination of silicate with special reference to sea and natural waters. Analytica Chimica Acta 27, 162-176.

Ruttenberg K. C. (1992) Development of a sequential extraction method for different forms of phosphorus in marine sediments. Limnology and Oceanography 37(7), 1460-1482.

Tamburini F. (2001) Phosphorus in marine sediments during the last 150,000 years: exploring relationships between continental weathering, productivity, and climate., University of Neuchatel.

APPENDIX C
CONFERENCE ABSTRACTS

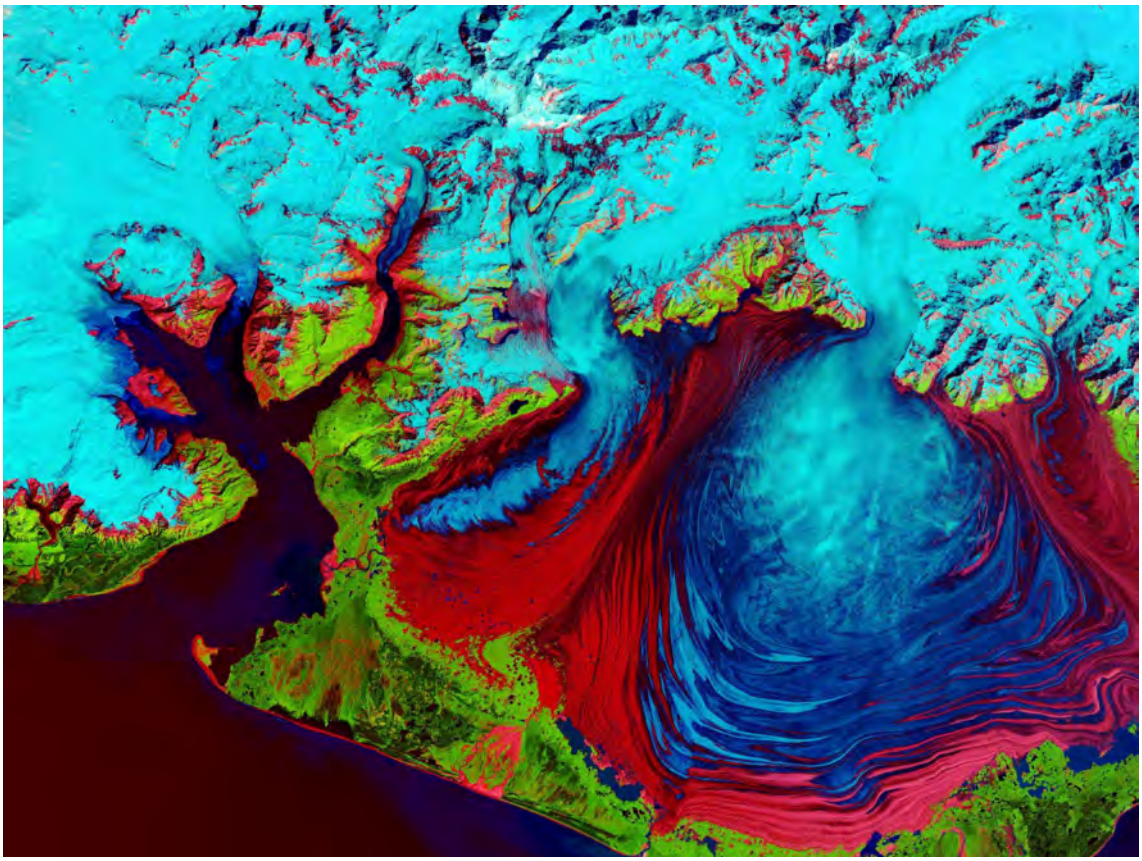

Appendix C: Conference Abstracts

First author presentations

Abstract for oral presentation at SwissSed 2000, Fribourg:

Present-day (bio)geochemical weathering in glaciated areas

K. Arn, R. Hosein, K.B. Föllmi, P. Steinmann

The influence of glacial activity on (bio-)geochemical weathering and its rates was studied in the two catchment areas of the Rhone and Oberaar glaciers. In a first-year field campaign (1999) water was measured and sampled five days a week at Rhone and twice a week at Oberaar glacier, always at 10 am and 5 pm, that is during those parts of the day in which water discharge reaches its minimum and maximum, respectively.

Results of the first field season show that concentrations of major cations and anions (Ca, Mg, Na, K, Al, Si, P, Cl, NO_3, SO_4, HCO_3) are generally higher (up to 10-40%) at minimum flow (10am) than at maximum flow (5pm). Concentrations are also lower from the middle of July until the beginning of September this year, probably relating to the seasonal evolution of daily mean temperature. Chloride and pH don't follow this trend. Increases in chloride are more likely to correspond to rain events. The big rain event at the beginning of July corresponds to the highest estimated discharge values. This in turn lead to a dilution of solutes; bedload transport was obvious.

Suspension load was estimated from filtering water samples. Grainsize and x-ray analyses will be performed and presented.

An initial comparison of phosphate values from this two glaciated catchment areas and from a tropical weathering regime (Orinoco basin, Venezuela) is presented in a related talk by Rachel Hosein.

Abstract for oral presentation at EGS 25, 2000, Nice:

Present-day glacial activity and geochemical weathering

K. Arn, R. Hosein, K.B. Föllmi, and P. Steinmann

The influence of glacial activity on (bio-)geochemical weathering and its rates was studied in the two catchment areas of the Rhone and Oberaar glaciers, both in the Swiss Alps. In a first-year field campaign (1999) water was measured and sampled five days a week at Rhone and twice a week at Oberaar glacier, always at 10 am and 5 pm, that is during those parts of the day in which water discharge reaches its minimum and maximum, respectively.

Results of the first field season show that concentrations of major cations and anions (Ca, Mg, Na, K, Al, Si, P, Cl, NO_3, SO_4, HCO_3) are generally higher (up to 10-40%) at minimum flow (10am) than at maximum flow (5pm). Concentrations are also lower from the middle of July until the beginning of September this year, probably relating to the seasonal evolution of daily mean temperature. Chloride and pH don't follow this trend. Increases in chloride are more likely to correspond to rain events. A big rain (and snowmelt) event at the beginning of July corresponds to the highest estimated discharge values what lead to a dilution of solutes.

Suspension load was estimated from filtering water samples. Suspension concentration seems to follow the discharge hydrograph and therefore also corresponds to rain events. Grainsize and x-ray analyses will be performed and presented to show the mineralogical evolution of the weathering environment over an ablation season.

Abstract for oral presentation at IGS BB Annual Meeting 2000, Southampton:

The importance of lithology in mass balance calculations of glaciated areas

K. Arn, R. Hosein, K.B. Föllmi, and P. Steinmann

The influence of glacial activity on (bio-)geochemical weathering and its rates is studied in the two catchment areas of the Rhone and Oberaar glaciers (Swiss Alps). The two areas were chosen because of their homogeneous lithology, both are lying in the crystalline rocks of the Aar massif. That should simplify the comparison of the dissolved chemistries between the two areas. Glacial meltwater was measured and sampled regularly over more than one ablation season, always at 10 am and 5 pm, that is during those parts of the day in which water discharge reaches its minimum and maximum, respectively.

In both areas the dissolved chemistry is showing the well known trends of higher concentrations during minimum discharge (10 am) than during maximum discharge (5 pm). Furtheron concentrations are also lower from middle of July until beginning of September, relating to the seasonal evolution of daily mean temperature. Chloride and pH don't follow this trend. Increases in chloride are more likely to correspond to rain events. The big rain event at the beginning of July 1999 corresponds to the highest estimated discharge values. This in turn leads to a dilution of solutes; bedload transport was obvious.

A preliminary comparison of the results from the two catchments shows that concentrations of major cations and anions (Ca, Mg, Na, K, PO_4, Cl, NO_3, SO_4, HCO_3) are generally higher at Oberaar glacier than at Rhoneglacier and therefore, the fluxes seem to be independent on the ratio of glacier cover (glacier cover Oberaar < Rhoneglacier). The Si fluxes of the two areas on the other hand are in the same order of magnitude. This observations imply that the lithology of the Oberaar catchment has to be less homogeneous. Specially Na-normalized Mg–Ca as well as HCO_3–Ca plots are showing a generally more pure granitic solute source in Rhone catchment, whereas a small portion of a gneissic-schisty zone in Oberaar catchment seems to be of a major importance for the dissolved chemistry.

Suspension load was estimated from weighing sample filters and from measuring turbidity during ablation season 2000. Particulate output and therefore physical erosion is also higher at Oberaar glacier. Local to regional weather patterns and their flushing influences are observed in both neighbouring catchments.

Abstract for poster presentation at EUG 11, 2001, Strasbourg:

Subglacial vs secondary weathering in two glaciated areas in the Swiss Alps

K. Arn, R. Hosein, T. Adatte, K.B. Föllmi, and P. Steinmann

The influence of glacial activity on (bio-)geochemical weathering and its rates is studied in the two catchment areas of the Rhone and Oberaar glaciers (Swiss Alps). In sampling glacial meltwaters and measuring their dissolved chemistry two main questions arose: (1) Are they a result of primary weathering, that means of dissolution of freshly ground fines or are there also reworking processes going on (weathering of soils and moraines up in the catchments)? (2) Can secondary weathering, after the deposition of moraines, be visible in the mineralogy of such deposits?

Suspended sediment from two ablation seasons was collected when filtering meltwaters: Whole rock mineralogy (filters) as well as the <2 μm grainsize fraction represent mainly the lithology of the catchment. There is no sign of secondary products like vermiculite. Therefore the suspended sediment has to origin from subglacial mechanical erosion of fresh bedrock.

Several profiles within moraine walls of different age (mainly walls from little ice age 1600-1850 as well as walls more than 500 years old) showed secondary weathering: The ratios of mica/clorite and K-Feldspar/Plagioclase respectively, increase with increasing age from 1.5 (value from recent sediment) to 2-3 and from 0.2 to 0.5-0.85 respectively. The older moraines showed an especially high vermiculite content of 5-30 % compared to mica and chlorite. The appearance of these secondary clay minerals seems to be dependent also on siltosity of the moraines (if compared with the granulometry).

This shows that alteration occurs in moraine deposits in a temperate alpine environment, even though

the moraines are at altitudes of more than 2000 m a.s.l. and at low yearly average temperatures. Therefore in calculating regional to global weathering fluxes from glaciated areas, secondary weathering should not be neglected.

Abstract for oral presentation at Earth System Processes, 2001, Edinburgh:

The importance of gradual chemical weathering on nutrient release in two glaciated areas in the Swiss Alps

K. Arn, R. Hosein, T. Adatte, K.B. Föllmi, and P. Steinmann

In order to identify processes and rates of alteration of moraine material in the glacier forefield, we studied chemical weathering processes of glacial sediments and rates in the two catchment areas of the Rhone and Oberaar glaciers (Swiss Alps).

We use mineralogy and bulk chemistry (XRD and XRF data) of glacial sediments of different ages from both glaciers; i.e. suspended sediment in meltwater, recent englacial melt-out sediment, terminal moraines dating from little ice age LIA (1300-1850), and older tills. Two of the main questions are: (1) How much does subsequent weathering of sediment after deposition contribute to the overall chemical denudation rate of a catchment? (2) How long is its influence significant? The answers could be used to assess weathering rates during glacial periods.

XRD data show an increase of pedogenic formed vermiculite and a continuous decrease of biotite with increasing age of the sediment. Chlorite seems to be more or less stable in tills up to LIA, in the oldest deposited tills there is a significant decrease. Suspended sediment is fresh, secondary weathering products are missing. Melt-out sediment contains vermiculite suggesting it may be derived from reworked lateral moraines that were previously weathered.

XRF element distributions have been compared to mineralogy in our profiles, which should give an insight in nutrient leaching processes. The distribution of some elements can directly be related to mineral weathering reactions, eg. biotite => vermiculite: The concentration of Fe_2O_3, K_2O, and MgO decreases as biotite content becomes less. In the pre-LIA tills Fe2O3 is completely leached in the top 30 cm of the profile.

This gradual convergence of biotite to vermiculite over a time scale of 100's of years emphasises the importance of secondary weathering in glaciated cachments. This pedogenic processes allow the slow release of Fe, probably biolimiting nutrient in proglacial alpine areas.

Abstract for oral presentation at 12th Goldschmidt Conference, 2002, Davos:

Sr isotope systematics in two glaciated crystalline catchments in the Swiss Alps

K. Arn, R. Hosein, K.B. Föllmi, and P. Steinmann, J. Kramers,[†] D. Aubert[§]

[†] Gruppe Isotopengeologie, Geol. Inst., Uni Bern, Erlachstrasse 9a, CH-3012 Bern

[§] EOST, ULP/CNRS, Centre de Géochimie de la Survace, UMR 7517, 1 rue Blessig, F-67084 Strasbourg

The Sr isotope systematics are useful in the identification of the relative importance of different sources contributing to chemical weathering fluxes. We studied subglacial chemical weathering processes and the Sr isotope composition of runoff and particulate material in the two glaciated catchments of Oberaar (OA) and Rhone (RH) glacier (Swiss Alps). Both areas are contained within the crystalline rocks of the Aar Massif, and the lithologies are quite homogeneous and comparable, except for the presence of a zone of highly deformed variscide basement gneisses and schists in the Oberaar cachment.

We analysed meltwaters (RH $^{87}Sr/^{86}Sr$ = 0.7257 / OA 0.7155), suspended sediment (RH 0.7292 / OA 0.7134), precipitation (0.7104) and dust (0.7109), local bedrock (0.7101 – 0.7377), and subglacially precipitated calcite that is now exposed in front of the glaciers (RH 0.7182 / OA 0.7164).

RH meltwater ratio is smaller than RH suspended sediment (total digestions) which can be interpreted as a mixture of granodiorite (0.7101) and granite (0.7377). We explain this by the preferential weathering of calcite (disseminated or in veins), which has a relatively low $^{87}Sr/^{86}Sr$ ratio. An enrichment in Ca relative to Na in the meltwaters compared to suspended sediments is

visible in both areas (OA > RH). In addition meltwaters could also be influenced by atmospheric input. The role of this will be assesed by mass balance calculations. The fact that OA meltwaters show an increased ratio compared to OA suspended sediment points to a minor atmospheric influence on our meltwaters: Increased OA meltwater ratios are better explained by the weathering of freshly ground biotite. The concentration of suspended sediment is higher for OA than for RH. OA suspended sediment contains more biotite due to the gneissic rocks within this catchment, what is also visible in the more elevated K flux.

The first order reaction in our catchments is weathering of calcite, but in addition, in the OA catchment biotite weathering exerts an other major influence on the meltwater $^{87}Sr/^{86}Sr$ ratio.

Abstract for oral presentation at IGS BB Annual Meeting 2002, Glasgow:

Quantifying the impact of accessory calcite on meltwater chemistries draining two crystalline catchments, the Rhone and Oberaar glaciers, Switzerland

K. Arn, R. Hosein, P. Steinmann, T. Adatte, K.B. Föllmi

Annual suspended sediment and dissolved fluxes have been calculated for the presently glaciated Rhone and Oberaar catchments. The catchments lie on the crystalline rocks of the Aar massif in central Switzerland. There are minor lithological differences between the two catchments; The central section of Oberaar catchment is underlain by a schistose zone containing < 5 % calcite, whereas the Rhone catchment only contains granitic and granodioritic bedrock with < 1 % calcite.

Metlwaters from the two catchments were sampled over two years (1999-2001). Monthly samples were taken during the accumulation period (winter) whereas during the ablation period (summer) samples were taken twice daily. There is a considerable difference in the total dissolved fluxes from the two catchments, which is principally the calcium flux from the Oberaar catchment being 5 – 6 times higher than that from the Rhone. We attribute this to the elevated calcite flux from the Oberaar glacier: Calcite concentrations are 3 times higher in the Oberaar suspended sediment and 1.6 – 2 times as much suspended sediment is exported from the Oberaar catchment than from the Rhone. This leads to a calcite flux of approximately 16 t km-2 yr-1 from the Oberaar catchment, whereas the calcite flux from the Rhone catchment is only 3 t km-2 yr-1. The calcium fluxes from these alpine glaciers is directly proportional to the calcite content of their suspended sediment, and the higher calcite content of the Oberaar sediment causes 3 times more atmospheric CO_2 to be sequestered in the Oberaar catchment compared to the Rhone.

Second author presentations

Abstract for oral presentation at Swissed 2000, Fribourg:

A comparison of soluble reactive and total dissolved phosphate concentrations and dynamics, in temperate-glacial and humid-tropical fluvial systems.

R. Hosein, K. Arn, K.B. Föllmi, P. Steinmann

Soluble reactive phosphate (SRP) and total dissolved phosphate (TDP) concentrations have been studied in two contrasting weathering environments:

a) two small, temperate, mountain glacier catchments; the Rhone and Oberaar glaciers, in Switzerland over a one-year ablation period

b) A large, humid-tropical watershed, the Apure river system, Venezuela, which runs from the Venezuelan Andes to the Orinoco river. The Venezuelan watershed was sampled once during the dry season (February) and once at the end of the rainy season (September).

Comparing present-day biogeochemical weathering in glacial and tropical environments may initially seem counter-intuitive. Classically chemical weathering studies looked to the tropics, following the rational that a 10∞C increase in temperature doubles chemical reaction rates. But another physical control of reaction rates is the reactive surface area of the “chemicals”. Glacier milks contain particles of high surface area to volume ratio. In temperate glaciers such particles may remain

in isolated contact with subglacial waters for periods of months.

Our initial results suggest that SRP and TDP concentrations in the two environments are comparable. Oberaar glacier values lie between 35 and 65 μg/l, those of the Rhone glacier are between 10 and 40 μg/l . February tropical values are consistently lower than or equal to temperate values, whereas the September tropical data falls into the same range as the temperate results.

In this light we suggest that the importance of biogeochemical weathering in glaciated environments might be greater than is presently recognised.

Abstract for oral presentation at EGS 25, 2000, Nice:

Can icehouse-greenhouse transitions be modeled by extrapolating data sets from temporate-glacial and humid tropical environments?

R. Hosein, K. Arn, K.B. Föllmi, P. Steinmann, C.J. Burton†, M.J. Russell†

† Division of Earth Sciences, Gregory Building, Lilybank Gardens, University of Glasgow, Glasgow G12 8QQ, UK

How, in a greenhouse climate, could late Ordovician temperature drop by 10°C (Brenchley 1995), creating an icehouse period of less than 1my? ∂C13 curves demonstrate increased productivity at the glacial maximum. Contemporaneous excursions in our chemostratigraphy (P_2O_5, Fe_2O_3) support the argument for increased nutrient supply driving productivity and thus CO_2 drawdown. If nutrient supply had an important role in climate change (albedo can only explain 47% of temperature change) then identifying the nutrient source may improve our understanding of climate forcing.

Here we have explored a glaciated continent's potential to be a significant nutrient source by analysing phosphate in waters from a humid-tropical and two temporate glacial catchments. Initial results suggest that concentrations of soluble reactive (SRP) phosphate in temporate glacial waters are comparable with concentrations in tropical waters (10-65 μg/l & 5-30 μg/l SRP respectively). We suggest glacial, bio-geochemical weathering rates may be greater than presently recognised and encour-age the inclusion of the continental weathering data in models of climate change.

Abstract for oral presentation at EGS 25, 2000, Nice:

Weathering and climate change

K.B. Föllmi, R. Hosein, K. Arn, F. Tamburini, T. van Westrenen, B. van de Schootbrugge, P. Steinmann, T. Adatte

Weathering is important in regulating the long-term carbon cycle. Temporal changes in biogeochemical weathering rates modulate the uptake of atmospheric CO_2, and changes in biogeochemical weathering rates lead to changes in the release rates of biophile elements (such as P, Si, Ca, Fe), which modulate transformation rates of in-organic carbon into organic carbon through photosynthesis. Variations in weathering may, therefore, exert an important control on a row of globally interlinked processes such as productivity, transformation of inorganic carbon into organic carbon, oxygen contents, as well as climate.

Presently, in the field of research on weathering, several main topics have been identified as partially unresolved: 1) Quantification of weathering rates in the geolo-gical past; 2) The degree of dependency of biogeochemical weathering rates on total weathering rates; and 3) The influence of glaciation on total and biogeochemical weathering rates. These topics are relevant to several open questions, such as 1) to what extend continental weathering did contribute to phases of enhanced marine productivity during the Neogene and Quaternary, dependent on climate change; and 2) which types of feedback mechanisms may have developed between weathering and climate change in the case glaciation events did contribute to enhanced biogeo-chemical weathering.

Abstract for oral presentation at IGS BB Annual Meeting 2000, Southampton:

Comparing phosphate weathering rates in glacial and tropical environments: Implications for feedbacks to global climate through coupled phosphate-carbon cycles

R. HOSEIN, K. ARN, K.B. FÖLLMI, P. STEINMANN

Raymo (1991) has highlighted the importance of feedbacks between silicate weathering and CO_2 drawdown in climate change models. It is suggested that silicate weathering rates are strongly temperature dependent (Brady 1991). Therefore although glacial environments do sequester CO_2 (Sharp et al 1995) the global rate of CO_2 removal from the atmosphere could be anticipated to decrease during a glaciation, reducing the potential for a negative feedback. A second mechanism of CO_2 drawdown could be a biogeochemical one; Given phosphate would be the limiting factor and applying Redfield molar ratios 106 moles of CO_2 could be taken up by aquatic biomass for every mole of phosphate available to them.

We compare phosphate fluxes (as soluble reactive phosphate-SRP) from glacial and tropical environments to see whether temperature is clearly the limiting factor in weathering phosphate-bearing minerals. The values from both environments fall into a similar range. We suggest that the crushing, grinding action of glaciers plays an important role in increasing the surface area of minerals and that surface area may, in part, control the rate of phosphate weathering.

On paper the effieciency of phosphate limited CO_2 drawdown depends on the C:P molar ratio chosen for calculations. In the Oberaar and Rhone catchments, multiplying the P flux values, 17 and 29 kg/km^2/year respectively, by the Redfield molar ratio (draw down by living algae) implies that 1416 and 696 kg-C/km^2/yr respectively of carbon could be sequestered from the atmosphere. If a higher C:P molar ratio ,e.g 1:500, as found in the decayed organic matter of land plants, is chosen the CO_2 draw down increases considerably. This would suggest glacial P fluxes could have an impact on pCO_2 ,if the organic matter was not reoxidised, at a similar order of magnitude to silicate weathering 2137 kg-C/km^2/yr (Sharp et al 1995) in the glacial environment.

Abstract for poster presentation at EUG 11, 2001, Strasbourg:

Adsorbed cation fluxes from the Rhone and Oberaar Glaciers

R. HOSEIN, K. ARN, K.B. FÖLLMI, P. STEINMANN

Suspended sediment samples were taken during the 1999 ablation season from the Rhone and Oberaar glacier meltwater streams. 40 of these samples were leached with 3 x 10 ml aliquots of 1N ammonium acetate. This leachate was measured for Ca^{2+},Mg^{2+}, Na^+ and K^+ ions using a flame AAS.

We found, firstly that the adsorbed cation concentration was not constant during the ablation season for any ion. On an annual scale sediment exported during "flushing events", namely days with high rain fall, contained elevated concentrations of adsorbed ions (mg/g). The change in the adsorbed ions can also be seen on an hourly scale, during a 24h study of a rain event. On the 27/7/99-28/7/99 heavy rain fell on the Rhone catchment between 19.00 and 04.00. An increase in the Ca^{2+} and Na+ adsorbed load was observed at 23.00 and 01.00. Post rainstorm adsorbed cation concentrations returned to their lower values.

Secondly the ratio of dissolved to adsorbed ion concentrations does not appear constant during the ablation season and is also perturbed by flushing events.

We suggest the concentration of adsorbed ion cations can be up to 100% of the dissolved load. This observation has important implications for chemical mass balance studies in glaciated areas. Potential CO_2 draw-down by chemical weathering in glaciated areas may be higher if the total concentration of the adsorbed weathering products has previously been underestimated.

Abstract for oral presentation at Earth System Processes, 2001, Edinburgh:

A SEM study of the chemical weathering rates of apatites in two glaciated catchments in the Swiss Alps

R. Hosein, M. Lee†, K. Arn, K.B. Föllmi, P. Steinmann

† Division of Earth Sciences, Gregory Building, Lilybank Gardens, University of Glasgow, Glasgow G12 8QQ, UK

Apatite is a common phosphorus-bearing mineral. Quantifying its weathering rate is important as phosphorus (as PO_4) is a biolimiting nutrient whose only source is rock weathering (it has no geseous phase). Its rate of supply to the environment may affect the rate which carbon is taken up biologically. Using a mass balance method (inputs of phosphate in the form of rain and snow subtracted from its output in river water) we calculate an annual weathering flux of 10-12 kg/km2/ year for the catchments of the Rhone and Oberaar glaciers, Switzerland. Both areas have a granitic bedrock.

An alternative way to estimate weathering rates is to look at mineral etching, using scanning electron microscope imaging. If sediment age and pit depth is known, then a weathering rate can be calculated for the individual minerals in the sediment. This method is used here as a first-order test to constrain the weathering rates estimated by the mass balance method. It may also demonstrate varying weathering rates in different environments (periglacial, subglacial) in the same catchment.

We hope to compare the degree of etching in glacial sediments of different ages, taken from within our catchments. Apatites have been isolated from recent glacial-fluvial, lacustrine and melt-out sediment, from 1850-moraines and moraine dating from before 1300. Apatites from the oldest moraine, which is all we have analysed to date, show evidence of etching, possibly following previous weakenings in the crystal lattice caused by fission tracks. Results will be presented as weathering rates of phosphorus for the apatite grains and compared to our mass balance rate results.

Abstract for oral presentation at 12th Goldschmidt Conference, 2002, Davos:

Detrital phosphorus weathering rates and mechanisms: comparing tropical and glacial catchments.

R. Hosein, K. Arn, S. Huon†, K.B. Föllmi

† Univ. P.M. Curie, Lab. Biogéochimie isotopique (LBI), UMR 7618, Paris

Continental biogeochemical weathering of apatite is the primary source of phosphorus (P). Variations in weathering intensity may influence the global P flux and therefore primary production rates, which are important with regard to the carbon cycle and climate change. To assess the relative importance of the phosphorus flux in tropical and glacial environments we compared the distribution of phosphorus phases in suspended sediments from the Apure river system, Venezuela with those from meltwater streams of the Oberaar and Rhone glaciers, central Switzerland. Additionally two chronosequences were sampled in the forefields of the Oberaar and Rhone glaciers, comprising Little Ice Age moraines and tills of the Younger Dryas. Iron-bound P, organic P, and detrital P phases are quantified by a sequential extraction (SEDEX) method. In the glacial suspended sediment detrital P is the main phase. The Apure system suspended sediment becomes impoverished in detrital P and enriched in iron and organic bound P in rivers further from the source. In the glacial Younger Dryas samples the detrital P phase is replaced by organic and iron-bound P. Initial calculations give approximate apatite weathering rates of 0.3 $gm^{-2}yr^{-1}$ for the Little Ice Age moraines and 0.01 g P $m^{-2}yr^{-1}$ for the Younger Dryas tills. These weathering rates are one order of magnitude higher than the continental average value. Our results show that alpine glaciers have potential to accelerate detrital P weathering, especially in the first 100's of years after deposition of glacial sediment. Finally we present a global data set demonstrating that the flux of Total P in meltwaters from presently glaciated catchments is elevated when compared to riverine fluxes from presently non-glaciated catchments.

Abstract for oral presentation at IGS BB Annual Meeting 2002, Glasgow:

Phosphorus phases in 2 alpine glacial meltwater streams and a proglacial tributary draining crystalline catchments in the Swiss Alps

R. HOSEIN, K. ARN, P. STEINMANN, K.B. FÖLLMI

The bio-availability of phosphorus (P) and its potential impact on bio-productivity and atmospheric CO_2 sequestration varies, depending on the form and the environment it is in. Detrital P is the primary source of P to the biosphere and physical erosion rates control detrital P supply. Total P concentrations in the Rhone and Oberaar glacier meltwaters are directly proportional to their suspended sediment concentrations. We calculate present-day detrital P fluxes from the Rhone and Oberaar glaciers of 7 and 11 kmol km^{-2} yr^{-1} respectively, representing 93 – 95 % of the total P flux. These fluxes are among the highest recorded particulate P fluxes in the world. But retention of detrital P minerals in terrestrial deposits may be vital to convert them into bio-available forms, as detrital P is not bio-available in aquatic environments. Protosols develop on alpine glacial deposits within a timespan of hundreds of years and the low pH and biological processes associated with the pedosphere enhances dissolution of the main detrital P bearing mineral, apatite. Soluble reactive P (SRP) concentrations in the Rhone and Oberaar glacier meltwaters are lower than SRP concentrations in the Rhone tributary that drains 11.6 kyr (Younger Dryas aged) sediments on which alpine meadow has developed. We calculate an SRP weathering flux from the Rhone tributary of 0.36 kmol km^{-2} yr^{-1}, whereas the Rhone and Oberaar glacier SRP flux is 0.16 kmol km^{-2} yr^{-1}. This implies that apatite dissolution is faster in the proglacial environment. The released SRP is biologically available. The ironbound and organically bound P phases, which have accumulated in the 11.6 kyr sediment, are also more bio-available than detrital P in freshwater and marine environments.

APPENDIX D
CURRICULUM VITAE

Appendix D: Curriculum Vitae

Name:	Arn	
First name:	Kaspar Samuel	
Nationality:	Swiss	
Address:	Bucheggstrasse 6	c/o Marlen Schaller, Postheiriweg 5
	CH-4581 Küttigkofen	CH-4500 Solothurn
phone:	032 / 718 26 42 (office), 032 / 677 13 33; 032 / 623 42 74 (home)	
fax:	032 / 718 26 01 (office)	
e-mail:	kaspar.arn@unine.ch ; kaspar1@bluewin.ch	
birth date:	7 September 1973	

Education

1998 - 2002: PhD thesis at the Geological Institute of the University of Neuchâtel, Switzerland (Prof. Karl B. Föllmi)
Thesis title: "The relative impact of sub- and proglacial weathering on primary minerals in crystalline rocks."

1993 - 1998 Studies in Earth sciences at the Geological Institute of the University of Berne, Switzerland, with Masters in Quaternary Geology. Masters thesis: "Quaternary Geology in the Binnvalley (VS) and in Southern Chile (42 °S)."

Post-grade course:

March 2000 Controls on rock weathering and continental erosion, University of Berne, Switzerland.

Further education in applied Geology:

April/May 2002: "Hydrogeochemie des Grundwassers" (NDK 19, ETHZ)

October 2002: "Geotechnik der Quartären Lockergesteine" (NDK 20, ETHZ)

Teaching

1999 -2002: Undergraduate and graduate courses (Teaching assistantship, in French). Subjects: General Introduction to Geology; Sedimentology; Glaciology/Quaternary; Geophysiology.
Guidance/coordination of several fieldtrips: Southern Germany, Swiss Alps, Mexico.

Practical experience

May 2001: Participation on workshop: Changements in the lake Brienz ecosystem; organised by the Canton of Berne, Brienz (BE), Switzerland.

1998 - 2002: Diverse lab works in GEA laboratory at the Geological Institute of the University of Neuchatel, mainly water analysis.

1999: Field assistance on geochemical mission in Venezuela in collaboration with Dr. S. Huon, Paris: Handling of a sonde, water/sediment sampling along Orinoco river system, mainly technical works.

June 1998: Internship in geology consulting office (Kellerhals und Häfeli, Berne): Revision of printing

	model of geological atlas of Switzerland (sheets Berne and Worb); completion of legend and diverse wells from various archives.
1997:	Field assistance in framework of international research project in Lake Region in southern Chile (Universities of Maine and Berne; Prof. G. Denton, Prof. T. Lowell, Prof. C. Schlüchter). Logging of diverse sections in quaternary deposits along the construction site of Routa 5 and sampling of glacial diamictons.
1996 – 1997:	Assistance at the Geological Institute of the University of Berne: Organisation of a workshop (on overdeepened valleys in Switzerland) and elaboration and presentation of one subject (overview on current work on overdeepened valleys in Switzerland).
1995 - 1997:	Daywise field assistance with geology consulting office (Kellerhals und Häfeli, Berne): Tunnel construction site Lötschberg, Frutigen (NEAT), highway construction sites (A16, A5, Sion), well logging (various regions of Swiss plateau). The works mainly consisted of tunnel mapping and logging of quaternary deposits as well as diverse well measuring sessions.
1995 - 1996:	Diverse field assistantships with PhD students, sampling of water, rock, and quaternary deposits.

Memberships

CHGeol
S-Quat
International Glaciological Society
International Association of Hydrological Science
European Union of Geosciences
European Association of Geochemistry / The Geochemical Society

Awards

John Glenn Price for best oral presentation at the International Glaciological Society British Branch Annual Meeting 2002, Glasgow.

Computer skills

Good knowledge of the Macintosh system, experience with PC. Word processing, and calculation (Microsoft Office). Graphic design and publishing (Adobe Illustrator, Photoshop, Acrobat, InDesign, AutoCAD (R14)). Web design (Adobe Golive).

Languages

German:	mother tongue
English:	fluent, speaking and writing
French:	fluent, speaking and writing
Italian:	speaking fluency

References

Prof. Dr. K. B. Föllmi
Geochemical and Environmental Analysis GEA
Institut de Géologie, Université de Neuchâtel
Rue Emile-Argand 11
CH-2007 Neuchâtel

Prof. Dr. Ch. Schlüchter
Quaternary Geology (Happy Ice Age group)
Geological Institute, University of Berne
Baltzerstrasse 1
CH-3012 Berne

APPENDIX E
COLOR PLATES

Contents Appendix E: Color plates

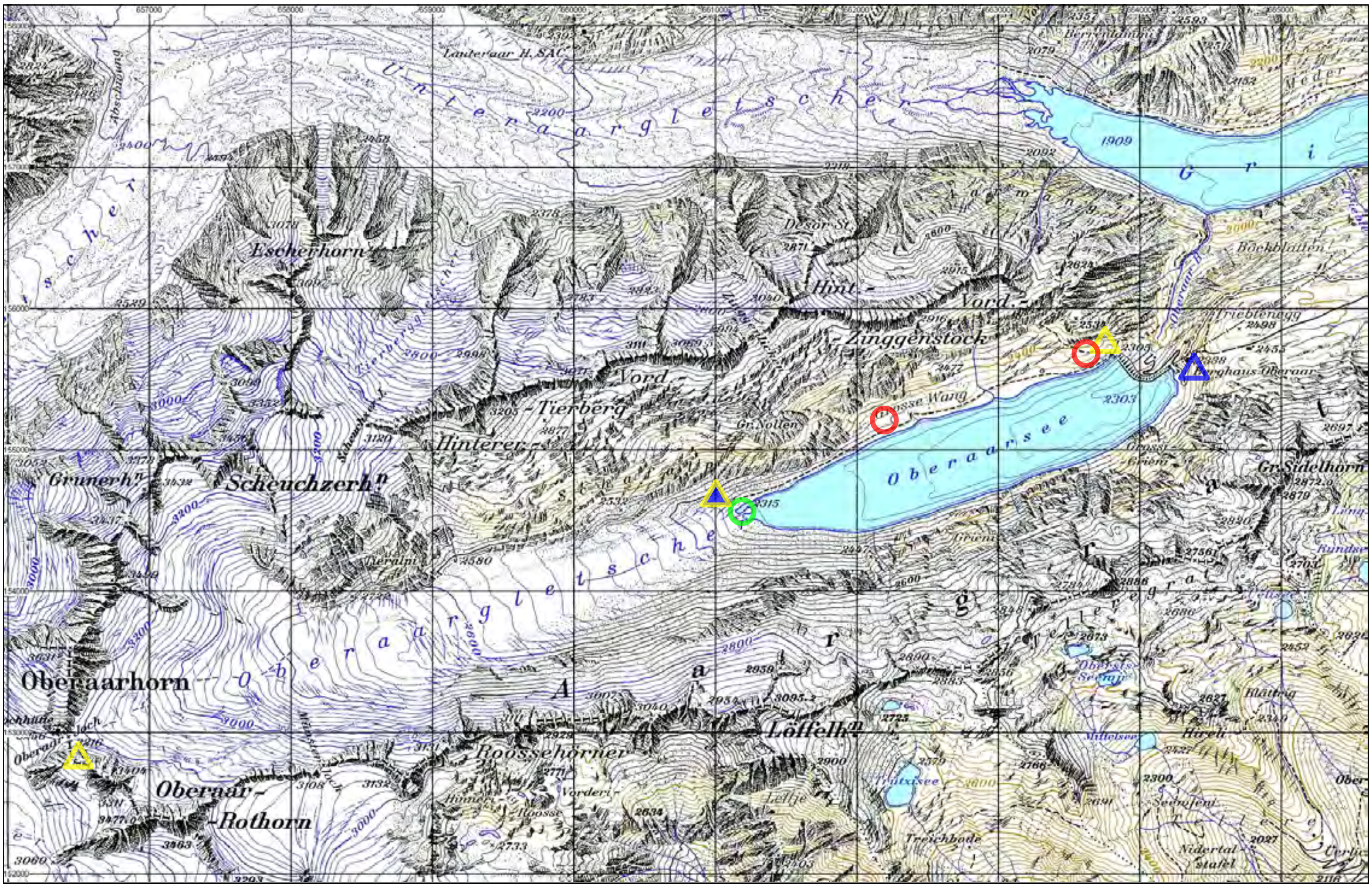

Sampling point meltwater, Soil profiles, Totalisators, Raingauge, Rain sampling

Fig. 1.3a: Oberaar overview with sampling points (1:50'000).
Reproduced with permission of the Swiss Federal Office of Topography (BA024559).

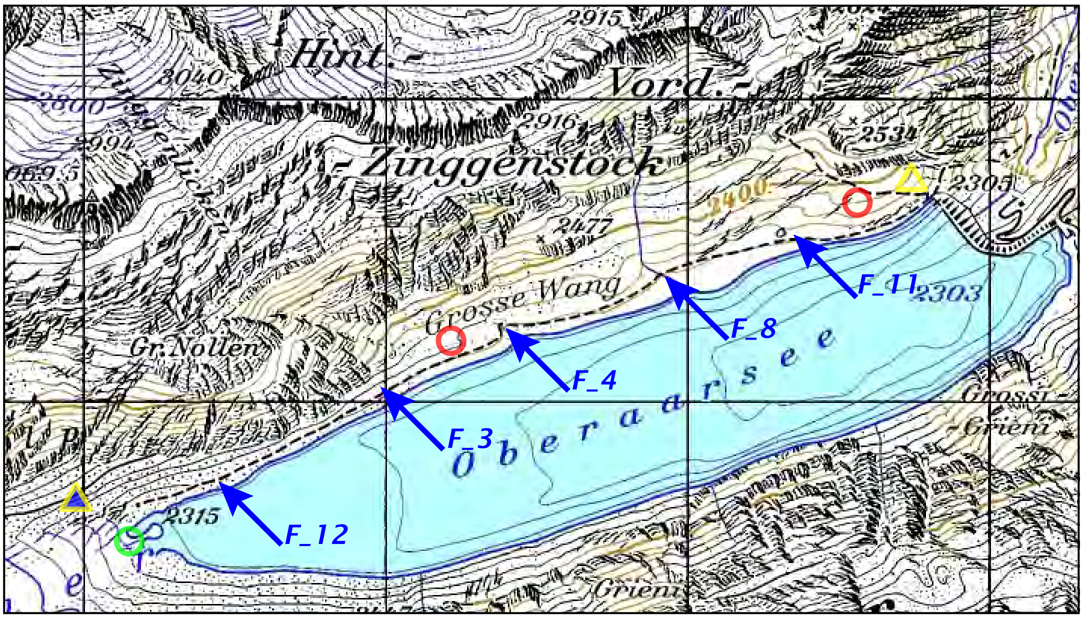

Sampling point meltwater, Soil profiles, Totalisators, Raingauge, Sidestreams

Fig. 1.3b: Oberaar detail map with sampling points and sidestreams.
Reproduced with permission of the Swiss Federal Office of Topography (BA024559).

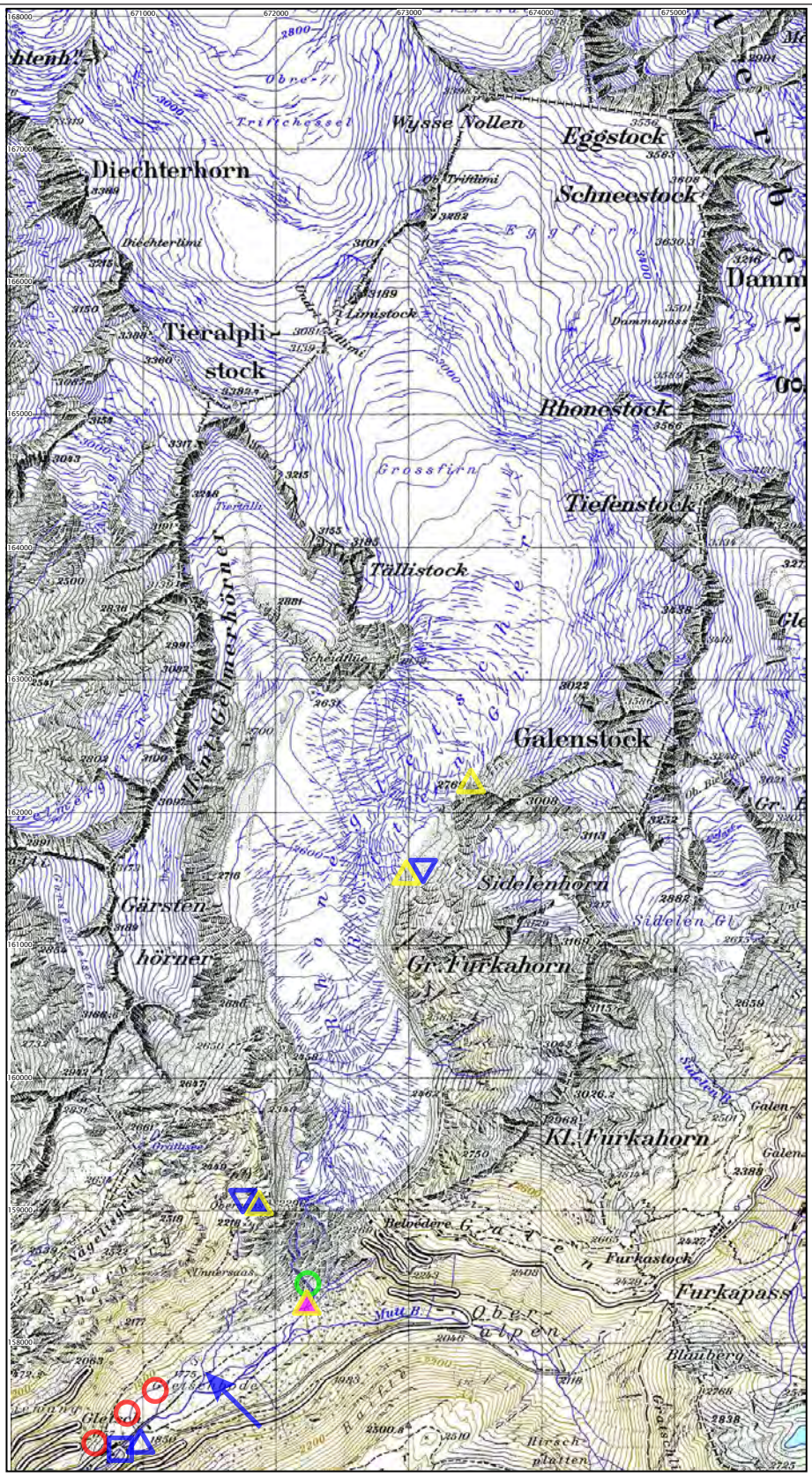

Fig. 1.3c: Rhone overview with sampling points (1:50'000).
Reproduced with permission of the Swiss Federal Office of Topography (BA024559).

Fig. 1.7A: Oberaar glacier with lake I.

Fig. 1.7B: Oberaar glacier with lake II.

Fig. 1.7C: Oberaar glacier snout I.

Fig. 1.7D:Oberaar Joch.

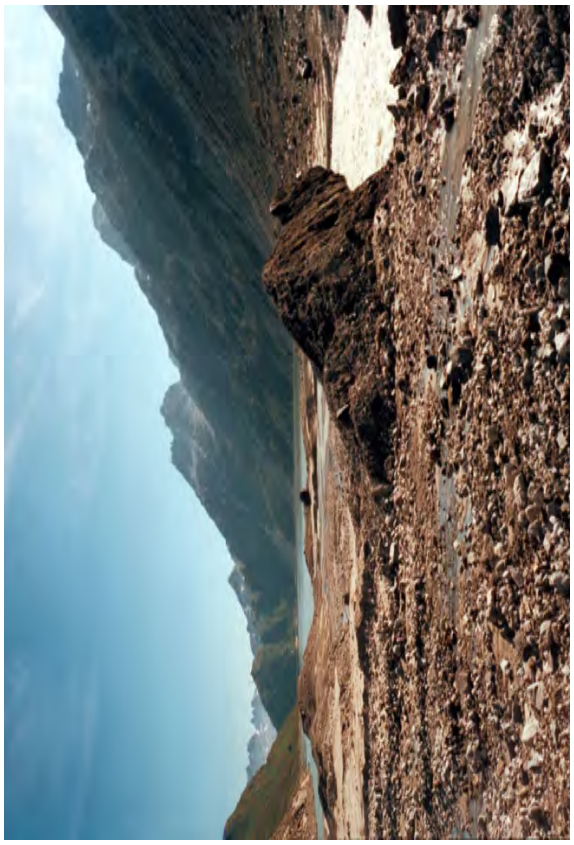

Fig. 1.7F: Oberaar glacier "Press-Schuppen".

Fig.1.7H: Water filtering in front of glacier.

Fig. 1.7E: Oberaar glacier snout II.

Fig. 1.7G: Oberaar glacier snout III.

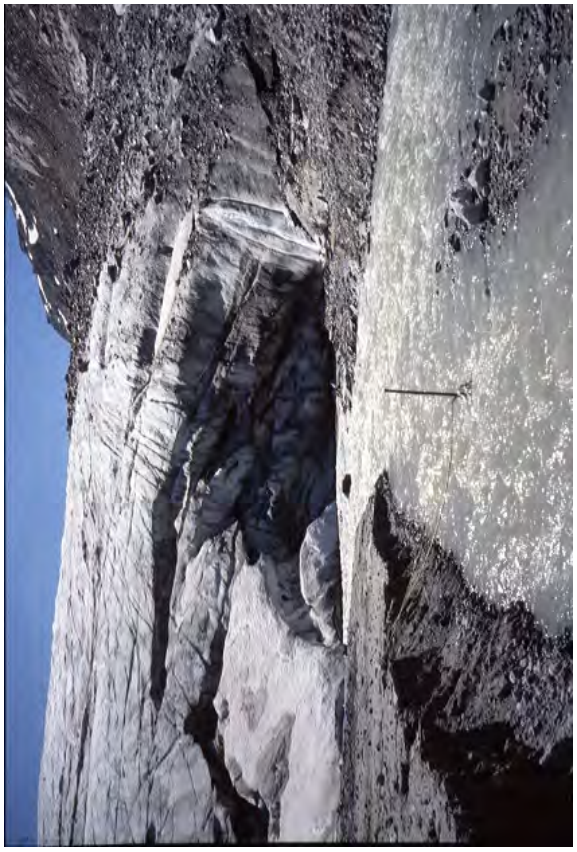

Fig. 1.7J: Turbiditymeter in the river.

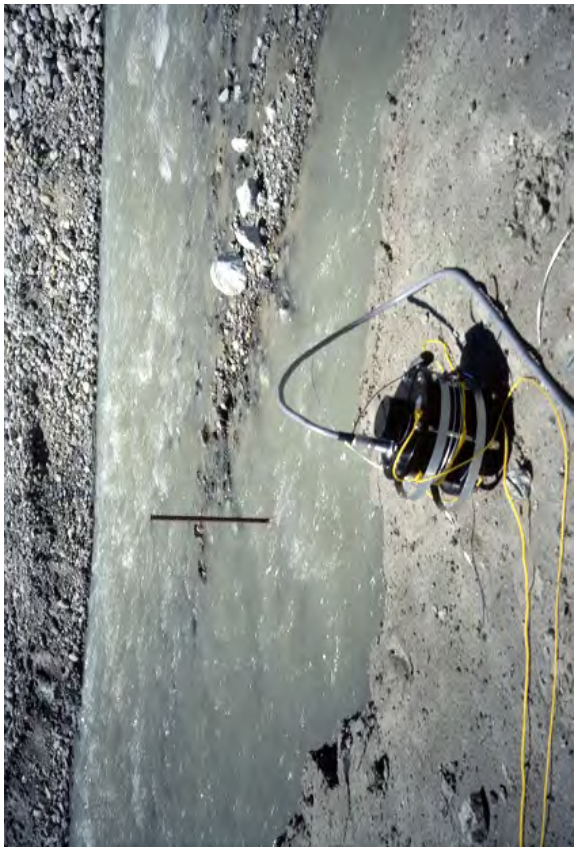

Fig. 1.7L: Turbiditymeter on land.

Fig. 1.7I: Oberaar glacier snout IV.

Fig. 1.7K: Rain sampling.

Fig. 1.7N: Profile Oberaar LIA A.

Fig. 1.7P: Profile Oberaar YD.

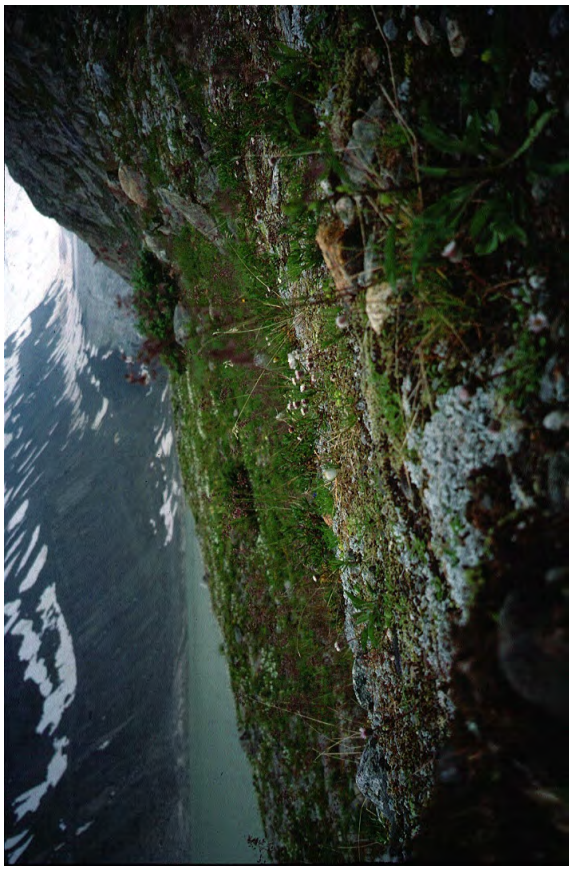

Fig. 1.7M: LIA moraine ridge.

Fig. 1.7O: Profile Oberaar LIA B.

Fig. 1.8C: Getting there...

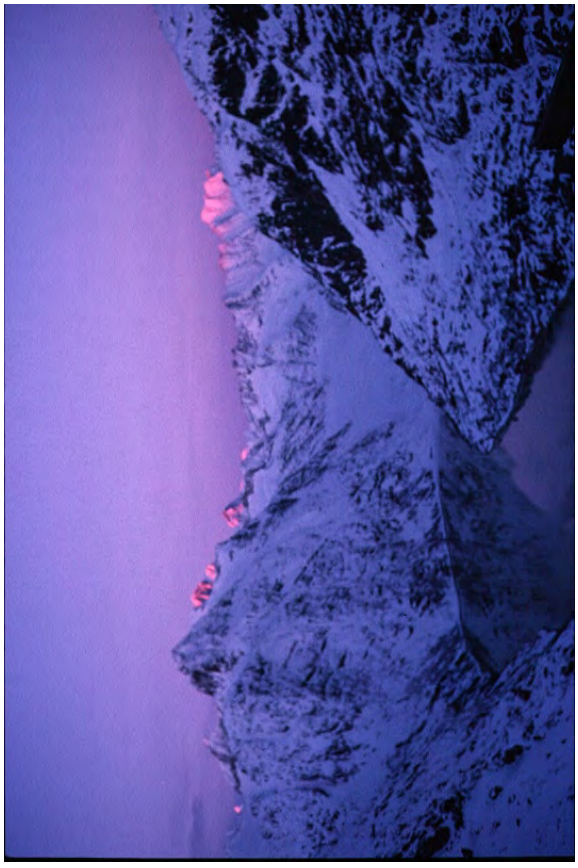

Fig. 1.8A: Winter morning view at Unteraargletscher.

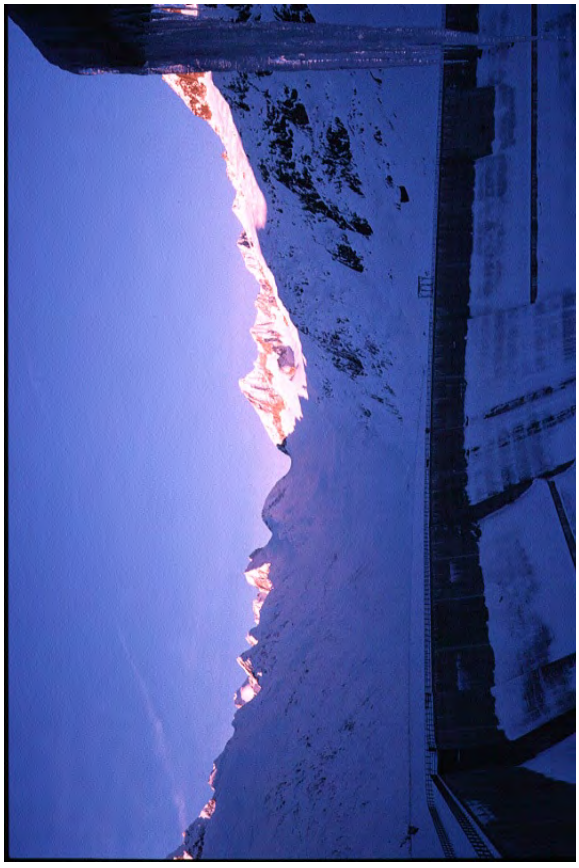

Fig. 1.8B: Winter morning view at Oberaar glacier.

Fig. 1.2.8E: Digging I.

Fig. 1.8G: Water sampling at 4 m depth.

Fig. 1.8D: Walking to the glacier.

Fig. 1.8F: Digging II.

Fig. 1.8I: Raingauge.

Fig. 1.8K: Getting back safely II.

Fig. 1.8H: Frozen lake.

Fig. 1.8J: Getting back safely I.

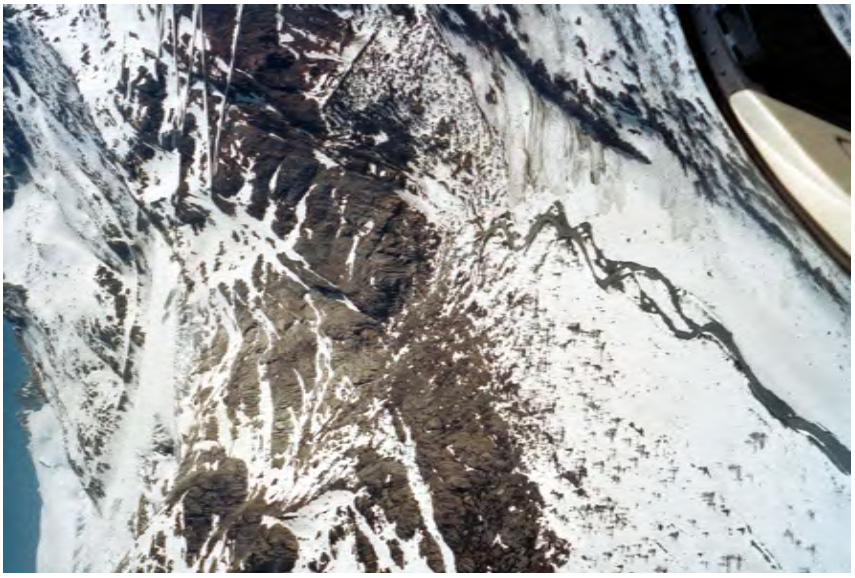

Fig. 1.9C: Rhone glacier in early spring.

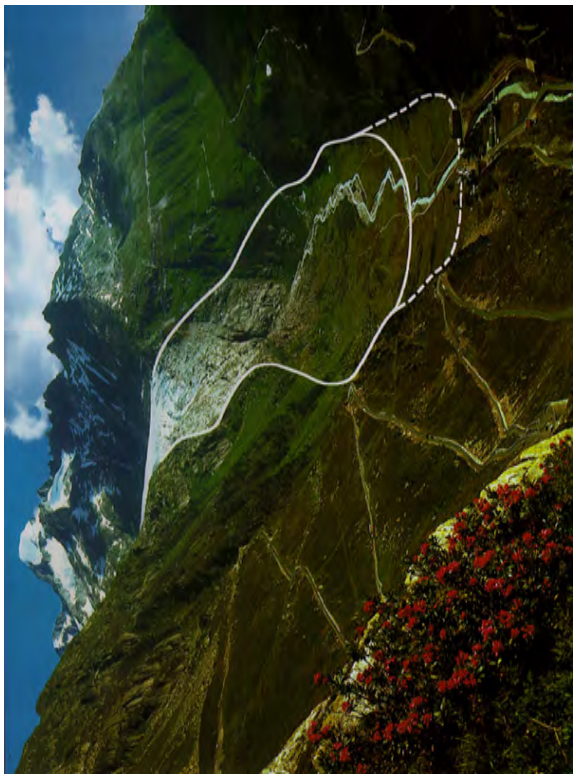

Fig. 1.9A: Rhone glacier.

Fig. 1.9B: Rhone glacier snout.

Fig. 1.9E: Rhone LIA moraine profile.

Fig. 1.9D: Sonde station Rhone meltwater river.

Fig. 1.10A: Rhone forefield in winter.

Fig. 1.10B: Winter sampling I (Martin Burkhard & Rachel Hosein).

Fig. 1.10C: Rhone winter sampling II

Fig. 1.10D: Rhone winter sampling III.

Fig. 1.10E: Rhone winter sampling IV.

LA VERDAD
ZULIA
Sociedad Civil - Comunidad
Salud - Educación - Universitas
Profesionales - Cultura
Controversia, Tribunales y Sucesos
LA VERDAD.COM
Pioneros en un nuevo mundo
www.laverdad.com
Maracaibo, martes 14 de septiembre de 1999

Está la propuesta de investigar las fuentes de carbono que entran a la cuenca

El Iclam y científicos europeos estudian la falta de oxígeno en el Lago de Maracaibo

Judith Chirino Nava
• LA VERDAD

En el Lago de Maracaibo hay separación de masas de agua de diferente densidad, inducidas por la salinidad que entra por el canal de navegación, esto conlleva a fenómenos como la anoxia o falta de oxígeno, principalmente en el volumen central de esta cuenca.

Precisamente en un punto afectado por esta situación anclo el barco laboratorio "Bergantín Maracaibo", con investigadores del Instituto de Conservación del Lago de Maracaibo y un equipo europeo conformado por Vincent Vallés, del Instituto Nacional de Investigaciones Agronómicas de Francia, y Sylvain Huon, de la Universidad de Aviñón, París. También Raquel Hosein y Kaspar Arn, ambos estudiantes de PHD de geoquímica del fosfato de la Universidad de Neuchatel, en Suiza. El objetivo de la misión es tomar muestras del agua para posteriormente intercambiar la información, lo que abre la posibilidad de un proyecto de investigación conjunto.


ELVIA DURÁN


ELVIA DURÁN

Propuesta inicial

El grupo de investigadores extranjeros fue invitado por el ministro del Ambiente, Jesús Pérez, para que conociera el trabajo del Iclam y tomara muestras del agua, aunque realmente están en el país con el auspicio de Francia para estudiar el flujo de los elementos químicos de los sedimentos en los ríos desde Trujillo, los Llanos y hasta el Orinoco.

El jefe de calidad de agua del Iclam, Federico Troncone, señala que los investigadores invitados trabajan con una técnica de isótopos radioactivos que permite conocer el origen de un cuerpo de agua. Por ejemplo, en el caso de la materia orgánica, compuestos que tienen carbono, de alguna manera se puede establecer el origen de la materia que cae en el Lago de Maracaibo.

Después de compartir información nació la propuesta de este tipo de estudio en nuestra cuenca, utilizando la técnica del isótopo radiactivo del carbono. Así con esta especie de huella digital se establecerá si es vegetal o fósil, además de tener una idea de saber cuál de esas fuentes contribuye con el carbono que cae en el Lago.

Cuando las aguas se unen

El profesor Vincent Vallés señala que los investigadores del Iclam tienen mucha información, equipos sofisticados y un alto nivel en su personal, pero se pueden obtener datos más precisos y comparar. "La salinidad afecta a los suelos en la orillas cuando es un clima muy seco. En el Lago impide la mezcla del fondo con la superficie, hay desarrollo excesivo de algas y materia orgánica, por eso el color verde; con un método isotópico se puede entender el origen de la materia, saber de dónde proviene el alga y cómo se descompone", señala.

Vallés aclara que realmente están en Venezuela estudiando los elementos químicos de los sedimentos: el arrastre, el transporte, las mezclas y depósito en las represas y también el proceso que ocurre durante el recorrido desde los ríos llaneros hasta el Orinoco, pero, según el experto, no tienen grandes ambiciones porque sólo cuentan con los recursos aportados por Francia.

En su última estadía en Venezuela tomaron muestras en el Apure y Orinoco, "no es tiempo de dar resultados, con un mes de trabajo de campo hay un año de trabajo de laboratorio". En Francia trabajan -afirma- 100 por ciento para el proyecto de Venezuela, quedan seis meses de laboratorio para tener una visión seria de los resultados. Todo con el apoyo logístico en Venezuela del Ministerio del Ambiente, Cadafe y la Universidad de Los Andes, en el núcleo de Boconó.

El caso Boconó

Vallés destaca que en un estudio realizado con la investigadora venezolana Mirla Cornelle, en la zona de Niquitao, se determinó la presencia de metales tan dañinos como cobalto, manganeso, uranio y níquel. Es un problema localizado, que si se quiere con cal se neutraliza, de lo contrario puede ser muy dañino, por lo que le informaron a las autoridades sanitarias de Trujillo y a Hidroandes, porque puede convertirse en un problema de salud en la población de la zona.

Esos tóxicos son el resultado de un proceso natural, por la calidad de la roca que es muy frecuente en los ríos andinos, por lo que se supone que esto ocurre en otros sitios, más allá de la cuenca de Boconó, pero se sabe cómo neutralizar la acidez.

En el barco laboratorio "Bergantín Maracaibo" los científicos intercambiaron información sobre la anoxia o falta de oxígeno que está afectando a la cuenca, aunque los invitados están en Venezuela estudiando el flujo de elementos químicos en los ríos de Trujillo, los Llanos y hasta el Orinoco

El Bergantín Maracaibo levó anclas

Tripulación: Capitán, Juan Galbán; maquinista, Norberto Robles; marinos timoneles: Emilio Díaz y Ramón Navas.

Del Iclam en esta oportunidad: jefe de calidad de agua, Federico Troncone; biólogos: Enrique Ochoa y Enrique Márquez; asistentes biólogos: Rómulo Márquez y Mangleo Balzán.

Según Vallés, en términos de costo no merece la pena actuar, sino que se prohíba la utilización del agua de ese sector, porque existe un mapa de la caída del agua -con alta precisión- de la cuenca de Boconó, así se sabe qué zona es muy buena.

Puntos de encuentro

Entre los puntos comunes de estudio - señala Vallés- está la eutroficación en las represas, en el Lago se acentúa por la entrada de agua salina, una de las características es la falta de oxígeno. En la toma de aguas en Boconó-Tucupido para alimentar la zona de Guanare huele muy mal y esto se debe a sulfuros y es igual lo que pasa dentro del Lago.

No es un proceso de acidez, es una falta de oxígeno llamada anoxia, esto induce a la disolución de metales que pueden ser tóxicos; manganeso, hierro, entre otros. Se generan sólo microorganismos como las bacterias, los peces huyen porque el agua se carga de amonio y es tóxico.

Estos científicos estudian el flujo de elementos químicos en el intercambio continente-océano y en los embalses, pero en los casos donde han encontraron elementos dañinos para la salud pública informaron a las autoridades, además de exponer las recomendaciones.

¡Oxígeno, por favor!

En el Lago de Maracaibo hay varias capas de masas de agua de diferente salinidad, esto genera un problema porque impide el flujo de agua y el oxígeno que está en la parte más profunda se agota, las capas impiden la circulación del agua, una especie de candado, generando las llamadas cuencas anóxicas. Troncone explica que esto ocupa entre el 30 a 35 por ciento, a veces un poco más; cada vez se hace más anóxico, hasta ahora se ha incrementado la anoxia en algunas áreas y cambia de tamaño.

El fenómeno, llamado también hipolimion, cuando inicialmente fue descrito los investigadores afirmaban que se formaba y luego desaparecía, pero los valores de salinidad no eran muy altos. Los estudios del Iclam -desde 1992 hasta la fecha- señalan que el hipolimion no ha disminuido; "a principio de los años sesenta se decía que desaparecía con las lluvias, ahora es permanente porque es un problema crónico", señala.

Troncone explica que a través de los ríos viene un exceso de nitrógeno producto del abono, también entran pesticidas, elementos tóxicos; de las áreas agrícolas son arrastrados por el río. El nitrógeno es uno de los macronutrientes, como el carbono. El exceso de algas que hay en el Lago, una especie de verdín, emana mal olor producto de su descomposición, un reflejo del grado de degradación que tiene la cuenca y una de las causas principales es el exceso de nitrógeno que llega a la cuenca a través de las aguas negras y por el manejo inadecuado de las prácticas agrícolas y esto puede mejorar si se determinan los sitios y son intervenidos.

Carbono en la mira

En relación al carbono, el Iclam todavía no maneja tantos datos, por eso la propuesta de estudiar el balance del macronutriente. Esto se hace para diseñar sistemas para reducir el elemento; si saben por cuál zona están entrando niveles muy altos de un compuesto de carbono se toman acciones.

El ciclo del carbono tiene varias vías en diferentes compuestos y de las vías que tome dependen los procesos que podrían estudiar conjuntamente con los europeos, el potencial de oxidorreducción. Por ejemplo, en tantos metros lo que pasa es que va oxidar a mono o bióxido de carbono, en otro lado se puede formar metano, por los valores negativos del potencial de oxidorreducción, entre otras informaciones valiosas. Según Troncone si este trabajo logra financiamiento, por lo menos se requieren entre cuatro a cinco años para obtener información científicamente aceptable.


ELVIA DURÁN


ELVIA DURÁN

Fig. 1.11: Venezuelan Newspaper report.

Fig. 1.12A: The region near Bocono I.

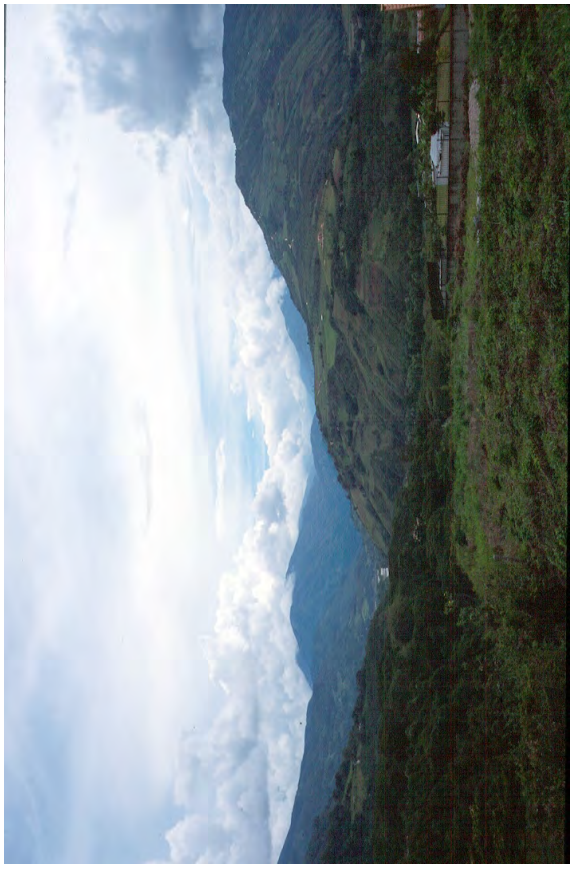

Fig. 1.12B: Apure headwater rivers.

Fig. 1.12C: Apure headwater river sampling (Sylvain Huon & Rachel Hosein)

Fig. 1.12D: The region near Bocono II.

Fig. 1.12F: Sampling Guanare.

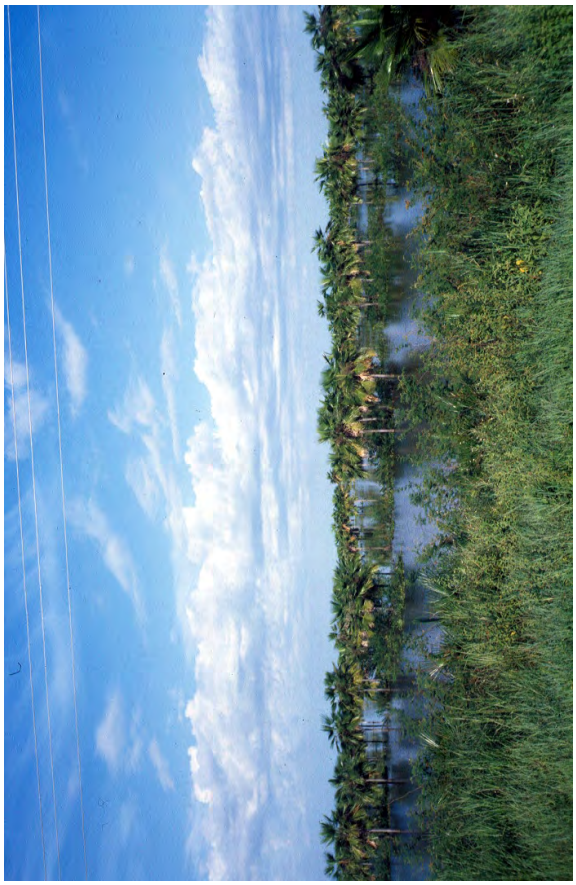

Fig. 1.12H: Flooded plains of Los Llanos.

Fig. 1.12E: Lago Bocono.

Fig. 1.12G: Sampling Portuguesa.

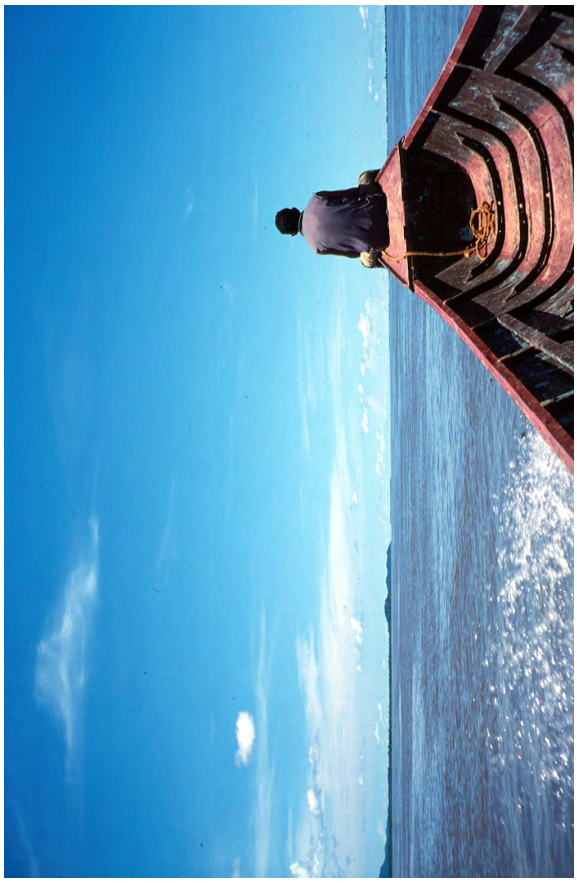

Fig. 1.12J: Orinoco boat ride.

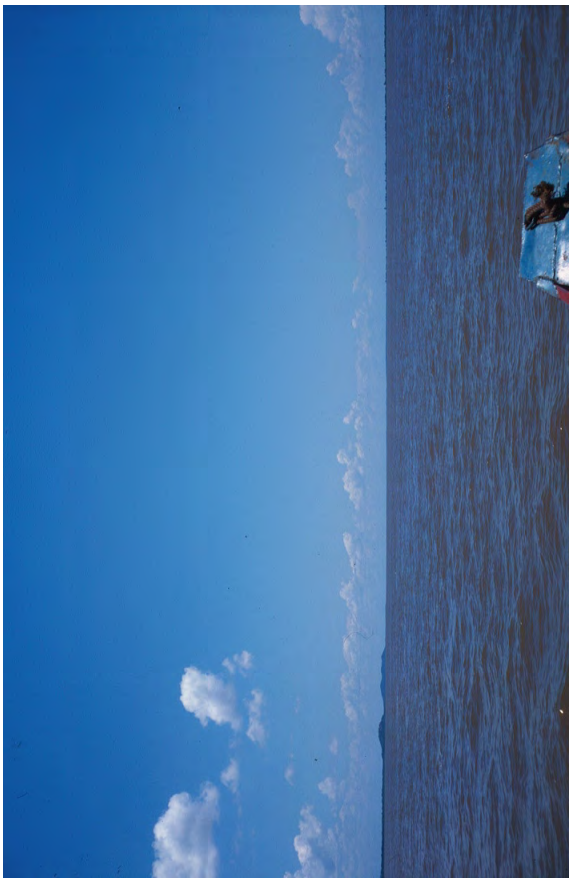

Fig. 1.12L: Orinoco.

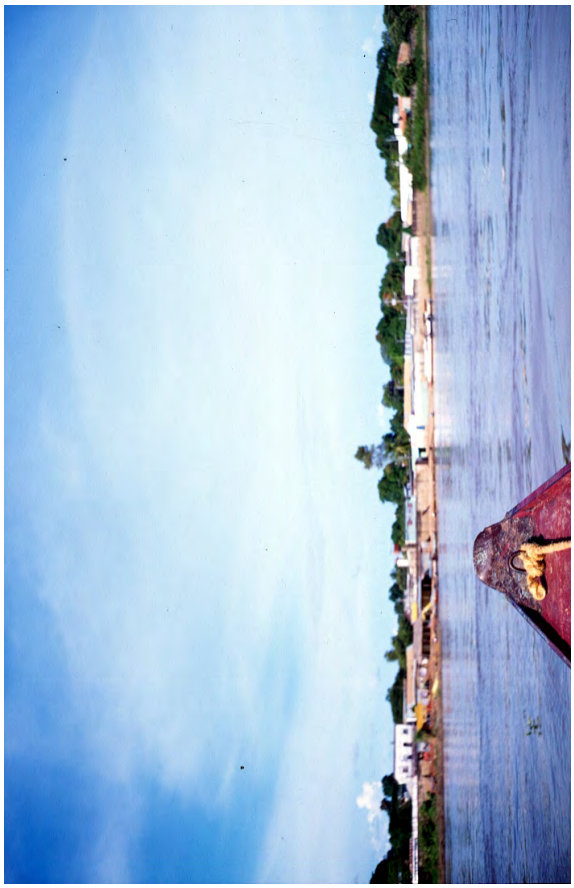

Fig. 1.12I: Getting back to Cabrutta.

Fig. 1.12K: Orinoco bank I.

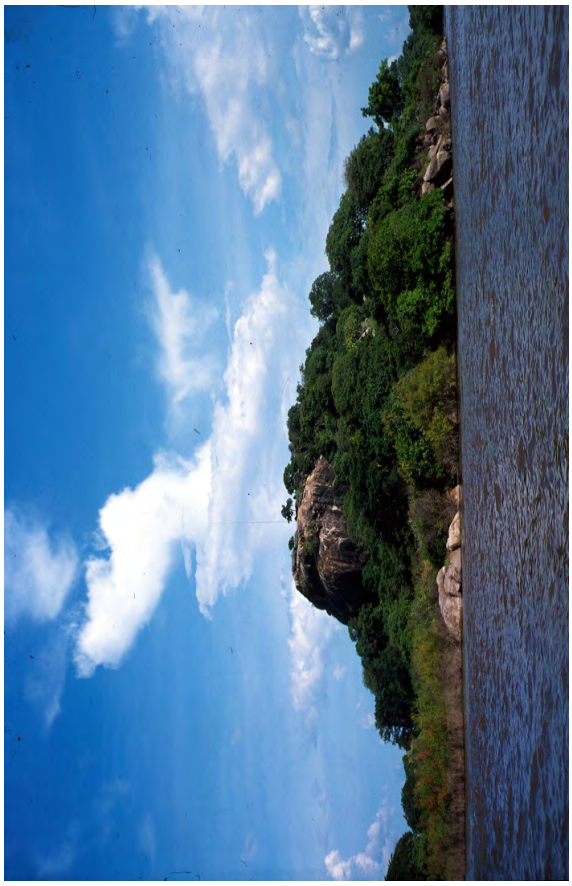

Fig. 1.12N: Orinoco bank II.

Fig. 1.12P: The famous sonde on Orinoco.

Fig. 1.12M: Preparing the water velocity measurment.

Fig. 1.12O: The team: Sylvain Huon, Driver Gerardo, Rachel Hosein, myself (f.l.t.r.)